Syntheses of Novel Nickel and Palladium Complexes: Catalytic C–H Functionalizations and Mechanistic Studies

Thesis

Submitted to AcSIR for the Award of the Degree of

DOCTOR OF PHILOSOPHY

in

Chemical Sciences

by

Shrikant Manmathappa Khake

(Reg. No: 10CC12J26019)

under the guidance of

Dr. Benudhar Punji

CSIR-National Chemical Laboratory

Pune-411 008, INDIA

2017

Dedicated to My Parents and Teachers

राष्ट्रीय रासायनिक प्रयोगशाला
(वैज्ञानिक तथा औद्योगिक अनुसंधान परिषद)
डॉ. होमी भाभा मार्ग, पुणे - 411 008. भारत
NATIONAL CHEMICAL LABORATORY
(Council of Scientific & Industrial Research)
Dr. Homi Bhabha Road, Pune - 411 008. India.
हीरक जयन्ती वर्ष 2009-10

Dr. Benudhar Punji
Senior Scientist and Assistant Professor (AcSIR)
CSIR-National Chemical Laboratory
b.punji@ncl.res.in
+91 20 2095 2733

Thesis Certificate

This is to certify that the work incorporated in this Ph.D. thesis entitled "**Syntheses of Novel Nickel and Palladium Complexes: Catalytic C–H Functionalizations and Mechanistic Studies**" submitted by Mr. Shrikant Manmathappa Khake to the Academy of Scientific and Innovative Research (AcSIR) in fulfillment of the requirements for the award of the Degree of the Doctor of Philosophy, embodies original research work under my supervision. I further certify that this work has not been submitted to any other University or Institution in part or full for the award of any degree or diploma. Research material obtained from other sources has been duly acknowledged in the thesis. Any text, illustration, table, etc., used in the thesis from other sources, have been duly cited and acknowledged.

Shrikant Manmathappa Khake
(Research Student)

17/7/2017
Dr. Benudhar Punji
(Research Supervisor)

Declaration by the Candidate

I hereby declare that the original research work embodied in this thesis entitled, "**Syntheses of Novel Nickel and Palladium Complexes: Catalytic C–H Functionalizations and Mechanistic Studies**" submitted to the Academy of Scientific and Innovative Research for the award of the degree of the Doctor of Philosophy (Ph.D.) is the outcome of experimental investigations carried out by me under the supervision of Dr. Benudhar Punji, Senior Scientist, CSIR-National Chemical Laboratory, Pune. I affirm that the work incorporated is original, and has not been submitted to any other academy, university or institute for the award of any degree or diploma.

July 2017
CSIR-National Chemical Laboratory
Pune-411008

Shrikant Manmathappa Khake
(Research Student)

Acknowledgement

Any human achievement is the culmination of numerous contributions and endeavors. There are many helping hands in one's success, and the present thesis is not an exception. As I completed my journey towards the most cherished dream, it gives immense pleasure and sense of satisfaction to record my heartfelt gratitude to all the persons who have made this possible for me. First and foremost, I wish to express my heartfelt gratitude to my research supervisor, **Dr. Benudhar Punji** for believing in my abilities and providing me an incredible opportunity to pursue my career as a Ph. D. student. I thank him for his excellent guidance, constant encouragement, sincere advice, understanding and unstinted support during all the times of my doctoral research. He is a fantastic mentor who was influential for my interest, and my ability to grasp the essence of organometallic chemistry. He taught me everything he knows and always encourages me to think creatively and be prepared to learn new scientific methods. I am grateful to him for all the ways in which he has prepared me to move forward in my career as well as life. I consider very fortunate for my association with him, which has given a decisive turn and a significant boost in my career. Although I am sad to be leaving, I am looking forward to the future and will enjoy watching the lab develop during the upcoming years.

I wish to express my sincere thanks to the Doctoral Advisory Committee members, Dr. Samir H. Chikkali, Dr. Kumar Vanka, Dr. Sayam Sen Gupta and Dr. E. Balaraman for their continued support, guidance, and suggestions. I am grateful to Prof. A. K. Nangia, Director, NCL, Dr. V. K. Pillai and Prof. S. Pal (Former Director, NCL), Dr. S. Tambe, Head, CEPD Division, and Dr. Ranade (Former HoD, CEPD Division) for giving me this opportunity and providing all necessary infrastructure and facilities.

I was very fortunate to work with a fantastic group of colleagues in the **Punji's** research group. My sincere thanks to **Hanuman**, **Vineeta**, **Ulhas**, **Dilip**, **Rahul**, and **Dipesh** for devoting their help and made many valuable suggestions. I would like to thank summer trainee **Fathima**, **Shreya**, **Anupriya** and **Haripriya** for their help during work. Also, I am thankful to Dr. Chikkali's group members Dr. Ketan Patel, Dr. Shilpi Kushwaha, Dr. Dipa Mandal, Vijay, Shahji, Bhausaheb, Satej, Swechchha, Nilesh, Anirban, Dynaneshwar, Ravi and Rohit who helped me during my Ph. D. work.

I would like to acknowledge my senior colleagues for their helping hands and friendly affection including Drs. Rahul Patil, Kishor Harale, Ravi Jagtap, Sachin Mali, Prakash

Sultane, Prakash Chavan, Kailash Pawar, Govind Pawar, Rohan Erande, Manoj Mane, Santosh Chavan, Sambhaji Dhumal, Amarsinh Deshmukh and Suhas Bhosale throughout my tenure in Pune and Aurangabad.

I wish to thank Dr. Sachin Bhojgude, Dr. Sachin Thawarkar, Bharat, Balasaheb, Sakharam, Govind, Nagesh, Pradnya, Rohini, Sachin, Yuvraj, Shailja for helping me in various stage of work in NCL. Help from my senior friends from NCL including Dr. Mahesh Bhure, Munmun, Satywan and Amol are gratefully and sincerely appreciated. I would like to extend my thanks to Dr. Rajamohanan, Amol, Mayur, Shrikant, Dinesh for their timely help with NMR recording, Dr. R. Gonnade, Shridhar, Ekta, Samir for the X-ray analysis, Mrs. Shantakumari for Mass/HRMS facility, and Dr. Borikar for GCMS analysis. Help from elemental analysis facility is also acknowledged. I would like to express my sincere appreciation to the Council of Scientific & Industrial Research (CSIR)-New Delhi for providing JRF and SRF fellowships, without this Ph. D. would not have been possible.

Finally, I dedicate this thesis to the people who mean the most to me, my dear respected parents, beloved brother Ashok and sister Meenakshi, and all my well-wishers whose continuous encouragement and support have been a source of inspiration in the completion of this tough task.

Shrikant Manmathappa Khake

Abstract

Chapter 1 deals with the detailed literature survey on the pincer-based palladium complexes, and their applications in various cross-coupling reactions. Mechanistic aspect of the pincer palladium-catalyzed coupling reaction is also reviewed. Further, the C–H bond arylation of azoles by various catalytic systems has been described. Similarly, this chapter includes reports on the Ni-catalyzed C–C bond forming reaction *via* C–H activation, and their catalytic pathways.

In Chapter 2, several hybrid amino-phosphinite based pincer ligands with different steric and electronics properties have been synthesized. The metalation of all the pincer ligands with palladium precursors has been performed to synthesize the pincer palladium complexes. The amino-phosphinite pincer ligands 1-(R_2PO)-C_6H_4-3-($CH_2N^iPr_2$) [$^{R2}POCN^{iPr2}$–H; R = ^{i}Pr or ^{t}Bu] were synthesized in two steps starting from 3-hydroxy benzyl bromide. The treatment 3-hydroxy benzyl bromide with the diisopropylamine gave hydroxylamine, which on further reaction with the dialkylchlorophosphine afforded ($^{R2}POCN^{iPr2}$)–H ligands. The ($^{R2}POCN^{iPr2}$)–H on metalation with (COD)$PdCl_2$ produces the pincer complexes, {2-(R_2PO)-C_6H_3-6-($CH_2N^iPr_2$)}PdCl [($^{R2}POCN^{iPr2}$)PdCl; R = ^{i}Pr, ^{t}Bu] in good yields. Both the ($^{R2}POCN^{iPr2}$)–H ligands and ($^{R2}POCN^{iPr2}$)PdCl complexes were characterized by ^{1}H, ^{13}C, and ^{31}P NMR spectroscopy. Further, the ($^{R2}POCN^{iPr2}$)PdCl complexes were characterized by X-ray diffraction study and elemental analysis. Treatment of palladium complex ($^{iPr2}POCN^{iPr2}$)PdCl with KI gave ($^{iPr2}POCN^{iPr2}$)PdI complex. The reactions of ($^{R2}POCN^{iPr2}$)PdCl with AgOAc, AgOTf, and $AgSbF_6$ in THF at room temperature produced ($^{R2}POCN^{iPr2}$)PdOAc, ($^{R2}POCN^{iPr2}$)Pd(OTf) and ($^{iPr2}POCN^{iPr2}$)Pd(SbF_6) complexes, respectively. All these pincer palladium complexes were screened and employed for the C–H bond arylation of azoles with aryl halides.

Similarly, the synthesis of electronically and sterically distinct pincer palladium complexes, {2-(R_2PO)-C_6H_3-6-(CH_2NEt_2)}PdCl [($^{R2}POCN^{Et2}$)PdCl; R = ^{i}Pr, Ph] and their catalytic activity for the C–H bond arylation of azoles have been described in Chapter 3. Firstly, the precursor for the ligand, 3-((diethylamino)methyl)phenol was synthesized by the reaction of 3-hydroxy benzyl bromide with diethylamine. The 3-((diethylamino)methyl)phenol on phosphinations with dialkylchlorophosphine and diarylchlorophosphine afforded corresponding ($^{R2}POCN^{Et2}$)–H [R = ^{i}Pr, Ph] ligands. The complexation of ($^{R2}POCN^{Et2}$)–H with (COD)$PdCl_2$ provided ($^{R2}POCN^{Et2}$)PdCl (R = ^{i}Pr, Ph) complexes. All the ($^{R2}POCN^{Et2}$)–H ligands and ($^{R2}POCN^{Et2}$)PdCl complexes were

characterized by various analytical techniques. Further, the molecular structures of both the Pd-complexes are established by the X-ray diffraction study. The complex (^{iPr2}POCN^{Et2})PdCl was found to be an efficient catalyst for the arylation of benzothiazole and benzoxazole using mild base, K_3PO_4. This reaction tolerates the important functional groups like –OMe, –CF_3, –COOMe, –F, and –Cl. The rate of the arylation using various (^{R2}POCN^{R2})PdCl catalysts was compared, and the complex (^{iPr2}POCN^{Et2})PdCl was found to be much superior for the arylation of azoles.

The detailed mechanism of the (^{iPr2}POCN^{Et2})Pd-catalyzed arylation of benzothiazole with aryl iodides is discussed in Chapter 4. Preliminary experiments have been performed to know the homogeneous *verses* heterogeneous nature of the catalyst, wherein the effect of external additives, such as PPh_3, pyridine, $^{n}Bu_4NBr$, PVPy and Hg on the arylation was examined. To gain more insight into the mechanism, kinetics of the arylation reaction was performed, including the induction period analysis, rate of the reaction and order of the reaction with various reaction components. The kinetic isotope effect (KIE) experiment has been performed to understand the C–H bond activation process during the catalysis. The initial rates for the arylation reaction of benzothiazole with electronically different *para*-substituted aryl iodides were determined to understand the electronic influence of the substrate on the arylation. Hammett plot analysis suggested the electrophilic nature of the active Pd-catalyst. The catalytic active (^{iPr2}POCN^{Et2})Pd(benzothiazolyl) intermediate has been isolated and characterized by NMR, elemental analysis, and X-ray diffraction study. The controlled reactivity study of (^{iPr2}POCN^{Et2})Pd(benzothiazolyl) with substituted aryl iodides suggest that the oxidative addition of aryl iodide could be the slow step during the catalysis. To understand the feasibility of the catalytic process the DFT calculation was carried out, which shows reasonable energy barrier (32.9 kcal/mol) for the oxidative addition of aryl iodide to Pd(II). All these studies suggested that the catalysis follows a Pd(II)/Pd(IV)/Pd(II) pathway.

Chapter 5 describes a general nickel-catalyzed method for the alkynylation of heteroarenes *via* monodentate chelation-assistance. The *in-situ* generated catalyst obtained from $(THF)_2NiBr_2$ and 1,10-phenanthroline (Phen) catalyzes the alkynylation of heteroarenes with alkynyl bromide. This approach allowed the coupling of various heteroarenes like indoles, pyrroles, benzimidazole, imidazoles and pyrazole with (triisopropyl)silylalkynyl bromide. This methodology tolerates the synthetically valuable functional groups, such as –OMe, –CF_3, –NO_2, –CN, –F and –Br on indole moiety. This represents the first report for the alkynylation of heteroarenes using Ni-catalyst *via* monodentate chelation assistance. The

synthetic applicability of this Ni-catalyzed method has been demonstrated by the removal of (triisopropyl)silyl (–Si^{i}Pr$_3$) group upon treating with tetra-butyl ammonium bromide. Further, the functionalization of the alkynyl-indole with benzyl azide produced triazolyl compounds. Sonogashira coupling reaction of the deprotected alkynyl-indole with aryl iodide afforded alkynyl arene, whereas the reaction of alkynyl-indole with 2-hydroxy aryl iodide produced benzofuran derivatives.

The mechanistic aspect of the Ni-catalyzed C(2)–H alkynylation of indoles is described in Chapter 6. The *in-situ* generated Ni-catalyst (THF)$_2$NiBr$_2$/Phen efficiently catalyzed the alkynylation of indoles. Hence, the [(Phen)$_3$Ni].NiBr$_4$, (Phen)$_2$NiCl$_2$ and [(Phen)$_3$Ni].NiCl$_4$ complexes were independently synthesized, and characterized by X-ray diffraction study and elemental analysis. These complexes were as reactive as the *in-situ* generated catalyst for the alkynylation of indoles. The reactivity of the isolated complexes has been investigated. Various controlled and additive experiments were performed to understand the probable pathway for the alkynylation reaction. To gain more insight, the detailed kinetics of the alkynylation reaction was performed, including the rate order determination. DFT calculation was performed to support the experimental evidence of the alkynylation reaction. Finally, a probable mechanistic cycle for the Ni-catalyzed alkynylation of indole was presented.

Abbreviations

acac	Acetylacetonate
AgOTf	Silver trifluoromethanesulfonate
$AgPF_6$	Silver hexafluorophosphate
$AgSbF_6$	Silver hexafluoroantimonate
bathocuproine	2,9-Dimethyl-4,7-diphenyl-1,10-phenanthroline
bipy	2,2'-Bipyridine
BDMAE	Bis(2-dimethylaminoethyl) ether
BnN_3	Benzyl azide
BINOL	1,1'-Bi-2-naphthol
Cp	Cyclopentadienyl
COD	1,5-cyclo-octadiene
Cy	Cyclohexyl
Davephos	2-Dicyclohexylphosphino-2′-(*N*,*N*-dimethylamino)biphenyl
DCE	1,2-dichloroethane
dcype	Dicyclophosphinoethane
DFT	Density functional theory
DME	Dimethoxy ethane
DMA	*N*,*N*-dimethylacetamide
DMAP	4-Dimethylaminopyridine
DMF	*N*,*N*-dimethylformamide
DMSO	Dimethyl sulfoxide
D*t*BEDA	*N*,*N'*-Di-*tert*-butyl ethylenediamine
dtbpy	4,4-Di-*tert*-butyl bipyridine
dppf	1,1'-Bis(diphenylphosphino)ferrocene
dppz	Dipyrido[3,2-a:2′,3′-c]phenazine
dppbz	1,2-Bis(diphenylphosphanyl)benzene
F-SPE	Fluorous-solid phase extraction technique
Galvinoxyl	2,6-Di-*tert*-butyl-α-(3,5-di-*tert*-butyl-4-oxo-2,5-cyclohexadien-1-ylidene)-*p*-tolyloxy
HRMS	High resolution mass spectrometry
LA	Lewis Acid

LiHMDS	Lithium bis(trimethylsilyl)amide
$Me_2S{\cdot}CuBr$	Copper(I) bromide dimethyl sulphide
MeSCOOH	2,4,6-trimethylbenzoic acid
Neocuproine	2,9-dimethyl-1,10-phenanthroline
$(DME)NiCl_2$	Nickel(II) chloride ethylene glycol dimethyl ether
$(dppp)NiCl_2$	Dichloro(1,3-bis(diphenylphosphino)propane)nickel
n-Bu_4NBr	*n*-Tetrabutyl ammonium bromide
NMP	1-Methyl-2-pyrrolidone
OLED	Organic light emitting diodes
ORTEP	Oak ridge thermal-ellipsoid plot program
OTf	Trifluoromethanesulfonate
$Pcyp_3$	Tricyclo pentyl phosphine
$Pd_2(dba)_3$	Tris(dibenzylideneacetone)dipalladium(0)
$Pd(COD)Cl_2$	Dichloro(1,5 cyclooctadiene)palladium(II)
Phen	1.10-Phenanthroline
PIP	2-Pyridinyl isopropyl
Piv	Pivalate
PMe_3	Trimethyl phosphine
PvPy	Poly(vinylpyridine)
Py	Pyridinyl
$P(^iPr)_3$	*tri*-Isopropyl phosphine
$[RhCl(coe)_2]_2$	Chlorobis(cyclooctenerhodium(I)
TADDOL	α,α,α,α-Tetraaryl-1,3-dioxolane-4,5- dimethanols
t-AmOH	*tert*-Amylalcohol
TBHP	*tert*-Butylhydroperoxide
TBAF	tetra-*n*-Butylammonium fluoride
TEMPO	(2,2,6,6-Tetramethylpiperidin-1-yl)oxyl
TFA	Trifluoroacetic acid
TFE	Trifluoroethanol
TIPS	Triisopropylsilyl
TOF	Turnover frequency
TON	Turnover number

List of tables

2.1	Selected bond lengths (Å) and bond angles (^{o}) for **4** and **5**	59
2.2	Optimization of reaction conditions for arylation of azole	60
3.1	Selected bond lengths (Å) and bond angles (^{o}) for **20**, **22**, **23** and **24**	86
3.2	Optimization of reaction conditions for arylation of azole	88
3.3	Rate of the arylation reaction with various (POCN)PdCl catalysts	89
4.1	Added ligand experiments	102
4.2	Rate of arylation reaction with varying concentration of benzothiazole	105
4.3	Rate of arylation reaction with varying concentration of 4-iodotoluene	105
4.4	Rate of arylation reaction with varying concentration of ($^{i\mathrm{Pr2}}$POCN$^{\mathrm{Et2}}$)PdCl	106
4.5	Rate of arylation reaction with varying concentration of CuI	106
4.6	Rate arylation reaction with varying concentration of K_3PO_4	107
4.7	Rate of arylation reaction at same [excess] concentration of substrate	110
4.8	Selected bond lengths (Å) and bond angles (^{o}) for **25**	118
5.1	Optimization of reaction conditions for alkynylation	133
6.1	Selected bond lengths (Å) and bond angles (^{o}) for **36**, **37** and **38**	166
6.2	Rate of alkynylation reaction with varying concentration of **27a**	172
6.3	Rate of alkynylation reaction varying concentration alkynyl bromide (**28**)	172
6.4	Rate of alkynylation reaction at different loading of LiO^{t}Bu	172
6.5	Rate of alkynylation reaction at different loading of **36**	173
	Crystal data and structure refinement for complexes **4**, **5** and **20**	188
	Crystal data and structure refinement for complexes **22**, **23** and **24**	189
	Crystal data and structure refinement for complexes **25** and **36**	190
	Crystal data and structure refinement for complexes **37** and **38**	191

List of figures

1.1	Schematic representation of pincer ligand	2
1.2	General representation of pincer complexes	3
1.3	Pincer complexes by Shaw and co-workers	3
1.4	A) NCN pincer ligand by van Koten; B) PNP pincer system by Fryzuk	4
1.5	Representative symmetrical pincer ligands	4
1.6	Representative non-symmetric pincer ligands	5
1.7	Representative pincer palladium complexes	6
1.8	Chiral pincer palladium complexes *via* C–I bond activation	8
2.1	Hybrid POCN pincer ligand and POCN pincer palladium complexes	55
2.2	Thermal ellipsoid of (^{iPr2}POCN^{iPr2})PdCl (**4**)	58
2.3	Thermal ellipsoid of (^{tBu2}POCN^{iPr2})PdCl (**5**)	58
3.1	ORTEP diagram of complexes **20**, **22**, **23** and **24**	85
3.2	Time-dependent formation of **14aa** using various (POCN)PdX catalysts	89
4.1	Mechanism for arylation of azoles *via* Pd(0)/Pd(II) or Pd(II)/(IV) pathway	100
4.2	Reaction profile for arylation of benzothiazole with 4-iodotoluene	104
4.3	(A) Formation of **14aa** with varying concentration of benzothiazole. (B) Plot of log(rate) *vs* log(conc. benzothiazole)	107
4.4	(A) Formation of **14aa** with varying concentration 4-iodotoluene. (B) Plot of log(rate) *vs* log(conc. 4-iodotoluene)	108
4.5	(A) Formation of **14aa** at different concentration of **20**. (B) Plot of log(rate) *vs* log(conc. **20**)	108
4.6	(A) Formation of **14aa** at different conc. of CuI. (B) Plot of log(rate) *vs* log(conc. CuI)	108
4.7	(A) Formation of **14aa** at different loading of K_3PO_4. (B) Plot of log(rate) *vs* log(equiv. K_3PO_4)	109
4.8	Formation of **14aa** at same [excess] concentrations of benzothiazole and 4-iodotoluene	110
4.9	Formation of **14aa** using 2-*H/D*-benzothioazole with 4-iodotoluene	111

4.10 Kinetics for reaction of 6-ethoxybenzothiazole, benzothiazole and 6-fluorobenzothiazole with 4-iodotoluene 113
4.11 (A) Arylations using different *para*-substituted aryl iodides with benzothiazole. (B) Hammett plot correlation 114
4.12 ORTEP diagram of (^{iPr2}POCN^{Et2})Pd(benzothiazolyl) (**25**) 118
4.13 Formation of (^{iPr2}POCN^{Et2})PdI (**22**) from **25** and aryl iodides 120
4.14 Possible transition states for the oxidative addition of RC1 to **25** 121
4.15 Free energy profile for the reaction of phenyl iodide (RC1) with **25** 122
4.16 Proposed arylation pathway using (POCN)PdX 123

6.1 ORTEP diagram of $[(Phen)_3Ni]\cdot NiBr_4$ (**36**) 165
6.2 ORTEP diagram of $[(Phen)_3Ni]\cdot NiCl_4$ (**37**) 165
6.3 ORTEP diagram of $(Phen)_2NiCl_2$ (**38**) 165
6.4 Formation of **29a** using 1-(pyridin-2- yl)-1*H*-indole (**27a**) and **28** 170
6.5 Formation of **29a** from the reaction of **27a** with **28** 171
6.6 (A) Product **29a** at different initial concentration of **27a**. (B) Plot of log(rate) *vs* log(conc. **27a**) 173
6.7 (A) Formation of **29a** with varying concentration of **28**. (B) Plot of log(rate) *vs* log(conc. **28**) 174
6.8 (A) Formation of **29a** at different loading of LiO^tBu. (B) Plot of log(rate) *vs* log(equiv. LiO^tBu) 174
6.9 (A) Formation of **29a** at different loading of **36**. (B) Plot of log(rate) *vs* log(equiv. **36**) 174
6.10 Formation of the product **29a** from the reactions of [**27a**]-H or [**27a**]-D with **28** 175
6.11 Free energy profile for the Ni(II)-catalyzed alkynylation of indoles 178
6.12 Probable catalytic cycle for alkynylation reaction 179

List of schemes

1.1	Synthesis of (NCN)PdBr by oxidative addition of C–Br bond	7
1.2	Synthesis of (POCOP)PdBr by oxidative addition approach	7
1.3	Synthesis of (PCP)Pd-pincer complex *via* C–H activation process	9
1.4	Synthesis of pincer palladium complex *via* C–H activation process	9
1.5	Synthesis of pincer palladium complex by transcyclometalation	10
1.6	Synthesis of chiral pincer palladium complex by C–H activation	10
1.7	Synthesis of chiral NCN pincer palladium *via* ligand introduction route	11
1.8	Heck coupling reaction using **1.26** complex	12
1.9	Heck coupling reaction using **1.27** complex	12
1.10	Heck coupling reaction using **1.28** complex	13
1.11	Heck coupling reaction using hemilabile Pd-pincer **1.29** complex	13
1.12	Suzuki coupling reaction using **1.30** complex	14
1.13	Suzuki coupling reaction using chiral pincer complex **1.32**	14
1.14	Cross-coupling of aryl boronate with aziridine using complex **1.33**	15
1.15	Cross-coupling of vinyl boronate with vinyl epoxide using complex **1.34**	15
1.16	Suzuki coupling reaction using bis(azole) pincer palladium complex **1.35**	15
1.17	Suzuki coupling using amido-phosphine palladium pincer complex **1.36**	16
1.18	Hiyama cross coupling using unsymmetrical pincer complex **1.37**	16
1.19	Stille reaction using PCP pincer complex **1.38**	17
1.20	Negishi coupling reaction using pincer complex **1.41**	17
1.21	Cross-coupling reaction of aryl bromide with aryl zinc using pincer complex **1.42**	17
1.22	Cross-coupling of aryl iodide with terminal alkynes using complex **1.43**	18
1.23	Pincer palladium complex **1.44** catalyzed Sonogashira reaction	19
1.24	Sonogashira reaction using unsymmetrical pincer palladium complex **1.45**	19
1.25	Enantioselective synthesis of oxazoline using chiral pincer complex **1.46**	19
1.26	Catalytic generation of nucleophilic bis(allyl)Pd-species	20
1.27	Catalytic generation of nucleophilic η^1-allyl palladium pincer species	20
1.28	Allylation of aldehyde using selenium based complex **1.50**	21
1.29	Allylation of aldehyde using porphyrin-based pincer palladium complex **1.51**	21
1.30	Heck reaction using pincer palladium complex **1.52** as dispenser of Pd(0) nanoparticles	22

1.31	Heck coupling *via* Pd(0)/Pd(II) classical catalytic cycle	23
1.32	Proposed pathway for decomposition of pincer palladium	24
1.33	Reduction of **1.55a** and **1.55b** to form **1.55c** and it's oxidation to regenerate pincer complex	25
1.34	Oxidation of Pd(II) pincer to Pd(IV) complexes using hypervalent iodine salts	26
1.35	Heck coupling of iodonium salt and allyl acetate using complex **1.59**	27
1.36	Catalytic cycle for Heck coupling *via* Pd(II)/Pd(IV) pathway	27
1.37	Catalytic cycle for Suzuki reaction using complex **1.62**	28
1.38	Direct C–H arylation of azoles using palladium catalyst	29
1.39	Arylation of azole using nickel-catalyst	30
1.40	Arylation of benzoxazole using CuI catalyst	30
1.41	Direct C(2)-arylation of azole using palladium as catalyst	31
1.42	Arylation of benzimidazole using rhodium as a catalyst	31
1.43	Arylation of azole using Pd as catalyst and Cu as co-catalyst	31
1.44	Synthesis of organonickel species	32
1.45	Nickel-catalyzed alkylation of aromatic heterocycle with an alkyl halide	33
1.46	Alkylation of azoles using (NNN)Ni-pincer complex	33
1.47	Ni-catalyzed alkylation of benzamide using bidentate directing group	33
1.48	Nickel-catalyzed alkylation of C(sp^3)–H bond of aliphatic amide	34
1.49	Nickel-catalyzed *ortho*-alkylation of aniline *via* monodentate chelation assistance	34
1.50	Direct C(2)–H alkylation of indoles using (NNN)Ni-catalyst with alkyl halides	35
1.51	Nickel-catalyzed addition of pyridine-*N*-oxide to alkyne	35
1.52	Nickel-catalyzed alkenylation of pentafluorobenzene	36
1.53	Direct C(2)–H alkenylation of pyridine using nickel and Lewis acid system	36
1.54	Nickel-catalyzed arylation of azoles with aryl halide or aryl triflate	37
1.55	Nickel-catalyzed arylation of azoles with aryl bromide	37
1.56	Nickel-catalyzed arylation of azoles using $Mg(O^tBu)_2$ in DMF	37
1.57	Nickel-catalyzed Ar–H/Ar–O cross-coupling reaction	38
1.58	Nickel-catalyzed C–H arylation of heteroarenes with the organosilicon compounds	39
1.59	Nickel-catalyzed C–H arylation of heteroarenes with aryl boronic acid	39
1.60	Nickel-catalyzed C(sp^2)–H arylation of purines with aryl magnesium bromide	39
1.61	Nickel-catalyzed direct C(sp^3)–H bond arylation of aliphatic amides	40
1.62	Solvent-free nickel-catalyzed C(sp^2)–H bond arylation of bezo[*H*]quinoline	40

1.63	Nickel-catalyzed direct alkynylation of azoles with alkynyl bromide	41
1.64	Nickel-catalyzed direct cross coupling of azoles with various alkynes	41
1.65	Nickel-catalyzed alkynylation of a C(sp^2)–H bond of aryl amide	42
1.66	Nickel-catalyzed alkynylation of aryl amide	42
1.67	Nickel-catalyzed oxidative cross-coupling of C(sp^3)–H bond of the aliphatic amide with alkyne	42
1.68	Nickel-catalyzed sulfenylation of C(sp^2)–H bond of the benzamide with diaryl disulfide	43
1.69	Nickel-catalyzed sulfenylation of C(sp^3)–H bond of the aliphatic amide	43
1.70	Plausible mechanism for nickel-catalyzed alkylation of azole	45
1.71	Plausible catalytic cycle for alkylation of C(sp^3)–H bond of the aliphatic amide with an alkyl halide	46
1.72	Plausible mechanism for nickel catalyzed alkenylation of pyridine-*N*-oxide with alkynes	46
1.73	Catalytic cycle for arylation of benzothiazole using nickel catalyst	47
1.74	Plausible mechanism for arylation of C(sp^3)–H bond in aliphatic amide using nickel catalyst	48
1.75	Catalytic cycle for direct alkynylation of azoles using nickel catalyst	49
1.76	Plausible mechanism for nickel-catalyzed alkynylation of the aromatic amide	50
2.1	Synthesis of (^{R2}POCN^{iPr2})–H ligands	56
2.2	Synthesis of (^{R2}POCN^{iPr2})PdCl complexes	56
2.3	Synthesis of (^{iPr2}POCN^{iPr2})PdI complex	57
2.4	Synthesis of ($^{R'2}$POCN^{iPr2})PdX derivatives	57
2.5	Substrate scope for (^{iPr2}POCN^{iPr2})PdCl catalyzed arylation of azoles	62
2.6	Substrate scope for (^{iPr2}POCN^{iPr2})PdCl catalyzed arylation of 5-substituted azole	62
3.1	Synthesis of (^{R2}POCN^{Et2})–H ligand	82
3.2	Synthesis of (^{R}POCN^{Et2})PdCl complexes	83
3.3	Synthesis of (^{iPr2}POCN^{Et2})PdX complexes	83
3.4	Substrate scope of the (^{iPr2}POCN^{Et2})PdCl (**20**)-catalyzed arylation of azoles	90
3.5	Coupling of 5-substituted oxazole with aryl iodide using ^{iPr2}POCN^{Et2})PdCl	91
4.1	Recycling experiments of the catalyst **20**	109
4.2	H/D scrambling experiment	112

4.3	Intermolecular competition experiments	113
4.4	Stoichiometric reaction and resting state of catalyst **20**	116
4.5	Synthesis of catalyst (^{iPr2}POCN^{Et2})Pd-benzothiazolyl (**25**)	117
4.6	Reactivity of (^{iPr2}POCN^{Et2})Pd-benzothiazolyl with electrophiles	119
5.1	Screening of *N*-substituent at indole	134
5.2	Scope of nickel-catalyzed alkynylation of indoles and pyrroles	136
5.3	Scope of nickel-catalyzed alkynylation of benzimidazole, imidazole, and pyrazole	137
5.4	Deprotection silyl group	138
5.5	Synthesis of triazole derivatives	138
5.6	Synthesis of alkynyl-arenes	138
5.7	Synthesis of benzofuranyl derivative	139
6.1	Synthesis of $[(Phen)_3Ni]\cdot NiBr_4$ (**36**) complex	164
6.2	Synthesis of $[(Phen)_3Ni]\cdot NiCl_4$ (**37**) complex	164
6.3	Synthesis of $(Phen)_2NiCl_2$ (**38**) complex	167
6.4	Alkynylation with the isolated nickel-catalysts	167
6.5	Reaction in presence of external additive	168
6.6	H/D scrambling experiment	176
6.7	Intermolecular competition experiment	177
6.8	Reactivity study of $(THF)_2NiBr_2$/Phen with (pyridin-2-yl)-1*H*-indole (**27a**)	177

Chapter 1

Introduction

1.1 Classification, nomenclature, and properties of pincer system 2

1.1.1 Definition and nomenclature of pincer complex 2

1.1.2 Basic properties of pincer palladium complexes 6

1.2 Syntheses and catalytic application of pincer based palladium complexes 6

1.2.1 Synthesis of pincer palladium complexes 6

1.2.1.1 Pincer palladium complex *via* C–X activation 7

1.2.1.2 Synthesis of pincer palladium complexes *via* C–H activation 8

1.2.1.3 Synthesis of pincer palladium complex by ligand introduction route 10

1.2.2 Catalytic application of pincer palladium complexes 11

1.2.2.1 Heck coupling reaction 11

1.2.2.2 Suzuki-Miyaura coupling reaction 13

1.2.2.3 Hiyama coupling reaction 16

1.2.2.4 Stille coupling reaction 16

1.2.2.5 Negishi coupling reaction 17

1.2.2.6 Sonogashira coupling reaction 18

1.2.2.7 Aldol and Michael reaction by pincer palladium complexes 19

1.2.2.8 Allylation of aldehydes and imines 20

1.3 Mechanistic aspect of pincer palladium-catalyzed cross-coupling reactions 21

1.3.1 Mechanistic insight for Heck reaction 22

1.3.2 Mechanistic pathway for Suzuki-Miyaura cross-coupling reaction 27

1.4 C–H bond arylation of azoles by various catalytic systems 29

1.5 Nickel-catalyzed C–H activation and functionalizations 31

1.5.1 C–C bond forming reaction using nickel catalyst 32

1.5.1.1 Nickel-catalyzed C–H alkylation of (hetero)arenes 32

1.5.1.2 Nickel-catalyzed C–H alkenylation of (hetero)arenes 35

1.5.1.3 Nickel-catalyzed C–H arylation of (hetero)arenes 36

1.5.1.4 Nickel-catalyzed alkynylation of (hetero)arenes 40

1.5.2 Nickel-catalyzed thiolation of (hetero)arenes 43

1.6 Mechanistic aspect of nickel-catalyzed C–C bond forming reactions through C–H bond activation 44

1.6.1 Mechanistic pathway for nickel-catalyzed alkylation reaction 44

1.6.2 Mechanistic pathway for nickel-catalyzed alkenylation reaction 45

1.6.3 Mechanism of nickel-catalyzed arylation 47

1.6.4 Mechanistic pathway for nickel-catalyzed alkynylation reaction 49

Chapter 2

Design and development of hybrid POCN-pincer palladium complexes for arylation of azoles

2.1 Introduction 54

2.2 Results and discussion 55

2.2.1 Synthesis of {1-(R_2PO)-C_6H_4-3-($CH_2N^iPr_2$)} ($^{R2}POCN^{iPr2}$)–H ligands 55

2.2.2 Synthesis of ($^{R2}POCN^{iPr2}$)-palladium complexes 56

2.2.3 Crystal structure description 57

2.2.4 Catalytic activity of ($^{R2}POCN^{iPr2}$)PdCl for C–H bond arylation of azoles 59

2.2.4.1 Optimization of catalytic condition 59

2.2.4.2 Substrate scope for arylation of azoles 61

2.3 Conclusion 63

2.4 Experimental section 63

2.4.1 Synthesis of 3-((diisopropylamino)methyl)phenol (**1**) 64

2.4.2 Synthesis of ($^{R2}POCN^{iPr2}$)–H ligands and characterization data 65

2.4.3 Synthesis of ($^{R2}POCN^{iPr2}$)PdCl complexes and characterization data 66

2.4.4 Synthesis and characterization of ($^{R2}POCN^{iPr2}$)PdX derivatives 67

2.4.5 Procedure for azole arylation and characterization data 70

Chapter 3

Synthesis of sterically distinct (POCN)-pincer palladium for C–H bond arylation of azoles

3.1 Introduction 81

3.2 Results and discussion 81

3.2.1 Synthesis of {1-(R_2PO)-C_6H_4-3-(CH_2NEt_2)} ($^{R2}POCN^{Et2}$)–H ligands 81

3.2.2 Synthesis of ($^{R2}POCN^{Et2}$)PdCl complexes and their derivatives 82

3.2.3 Crystal structure description 84

3.2.4 Catalytic activity for arylation of azoles 87

3.2.4.1 Optimization of catalytic condition 87
3.2.4.2 Comparison of catalytic activity of (^{R2}POCN$^{R'2}$)PdX complexes 88
3.2.4.3 Substrate scope for arylation of azoles using ($^{i\text{Pr}2}$POCN$^{\text{Et}2}$)PdCl (**20**) 89
3.3 Conclusion 91
3.4 Experimental section 92
3.4.1 Synthesis of 3-((diethylamino)methyl)phenol 92
3.4.2 Synthesis and characterization of (^{R2}POCN^{Et2})–H ligands 92
3.4.3 Synthesis of (^{R2}POCN^{Et2})PdX complexes 93
3.4.4 Procedure for arylation and characterization data 96
3.4.5 Procedure for rate measurement of arylation reaction 97

Chapter 4

Mechanistic aspects of (^{R2}POCN^{R2})Pd-catalyzed arylation of azoles

4.1 Introduction 99
4.2 Results and discussion 100
4.2.1 External additive experiments 101
4.2.2 Kinetic analysis for arylation of azoles by ($^{i\text{Pr}2}$POCN$^{\text{Et}2}$)PdCl (**20**) 103
4.2.3 Rate order determination with various reaction components 104
4.2.4 Catalyst stability and product inhibition study 109
4.2.5 Isotope labelling experiments 110
4.2.6 Electronic effect on arylation reaction 112
4.2.7 Role of CuI and (POCN)PdX in arylation reaction 115
4.2.8 Controlled reactivity of ($^{i\text{Pr}2}$POCN$^{\text{Et}2}$)PdCl 115
4.2.9 Synthesis and reactivity of intermediate ($^{i\text{Pr}2}$POCN$^{\text{Et}2}$)Pd(benzothiazolyl) (**25**) 117
4.2.10 DFT study and energy profile diagram 120
4.2.11 Probable catalytic cycle 122
4.3 Conclusion 123
4.4 Experimental section 124
4.4.1 General procedure for added ligand experiments 124
4.4.2 Kinetic measurements for arylation reaction 124
4.4.3 Catalyst stability and product inhibition study 125
4.4.4 Isotope labelling experiments 126

4.4.5 Procedure for electronic effect study 126

4.4.6 Catalyst reactivity study 127

4.4.7 Procedure for synthesis of (^{iPr2}POCN^{Et2})Pd-benzothiazolyl (**25**) 128

4.4.8 Reactivity of (^{iPr2}POCN^{Et2})Pd-benzothiazolyl (**25**) 128

Chapter 5

Nickel(II)-catalyzed C(2) selective C–H alkynylation of heteroarenes with alkynyl bromide

5.1 Introduction 131

5.2 Result and discussion 132

5.2.1 Optimization of catalytic condition 132

5.2.2 Screening of *N*-substituent at indole 134

5.2.3 Scope of nickel-catalyzed alkynylation of heteroarenes 135

5.2.3.1 Scope of nickel-catalyzed alkynylation of indoles and pyrroles 135

5.2.3.2 Scope of nickel-catalyzed alkynylation of benzimidazole, imidazole and pyrazole 136

5.2.4 Synthetic utility of Ni-catalyzed alkynylation reaction 137

5.3 Conclusion 139

5.4 Experimental section 139

5.4.1 Synthesis and characterization of starting precursors 140

5.4.2 Representative procedure for alkynylation and characterization data 141

5.4.3 Deprotection and functionalization 155

Chapter 6

Mechanistic aspects of nickel-catalyzed C(2)–H alkynylation of indoles

6.1 Intorduction 163

6.2 Result and discussion 163

6.2.1 Synthesis of $(Phen)_nNiX_n$ complexes 163

6.2.2 Catalytic competency of isolated nickel complexes 167

6.2.3 External additive experiments 167

6.2.4 Kinetic analysis of alkynylation reaction 168

6.2.5 Rate order determination 171

6.2.6 Isotope labelling experiments 175

6.2.7 Electronic effect on alkynylation 176

6.2.8 Control reactivity study 177
6.2.9 DFT calculation 178
6.2.10 Probable catalytic cycle 178
6.3 Conclusion 180
6.4 Experimental section 181
6.4.1 Synthesis of $NiBr_2(Phen)_n$ complexes 181
6.4.2 Procedure for external additive experiments 181
6.4.3 Kinetics of alkynylation reaction 182
6.4.4 Procedure for order determination 183
6.4.5 Isotope labelling experiments 185
6.4.6 Procedure for intermolecular competition experiment 185
6.4.7 Procedure for controlled reaction 186

X-ray structure determination 187
References 192
NMR and HRMS spectra of complexes 211
List of publications 238

Chapter 1

Introduction

Introduction

Chapter 1 describes the general classification, nomenclature, and properties of pincer ligand systems and pincer complexes. The main focus is on the pincer palladium systems and their applications. In this regards, the fundamental properties and synthetic routes of the pincer palladium complexes were discussed. The utilization of pincer palladium complexes in various catalytic transformations and their mechanistic study is documented in details. Similarly, the role of nickel as catalyst in the C–H bond activation reaction is discussed. More focus is given on the nickel-catalyzed C–H alkynylations and their mechanistic aspects.

1.1 Classification, nomenclature, and properties of pincer system

1.1.1 Definition and nomenclature of pincer complex

The development of well-defined ligand system, which can tune and control the properties of a transition metal, is the eventual aim of inorganic and organometallic chemistry. An ideal catalyst has the properties like good stability, should produce high selectivity, should give high turnover numbers (TON) and permits low catalyst loading. Also, ligand should be amenable to rational design, which can fine tune the catalytic properties of metal center. These properties can be addressed by the appropriate choice of the ligands. Among various ligand systems available in the literature, the pincer ligand and their complexes have attracted considerable attention because of their high strength, reactivity, and variability. The pincer ligand is the system containing a tridentate chelating organic compound, which generally has two co-ordinating moieties like amine, phosphine, thioether, carbene, etc., and one anionic moiety like alkyl, aryl, phosphide, silyl, amide or a neutral donor moiety (Figure 1.1).

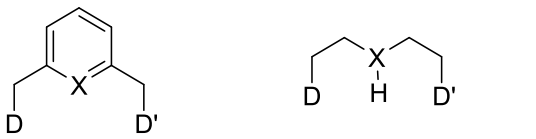

D and D' = $-NR_2$, $-PR_2$, -SR, -OR or Carbene

X = N, P, SiR, CH

Figure 1.1 Schematic representation of pincer ligand.

General representation of pincer ligand is shown in Figure 1.1, where D and D’ are the co-ordinating groups and X is an anionic or a neutral atom. Various type of pincer ligand systems known in the literature. The pincer ligands have been classified into two different

types on the basis of co-ordinating atoms: symmetrical and non-symmetrical. If the co-ordinating atoms D and D' are same, then it is referred as a symmetric pincer ligand, if not then non-symmetrical.

The pincer complex is the system in which the ligand is coordinated to metal through three sites, wherein metal is directly attached with an anionic moiety or a neutral atom and coordinated by two neutral atoms (Figure 1.2). If both neutral species are same then is called symmetrical pincer complex, if they are different then unsymmetrical pincer complex. The pincer backbone affects the properties of pincer metal complexes in the catalytic reactions. As the pincer ligand coordinates to the metal through three sites, it increases the thermal stability as well as the selectivity during catalysis. In the case of pincer complex three sites are occupied by ligand and less number of sites are available for the catalysis, which minimizes the formation of unwanted side products arises from shuffling of ligand during the processes. The first pincer system was described by Shaw and co-workers in 1976.[1] The complexes were reported with various transition metals, such as Ni, Pd, Pt, Rh, Ir and were based on the $PC_{sp2}P$ pincer system as shown in Figure 1.3. These pincer complexes have high potential in the catalytic application, and have the features like thermal stability and ability to sustain unusual oxidation states.

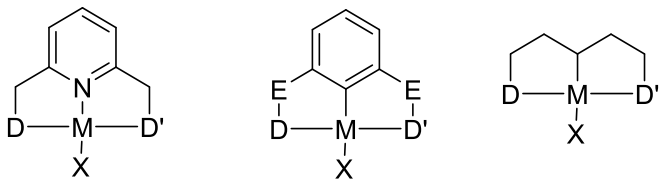

Figure 1.2 General representation of pincer complexes.

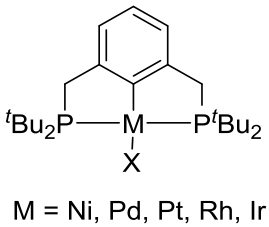

Figure 1.3 Pincer complexes by Shaw and co-workers.

After the introduction of pincer complexes by Shaw, this chemistry was not much explored. Later, in 1979, van Koten came up with the NCN pincer ligand to continue the pincer chemistry (Figure 1.4a).[2] They have synthesized various pincer complexes of NCN

ligand with Ni, Pd and Pt-transition metals. First time, these complexes were structurally characterized and (NCN)Ni(II)-complex was utilized in the Kharasch addition reaction.[2] In addition, they have characterized the Ni(III) complex featuring Ni–C linkage, and highlighted the importance of this oxidation state of the nickel for the catalytic activities in Kharasch addition reaction.[2]

In 1982, Fryzuk and co-worker described an interesting example of the aliphatic hybrid "PNP" pincer ligand, which contains soft phosphine as neutral donor and hard nitrogen as anionic donor atom (Figure 1.4b).[3] Additionally, this ligand contains two dimethylsilyl moieties at *β*-position to metal, which diminishes the probability of reductive elimination or oxidation of metal. They have synthesized and structurally characterized the complexes of nickel and palladium with the aliphatic PNP pincer ligand system.

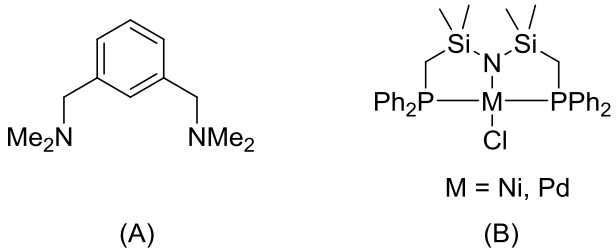

Figure 1.4 A) NCN pincer ligand by van Koten; B) PNP pincer system by Fryzuk.

Later, various symmetric pincer ligands systems, such as PCP, NCN,[2,4,5] POCOP,[6-10] PNCNP,[11] SCS, CCC[12] were developed and their complexes were structurally characterized (Figure 1.5). Among them, the POCOP ligand system has extensively been studied compared to other symmetric ligands, which was first introduced by Jensen and co-workers in 1998.[13] The (POCOP)Ir or (PCP)Ir-pincer complexes gave very interesting reactivity for dehydrogenation of alkanes to olefins.[14-16] Similarly, the asymmetric pincer ligands, such as PCN[17], NCS[18] and PCS[18] were developed (Figure 1.6). The chemistry of non-symmetric ligands is less explored compared to the symmetric pincer ligands.

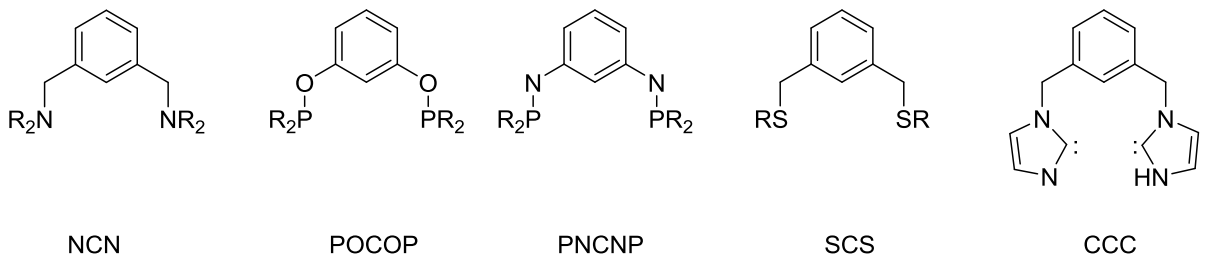

Figure 1.5 Representative symmetrical pincer ligands.

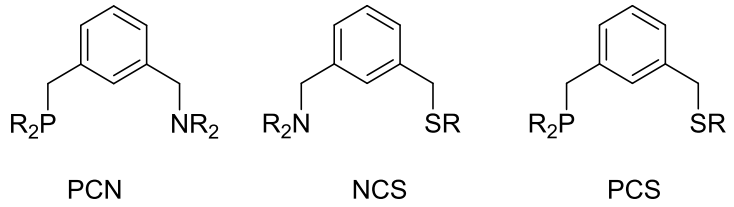

Figure 1.6 Representative non-symmetric pincer ligands.

In the case of non-symmetric ligand system, it is very easy to tune the electronic features of the metal by varying the donor substituents. The hemilabile nature of non-symmetrical pincer ligand, which has control over other catalytic pathways during catalysis, significantly increases the number of active sites on metal and consequently enhances the rate of reaction. However, the use of hemilabile ligands has drawbacks that the irreversible dissociation from the metal system can lead to the decomposition of metal complexes.[19]

Various pincer complexes of transition metals have been developed and studied in different catalytic processes. Among them, pincer palladium has the attractive synthetic features as it has broad synthetic scope and has the ability to control the selectivity of catalytic transformation. The pincer palladium complex that contains at least one metal-carbon is also called palladacycle.[20-23] Generally, the pincer palladium complexes are the subclass of palladacycles, which contain two fused cyclic rings. There are other interesting pincer palladium complexes, where the palladium-carbon bond is replaced with other isoelectronic structure elements, such as palladium-silicon and palladium-phosphorous bond as shown in Figure 1.7.[24-26] There are some pincer palladium systems, in which the palladium-carbon anionic bond is replaced by a neutral sp^2 nitrogen atom (Figure 1.7).[27-29] Such replacement of Pd–C bond with isoelectronic species (Si, P, N) sometimes improves the reactivity of metal. Mostly, in pincer palladium complexes, the pincer skeleton is aryl anion, which directly binds with palladium through σ-bond; substituent *ortho* to σ-bond adhere tight position and can coordinate through N, S, O, P neutral atoms. The donor atoms and their substituents can control the approach of the promising substrate and tune the electronic property around the metal center. Also, it is possible to introduce stereochemical information at benzylic carbon in the generic pincer complex, which creates stereoselective catalyst.[30] The symmetrical pincer complexes are more explored compared to unsymmetrical complex because of the easier synthesis of former. In last decades, number of reviews have been published based on the pincer palladium complexes, wherein the pincer palladium complexes

were studied for the catalytic applications, switches, sensors for SO_2 absorption and so on.[31-37]

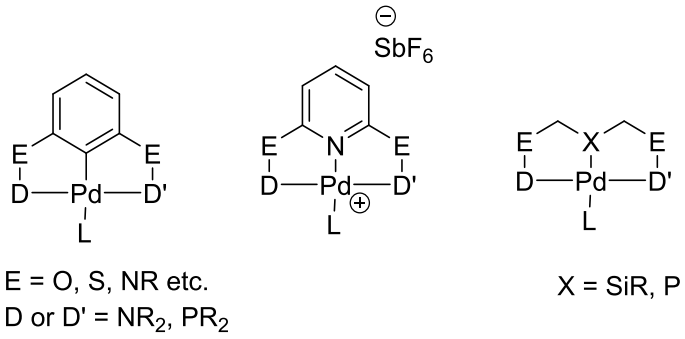

Figure 1.7 Representative pincer palladium complexes.

1.1.2 Basic properties of pincer palladium complexes

In pincer palladium complex, the strong tridentate coordination increases the thermal stability of the complex. Most of the complexes are moisture- and air-stable, which makes them easy to handle and storage. In case of pincer complex, the metal and ligand stay together during the catalysis, consequently all the steric and electronic features of ligand transfer to the metal, which increases the reactivity of the metal. In such complex, metal is attached through three sites with ligand in a co-planar fashion and only one site is accessible for the catalysis; which increases the selectivity for the formation of desired product. Under the harsh reaction condition, the reduction of Pd–C bond of pincer palladium to Pd(0) can occur irreversibly, in that case the palladium complex does not act as a direct catalyst, but acts as the pre-catalyst for the reaction.[38,39] In other way, instead of the reduction of Pd(II) to Pd(0); it's oxidation to Pd(IV) can be possible during the catalytic reaction, which avoid the cleavage of Pd-anionic carbon bond of the pincer complex.[40-43] The strong tridentate coordination of ligand around the palladium in pincer complex sustains the higher oxidation state at the palladium metal compared to other palladium precursors, such as $PdCl_2$, $Pd(OAc)_2$.

1.2 Syntheses and catalytic applications of pincer based palladium complexes

1.2.1 Synthesis of pincer palladium complexes

The synthesis of pincer palladium complexes is a tedious process, which some times limits their application for the catalysis. In pincer palladium synthesis, the main step is the cyclometalation of the ligand with palladium to form palladacycle. The cyclometalation can occur through the chelation of pincer ligand to palladium center to form two metallocycles in

B-shape. There are many methods known for this transformation to achieve the pincer-palladium complexes.

1.2.1.1 Pincer palladium complex *via* C–X activation

The synthesis of pincer palladium complex *via* C–halide functionalization is the simplest and most convenient way to develop pincer palladium complex; wherein the oxidative addition of the C–halogen bond of the pincer proligand to the low valent palladium precursors like $Pd(PPh)_4$, $Pd_2(dba)_3$ occurs. Several reports described the use of low oxidation state metal for C–X activation that leads to the formation of pincer complex.[44,45] van Koten described the synthetic route for the NCN pincer palladium complexes by the functionalization of C–Br bond (Scheme 1.1).[44] This process starts by the reaction of dimethylamine with tribromide **1.1** to form the diaminated compound **1.2**. The compound **1.2** on oxidative addition with $Pd_2(dba)_3$ produces the complex (NCN)PdBr (**1.3**). This NCN pincer complex **1.3** is moisture and air-stable compared to the starting metal precursor. Similarly, the phosphine containing PCP pincer complexes can be easily prepared by the C–halogen bond activation at low valent metal. The synthesis of phosphinite based POCOP complex **1.6** can be obtained from resorcinol derivative **1.4** and chlorodiphenylphosphine (Scheme 1.2).[45] The first step, synthesis of ligand **1.5** is sensitive to moisture, and is carried out under inert atmosphere. The compound **1.5** on oxidative addition with $Pd_2(dba)_3$ gives (POCOP) complex **1.6**.

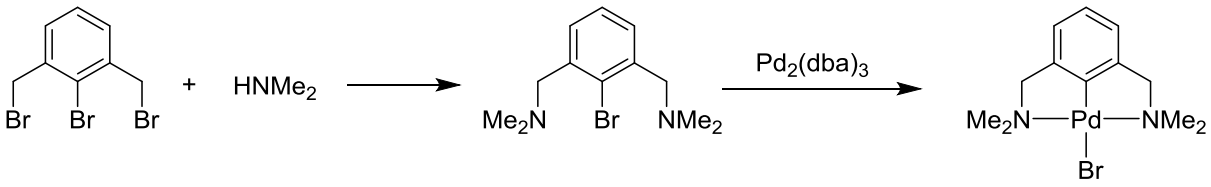

1.1 **1.2** **1.3**

Scheme 1.1 Synthesis of (NCN)PdBr by oxidative addition of C–Br bond

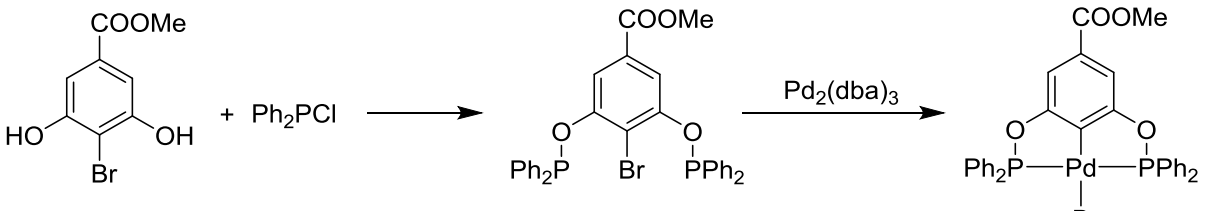

1.4 **1.5** **1.6**

Scheme 1.2 Synthesis of (POCOP)PdBr by oxidative addition approach

Similar strategy has been utilized for the synthesis of various chiral PCP pincer complexes which contains TADDOL (**1.7**),[46] BINOL (**1.8-1.11**),[46-48] and bis(phenanthrol) (**1.12**)[47] bulky backbone (Figure 1.8). All these chiral complexes **1.7-1.12** are air- and moisture-stables.

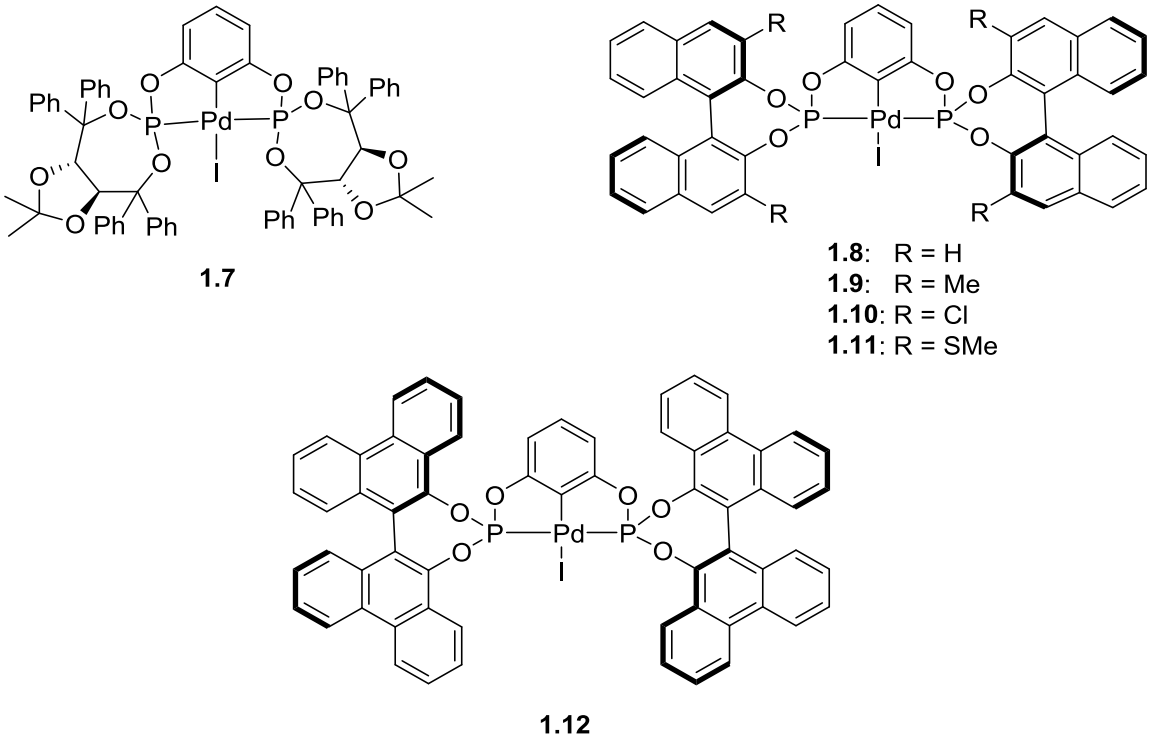

Figure 1.8 Chiral pincer palladium complexes *via* C–I bond activation.

1.2.1.2 Synthesis of pincer palladium complexes *via* C–H activation

The cyclometalation *via* the C–H activation is an important strategy commonly used for the synthesis of pincer palladium complexes.[49,50] This method involves the C–H activation process which requires simple metal precursor compared to the procedure based on C–X bond activation. The success of this method is mostly based on the electronic properties and bulkiness on the side arm of the pincer ligands. One of the most important difference between C–X and C–H bond activation method is the use of different oxidation state metal precursors. In the case of oxidative addition strategy, the oxidative addition of C–X performed with Pd(0) species [$Pd(PPh_3)_4$ or $Pd_2(dba)_3$], while in the case of C–H bond activation the reaction achieved with Pd(II) precursors. The C–H activation process generally depends on the ligand moieties attached to Pd(II) metal precursors. It was demonstrated that efficient C–H functionalization can be achieved using Pd(II) salt having weakly co-ordinating ligands, such as $Pd(OCOCF_3)_2$[51,52] or $Pd(BF_4)_2(CH_3CN)_4$.[18,39,45,53] In 1997, Milstein described the synthesis

of (PCP)Pd-complex **1.14** *via* the C–H activation of PCP pincer ligand **1.13** with $Pd(TFA)_2$ salt (Scheme 1.3).[51] Later, Aydin synthesized (SeCSe)Pd-pincer complex (**1.16**) *via* C–H activation from SeCSe pincer ligand (**1.15**) with $Pd(BF_4)_2(CH_3CN)_4$ (Scheme 1.4).[53]

The transcyclometalation reaction is an alternative way to synthesize the pincer palladium complexes.[54] The transcyclometalation strategy can also be used for the preparation of PCP pincer palladium complex (Scheme 1.5);[55] wherein the use of commercially available transcyclometal complex **1.18** acts as an efficient source for palladium precursor.[56] Hence, the PCP complex **1.19** can be synthesized in two steps starting from phosphorylation of resorcinol with chlorophosphine, followed by the transcyclometalation of the complex **1.18** with phoshinite proligand **1.17** (Scheme 1.5). Welch and co-worker also reported the derivative of complex **1.19** by the reaction of **1.17** with $Pd(OCOCF_3)_2$.[52]

The C–H activation methodology has been used for the synthesis of chiral pincer complex **1.22** by Wingad and co-workers (Scheme 1.6).[50] Thus, the treatment of *tert*-butyl resorcinol derivatives with chlorophosphite **1.20** produced the proligand **1.21**, which on metalation with $PdCl_2(CH_3CN)_4$ afforded complex **1.22**. Herein, the *tert*-butyl group on aromatic accelerates the C–H activation process.[50]

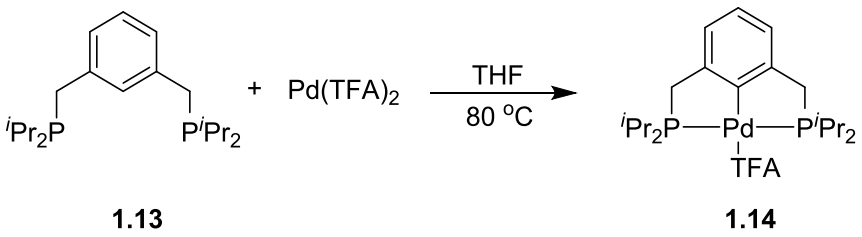

Scheme 1.3 Synthesis of (PCP)Pd-pincer complex *via* C–H activation process

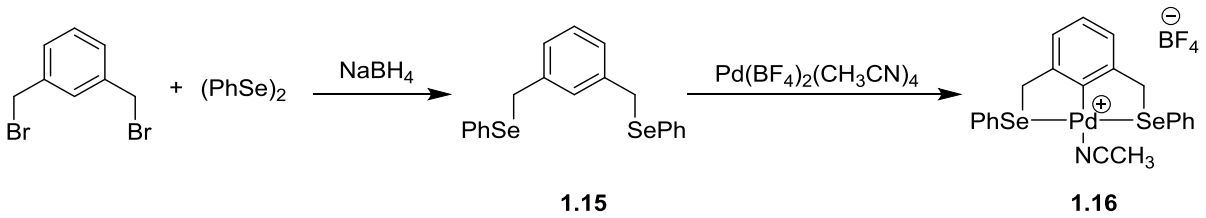

Scheme 1.4 Synthesis of pincer palladium complex *via* C–H activation process

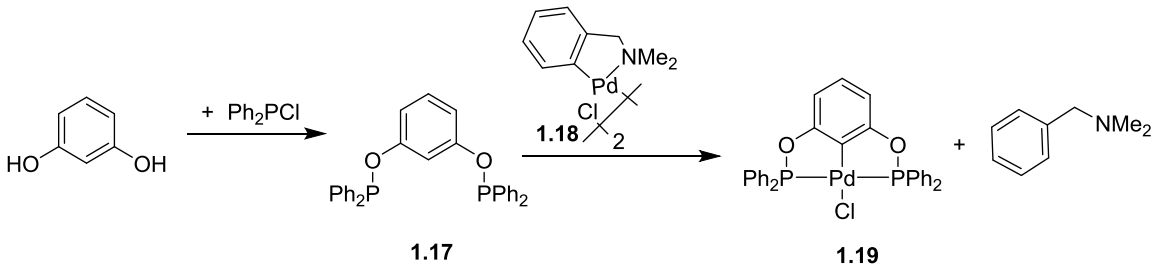

Scheme 1.5 Synthesis of pincer palladium complex by transcyclometalation

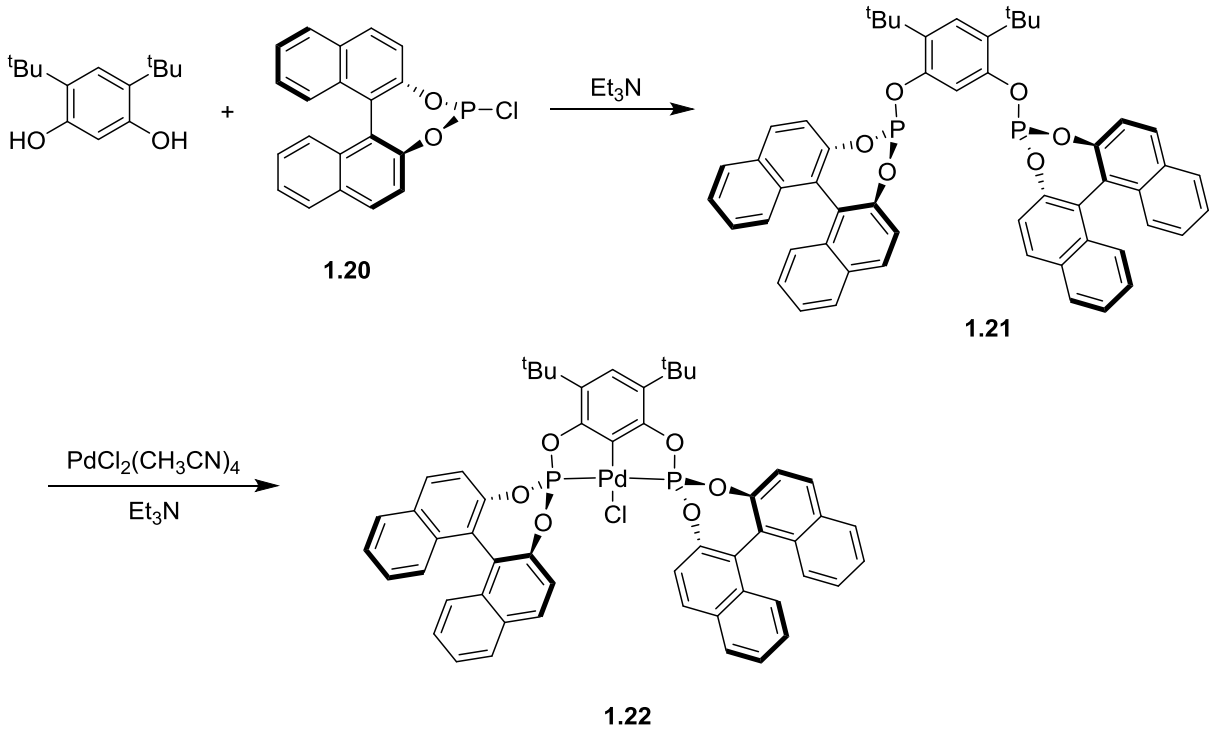

Scheme 1.6 Synthesis of chiral pincer palladium complex by C–H activation method

1.2.1.3 Synthesis of pincer palladium complex by ligand introduction route

All the mentioned methods for the preparation of pincer palladium complexes are mostly dependent on a synthesis of pincer pro-ligand, followed by the palladation of C–X or C–H bond with Pd(0) or Pd(II) species. In these methods, the palladium metal was introduced at the last step, thus this technique is also called ‘metal introduction method’. These methods give easy access to the synthesis of pincer complexes, however, sometimes they are sensitive to the sterically hindered substituent on the side arm of the pincer ligands. Uozumi and co-workers has demonstrated an interesting method, which overcomes the problem caused by the bulky substituents on the side arm of the pincer ligands.[57-60] In this method, the palladium atom is introduced at an early stage of the complex synthesis, and thus, this technique is

called as “ligand introduction route”. Uozumi has synthesized the chiral NCN-pincer complex **1.25** by the ligand introducing method (Scheme 1.7).[57,58] Herein, the key step is the synthesis of complex **1.24** by the oxidative addition of C–OTf bond of **1.23** to $Pd_2(dba)_3$ in the presence of triphenylphosphine and LiCl salt. The next step is the addition of proline to give complex **1.25**. Various NCN and PCP pincer complexes were developed using the ligand introduction method. Frech and co-workers reported hybrid aminophosphine-based pincer palladium complexes using the same method.[61]

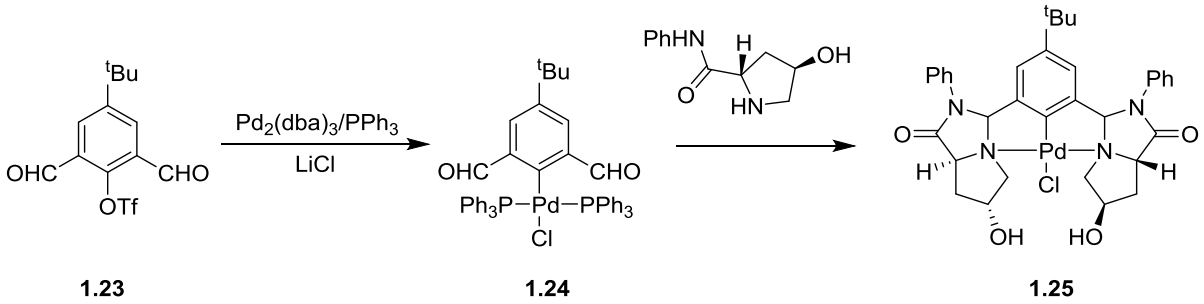

1.23 **1.24** **1.25**

Scheme 1.7 Synthesis of chiral NCN pincer palladium *via* ligand introduction route

1.2.2 Catalytic application of pincer palladium complexes

High thermal stability and well defined nature of the pincer palladium complexes make them unique catalysts for practical applications. The literature reports highlighted that the pincer palladium complexes have mostly been used for the cross-coupling reaction, as the cross coupling reaction represents the most important type of C–C bond forming reaction.[62, 63] Milstein and co-workers reported the Heck reaction catalyzed by pincer palladium catalyst.[51] After this, number of publications have appeared on cross-coupling reactions, such as Heck coupling or Heck type reaction,[64-84] Suzuki-Miyaura reaction,[85-105] Sonogashira reaction,[106-114] Stille coupling,[70,115] Hiyama,[106] Negishi coupling[28,116,117] using pincer palladium complex as catalyst. In addition, these pincer complexes have other applications, such as use in light harvesting, OLED devices as well as molecular sensors and switches.[118-120]

1.2.2.1 Heck coupling reaction

Heck coupling reaction provides easy access for various substituted alkenes, and for the preparation of highly conjugated and luminescent organic materials that can be used in OLED display. In 1997, Milstein described the pincer palladium **1.26** catalyzed Heck reaction of aryl iodide with methyl acrylate with high turnover numbers (Scheme 1.8).[51] The most challenging coupling reagent for Heck reaction, such as aryl bromide and aryl chloride can be

coupled with olefin by using pincer palladium complex. Frech and co-worker reported coupling of bromobenzene with styrene catalyzed by pincer palladium complex **1.27** with TON's 4980 000 (Scheme 1.9).[121] Similarly, Jensen and co-worker have reported coupling reaction of most challenging aryl chloride with olefin employing five-membered phosphinito pincer palladium **1.28** in good yields (Scheme 1.10).[6] Kumar *et al* achieved efficient cross-coupling of electron-deficient aryl halide with acrylic acid using (ENO; E = S, Se, Te) pincer palladium complex under aerobic conditions.[72] In 2012, Dominguez and co-worker have developed CNC pincer palladium complexes for Mizoroki-Heck coupling reaction in H_2O and DMF.[79] Cai and co-workers described the efficient Heck coupling of perfluoroalkyl-substituted ethylene with aryl halide by PCP pincer palladium complex; wherein they showed the catalyst can be separated from the reaction by F-SPE technique and catalyst can be reused for three times without change in the catalytic activity.[80] Sobhani *et al* developed bis(imino)pyridine pincer-Pd complex which supported on γ-Fe_2O_3@SiO_2 magnetic nanoparticles for the Heck coupling of aryl iodide, bromide, and chloride with alkyl acrylate and styrene, where the catalyst was recovered and reused ten times without decrease in the catalytic activity.[83] Recently, Laguna group reported hemilabile palladium complex of SPS-pincer ligand which shows high activity for Mizoroki-Heck coupling of aryl iodide with methyl acrylate or styrene (Scheme 1.11).[122]

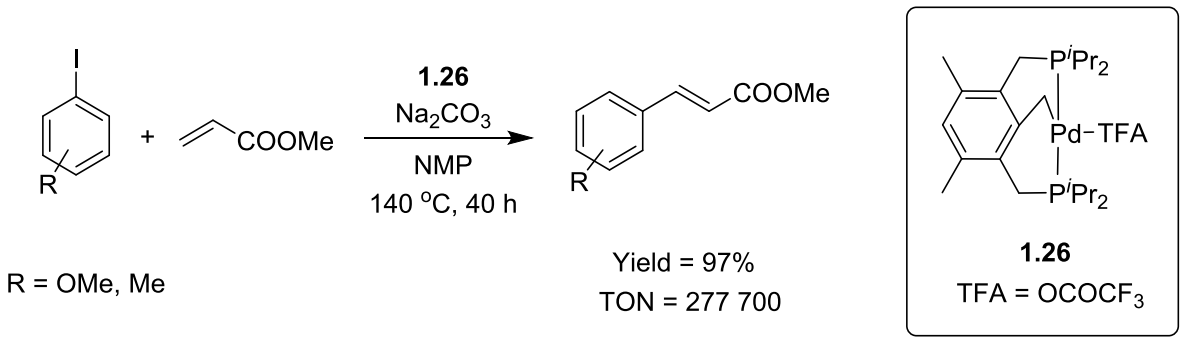

Scheme 1.8 Heck coupling reaction using complex **1.26**

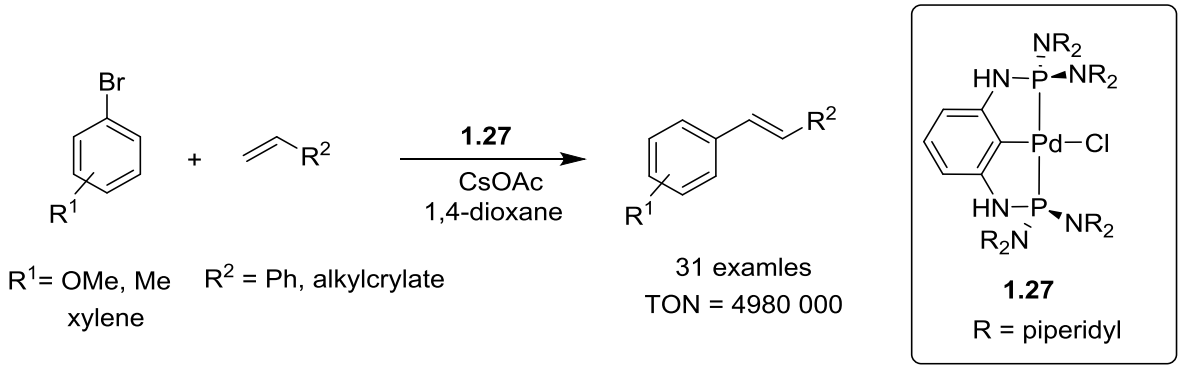

Scheme 1.9 Heck coupling reaction using complex **1.27**

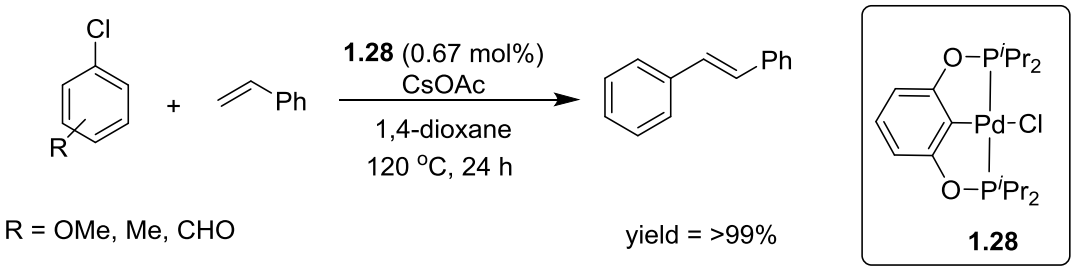

Scheme 1.10 Heck coupling reaction using complex **1.28**

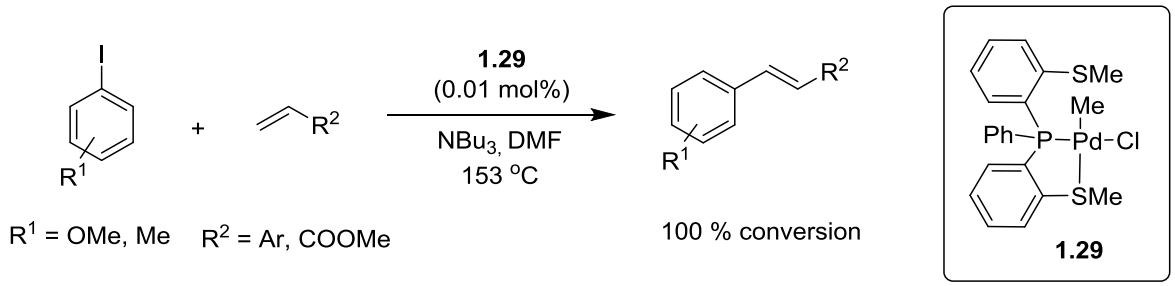

Scheme 1.11 Heck coupling reaction using hemilabile Pd-pincer complex **1.29**

1.2.2.2 Suzuki-Miyaura coupling reaction

Suzuki-Miyaura coupling is one of the most significant carbon-carbon bond forming reaction, which is based on the coupling of arylboronic acid with aryl halide under basic condition.[123] Pincer palladium complexes are among the most effective for Heck and Suzuki coupling and constantly increases the attention because of their particular balance between reactivity and stability. Apparenlty, slight modifications in steric and electronic of the pincer core or the phosphine substituent's can dramatically prominence their catalytic activities for Suzuki-Miyaura reaction.[85-105] The significant difference between the Suzuki-coupling and Heck-coupling is that in case of Suzuki reaction, the crucial steps is transmetalation[123] of the organoboronate with a Pd(II) species, which does not involve redox reaction. In the context of pincer palladium this is important, because this catalytic step does not change the oxidation state of Pd(II) as in the pincer palladium.

Welch group have described the first cross-coupling reaction of aryl iodide with boronic acid using PCP pincer palladium complex **1.30** (Scheme 1.12).[52] In this, the efficient cross-coupling of aryboronic acid with aryl bromide was carried out by the pincer palladium complex **1.30**, which resulted with turnover numbers (TON's) of 190 000.

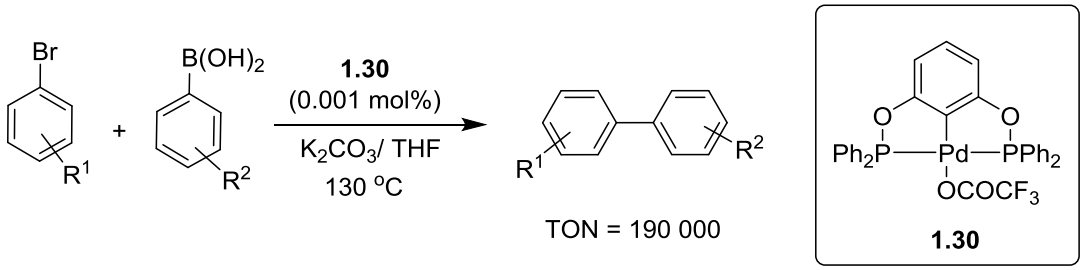

Scheme 1.12 Suzuki coupling reaction using complex **1.30**

Nishiyama and co-workers[124] reported an interesting example of asymmetric Suzuki-Miyaura coupling reaction catalyzed by the chiral pincer palladium complex **1.32** based on bisoxazoline ligand backbone. In this case, the coupling product **1.31** was obtained from the reaction of aryl iodide with aryl boronic acid and resulted with 46% ee (Scheme 1.13). The catalyst **1.32** gives TON's up to 900 000 for nonchiral Suzuki-Miyaura coupling reaction.

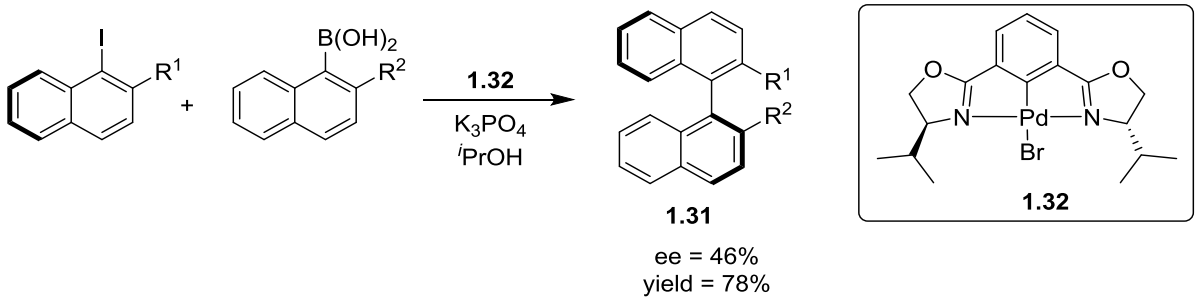

Scheme 1.13 Suzuki coupling reaction using chiral pincer complex **1.32**

The Szabó group has reported an interesting example of Suzuki coupling reaction, wherein the pincer complex **1.33** catalyzed the coupling of aryl boronates and vinyl aziridines with the opening of three-membered aziridine ring to obtained linear allylic amines (Scheme 1.14).[86] Similarly, van Koten group has demonstrated the cross-coupling reactions of vinyl boronates with epoxides by using pincer complex **1.34** to give linear allylic alcohol (Scheme 1.15).[92] The use of pincer palladium complex increases the regioselectivity for opening of aziridine and epoxide, providing linear allylic amine and allylic alcohol, respectively. Odinet and co-workers developed hybrid thiophosphoryl-benzothiazole (SCN) pincer palladium complex for the Suzuki coupling of electron-deficient aryl bromide with phenylboronic acid in excellent yield.[94] In 2012, Xiao *et al* showed the symmetrical bis(thiazole) (NCN) pincer palladium **1.35** efficiently catalyzes the Suzuki-Miyaura coupling of aryl iodides, bromides, and chlorides with high TON's (Scheme 1.16).[95] Ramírez-Rave *et al* synthesized the non-

symmetrical pincer Pd-complexes based on thioether functionalized iminophosphoranes pincer ligand, and utilized them for the Suzuki-Miyaura coupling of a series of *para*-substituted aryl bromide.[99] In 2016, Song and co-workers developed amido-phosphine pincer palladium complex **1.36** for the Suzuki-Miyaura reaction of both activated and deactivated (hetero)aryl bromide and iodides with *ortho*-substituted aryl boronic acid under aerobic condition in aqueous solution (Scheme 1.17).[103] Recently, Menteş *et al* reported biopolymer (chitosan) based pincer palladium complex for Suzuki cross-coupling, which showed remarkable product yield with high TON's and TOF.[104]

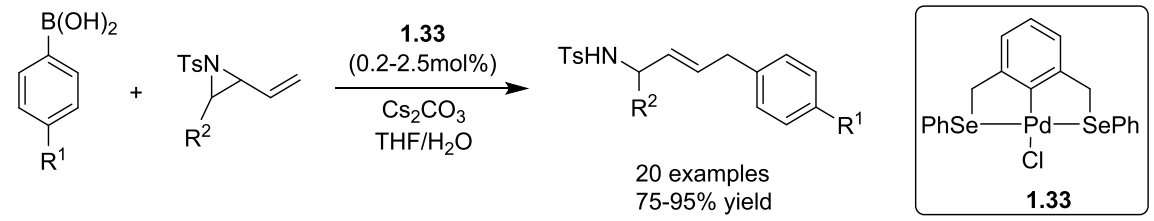

Scheme 1.14 Cross-coupling of aryl boronate with aziridine using complex **1.33**

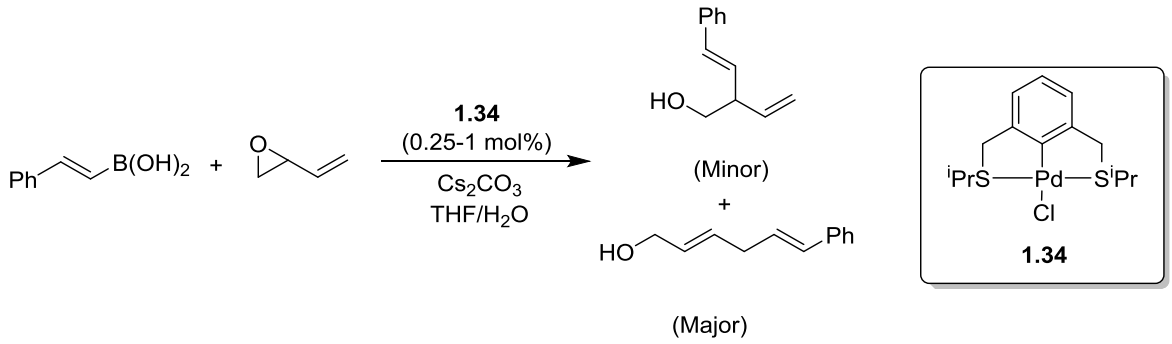

Scheme1.15 Cross-coupling of vinyl boronate with vinyl epoxide using complex **1.34**

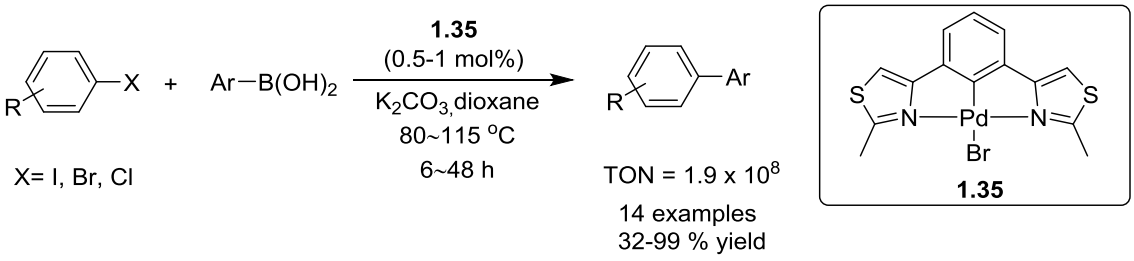

Scheme 1.16 Suzuki coupling using bis(azole) pincer palladium complex **1.35**

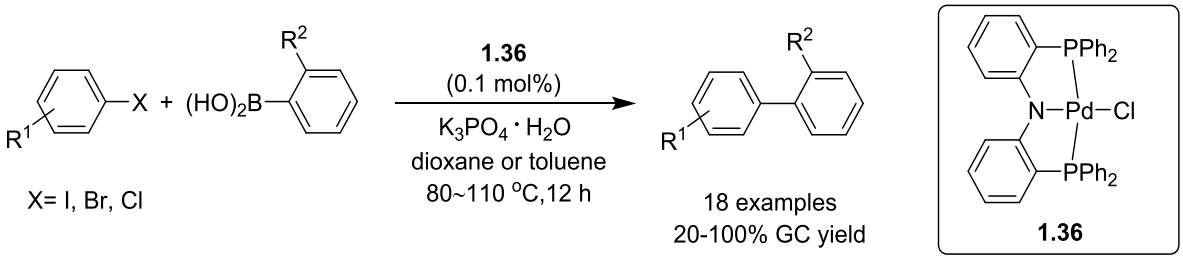

Scheme 1.17 Suzuki coupling reaction using amido-phosphine palladium pincer complex **1.36**

1.2.2.3 Hiyama coupling reaction

Hiyama coupling reaction is the cross-coupling reaction of organosilane with an aryl halide in the presence of fluoride ion as a promoter. SanMartin and Domínguez have reported the first Hiyama coupling reaction of organosilane with aryl bromide using unsymmetrical pincer palladium complex **1.37** to produce the coupled product (Scheme 1.18).[106] This coupling reaction was carried out in water in the presence of NaOH as an activator. In this catalysis, the status of catalyst was not clear.

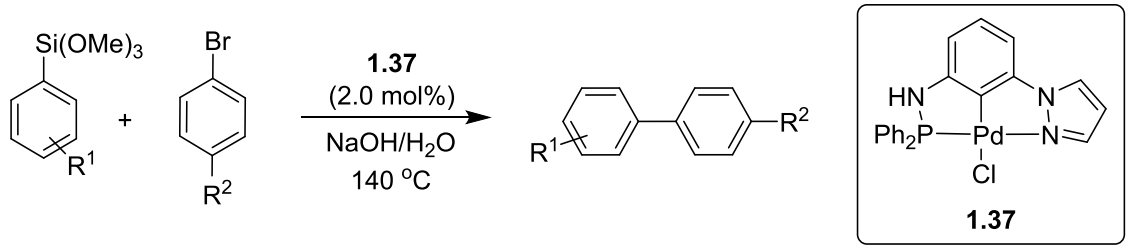

Scheme 1.18 Hiyama cross-coupling reaction using unsymmetrical pincer complex **1.37**

1.2.2.4 Stille coupling reaction

The cross-coupling reaction of organotin reagent with a C_{sp2} organic halide has been reported using pincer palladium catalyst. Wendt group described that the PCP pincer complex **1.38** catalyzes the coupling of aryl tin with aryl bromide (Scheme 1.19).[115] The process is very efficient to produce the coupled product with low catalyst loadings and resulted with very high TON's.

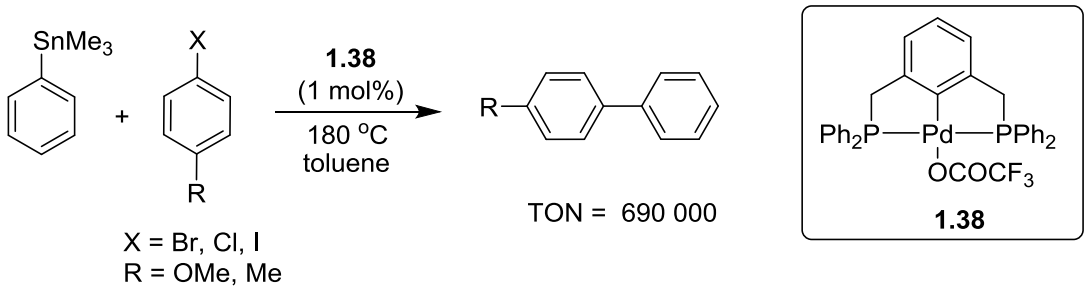

Scheme 1.19 Stille reaction using PCP pincer complex **1.38**

1.2.2.5 Negishi coupling reaction

In addition to other cross-coupling reactions, the Negishi coupling is also a synthetically important coupling reaction. Lei and co-workers have reported the Negishi coupling using pincer palladium complex, wherein they have described a mechanistic aspect of the reaction. The cross-coupling of aryl iodide with aryl zinc derivatives was achieved using pincer palladium catalyst **1.41**, which provide high selectivity for desired product **1.39** with dehalogenated product **1.40** (Scheme 1.20).[28,116] Frech *et al* developed an aliphatic phosphine based pincer palladium complex **1.42** for the Negishi reaction, wherein the coupling of electronically diverse, activated and non-activated, sterically bulky and functionalized aryl bromides with diaryl zinc were achieved (Scheme 1.21).[117]

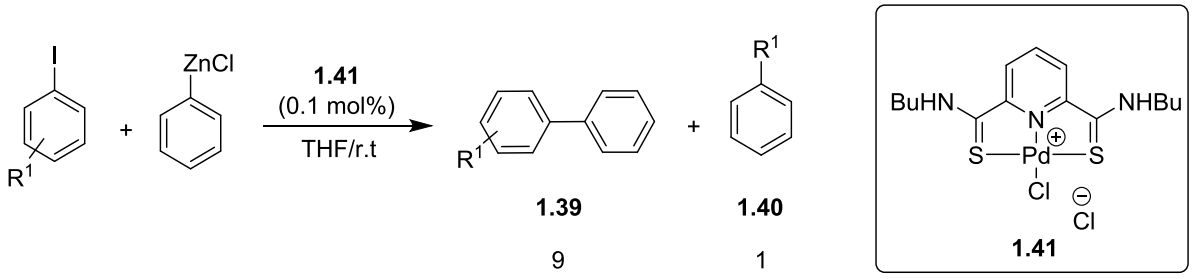

Scheme 1.20 Negishi coupling reaction using pincer complex **1.41**

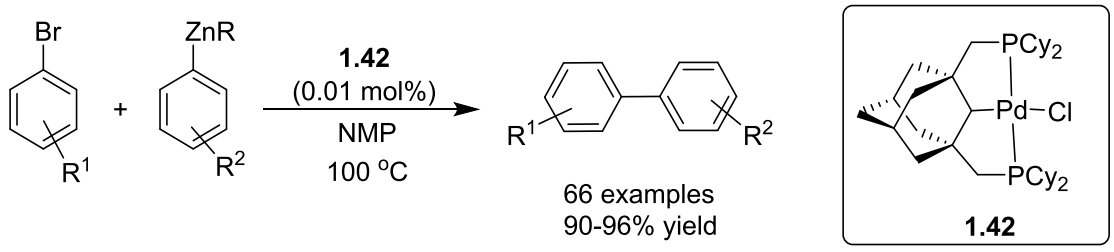

Scheme 1.21 Cross-coupling reaction aryl bromide with aryl zinc using pincer complex **1.42**

1.2.2.6 Sonogashira coupling reaction

Sonogashira reaction is the coupling reaction of alkynes and aryl halide catalyzed by palladium.[125,126] Due to the synthetic importance of coupled product of alkyne with aryl halide, various studies are demonstrated, and the development of this reaction can be achieved using pincer palladium catalysts.[106-114] Frech and co-workers have developed aminophosphine based pincer palladium catalyst **1.43** for the coupling of aryl iodide with phenyl acetylene to obtain aryl-alkyne coupled products (Scheme 1.22).[107] This reaction provides excellent TON (2 x 10^6) and a quantitative yield without the use of copper as co-catalyst. The coupling reaction shows negative mercury drop test, therefore, it is ambiguous whether **1.43** is the direct catalyst for the reaction. Gu and Chen have demonstrated that carbene based pincer catalysts efficiently performs Sonogashira cross-coupling reactions without the use of copper.[108]

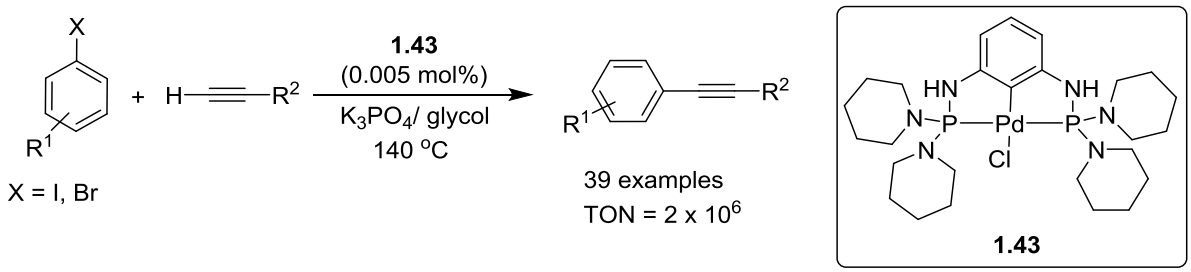

Scheme 1.22 Cross-coupling of aryl iodide with terminal alkynes using complex **1.43**

Later, Lee group developed di(1,2,4-triazolin-5-ylidene)Pd(II) pincer complex **1.44** for Sonogashira coupling reaction of aryl bromide with phenyl acetylene under copper and amine-free condition (Scheme 1.23).[109] Liang *et al* showed efficient cross coupling of differently substituted terminal alkynes with electronically variable aryl iodides and bromides using (PNP)PdCl catalyst under mild reaction condition.[111] In 2015, Wang group developed substituted diimino pincer palladium complex for Sonogashira reaction; wherein they observed that electron-withdrawing group on aromatic backbone of the pincer palladium complex enhances its catalytic activity.[112] Recently, Singh and co-workers described cross-coupling reaction of aryl halide and terminal alkyne using oxine based unsymmetrical (ONSe) pincer palladium(II) complex **1.45** (Scheme 1.24).[114]

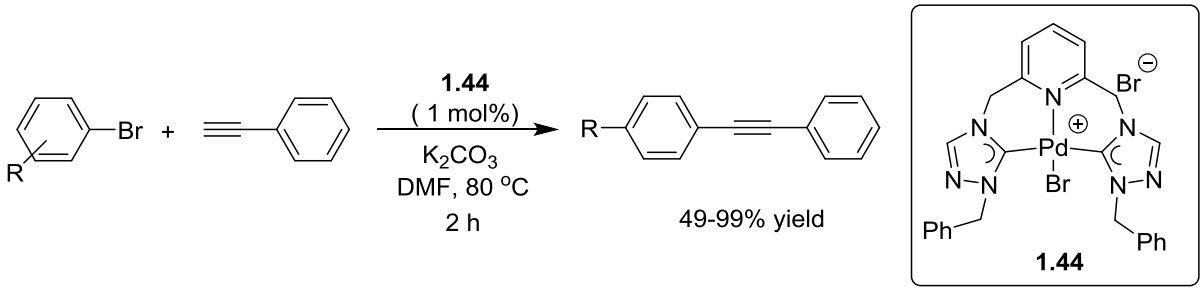

Scheme 1.23 Pincer palladium complex **1.44** catalyzed Sonogashira reaction

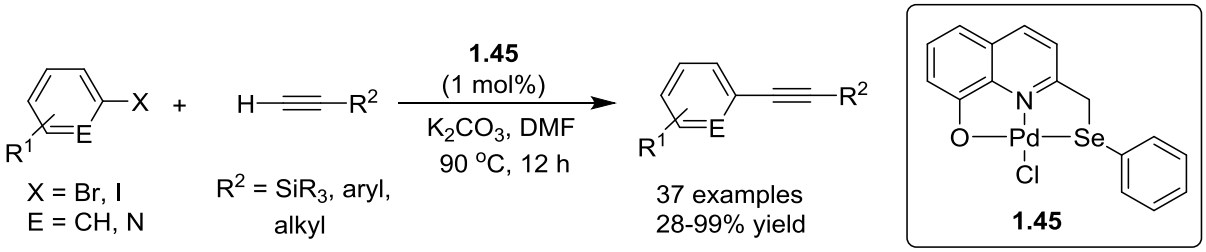

Scheme 1.24 Sonogashira reaction using unsymmetrical pincer palladium complex **1.45**

1.2.2.7 Aldol and Michael reaction by pincer palladium complexes

Richards and co-workers[127,128] have shown that pincer palladium complexes can be used as Lewis acid catalysts in Aldol[18,45,127] and Michael[57,127-129] types of reactions. The aldol and Michael reactions are synthetically significant process because they involve C–C bond formation and generate new stereocentre at the carbon. The high enantioselectivity for Aldol and Michael reaction has been achieved using chiral pincer palladium complexes.[130-132] Shang and co-worker have described a straight forward preparation of chiral PCP-complex **1.46**, which was used as catalyst for the coupling of methyl isocyanoacetate and different aldehydes to affords *cis* and *trans* isomers of oxazoline product (Scheme 1.25).[30]

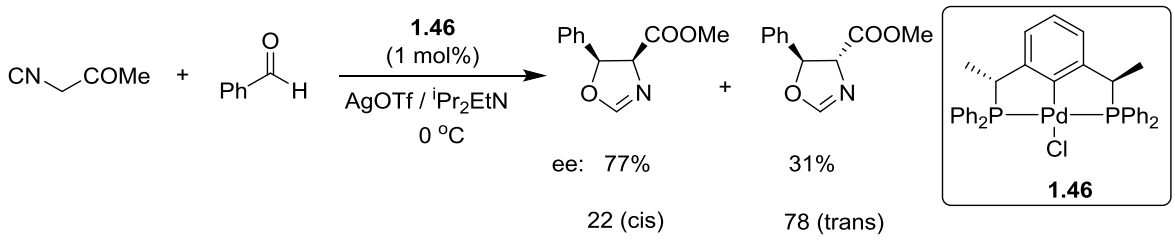

Scheme 1.25 Enantioselective synthesis of oxazoline using chiral pincer complex **1.46**

1.2.2.8 Allylation of aldehydes and imines

The allylation of aldehyde and imine is an important cross-coupling reaction catalyzed by the transition metal to produce the homoallylic alcohol and imine. Various reports are published on allylation of aldehyde and imine using pincer palladium complexes.[133-137] Yamamoto group have described the electrophilic allylation of aldehydes and imines by using bis-allyl palladium complex.[138-142] The bis-allyl palladium complex **1.47** was generated from the reaction of allylic stannane with monoallyl palladium complex *via* transmetalation process (Scheme 1.26).[143] The DFT modeling study demonstrated that the η^1-coordinated allyl-Pd moiety in **1.48** has a more nucleophilic character, and hence it can easily react with electrophiles, such as aldehydes, imines, Michael acceptors, and related reagents.[144-146] Szabó and other group studied that the pincer palladium complexes can efficiently replace monoallyl palladium species and provide nucleophilic allyl species under catalytic conditions (Scheme 1.26).[45,46] There are many reports which show that pincer palladium complexes efficiently catalyzes the electrophilic allylation of aldehydes and imines with allylic stannanes.[147,148] The use of pincer palladium catalysts for the allylation process is more beneficial compared to bis-allyl palladium complex.[149] The tridentate coordination of the ligand forces the allyl moiety into a η^1-coordination mode **1.49**, which prevents the regioselective issues that may occur with complex **1.48** bearing two different allylic moieties (Scheme 1.27).

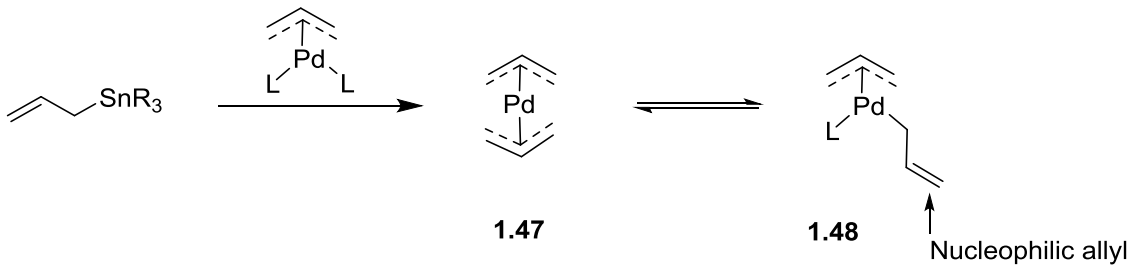

Scheme 1.26 Catalytic generation of nucleophilic bis-allyl Pd-species

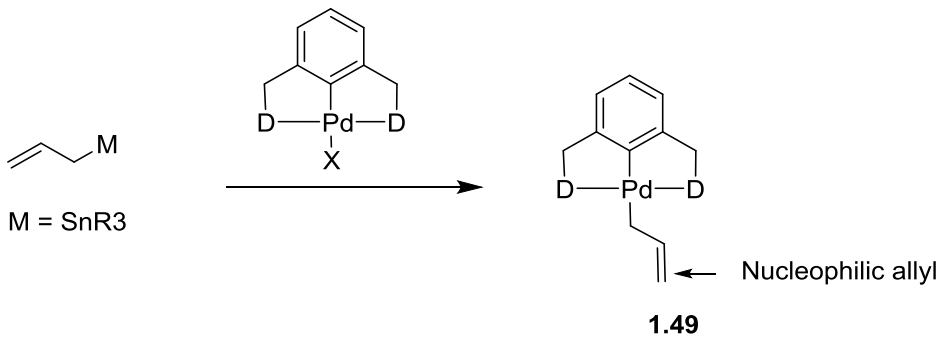

Scheme 1.27 Catalytic generation of nucleophilic η^1-allyl palladium pincer species

In 2006, Sheets and co-workers reported the allylation of aromatic aldehydes by selenium-based pincer complex **1.50**.[150] Herein, the efficient allylation of aromatic aldehydes was achieved with allyl tributyltin using **1.50** pincer palladium catalyst (Scheme 1.28). This methodology shows tolerance of sensitive functional groups, such as NO_2, CN, OMe, Br on aromatic aldehyde. Later, Osuka group developed porphyrin-based PCP pincer palladium complex **1.51** for the allylation of aldehyde with allylstannane (Scheme 1.29).[137]

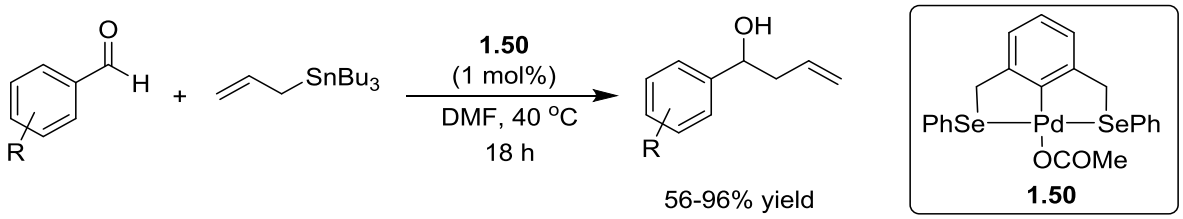

Scheme 1.28 Allylation of aldehyde using selenium based pincer complex **1.50**

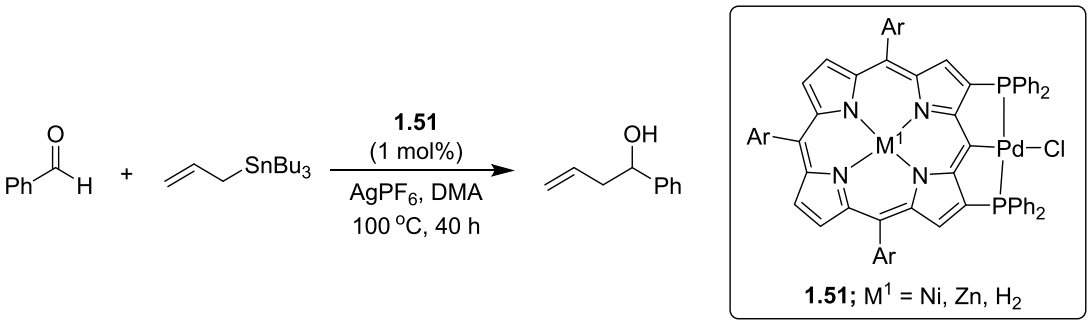

Scheme 1.29 Allylation of aldehyde using porphyrin-based pincer palladium complex **1.51**

1.3 Mechanistic aspect of pincer palladium-catalyzed cross-coupling reactions

The pincer palladium complexes have been used for number of C–C bond forming reactions, such as Heck reaction[64- 84] Suzuki-Miyaura reaction,[85-105] Sonogashira reaction,[106-114] Stille coupling,[70,115] Hiyama coupling,[106] Negishi coupling[28,116,117] and allylation of aldehyde and imines.[46,45,137,147,148] Hence, the mechanistic pathway of the pincer palladium catalyzed cross-coupling reaction is well studied, even though the actual role of pincer palladium complex is debatable. There are reports which demonstrate that the pincer complexes directly involved in the catalysis as an active catalyst. In such cases, during the cross coupling reaction palladium undergo redox process and proceeds *via* Pd(II)/Pd(IV) pathway.[71,75,86,90,92,121,124,151] In contrast, many studies demonstrated that the pincer palladium complexes decomposes to Pd(0) under harsh condition[23,38,39,68,97,152-154] and the catalytic activity appears from the palladium(0), such as Pd(0) nanoparticles or colloidal palladium. In

this case, the pincer palladium complex does not act as direct catalyst, but behaves as the pre-catalyst and releases the palladium(0) nanoparticles or homogeneous palladium(0) that act as the catalyst. Various methods are known to detect the formation of palladium (0) nanoparticles.[38,68,97,98,153,154]

1.3.1 Mechanistic insight for Heck reaction

There are many reports on the Heck reaction which is catalyzed by the pincer palladium complexes with high yield.[64-84] As mentioned, the pincer palladium complexes decompose to form Pd(0) nanoparticles or clusters upon Pd–C bond cleavage. Hence, Pd(0) species don't have pincer backbone. There are many reports, which show that under basic condition and high temperature, the pincer palladium complex decomposes to form colloidal Pd(0) clusters or nanoparticles[23,38,39,68,76,152-154] which catalyze the reaction. Gladysz *et al*[68] have demonstrated that the cross-coupling of phenyl iodide and methyl acrylate does not catalyze directly by fluorous pincer complex **1.52**, but by the dispenses Pd(0) nanoparticles (Scheme 1.30). They have observed that the colloidal Pd(0) nanoparticles generally exhibit reddish colour of the reaction mixture. The nanoparticle catalyzes the cross-coupling reaction following the Pd(0)/Pd(II) mechanistic pathway, which is shown in Scheme 1.31. Jones and co-workers independently carried out several experimental studies for the mechanistic pathway of the reaction.[39,152,153] They observed that the reaction is catalyzed by Pd(0) nanoparticles that released from pincer palladium complex. The classical catalytic cycle of the Heck coupling based on the oxidative addition of aryl halide to the Pd(0) catalyst **1.53**, which released from pincer palladium complex **1.52**, is shown in Scheme 1.31. The first step is the oxidative addition of aryl halide to Pd(0) to form Pd(II) complex **1.53a**. In second step, the ligand exchanges with olefin to give **1.53b**, which undergoes insertion of olefin into Pd−Ar bond, and affords η^1−alkyl-Pd complex **1.53c**. The *β*-hydride elimination generates the coupled product and hydrido palladium complex **1.53d**, which upon deprotonation with base produce the Pd(0) catalyst **1.53**.

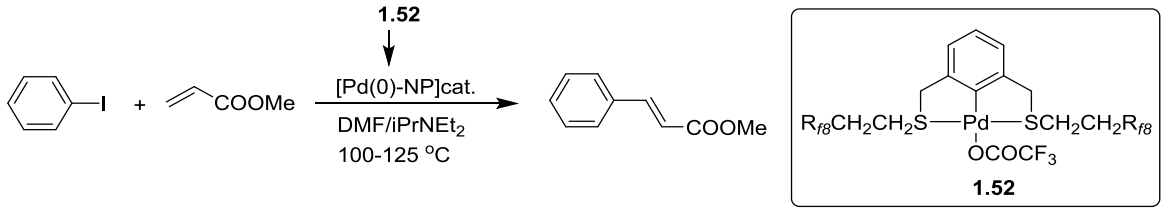

Scheme 1.30 Heck reaction using pincer cpalladium complex **1.52** as dispenser of Pd(0) nanoparticles (R_f indicates polyfluorinated chain)

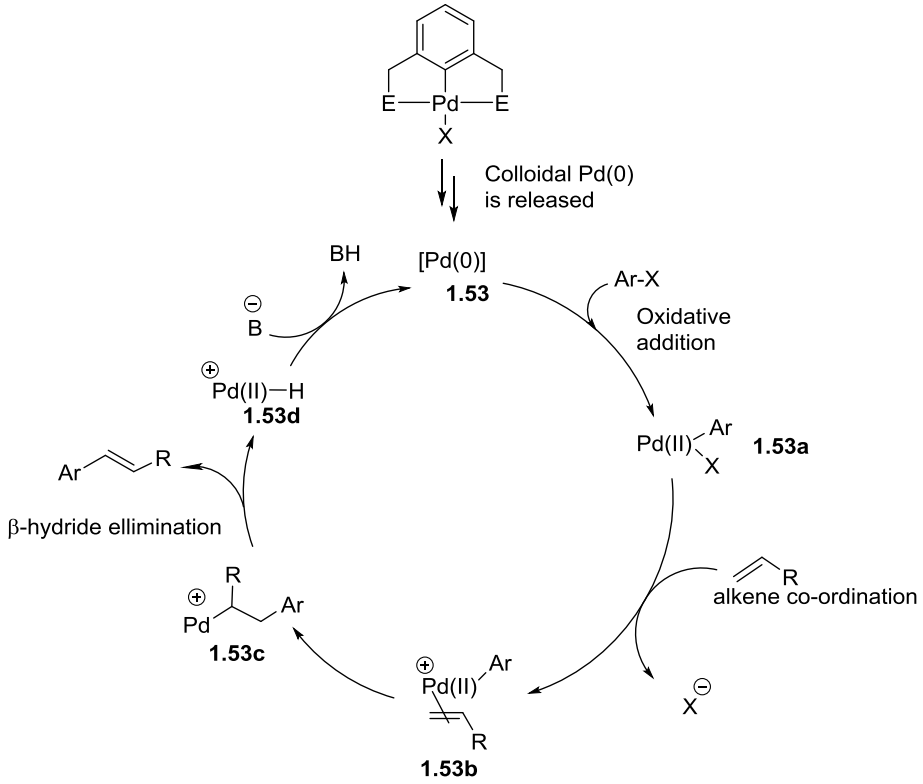

Scheme 1.31 Heck coupling *via* Pd(0)/Pd(II) classical catalytic cycle

Heck coupling reaction demonstrated by Gladysz and Jones shows that the pincer palladium is not the actual catalyst, but acts as pre-catalyst for the formation of active Pd(0) particles. In this, the use of co-ordinating base such as triethylamine, and high temperature would favours for the decomposition of pincer palladium to Pd(0) nanoparticles. In 2005, Weck and co-workers hypothesized the decomposition pathway for the PCP pincer palladium complex **1.54** under applied reaction condition, wherein the first step is the co-ordination of triethyl amine to palladium with opening one of the side arm [**1.54a**] (Scheme 1.32).[39] The second step is *β*-hydride elimination to form an anionic complex **1.54b**, which on further co-ordination with triethylamine forms **1.54c**. The species **1.54c** on *β*-hydride elimination forms palladium(0) nanoparticles. The decomposition pathway was supported by NMR, MS and DFT study. The high temperature is the most probable factor to irreversible decomposition pathway for the pincer complexes. Milstein *et al* reported that under mild reaction condition, the pincer palladium complexes collapses to Pd(0) and further regenerates the Pd(II) upon reaction with organic halide.[155] They have reported novel process which shows the easy collapse of a thermally stable d^8 Pd(II) pincer system under reducing conditions. In this process, the reduction of complex **1.55a** and **1.55b** by sodium metal generates a novel binuclear Pd(0)/Pd(II) complex **1.55c** containing a 14-electron linear Pd(0) moiety and a

completely nonplanar, “butterfly” type Pd(II) 16-electron moiety (Scheme 1.33). The complex is diamagnetic, and the mechanistic studies for the formation of **1.55c** have not clearly understood. A probable pathway for the formation of **1.55c** might involve a single electron transfer from sodium to Pd(II) to form a tri-coordinate PdI intermediate with the precipitation of NaX. The tri-coordinate PdI intermediate which is likely to undergo dimerization followed by successive disproportionation to form Pd(0) and Pd(II), and the rearrangement involving pincer ligands. Two different ways for the conversion of binuclear **1.55c** to mononuclear pincer palladium complex have been mentioned. One way in which reaction of complex **1.55c** with iodobenzene produces the formation of complex(PCP)PdI and dimer of arenes, but with slower reaction rate. It indicates that reaction proceeds *via* electron transfer from the Pd(0) center to the aryl halide. To support the electron-transfer reaction (other possibility), the reaction of a THF solution of **1.55c** with AgOTf resulted in the immediate formation of the monomeric (PCP)PdOTf complex and silver metal. The binuclear complex **1.55c** shows high catalytic activity for Heck reaction, and is probably based on the formation of the corresponding monomeric (PCP)PdI complex. They assume that the Heck reaction by (PCP)Pd(II) complex follows different mechanism for reaction than the classical Pd(0)/Pd(II) catalytic process.

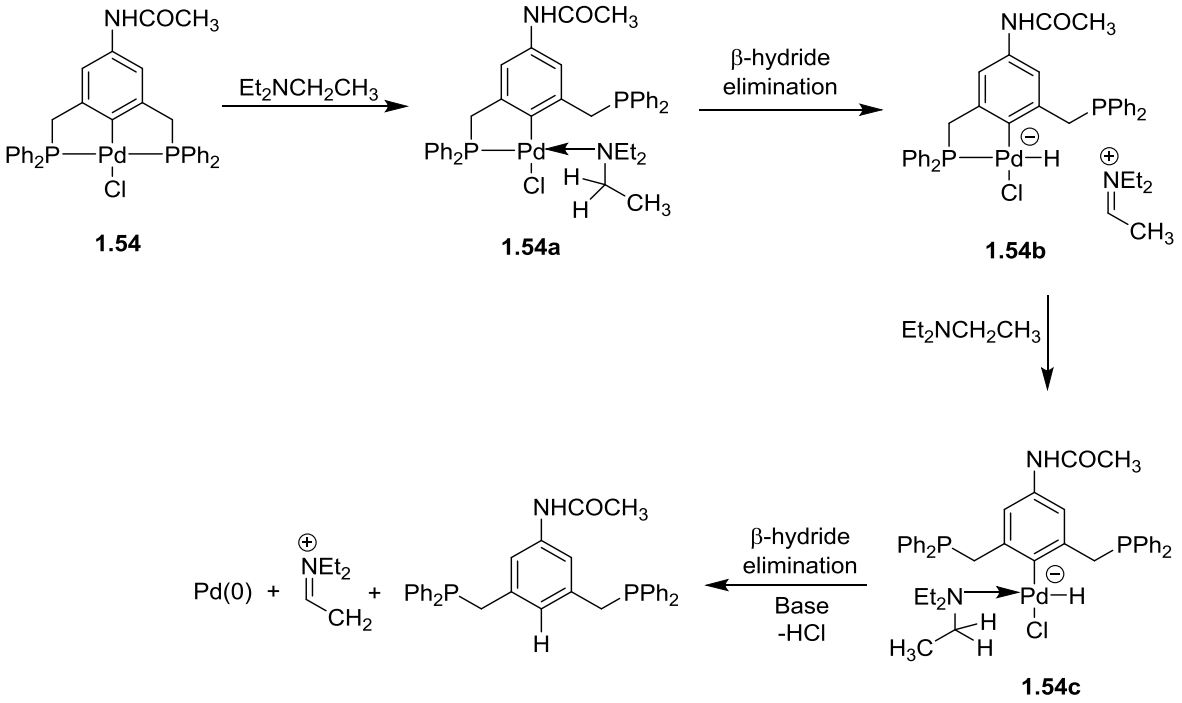

Scheme 1.32 Proposed pathway for decomposition of pincer palladium

Mercury drop test is a typical qualitative method to verify colloidal Pd(0) particles.[38] In this test, colloidal Pd(0) nanoparticles react with Hg(0) to form an amalgamate, and if there is release of palladium nanoparticles from the pincer palladium complex then mercury binds with nanoparticles and quenches the rection. If catalytic reaction stopped or slow down, it suggest that the Pd(0) particles arises from the decomposition of the pincer are the actual catalyst in the reaction. Similalry, the cross-linked poly(vinyl pyridine) (PVPy) which co-ordinate to soluble nanoparticles of palladium metal, and hence quenches the reaction.[38]

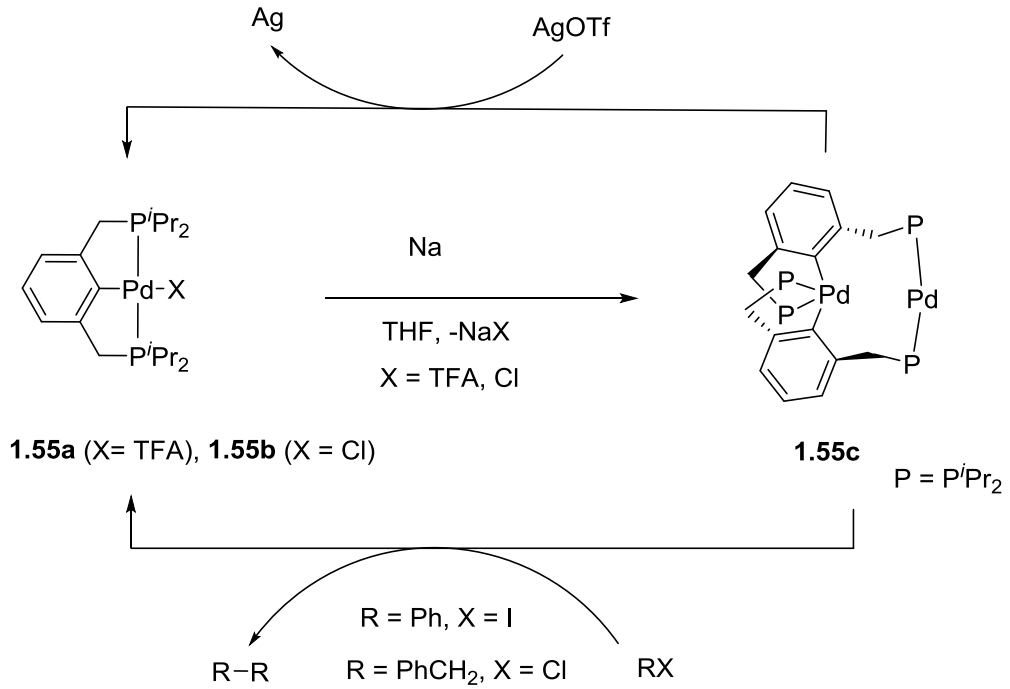

Scheme 1.33 Reduction of **1.55a** and **1.55b** to form **1.55c** and it's oxidation to regenerate pincer complex

As shown in Scheme 1.31, the oxidative addition of the aryl halide to Pd(0) catalyst to form Pd(II) is the main step in the Heck coupling reaction. The same reaction can be possible at the Pd(II) species which upon oxidative addition with aryl halide can generate Pd(IV) intermediate.[6,51,67,75] The oxidation potential of aryl iodide is very low to oxidize the Pd(II) to Pd(IV) species, however, this can be achieved by the specific modification in the complexes. Till date, there is no strong evidence for the pincer palladium complex to be the direct catalyst in Heck coupling that follows Pd(II)/Pd(IV) pathway. DFT study also shows that the oxidation of palladium atom of pincer complex to Pd(IV) with aryl iodide is less likely under the reaction condition for Heck coupling.[71,75,121]

The strong oxidants, like hypervalent iodine salts, can efficiently oxidize the pincer palladium complexes. Canty[156] and van Koten[40] have demonstrated that the hypervalent iodines easily oxidize the NCN pincer Pd(II) complex **1.56** to the corresponding Pd(IV) complex (Scheme 1.34). Inspired by these studies, Szabó and co-worker developed pincer complex **1.59** that catalyzes Heck coupling of hypervalent iodine and allyl acetate to obtained coupled product through Pd(IV) complex **1.60** (Scheme 1.35).[71] The formation Pd(0) species has not observed using the strong oxidant like aryl iodonium salt, and the reaction mostly proceeded through Pd(II)/Pd(IV) pathway.

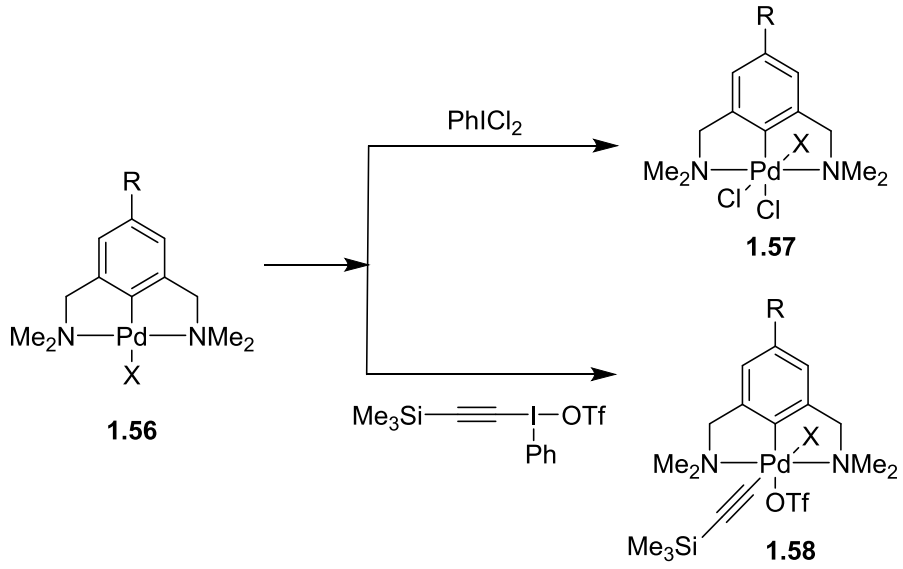

Scheme 1.34 Oxidation of Pd(II) pincer to Pd(IV) complexes using hypervalent iodine salts

Jenson *et al* have described Heck coupling reaction catalyzed by the (PCP)Pd-complex in which the reaction proceeds through Pd(II)/Pd(IV) catalytic cycle (Scheme 1.36).[6] This catalytic process initiated with the oxidative addition of a vinyl C−H bond of the alkene to Pd(II) pincer complex **1.61** to generate Pd(IV) species **1.61a**, which upon reductive elimination of HCl to give **1.61b**. Species **1.61b** undergoes oxidative addition with aryl halide to form **1.61c**, which undergoes reductive elimination of coupled product to regenerate the pincer catalyst **1.61**. Unfortunately, this proposal has been made without any experimental evidence.

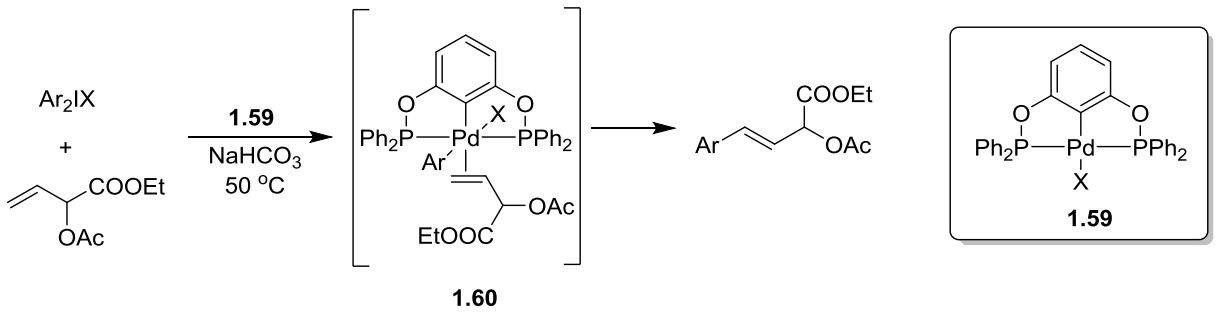

Scheme 1.35 Heck coupling of iodonium salt and allyl acetate using complex **1.59**

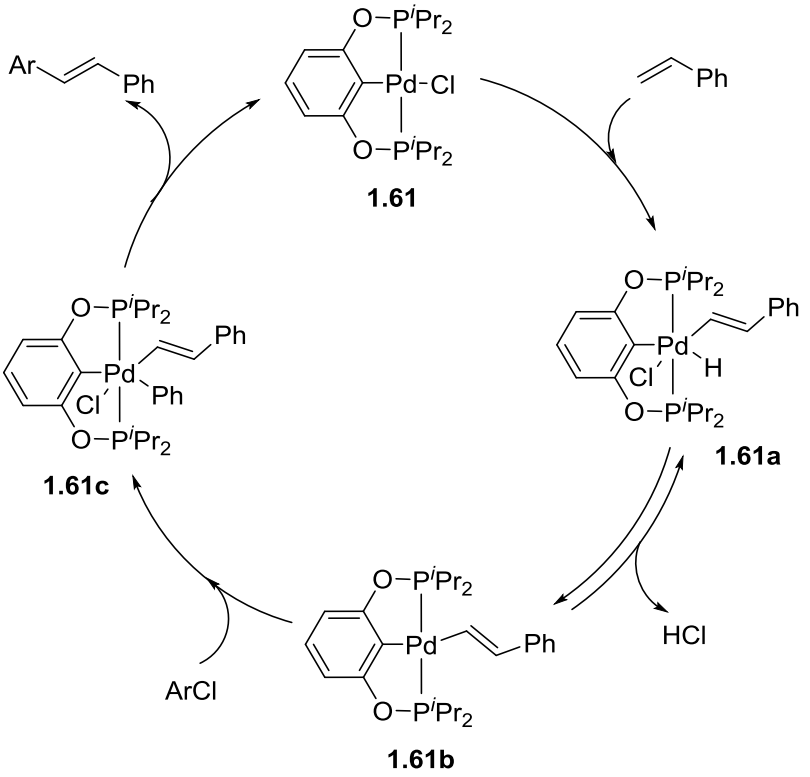

Scheme 1.36 Catalytic cycle for Heck coupling *via* Pd(II)/Pd(IV) pathway

1.3.2 Mechanistic pathway for Suzuki-Miyaura cross-coupling reaction

Recently, Wendt[91] and Nishiyama[124] group independently described the Suzuki-Miyaura cross-coupling reaction of aryl boronates with an aryl halide, wherein they observed that the reaction does not proceed through the classical Pd(0)/Pd(II) pathway. In this, the palladium atom of the pincer complex maintains its oxidation state, and decomposition of pincer complex does not occur. Similarly, Liu[93] and Nishioka[101] group showed that pincer palladium complexes are the main catalyst for the Suzuki-Miyuara coupling reaction, and does not form any Pd(0) nanoparticles.

Frech and co-workers reported Suzuki coupling reaction of aryl boronic acid with aryl halides in the presence of water using aliphatic phosphine based pincer palladium complex

1.62.[157] The substitution of chloride ligand of **1.62** with bromide to give corresponding bromide palladium complex **1.62b** was observed during the control reaction (Scheme 1.37). After the completion of the reaction, catalyst remains highly active and catalysis was continued by the addition of more substrates which afforded the desired coupled product without a decrease in catalytic activity, which indicated the homogeneous catalysis and less likely the formation of palladium nanoparticles. They have proposed a catalytic cycle, wherein the first step is the formation of complex **1.62a** from the reaction of **1.62** with phenylboronic acid in the presence of NaOH. The hydroxide ion activates the phenylboronic acid that promotes phenyl group transfer to the palladium center. The next step involves the oxidative addition of aryl bromide to **1.62a**, which forms a neutral hexacoordinated pincer Pd(IV) species [Pd(Ar)(Br)(Ph)]. The hexacoordinated Pd(IV) species upon the reductive elimination of the desired coupled product gives back Pd(II) active catalyst (Scheme 1.37; path **A**). Alternately, the direct biaryl product formation at the Pd(II) center through a four-centered transition state has been proposed (Scheme 1.37; path **B**).

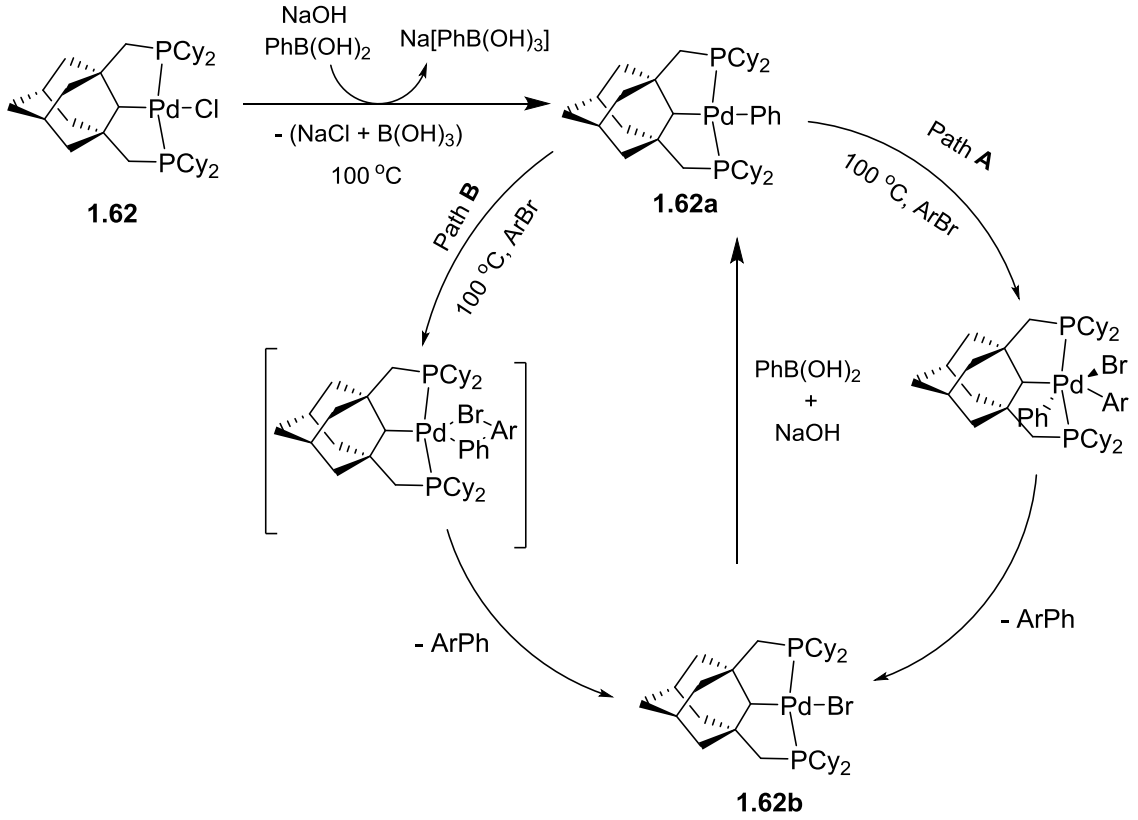

Scheme 1.37 Catalytic cycle for Suzuki reaction using complex **1.62**

Similarly, the aminophosphinate pincer catalyst has been developed by Frech for the Suzuki-Miyaura reaction.[58,158] In this case, Hg drop test shows negative indicating the catalysis proceeded through a Pd(II)/Pd(IV) process. In many cases, the cross-coupling reactions by the pincer palladium complexes show the positive Hg drop test, which suggests the decomposition of the pincer palladium catalyst to Pd(0) nanoparticles, and Pd(0) nanoparticles are the active catalyst for the reaction.[29,98,159]

1.4 The C–H bond arylation of azoles by various catalytic systems

The arylated azoles have attracted particular attention as they are fundamental unit of many naturally occurring compounds as well as pharmaceutical products.[160-163] The selectively C-2 arylation of azoles has been achieved using various transition metal salts, such as Cu,[164-170] Pd,[171-187] Ni,[188-190] Ru,[191] Rh,[192-196] with the added ligands. In 1990, Ohta *et al* demonstrated the first example of direct C–H bond arylation of various azoles using palladium catalyst.[197] They observed the selective C-5 arylation of oxazole with chloropyrazine using $Pd(PPh_3)_4$ as catalyst and KOAc as base (Scheme 1.38). Later on, Itami and co-workers reported the C-2 arylation of azoles using most convenient and less expensive nickel catalyst (Scheme 1.39).[190] The arylation of azole with an aryl halide or aryl triflate was carried out using $Ni(OAc)_2$/bipyridine catalyst system to obtain arylated product **1.63**. Similarly, Daugulis[164] described the arylation of heterocycles using easily available and less expensive copper metal (Scheme 1.40). Herein, the use of simple CuI metal efficiently catalyzed the arylation of benzoxazole with aryl halide to give arylated product **1.64** in the presence of LiO^tBu.

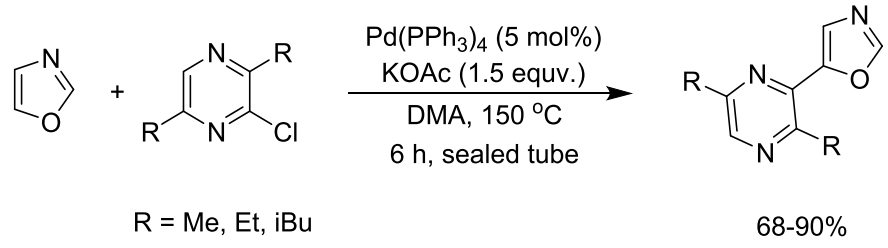

Scheme 1.38 Direct C(5)–H arylation of azoles using palladium catalyst

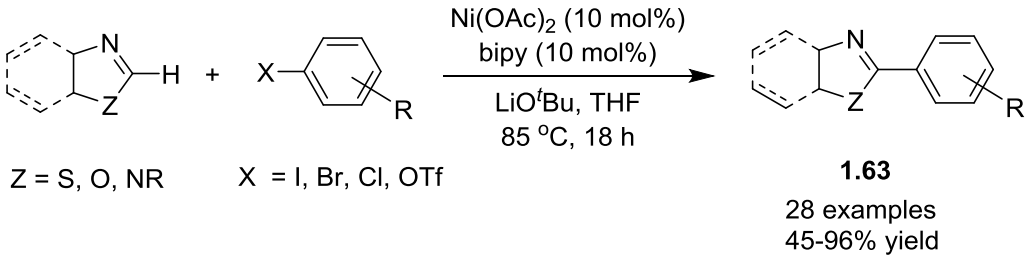

Scheme 1.39 C(2)–H arylation of azole using nickel-catalyst

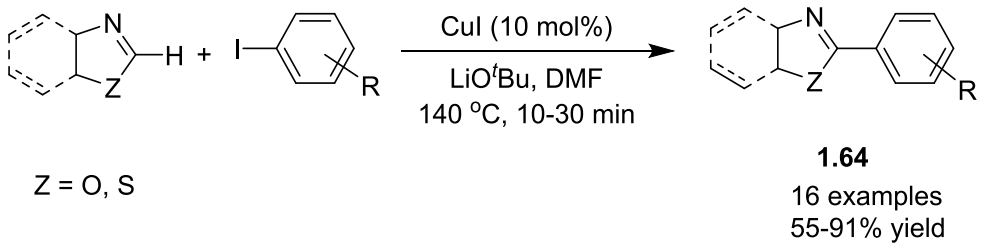

Scheme 1.40 Arylation of benzoxazole using CuI as catalyst

The arylation of azole using nickel and copper catalyst gave the important development from the economical perspective for the large scale synthesis. However, in most of these cases, the use of strong base and high reaction temperature limit the methodologies. The arylation of azoles under mild reaction condition has been reported using precious transition metals, such as Ru,[191] Rh,[192-196] Pd[171-187]. In 2006, Bellina *et al* described the first direct C-2 arylation of azoles with aryl iodides by the palladium catalyst and CuI as co-catalyst under base-free reaction. The azoles containing free NH, such as imidazole, benzimidazoles, and indoles efficiently undergoes arylation with differently substituted aryl halides (Scheme 1.41).[172] In 2008, Ellman and co-worker demonstrated the rhodium-catalyzed arylation of benzimidazole with aryl bromide to provide coupled product **1.66** with good yield (Scheme 1.42).[195] Later, Haung *et al* reported the arylation of azoles with a difficult arylating reagent, such as aryl bromide using palladium as catalyst and Cu as co-catalyst for the reaction (Scheme 1.43).[180] In this, they have isolated Cu(xanthphos)(benzothiazole)I intermediate and studied the reaction mechanism for the arylation reaction. From the various reactivity study of the Cu(xanthphos)(benzothiazole)I complex, they observed that the transmetalation is crucial step during the catalysis.

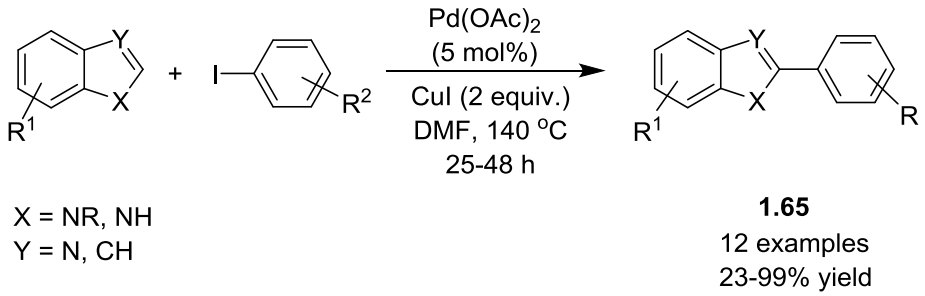

Scheme 1.41 Direct C(2)-arylation of azole using palladium as catalyst

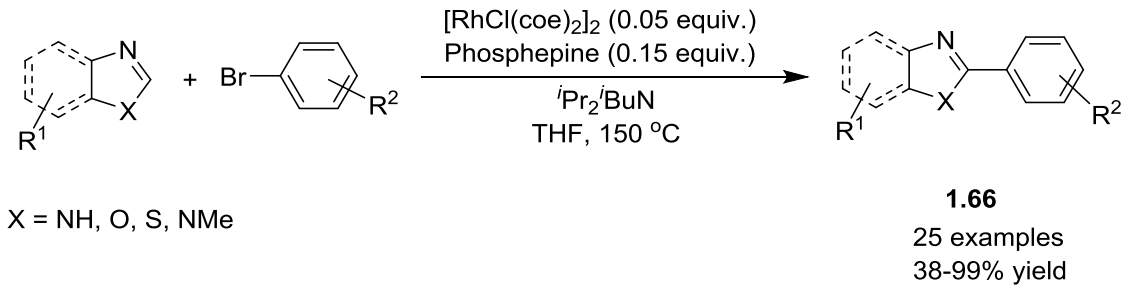

Scheme 1.42 Arylation of benzimidazole using rhodium as catalyst

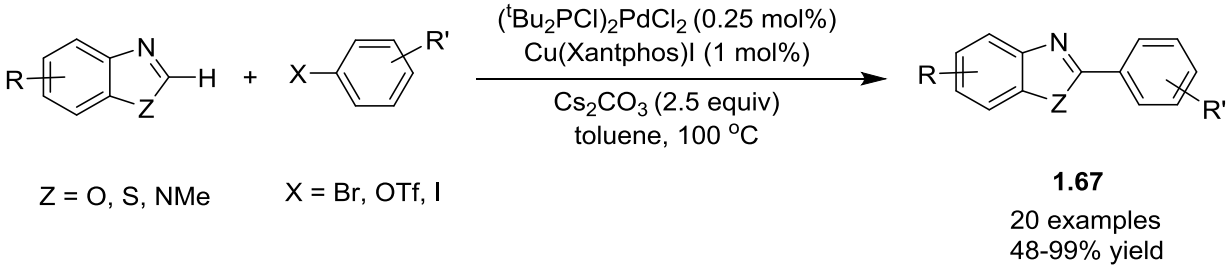

Scheme 1.43 Arylation of azole using Pd catalyst and Cu co-catalyst

1.5 Nickel-catalyzed C–H activation and functionalizations

Direct C–H bond functionalization of the organic compound to form C–C or C–heteroatom bond by the transition metal catalyst is a powerful and attractive method.[198-209] In the last few decades, the late and noble transition metal catalysts are extensively used in the inert C–H bond activation and functionalization; however, less abundance and expensiveness of these noble metal limits their broad application. Compared to the 4d and 5d transition metals, 3d transition metals have high abundance, low cost, and unique reactivity. However, the 3d transition metals are not much explored compared to 4d and 5d transition metals in various catalytic applications. Among the 3d metals, the nickel (Ni) has excessive activity and versatile reactivity. In 1922, Sabatier group described that "nickel can do all kind of work and maintain it's activity for a long time". The development of organo-nickel

chemistry led to discovering several catalytic systems and much practical application.[210-215] The nickel complexes have been used as catalyst in many organic transformations, such as cycloaddition, carbonylation, decarbonylation, alkene polymerization, which contributes both in academic as well as in the industry.[216-220]

The first nickel-mediated aromatic C–H bond activation was described by Kleinman and Dubeck group in 1964.[221] They observed that the heating of dicyclopentadienyl nickel with an excess of diazo-benzene afforded purple blue organo-nickel species (Scheme 1.44). Till then there are several publications appeared on the nickel-catalyzed C–H bond activation and functionalization. In this section, various C–H bond functionalization reactions catalyzed by nickel is summarized.

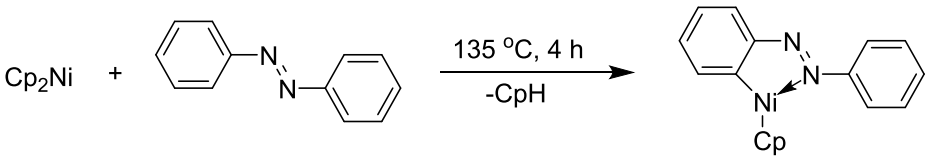

1.70

Scheme 1.44 Synthesis of organonickel species

1.5.1 Carbon-carbon bond forming reaction using nickel catalyst

The less expensiveness, high abundance and unique reactivity of nickel make it beneficial to utilize in various organic transformation compared to the 4d and 5d transition metals. Nickel as a catalyst has been utilized in various C–C bond forming reactions, such as alkylation,[222-233] alkenylation,[234-236] arylation,[188-190, 237-241] alkynylation.[242-246]

1.5.1.1 Nickel-catalyzed C–H alkylation of (hetero)arenes

The alkylated arenes and heteroarenes are important backbone of many natural molecules, biologically relevant compounds, and organic materials.[247-249] In 2010, Hu group reported the nickel-catalyzed C–H bond alkylation of aromatic heterocycles with unactivated alkyl halides containing the *β*-hydrogens (Scheme 1.45).[223] With the optimization conditions, the coupling of various substituted heterocycles with diversely substituted alkyl iodide was achieved using catalyst **1.71** and CuI co-catalyst in the presence of LiO^{t}Bu. This methodology tolerates various functional groups, such as –OMe, –Cl, –Br on oxazole and –OAr, –OCOAr, –SAr, –CO, –CN groups on alkyl halide moiety, and shows excellent chemo and regioselectivity for the product formation. Punji and co-workers developed a quinolinyl-based

NNN pincer nickel complex for the direct C–H bond alkylation of azole under mild reaction conditions; wherein the coupling of azoles with alkyl halide achieved using complex **1.72** at 100 ^{o}C without CuI co-catalyst (Scheme 1.46).[232] The catalyst **1.72** is robust in nature, which was recycled and reused five time for the alkylation without affecting the catalytic activity. This catalysis shows broad substrate scope for differently substituted azoles and alkyl halides. Chatani *et al* developed a new strategy for the direct alkylation of benzamide and acrylamide with alkyl halide by nickel catalyst using 8-aminoquinoline as a bidentate directing group (Scheme 1.47).[226] The coupling of benzamide with alkyl halide was achieved using $Ni(OTf)_2/PPh_3$ catalyst system in the presence of Na_2CO_3 in toluene. This methodology provideed broad substrate scope for various benzamides and tolerated important of functional groups on the aromatic backbone and on the alkyl halides. The reaction is highly selective for less hindered C–H alkylation of the *meta*-substituted aromatic amides.

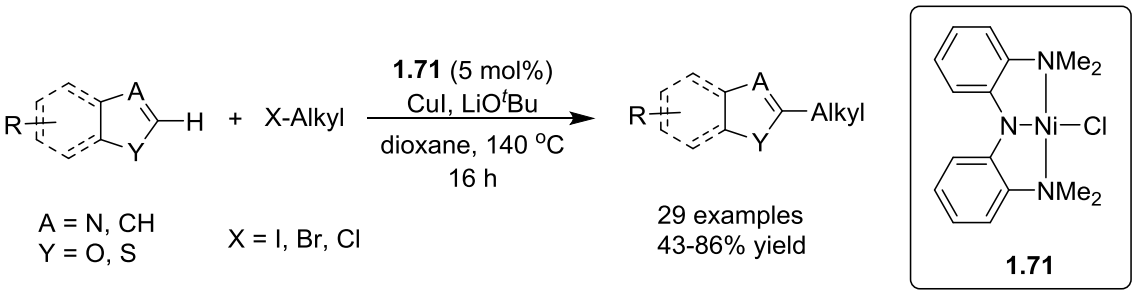

Scheme 1.45 Nickel-catalyzed alkylation of aromatic heterocycle with alkyl halide

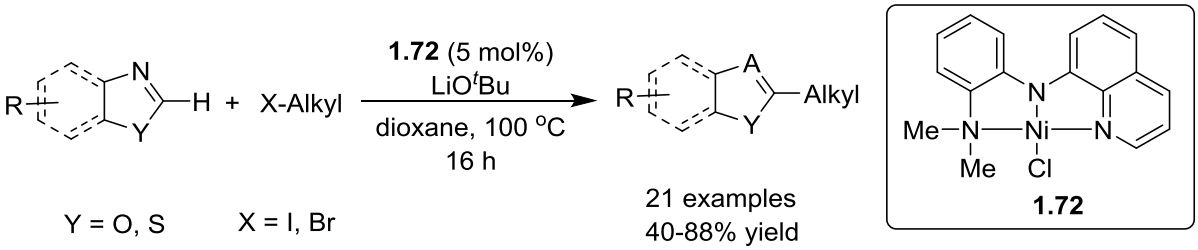

Scheme 1.46 Alkylation of azoles using (NNN)Ni-pincer complex

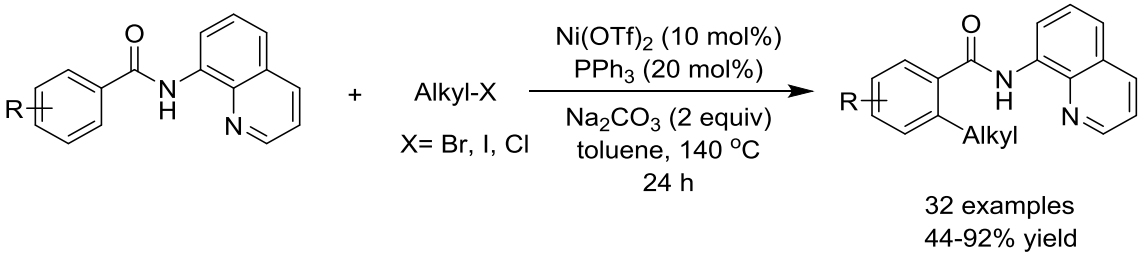

Scheme 1.47 Ni-catalyzed alkylation of benzamide using bidentate directing group

In 2014, Ge *et al* showed the direct alkylation of unactivated C(sp^3)–H bond of alkyl amides with alkyl halides using nickel catalyst *via* the bidentate chelation assistance (Scheme 1.48).[228] This method is highly selective for C–H bond alkylation of methyl group over the methylene C–H bond of the aliphatic amide. Important functional groups like alkenyl, cyano, ester, and trifluoromethyl were tolerated on aliphatic amides. Recently, Ackerman and co-workers developed a new methodology for *ortho* C–H alkylation of aniline with alkyl bromide using nickel catalyst *via* monodentate chelation assistance (Scheme 1.49).[230] Herein, the efficient cross coupling of anilines bearing a monodentate *N*-pyrimidyl substituent with alkyl bromide can be achieved using (DME)$NiCl_2$/D*t*BEDA catalyst system. This methodology provided broad substrate scope for *ortho*, *meta* and *para*-substituted aniline with the tolerance of important functional groups, such as –OMe, –CF_3, –F, –Cl, –COOEt. This method is not only limited to the primary alkyl bromides, it also efficiently works for the secondary alkyl bromides. Recently, Punji and co-workers described the direct C(2)-alkylation of indole through monodentate chelation assistance using (quinolinyl)amido-nickel catalyst with alkyl halides.[233] In this case, the efficient coupling of indole with primary and secondary alkyl halide was achieved using (NNN)Ni-catalyst **1.73** (Scheme 1.50). This methodology provided broad substrate scope for the primary as well as secondary alkyl halides.

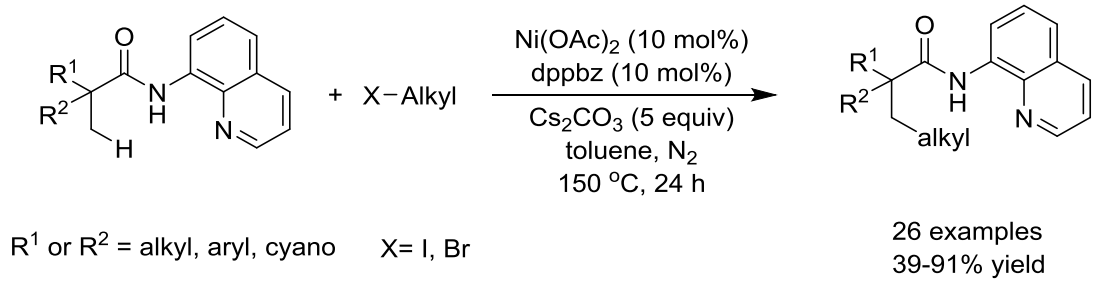

Scheme 1.48 Nickel-catalyzed alkylation of C(sp^3)–H bond of the aliphatic amide

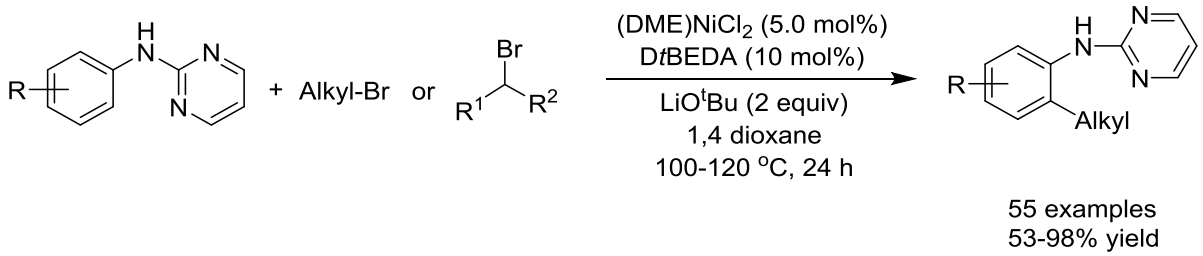

Scheme 1.49 Nickel-catalyzed *ortho*-alkylation of aniline *via* monodentate chelation assistance

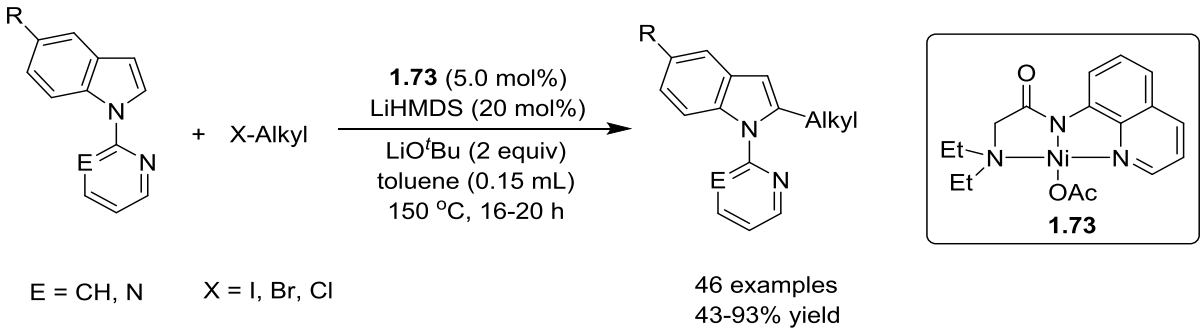

Scheme 1.50 Direct C(2)–H alkylation of indoles using (NNN)Ni-catalyst with alkyl halides

1.5.1.2 Nickel-catalyzed C–H alkenylation of (hetero)arenes

In 2007, Hiyama reported the direct C–H bond functionalization of pyridine *N*-oxide.[234] The addition of pyridine-*N*-oxide across various alkyne was achieved using nickel as a catalyst (Scheme 1.51). This addition was chemoselective and occurred particularly at the C-2 position of the pyridine-*N*-oxide through C–H bond activation under mild reaction condition. The addition of substituted pyridine-*N*-oxide to symmetrical alkynes affords good yield and good E/Z selectivity of products. Also, the E-selectivity for the product can be obtained by using unsymmetrical alkynes as coupling partner.

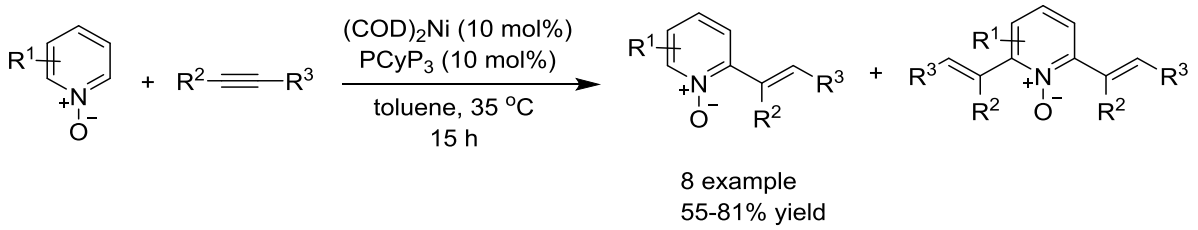

Scheme 1.51 Nickel-catalyzed addition of pyridine-*N*-oxide to alkyne

There has been great demand to develope a method for the introduction of F-containing group in organic compound due to the unique effect of F-substituent in pharmaceutical, agrochemicals and material sciences.[250] Mostly, the functionalization of polyfluoro arenes can be achieved by the deprotonation of acidic protons using the stoichiometric amount of organometallic bases, and the reaction followed by the electrophilic addition of electrophiles.[251] The direct C–H bond activation of polyfluoro arenes using transition metal complex appears to be the ideal catalytic system.[252,253] Recently, Hiyama and co-workers reported the alkenylation of pentafluoro arenes *via* the C–H bond functionalization using inexpensive nickel catalyst.[235] They observed the smooth coupling of polyfluoro arenes with a

symmetrical alkyne to afford a good yield of the coupled product (Scheme 1.52). With the excess use of alkyne and upon increasing the reaction time, they have observed dialkenylated product in good yield. The reaction shows high regio- and stereoselectivity for the insertion of alkyne to C–H bond over the C–F bond.

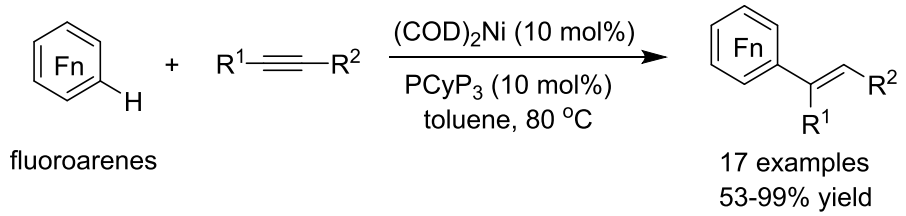

Scheme 1.52 Nickel-catalyzed alkenylation of pentafluorobenzene

The same group reported C(2)-selective alkenylation of pyridine, which is difficult to undergo C–H functionalization.[236] They observed that the coupling of pyridine with alkyne produces an excellent yield of coupled product using nickel and a Lewis acid catalyst (LA) (Scheme 1.53). It is assumed that the pyridine is activated by the co-ordination of pyridine nitrogen to a Lewis acid catalyst. The combination of Ni-catalyst and Lewis acid catalyst gives selective C(2)–H alkenylation product in good yield. This methodology provides a wide range of alkenylated pyridines in chemo-, regio-, and stereoselective manner under the mild reaction conditions.

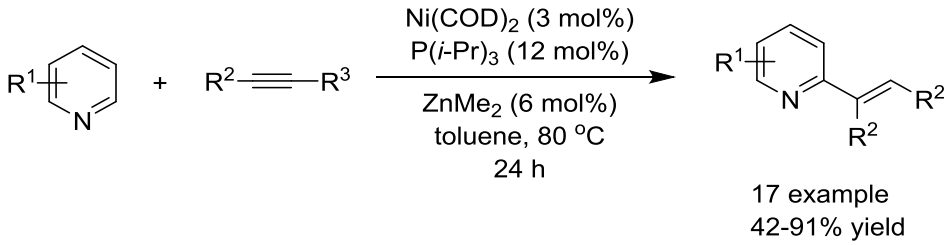

Scheme 1.53 Direct C(2)–H alkenylation of pyridine using nickel and Lewis acid system

1.5.1.3 Nickel-catalyzed C–H arylation of (hetero)arenes

In 2009, the nickel-catalyzed C–H bond arylation of azoles with aryl halide was reported by Itami[188] and Miura,[189] independently. Itami group described the cross-coupling of azole with aryl halides and aryl triflate using $Ni(OAc)_2$/bipy or $Ni(OAc)_2$/dppf catalyst in the presence of LiO^tBu (Scheme 1.54).[188] A number of structurally diverse heteroarenes, such as thiazole, benzothiazole, oxazole, benzoxazole, and benzimidazole can be efficiently coupled

with differently substituted aryl halides. Similarly, Miura *et al* demonstrated the arylation reaction of various azoles with aryl bromide (Scheme 1.55).[189] They have achieved the coupling of azoles with aryl bromide using $NiBr_2$·diglyme/Phen catalyst system and LiO^tBu. It was observed that the use of Zn powder increases the reaction rate by reducing N(II) to Ni(0) active species.

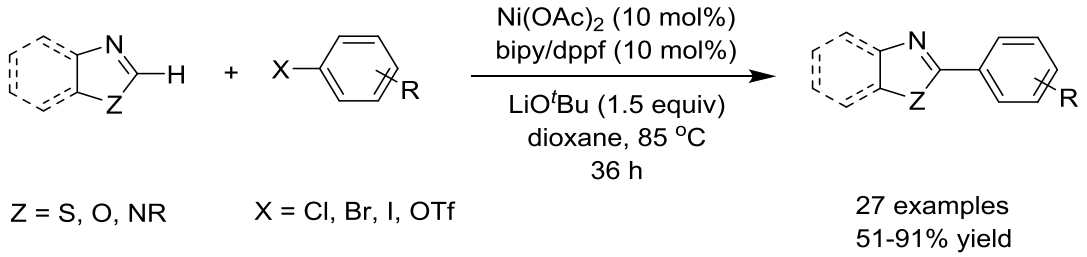

Scheme 1.54 Nickel-catalyzed arylation of azoles with aryl halide or aryl triflate

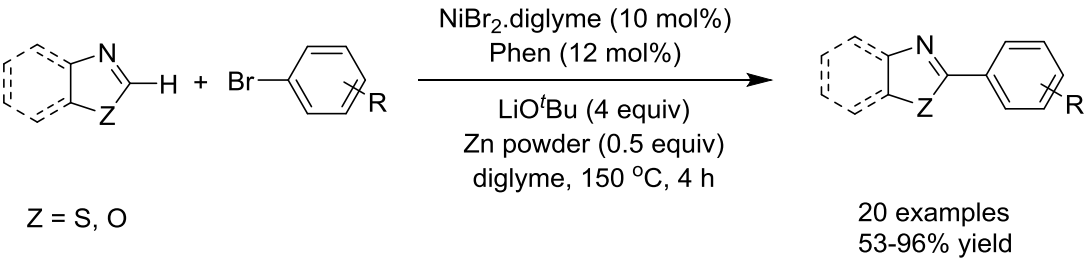

Scheme 1.55 Nickel-catalyzed arylation of azoles with aryl bromide

The arylation of azoles by Itami and Miura groups demonstrated that the nickel has the potential to allow the access of a wide range of 2-arylated azoles with substituted aryl halides or triflates. However, in both the cases, the utilization of strong base LiO^tBu limits the methods. Itami group developed a new strategy for the arylation of azole using $Mg(O^tBu)_2$ base in DMF (Scheme 1.56).[190] Herein, they have developed two different conditions for the arylation of azoles using $Ni(OAc)_2$/Phen catalyst system: i) LiO^tBu/dioxane works very well for the robust substrate, ii) $Mg(O^tBu)_2$/DMF works for substrates which contain base, sensitive groups, like nitro and ester.

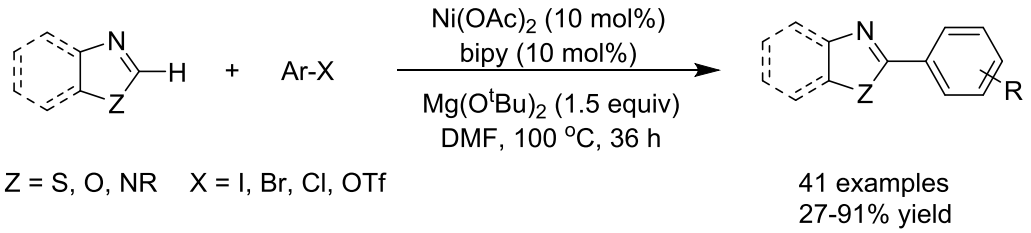

Scheme 1.56 Nickel-catalyzed arylation of azoles using $Mg(O^tBu)_2$ in DMF

Various catalytic systems were reported for the coupling reaction of (hetero)arenes with aryl halide using nickel as catalyst, but the use of aryl halide is still a drawback.[188-190] The coupling of arenes with phenol derivatives would be more beneficial since the phenol and their derivatives are commercially available and less expensive. In 2012, Itami group demonstrated the first nickel-catalyzed Ar–H/Ar–O coupling reaction (Scheme 1.57).[238] In this, they have achieved the cross coupling of variously substituted 1,3-azole and benzoxazole with phenol derivatives using $Ni(COD)_2$/dcype as catalyst in the presence of Cs_2CO_3. This protocol provides efficient coupling of azoles with various phenol derivatives, such as pivalates, triflates, tosylates, mesylates, carbamates, carbonates, and sulfamates, with the tolerance of functional groups –OMe and –COOMe on azoles.

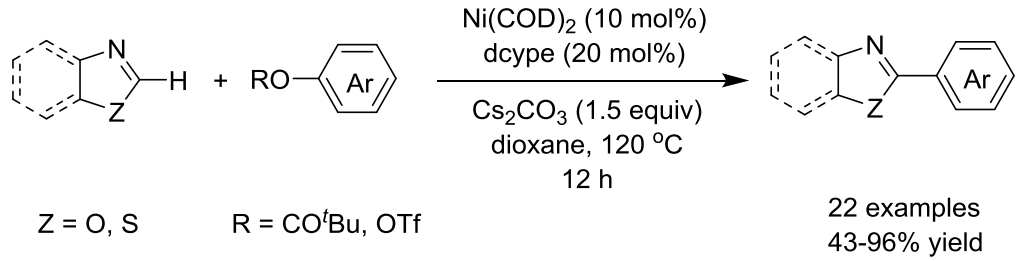

Scheme 1.57 Nickel-catalyzed Ar–H/Ar–O cross-coupling reaction

Similarly, the transition-metal-catalyzed arylation of heteroarenes can be achieved by using aryl silane or aryl boronic acid as coupling partner instead of aryl halide or triflate. In 2010, Miura *et al* described the nickel-catalyzed cross-coupling of azoles with organosilicon as coupling reagent (Scheme 1.58).[239] Herein, the $NiBr_2$·diglyme/bipy catalyst system efficiently coupled the 1,3-azole with trimethoxyarylsilane in the presence of CsF and CuF_2 as additives. Using this strategy the coupling of various 1,3-azoles, such as benzothiazole, benzoxazoles, benzimidazoles, thiazoles, oxazoles with aryl silane was achieved. In 2010, the same group has reported the nickel-catalyzed azole arylation using aryl boronic acid as a coupling partner in the presence of air (Scheme 1.59).[240] Hence, the treatment of 1,3-azole with aryl boronic acid in the presence of $NiBr_2$/bpy catalyst and K_3PO_4 provided the desired coupled product. Guo group reported a novel strategy for the $C(sp^2)$–H bond arylation of purines using nickel catalyst.[241] Herein, the coupling of *N*-containing heterocycle with aryl magnesium bromide was achieved using (dppp)$NiCl_2$ catalyst in DCM/THF at room temperature (Scheme 1.60). This strategy provided excellent tolerance of electron donating group on the Grignard reagent.

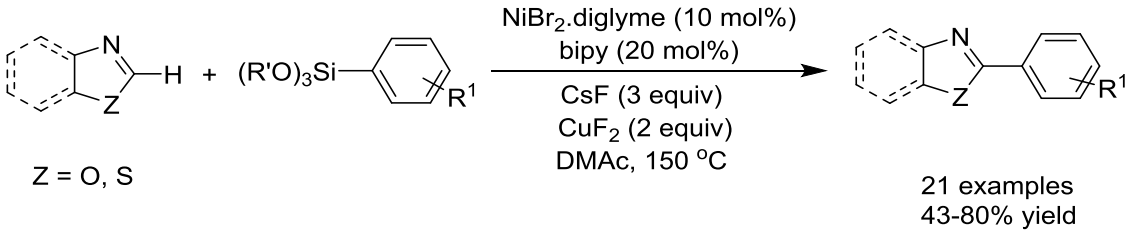

Scheme 1.58 Nickel-catalyzed C–H arylation of heteroarenes with the organosilicon compound

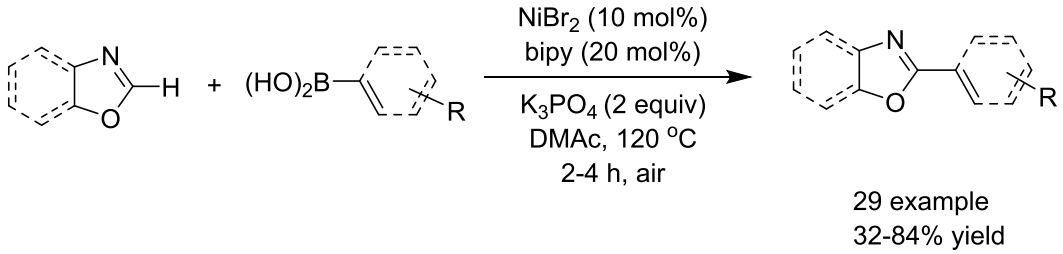

Scheme 1.59 Nickel-catalyzed C–H arylation of heteroarenes with aryl boronic acid

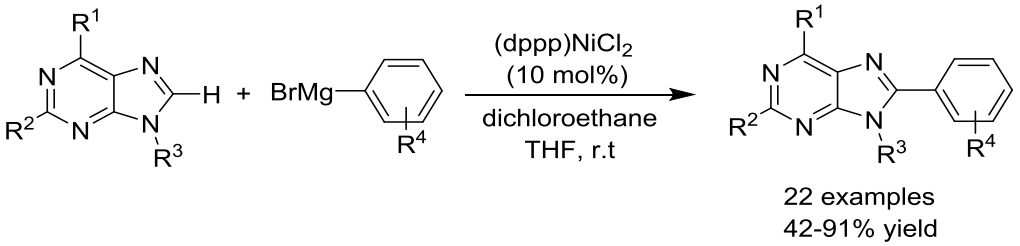

Scheme 1.60 Nickel-catalyzed C(sp^2) –H arylation of purines with aryl magnesium bromide

A wide variety of catalytic systems were developed for the C(sp^2)–H bond arylation of arenes and heteroarenes, but the C(sp^3)–H bond arylation remained challenging. In 2014, Chatani *et al* developed the nickel-catalyzed arylation of unactivated C(sp^3)–H bond in aliphatic amide using bidentate chelation assistance (Scheme 1.61).[237] Herein, the arylation of aliphatic amide containing 8-aminoquinoline as directing group with various aryl iodide was achieved using $Ni(OTf)_2$ as catalyst. This reaction is highly selective for the methyl group arylation, and the methylene and benzene C–H bond remain unreacted.

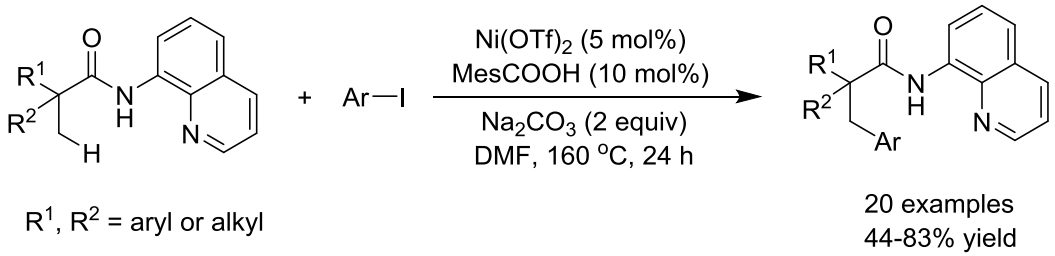

Scheme 1.61 Nickel-catalyzed direct C(sp^3)–H bond arylation of aliphatic amides

Recently, Punji and co-workers developed an efficient solvent-free method for the arylation of arenes and indoles using nickel catalyst through the chelation assistance (Scheme 1.62).[254] In this case, efficient coupling of benzo[*H*]quinoline with aryl halide was achieved using a quinolinyl based pincer nickel complex **1.73** without the use of a solvent. This methodology also works with indole and phenyl pyridine derivatives for the arylation. This method provided a broad substrate scope for the arylation of arenes/heteroarenes and indole with various aryl halides with the tolerance of functional groups. This method is highly selective for monoarylation for phenyl pyridine derivatives.

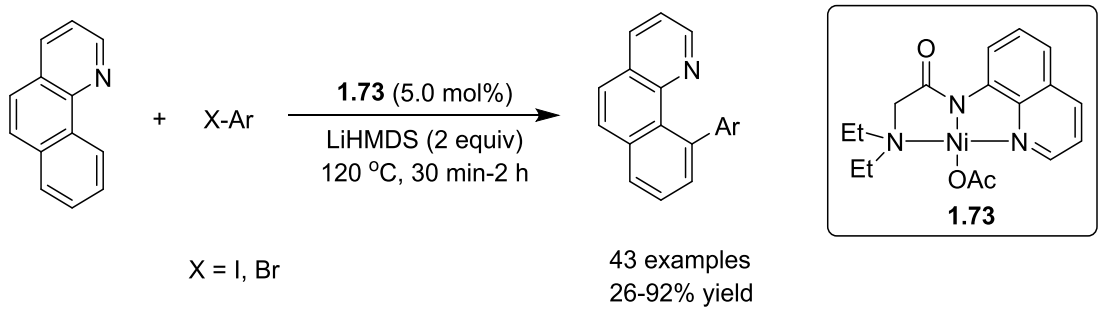

Scheme 1.62 Solvent-free nickel-catalyzed C(sp^2)–H bond arylation of bezo[*H*]quinoline

1.5.1.4 Nickel-catalyzed alkynylation of (hetero)arenes

The alkynylated heteroarenes are the most fundamental and important composition of many natural products, materials, and pharmaceutical compounds.[255,256] Various Ni-catalyst systems were developed for the direct C(sp^2)–H arylation and alkenylation reactions; however, only a few systems were reported for the C(sp^2)–H alkynylation of arenes and heteroarenes using nickel catalyst.[243-246] In 2009, Miura described the nickel-catalyzed direct alkynylation of azole with alkynyl bromide (Scheme 1.63).[242] Efficient coupling of azole with alkynyl bromide was achieved using $Ni(COD)_2$/dppz catalyst and LiO^tBu base in toluene. This methodology works for diverse alkynyl bromides bearing aryl, alkenyl, alkyl and silyl

groups. Similarly, this method was applied for the direct alkynylation of various azoles, such as benzothiazole, benzoxazole, 5-substituted oxazole and benzimidazole and the desired products were obtained with good yield and excellent functional group tolerability.

Miura also reported the nickel-catalyzed direct coupling of azoles and alkynes through double C–H bond activation, which is a highly challenging task due to the difficulties of catalyst control in activation of two different C–H bonds (Scheme 1.64).[243] Herein, various azoles were coupled with alkynes in the presence of $NiBr_2$·diglyme/dtbpy and LiO^tBu under O_2 atmosphere. This method furnishes a new approach for the direct coupling of azoles and alkynes without preactivation of the substrate under the O_2 atmosphere, which is beneficial from the economical prospective.

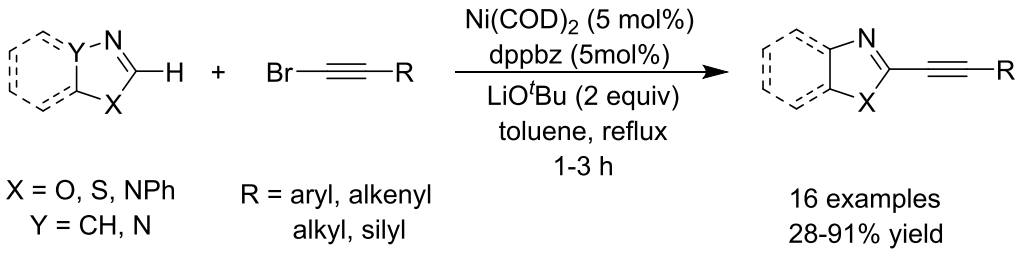

Scheme 1.63 Nickel-catalyzed direct alkynylation of azoles with alkynyl bromide

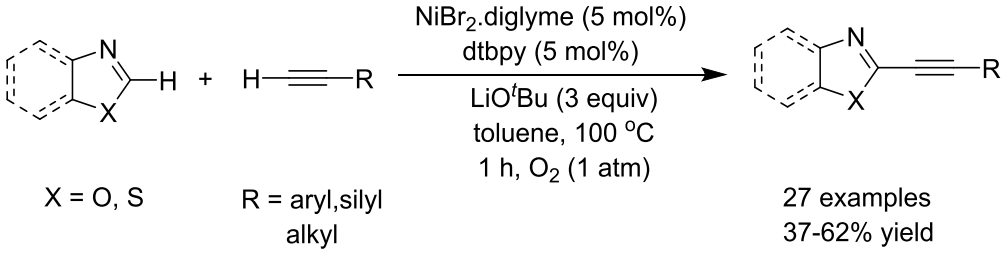

Scheme 1.64 Nickel-catalyzed direct cross coupling of azoles with various alkynes

In 2015, Li described an efficient method for the *ortho*-C(sp^2)–H bond alkynylation of aromatic amides using nickel catalyst *via* the chelation-assistance of 8-aminoquinoline (Scheme 1.65).[244] They found that $NiCl_2$/BDMAE catalyst system efficiently catalyzes the coupling aromatic amide with alkynyl bromide in the presence of Na_2CO_3 at 100 ^oC to provide desired coupled products in good yields. This protocol shows good reactivity for a range of (hetero)aryl amide, and for the *α, β*-unsaturated alkenyl amides.

Recently, Balaraman and co-workers demonstrated the nickel-catalyzed C(sp^2)–H alkynylation of substituted benzamide with alkynyl bromide using 8-aminoquinoline as

directing group (Scheme 1.66).[245] In this methodology, they observed slight variation of substituent on aromatic ring increases the selectivity for mono alkynylation as well as dialkynylation. This methodology provided broad substrate scope and tolerance of sensitive functional group on aromatic amides.

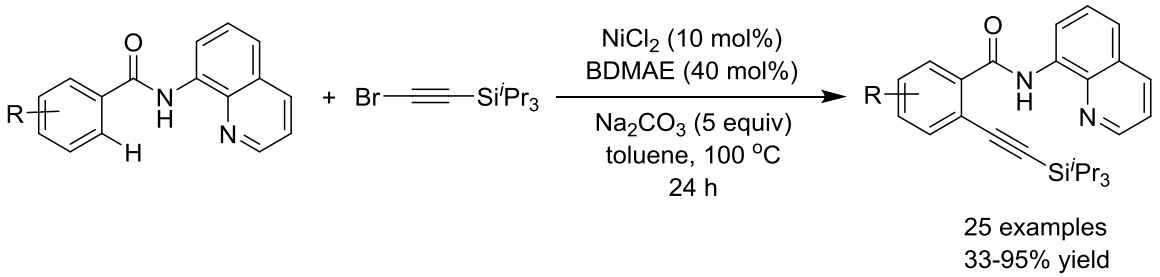

Scheme 1.65 Nickel-catalyzed alkynylation of C(sp^2)–H bond of aryl amide

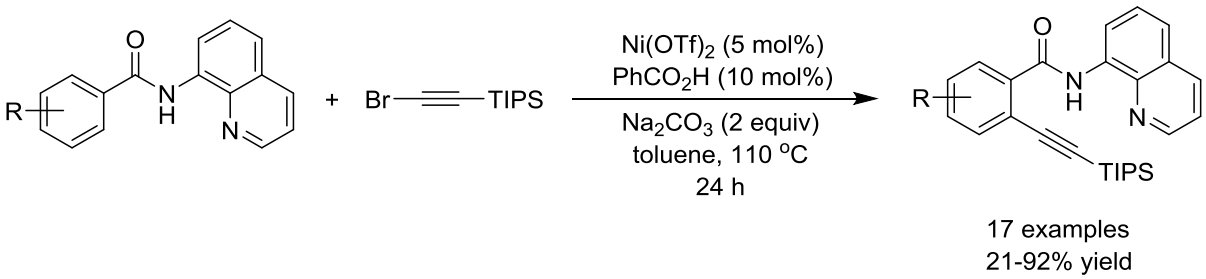

Scheme 1.66 Nickel-catalyzed alkynylation of aryl amide

Recently, Shi and co-worker reported the nickel-catalyzed oxidative cross-coupling of unactivated C(sp^3)–H bond in aliphatic amide with alkynes using 8-aminoquinoline directing group (Scheme 1.67).[246] The oxidative coupling was carried out by the treatment of aliphatic amide with triisopropylsilyl alkyne in the presence of $Ni(acac)_2$/DPPBz catalyst. In this reaction, the $Me_2S{\cdot}CuBr$ was used as a transmetalating reagent and $Cu(OAc)_2$ as the oxidant. This reaction shows good compatibility with differently substituted aliphatic amides. The reaction is stereoselective for the methyl group over the secondary C(sp^3)–H bond and benzyl methylene group.

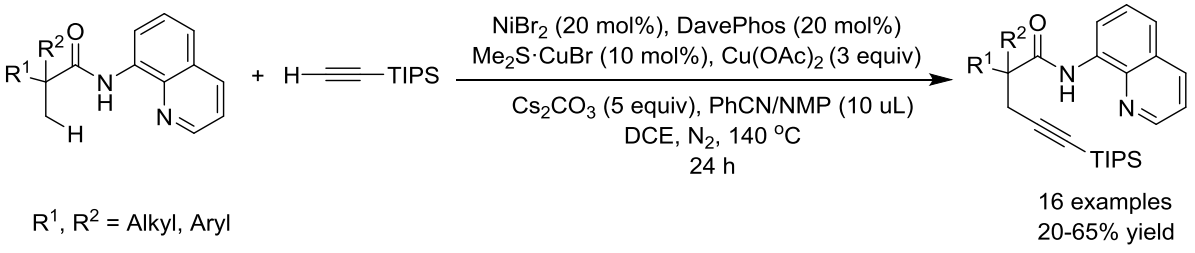

Scheme 1.67 Nickel-catalyzed oxidative cross-coupling of C(sp^3)–H bond of the aliphatic amide with an alkyne

1.5.2 Nickel-catalyzed thiolation of (hetero)arenes

Diaryl sulphide and their derivatives are found in many biologically active compounds, natural products and pharmaceuticals compounds. There are various synthetic routes known to synthesize the diarylsulfide, among them the transition-metal-catalyzed cross-coupling aryl thiols or their metal salts (ArSM) with aryl–X (X = Cl, Br, I, OTf) is one of the most convenient and effective method.[257-259] In 2015, Kambe *et al* reported the sulfenylation of C(sp^2)–H bond of benzamide with nickel catalyst using 8-aminoquinoline moiety as a bidentate directing group.[260] The sulfenylation of benzamide was achieved using $NiCl_2$ as catalyst with diaryl sulfides in the presence of Cs_2CO_3 (Scheme 1.68). This protocol provided broad substrate scope for benzamide derivatives and tolerates functional groups on diarydisulfide electrophiles. Similarly, Shi group developed a new method for the sulfenylation of C(sp^3)–H bond of aliphatic amides *via* bidentate chelation assistance.[261] Herein, the efficient coupling of the aliphatic amide with diaryldisulfide was achieved using $Ni(OTf)_2$ catalyst in DMF (Scheme 1.69). Other metals, such Cu, Fe, Rh, Pd, Co are ineffective to give the desired sulfenylated product under the identical condition. Also, this protocol gives oxidative cross-coupling of C(sp^2)–H bond of benzamides and ArSH in the presence of air. This methodology has broad substrate scope for the aliphatic and aromatic amides and tolerates the important functional groups, such as –OMe, –CF_3, –Cl, –F on amide substrate. Shi and co-worker also reported the sulfenylation of unactivated arenes bearing PIP as the directing group using the nickel catalyst.[262]

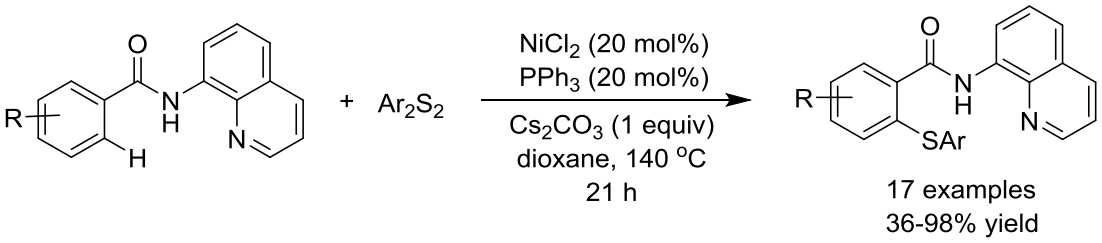

Scheme 1.68 Nickel-catalyzed sulfenylation of C(sp^2)–H bond of the benzamide with diaryldisulfide

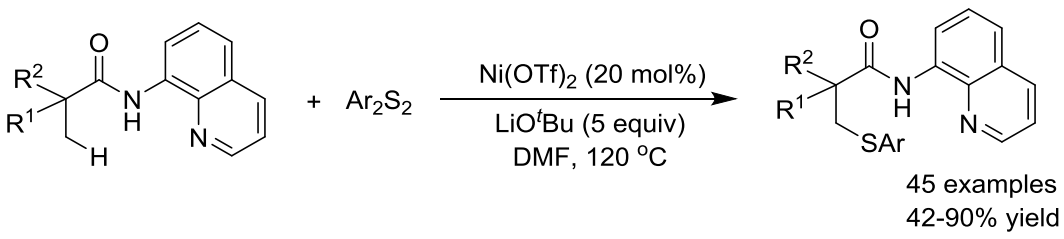

Scheme 1.69 Nickel-catalyzed sulfenylation of C(sp^3)–H bond of the aliphatic amide

1.6 Mechanistic aspect of nickel-catalyzed C–C bond forming reactions through C–H bond activation

Generally, the organonickel species are highly reactive, and hence, they lead to the discovery of new reaction pathways. The homolytic bond cleavage in Ni–C occurs faster than the Pd–C and Pt–C,[263,264] hence, in group 10 metals the contribution of radical processes is favorable in nickel species compared to the Pd and Pt metals. Because of the involvement of one-electron process,[211] the nickel species shows easy access to the different oxidation states, such as Ni(0), Ni(I), Ni(II), Ni(III) and Ni(IV) during the catalytic transformation. These diverse oxidation states discover new reactive pattern beyond the traditional framework of the noble metal. There are many reports on the C–C bond forming reaction using nickel as catalyst. In this section, the mechanistic aspect of nickel-catalyzed C–H functionalization will be briefly discussed.

1.6.1 Mechanistic pathway for nickel-catalyzed alkylation reaction

Miura and co-worker reported the C–H bond alkylation of benzothiazole with alkyl bromide using nickel catalyst; wherein they have carried out preliminary experiments to know the working mode of the catalyst.[224] On the basis of the preliminary experiments and previous report, a catalytic cycle for the arylation of azoles is shown in Scheme 1.70. First, the formation electron-rich heteroaryl nickel [Ni(0)] **1.74** occurs by the combination of $NiBr_2$·diglyme, benzothiazole, and LiO^tBu. The generation of an alkyl radical by the single electron transfer takes place from the species **1.74** to form Ni(I) species **1.74a**. The species **1.74a** on recombination with an alkyl radical forms Ni(II) species **1.74b**, which upon reductive elimination produce the alkylated coupled product with the regeneration of species **1.74**.

Chatani *et al* described the nickel-catalyzed alkylation of $C(sp^3)$–H bond of the aliphatic amide with alkyl halide *via* the bidentate chelation assistance.[228] They have proposed two different pathways for the catalysis: a) Ni(II)/Ni(IV) or b) Ni(II)/Ni(III) (Scheme 1.71). The first step involves the coordination of aliphatic amide **1.75** to the Ni(II) species, which undergoes ligand transfer process in the presence of Cs_2CO_3 to form nickel species **1.76**. This species undergoes deprotonation in the presence of Cs_2CO_3 to form nickelacylce intermediate **1.76a**. The oxidative addition of alkyl halide to intermediate **1.76a** form the Ni(IV) species **1.76b**, which upon reductive elimination affords species **1.76c**. The protonation of **1.76c** produces the desired coupled product **1.77** and regenerates the Ni(II) active catalyst. Alternatively, the intermediate **1.76a** could form Ni(III) species **1.76d** upon addition of alkyl

radical, which on reductive elimination forms Ni(I) species **1.76e**. The species **1.76e** on protonation produces coupled product **1.77** and generate Ni(I) species **1.76f**. They have performed deuterium scrambling and kinetic isotope effect experiments, which suggested that the rate determining step is cyclometalation of amide **1.75** with nickel species. The standard catalytic reaction was performed using $Ni(COD)_2$ as catalyst, wherein the low yield of desired product indicated the low probability of Ni(0) active species. Further, radical trapping experiment in the presence of TEMPO resulted in a low yield of the desired product, which indicated that the reaction proceeds through Ni(II)/Ni(III) pathway.

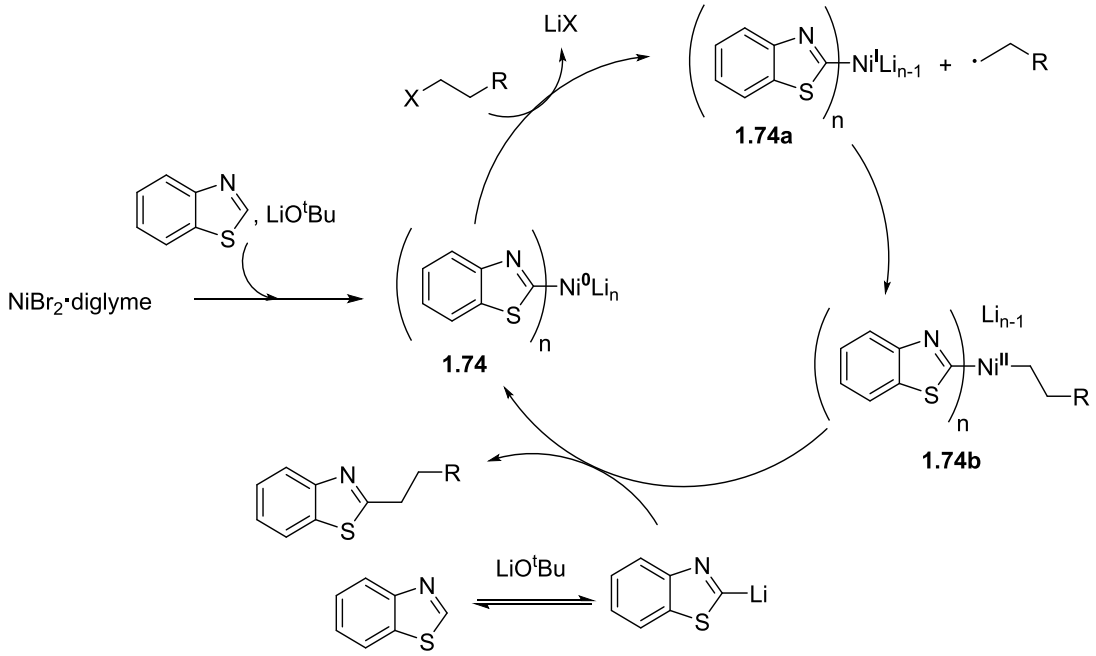

Scheme 1.70 Plausible mechanism for nickel-catalyzed alkylation of azole

1.6.2 Mechanistic pathway for nickel-catalyzed alkenylation reaction

Hiyama group reported the addition of pyridine-*N*-oxide to the alkyne through C–H bond functionalization to produce C(2)-alkenylated product.[234] They have proposed a plausible mechanism which is shown in Scheme 1.72. The first step is considered as the coordination of alkyne to Ni(0) to form species **1.78**, which upon oxidative addition with C(2)–H of pyridine-*N*-oxide form the pyridyl(hydride)nickel species **1.78a**. After hydride addition to alkyne, it provides alkenyl(pyridinyl)nickel intermediate **1.78b**. The reductive elimination of 2-alkenylated pyridine-*N*-oxide from **1.78b** followed by the alkyne coordination generates the nickel (0) species **1.78**. Here, the *N*-oxide moiety plays an important role, which directs the metal catalyst proximal to the C(2)–H bond and makes C–H bond more acidic, and C(2)–H bond easily undergo oxidative addition to Ni(0) species.

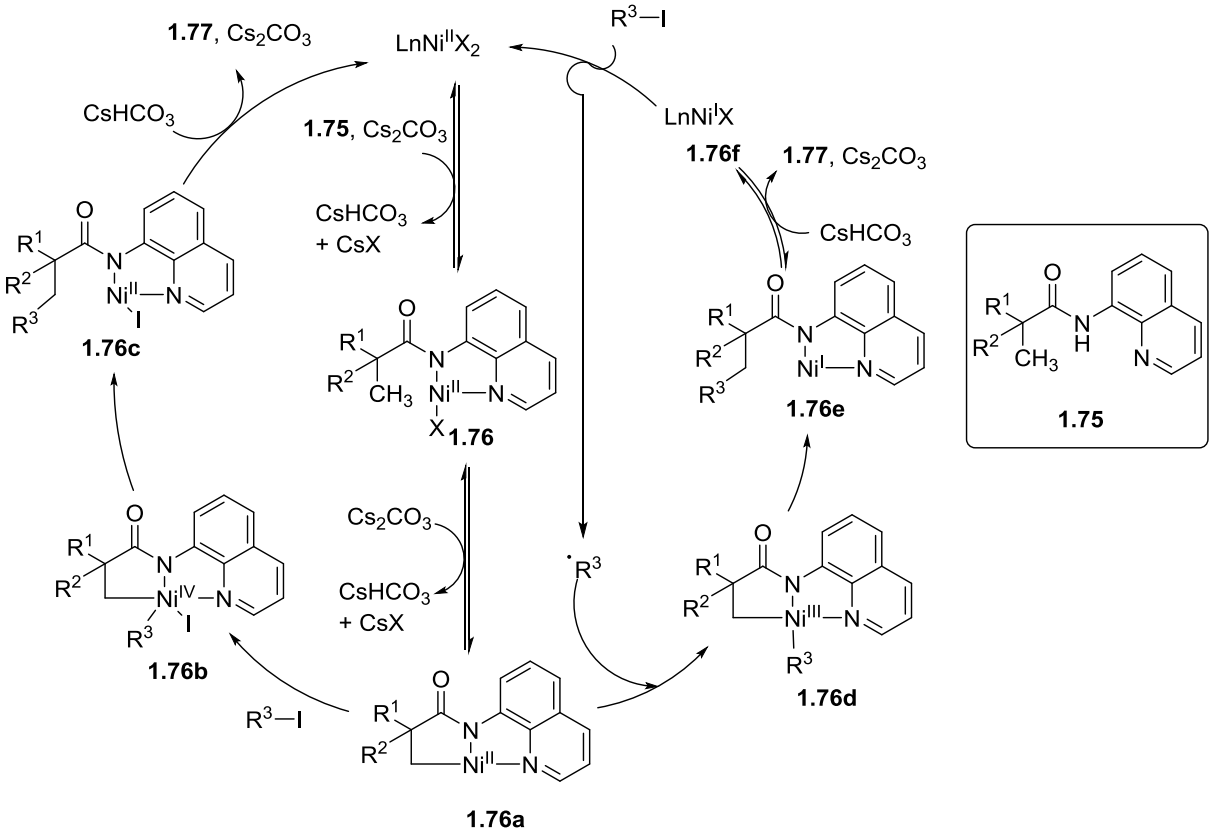

Scheme 1.71 Plausible catalytic cycle for alkylation of C(sp^3)–H bond of the aliphatic amide with an alkyl halide

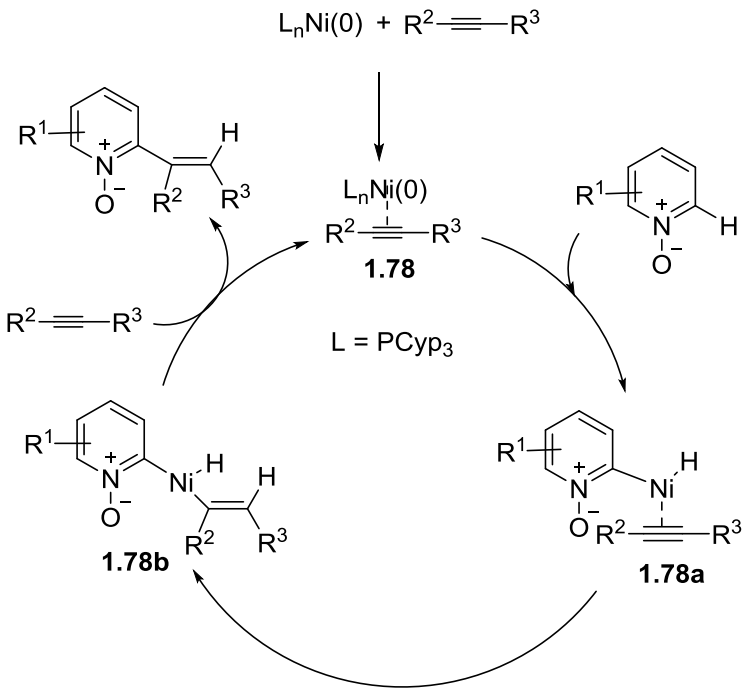

Scheme 1.72 Plausible mechanism for nickel-catalyzed alkenylation of pyridine-*N*-oxide with alkynes

1.6.3 Mechanism of nickel-catalyzed arylation

Miura has proposed a plausible catalytic cycle for the arylation of azoles using nickel catalyst as shown in Scheme 1.73.[189] The first step is considered as the generation of Ni(0) species **1.79** by the reduction of $NiBr_2$ in the presence of benzothiazole/LiO^tBu or Zn in diglyme. The oxidative addition of aryl bromide to Ni(0) produces Ni(II) species **1.79a**. The Ni(II) species on transmetalation with benzothiazole lithium gives the corresponding diaryl nickel species **1.79b**, which upon reductive elimination furnish the arylated benzothiazole and regenerates the active catalyst species **1.79**. In this case, the reaction mixture shows a small amount of homocoupled product of benzothiazole, which indicates the deprotonation of benzothiazole by Ni-catalyzed is less likely. The catalytic cycle follows a Ni(0)/Ni(II) redox pathway for the reaction.

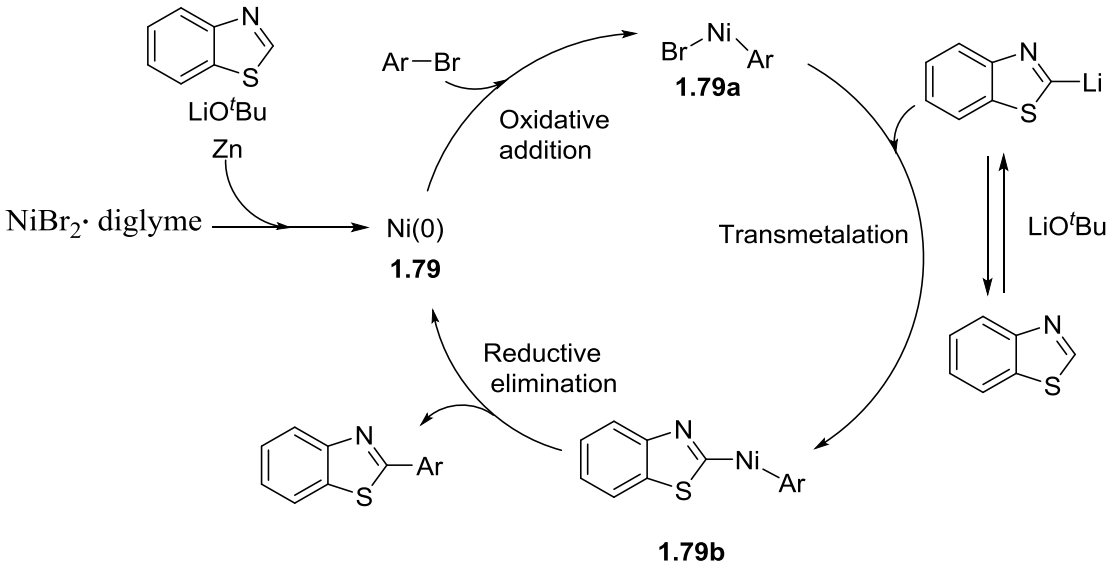

Scheme 1.73 Catalytic cycle for arylation of benzothiazole using nickel catalyst

Chatani *et al* described the arylation of the aliphatic amide with aryl halide using bidentate directing group strategy, wherein they did an extensive mechanistic study for the reaction.[237] The deuterium labelling experiments show that the C–H bond breaking is reversible process during the reaction. The product distribution study was performed to understand the difference between Ni(0) and Ni(II) catalyzed reaction. The experiment suggests that the catalysis involves Ni(II) as active species, and not the Ni(0). On the basis of these experimental studies, they proposed the catalytic cycle which is shown in Scheme 1.74. The catalytic cycle starts with the coordination of amide **1.80** to Ni-centre followed by the ligand exchange in the presence of Na_2CO_3 to produce Ni-species **1.81**, which undergoes

reversible cyclometalation to give nickel species **1.81a** *via* the concerted-metalation-deprotonation pathway. The oxidative addition of iodobenzene to Ni(II) species **1.81a** forms high valent Ni(IV) species **1.81b**, which on reductive elimination afforded species **1.81c**. The species **1.81c** on protonation gives the desired arylated product and regenerates the Ni(II) active species. The catalytic cycle follows the Ni(II)/Ni(IV) pathway.

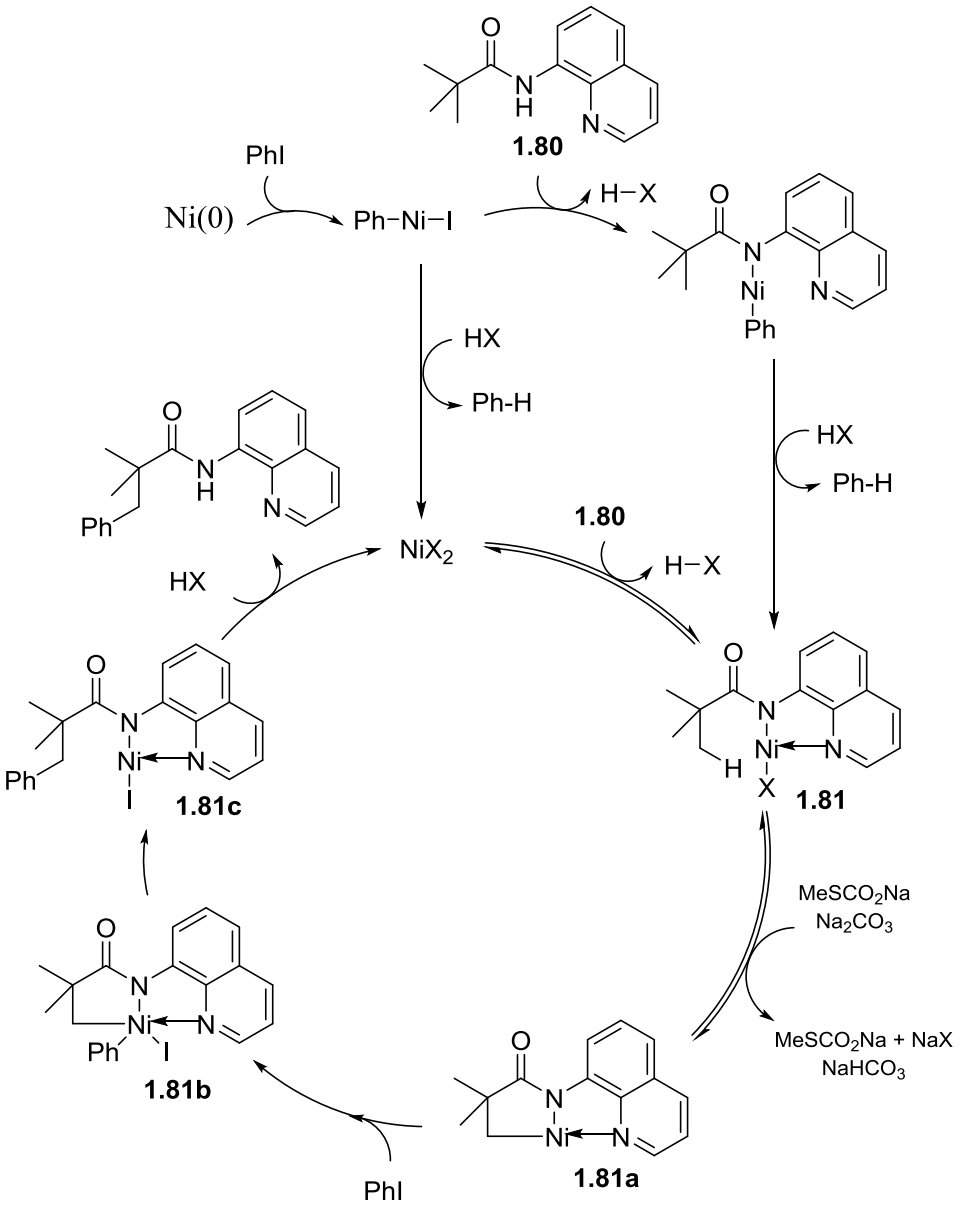

Scheme 1.74 Plausible mechanism for arylation of C(sp^3)–H bond in aliphatic amide using nickel catalyst

1.6.4 Mechanistic pathway for nickel-catalyzed alkynylation reaction

Miura and co-workers demonstrated the direct alkynylation of azoles with alkynyl bromide using nickel as catalyst; wherein the reaction was proposed to proceeds *via* a Ni(0)/Ni(II) redox pathway as shown in Scheme 1.75.[242] The first step is the oxidative addition of alkynyl bromide to Ni(0) species to affords (alkynyl)Ni(II) intermediate **1.82**, followed by the transmetalation with heteroaryl lithium to produce (heteroaryl)(alkynyl)Ni(II) (**1.82a**) species. The (heteroaryl)(alkynyl)Ni(II) species **1.82a** on reductive elimination produces the corresponding alkynylated azoles and regenerates the Ni(0) catalyst.

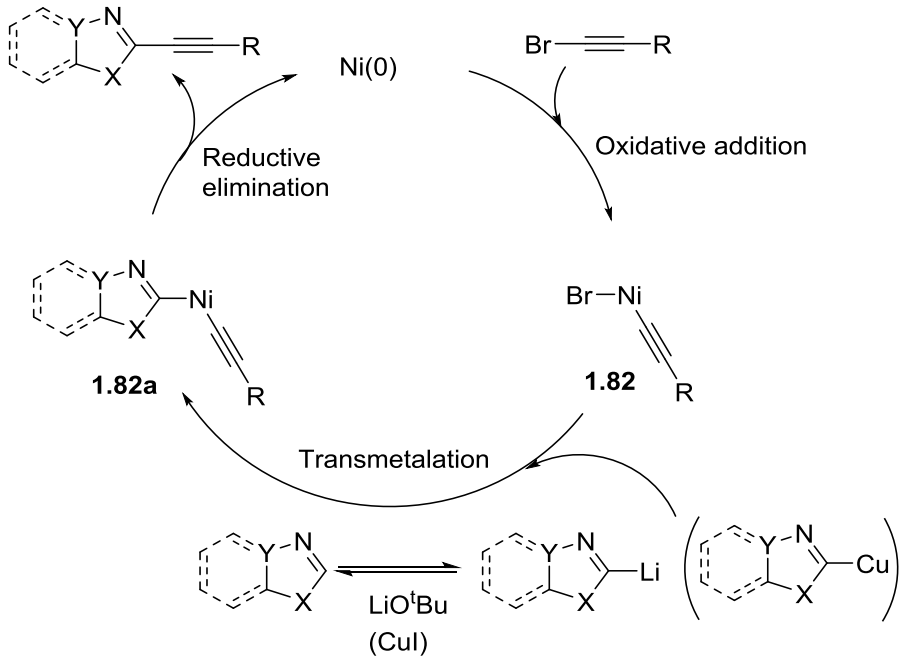

Scheme 1.75 Catalytic cycle for direct alkynylation of azoles using nickel catalyst

Li group developed an efficient nickel system for the alkynylation of C(sp^2)–H of the amide with alkynyl bromide.[244] To understand the mechanism, they have performed kinetic isotope (KIE) experiment, radical trapping experiment and competition experiments with the differently substituted group on amides. The KIE observed was 3.2, which suggests that *ortho* C–H bond cleavage of amide involves in the rate determining step during the reaction. The competition experiment with electron-donating and electron-withdrawing substituents on amide shows that the reaction is faster with the electron-withdrawing group on amide. The KIE and competition experiments suggest that the breaking of *ortho* C–H bond occurs through the concerted metalation-deprotonation pathway.[228,265,266] The radical trapping experiment in the presence of TEMPO does not affect the yield of desired product, which

indicates the single electron transfer pathway for the reaction is unlikely. On the basis of these crucial experiments and previous report, they proposed a plausible catalytic cycle as shown in Scheme 1.76. The reaction starts with the coordination of amide **1.83** to nickel in the presence of Na_2CO_3, followed by the ligand exchange to form species **1.84**. The species **1.84** on deprotonation with base forms metalacycle intermediate **1.84a**. The oxidative addition of alkynyl bromide with **1.84a** affords high valent Ni(IV) species **1.84b**, which upon the reductive elimination gives desired alkynylated product **1.85** and regenerates the Ni(II) catalyst. The catalytic cycle follows a Ni(II)/Ni(IV) redox pathway.

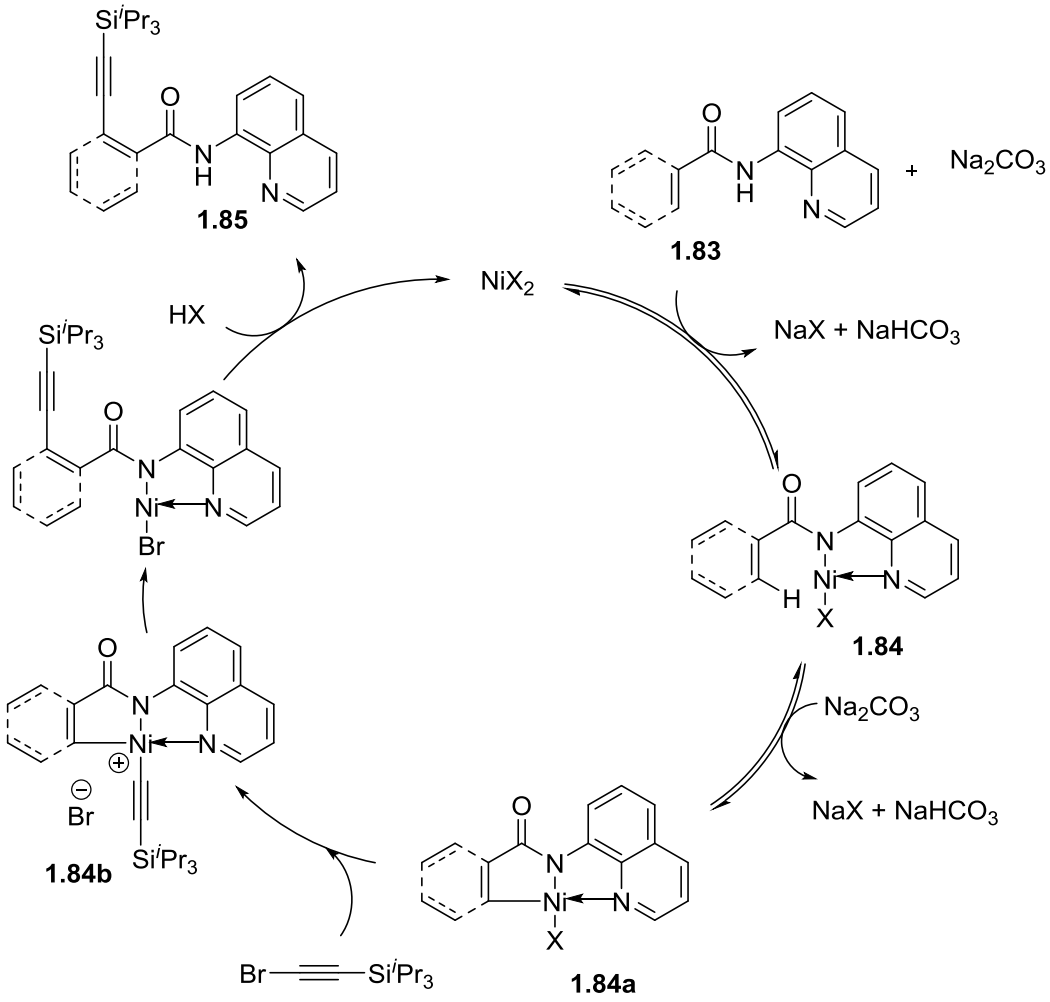

Scheme 1.76 Plausible mechanism for nickel-catalyzed alkynylation of the aromatic amide

Objectives of the present study

Literature survey shows that the pincer palladium catalyzed reactions are more efficient than the non-pincer palladium catalyzed methods. The pincer complexes have the well-defined structure, which enhances the selectivity during the catalysis. During the catalysis, the pincer system keeps the metal and ligand together in each catalytic step, hence the steric and electronic properties of the ligand influences the reactivity of the catalyst for better selectivity. The POCOP, PCP and NCN pincer palladium complexes are well explored because of their easy synthetic pathway. The POCOP pincer palladium complex would favor the cyclometalation/transmetalation during the catalytic reaction, while NCN pincer system makes the metal center electron-rich, and can favor electrophilic addition. As many pincer palladium-catalyzed cross-coupling reactions assumed to follow Pd(II)/Pd(IV)/Pd(II) pathway, the strong σ-donor ligand will favour oxidative addition at Pd(II) center and can stabilize Pd(IV) intermediate during the catalysis. While the electron-deficient pincer palladium complexes might favour the transmetalation during the catalysis. In this regard, the objective of the current study is to synthesize novel and efficient amino-phosphinite (POCN) ligand and their pincer palladium complexes for C–C bond forming reaction through C–H bond activation (Figure 1.9). In the POCN system, the electron-rich amino side would favour the oxidative addition of electrophile while electron-deficient phosphinite might favour the transmetalation during the reaction. Hence, the POCN pincer could be the ideal system for performimg the catalytic C–H functionalization involving the high oxidation state metal species.

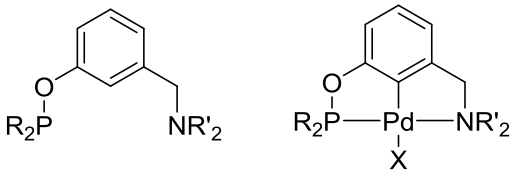

R = ^{i}Pr, ^{t}Bu, Ph; R' = ^{i}Pr, Et

Figuree 1.9 Hybrid POCN ligands and complexes described in the thesis.

The results obtained from the investigation are discussed in Chapters 2, 3 and 4. The second chapter describes the design and syntheses of hybrid phosphinite-amine pincer ligands, 1-(R_2PO)-C_6H_4-3-($CH_2N^iPr_2$) [(^{R2}POCN^{iPr2})–H], their pincer palladium complexes and application of the pincer-palladium complexes for the C–H bond arylation of azoles with aryl halides. The third chapter deals with the synthesis of electronically and sterically distinct

(^{R2}POCN^{Et2})-pincer palladium complexes for the C–H bond arylation of azoles. Chapter 4 describes the detail mechanistic study of (POCN)Pd-catalyzed arylation of azoles.

Similarly, the literature survey shows that the nickel catalyst systems are highly active, and are efficient catalysts for the transformation of unreactive substrates. The nickel catalyst systems have been used for many C–C bond forming reactions, such as alkenylation, alkylation, arylation, and alkynylation. Herein, the objective was to develop a new nickel catalyst system for alkynylation of indole with alkynyl bromide using monodentate chelation assistance. The results obtained from the investigation are discussed in Chapter 5. Chapter 5 describes the optimization of reaction condition for the alkynylation of indole, and the substrate scope for the alkynylation of indole, imidazole, pyrrole, pyrazole, and benzimidazoles with alkynyl bromide. In addition, the synthetic applicatibility of nickel-catalyzed method is demonstrated by synthesizing various important compounds. Chapter 6 describes the detailed mechanistic investigation of the nickel-catalyzed alkynylation of indole with alkynyl bromide. The catalytically pertinent nickel complexes were synthesized and fully characterized. Kinetic analysis of the alkynylation reaction, isotope labelling studies, and controlled reactivity studies were preformed to understand the working mode of the catalyst. Further, the experimental results were supported by the DFT energy calculations.

Chapter 2

Design and development of hybrid POCN-pincer palladium complexes for arylation of azoles

2.1 Introduction

Direct C–H bond functionalization of heteroarenes has raised much interest as an alternative to traditional cross-coupling reactions, because such process bypasses the pre-activation steps, such as halogenation or metalation of heteroarenes.[267,268] The transition metal-catalyzed C–H bond functionalizations, like arylation, alkenylation, alkynylation and alkylation of various heteroarenes have been widely explored since last few years.[269-275] In particular, the arylation of azoles has received much more attention, because arylated azoles are essential backbone of diverse biological and pharmaceutical compounds.[160-163] The C-2 arylation of azoles has been achieved by the employment of various transition metal salts with suitable ligand system.[276] The use of most abundant and less expensive transition metal catalysts, such as Ni[188-190,239,240,277] and Cu[164,278,279] represent very important development for the azole arylation in terms of catalyst cost for large scale synthesis. However, most of the cases involve the use of strong base and harsh reaction condition, which limits further development of these methodologies. The azole arylations have also been reported under mild conditions employing precious metal catalysts, such as Ru,[191] Rh[192,194,196] and Pd[171-282] wherein high loading of catalysts (> 5 mol %) are essential for the completion of reactions. Moreover, many of these catalysts were generated in-situ (not "well-defined") with few exception;[180] hence difficult to understand the catalyst reactivity and reaction system. Although many of these in-situ catalysts perform conveniently for arylation of various azoles, still there is a demand to develop a well-defined catalyst which can execute the same with minimal catalyst loading. Herein, the objective is to develop well-defined and competent palladium catalysts for the direct C–H bond arylation of azoles, as in many cases such complexes are more efficient than the transformations carried out by metal salts and added ligands.[23]

As discussed in Chapter 1, the pincer-ligated transition metal catalysts have shown exceptionally high thermal stability and catalytic activity for various organic transformations than the traditional mono- or bi-dentate ligated transition metal catalysts.[32,283,284] Further, some cases pincer palladium catalysts follow a probable Pd(II)-Pd(IV)-Pd(II) catalytic pathway during cross-coupling reaction,[6,51,157] hence, a pincer-ligated palladium complex having strong electron donor atom on ligand would enhance electrophilic oxidative addition at Pd(II) center and will stabilize Pd(IV) species.[285] Further, the transmetallation and electrophilic oxidative addition have opposite electron demand during such catalysis. Hence, it is anticipated that an amino-phosphinite ligand, where electron-rich hard donor amino-side

and phosphinite segment would assist electrophilic addition and transmetallation, respectively; could be an ideal system to stabilize the catalytically active palladium species in higher oxidation state, which can lead to high conversion rate with low catalyst loading. With this hypothesis, this chapter describes the design and synthesis of amino-phosphinite ligands, and their pincer palladium complexes (Figure 2.1).[286] Also, these synthesized "hybrid" pincer palladium catalyst systems were utilized for the C–H bond arylation of various azoles with aryl iodides under low catalyst loading in the presence of CuI co-catalyst.

(^{R2}POCN$^{R'2}$)-H (^{R2}POCN$^{R'2}$)PdX

R = ^{i}Pr, ^{t}Bu; R' = ^{i}Pr

Figure 2.1 Hybrid POCN pincer ligand and POCN pincer palladium complexes

2.2 Results and discussion

2.2.1 Synthesis of {1-(R_2PO)-C_6H_4-3-($CH_2N^iPr_2$)} (^{R2}POCN^{iPr2})–H ligands

The {1-(R_2PO)-C_6H_4-3-($CH_2N^iPr_2$)} (^{R2}POCN^{iPr2})–H ligands were synthesized in two steps starting from 3-hydroxy benzyl bromide (Scheme 2.1). First, 3-hydroxy benzyl bromide was treated with two equivalent of di-isopropyl amine in acetone to obtain a colorless product of 3-((diisopropylamino)methyl) phenol **1** in 82% isolated yield. The compound **1** was characterized by ^{1}H and ^{13}C NMR as well as by the HRMS. The treatment of 3-((diisopropylamino)methyl)phenol **1** with NaH, followed by the reaction with dialkyl chlorophosphine, R_2PCl (R = ^{i}Pr, ^{t}Bu) provides the ligands, {1-(R_2PO)-C_6H_4-3-($CH_2N^iPr_2$)} (^{R2}POCN^{iPr2})–H (R = ^{i}Pr, **2**; R = ^{t}Bu, **3**) as colorless viscous liquids in excellent yields. The (^{R2}POCN^{iPr2})–H (R = ^{i}Pr, **2**; R = ^{t}Bu, **3**) ligands were characterized by ^{1}H, ^{13}C, and ^{31}P NMR spectroscopy. The ^{31}P NMR spectrum of **2** displays a single resonance at 148.8 ppm (for O–P^{i}Pr$_2$ moiety), whereas that of **3** shows a single resonance at 154.3 ppm (for O–P^{t}Bu$_2$ moiety). These ^{31}P NMR values are consistent with the similar compounds reported *i.e.* (^{iPr2}POCOP^{iPr2})–H[7] (cf. δ 149.0 ppm) and (^{tBu2}POCOP^{tBu2})–H[14] (cf. δ 153.1 ppm), respectively. The crude viscous liquid compounds **2** and **3** were used for the metalation reactions without further purification.

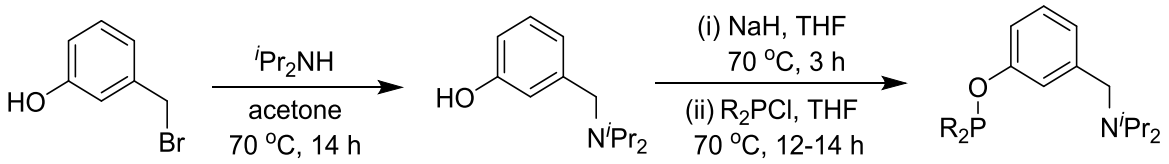

1 (R = ^{i}Pr; **2**; R = ^{t}Bu; **3**)

Scheme 2.1 Synthesis of (^{R2}POCN^{iPr2})–H ligands

2.2.2 Synthesis of (^{R2}POCN^{iPr2}) palladium complexes

The complexation of ligand (^{iPr2}POCN^{iPr2})–H (**2**) with Pd(COD)Cl$_2$ in the presence of K$_3$PO$_4$ in 1,4-dioxane under reflux condition gave {2-(^{i}Pr$_2$PO)-C$_6$H$_3$-6-(CH$_2$N^{i}Pr$_2$)}PdCl, (^{iPr2}POCN^{iPr2})PdCl (**4**) as an air-stable light yellow solid (Scheme 2.2). The ^{31}P{^{1}H} NMR spectrum of **4** shows a singlet at δ 198.9 ppm (cf. (^{iPr2}POCOP^{iPr2})PdCl,[6] δ 187.7 ppm). The ^{1}H NMR spectrum of compound **4** shows signal only for three protons in the aromatic region with the disappearance of the signal for apical proton, which clearly indicates the formation of pincer-palladium complex. Similarly, the complexation of (^{tBu2}POCN^{iPr2})–H (**3**) with Pd(COD)Cl$_2$ in the presence of K$_3$PO$_4$ in toluene under reflux condition produce {2-(^{t}Bu$_2$PO)-C$_6$H$_3$-6-(CH$_2$N^{i}Pr$_2$)}PdCl, [(^{tBu2}POCN^{iPr2})PdCl] (**5**) as yellow solid in 90% yield (Scheme 2.2). The ^{31}P{^{1}H} NMR spectrum of **5** shows a singlet at δ 204.9 ppm (cf. (^{tBu2}POCOP^{tBu2})PdCl,[287] δ 192.1 ppm). The complexes **4** and **5** were well characterized by ^{1}H and ^{13}C NMR as well as by elemental analyses. Further, the complexes (^{iPr2}POCN^{iPr2})PdCl (**4**) and (^{tBu2}POCN^{iPr2})PdCl (**5**) were characterized by the single crystal XRD technique.

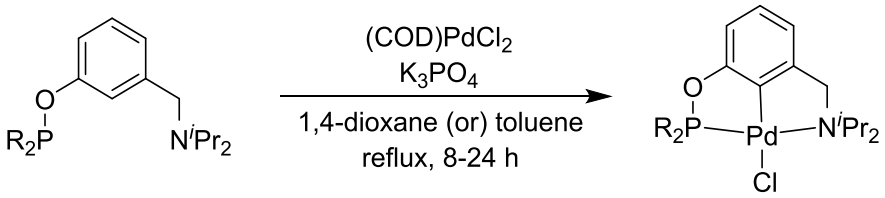

R = ^{i}Pr, **2**; R = ^{t}Bu, **3** R = ^{i}Pr, **4**; R = ^{t}Bu, **5**

Scheme 2.2 Synthesis of (^{R}POCN^{iPr2})PdCl complexes

The derivatives (^{R2}POCN^{iPr2})Pd(X) (X = I, OAc, OTf, SbF$_6$) were synthesized from the reaction of the corresponding (^{R2}POCN^{iPr2})PdCl complexes with a metal salt. Treatment of (^{iPr2}POCN^{iPr2})PdCl (**4**) with KI in dichloromethane and methanol solvent mixture in J-Young NMR tube at 40 °C afforded the complex (^{iPr2}POCN^{iPr2})PdI (**6**) (Scheme 2.3). The ^{31}P NMR spectrum of **6** shows a single resonance at 203.9 ppm. The reactions of (^{iPr2}POCN^{iPr2})PdCl

with AgOAc, AgOTf, and $AgSbF_6$ in THF at room temperature gave (^{iPr2}POCN^{iPr2})PdOAc (**7**), (^{iPr2}POCN^{iPr2})Pd(CH_3CN)OTf (**8**) and (^{iPr2}POCN^{iPr2})Pd(CH_3CN)SbF_6 (**9**), respectively (Scheme 2.4). The complexes **7**, **8** and **9** show ^{31}P NMR signals at 196.7, 199.1 and 199.1 ppm, respectively. Further, the complexes **7**, **8** and **9** were characterized by ^{1}H and ^{13}C NMR spectroscopy as well as by HRMS technique. Similarly, the complexes (^{tBu2}POCN^{iPr2})PdOAc (**10**) and (^{tBu2}POCN^{iPr2})Pd(CH_3CN)SbF_6 (**11**) were synthesized by the reactions of (^{tBu2}POCN^{iPr2})PdCl (**5**) with AgOAc and $AgSbF_6$, respectively in THF. The complexes **10** and **11** show ^{31}P NMR signal at 200.8 and 205.7 ppm, respectively. Also, the complexes **10** and **11** were characterized by ^{1}H and ^{13}C NMR spectroscopy. ^{1}H and ^{13}C NMR spectra of complexes **8**, **9** and **11** show that the solvent acetonitrile is coordinated to palladium.

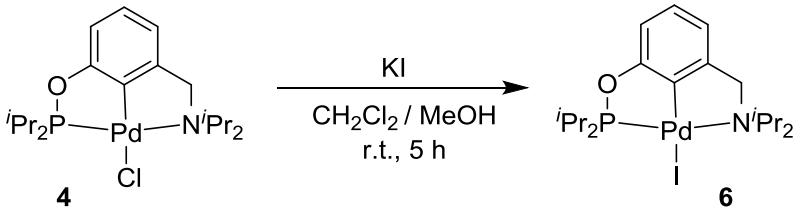

Scheme 2.3 Synthesis of (^{iPr2}POCN^{iPr2})PdI complex

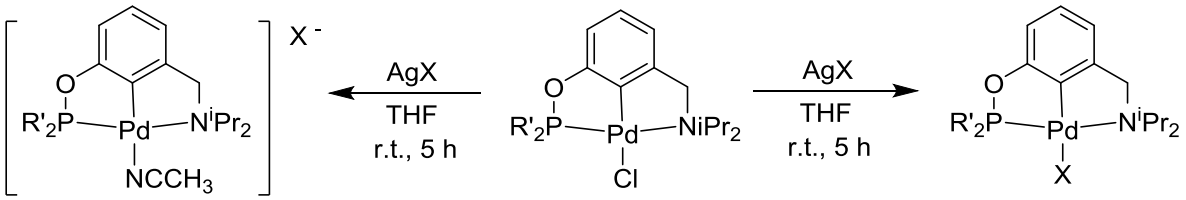

R' = ^{i}Pr, X = OTf; **8**
R' = ^{i}Pr, X = SbF_6; **9**
R' = ^{t}Bu, X = SbF_6; **11**

4; R' = ^{i}Pr
5; R' = ^{t}Bu

R' = ^{i}Pr, X = OAc; **7**
R' = ^{t}Bu, X = OAc; **10**

Scheme 2.4 Synthesis of ($^{R'2}$POCN^{iPr2})PdX derivatives

2.2.3 Crystal structure description

The single X-ray crystal structure of complexes **4** and **5** are shown in Figures 2.2 and 2.3. Selected bond lengths and bond angles are listed in Table 2.1. The coordination geometry around the palladium is distorted square-planar in (^{iPr2}POCN^{iPr2})PdCl (**4**) complex (Figure 2.2). In the structure **4**, the Pd–C(*ipso*) bond length is 1.956(2) Å, slightly shorter than the Pd–C bond length 1.974(±1) Å of (^{iPr2}POCOP^{iPr2})PdCl; whereas the Pd–Cl bond length (2.3922(6) Å) is slightly longer than the corresponding bond length (2.371(2) Å) of (^{iPr2}POCOP^{iPr2})PdCl.[6] This could be due to the strong σ-donor strength of (^{iPr2}POCN^{iPr2})

moiety exerted towards palladium in **4** than the (^{iPr2}POCOP^{iPr2}) moiety towards (^{iPr2}POCOP^{iPr2})PdCl complex. Interestingly, the Pd–P bond length 2.1890(6) Å in **4** is significantly shorter than the corresponding Pd–P bond lengths (2.276(±2), 2.284(±2) Å) reported for (^{iPr2}POCOP^{iPr2})PdCl. The Pd–N bond length 2.2204(17) Å in **4** is slightly longer than the Pd–N bond length (2.159(±2) Å) observed for a similar palladium complex, (3-MeO-^{Ph2}POCN^{Me2})PdCl.[14] The P–Pd–N bond angle 162.10(5)° of **4** is slightly greater than that observed for (3-MeO-^{Ph2}POCN^{Me2})PdCl (P–Pd–N, 159.53(5)°). The C–Pd–P bond angle 80.35(7)° of **4** is comparable with that observed for (^{iPr2}POCOP^{iPr2})PdCl (C–Pd–P; 80.500(±2) and 79.920(±2)°). The C–Pd–N bond angle (81.84(8)°) is slightly greater than the C–Pd–P bond angle (80.35(7)°) for **4**.

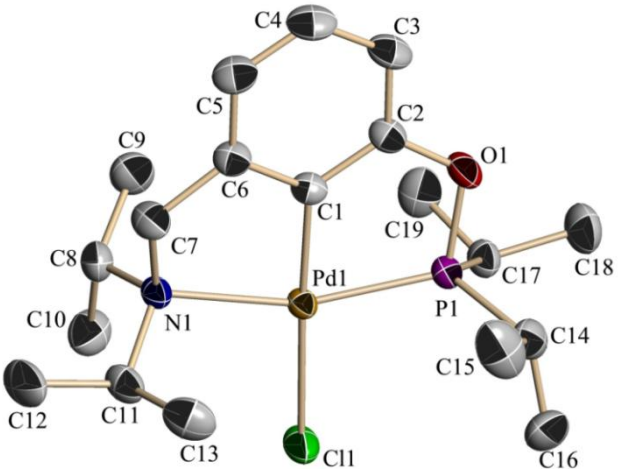

Figure 2.2 Thermal ellipsoid of (^{iPr2}POCN^{iPr2})PdCl (**4**). All the hydrogen atoms are omitted for clarity.

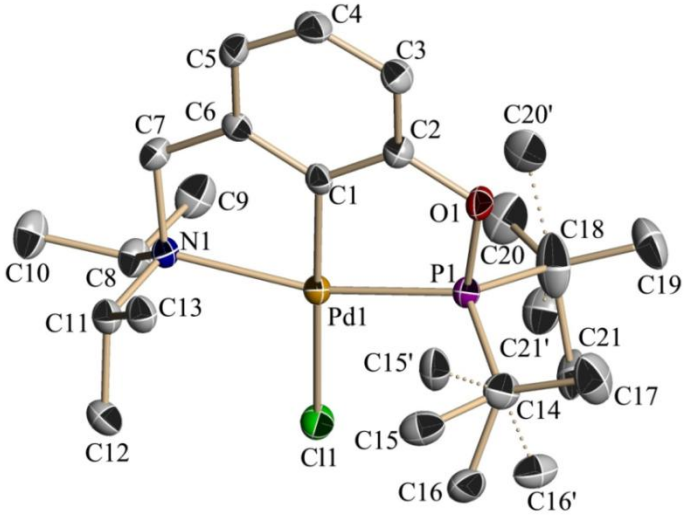

Figure 2.3 Thermal ellipsoid of (^{tBu2}POCN^{iPr2})PdCl (**5**). All the hydrogen atoms are omitted for clarity.

Similarly, in the case of (^{tBu2}POCN^{iPr2})PdCl (**5**), the coordination geometry around palladium is distorted square-planar (Figure 2.3). Two methyl groups (C15, C16, and C20, C21) of each *tert*-butyl groups showed large anisotropic displacement parameters (ADP) due to orientational disorder. The Pd–C(*ipso*) and Pd–Cl bond lengths in **5** are 1.958(4) and 2.3943(11) Å, respectively; comparable with the corresponding bond lengths of **4**. The Pd–P bond length 2.2090(11) Å in **5** is slightly longer than the Pd–P bond length of **4**, whereas the Pd–N bond length 2.229(3) Å in **5** is comparable with that observed for **4**. The P–Pd–N (161.65(9)°), C–Pd–P (80.56(12)°) and C–Pd–N (81.35(15)°) bond angles of **5** are comparable with corresponding bond angles in **4**.

Table 2.1 Selected bond lengths (Å) and bond angles (^{o}) for **4** and **5**

Bond length (Å)		**Bond angles (^{o})**	
Complex 4			
Pd(1)–C(1)	1.9560(2)	C(1)–Pd(1)–P(1)	80.35(7)
Pd(1)–P(1)	2.1890(6)	C(1)–Pd(1)–N(1)	81.84(8)
Pd(1)–N(1)	2.2204(17)	P(1)–Pd(1)–N(1)	162.10(5)
Pd(1)–Cl(1)	2.3922(6)	C(1)–Pd(1)–Cl(1)	177.32(7)
		P(1)–Pd(1)–Cl(1)	97.04(2)
		N(1)–Pd(1)–Cl(1)	100.79(5)
Complex 5			
Pd(1)–C(1)	1.9580(4)	C(1)–Pd(1)–P(1)	80.56(12)
Pd(1)–P(1)	2.2090(11)	C(1)–Pd(1)–N(1)	81.35(15)
Pd(1)–N(1)	2.2290(3)	P(1)–Pd(1)–N(1)	161.65(9)
Pd(1)–Cl(1)	2.3943(11)	C(1)–Pd(1)–Cl(1)	177.93(13)
		P(1)–Pd(1)–Cl(1)	99.18(4)
		N(1)–Pd(1)–Cl(1)	99.00(9)

2.2.4 Catalytic activity of (^{R2}POCN^{iPr2})PdCl for C–H bond arylation of azoles

2.2.4.1 Optimization of catalytic condition

The newly synthesized hybrid pincer palladium complexes, (^{iPr2}POCN^{iPr2})PdCl (**4**) and (^{tBu2}POCN^{iPr2})PdCl (**5**) are optimized and employed for the direct C–H bond arylation of azoles with aryl iodides. Optimization started with the use of benzothiazole **12a**, and 4-iodotoluene **13a** as a standard coupling partner. Initially, the complex **4** was screened for C–H bond arylation of benzothiazole (**12a**) with 4-iodotoluene (**13a**) as an electrophile, employing CuI as co-catalyst. After investigating various experimental parameters, it was found that the

coupled product 2-(*p*-tolyl)benzothiazole (**14aa**) could be obtained in 97% isolated yield employing 0.5 mol% of catalyst **4** and 5.0 mol% of CuI, in the presence of Cs_2CO_3 as a base in DMF (Table 2.2). Other carbonate bases, such as K_2CO_3, Na_2CO_3 as well as cesium source like CsOAc are found to be less effective to give the coupled product **14aa** (5 - 34%). The use of K_3PO_4 base also gives good yield (88%). The polar aprotic solvent DMF is found to be the solvent of choice, whereas solvents like 1,4-dioxane, toluene are reluctant to give coupled product. The presence of CuI as co-catalyst is very much essential to obtain good conversion rate. Direct arylation proceeded even in absence of CuI co-catalyst, however with a low yield of coupled product (21% of **14aa**). The CuI is most likely enhances the transmetallation of azoles to the palladium center.[180] The presence of palladium catalyst **4** under the standard condition (**12a**, 0.50 mmol; **13a**, 0.75 mmol; Cs_2CO_3, 0.75 mmol; CuI, 5 mol% in DMF at 120 ^oC) was necessary; in it's absence the arylation product **14aa** formed in < 2% ^1H NMR yield, which is non-catalytic with CuI. The reaction also proceeded with low catalyst loading (0.1 mol%) giving product **14aa** with a TON's of 650 after 48 h. The employment of bulky pincer palladium catalyst, (^{t}Bu2POCN^{i}Pr2)PdCl (**5**) is less efficient to produce the coupled product **14aa** in 47% yield; which could be due to the more steric constraint in the complex.

Table 2.2 Optimization of reaction conditions for arylation of azole

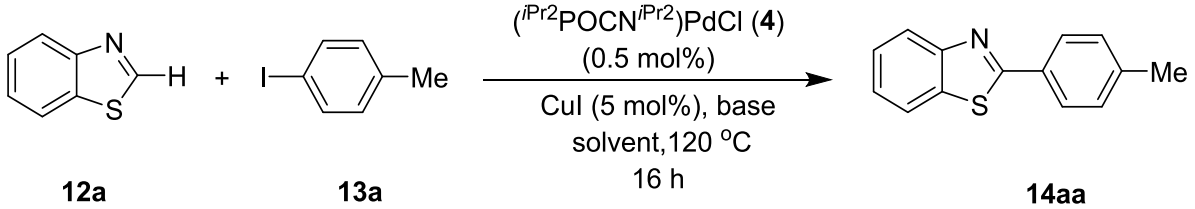

12a **13a** **14aa**

Entry	Base	Solvent	Yield (%)[a]	Entry	Base	Solvent	Yield (%)[a]
1	Na_2CO_3	DMF	< 5[b]	8	Cs_2CO_3	dioxane	14
2	K_2CO_3	DMF	34	9	Cs_2CO_3	toluene	< 5[b]
3	K_3PO_4	DMF	88	10[c]	Cs_2CO_3	DMF	65
4	**Cs_2CO_3**	**DMF**	**97**	11[d]	Cs_2CO_3	DMF	21
5	CsOAc	DMF	11	12[e]	Cs_2CO_3	DMF	–
6	Cs_2CO_3	DMSO	47	13[f]	Cs_2CO_3	DMF	47
7	Cs_2CO_3	DMAc	11				

Conditions: Benzothiazole (0.0675 g, 0.5 mmol), 4-iodotoluene (0.163 g, 0.75 mmol), base (0.75 mmol), solvent (1 mL). [a] Isolated yields, [b] NMR yields, [c] 0.1 mol% of (^{i}Pr2POCN^{i}Pr2)PdCl (**4**) after 48 h, [d] without CuI, [e] without cat (^{i}Pr2POCN^{i}Pr2)PdCl (**4**), [f]employing (^{t}Bu2POCN^{i}Pr2)PdCl (**5**) catalyst.

2.2.4.2 Substrate scope for arylation of azoles

The optimized reaction condition was applied to the C–H bond arylation of benzothiazoles and oxazoles **12** with diversely substituted aryl iodide electrophiles (Scheme 2.5). By employing only 0.5 mol% of catalyst **4** and 5 mol% of CuI, benzothiazole **12a** was very efficiently arylated in DMF at 120 °C. Thus, electron-rich aryl iodides were effectively employed as coupling partner including sterically demanding *ortho*-substituted partner (**13j**). The coupling of electron-deficient aryl iodides with benzothiazole was less effective, giving the products (**14af**, **14ag**) in moderate to low yields. This methodology provides tolerance of functional groups, such as –OMe, –F, –Cl, –Br, $–CF_3$, $–COCH_3$ on aryl iodide. The tolerability of functional groups, like –Cl, –Br in the product (**14ad**, **14ai**) is significant, as they can be used for further functionalization. Also, this methodology provides coupling of heteroarene electrophiles, such as iodopyridine and 2-iodo-pyrazine with benzothiazole to give coupled products **14al** and **14am** with moderate to good conversion rate. On contrary, the aryl bromides or chloride as electrophilic coupling partner did not produce any arylated product. Similar to benzothiazole, substituted-benzoxazoles also reacted smoothly yielding the products **14ba**, **14ca** in good yields.

Furthermore, the catalyst **4** was utilized for arylation of various 5-substituted oxazoles with aryl iodides (Scheme 2.6). It was observed that, azoles containing both electron donating as well as electron withdrawing group (**15a** and **15c**) on aryl backbone smoothly reacted with aryl iodide to provide 2-arylated product in good yield. This methodology provides tolerance of functional groups, like chloro and methoxy, as well as heteroarenes substituents like pyridine, on azole substrates. Interestingly, the electron-deficient aryl iodides that showed moderate performance in coupling with benzothiazole, reacted efficiently with a 5-pyridinyl azole, giving the arylated product **16ef** in good yield.

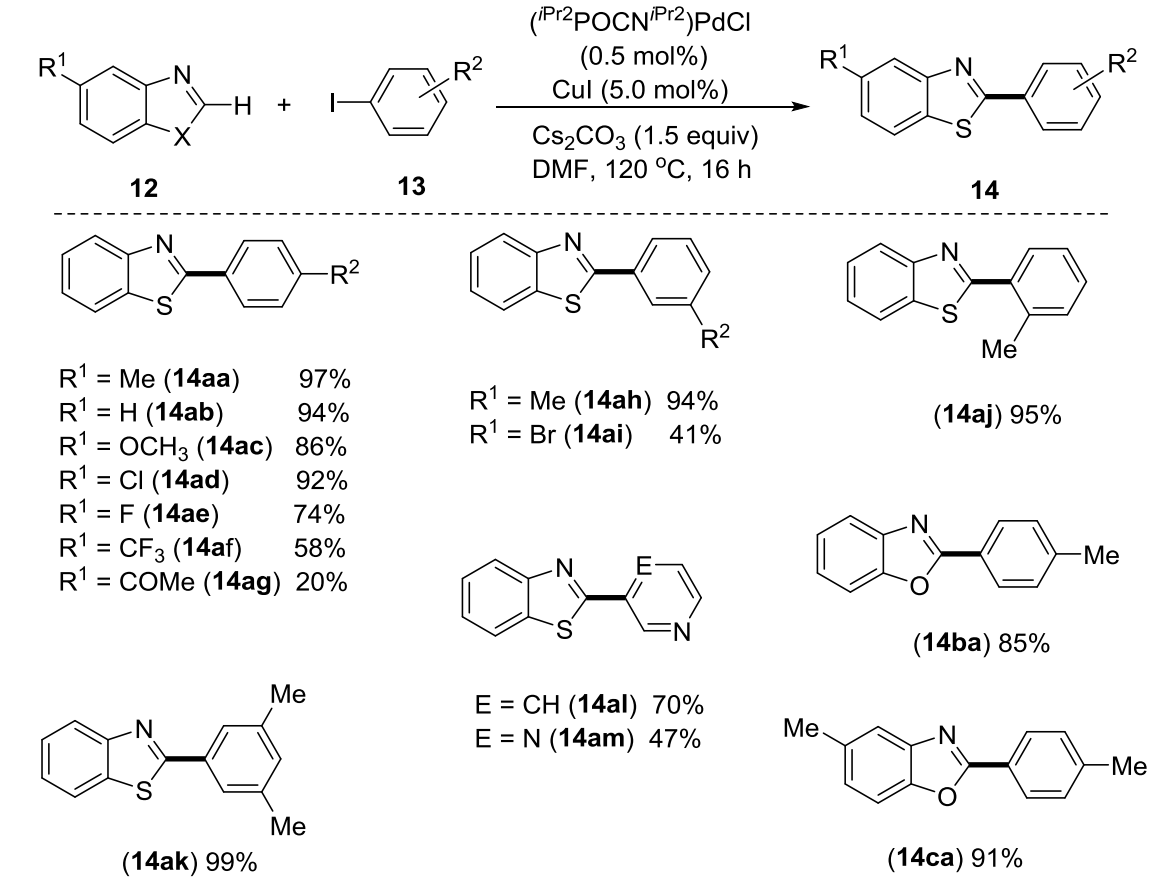

Scheme 2.5 Substrate scope for (^{iPr2}POCN^{iPr2})PdCl catalyzed arylation of azoles

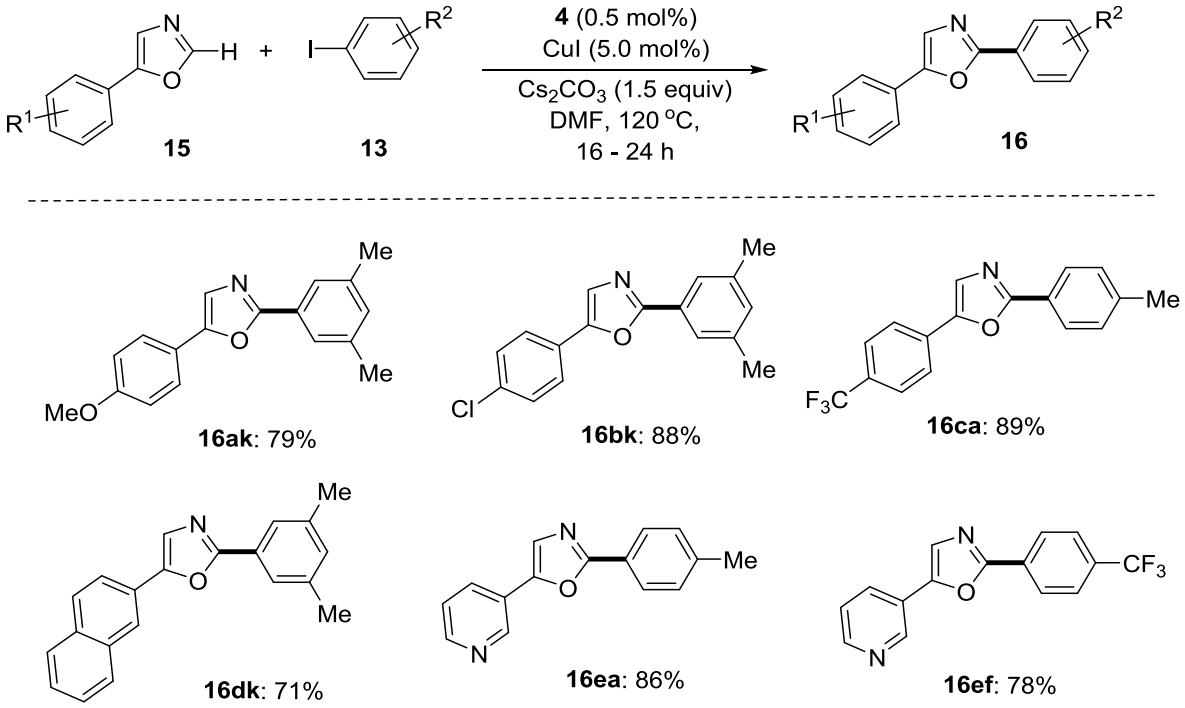

Scheme 2.6 Substrate scope for (^{iPr2}POCN^{iPr2})PdCl catalyzed arylation of 5-substituted azole

2.3 Conclusion

In this chapter, the synthesis and characterization of new unsymmetrical pincer palladium complexes ($^{i\text{Pr2}}$POCN$^{i\text{Pr2}}$)PdCl and ($^{t\text{Bu2}}$POCN$^{i\text{Pr2}}$)PdCl is described. The derivatives of both the complexes, such as ($^{i\text{Pr2}}$POCN$^{i\text{Pr2}}$)PdOAc, ($^{i\text{Pr2}}$POCN$^{i\text{Pr2}}$)Pd(CH_3CN)OTf, ($^{i\text{Pr2}}$POCN$^{i\text{Pr2}}$)Pd(CH_3CN)SbF_6, ($^{t\text{Bu2}}$POCN$^{i\text{Pr2}}$)PdOAc and ($^{t\text{Bu2}}$POCN$^{i\text{Pr2}}$)Pd(CH_3CN)SbF_6 were efficiently synthesized in good to excellent yields. All the complexes were fully characterized by ^{1}H, ^{13}C, ^{31}P NMR and elemental analyses. Further the molecular structure of ($^{i\text{Pr2}}$POCN$^{i\text{Pr2}}$)PdCl and ($^{t\text{Bu2}}$POCN$^{i\text{Pr2}}$)PdCl were established by the X-ray diffraction studies. Complexes ($^{i\text{Pr2}}$POCN$^{i\text{Pr2}}$)PdCl and ($^{t\text{Bu2}}$POCN$^{i\text{Pr2}}$)PdCl were efficiently demonstrated for the C–H bond arylation of azoles. This represents the first pincer-palladium complex that has been employed for the C–H bond arylation of azoles. In particular, the sterically less demanding complex ($^{i\text{Pr2}}$POCN$^{i\text{Pr2}}$)PdCl catalyzes the coupling of a variety of activated, unactivated and functionalized azoles with diverse aryl iodides with very low catalyst loading. Various functional groups, such as –F, –Cl, –Br, –OMe, –$COCH_3$ were tolerated on the aryl backbone to give the coupled products in moderate to excellent yields. Notably, the electron-rich aryl iodide electrophiles perform better than the electron-poor counter parts, these results are complementary to the traditional Pd(0)-catalyzed reactions.

2.4 Experimental section

General experimental

All manipulations were conducted under an argon atmosphere either in a glove box or using standard Schlenk techniques in pre-dried glass wares. The catalytic reactions were performed in flame-dried reaction vessels with teflon screw cap. Solvents were dried over Na/benzophenone or CaH_2 and distilled prier to use. DMF was dried over CaH_2, distilled under vacuum and stored over 4 Å molecular sieves. Liquid reagents were flushed with argon prior to use. 3-hydroxy benzyl bromide,[288] 5-methyl benzoxazole,[289] and 5-aryl azoles[290] were synthesized according to previously described procedures. All other chemicals were obtained from commercial sources and were used without further purification. Yields refer to isolated compounds, estimated to be > 95% pure as determined by ^{1}H-NMR. TLC: TLC Silica gel 60 F_{254}. Detection under UV light at 254 nm. Chromatography: Separations were carried out on Spectrochem Silica gel (0.120-0.250 mm, 60-120 mesh). All IR spectra were recorded on a Perkin-Elmer 1615 FT Infrared Spectrophotometer Model 60B. High-resolution mass spectroscopy (HRMS) mass spectra were recorded on a Thermo Scientific Q-Exactive,

Accela 1250 pump. M. p.: Büchi 540 capillary melting point apparatus, values are uncorrected. NMR (^{1}H and ^{13}C) spectra were recorded at 400 or 500 (^{1}H), 100 or 125 {^{13}C, DEPT (Distortionless enhancement of polarization transfer)}, 377 (^{19}F) and 162 or 202 MHz ($^{31}P\{^{1}H\}$), respectively on Bruker AV 400 and AV 500 spectrometers in $CDCl_3$ solutions, if not otherwise specified; chemical shifts (δ) are given in ppm. The ^{1}H and ^{13}C NMR spectra are referenced to residual solvent signals ($CDCl_3$: δ H = 7.26 ppm, δ C = 77.2 ppm) and $^{31}P\{^{1}H\}$ NMR chemical shifts are referenced to an external standard, Me_3P in *p*-xylene-d_{10} solvent (δ –62.4 ppm), in a sealed capillary tube.

GC Method. Gas Chromatography analyses were performed using a Shimadzu GC-2010 gas chromatograph equipped with a Shimadzu AOC-20s autosampler and a Restek RTX-5 capillary column (30 m x 250 μm). The instrument was set to an injection volume of 1 μL, an inlet split ratio of 10:1, and inlet and detector temperatures of 250 and 320 °C, respectively. UHP-grade argon was used as carrier gas with a flow rate of 30 mL/min. The temperature program used for all the analyses is as follows: 80 °C, 1 min; 30 °C/min to 200 °C, 2 min; 30 °C/min to 260 °C, 3 min; 30 °C/min to 300 °C, 3 min.

Response factors for all the necessary compounds with respect to standard mesitylene were calculated from the average of three independent GC runs.

2.4.1 Synthesis of 3-((diisopropylamino)methyl)phenol (**1**)

To a solution of 3-hydroxy benzyl bromide (5.0 g, 26.73 mmol) in acetone (50 mL) was added diisopropylamine (7.6 mL, 53.46 mmol) at room temperature. The resultant reaction mixture was refluxed at 70 ^{o}C for 14 h under argon atmosphere. After cooling the reaction mixture to room temperature, the solvent was evaporated under reduced pressure and crude product obtain was treated with 10% aqueous solution of $NaHCO_3$ (70 mL). The product was extracted with Et_2O (20 mL x 3) and combined extracts were dried over $MgSO_4$. Filtration and evaporation of all the volatile gave colorless viscous product. Yield: 4.52 g 82%. ^{1}H-NMR (200 MHz, $CDCl_3$): δ = 7.14 (vt, *J* = 7.8 Hz, 1H, Ar–H), 6.94-6.90 (m, 2H, Ar–H), 6.68 (dd, *J* = 8.1, 2.2 Hz, 1H, Ar–H), 3.59 (s, 2H, C*H*$_2$), 3.02 (sept, *J* = 6.7 Hz, 2H, N{C*H*$(CH_3)_2\}_2$), 1.02 (d, *J* = 6.7 Hz, 12H, N{CH(C*H*$_3)_2\}_2$). ^{13}C-NMR (50 MHz, $CDCl_3$): δ = 155.8 (C_q), 145.3 (C_q), 129.2 (CH), 120.4 (CH), 115.0 (CH), 113.5 (CH), 49.0 (CH_2), 48.1 (2C, N{*C*H$(CH_3)_2\}_2$), 20.8 (4C, N{CH(*C*H$_3)_2\}_2$). HRMS (ESI): *m/z* calcd for $C_{13}H_{21}NO+H^+$ $[M+H]^+$ 208.1701, found 208.1694.

2.4.2 Synthesis of (^{R2}POCN^{iPr2})–H ligands and characterization data

(^{iPr2}POCN^{iPr2})–H (2): To the suspension of NaH (0.56 g, 23.3 mmol) in THF (10 mL) was added a solution of appropriate amount of 3-((diisopropylamino)methyl)phenol (4.0 g, 19.3 mmol) in THF (20 mL) and the resulting mixture was refluxed at 70 ^{o}C for 3 h. After 3h, the reaction mixture was cooled to room temperature, a solution of chlorodiisopropylphosphine, $^{i}Pr_2PCl$ (3.2 mL, 20.1 mmol) in THF (20 mL) was added and resulting reaction mixture was further refluxed at 70 ^{o}C for 12 h. The reaction mixture was cooled to ambient temperature and volatile were evaporated under reduced pressure. The compound was extracted with *n*-hexane (60 mL x 3) and combined *n*-hexane solutions were evaporated under vacuum to obtain an oily product of (^{iPr2}POCN^{iPr2})–H (**2**). Yield: 5.40 g 87%. ^{1}H-NMR (400 MHz, $CDCl_3$): δ = 7.20-7.16 (m, 2H, Ar–H), 7.01 (d, J = 7.3 Hz, 1H, Ar–H), 6.94 (d, J = 5.8 Hz, 1H, Ar–H), 3.64 (s, 2H, CH_2), 3.04 (sept, J = 6.5 Hz, 2H, N{C*H*$(CH_3)_2$}$_2$), 1.94 (d of sept, J = 6.8, 2.5 Hz, 2H, P{C*H*$(CH_3)_2$}$_2$), 1.21 (dd, J = 10.5, 6.8 Hz, 6H, PCH(C*H*$_3$)$_2$), 1.14 (dd, J = 15.8, 7.3 Hz, 6H, PCH(C*H*$_3$)$_2$), 1.05 (d, J = 6.5 Hz, 12H, N{CH(C*H*$_3$)$_2$}$_2$). ^{13}C-NMR (100 MHz, $CDCl_3$): δ = 159.5 (d, J_{P-C} = 8.4 Hz, C_q), 145.2 (C_q), 128.8 (CH), 121.2 (CH), 118.2 (d, J_{P-C} = 10.3 Hz , CH), 116.6 (d, J_{P-C} = 9.9 Hz , CH), 48.9 (CH_2), 47.9 (2C, N{*C*H$(CH_3)_2$}$_2$), 28.5 (d, J_{P-C} = 17.6 Hz, 2C, P{*C*H$(CH_3)_2$}$_2$), 20.9 (4C, N{CH(*C*H$_3$)$_2$}$_2$), 18.0 (d, J_{P-C} = 20.5 Hz, 2C, PCH(*C*H$_3$)$_2$), 17.2 (d, J_{P-C} = 8.4 Hz, 2C, PCH(*C*H$_3$)$_2$). ^{31}P{^{1}H}-NMR (162 MHz, $CDCl_3$): δ = 148.8 (s).

(^{tBu2}POCN^{iPr2})–H (3): To the suspension of NaH (0.42 g, 17.5 mmol) in THF (10 mL) was added a solution of an appropriate amount of 3-((diisopropylamino)methyl)phenol (3.0 g, 14.5 mmol) in THF (20 mL) and the resulting mixture was refluxed at 70 ^{o}C for 3 h. The reaction mixture was cooled to room temperature and a solution of chlorodi-*tert*-butylphosphine, $^{t}Bu_2PCl$ (2.90 mL, 15.3 mmol) in THF (20 mL) was added, and resulting reaction mixture was further refluxed at 70 ^{o}C for 12 h. The reaction mixture was cooled to ambient temperature and volatiles were evaporated under reduced pressure. The compound was extracted with *n*-hexane (60 mL x 3) and combined *n*-hexane solutions were evaporated under vacuum to obtain an oily product of (^{tBu2}POCN^{iPr2})–H (**3**). Yield: 4.58 g, 90%. ^{1}H-NMR (400 MHz, $CDCl_3$): δ = 7.21 (br s, 1H, Ar–H$_{ipso}$), 7.15 (t, J = 7.8 Hz, 1H, Ar–H), 6.98 (d, J = 7.8 Hz, 2H, Ar–H), 3.62 (s, 2H, CH_2), 3.02 (sept, J = 6.4 Hz, 2H, N{C*H*$(CH_3)_2$}$_2$), 1.17 (d, J = 11.5 Hz, 18H, P{C(C*H*$_3$)$_3$}$_2$), 1.02 (d, J = 6.4 Hz, 12H, N{CH(C*H*$_3$)$_2$}$_2$). ^{13}C-NMR (100 MHz, $CDCl_3$): δ = 160.0 (d, J_{P-C} = 8.6 Hz, C_q), 145.2 (C_q), 128.8 (CH), 120.9 (CH), 118.0 (d, J_{P-C} = 9.6 Hz, CH), 116.4 (d, J = 10.5 Hz, CH), 48.9 (*C*H$_2$), 47.9 (2C,

N{*C*H(CH$_3$)$_2$}$_2$), 35.8 (d, J_{P-C} = 25.9 Hz, 2C, P{*C*(CH$_3$)$_3$}$_2$), 27.6 (d, J_{P-C} = 15.3 Hz, 6C, P{C(*C*H$_3$)$_3$}$_2$), 20.9 (4C, N{CH(*C*H$_3$)$_2$}$_2$). ^{31}P{^{1}H}-NMR (162 MHz, CDCl$_3$): δ = 154.3 (s).

2.4.3 Synthesis (^{R2}POCN^{iPr2})PdCl complexes and characterization data

(^{iPr2}POCN^{iPr2})PdCl (4): A mixture of (COD)PdCl$_2$ (0.84 g, 2.94 mmol), (^{iPr2}POCN^{iPr2})–H (1.0 g, 3.09 mmol) and K$_3$PO$_4$ (0.749 g, 3.53 mmol) were taken in a Schlenk flask and 1,4-dioxane (30 mL) was added into it. The reaction mixture was heated at reflux temperature 100 ^{o}C for 8 h under argon atmosphere. The yellowish-black suspension formed was formed. The reaction mixture was cooled to room temperature and the volatile were evaporated under reduced pressure. The compound was extracted with *n*-hexane (30 mL x 6) and combined organic solution was evaporated under reduced pressure to obtain compound **4** as light yellow crystalline solid. The compound **4** was recrystallized from *n*-hexane solution by slow evaporation to obtain an X-ray quality crystals. Yield: 0.818 g, 60%. M.p. = 143–144 ^{o}C. ^{1}H-NMR (400 MHz, CDCl$_3$): δ = 6.91 (vt, *J* = 7.8 Hz, 1H, Ar–H), 6.62 (d, *J* = 7.3 Hz, 1H, Ar–H), 6.56 (d, *J* = 7.8 Hz, 1H, Ar–H), 4.07 (s, 2H, CH$_2$), 3.55 (apparent octet,^{291} *J* = 6.4 Hz, 2H, N{C*H*(CH$_3$)$_2$}$_2$), 2.43 (apparent octet,^{291} *J* = 7.0 Hz, 2H, P{C*H*(CH$_3$)$_2$}$_2$), 1.65 (d, *J* = 6.8 Hz, 6H, NCH(C*H*$_3$)$_2$), 1.42 (dd, *J* = 18.8, 7.3 Hz, 6H, PCH(C*H*$_3$)$_2$), 1.30 (dd, *J* = 15.8, 7.1 Hz, 6H, PCH(C*H*$_3$)$_2$), 1.21 (d, *J* = 6.4 Hz, 6H, NCH(C*H*$_3$)$_2$). ^{13}C-NMR (100 MHz, CDCl$_3$): δ = 163.6 (d, J_{P-C} = 6.9 Hz, C$_q$), 153.5 (C$_q$), 143.2 (d, J_{P-C} = 1.5 Hz, C$_q$), 126.3 (CH), 114.9 (CH), 108.2 (d, J_{P-C} = 16.2 Hz, CH), 61.1 (*C*H$_2$), 57.3 (2C, N{*C*H(CH$_3$)$_2$}$_2$), 29.4 (d, J_{P-C} = 25.4 Hz, 2C, P{*C*H(CH$_3$)$_2$}$_2$), 22.5 (2C, NCH(*C*H$_3$)$_2$), 19.4 (2C, NCH(*C*H$_3$)$_2$), 17.7 (d, *J* = 5.4 Hz, 2C, PCH(*C*H$_3$)$_2$), 16.9 (2C, PCH(*C*H$_3$)$_2$). ^{31}P{^{1}H}-NMR (162 MHz, CDCl$_3$): δ = 198.9 (s). HRMS (ESI): *m/z* calcd for C$_{19}$H$_{33}$ClNOPPd–Cl$^+$ [M–Cl]$^+$ 428.1335, found 428.1331. Anal. calcd for C$_{19}$H$_{33}$ClNOPPd: C, 49.15; H, 7.16; N, 3.02. Found: C, 49.07; H, 7.16; N, 2.77.

(^{tBu2}POCN^{iPr2})PdCl (5): A mixture of (COD)PdCl$_2$ (0.155 g, 0.54 mmol), (^{t}Bu^{2}POCN^{iPr2})–H (0.20 g, 0.568 mmol) and K$_3$PO$_4$ (0.137 g, 0.645 mmol) were taken in a Schlenk flask and toluene (30 mL) was added into it. The reaction mixture was heated at reflux temperature 110 ^{o}C for 24 h under argon atmosphere. The yellowish-black suspension formed was formed. The reaction mixture was cooled to room temperature and the volatiles were evaporated under reduced pressure. The compound was extracted with THF (40 mL x 2) and combined organic solution was evaporated under reduced pressure to obtain compound **5** as light yellow crystalline solid. The compound was recrystallized from CH$_2$Cl$_2$/*n*-hexane solvent to obtain X-ray quality crystals. Yield: 0.237 g, 89%. M.p. = 167–169 ^{o}C. ^{1}H-NMR (400 MHz, CDCl$_3$): δ = 6.91 (vt, *J* = 7.8, 7.5 Hz, 1H, Ar–H), 6.58 (vt, *J* = 7.7 Hz, 2H, Ar–H),

4.04 (s, 2H, CH_2), 3.58 (apparent octet,[291] J = 6.4 Hz, 2H, N{CH(CH_3)$_2$}$_2$), 1.65 (d, J = 6.4 Hz, 6H, NCH(CH_3)$_2$), 1.46 (d, J = 15.3 Hz, 18H, P{C(CH_3)$_3$}$_2$), 1.19 (d, J = 6.4 Hz, 6H, NCH(CH_3)$_2$). ^{13}C-NMR (100 MHz, $CDCl_3$): δ = 164.3 (d, J_{P-C} = 5.7 Hz, C_q), 153.5 (C_q), 143.4 (C_q), 126.1 (CH), 114.7 (CH), 108.2 (d, J_{P-C} = 16.2 Hz, CH), 61.1 (CH_2), 57.2 (2C, N{CH(CH_3)$_2$}$_2$), 40.1 (d, J_{P-C} = 16.2 Hz, 2C, P{C(CH_3)$_3$}$_2$), 28.1 (d, J_{P-C} = 4.5 Hz, 6C, P{C(CH_3)$_3$)}$_2$), 22.6 (2C, NCH(CH_3)$_2$), 19.4 (2C, NCH(CH_3)$_2$). ^{31}P{^{1}H}-NMR (162 MHz, $CDCl_3$): δ = 204.9 (s). HRMS (ESI): *m/z* calcd for $C_{21}H_{37}ClNOPPd–Cl^+$ $[M–Cl]^+$ 456.1648, found 456.1643. Anal. calcd for $C_{21}H_{37}ClNOPPd$: C, 51.23; H, 7.57; N, 2.84. Found: C, 49.87; H, 7.26; N, 1.96.[292]

2.4.4 Synthesis and characterization data of (^{R2}POCN^{iPr2})PdX derivatives

(^{iPr2}POCN^{iPr2})PdI (6): To the mixture of 2,6-(^{i}Pr$_2$PO)(C_6H_3)(CH_2-N^{i}Pr$_2$)PdCl (**4**) (0.015 g, 0.032 mmol) and KI (0.008 g, 0.048 mmol) in a J-Young NMR tube was added CH_2Cl_2 (0.3 mL) and methanol (0.3 mL). Upon warming the reaction mixture at 40 ^{o}C for 5 h, the chloro-derivative **4** is completely converted to iodo-derivative (^{iPr2}POCN^{iPr2})PdI (**6**). At ambient temperature the volatiles were removed under vacuum to obtain light yellow compound. M.p. = 159–160 ^{o}C. ^{1}H-NMR (400 MHz, $CDCl_3$): δ = 6. 94 (vt, J = 8.0, 7.5 Hz, 1H, Ar–H), 6.64 (d, J = 7.5 Hz, 1H, Ar–H), 6.61 (d, J = 8.0 Hz, 1H, Ar–H), 4.09 (s, 2H, CH_2), 3.61 (apparent octet,[291] J = 6.3 Hz, 2H, N{CH(CH_3)$_2$}$_2$), 2.54 (apparent octet,[291] J = 7.0 Hz, 2H, P{CH(CH_3)$_2$}$_2$), 1.66 (d, J = 6.3 Hz, 6H, NCH(CH_3)$_2$), 1.45 (dd, J = 18.8, 7.3 Hz, 6H, PCH(CH_3)$_2$), 1.28 (dd, J = 15.8, 7.0 Hz, 6H, PCH(CH_3)$_2$), 1.19 (d, J = 6.3 Hz, 6H, NCH(CH_3)$_2$). ^{13}C-NMR (100 MHz, $CDCl_3$): δ = 162.9 (d, J_{P-C} = 6.2 Hz, C_q), 153.8 (C_q), 147.1 (d, J = 6.9 Hz, C_q), 126.4 (CH), 115.1 (CH), 108.1 (d, J_{P-C} = 16.9 Hz, CH), 61.1 (CH_2), 58.2 (2C, N{CH(CH_3)$_2$}$_2$), 30.3 (d, J_{P-C} = 26.9 Hz, 2C, P{CH(CH_3)$_2$}$_2$), 23.7 (2C, NCH(CH_3)$_2$), 19.5 (2C, NCH(CH_3)$_2$), 18.8 (d, J = 3.9 Hz, 2C, PCH(CH_3)$_2$), 16.9 (s, 2C, PCH(CH_3)$_2$). ^{31}P{^{1}H}-NMR (162 MHz, $CDCl_3$): δ 203.9 (s). HRMS (ESI): *m/z* calcd for $C_{19}H_{33}INOPPd–I^+$ $[M–I]^+$ 428.1329, found 428.1330.

(^{iPr2}POCN^{iPr2})Pd(OCOCH$_3$) (7): The mixture of 2,6-(^{i}Pr$_2$PO)(C_6H_3)(CH_2-N^{i}Pr$_2$)PdCl (0.03 g, 0.065 mmol) and AgOAc (0.012 g, 0.072 mmol) in THF (10 mL) was stirred at room temperature for 5 h. The resultant suspension was filtered through celite and volatile were evaporated under reduced pressure to obtain light yellow compound **7**. Yield: 0.023 g, 73%. M.p. = 134–135 ^{o}C. ^{1}H-NMR (400 MHz, $CDCl_3$): δ 6.89 (vt, J = 7.8, 7.5 Hz, 1H, Ar–H), 6.56 (d, J = 7.5 Hz, 1H, Ar–H), 6.52 (d, J = 7.8 Hz, 1H, Ar–H), 4.05 (s, 2H, CH_2), 3.43 (apparent octet,[291] J = 6.3 Hz, 2H, N{CH(CH_3)$_2$}$_2$), 2.66 (apparent octet,[291] J = 7.0 Hz, 2H,

P{C*H*(CH_3)$_2$}$_2$), 1.92 (s, 3H, COC*H*$_3$), 1.55 (d, *J* = 6.3 Hz, 6H, NCH(C*H*$_3$)$_2$), 1.32 (dd, *J* = 19.6, 7.3 Hz, 6H, PCH(C*H*$_3$)$_2$), 1.26 (dd, *J* = 14.7, 7.0 Hz, 6H, PCH(C*H*$_3$)$_2$), 1.23 (d, *J* = 6.3 Hz, 6H, NCH(C*H*$_3$)$_2$). ^{13}C-NMR (100 MHz, $CDCl_3$): δ 176.5 (*C*OCH$_3$), 164.2 (d, J_{P-C} = 7.6 Hz, C_q), 153.4 (C_q), 140.7 (C_q), 126.0 (CH), 114.4 (CH), 107.9 (d, J_{P-C} = 15.3 Hz, CH), 60.8 (*C*H$_2$), 56.9 (2C, N{*C*H(CH_3)$_2$}$_2$), 29.9 (d, J_{P-C} = 25.8 Hz, 2C, P{*C*H(CH_3)$_2$}$_2$), 24.2 (COCH_3), 21.9 (2C, NCH(*C*H$_3$)$_2$), 19.3 (2C, NCH(*C*H$_3$)$_2$), 18.1 (d, *J* = 6.7 Hz, 2C, PCH(*C*H$_3$)$_2$), 16.9 (d, J_{P-C} = 2.9 Hz, 2C, PCH(*C*H$_3$)$_2$). ^{31}P{^{1}H}-NMR (162 MHz, $CDCl_3$): δ = 196.7 (s). IR (neat): 1598 cm^{-1} (C=O). HRMS (ESI): *m/z* calcd for $C_{21}H_{36}NO_3PPd-OCOCH_3^+$ $[M-OCOCH_3]^+$ 428.1335, found 428.1329. Anal.calcd for $C_{21}H_{36}NO_3PPd$: C, 51.70; H, 7.44; N, 2.87. Found: C, 51.29; H, 7.46; N, 1.91.[292]

(*i*Pr2POCN*i*Pr2)Pd(CH_3CN)(OTf) (8): The compound **8** was synthesized following the procedure similar to **7**, using compound **4** (0.030 g, 0.0646 mmol) and AgOTf (0.0192 g, 0.071 mmol). The compound was recrystallized from CH_3CN at room temperature. Yield: 0.032 g, 86%. ^{1}H-NMR (400 MHz, $CDCl_3$): δ 6.95 (t, *J* = 7.8 Hz, 1H, Ar–H), 6.6 (d, *J* = 7.5 Hz, 1H, Ar–H), 6.55 (d, *J* = 7.8 Hz, 1H, Ar–H), 4.05 (s, 2H, –CH_2), 3.47 (sept, 2H, N{C*H*(CH_3)$_2$}$_2$), 2.62 (sept, 2H, P–C*H*(CH_3)$_2$), 2.43 (s, 3H, C*H*$_3$CN), 1.58 (d, 6H, 2 x CH_3, –N{CH(C*H*$_3$)$_2$}), 1.41 (dd, J_{P-H} = 20.0 Hz, 7.2 Hz, 6H, 2 x CH_3, –P{CH(C*H*$_3$)$_2$}$_2$), 1.29 (dd, J_{P-H} = 15.3 Hz, 7.0 Hz, 6H, 2 x CH_3, –P{CH(C*H*$_3$)$_2$}$_2$), 1.20 (d, 6H, 2 x CH_3, –N{CH(C*H*$_3$)$_2$}). ^{13}CNMR{^{1}H}-NMR (100 MHz, $CDCl_3$): δ 163.8 (d, J_{P-c}= 6.1 Hz, C_q), 153.1 (C_q), 139.6 (C_q), 128.0 (CH), 124.9 (s, CH_3*C*N), 115.7 (CH), 109.1 (d, J_{P-c} = 15.4 Hz, CH), 60.5 (*C*H$_2$), 57.8 (2 x CH, N{*C*H(CH_3)$_2$}$_2$), 29.5 (d, J_{P-c} = 23.8 Hz, 2 x CH, P{*C*H(CH_3)$_2$}$_2$), 22.4 (2 x CH_3, –NCH(*C*H$_3$)$_2$), 19.4 (2 x CH_3, –NCH(*C*H$_3$)$_2$), 17.9 (d, *J* = 6.1 Hz, 2 x CH_3, –P{CH(*C*H$_3$)$_2$}), 16.8 (d, J_{P-c} = 2.3 Hz, 2 x CH_3, –P{CH(*C*H$_3$)$_2$}), 2.8 (s, CH_3, *C*H$_3$CN). ^{31}P{^{1}H}-NMR (161 MHz, $CDCl_3$): δ 199.1(s). Anal. calcd for $C_{21}H_{36}NO_3PPd$: C, 51.70; H, 7.44; N, 2.87. Found: C, 51.29; H, 7.46; N, 1.91.[292]

(*i*Pr2POCN*i*Pr2)Pd(CH_3CN)SbF_6 (9): The compound **9** was synthesized following the procedure similar to **7**, using **4** (0.030g, 0.0646 mmol) and $AgSbF_6$ (0.0243g, 0.071 mmol), and the reaction mixture was stirred for 5 h. The compound was crystallized in acetonitrile/hexane to obtain yellow cryatalline solid. Yield: 0.042 g, 92%. ^{1}H-NMR (500 MHz, $CDCl_3$): δ 7.00-6.97 (m, 1H, Ar–H), 6. 65 (d, *J* = 7.6 Hz, 1H, Ar–H) 6.59 (d, *J* = 7.9 Hz, 1H, Ar–H), 4.05 (s, 2H, –CH_2), 3.45 (sept, 2H, N{C*H*(CH_3)$_2$}$_2$), 2.48 (m, 2H, P–C*H*(CH_3)$_2$), 2.43 (s, 3H, C*H*$_3$CN), 1.57 (d, 6H, 2 x CH_3, –N{CH(C*H*$_3$)$_2$}), 1.38–1.28 (m, {(CH_3)$_2$CH}$_2$–P, 12H), 1.22 (d, 6H, 2 x CH_3, –N{CH(C*H*$_3$)$_2$}). ^{13}CNMR{^{1}H}-NMR (125

MHz, $CDCl_3$): δ 163.9 (d, J_{P-c}= 5.7 Hz, C_q), 154.1 (C_q), 149.2 (C_q), 128.0 (CH), 124.6 (s, CH_3CN), 115.7 (CH), 109.1 (d, J_{P-c} = 16 Hz, CH), 60.5 (CH_2), 57.8 (2 x CH, N{$CH(CH_3)_2$}$_2$), 29.5 (d, J_{P-c} = 25.6 Hz, 2 x CH, P{$CH(CH_3)_2$}$_2$), 22.4 (2 x CH_3, –$NCH(CH_3)_2$), 19.4 (2 x CH_3, –$NCH(CH_3)_2$), 17.5 (d, J = 5.7 Hz, 2 x CH_3, –P{$CH(CH_3)_2$}), 16.8 (s, 2 x CH_3, –P{$CH(CH_3)_2$}), 2.8 (s, CH_3, CH_3CN). $^{31}P\{^1H\}$-NMR (201.2 MHz, $CDCl_3$): δ 199.1 (s). Anal. calcd for $C_{21}H_{36}F_6N_2OPPdSb$: C, 35.74; H, 5.14; N, 3.97. Found: C, 36.42; H, 5.03; N, 3.45.

(^{tBu2}POCN^{iPr2})PdOAc (10): The (^{tBu2}POCN^{iPr2})PdCl (**5**; 0.050 g, 0.1015 mmol) and AgOAc (0.027 g, 0. 1624 mmol) was taken in a Schlenk flask. In that, 10 mL THF was added and the reaction mixture was stirred at room temperature for 5 h. The solution was filtered to a different flask and volatile were evaporated under reduced pressure to obtain the yellow compound **10**. Yield: 0.045 g, 87%. ^{1}H-NMR (500 MHz, $CDCl_3$): δ 6.89 (d, J = 7.6 Hz, 7.6 Hz, 1H, Ar–H), 6.55-6.52 (m, 2H, Ar–H), 4.05 (s, 2H, –CH_2), 3.38 (sept, 2H, N{$CH(CH_3)_2$}$_2$), 1.91 (s, 3H, {CH_3CO}), 1.60 (d, 6H, 2 x CH_3, –N{$CH(CH_3)_2$}), 1.42 (d, 18H, J_{P-H} = 15.2 Hz, −P{2 x $C(CH_3)_3$}, 1.24 (d, 6H, 2 x CH_3, –N{$CH(CH_3)_2$. ^{13}C-NMR (100 MHz, $CDCl_3$): δ 176.3 ($COCH_3$), 164.7 (d, J_{P-C} = 5.7 Hz, C_q), 153.7 (C_q), 139.9 (C_q), 125.9 (CH), 114.5 (CH), 108.0 (d, J_{P-C} = 15.3 Hz, CH), 60.9 (CH_2), 57.4 (2C, N{$CH(CH_3)_2$}$_2$), 39.7 (d, J_{P-C} = 16.2 Hz, 2C, P{$C(CH_3)_3$}$_2$), 27.6 (d, J = 5.7 Hz, 6 x CH_3, –P{$C(CH_3)_3$}$_2$), 25.1 ($COCH_3$), 21.9 (2C, $NCH(CH_3)_2$), 19.2 (2C, $NCH(CH_3)_2$). $^{31}P\{^1H\}$-NMR (201 MHz, $CDCl_3$): δ 200.8 (s). HRMS (ESI): *m/z* calcd for $C_{23}H_{40}NO_3PPd-OCOCH_3^+$ $[M-OCOCH_3]^+$ 456.1642, found 456.1651. Anal. calcd for $C_{23}H_{40}NO_3PPd$: C, 53.54; H, 7.81; N, 2.71. Found: C, 54.53; H, 7.64; N, 1.75.

(^{tBu2}POCN^{iPr2})Pd(CH_3CN)(SbF_6) (11): The compound **11** was prepared following the procedure similar to **10**, using **5** (0.050 g, 0.1015 mmol) and $AgSbF_6$ (0.055 g, 0. 1624 mmol) in THF (1.0 mL), and the reaction mixture was stirred at room temperature for 5 h. The solution was filtered another flask and volatile were evaporated under reduced pressure, and compound was recrystallized in acetonitrile to obtain compound **11**. Yield: 0.064 g, 86%. ^{1}H-NMR (500 MHz, $CDCl_3$): δ 7.00-6.97 (m, 1H, Ar–H), 6. 64 (d, J = 7.6 Hz, 1H, Ar–H) 6.62 (d, J = 7.9 Hz, 1H, Ar–H), 4.07 (s, 2H, –CH_2), 3.47 (sept, 2H, –N{$CH(CH_3)_2$}$_2$), 2.47 (s, 3H, CH_3CN), 1.58 (d, 6H, 2 x CH_3, –N{$CH(CH_3)_2$}), 1.41 (d, 18H, J_{P-H} = 15.6 Hz, −P{2 x $C(CH_3)_3$}), 1.21 (d, 6H, 2 x CH_3, –N{$CH(CH_3)_2$}). ^{13}CNMR{^{1}H}-NMR (125 MHz, $CDCl_3$): δ 164.6 (d, J_{P-c}= 4.8 Hz, C_q), 153.9 (C_q), 139.3 (C_q), 127.8 (CH), 124.8 (s, C_q, CH_3CN), 115.4 (CH), 109.0 (d, J_{P-c} = 16.2 Hz, CH), 60.3 (CH_2), 57.6 (2 x CH, N{$CH(CH_3)_2$}$_2$), 40.1

(d, J_{P-c} = 17.1 Hz, 2 x C_q, P{*C* (CH_3)$_3$}$_2$), 27.5 (d, *J* = 4.7 Hz, 6C, –P{C(*C*H_3)$_3$}$_2$), 22.3 (2C, –NCH(*C*H_3)$_2$), 19.1 (2C, –NCH(*C*H_3)$_2$), 2.7 (s,CH_3, *C*H_3CN). ^{31}P{^{1}H}-NMR (201.2 MHz, $CDCl_3$): δ 205.7 (s). HRMS (ESI): *m/z* calcd for $C_{23}H_{40}F_6N_2OPPdSb-OTf^+$ $[M-OTf]^+$ 456.1642, found 456.1642. Anal. calcd for $C_{23}H_{40}F_6N_2OPPdSb$: C, 37.65; H, 5.50; N, 3.82. Found: C, 25.37; H, 4.09; N, 2.61.[292]

2.4.5 Procedure for azoles arylation and characterization data

Representative procedure for azole arylation: Synthesis of 2-(*p* tolyl)benzo[*d*]thiazole (14aa): To a flame-dried screw-capped Schlenk tube equipped with magnetic stir bar was introduced 4-iodotoluene (**13a**; 0.164 g, 0.75 mmol), Cs_2CO_3 (0.244 g, 0.75 mmol) and CuI (0.005 g, 0.025 mmol, 5.0 mol%) under argon. The screw-capped Schlenk tube with mixture was then evacuated and refilled with argon. To the above mixture was added benzothiazole (**12a**; 0.068 g, 0.50 mmol) and (^{iPr2}POCN^{iPr2})PdCl (0.0025 mmol, 0.5 mol%, 1.0 mL of 0.0025 M stock solution in DMF) in DMF under argon. The resultant reaction mixture was then degassed, refilled with argon and was stirred at 120 ^{o}C in a pre-heated oil bath for 16 h. At ambient temperature, H_2O (15 mL) was added and the reaction mixture was extracted with *t*-BuOMe (20 mL x 3). The combined organic layers were dried over $MgSO_4$ and the solvent was evaporated *in vacuo*. The remaining residue was purified by column chromatography on silica gel (petroleum ether/EtOAc: 30/1→ 20/1) to yield **14aa** as an off-white solid.

Characterization data for compounds 14

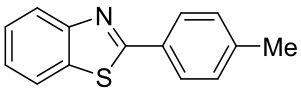

2-(*p*-Tolyl)benzo[*d*]thiazole (14aa):[180] Yield: 0.109 g, 97%. M.p. = 85–87 ^{o}C. ^{1}H-NMR (400 MHz, $CDCl_3$): δ = 8.07 (d, *J* = 8.2 Hz, 1H, Ar–H), 7.99 (d, *J* = 8.2 Hz, 2H, Ar–H), 7.89 (d, *J* = 8.2 Hz, 1H, Ar–H), 7.49 (vt, *J* = 8.1 Hz, 1H, Ar–H), 7.37 (vt, *J* = 7.9 Hz, 1H, Ar–H), 7.30 (d, *J* = 8.2 Hz, 2H, Ar–H), 2.43 (s, 3H, CH_3). ^{13}C-NMR (100 MHz, $CDCl_3$): δ = 168.5 (C_q), 154.2 (C_q), 141.7 (C_q), 135.0 (C_q), 131.0 (C_q), 129.9 (2C, CH), 127.7 (2C, CH), 126.5 (CH), 125.2 (CH), 123.2 (CH), 121.8 (CH), 21.7 (CH_3). IR (neat): ν_{max}/cm^{-1} 2961, 2918, 2851, 1478, 1428, 1257, 1224, 1084, 1013, 958, 793. HRMS (ESI): *m/z* calcd for $C_{14}H_{11}NS+H^+$ $[M+H]^+$ 226.0690, found 226.0685.

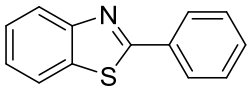

2-Phenylbenzo[*d*]thiazole (14ab):[180] The representative procedure was followed, using **12a** (0.068 g, 0.5 mmol) and iodobenzene (**13b**; 0.153 g, 0.75 mmol). Purification by column chromatography on silica gel (petroleum ether/EtOAc: 25/1) yielded **14ab** as a white solid. Yield: 0.099 g, 94%. M.p. = 117–118 ^{o}C. ^{1}H-NMR (400 MHz, $CDCl_3$): δ = 8.13-8.08 (m, 3H, Ar–H), 7.91 (d, J = 7.8 Hz, 1H, Ar–H), 7.53-7.48 (m, 4H, Ar–H), 7.39 (dvt, J = 8.0, 1.0 Hz, 1H, Ar–H). ^{13}C-NMR (100 MHz, $CDCl_3$): δ = 168.3 (C_q), 154.2 (C_q), 135.2 (C_q), 133.7 (C_q), 131.2 (CH), 129.2 (2C, CH), 127.7 (2C, CH), 126.5 (CH), 125.4 (CH), 123.4 (CH), 121.8 (CH). IR (neat): ν_{max}/cm^{-1} 2922, 2850, 1472, 1426, 1218, 956, 756, 680. HRMS (ESI): *m/z* calcd for $C_{13}H_{10}NS+H^+$ $[M+H]^+$ 212.0534, found 212.0527.

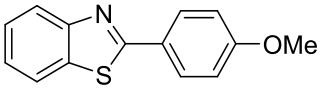

2-(4-Methoxyphenyl)benzo[*d*]thiazole (14ac):[180] The representative procedure was followed, using **12a** (0.067 g, 0.5 mmol) and 4-iodoanisole (**13c**; 0.176 g, 0.75 mmol). Purification by column chromatography on silica gel (petroleum ether/EtOAc: 20/1 → 10/1) yielded **14ac** as a white solid. Yield: 0.103 g, 86%. M.p. = 125–126 ^{o}C. ^{1}H-NMR (400 MHz, $CDCl_3$): δ = 8.04-8.01 (m, 3H, Ar–H), 7.87 (d, J = 7.8 Hz, 1H, Ar–H), 7.47 (dvt, J = 7.1, 1.4 Hz, 1H, Ar–H), 7.35 (dvt, J = 7.8, 1.4 Hz, 1H, Ar–H), 6.99 (d, J = 8.7 Hz, 2H, Ar–H), 3.87 (s, 3H, OCH_3). ^{13}C-NMR (100 MHz, $CDCl_3$): δ = 168.0 (C_q), 162.1 (C_q), 154.4 (C_q), 135.0 (C_q), 129.3 (2C, CH), 126.6 (C_q), 126.4 (CH), 124.9 (CH), 122.9 (CH), 121.7 (CH), 114.5 (2C, CH), 55.6 (CH_3). IR (neat): ν_{max}/cm^{-1} 2996, 2936, 2836, 1591, 1521, 1466, 1412, 1286. HRMS (ESI): *m/z* calcd for $C_{14}H_{11}NOS+H^+$ $[M+H]^+$ 242.0640, found 242.0636.

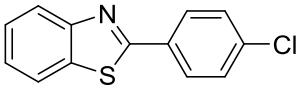

2-(4-Chlorophenyl)benzo[*d*]thiazole (14ad):[188] The representative procedure was followed, using **12a** (0.065 g, 0.481 mmol) and 1-chloro-4-iodobenzene (**13d**; 0.18 g, 0.75 mmol). Purification by column chromatography on silica gel (petroleum ether/EtOAc: 30/1 → 20/1) yielded **14ad** as a white solid. Yield: 0.109 g, 92%. M.p. = 118–119 ^{o}C. ^{1}H-NMR (400 MHz, $CDCl_3$): δ = 8.07 (d, J = 7.7 Hz, 1H, Ar–H), 8.02 (d, J = 8.7 Hz, 2H, Ar–H), 7.90 (d, J = 7.3 Hz, 1H, Ar–H), 7.50 (dvt, J = 7.2, 1.4 Hz, 1H, Ar–H), 7.46 (d, J = 8.2 Hz, 2H, Ar–H),

7.40 (dvt, J = 7.6, 1.4 Hz, 1H, Ar–H). ^{13}C-NMR (100 MHz, $CDCl_3$): δ = 166.8 (C_q), 154.2 (C_q), 137.2 (C_q), 135.2 (C_q), 132.3 (C_q), 129.4 (2C, CH), 128.9 (2C, CH), 126.7 (CH), 125.6 (CH), 123.5 (CH), 121.8 (CH). IR (neat): ν_{max}/cm^{-1} 2960, 2922, 2849, 1469, 1429, 1256, 1081, 1012, 797, 755. HRMS (ESI): *m/z* calcd for $C_{13}H_8ClNS+H^+$ $[M+H]^+$ 246.0144, found 246.0141.

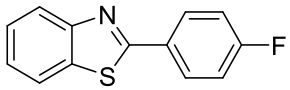

2-(4-Fluorophenyl)benzo[*d*]thiazole (14ae):[188] The representative procedure was followed, using **12a** (0.072 g, 0.533 mmol) and 1-fluoro-4-iodobenzene (**13e** ; 0.167 g, 0.75 mmol). Purification by column chromatography on silica gel (*n*-hexane/EtOAc: 30/1 → 25/1) yielded **14ae** as a white solid. Yield: 0.090 g, 74%. M.p. = 102–103 ^{o}C. ^{1}H-NMR (500 MHz, $CDCl_3$): δ = 8.10-8.05 (m, 3H, Ar–H), 7.90 (d, J = 7.8 Hz, 1H, Ar–H), 7.50 (vt, J = 7.3 Hz, 1H, Ar–H), 7.39 (vt, J = 7.7 Hz, 1H, Ar–H), 7.19 (vt, J = 8.5 Hz, 2H, Ar–H). ^{13}C-NMR (125 MHz, $CDCl_3$): δ = 166.9 (C_q), 164.6 (d, $^1J_{C–F}$ = 251.8 Hz, C_q), 154.3 (C_q), 135.2 (C_q), 130.1 (d, $^4J_{C–F}$ = 2.9 Hz, C_q), 129.7 (d, $^3J_{C–F}$ = 8.6 Hz, 2C, CH), 126.6 (CH), 125.4 (CH), 123.4 (CH), 121.8 (CH), 116.3 (d, $^2J_{C–F}$ = 21.9 Hz, 2C, CH). ^{19}F-NMR (377 MHz, $CDCl_3$): δ = −108.8 (s). IR(neat): ν_{max}/cm^{-1} 3055, 2924, 2853, 1605, 1483, 1435, 1233, 969, 837, 756. HRMS (ESI): *m/z* calcd for $C_{13}H_8FNS+H^+$ $[M+H]^+$ 230.0440, found 230.0434.

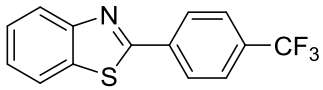

2-(4-(Trifluoromethyl)phenyl)benzo[*d*]thiazole (14af):[180] The representative procedure was followed, using **12a** (0.065 g, 0.481 mmol) and 1-iodo-4-(trifluoromethyl)benzene (**13f**; 0.20 g, 0.75 mmol). Purification by column chromatography on silica gel (petroleum ether/EtOAc: 30/1 → 25/1) yielded **14af** as a white solid. Yield: 0.031 g, 23%. M.p. = 157–158 ^{o}C. ^{1}H-NMR (400 MHz, $CDCl_3$): δ = 8.20 (d, J = 8.1 Hz, 2H, Ar–H), 8.11 (d, J = 8.1 Hz, 1H, Ar–H), 7.93 (d, J = 8.1 Hz, 1H, Ar–H), 7.75 (d, J = 8.3 Hz, 2H, Ar–H), 7.53 (dvt, J = 8.0, 1.2 Hz, 1H, Ar–H), 7.43 (dvt, J = 8.1, 1.0 Hz, 1H, Ar–H). ^{13}C-NMR (100 MHz, $CDCl_3$): δ = 166.2 (C_q), 154.2 (C_q), 136.9 (C_q), 135.4 (C_q), 132.7 (q, $^2J_{C–F}$ = 32.4 Hz, C_q), 127.9 (2C, CH), 126.9 (CH), 126.2 (q, $^3J_{C–F}$ = 3.8 Hz, 2C, CH), 125.9 (CH), 124.0 (q, $^1J_{C–F}$ = 272.8 Hz, CF_3), 123.8 (CH), 121.9 (CH). ^{19}F-NMR (377 MHz, $CDCl_3$): δ = −62.9 (s). IR(neat): ν_{max}/cm^{-1} 3058,

2995, 2917, 1594, 1485, 1408, 1231. HRMS (ESI): *m/z* calcd for $C_{14}H_8F_3NS+H^+$ $[M+H]^+$ 280.0408, found 280.0415.

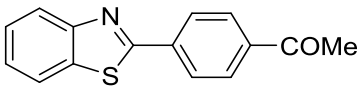

1-(4-(Benzo[*d*]thiazol-2-yl)phenyl)ethan-1-one (14ag): The representative procedure was followed, using **12a** (0.071 g, 0.525 mmol) and 4-iodoacetophenone (**13g**; 0.184 g, 0.75 mmol). Purification by column chromatography on silica gel (petroleum ether/EtOAc: 10/1 → 5/1) yielded **14ag** as a white solid. Yield: 0.026 g, 20%. M.p. = 185–186 °C. ^{1}H-NMR (400 MHz, $CDCl_3$): δ = 8.20 (d, *J* = 8.6 Hz, 2H, Ar–H), 8.12 (d, *J* = 8.3 Hz, 1H, Ar–H), 8.08 (d, *J* = 8.6 Hz, 2H, Ar–H), 7.94 (d, *J* = 7.8 Hz, 1H, Ar–H), 7.53 (dvt, *J* = 8.3, 1.2 Hz, 1H, Ar–H), 7.43 (dvt, *J* = 7.8, 0.7 Hz, 1H, Ar–H), 2.66 (s, 3H, $COCH_3$). ^{13}C-NMR (100 MHz, $CDCl_3$): δ = 197.6 (C_q), 166.7 (C_q), 154.2 (C_q), 138.8 (C_q), 137.6 (C_q), 135.4 (C_q), 129.2 (2C, CH), 127.9 (2C, CH), 126.9 (CH), 126.0 (CH), 123.8 (CH), 121.9 (CH), 27.0 (CH_3). IR(neat): ν_{max}/cm^{-1} 2923, 2852, 1676, 1554, 1260, 1106, 964, 823, 763. HRMS (ESI): *m/z* calcd for $C_{15}H_{11}NOS+H^+$ $[M+H]^+$ 254.0640, found 254.0643.

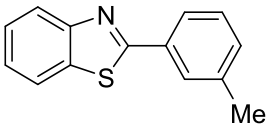

2-(*m*-Tolyl)benzo[*d*]thiazole (14ah): The representative procedure was followed, using **12a** (0.072 g, 0.533 mmol) and 3-iodotoluene (**13h**; 0.164 g, 0.75 mmol). Purification by column chromatography on silica gel (petroleum ether/EtOAc: 30/1 → 25/1) yielded **14ah** as a white solid. Yield: 0.113 g, 94%. M.p. = 76–78 °C. ^{1}H-NMR (400 MHz, $CDCl_3$): δ = 8.09 (d, *J* = 7.8 Hz, 1H, Ar–H), 7.95 (s, 1H, Ar–H), 7.91-7.86 (m, 2H, Ar–H), 7.50 (vt, *J* = 7.3 Hz, 1H, Ar–H), 7.38 (vt, *J* = 7.5 Hz, 2H, Ar–H), 7.30 (d, *J* = 7.6 Hz, 1H, Ar–H), 2.46 (s, 3H, CH_3). ^{13}C-NMR (100 MHz, $CDCl_3$): δ = 168.5 (C_q), 154.3 (C_q), 139.0 (C_q), 135.2 (C_q), 133.7 (C_q), 132.0 (CH), 129.1 (CH), 128.2 (CH), 126.5 (CH), 125.3 (CH), 125.0 (CH), 123.3 (CH), 121.8 (CH), 21.5 (CH_3). IR(neat): ν_{max}/cm^{-1} 3056, 2923, 2854, 1610, 1503, 1433, 1290, 887, 791 HRMS (ESI): *m/z* calcd for $C_{14}H_{11}NS+H^+$ $[M+H]^+$ 226.0690, found 226.0686.

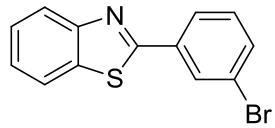

2-(3-Bromophenyl)benzo[*d*]thiazole (14ai): The representative procedure was followed, using **12a** (0.063 g, 0.466 mmol) and 3-bromo-4-iodobenzene (**13i**; 0.212 g, 0.75 mmol), and reaction was heated for 24 h. Purification by column chromatography on silica gel (petroleum ether/EtOAc: 30/1 → 20/1) yielded **14ai** as a light yellow solid. Yield: 0.055 g, 41%. M.p. = 91–93 °C. ^{1}H-NMR (400 MHz, $CDCl_3$): δ = 8.28 (t, *J* = 1.7 Hz, 1H, Ar–H), 8.09 (d, *J* = 8.1 Hz, 1H, Ar–H), 7.99 (d, *J* = 7.8 Hz, 1H, Ar–H), 7.91 (d, *J* = 7.8 Hz, 1H, Ar–H), 6.61 (dd, *J* = 8.1, 1.0 Hz, 1H, Ar–H), 7.51 (dvt, *J* = 8.3, 1.2 Hz, 1H, Ar–H), 7.41 (dvt, *J* = 8.1, 1.0 Hz, 1H, Ar–H), 7.36 (t, *J* = 7.8 Hz, 1H, Ar–H). ^{13}C-NMR (100 MHz, $CDCl_3$): δ = 166.3 (C_q), 154.1 (C_q), 135.6 (C_q), 135.3 (C_q), 134.0 (CH), 130.7 (CH), 130.4 (CH), 126.7 (CH), 126.3 (CH), 125.8 (CH), 123.6 (CH), 123.4 (C_q), 121.9 (CH). IR (neat): ν_{max}/cm^{-1} 2959, 2922, 2851, 1458, 1421, 1216, 970, 788, 749. HRMS (ESI): *m/z* calcd for $C_{13}H_9BrNS+H^+$ [M+H$^+$] 289.9639, found 289.9644; [M+2+H]$^+$ 291.9619, found 291.9625.

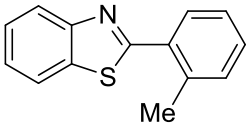

2-(*o*-Tolyl)benzo[*d*]thiazole (14aj): The representative procedure was followed, using **12a** (0.067 g, 0.50 mmol) and 2-iodotoluene (**13j**; 0.164 g, 0.75 mmol). Purification by column chromatography on silica gel (petroleum ether/EtOAc: 30/1 → 25/1) yielded **14aj** as white solid. Yield: 0.107 g, 95%. M.p. = 58–59 °C. ^{1}H-NMR (400 MHz, $CDCl_3$): δ = 8.12 (d, *J* = 8.2 Hz, 1H, Ar–H), 7.94 (d, *J* = 7.8 Hz, 1H, Ar–H), 7.77 (d, *J* = 7.8 Hz, 1H, Ar–H), 7.52 (dvt, *J* = 7.8, 1.4 Hz, 1H, Ar–H), 7.44-7.30 (m, 4H), 2.67 (s, 3H, CH_3). ^{13}C-NMR (100 MHz, $CDCl_3$): δ = 168.2 (C_q), 153.9 (C_q), 137.4 (C_q), 135.7 (C_q), 133.2 (C_q), 131.7 (CH), 130.7 (CH), 130.2 (CH), 126.3 (CH), 126.2 (CH), 125.3 (CH), 123.5 (CH), 121.5 (CH), 21.5 (CH_3). IR (neat): ν_{max}/cm^{-1} 2923, 2859, 1476, 1452, 1428, 1238, 1041, 951, 756. HRMS (ESI): *m/z* calcd for $C_{14}H_{11}NS+H^+$ [M+H]$^+$ 226.0690, found 226.0687.

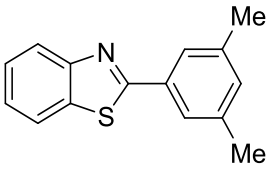

2-(3,5-Dimethylphenyl)benzo[*d*]thiazole (14ak): The representative procedure was followed, using **12a** (0.070 g, 0.518 mmol) and 1-iodo-3,5-dimethylbenzene (**13k**; 0.174 g,

0.75 mmol). Purification by column chromatography on silica gel (petroleum ether/EtOAc: 30/1 → 25/1) yielded **14ak** as white solid. Yield: 0.123 g, 99%. M.p. = 76–77 °C. ^{1}H-NMR (400 MHz, $CDCl_3$): δ = 8.09 (d, J = 8.0 Hz, 1H, Ar–H), 7.90 (d, J = 7.9 Hz, 1H, Ar–H), 7.73 (s, 2H, Ar–H), 7.49 (vt, J = 7.6 Hz, 1H, Ar–H), 7.38 (vt, J = 7.6 Hz, 1H, Ar–H), 7.14 (s, 1H, Ar–H), 2.42 (s, 6H, CH_3). ^{13}C-NMR (100 MHz, $CDCl_3$): δ = 168.8 (C_q), 154.2 (C_q), 138.8 (2C, C_q), 135.1 (C_q), 133.5 (C_q), 133.0 (CH), 126.4 (CH), 125.5 (2C, CH), 125.3 (CH), 123.3 (CH), 121.8 (CH), 21.4 (2C, CH_3). IR (neat): ν_{max}/cm^{-1} 3055, 2915, 2854, 1599, 1432, 1310, 1163, 842, 772. HRMS (ESI): *m/z* calcd for $C_{15}H_{13}NS+H^+$ $[M+H]^+$ 240.0847, found 240.0843.

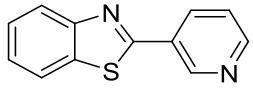

2-(Pyridin-3-yl)benzo[*d*]thiazole (14al):[180] The representative procedure was followed, using **12a** (0.069 g, 0.510 mmol) and 3-iodopyridine (**13l**; 0.154 g, 0.75 mmol) and reaction was heated for 24 h. Purification by column chromatography on silica gel (petroleum ether/EtOAc/Et_3N: 5/1/0.5 → 3/1/0.5) yielded **14al** as white solid. Yield: 0.070 g, 65%. M.p. = 131–133 °C. ^{1}H-NMR (400 MHz, $CDCl_3$): δ = 9.31 (br s, 1H, Ar–H), 8.73 (br s, 1H, Ar–H), 8.41 (d, J = 7.8 Hz, 1H, Ar–H), 8.11 (d, J = 8.3 Hz, 1H, Ar–H), 7.94 (d, J = 7.8 Hz, 1H, Ar–H), 7.54 (vt, J = 7.7 Hz, 1H, Ar–H), 7.48-7.43 (m, 2H, Ar–H). ^{13}C-NMR (100 MHz, $CDCl_3$): δ = 164.5 (C_q), 154.0 (C_q), 151.5 (CH), 148.5 (CH), 135.0 (C_q), 134.7 (CH), 129.8 (C_q), 126.7 (CH), 125.8 (CH), 123.9 (CH), 123.5 (CH), 121.8 (CH). IR (neat): ν_{max}/cm^{-1} 2959, 2922, 2851, 1419, 1259, 1091, 1015, 954, 802. HRMS (ESI): *m/z* calcd for $C_{12}H_8N_2S+H^+$ $[M+H]^+$ 213.0486, found 213.0491.

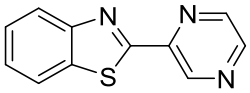

2-(Pyrazin-2-yl)benzo[*d*]thiazole (14am): The representative procedure was followed, using **12a** (0.063 g, 0.466 mmol) and 2-iodopyrazine (**13m**; 0.154 g, 0.75 mmol). Purification by column chromatography on silica gel (petroleum ether/EtOAc/Et_3N: 5/1/0.5 → 3/1/0.5) yielded **14am** as white solid. Yiled: 0.047 g, 47%. M.p. = 183–184 °C. ^{1}H-NMR (400 MHz, $CDCl_3$): δ = 9.61 (s, 1H, Ar–H), 8.66 (d, J = 9.8 Hz, 2H, Ar–H), 8.14 (d, J = 8.1 Hz, 1H, Ar–H), 7.98 (d, J = 8.1 Hz, 1H, Ar–H), 7.54 (vt, J = 7.6 Hz, 1H, Ar–H), 7.46 (vt, J = 7.6 Hz, 1H, Ar–H). ^{13}C-NMR (100 MHz, $CDCl_3$): δ = 166.6 (C_q), 154.4 (C_q), 147.2 (C_q), 146.0 (CH),

144.3 (CH), 142.6 (CH), 136.2 (C_q), 126.8 (CH), 126.4 (CH), 124.2 (CH), 122.2 (CH). IR (neat): ν_{max}/cm^{-1} 2957, 2921, 2850, 1501, 1392, 1259, 1010, 970, 758. HRMS (ESI): *m/z* calcd for $C_{11}H_7N_3S+H^+$ $[M+H]^+$ 214.0439, found 214.0440.

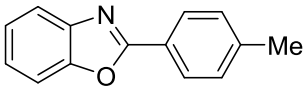

2-(*p*-Tolyl)benzo[*d*]oxazole (14ba): The representative procedure was followed, using **12b** (0.063 g, 0.528 mmol) and 4-iodotoluene (**13a**; 0.164 g, 0.75 mmol). Purification by column chromatography on silica gel (petroleum ether/EtOAc: 40/1) yielded **13ba** as a white solid. Yield: 0.094 g, 85%. M.p. = 115–116 ^oC. ^1H-NMR (400 MHz, $CDCl_3$): δ = 8.15 (d, J = 8.2 Hz, 2H, Ar–H), 7.79-7.75 (m, 1H, Ar–H), 7.59-7.55 (m, 1H, Ar–H), 7.37-7.32 (m, 4H, Ar–H), 2.44 (s, 3H, CH_3). ^{13}C-NMR (100 MHz, $CDCl_3$): δ = 163.5 (C_q), 150.8 (C_q), 142.3 (C_q), 142.2 (C_q), 129.8 (2C, CH), 127.8 (2C, CH), 125.1 (CH), 124.7 (CH), 124.5 (C_q), 120.0 (CH), 110.7 (CH), 21.8 (CH_3). IR (neat): ν_{max}/cm^{-1} 3058, 2923, 2856, 1548, 1445, 1240, 1047, 806, 687. HRMS (ESI): *m/z* calcd for $C_{14}H_{11}NO+H^+$ $[M+H]^+$ 210.0919, found 210.0913.

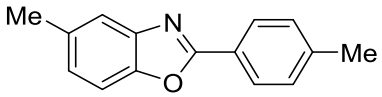

5-Methyl-2-(*p*-tolyl)benzo[*d*]oxazole (14ca): The representative procedure was followed, using **12c** (0.066 g, 0.50 mmol) and 4-iodotoluene (**13a**; 0.164 g, 0.75 mmol). Purification by column chromatography on silica gel (petroleum ether/EtOAc: 50/1 → 30/1) yielded **14ca** as a white solid. Yield: 0.102 g, 91%. M.p. = 139–140 ^oC. ^1H-NMR (400 MHz, $CDCl_3$): δ = 8.13 (d, J = 8.1 Hz, 2H, Ar–H), 7.54 (s, 1H, Ar–H), 7.43 (d, J = 8.2 Hz, 1H, Ar–H), 7.32 (d, J = 8.1 Hz, 2H, Ar–H), 7.14 (d, J = 8.2 Hz, 1H, Ar–H), 2.48 (s, 3H, CH_3), 2.43 (s, 3H, CH_3). ^{13}C-NMR (100 MHz, $CDCl_3$): δ = 163.6 (C_q), 149.1 (C_q), 142.5 (C_q), 142.1 (C_q), 134.4 (C_q), 129.8 (2C, CH), 127.7 (2C, CH), 126.1 (CH), 124.7 (C_q), 119.9 (CH), 110.0 (CH), 21.8 (CH_3), 21.7 (CH_3). IR (neat): ν_{max}/cm^{-1} 3031, 2922, 2863, 1564, 1489, 1264, 1185, 1053, 801. HRMS (ESI): *m/z* calcd for $C_{15}H_{13}NO+H^+$ $[M+H]^+$ 224.1075, found 224.1071.

Characterization data for compounds 16

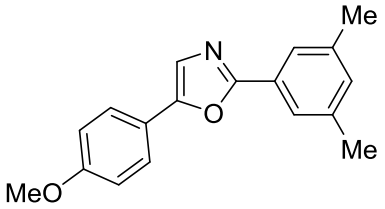

2-(3,5-Dimethylphenyl)-5-(4-methoxyphenyl)oxazole (16ak): The representative procedure was followed, using **15a** (0.088 g, 0.50 mmol) and 1-iodo-3,5-dimethylbenzene (**13k**; 0.174 g, 0.75 mmol). Purification by column chromatography on silica gel (petroleum ether/EtOAc: 10/1 → 5/1) yielded **16ak** as a white solid. Yield: 0.110 g, 79%. M.p. = 80–82 °C. ^{1}H-NMR (500 MHz, $CDCl_3$): δ = 7.72 (s, 2H, Ar–H), 7.66 (d, J = 8.5 Hz, 2H, Ar–H), 7.31 (s, 1H, Ar–H), 7.08 (s, 1H, Ar–H), 6.97 (d, J = 8.5 Hz, 2H, Ar–H), 3.85 (s, 3H, OCH_3), 2.39 (s, 6H, CH_3). ^{13}C-NMR (125 MHz, $CDCl_3$): δ = 161.1 (C_q), 159.9 (C_q), 151.3 (C_q), 138.6 (2C, C_q), 132.1 (CH), 127.5 (C_q), 125.9 (2C, CH), 124.1 (2C, CH), 121.9 (CH), 121.1 (C_q), 114.6 (2C, CH), 55.5 (OCH_3), 21.4 (2C, CH_3). IR (neat): ν_{max}/cm^{-1} 2958, 2916, 2836, 1607, 1497, 1457, 1244, 1176, 1026, 813, 728. HRMS (ESI): *m/z* calcd for $C_{18}H_{17}NO_2$+H^+ $[M+H]^+$ 280.1338, found 280.1332.

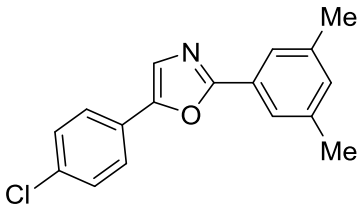

5-(4-Chlorophenyl)-2-(3,5-dimethylphenyl)oxazole (16bk): The representative procedure was followed, using **15b** (0.090 g, 0.50 mmol) and 1-iodo-3,5-dimethylbenzene (**13k**; 0.174 g, 0.75 mmol). Purification by column chromatography on silica gel (petroleum ether/EtOAc: 20/1 → 10/1) yielded **16bk** as a white solid. Yield: 0.110 g, 78%. M.p. = 129–131 °C. ^{1}H-NMR (400 MHz, $CDCl_3$): δ = 7.72 (s, 2H, Ar–H), 7.65 (d, J = 8.7 Hz, 2H, Ar–H), 7.43-4.40 (m, 3H, Ar–H), 7.10 (s, 1H, Ar–H), 2.40 (s, 6H, CH_3). ^{13}C-NMR (100 MHz, $CDCl_3$): δ = 161.9 (C_q), 150.2 (C_q), 138.7 (2C, C_q), 134.2 (C_q), 132.5 (CH), 129.3 (2C, CH), 127.1 (C_q), 126.7 (C_q), 125.5 (2C, CH), 124.3 (2C, CH), 123.9 (CH), 21.4 (2C, CH_3). IR (neat): ν_{max}/cm^{-1} 2959, 2915, 2851, 1531, 1478, 1259, 1085, 1011, 816, 728. HRMS (ESI): *m/z* calcd for $C_{17}H_{14}ClNO$+H^+ $[M+H]^+$ 284.0842, found 284.0837.

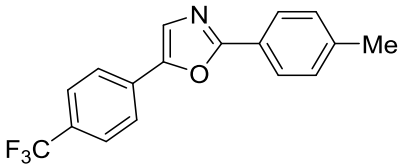

2-(*p*-Tolyl)-5-(4-(trifluoromethyl)phenyl)oxazole (16ca): The representative procedure was followed, using **15c** (0.106 g, 0.50 mmol) and 4-iodotoluene (**13a**; 0.164 g, 0.75 mmol) and the reaction was continued for 24 h. Purification by column chromatography on silica gel (*n* petroleum ether/EtOAc: 10/1 → 5/1) yielded **16ca** as a white solid. Yield: 0.135 g, 89%. M.p. = 157–158 ^{o}C. ^{1}H-NMR (400 MHz, $CDCl_3$): δ = 8.01 (d, J = 7.8 Hz, 2H, Ar–H), 7.80 (d, J = 8.1 Hz, 2H, Ar–H), 7.68 (d, J = 8.3 Hz, 2H, Ar–H), 7.53 (s, 1H, Ar–H), 7.30 (d, J = 7.8 Hz, 2H, Ar–H), 2.42 (s, 3H, CH_3). ^{13}C-NMR (100 MHz, $CDCl_3$): δ = 149.7 (C_q), 141.4 (2C, C_q), 131.5 (C_q), 130.1 (q, $^{2}J_{C–F}$ = 33.1 Hz, C_q), 129.8 (2C, CH), 126.6 (2C, CH), 126.1 (q, $^{3}J_{C–F}$ = 3.9 Hz, 2C, CH), 125.3 (CH), 124.5 (C_q), 124.3 (2C, CH), 124.1 (q, $^{1}J_{C–F}$ = 272.0 Hz, CF_3), 21.8 (CH_3). ^{19}F-NMR (377 MHz, $CDCl_3$): δ = −62.7 (s). IR (neat): ν_{max}/cm^{-1} 3047, 2925, 2862, 1613, 1489, 1326, 1121, 834, 730. HRMS (ESI): *m/z* calcd for $C_{17}H_{12}F_3NO+H^+$ $[M+H]^+$ 304.0949, found 304.0943.

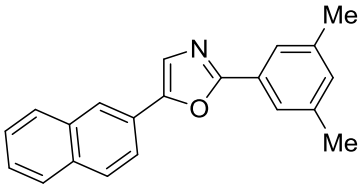

2-(3,5-Dimethylphenyl)-5-(naphthalen-2-yl)oxazole (16dk): The representative procedure was followed, using **15d** (0.098 g, 0.502 mmol) and 1-iodo-3,5-dimethylbenzene (**13k**; 0.174 g, 0.75 mmol). Purification by column chromatography on silica gel (petroleum ether/EtOAc: 20/1 → 10/1) yielded **16dk** as a white solid. Yield: 0.106 g, 71%. M.p. = 134–136 ^{o}C. ^{1}H-NMR (400 MHz, $CDCl_3$): δ = 8.21 (s, 1H, Ar–H), 7.93-7.89 (m, 2H, Ar–H), 7.86-7.84 (m, 1H, Ar–H), 7.79-7.77 (m, 3H, Ar–H), 7.55-7.48 (m, 3H, Ar–H), 7.12 (s, 1H, Ar–H), 2.43 (s, 6H, CH_3). ^{13}C-NMR (100 MHz, $CDCl_3$): δ = 161.9 (C_q), 151.4 (C_q), 138.7 (2C, C_q), 133.6 (C_q), 133.2 (C_q), 132.4 (CH), 128.9 (CH), 128.4 (CH), 128.0 (CH), 127.3 (C_q), 127.0 (CH), 126.7 (CH), 125.5 (C_q), 124.3 (2C, CH), 124.0 (CH), 123.0 (CH), 122.3 (CH), 21.5 (2C, CH_3). IR (neat): ν_{max}/cm^{-1} 2920, 2851, 1561, 1532, 1501, 1261, 1096, 1044, 812, 740. HRMS (ESI): *m/z* calcd for $C_{21}H_{17}NO+H^+$ $[M+H]^+$ 300.1388, found 300.1383.

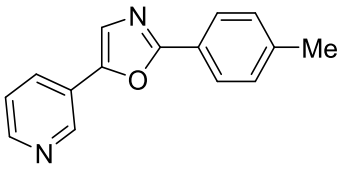

5-(Pyridine-3-yl)-2-(*p*-tolyl)oxazole (16ea): The representative procedure was followed, using **15e** (0.073 g, 0.5 mmol) and 4-iodotoluene (**13a**; 0.164 g, 0.75 mmol). Purification by column chromatography on silica gel (petroleum ether/EtOAc/Et_3N: 5/1/0.05 → 2/1/0.05 → 1/1/0.05) yielded **16ea** as a white solid. Yield: 0.102 g, 86%. M.p. = 81–83 ^oC. ^1H-NMR (400 MHz, $CDCl_3$): δ = 8.99 (s, 1H, Ar–H), 8.57 (s, 1H, Ar–H), 8.00-7.96 (m, 3H, Ar–H), 7.51 (s, 1H, Ar–H), 7.39-7.28 (m, 3H, Ar–H), 2.41 (s, 3H, CH_3). ^{13}C-NMR (100 MHz, $CDCl_3$): δ = 162.4 (C_q), 149.2 (CH), 148.2 (C_q), 145.6 (CH), 141.3 (C_q), 131.3 (CH), 129.8 (2C, CH), 126.6 (2C, CH), 124.8 (CH), 124.6 (C_q), 124.5 (C_q), 123.9 (CH), 21.7 (CH_3). IR(neat): ν_{max}/cm^{-1} 2920, 2854, 1493, 1423, 1327, 1136, 1020, 951, 823, 730. HRMS (ESI): *m/z* calcd for $C_{15}H_{12}N_2O+H^+$ $[M+H]^+$ 237.1028, found 237.1024.

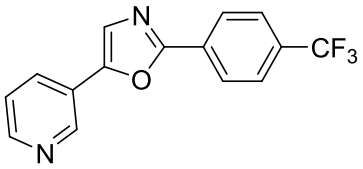

5-(Pyridine-3-yl)-2-(4-(trifluoromethyl)phenyl)oxazole (16ef): The representative procedure was followed, using (**15e**; 0.074 g, 0.506 mmol) and 1-iodo-4-(trifluoromethyl)benzene **13f** (0.20 g, 0.75 mmol). Purification by column chromatography on silica gel (petroleum ether/EtOAc/Et_3N: 5/1/0.05 → 2/1/0.05 → 1/1/0.05) yielded **16ef** as a white solid. Yield: 0.115 g, 78%. M.p. = 128–129 ^oC. ^1H-NMR (500 MHz, $CDCl_3$): δ = 9.01 (s, 1H, Ar–H), 8.61 (s, 1H, Ar–H), 8.22 (d, J = 8.2 Hz, 2H, Ar–H), 8.01 (d, J = 7.6 Hz, 1H, Ar–H), 7.75 (d, J = 7.9 Hz, 2H, Ar–H), 7.58 (s, 1H, Ar–H), 7.42-7.40 (m, 1H, Ar–H). ^{13}C-NMR (125 MHz, $CDCl_3$): δ = 160.7 (C_q), 149.7 (CH), 149.4 (C_q), 145.8 (CH), 132.5 (q, $^2J_{C–F}$ = 32.4 Hz, C_q), 131.7 (CH), 130.3 (C_q), 126.8 (2C, CH), 126.1 (q, $^3J_{C–F}$ = 3.8 Hz, 2C, CH), 125.3 (CH), 124.2 (C_q), 124.0 (CH), 123.9 (q, $^1J_{C–F}$ = 272.8 Hz, CF_3). ^{19}F-NMR (377 MHz, $CDCl_3$): δ = −62.9(s). IR(neat): ν_{max}/cm^{-1} 3061, 2924, 1563, 1482, 1413, 1328, 1119, 862, 701. HRMS (ESI): *m/z* calcd for $C_{15}H_9F_3N_2O+H^+$ $[M+H]^+$ 291.0745, found 291.0739.

Chapter 3

Sterically and electronically distinct (POCN)-pincer palladium for C–H bond arylation of azoles

3.1 Introduction

Chapter 2 demonstrated that the hybrid POCN ligated palladium complexes efficiently catalyze the arylation of azoles with aryl halides. The sterically less bulky catalyst ($^{i\text{Pr2}}$POCN$^{i\text{Pr2}}$)PdCl (**4**) was found to be better than the bulky analog ($^{t\text{Bu2}}$POCN$^{i\text{Pr2}}$)PdCl (**5**) for the direct arylation of azoles. Hence, it was hypothesized that the sterically even less bulky and electronically distinct complexes, such as ($^{i\text{Pr2}}$POCN$^{\text{Et2}}$)PdCl and ($^{\text{Ph2}}$POCN$^{\text{Et2}}$)PdCl might be superior than the previously employed pincer palladium complexes for the arylation of azoles. In this regards, this chapter describes the synthesis and characterization of sterically less hindered and electronically different pincer palladium complexes, ($^{i\text{Pr2}}$POCN$^{\text{Et2}}$)PdCl (**20**), ($^{\text{Ph2}}$POCN$^{\text{Et2}}$)PdCl (**21**) and their derivatives.[293] The catalytic activity of these complexes was studied for the arylation of azole with aryl iodides, and the catalyst **20** was found to be superior than the complexes **4** and **5**. In addition, the catalysis was performed using a mild and inexpensive base K_3PO_4 employing the catalyst **20**.

3.2 Results and discussion

3.2.1 Synthesis of {1-(R_2PO)-C_6H_4-3-(CH_2NEt_2)} ($^{\text{R2}}$POCN$^{\text{Et2}}$)–H ligands

The {1-($^{i}Pr_2$PO)-C_6H_4-3-(CH_2NEt_2)} ($^{i\text{Pr2}}$POCN$^{\text{Et2}}$)–H (**18**) ligand was prepared by the slight modification of the procedure reported for the same by Zargarian and van der Est (Scheme 3.1).[294] First, the 3-hydroxy benzyl bromide was treated with two equivalents of diethylamine in acetone to obtain the colorless product of 3-((diethylamino)methyl)phenol (**17**) in excellent yield. The 3-((diethylamino)methyl)phenol was well characterized by ^{1}H and ^{13}C NMR spectroscopy. The treatment of **17** with NaH at 70 ^{o}C followed by the phosphination with chlorodiisopropylphosphine ($^{i}Pr_2$PCl) produced the ligand ($^{i\text{Pr2}}$POCN$^{\text{Et2}}$)–H (**18**) as a viscous liquid in 86% yield. The ^{31}P{^{1}H} NMR spectrum of **18** showed a single resonance at 146.6 ppm (for O-P$^{i}Pr_2$ moiety). The ^{1}H, ^{13}C and ^{31}P NMR data of compound **18** are in good agreements with that reported for the same by Zargarian and van der Est.[294]

The in-situ generation of {1-(Ph_2PO)-C_6H_4-3-(CH_2NEt_2)} ($^{\text{Ph2}}$POCN$^{\text{Et2}}$)–H (**19**) ligand was reported by the Song and co-workers,[295] without the isolation and characterization of the same. Herein, the ($^{\text{Ph2}}$POCN$^{\text{Et2}}$)–H (**19**) ligand was synthesized and well characterized. Similar to the synthesis of **18**, the ligand precursor ($^{\text{Ph2}}$POCN$^{\text{Et2}}$)–H (**19**) was synthesized from the reaction of 3-((diethylamino)methyl)phenol (**17**) with the chlorodiphenylphosphine (Ph_2PCl) (Scheme 3.1). The compound **19** was obtained as a viscous liquid in 77% yield. The ^{31}P{^{1}H} NMR spectrum of **19** displayed a singlet at 110.1 ppm (for O-PPh_2 moiety), which is

consistent with the ^{31}P NMR data reported for the analog compound *i.e.* (^{Ph2}POCOP^{Ph2})–H[296] (δ 112.0 ppm). The compound **19** was characterized by ^{1}H and ^{13}C NMR spectroscopy. The crude compounds **18** and **19** were used for the complexation reactions without further purification.

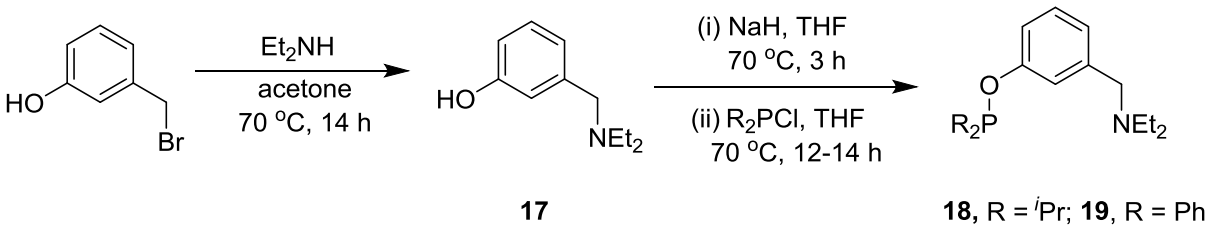

17 **18,** R = ^{i}Pr; **19**, R = Ph

Scheme 3.1 Synthesis of (^{R2}POCN^{Et2})–H ligands

3.2.2 Synthesis of (^{R2}POCN^{Et2})PdCl complexes and their derivatives

The complexation of the crude ligand **18** with (COD)$PdCl_2$ in the presence of K_3PO_4 in 1,4-dioxane at 70 °C afforded the complex [{2-(^{i}Pr$_2$PO)-C_6H_3-6-(CH_2NEt_2)}PdCl] (^{iPr2}POCN^{Et2})PdCl (**20**) as a light yellow solid after purification by column chromatography on neutral alumina (Scheme 3.2). The ^{31}P{^{1}H} NMR spectrum of **20** shows a singlet at δ 199.3 ppm, which is comparable with the ^{31}P NMR data reported for the similar compound (^{iPr2}POCN^{iPr2})PdCl (δ_P 198.9 ppm). In the ^{1}H NMR spectrum of **20**, the splitting pattern in the aromatic region clearly suggested the formation of a pincer-palladium complex, which is again evident from the disappearance of the peak corresponding to the apical proton. In the ^{1}H NMR spectrum of **20**, four protons on two $–CH_2$ groups of $–NEt_2$ appeared as a distinct sextet and a septet, against a single quartet for the same protons in the spectrum of the free-ligand **18**. This noticeable change in the splitting pattern of the $–CH_2$ peak in the ^{1}H NMR spectrum could be treated as an evidence of the N-arm coordination of the ligand to the palladium center. The ^{13}C NMR, HRMS, and elemental analysis data of **20** are in good agreement with the assigned molecular structure.

Complex (^{Ph2}POCN^{Et2})PdCl (**21**) was previously reported *via* the one-pot phosphorylation/palladation synthetic route, starting from 3-((diethylamino)methyl)phenol, diphenylchlorophosphine and palladium chloride by Song and co-workers,[295] without the isolation and characterization of the ligand precursor (^{Ph2}POCN^{Et2})–H (**19**). Herein, the ligand (^{Ph2}POCN^{Et2})–H (**19**) was synthesized and characterized, and the complexation was carried out by the modification of the reported procedure (Scheme 3.2). Metalation of the compound

19 with $Pd(COD)Cl_2$ in the presence of K_3PO_4 in 1,4-dioxane at 70 ^oC produced the complex [{2-(Ph_2PO)-C_6H_3-6-(CH_2NEt_2)}PdCl] ($^{Ph2}POCN^{Et2}$)PdCl (**21**). The $^{31}P\{^1H\}$ NMR spectrum of **21** showed a single peak at δ 151.5 ppm. The ^1H and ^{13}C NMR data of **21** are consistent with the literature reported data for the same compound by Song and co-workers.[295]

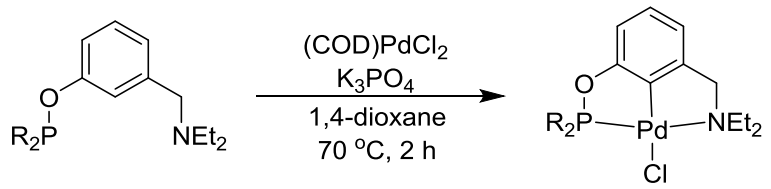

18, R= ^{i}Pr; **19**, R = Ph **20**, R= ^{i}Pr; **21**, R = Ph

Scheme 3.2 Synthesis of ($^{R2}POCN^{Et2}$)PdCl complexes

The palladium derivatives ($^{iPr2}POCN^{Et2}$)PdX (X = I, OAc, OTf) were synthesized from the complex ($^{iPr2}POCN^{Et2}$)PdCl to understand the reactivity pattern. Thus, the treatment of ($^{iPr2}POCN^{Et2}$)PdCl (**20**) with KI in dichloromethane and methanol solvent mixture in a round bottom flask gave ($^{iPr2}POCN^{Et2}$)PdI (**22**) at room temperature (Scheme 3.3). The reactions of ($^{iPr2}POCN^{Et2}$)PdCl with AgOAc and AgOTf in THF at room temperature afforded ($^{iPr2}POCN^{Et2}$)Pd(OAc) (**23**) and ($^{iPr2}POCN^{Et2}$)Pd(OTf) (**24**) in 99% and 79% yields, respectively (Scheme 3.3). The ^{31}P NMR spectrum of ($^{iPr2}POCN^{Et2}$)PdI **22** shows a single resonance at 205.3 ppm, whereas that of ($^{iPr2}POCN^{Et2}$)Pd(OAc) (**23**) and ($^{iPr2}POCN^{Et2}$)Pd(OTf) (**24**) resonates at 196.7 and 199.4 ppm respectively. All these ($^{iPr2}POCN^{Et2}$)PdX derivatives were characterized by ^1H, ^{13}C and HRMS spectroscopy. Further, the structures of all these complexes were elucidated by single crystal X-ray technique.

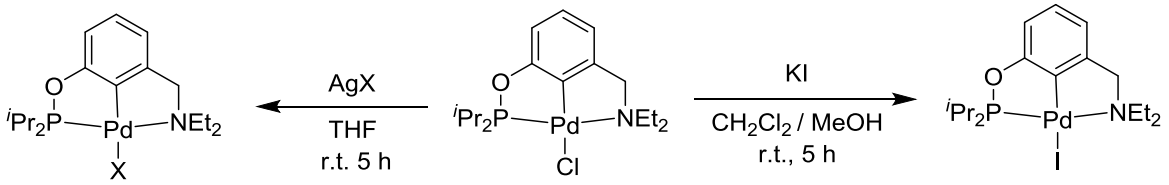

23; X = OAc; **24**; X = OTf **20** **22**

Scheme 3.3 Synthesis of ($^{iPr2}POCN^{Et2}$)PdX complexes

3.2.3 Crystal structure description

The single X-ray crystal structures of complexes **20**, **22**, **23**, and **24** are shown in Figure 3.1. Selected bond lengths and bond angles are listed in Table 3.1. The coordination geometry around palladium is approximately square-planar in ($^{i\text{Pr}2}$POCN$^{\text{Et}2}$)PdCl (**20**) complex (Figure 3.1 A). The Pd–P bond length in **20** is 2.1895(12) Å, almost the same as that observed in ($^{i\text{Pr}2}$POCN$^{i\text{Pr}2}$)PdCl (**4**) (Pd–P = 2.1890(6) Å). The Pd–N bond length is 2.192(4) Å, slightly shorter than that in ($^{i\text{Pr}2}$POCN$^{i\text{Pr}2}$)PdCl (Pd–N = 2.2204(17) Å). This value suggests that a stronger coordination of the amino group towards the Pd-center in **20** than the complex **4**. The Pd–C and Pd–Cl bond lengths are 1.955(4) and 2.3889(12) Å, respectively, which are comparable with the corresponding bond lengths in **4** (Pd–C = 1.956(2), Pd–Cl = 2.3922(6) Å). The P(1)–Pd(1)–N(1) bond angle (162.53(11)º) of **20** is comparable with that of **4** (162.10(5)º). The C(1)–Pd–N(1) bond angle is 82.4(2)º, slightly greater than that of ($^{i\text{Pr}2}$POCN$^{i\text{Pr}2}$)PdCl (81.84(8)º). The N(1)–Pd–Cl(1) bond angle of **20** (97.14(11)º) is significantly smaller than that of **4** (100.79(5)º), which indicates that the Pd–Cl bond is aligned more towards the amino group in **20** than the Pd–Cl bond in **4**. All these bond angles seem consistent with the less steric impact exerted by the –NEt_2 group in ($^{i\text{Pr}2}$POCN$^{\text{Et}2}$)PdCl than the –$N^{i}Pr_2$ group in ($^{i\text{Pr}2}$POCN$^{i\text{Pr}2}$)PdCl.

In the case of ($^{i\text{Pr}2}$POCN$^{\text{Et}2}$)PdI (**22**), the coordination geometry around palladium is distorted square planar (Figure 3.1 B). The Pd–C(*ipso*) bond length of **22** is 1.965(2) Å is similar to the Pd–C bond length 1.955(4) Å of ($^{i\text{Pr}2}$POCN$^{\text{Et}2}$)PdCl (**20**); whereas the Pd–I bond length (2.6825(2) Å) is slightly larger than the corresponding Pd–Cl bond length (2.3889(12) Å) of **20** (Figure 3.1). This could be due to the larger size of iodide atom. The Pd–N bond length 2.185(2) Å in **22** is comparable with the Pd–N bond length (2.192(4) Å) observed for **20**. The P–Pd–N bond angle 162.45 (6)° of **22** is similar to the palladium complex **20** (P–Pd–N, 162.53(11)°). The C–Pd–P bond angle 80.21(7)° of ($^{i\text{Pr}2}$POCN$^{\text{Et}2}$)PdI is similar with the ($^{i\text{Pr}2}$POCN$^{\text{Et}2}$)PdCl **20** (C–Pd–P; 80.08 (18)°). The Pd–C(*ipso*) bond length (1.965(2)) Å in ($^{i\text{Pr}2}$POCN$^{\text{Et}2}$)PdI is similar to the Pd–C(*ipso*) bond length (1.955(4)) Å for ($^{i\text{Pr}2}$POCN$^{\text{Et}2}$)PdCl.

For ($^{i\text{Pr}2}$POCN$^{\text{Et}2}$)PdOAc (**23**), the geometry around palladium is distorted square planar (Figure 3.1 C). The Pd–C(*ipso*) bond length is 1.946(2) Å is similar to the Pd–C bond length 1.955(4) Å of ($^{i\text{Pr}2}$POCN$^{\text{Et}2}$)PdCl; whereas the Pd–O bond length is the (2.0960(16) Å). This could be due to the electron withdrawing nature of acetate makes the shorter bond distance of Pd–O bond. The Pd–P bond length 2.2026(5) Å in **23** is slightly longer than the corresponding Pd–P bond length (2.1895(12) Å) in **20**. This could be due to the acetate group, as oxygen atom is directly bound to the palladium which makes Pd–P bond strong which

affect the elongation of the Pd–P bond. The Pd–N bond length 2.1633(17) Å in **23** is comparable with the Pd–N bond length (2.192(4) Å) observed for **20**.[286] The P–Pd–N bond angle 162.87(5)° of ($^{i\text{Pr2}}$POCN$^{\text{Et2}}$)PdOAc is similar to the palladium complex ($^{i\text{Pr2}}$POCN$^{\text{Et2}}$)PdCl (P–Pd–N, 162.53(11)°). The C–Pd–P bond angle (80.68(6)°) of **23** is similar with the **20** (C–Pd–P; 80.08 (18)°). The C–Pd–N bond angle (82.22(8)°) is slightly greater than the C–Pd–P bond angle (80.68(6)°) for ($^{i\text{Pr2}}$POCN$^{\text{Et2}}$)PdOAc.

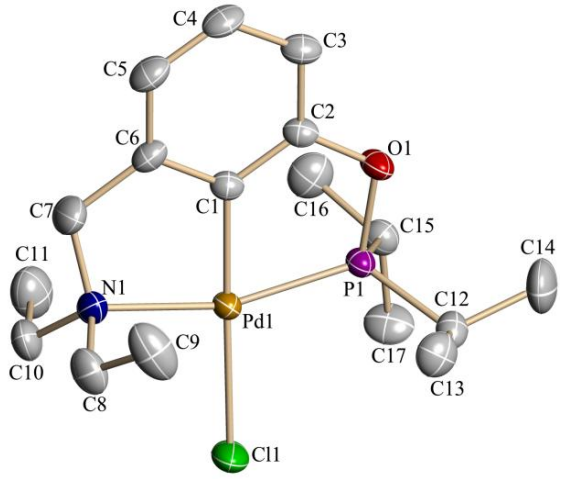

(**A**): ($^{i\text{Pr2}}$POCN$^{\text{Et2}}$)PdCl (**20**)

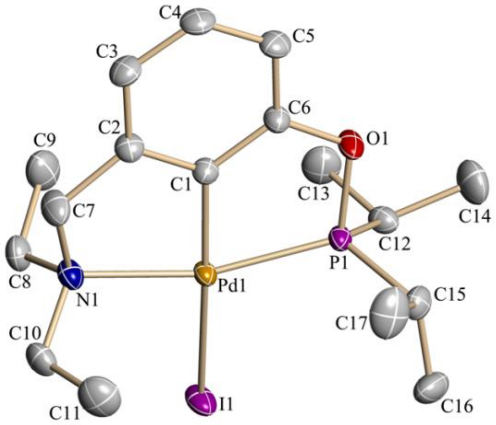

(**B**): ($^{i\text{Pr2}}$POCN$^{\text{Et2}}$)PdI (**22**)

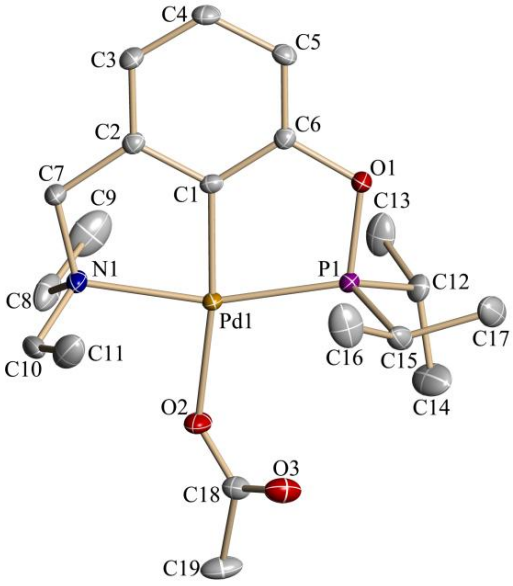

(**C**): ($^{i\text{Pr2}}$POCN$^{\text{Et2}}$)PdOAc (**23**)

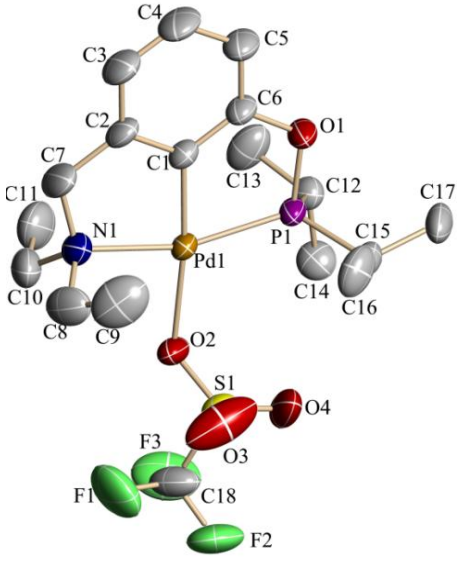

(**D**): ($^{i\text{Pr2}}$POCN$^{\text{Et2}}$)PdOTf (**24**)

Figure 3.1 ORTEP diagrams of complexes **20**, **22**, **23** and **24**.

Table 3.1 Selected bond lengths (Å) and bond angles (^{o}) for **20**, **22**, **23** and **24**

Bond length (Å)		Bond angles (^{o})	
Complex 20			
Pd(1)–C(1)	1.955(4)	C(1)–Pd(1)–P(1)	80.08(18)
Pd(1)–P(1)	2.1895(12)	C(1)–Pd(1)–N(1)	82.4(2)
Pd(1)–N(1)	2.192(4)	P(1)–Pd(1)–N(1)	162.53(11)
Pd(1)–Cl(1)	2.3889(12)	C(1)–Pd(1)–Cl(1)	175.41(13)
		P(1)–Pd(1)–Cl(1)	100.30(5)
		N(1)–Pd(1)–Cl(1)	97.14(11)
Complex 22			
Pd(1)–C(1)	1.965(2)	C(1)–Pd(1)–P(1)	80.21(7)
Pd(1)–P(1)	2.1959(7)	C(1)–Pd(1)–N(1)	82.25(9)
Pd(1)–N(1)	2.185(2)	P(1)–Pd(1)–N(1)	162.45(6)
Pd(1)–I(1)	2.6825(2)	C(1)–Pd(1)–I (1)	172.74(7)
		P(1)–Pd(1)–I (1)	99.531(18)
		N(1)–Pd(1)–I (1)	97.92(6)
Complex 23			
Pd(1)–C(1)	1.946(2)	C(1)–Pd(1)–P(1)	80.68(6)
Pd(1)–P(1)	2.2026(5)	C(1)–Pd(1)–N(1)	82.22(8)
Pd(1)–N(1)	2.1633(17)	P(1)–Pd(1)–N(1)	162.87(5)
Pd(1)–O(2)	2.0960(16)	C(1)–Pd(1)–O(2)	171.64(7)
C(18)–O(2)	1.271(3)	P(1)–Pd(1)–O(2)	106.30(5)
C(18)–O(3)	1.225(3)	N(1)–Pd(1)–O(2)	90.82(6)
Complex 24			
Pd(1)–C(1)	1.932(5)	C(1)–Pd(1)–P(1)	80.27(16)
Pd(1)–P(1)	2.219(14)	C(1)–Pd(1)–N(1)	82.5(2)
Pd(1)–N(1)	2.169(4)	P(1)–Pd(1)–N(1)	162.78(13)
Pd(1)–O(1)	2.176(3)	C(1)–Pd(1)–O(2)	174.12(18)
		P(1)–Pd(1)–O(2)	105.50(10)
		N(1)–Pd(1)–O(2)	91.68(16)

The X-ray structure for ($^{i\text{Pr}2}$POCN$^{\text{Et}2}$)PdOTf (**24**) is shown in Figure 3.1(D). The Pd–C(*ipso*) bond length is 1.932(5) Å is similar to the Pd–C bond length 1.946(2) Å of **24**; whereas the Pd–O bond length (2.176(3)) Å is slightly longer than the corresponding bond length (2.0960(12) Å) of ($^{i\text{Pr}2}$POCN$^{\text{Et}2}$)PdOAc (**23**). This could be due to the electron donation of oxygen which binds to Pd is decreased as it is attached to $–SO_2CF_3$. The Pd–P bond length (2.2195(14)) Å in **24** is similar to the corresponding Pd–P bond length (2.2026(5)

Å) for **23**. The Pd–N bond length 2.169(4) Å in **24** is comparable with the Pd–N bond length (2.1633(17) Å) observed for **23**. The C–Pd–N bond angle (82.5(2)°) is slightly greater than the C–Pd–P bond angle (80.27(16)°) for **24**. The Pd–C(*ipso*) bond length is 1.932(5) Å is slightly shorter than the corresponding Pd–C bond length 1.946(2) Å of ($^{i\text{Pr2}}$POCN$^{\text{Et2}}$)PdOAc (**23**).

3.2.4 Catalytic activity for arylation of azoles

3.2.4.1 Optimization of catalytic condition

Sterically and electronically distinct hybrid complexes ($^{i\text{Pr2}}$POCN$^{\text{Et2}}$)PdCl (**20**) and ($^{\text{Ph2}}$POCN$^{\text{Et2}}$)PdCl (**21**) along with the most common symmetrical complexes ($^{i\text{Pr2}}$PCP$^{i\text{Pr2}}$)PdCl and ($^{i\text{Pr2}}$POCOP$^{i\text{Pr2}}$)PdCl were screened and optimized for the direct arylation of azoles with aryl iodides. After screening various reaction parameters (see Table 3.2), it was found that 0.5 mol% of the catalyst ($^{i\text{Pr2}}$POCN$^{\text{Et2}}$)PdCl (**20**) along with CuI (1.0 mol%) catalyzed the arylation of benzothiazole (**12a**) with 4-iodotoluene (**13a**) to produce the arylated product 2-(*p*-tolyl)benzothiazole (**14aa**) in 98% yield in the presence of K_3PO_4 in DMF. Though the use of Cs_2CO_3 base with catalyst ($^{i\text{Pr2}}$POCN$^{i\text{Pr2}}$)PdCl (**4**) shows very efficient arylation of azoles,[286] the same base with ($^{i\text{Pr2}}$POCN$^{\text{Et2}}$)PdCl (**20**) catalyst is less effective (Table 3.2, entry 1). The most common symmetrical pincer palladium complexes ($^{i\text{Pr2}}$PCP$^{i\text{Pr2}}$)PdCl and ($^{i\text{Pr2}}$POCOP$^{i\text{Pr2}}$)PdCl were shown to have very poor catalytic performance for the arylation of benzothiazole with 4-iodotoluene and produced the coupled product **14aa** in 54% and 22% yields, respectively (Table 3.2 ; entries 11,12). The ($^{\text{Ph2}}$POCN$^{\text{Et2}}$)PdCl (**21**) is less effective for the formation of arylated product **14aa** (Table 3.2, entry 9). Other solvent such as DMSO gives a good yield for arylated product (Table 3.2, entry 7), while toluene gives diminished yield for the same (Table 2.4, entry 8).

Table 3.2 Optimization of reaction conditions for arylation of azole[a]

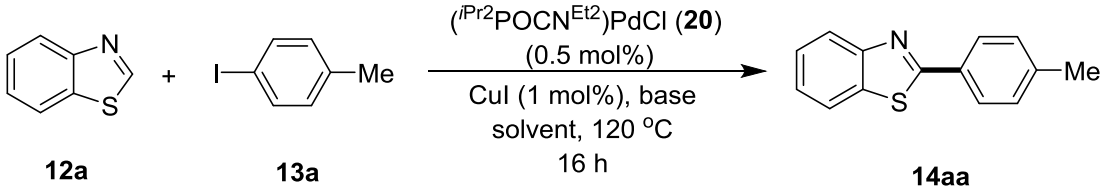

12a 13a 14aa

Entry	Pd-catalyst	Base	Solvent	Yield (%)[b]
1	**20**	Cs_2CO_3	DMF	76[c]
2	**20**	CsOAc	DMF	17
3	**20**	K_2CO_3	DMF	8
4	**20**	Na_2CO_3	DMF	6
5	**20**	**K_3PO_4**	**DMF**	**98**[c]
6	**20**	K_3PO_4	DMAc	83
7	**20**	K_3PO_4	DMSO	85[c]
8	**20**	K_3PO_4	Toluene	36
9	**21**	K_3PO_4	DMF	32
10	**5**	K_3PO_4	DMF	87[c]
11	(^{iPr2}PCP^{iPr2})PdCl	K_3PO_4	DMF	54
12	(^{iPr2}POCOP^{iPr2})PdCl	K_3PO_4	DMF	22

[a] Reaction Conditions: Benzothiazole (0.068 g, 0.5 mmol), 4-iodotoluene (0.163 g, 0.75 mmol), base (0.75 mmol), catalyst (0.0025 mmol), CuI (0.001 g, 0.005 mmol), solvent (2.0 mL). [b] GC yield using mesitylene as internal standard. [c] Yield of isolated compound.

3.2.4.2 Comparison of catalytic activity of (^{R2}POCN$^{R'2}$)PdX complexes

The rate of the arylation using various catalysts was measured to know their relative activity. All the kinetic experiments were performed in the flame-dried screw-capped tubes under an argon atmosphere. In the standard kinetic experiment, 1.25 mM of ($^{R'2}$POCN^{R2})Pd-catalyst, 2.50 mM of CuI, 0.108 M mesitylene (internal standard), benzothiazole (**12a**, 0.25 M), 4-iodotoluene (**13a**, 0.375 M) and K_3PO_4 (0.75 mmol) were taken, and DMF was added to make the total volume 2.0 mL. All the reactions were conducted at 120 ^{o}C, and the progress of the reaction was monitored by gas chromatography (GC) at regular intervals. The initial rates for the formation of arylated product **14aa** with different concentration of ($^{R'2}$POCN^{R2})Pd-catalyst have shown in Table 3.3.

Initial rates for the formation of arylated product **14aa** using different pincer palladium catalysts (^{iPr2}POCN^{Et2})PdCl, (^{iPr2}POCN^{iPr2})PdCl, (^{tBu2}POCN^{iPr2})PdCl, and (^{Ph2}POCN^{Et2})PdCl were measured to be 16.0 x 10^{-4}, 9.8 x 10^{-4}, 2.2 x 10^{-4} and 6.2 x 10^{-4} Mmin^{-1}, respectively

(Figure 3.2). Figure 3.2 clearly shows that the activity of a less bulky (^{iPr2}POCN^{Et2})Pd-catalyst is higher than the sterically bulky analogs, which supports the hypothesis. This catalyst system is much more efficient than the literature reported palladium-catalysts for the arylation of azoles in terms of higher turnover numbers.[172,176,181,280]

Table 3.3 Rate of the arylation reaction with various (POCN)PdCl catalysts

Experiment	Catalyst	Amount of catalyst (g)	Initial rate [Mmin^{-1}] x 10^{-3}
1	(^{iPr2}POCN^{Et2})PdCl	0.00109	1.33
2	(^{iPr2}POCN^{iPr2})PdCl	0.0011	1.10
3	(^{Ph2}POCN^{Et2})PdCl	0.00126	0.59
4	(^{tBu2}POCN^{iPr2})PdCl	0.00123	0.22

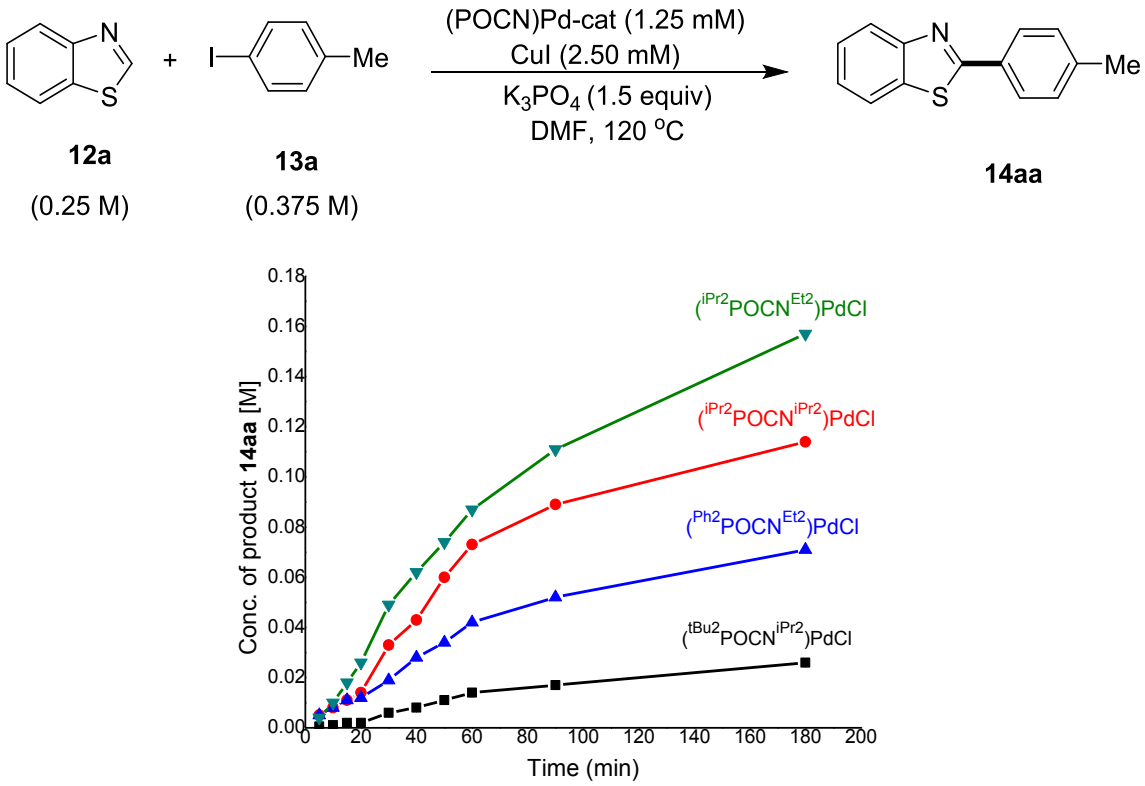

Figure 3.2 Time-dependent formation of **14aa** using various (POCN)Pd catalysts. Conditions: Benzothiazole (**12a**) (0.0675 g, 0.5 mmol), 4-iodotoluene (**13a**) (0.163 g, 0.75 mmol), K_3PO_4 (0.75 mmol), DMF (2 mL).

3.2.4.3 Substrate scope for arylation of azoles using (^{iPr2}POCN^{Et2})PdCl (20)

With the optimized reaction conditions in hand, the catalyst (^{iPr2}POCN^{Et2})PdCl (**20**) was employed for the arylation of various substituted-benzothiazoles and azoles with diverse aryl

iodides to obtain the desired products in moderate to good yields (Scheme 3.4). The coupling of electron-deficient aryl iodides **13f** and **13n** with benzothiazole gave coupled products **14af** and **14an** in moderate to good yields. Various functional groups, such as –OMe, –F, –Cl, –Br, $–CF_3$, –COOMe were tolerated on the aryl iodides backbone (**14ac**-**14an**). Aryl iodides containing heteroatoms were efficiently coupled with benzothiazole to afford the desired

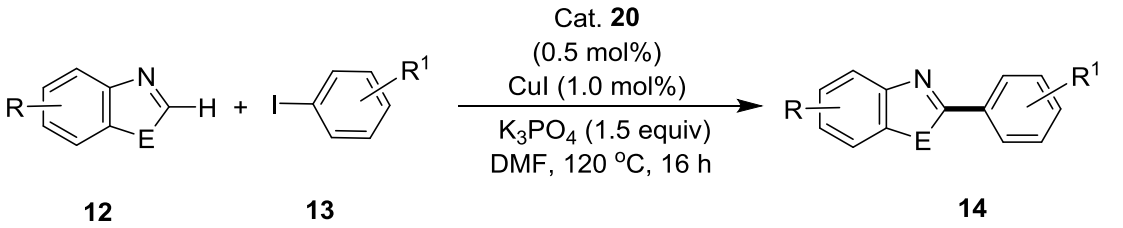

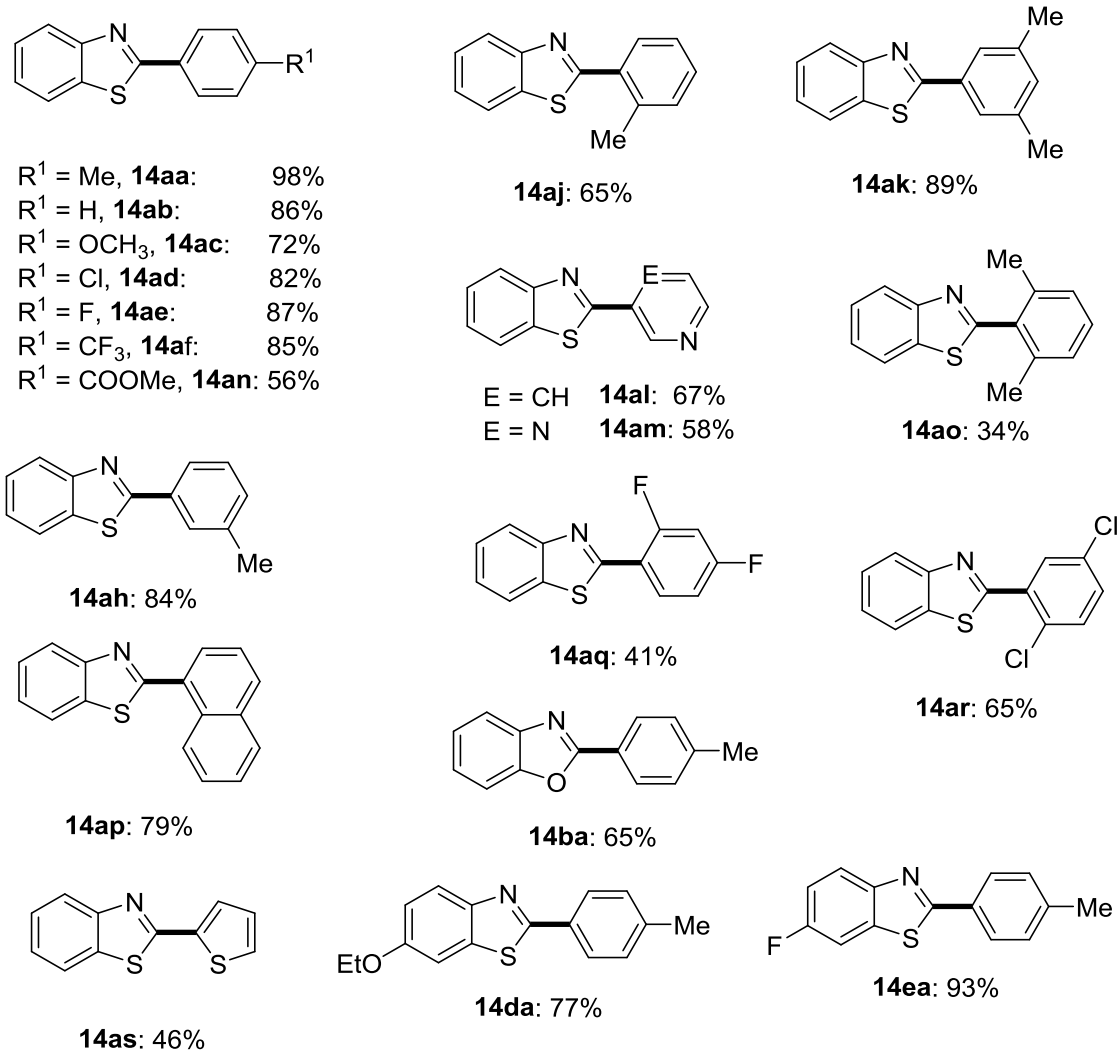

Scheme 3.4 Substrate scope of the (^{iPr2}POCN^{Et2})PdCl (**20**)-catalyzed arylations of azoles

coupling products **14al** and **14am** in good yields. This catalyst system shows coupling of sterically hindered *ortho*-disubstituted aryl iodide with benzothiazole to afford product **14ao** in moderate yield. However, the dichloro- and difluoro-substituted aryl iodides reacted with

the benzothiazole in moderate yields. Using this method, 5-substituted benzothiazoles (**14d**, **14e**) can be coupled with aryl iodide to give desired products. The aryl iodide such as 2-iodothiophene to provide coupled product **14as** in moderate yield (Scheme 3.4).

Similarly, this catalytic system was utilized for the arylation of 5-substituted oxazole with various aryl iodides (Scheme 3.5). Azoles containing electron electron-donating (**15a**) and electron-withdrawing substituents (**15c**) on aryl backbone reacted with aryliodide to gave **16aa** and **16ca** in good yield. Functional groups, such as –Cl and –OMe, as well as heteroarenes substituent like pyridine, were tolerated on azole substrate.

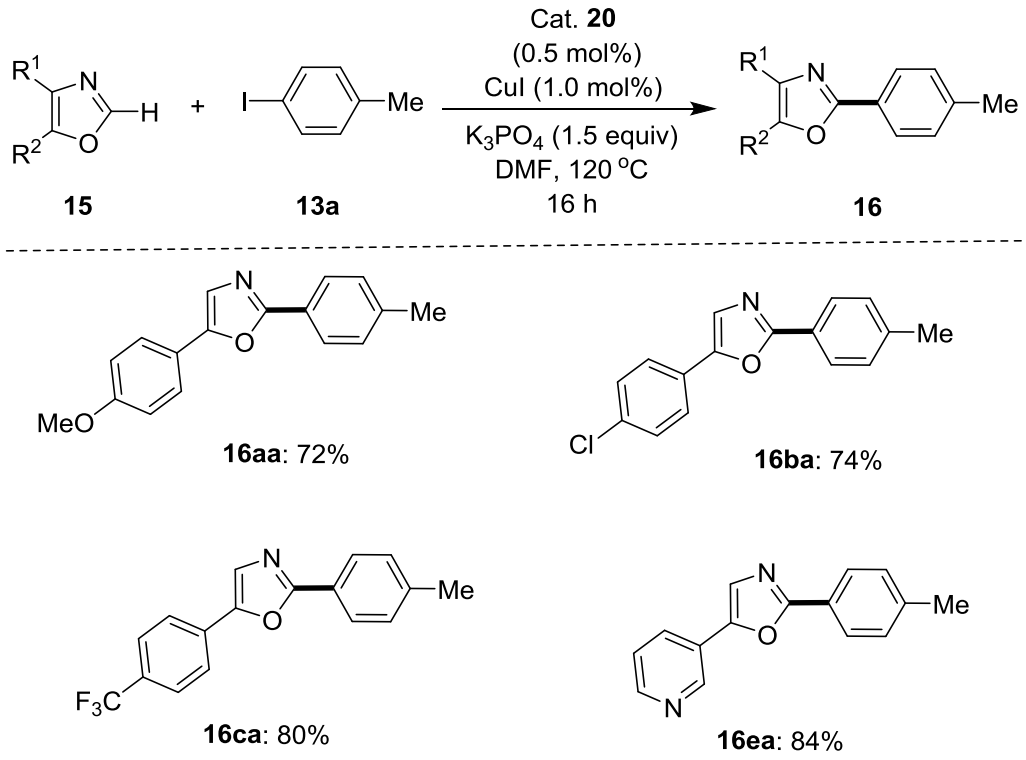

Scheme 3.5 Coupling of 5-substituted oxazole with aryl iodide using ($^{i\text{Pr}2}$POCN$^{\text{Et}2}$)PdCl

3.3 Conclusion

Synthesis and characterization of sterically less hindered pincer palladium complexes, ($^{i\text{Pr}2}$POCN$^{\text{Et}2}$)PdCl and ($^{\text{Ph}2}$POCN$^{\text{Et}2}$)PdCl is described. The derivatives of ($^{i\text{Pr}2}$POCN$^{\text{Et}2}$)PdCl, such as ($^{i\text{Pr}2}$POCN$^{\text{Et}2}$)PdI, ($^{i\text{Pr}2}$POCN$^{\text{Et}2}$)PdOAc and ($^{i\text{Pr}2}$POCN$^{\text{Et}2}$)PdOTf were conveniently synthesized in excellent yields. All the complexes were fully characterized by ^{1}H, ^{13}C, ^{31}P NMR spectroscopy and elemental analyses. Further the molecular structures of ($^{i\text{Pr}2}$POCN$^{\text{Et}2}$)PdCl, ($^{i\text{Pr}2}$POCN$^{\text{Et}2}$)PdI, ($^{i\text{Pr}2}$POCN$^{\text{Et}2}$)PdOAc, ($^{i\text{Pr}2}$POCN$^{\text{Et}2}$)PdOTf were established by the X-ray diffraction studies. The newly synthesized complexes were

employed for the C–H bond arylation of azoles with various aryl iodides. The complex ($^{i\text{Pr}2}$POCN$^{\text{Et}2}$)PdCl shows excellent reactivity compared to ($^{\text{Ph}2}$POCN$^{\text{Et}2}$)PdCl for the arylation reaction. The kinetic study for arylation reaction using the pincer complexes ($^{i\text{Pr}2}$POCN$^{i\text{Pr}2}$)PdCl, ($^{t\text{Bu}2}$POCN$^{i\text{Pr}2}$)PdCl, ($^{i\text{Pr}2}$POCN$^{\text{Et}2}$)PdCl and ($^{\text{Ph}2}$POCN$^{\text{Et}2}$)PdCl reveals that less hindered ($^{i\text{Pr}2}$POCN$^{\text{Et}2}$)PdCl complex show better rate for the formation of arylated product, which justified our hypothesis that the less hindered catalyst would perform better during the arylation reaction.

3.4 Experimental section

3.4.1 Synthesis of 3-((diethylamino)methyl)phenol

To a solution of 3-hydroxy benzyl bromide (5.0 g, 26.73 mmol) in acetone (40 mL) was added diethyl amine (3.91 g, 53.46 mmol) at room temperature. The resultant reaction mixture was refluxed at 60 ^{o}C for 14 h under argon atmosphere. After cooling the reaction mixture to ambient temperature, the solvent was evaporated under reduced pressure and the crude product obtained was treated with $NaHCO_3$ (50 mL, 10% aq solution). The product was extracted with ethyl acetate (20 mL x 3) and combined extracts were dried over $MgSO_4$. Filtration and evaporation of all the volatile gave the colorless liquid product. Yield: 4.11 g, 86%. ^{1}H-NMR (200 MHz, $CDCl_3$): δ = 7.11 (t, J = 7.9 Hz, 1H, Ar–H), 6.81-6.78 (m, 2H, Ar–H), 6.66-6.72 (m, 1H, Ar–H), 3.53 (s, 2H, CH_2), 2.56 (q, J = 7.2 Hz, 4H, CH_2CH$_3$), 1.04 (t, J = 7.2 Hz, 6H, CH$_2$CH_3). ^{13}C-NMR (50 MHz, $CDCl_3$): δ = 156.8 (C_q), 139.8 (C_q), 129.4 (CH), 121.2 (CH), 117.0 (CH), 115.0 (CH), 57.3 (CH_2), 46.5 (2C, CH$_2$CH$_3$), 11.1 (2C, CH$_2$$CH_3$).

3.4.2 Synthesis of $^{\text{R}2}$POCN$^{\text{Et}2}$–H ligands and characterization data

($^{i\text{Pr}2}$POCN$^{\text{Et}2}$)–H (18) [294]**:** To the suspension of NaH (1.023 g, 42.62 mmol) in THF (10 mL) was added a solution of 3-((diethylamino)methyl)phenol (6.366 g, 35.51 mmol) in THF (40 mL) and the resulting mixture was refluxed at 70 ^{o}C for 3 h. The reaction mixture was then cooled to room temperature and a solution of chlorodiisopropylphosphine, ^{i}Pr$_2$PCl (5.42 g, 35.51 mmol) in THF (40 mL) was added, and the resulting reaction mixture was further refluxed at 70 ^{o}C for 12 h. The reaction mixture was cooled to ambient temperature and volatile were evaporated under reduced pressure. The compound was extracted with *n*-hexane (60 mL x 3) and combined *n*-hexane solutions were evaporated under vacuum to obtain ($^{i\text{Pr}2}$POCN$^{\text{Et}2}$)–H (**18**) as a colorless oil. Yield: 9.0 g, 86%. ^{1}H-NMR (500 MHz, C_6D_6): δ =

7.49 (s, 1H, Ar–H), 7.22-7.18 (m, 2H, Ar–H), 7.05 (d, J = 6.7 Hz, 1H, Ar–H), 3.48 (s, 2H, CH_2), 2.45 (q, J = 7.3 Hz, 4H, CH_2CH$_3$), 1.79-1.88 (m, 2H, CH(CH$_3$)$_2$), 1.21 (dd, J = 10.4 Hz, J = 7.0 Hz, 6H, PCH(CH_3)$_2$), 1.05 (dd, $J_{P–H}$ = 15.6 Hz, $J_{H–H}$ = 7.0 Hz, 6H, PCH(CH_3)$_2$), 0.99 (t, J = 7.0 Hz, 6H, CH$_2$CH_3). ^{13}C{^{1}H}-NMR (100 MHz, C_6D_6): δ = 160.2 (d, $J_{P–C}$ = 8.8 Hz, C_q), 142.8 (C_q), 129.3 (CH), 122.2 (CH), 119.2 (d, $J_{P–C}$ = 10.6 Hz, CH), 117.3 (d, $J_{P–C}$ = 10.6 Hz, CH), 58.2 (CH_2), 47.3 (2C, CH$_2$CH$_3$), 28.7 (d, $J_{P–C}$ = 18.7 Hz, 2C, CH(CH$_3$)$_2$), 18.0 (d, $J_{P–C}$ = 20.9 Hz, 2C, CH(CH$_3$)$_2$), 17.2 (d, $J_{P–C}$ = 8.9 Hz, 2C, CH(CH$_3$)$_2$), 12.4 (2C, CH$_2$$CH_3$). ^{31}P{^{1}H}-NMR (202 MHz, C_6D_6): δ = 146.6 (s).

(^{Ph2}POCN^{Et2})–H (19): To the suspension of NaH (0.321 g, 13.38 mmol) in THF (10 mL) was added a solution of 3-((diethylamino)methyl)phenol (2.0 g, 11.15 mmol) in THF (40 mL) and the resulting mixture was refluxed at 70 ^{o}C for 3 h. The reaction mixture was then cooled to room temperature and a solution of chlorodiphenylphosphine, Ph_2PCl (2.46 g, 11.15 mmol) in THF (40 mL) was added and resulting reaction mixture was further refluxed at 70 ^{o}C for 12 h. The reaction mixture was cooled to ambient temperature and volatile were evaporated under reduced pressure. The compound was extracted with *n*-hexane (60 mL x 3) and combined *n*-hexane solutions were evaporated under vacuum to obtain compound ^{Ph2}POCN^{Et2}–H (**19**). Yield: 3.11 g, 77%. ^{1}H-NMR (500 MHz, $CDCl_3$): δ = 7.70-7.67 (m, 3H, Ar–H), 7.46-7.41 (m, 7H, Ar–H), 7.27-7.21 (m, 2H, Ar–H), 7.09-7.04 (m, 2H, Ar–H), 3.60 (s, 2H, CH_2), 2.59-2.52 (m, 4H, CH_2CH$_3$), 1.09 (t, J = 7.0 Hz, 6H, CH$_2$CH_3). ^{13}C{^{1}H}-NMR (50 MHz, $CDCl_3$): δ = 157.4 (d, $J_{P–C}$ = 9.9 Hz, C_q), 142.1 (C_q), 141.2 (d, $J_{P–C}$ = 17.9 Hz, 2C_q), 130.9 (2CH), 130.4 (2CH) 129.8 (2CH), 129.2 (CH), 128.6 (d, $J_{P–C}$ = 6.9 Hz, 4CH), 123.2 (CH), 119.4 (d, $J_{P–C}$ = 10.2 Hz, CH), 117.1 (d, $J_{P–C}$ = 11.3 Hz, CH), 57.5 (CH_2), 46.9 (2C, CH$_2$CH$_3$), 11.9 (s, 2C, CH$_2$$CH_3$). ^{31}P{^{1}H}-NMR (202 MHz, $CDCl_3$): δ = 110.1 (s).

3.4.3 Synthesis of (^{R2}POCN^{Et2})PdX complexes

(^{iPr2}POCN^{Et2})PdCl (20): A mixture of (COD)$PdCl_2$ (0.097 g, 0.34 mmol), compound **18** (0.1 g, 0.34 mmol) and K_3PO_4 (0.083 g, 0.39 mmol) was taken in a Schlenk flask, and 1,4-dioxane (10 mL) was added into it. The reaction mixture was heated at 70 ^{o}C under argon atmosphere for 2 h. The yellowish-black suspension formed was cooled to ambient temperature and filtered through cannula. The filtrate was evaporated under reduced pressure and the crude product was purified by column chromatography on neutral alumina (petroleum ether/EtOAc: 20/1 $\rightarrow$ 5/1) to obtain **20** as light yellow solid. Yield: 0.078 g, 53%. M.p. = 102–104 ^{o}C. ^{1}H-NMR (500 MHz, $CDCl_3$): δ 6.92 (t, J = 7.6 Hz, 1H, Ar–H), 6.64 (d, J = 7.3

Hz, 1H, Ar–H) 6.58 (d, J = 7.6 Hz, 1H, Ar–H), 4.10 (s, 2H, CH_2), 3.36 (app sextet, J = 5.5 Hz, 2H, CH_2CH$_3$), 2.76 (app septet, J = 6.4 Hz, 2H, CH_2CH$_3$), 2.35-2.42 (m, 2H, CH(CH$_3$)$_2$), 1.45 (t, J = 7.3 Hz, 6H, CH$_2$CH_3), 1.39 (dd, $J_{P–H}$ = 19.2 Hz, $J_{H–H}$ = 7.3 Hz, 6H, CH(CH_3)$_2$), 1.28 (dd, $J_{P–H}$ = 15.6 Hz, $J_{H–H}$ = 6.7 Hz, 6H, CH(CH_3)$_2$). ^{13}C{^{1}H}-NMR (100 MHz, CDCl$_3$): δ = 163.5 (d, $J_{P–C}$ = 6.6 Hz, C$_q$), 151.6 (C$_q$), 143.8 (C$_q$), 126.3 (CH), 115.7 (CH), 108.6 (d, $J_{P–C}$ = 15.4 Hz, CH), 65.4 (CH_2), 55.7 (2C, CH$_2$CH$_3$), 29.3 (d, $J_{P–C}$ = 25.4 Hz, 2C, CH(CH$_3$)$_2$), 17.6 (d, $J_{P–C}$ = 5.5 Hz, 2C, CH(CH$_3$)$_2$), 16.9 (2C, CH(CH$_3$)$_2$), 13.4 (2C, CH$_2C$H$_3$). ^{31}P{^{1}H}-NMR (202 MHz, CDCl$_3$): δ = 199.3 (s). HRMS (ESI): *m/z* calcd for $C_{17}H_{29}ClNOPPd–Cl^+$ $[M–Cl]^+$ 400.1020, found 400.1022. Anal. calcd for $C_{17}H_{29}ClNOPPd$: C, 46.80; H, 6.70; N, 3.21. Found: C, 47.07; H, 7.53; N, 2.77.[292]

(^{Ph2}POCN^{Et2})PdCl (21): The procedure similar to the synthesis of **20** was followed, employing (COD)PdCl$_2$ (0.086 g, 0.301 mmol), compound **19** (0.110 g, 0.302 mmol) and K_3PO_4 (0.074 g, 0.350 mmol) in 1,4-dioxane and the reaction mixture was heated at 70 ^{o}C for 3 h. The crude product was purified by column chromatography on neutral alumina (petroleum ether/EtOAc: 20/1 $\rightarrow$ 5/1) to obtain **21** as light yellow solid. Yield: 0.053 g, 35%. M.p. = 213–215 ^{o}C. ^{1}H-NMR (500 MHz, CDCl$_3$): δ 8.02-7.98 (m, 4H, Ar–H), 7.51-7.45 (m, 6H, Ar–H), 7.00 (t, J = 7.3 Hz, 1H, Ar–H), 6.77 (d, J = 7.9 Hz, 1H, Ar–H), 6.71 (d, J = 7.6 Hz, 1H, Ar–H), 4.18 (s, 2H, CH_2), 3.44 (app sextet, J = 6.4 Hz, 2H, CH_2CH$_3$), 2.86 (app septet, J = 6.7 Hz, 2H, CH_2CH$_3$), 1.48 (t, J = 7.3 Hz, 6H, CH$_2$CH_3). ^{13}C{^{1}H}-NMR (100 MHz, CDCl$_3$): δ = 162.2 (d, $J_{P–C}$ = 10.0 Hz, C$_q$), 151.4 (C$_q$), 145.1 (C$_q$), 133.8 (d, $J_{P–C}$ = 53.1 Hz, 2C$_q$), 132.0 (d, $J_{P–C}$ = 2.3 Hz, 2CH), 131.8 (2CH), 131.7 (2CH), 128.9 (d, $J_{P–C}$ = 11.5 Hz, 4CH), 126.9 (CH), 116.2 (CH), 109.6 (d, $J_{P–C}$ = 17.7 Hz, CH), 65.8 (d, $J_{P–C}$ = 2.3 Hz, CH$_2$), 55.8 (d, $J_{P–C}$ = 2.3 Hz, 2C, CH$_2$CH$_3$), 13.6 (2C, CH$_2C$H$_3$). ^{31}P{^{1}H}-NMR (202 MHz, CDCl$_3$): δ = 151.5 (s). HRMS (ESI): *m/z* calcd for $C_{23}H_{25}ClNOPPd–Cl^+$ $[M–Cl]^+$ 468.071; found 468.0709. Anal. calcd for $C_{23}H_{25}ClNOPPd$: C, 54.78; H, 5.00; N, 2.78. Found: C, 54.80; H, 5.01; N, 2.77.

(^{iPr2}POCN^{Et2})PdI (22): To the mixture of **20** (0.05 g, 0.115 mmol) and KI (0.028 g, 0.169 mmol) in a flask was added CH_2Cl_2 (5 mL) and methanol (5 mL), and the reaction mixture was stirred at room temperature for 5 h. The volatiles were evaporated under vacuum and the compound was extracted with diethyl ether (20 mL) and filtered through cannula. The filtrate was evaporated under reduced pressure to obtain compound **22** as light yellow solid. Yield: 0.052 g, 86%. M.p. = 128–130 ^{o}C. ^{1}H-NMR (500 MHz, CDCl$_3$): δ = 6.96 (t, J = 7.7 Hz, 1H, Ar–H), 6.64 (m, 2H, Ar–H), 4.16 (s, 2H, CH_2), 3.55 (app sextet, J = 7.3 Hz, 2H,

C*H*$_2$CH$_3$), 2.85 (app septet, *J* = 6.6 Hz, 2H, C*H*$_2$CH$_3$), 2.38-2.50 (m, 2H, C*H*(CH$_3$)$_2$), 1.45 (dd, J_{P-H} = 7.3 Hz, J_{H-H} = 3.9 Hz, 6H, CH(C*H*$_3$)$_2$), 1.41 (t, J_{H-H} = 7.6 Hz, 6H, CH$_2$C*H*$_3$), 1.27 (dd, J_{P-H} = 15.9 Hz, ^3J = 7.1 Hz, 6H, CH(C*H*$_3$)$_2$). ^{13}C{^{1}H}-NMR (100 MHz, CDCl$_3$): δ = 163.0 (d, J_{P-C} = 6.2 Hz, C$_q$), 152.4 (C$_q$), 147.9 (d, J_{P-C} = 3.9 Hz, C$_q$), 126.4 (CH), 115.4 (CH), 108.6 (d, J_{P-C} = 17.0 Hz, CH), 65.1 (CH$_2$), 57.4 (2C, *C*H$_2$CH$_3$), 29.9 (d, J_{P-C} = 26.2 Hz, 2C, *C*H(CH$_3$)$_2$), 18.6 (d, J_{P-C} = 4.6 Hz, 2C, CH(*C*H$_3$)$_2$), 16.9 (2C, CH(*C*H$_3$)$_2$), 13.8 (2C, CH$_2$*C*H$_3$). ^{31}P{^{1}H}-NMR (202 MHz, CDCl$_3$): δ 205.4 (s). HRMS (ESI): *m/z* calcd for C$_{17}$H$_{29}$INOPPd–I$^+$ [M–I]$^+$ 400.1022; found 400.1021. Anal. calcd for C$_{17}$H$_{29}$INOPPd: C, 38.69; H, 5.54; N, 2.65. Found: C, 39.67; H, 5.66; N, 2.62.

(iPr2POCNEt2)PdOAc (23): The mixture of **20** (0.06 g, 0.138 mmol) and AgOAc (0.044 g, 0.264 mmol) in THF (10 mL) was stirred at room temperature for 5 h. The volatile were evaporated under reduced pressure and the compound was extracted with diethyl ether (20 mL) and filtered through cannula. The filtrate was evaporated under reduced pressure to obtain compound **23** as light yellow solid. Yield: 0.063 g, 99%. M.p. = 125–127 ^{o}C. ^{1}H-NMR (500 MHz, CDCl$_3$): δ = 6.91 (t, *J* = 7.6 Hz, 1H, Ar–H), 6.61 (d, *J* = 7.6 Hz, 1H, Ar–H), 6.56 (d, *J* = 7.9 Hz, 1H, Ar–H), 4.07 (s, 2H, CH$_2$), 3.19-3.13 (m, 2H, C*H*$_2$CH$_3$), 2.82-2.74 (m, 2H, C*H*$_2$CH$_3$), 2.62-2.55 (m, 2H, C*H*(CH$_3$)$_2$), 1.95 (s, C(O)C*H*$_3$), 1.44 (t, *J* = 7.1 Hz, 6H, CH$_2$C*H*$_3$), 1.31 (dd, *J* = 19.5, 7.0 Hz, 6H, CH(C*H*$_3$)$_2$), 1.27 (dd, *J* = 15.0, 6.7 Hz, 6H, CH(C*H*$_3$)$_2$). ^{13}C{^{1}H}-NMR (100 MHz, CDCl$_3$): δ = 176.5 (CO), 164.2 (d, J_{P-C} = 6.9 Hz, C$_q$), 151.0 (C$_q$), 141.1 (d, *J* = 3.9 Hz, C$_q$), 126.1 (CH), 115.4 (CH), 108.3 (d, J_{P-C} = 15.4 Hz, CH), 64.9 (CH$_2$), 55.0 (2C, *C*H$_2$CH$_3$), 29.5 (d, J_{P-C} = 25.4 Hz, 2C, *C*H(CH$_3$)$_2$), 24.1 (C(O)*C*H$_3$), 17.9 (d, J_{P-C} = 6.2 Hz, 2C, CH(*C*H$_3$)$_2$), 16.8 (2C, CH(*C*H$_3$)$_2$), 13.1 (2C, CH$_2$*C*H$_3$). ^{31}P{^{1}H}-NMR (202 MHz, CDCl$_3$): δ = 197.94 (s). HRMS (ESI): *m/z* calcd for C$_{17}$H$_{29}$NOPPd–OAc$^+$ [M–OAc]$^+$ 400.1022; found 400.1021. Anal. calcd for C$_{19}$H$_{32}$NO$_3$PPd: C, 49.63; H, 7.01; N, 3.05. Found: C, 49.07; H, 7.16; N, 2.77.

(iPr2POCNEt2)PdOTf (24): The mixture of **20** (0.05 g, 0.115 mmol) and AgOTf (0.058 g, 0. 229 mmol) in THF (10 mL) was stirred at room temperature for 5 h. The volatiles were evaporated under reduced pressure and the compound was extracted with diethyl ether (20 mL). Filtration and evaporation of the solvent resulted in light yellow compound of **24**. Yield: 0.050 g, 79%. M.p. = 104–106 ^{o}C. H-NMR (500 MHz, CDCl$_3$): δ 6.97 (t, *J* = 6.82 Hz, 1H, Ar-H), 6.64 (d, *J* = 9.0 Hz, 1H, Ar-H) 6.59 (d, *J* = 7.9 Hz, 1H, Ar-H), 4.08 (s, 2H, C*H*$_2$), 3.26-3.19 (m, 2H, C*H*$_2$CH$_3$), 2.76 (apparent septet, *J* = 6.8 Hz, 2H, C*H*$_2$CH$_3$), 2.60-2.53 (m, 2H, C*H*(CH$_3$)$_2$), 1.48 (t, *J* = 7.0 Hz, 6H, CH$_2$C*H*$_3$), 1.40 (dd, J_{P-H} = 19.8, 7.5 Hz, 6H, CH(C*H*$_3$)$_2$),

1.28 (dd, J = 15.4, 7.0 Hz, 6H, CH(CH_3)$_2$). ^{13}C{^{1}H}-NMR (100 MHz, $CDCl_3$): δ = 164.0 (d, J_{P-C} = 6.7 Hz, C_q), 151.1 (C_q), 136.3 (d, J_{P-C} = 1.9 Hz, C_q), 127.2 (CH), 121.2 (q, J_{C-F} = 318.5 Hz, C_q), 116.2 (CH), 109.3 (d, J_{P-C} = 15.2 Hz, CH), 64.2 (CH_2), 55.5 (2C, CH_2CH_3), 29.2 (d, J_{P-C} = 24.8 Hz, 2C, $CH(CH_3)_2$), 17. 7 (d, J_{P-C} = 6.6 Hz, 2C, CH(CH_3)$_2$), 16.8 (s, 2C, CH(CH_3)$_2$), 13.2 (2C, CH_2CH_3). ^{31}P{^{1}H}-NMR (202 MHz, $CDCl_3$): δ = 199.4 (s). HRMS (ESI): *m/z* calcd for $C_{17}H_{29}NOPPd–OTf^+$ $[M–OTf]^+$ 400.102; found 400.1024. Anal. calcd for $C_{18}H_{29}F_3NO_4PPdS$: C, 49.63; H, 7.01; N, 3.05. Found: C, 49.07; H, 7.16; N, 2.77.

3.4.4 Procedure for arylation and characterization data

Representative procedure for azole arylation: Synthesis of 2-(*p*tolyl)benzo[*d*]thiazole (14aa): To a flame-dried screw-capped Schlenk tube equipped with magnetic stir bar was introduced CuI (0.001 g, 0.005 mmol, 1.0 mol%, from the stock solution in CH_3CN) and the solvent was evaporated to dryness under vacuum. Then, 4-iodotoluene (**13a**) (0.163 g, 0.75 mmol), K_3PO_4 (0.159 g, 0.75 mmol) and benzothiazole (**12a**) (0.068 g, 0.50 mmol) were added under argon. To the above mixture was added Pd-catalyst (0.0025 mmol, 0.5 mol%, from a stock solution in DMF) and DMF (2 mL) under argon. The resultant reaction mixture was then degassed, refilled with argon and was stirred at 120 ^{o}C in a pre-heated oil bath for 16 h. At ambient temperature, H_2O (15 mL) was added and the reaction mixture was extracted with EtOAc (20 mL x 3). The combined organic layers were dried over $MgSO_4$ and the solvent was evaporated *in vacuo*. The remaining residue was purified by column chromatography on silica gel (petroleum ether/EtOAc: 30/1→ 20/1) to yield **14aa** as an off-white solid.

Characterization data for new compounds

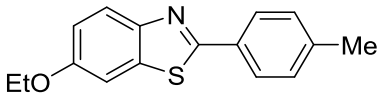

6-Ethoxy-2-(*p*-tolyl)benzo[*d*]thiazole (14ba): The representative procedure was followed, using **12b** (0.0896 g, 0.5 mmol) and 4-iodotoluene (**13a**; 0.163 g, 0.75 mmol). Purification by column chromatography on silica gel (petroleum ether/EtOAc: 10/1→ 2/1) yielded **14ba** as a white solid. Yield: 0.104 g, 77%. ^{1}H-NMR (400 MHz, $CDCl_3$): δ = 7.93-7.91 (m, 3H, Ar–H), 7.32 (d, J = 2.4 Hz, 1H, Ar–H), 7.27 (d, J = 8.1 Hz, 2H, Ar–H), 7.07 (dd, J = 9.0, 2.4 Hz, 1H, Ar–H), 4.08 (q, J = 6.9 Hz, 2H, –OCH_2CH_3), 2.41 (s, 3H, CH_3), 1.45 (t, J = 6.9 Hz, 3H, –OCH_2CH_3). ^{13}C-NMR (100 MHz, $CDCl_3$): δ = 165.8 (C_q), 157.1 (C_q), 148 .7 (C_q), 141.0

(C_q), 136.4 (C_q), 131.2 (C_q), 129.8 (2C, CH), 127.2 (2C, CH), 123.6 (CH), 116.0 (CH), 105.0 (CH), 64.2 (1C, O*C*$H_2$$CH_3$), 21.7 ($CH_3$), 15.0 (1C, O$CH_2$*C*$H_3$). HRMS (ESI): *m/z* calcd for $C_{16}H_{15}NOS+H^+$ $[M+H]^+$ 270.0947; found 270.0947.

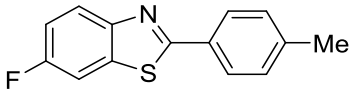

6-Fluoro-2-(*p*-tolyl)benzo[*d*]thiazole (14ca): The representative procedure was followed, using **12c** (0.0765 g, 0.5 mmol) and 4-iodotoluene (**13a**; 0.163 g, 0.75 mmol). Purification by column chromatography on silica gel (petroleum ether/EtOAc: 10/1→ 5/1) yielded **14ca** as a white solid.Yield: 0.113 g, 93%. ^{1}H-NMR (500 MHz, $CDCl_3$): δ = 7.98 (dd, *J* = 8.8, 4.8 Hz, 1H, Ar–H), 7.93 (d, *J* = 8.2 Hz, 2H, Ar–H), 7.54 (dd, *J* = 8.2, 2.7 Hz, 1H, Ar–H), 7.28 (d, *J* = 8.0 Hz, 2H, Ar–H), 7.23-7.19 (m, 1H, Ar–H), 2.42 (s, 3H, CH_3). ^{13}C-NMR (100 MHz, $CDCl_3$): δ = 168.1 (C_q), 160.5 (d, $^1J_{C–F}$ = 246.0 Hz, C_q), 150.9 (C_q), 141.6 (C_q), 136.1 (d, $^3J_{C–F}$ = 10.4 Hz, C_q), 130.8 (C_q), 129.9 (2C, CH), 127.5 (2C, CH), 124.0 (d, $^3J_{C–F}$ = 9.5 Hz, CH), 114.9 (d, $^2J_{C–F}$ = 24.8 Hz, CH), 107.9 (d, $^2J_{C–F}$ = 26.7 Hz, CH), 21.7 (CH_3). HRMS (ESI): *m/z* calcd for $C_{14}H_{10}FNS+H^+$ $[M+H]^+$ 244.0591; found 244.0590.

3.4.5 Procedure for rate measurement of arylation reaction

To the teflon-screw capped tube equipped with magnetic stir bar was introduced palladium catalyst (amount shown in Table 3.3, 0.0025 mmol, from a stock solution), CuI (0.0009 g, 0.005 mmol, from a stock solution), K_3PO_4 (0.159 g, 0.75 mmol), 4-iodotoluene (0.163 g, 0.75 mmol) and benzothiazole (0.0675 g, 0.5 mmol), and DMF (required amount) was added to make the total volume 2.0 mL. To the reaction mixture mesitylene (0.030 mL, 0.2154 mmol) was added as an internal standard. The reaction mixture was then stirred at 120 ^oC in a pre-heated oil bath. At regular intervals, the reaction vessel was cooled to ambient temperature and an aliquot of the sample was withdrawn to the GC vial. The sample was diluted with acetone and subjected to GC analysis. The concentration of the product **14aa** obtained in each sample was determined with respect to the internal standard mesitylene. The data of the concentration of the product *vs* time (min) plot was drawn (Figure 3.5) and fitted linear with Origin Pro 8, and the rate was determined by initial rate method (up to 90 minutes). The slope of the linear fitting represents the reaction rate.

Chapter 4

Mechanistic aspects of (^{R2}POCN^{R2})Pd-catalyzed arylation of azoles

4.1 Introduction

The direct arylation of azoles with aryl halides can be achieved by using transition metal catalysts, such nickel,[188-190,239,240,277] copper,[164,278,279] rhodium,[192,194] palladium [172,174,176, 179-181,275,280,282,297-306] to form the 2-arylated azoles. Among them, the palladium complexes as catalyst are predominantly utilized, because of the user-friendly nature of palladium precursors and the mild reaction conditions.[172,174,176,179-181,275,280,282,297-306] Although, palladium-catalyzed methods have significantly progressed, the in-depth mechanistic studies for the palladium-catalyzed arylation of azoles are unfortunately not available.[307-309] An insightful mechanistic understanding of the direct arylation of azoles is essential to the development of novel palladium catalyst systems that might show increased reactivity at a lower temperature and with the low catalyst loadings. The absence of a comprehensive mechanistic study for this reaction led to the consideration of diverse reaction pathways. For instance, an initial oxidative addition of aryl halides to palladium(0), followed by the electrophilic aromatic substitution of electron-rich azoles and subsequent reductive elimination has been proposed (Figure 4.1A).[175,280] Similarly, Huang and co-workers, as well as others, have described a crucial copper-benzothiazolyl transmetalation to the oxidatively added product $L_nPd(II)(Ar)I$ before the occurrence of the reductive elimination.[180] In contrast to other azoles, a ring-opening pathway in the Pd-catalyzed arylation of benzoxazole has been proposed, which is limited only to the benzoxazole system.[310] In all these proposed mechanisms for the arylation of azoles, special attention has been devoted to the C–H bond cleavage step, as the oxidative addition of Ar–X was proposed to occur at the Pd(0) center and the reaction was proposed to proceed *via* the classical Pd(0)-Pd(II)-Pd(0) catalytic cycle.

In contrast to this, a Pd(II)-Pd(IV)-Pd(II) catalytic cycle for the arylation of azoles can be envisioned if a suitable palladium catalyst system for the arylation reaction is applied. The arylations through the Pd(II)/Pd(IV) process will have many advantages over that with Pd(0)/Pd(II), as in the former, the active catalyst is expected to be highly air- and moisture-stable, and the reaction would exhibit complementary functional group tolerance.[311] Similar mechanistic observations have been made for the arylation of other (hetero)arenes, wherein the strong electrophilic reagents $[Ar_2I]X$,[312-317] or aryl halides with stoichiometric amount of external oxidants were employed.[318-323] Vicente *et al.* have shown the intramolecular $C(sp^2)$–I oxidative addition to a Pd(II)-species during the Heck-type reaction,[151,324] and the intermediacy of similar Pd(IV)-species is assumed in various other arylation reactions.[325,326] However, the arylation of azoles involving the oxidative addition of $C(sp^2)$–X electrophiles, such as aryl halides, to the Pd(II) derivative has not been documented; though the theoretical

work on Pd(II)/Pd(IV) process indicates that the oxidative addition of Ph–I to Pd(II) would be feasible if a suitable ligand system is present.[327]

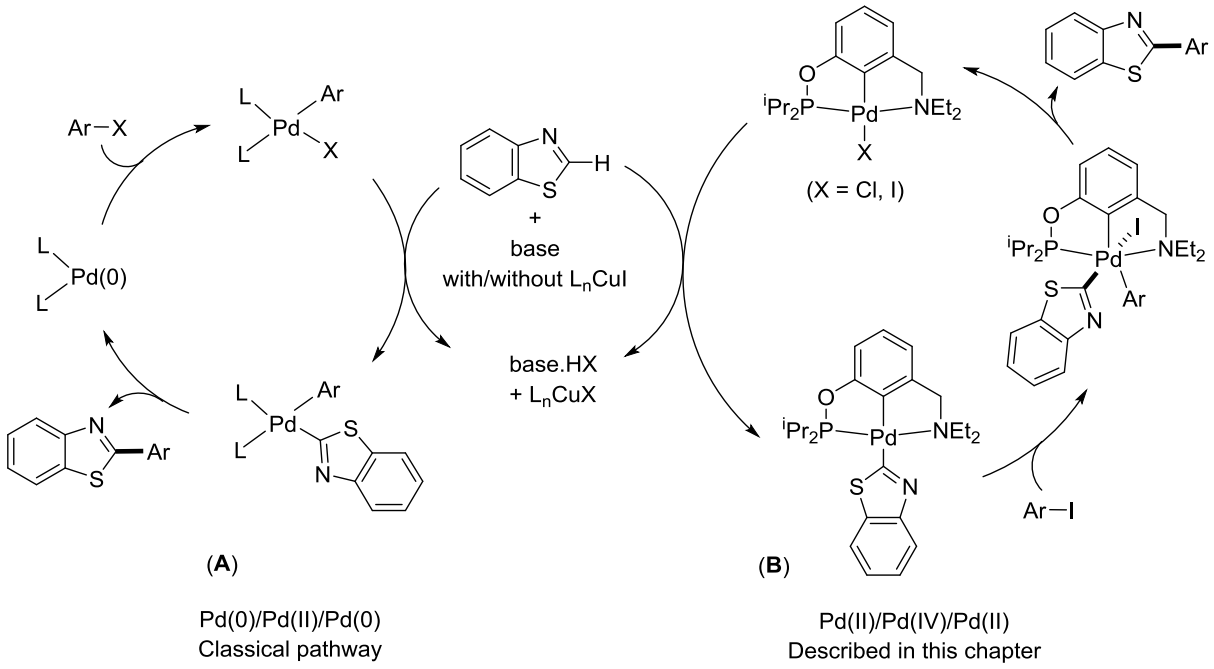

Figure 4.1 Mechanism for arylation of azoles *via* Pd(0)/Pd(II) or Pd(II)/(IV) pathway.

This chapter describes the detailed mechanism of the ($^{i\text{Pr2}}$POCN$^{\text{Et2}}$)Pd-catalyzed arylation of azoles with aryl iodides, wherein Pd(II)/Pd(IV) redox catalytic process has been interpreted (Figure 4.1B). In addition to the detailed kinetic and controlled reactivity studies, the isolation and reactivity of the intermediate species was performed to know the key elementary steps during the azoles arylation. The DFT calculation was carried out to obtain information about the energetically feasible intermediates during the azoles arylation. These investigations have led to the introduction of an advanced mechanistic pathway for the direct arylation of azoles with aryl iodides catalyzed by the ($^{i\text{Pr2}}$POCN$^{\text{Et2}}$)Pd-catalyst.[293]

4.2 Results and discussion

In the Chapters 2 and 3, the synthesis of arene-based hybrid pincer palladium complexes ($^{t\text{Bu2}}$POCN$^{i\text{Pr2}}$)PdCl, ($^{i\text{Pr2}}$POCN$^{i\text{Pr2}}$)PdCl, ($^{i\text{Pr2}}$POCN$^{\text{Et2}}$)PdCl and ($^{\text{Ph2}}$POCN$^{\text{Et2}}$)PdCl is described, and their application for the arylation of azoles with aryl iodides is discussed. These hybrid palladium systems were designed and developed with the assumption that the hemilabile character of POCN-backbone could provide suitable sterics, electronics and

coordination demands that are needed on the different steps of the arylation reaction. The described catalyst system is much efficient than the literature reported palladium-catalysts for the arylation of azoles in terms of higher turnover numbers.[172,176,181,280] Hence, the well-defined nature of the (POCN)Pd-catalyst prompted to carry out detail mechanistic investigation.

The palladium catalysts known for azole arylations generally undergo classical redox process, such as Pd(0)-Pd(II)-Pd(0) cycle. However, a similar cycle for ECE (E = donor atom) pincer complex will decompose the pincer catalyst when palladium enters to zero oxidation state; and concurrently the catalyst might transform to another active species, such as palladium(0) nanoparticles.[38,68,152-154,328] In such cases, the pincer complex do not catalyze the reaction directly, instead, serves as a precatalyst and releases active palladium(0) species. Alternatively, a hypothetical Pd(II)-Pd(IV)-Pd(II) catalytic cycle can be proposed for the arylation of azoles, wherein the pincer complex would directly catalyze the reaction; as the palladium(IV) pincer complexes are supposed to be the stable species.[7,51] In order to know the precise catalytic cycle involve for the (POCN)Pd-catalyst during the arylation of azole, a number of quantitative experiments, controlled reactivity study, kinetic analysis, isolation and reactivity of intermediate species, and DFT calculations were carried out.

4.2.1 External additive experiments

In order to know the precise nature of ($^{i\text{Pr2}}$POCN$^{i\text{Pr2}}$)PdCl (**4**) during the arylation of azoles, a number of added ligand experiments were carried out (See Table 4.1). The addition of Bu_4NBr (10 mol%), a salt known to stabilize the palladium(0) nanoparticles,[329,330] to the catalytic reaction did not enhance the rate of reaction as well as yield of product. Instead, a low yield of isolated product was observed in the presence of Bu_4NBr salt. This suggests that the Pd(0) particles are less likely the active catalyst during arylation reaction. The status of the catalytic species in the presence of Bu_4NBr during the catalytic reaction was monitored using ^{31}P NMR spectroscopy. Upon treatment of catalyst **4** (0.025 mmol) with benzothiazole (**12a**; 0.25 mmol) and 4-iodotoluene (**13a**; 0.375 mmol) in the presence of Bu_4NBr (0.05 mmol) under catalytic conditions at 100 °C for 3 h, three major species were observed in the solution are ($^{i\text{Pr2}}$POCN$^{i\text{Pr2}}$)PdI (**6**; 204.5 ppm, 43%), ($^{i\text{Pr2}}$POCN$^{i\text{Pr2}}$)PdCl (198.8 ppm, 24%) and a peak at 201.1 ppm (29%). The peak at 201.1 ppm is most likely from the ($^{i\text{Pr2}}$POCN$^{i\text{Pr2}}$)-PdBr compound, which was independently investigated by reacting ($^{i\text{Pr2}}$POCN$^{i\text{Pr2}}$)PdCl with Bu_4NBr (5 equiv). The observed low yield of the product in the presence of Bu_4NBr may be due to the impact of Bu_4NBr on CuX. The possible formation of co-ordinatively saturated

Cu(I) or Cu(II) species in equilibrium with CuX can be envisaged; a scenario which might hinder the action of Cu(I).

Table 4.1 Added ligand experiments

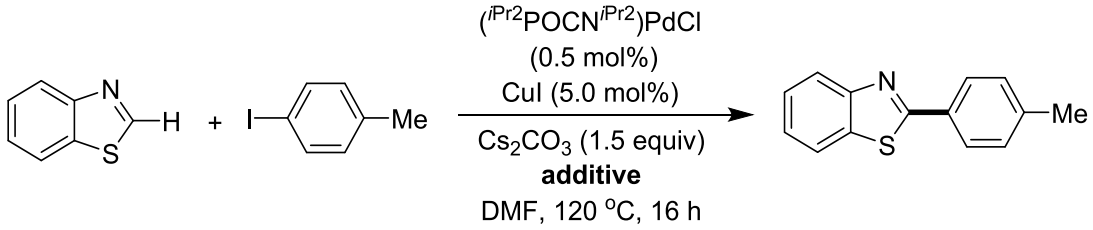

12a **13a** **14aa**

Entry	Additives	Yield	Observation
1	No additive	97%	
2	$^{n}Bu_4NBr$ (10 mol%)	40%	$^{n}Bu_4NBr$ should stabilize Pd-nanoparticles and should enhance the reaction: Less likely formation of Pd(0)
3	PPh_3 (1 equiv)	94%	PPh_3 should quench the Pd-nanoparticles and should shut down the reaction. No effect of PPh_3
4	Py (150 equiv)	76%	Py should quench the Pd-nanoparticles and should shut down the reaction. No effect of Py
5	PVPy (150 equiv)	80%	PVPy should remove the Pd(0) soluble nanoparticles, but no effect of PVPy. Less likely formation of Pd(0)
6	Hg (200 equiv)	42%	The reaction was not completely shut down: Less likely formation of heterogeneous Pd-nanoparticles during catalysis

The PPh_3 and molecular pyridine ligands are known to poison the Pd(0) nanoparticles. Generally, PPh_3 and pyridine binds to Pd(0) nanoparticles and shut down the catalytic activity of the catalyst. Hence, the standard catalytic reaction was performed in the presence PPh_3 (1.0 equiv w.r.t. **4**) or molecular pyridine (150 equiv w.r.t. **4**), and it was observed that the addition of PPh_3 (1.0 equiv w.r.t. **4**) or pyridine (150 equiv w.r.t. **4**) did not affect the yield of the product (See Table 4.1).[331-333] The catalytic reaction was also unaffected by the incorporation of 150 equiv of basic poison poly(vinyl pyridine) (PVPy), known to quenches homogeneous Pd(0) nanoparticles.[334,335] Moreover, the addition of 200 equiv of mercury to the catalytic reaction reduced the reaction yields remarkably, though it could not quench the reaction completely. Generally, mercury ceases the reaction completely, if the catalyst has heterogeneous in nature by forming an amalgam with palladium nanoparticles.[336,337] All these

experimental findings support the possibility of (^{iPr2}POCN^{iPr2})PdCl might directly involved in the catalytic reaction, and less likely transforming into another active catalytic species (palladium nanoparticles), though mercury drop experiment contradicts the other additive experiments.

4.2.2 Kinetic analysis for arylation of azoles by (^{iPr2}POCN^{Et2})PdCl (**20**)

The rate for the formation of arylated product **14aa** using sterically less hindered (^{iPr2}POCN^{Et2})PdCl (**20**) catalyst is faster compared to bulkier (^{iPr2}POCN^{iPr2})PdCl, (^{tBu2}POCN^{iPr2})PdCl and (^{Ph2}POCN^{Et2})PdCl pincer complexes. Hence, all the mechanistic and kinetic analysis for arylation of azole with aryl iodides were performed using (^{iPr2}POCN^{Et2})PdCl (**20**) complex. All the kinetic experiments were performed in the flame-dried screw-capped tubes under an argon atmosphere. In the standard kinetic experiment, 1.25 mM of (^{iPr2}POCN^{Et2})PdCl, 2.50 mM of CuI, 0.108 M mesitylene (internal standard), benzothiazole **12** (0.25 M), 4-iodotoluene **13** (0.375 M) and K_3PO_4 (0.75 mmol) were taken, and DMF was added to make the total volume 2.0 mL. All the reactions were conducted at 120 ^{o}C, and the progress of the reaction was monitored by gas chromatography (GC) at regular intervals. Reported values represent the average of the three independent experiments.

The reaction profile of the (^{iPr2}POCN^{Et2})PdCl-catalyzed arylation of benzothiazole with 4-iodotoluene over a period of 90 min is shown in Figure 4.2. The formation of coupled product **14aa** followed a linear line, indicates a constant reaction rate. After 5 and 10 min of the reaction, 4.0 mM and 10 mM of coupled product was formed accounting to 3 and 8 TON's, respectively; which suggests the absence of induction period for the arylation reaction. The absence of induction period indicates that there is no formation of any other active species from (^{iPr2}POCN^{Et2})PdCl, and (^{iPr2}POCN^{Et2})PdCl might directly involved in the catalytic reaction. At the end of 90 min, the conversion of benzothiazole was 48% and the product **14aa** formation was 44%.

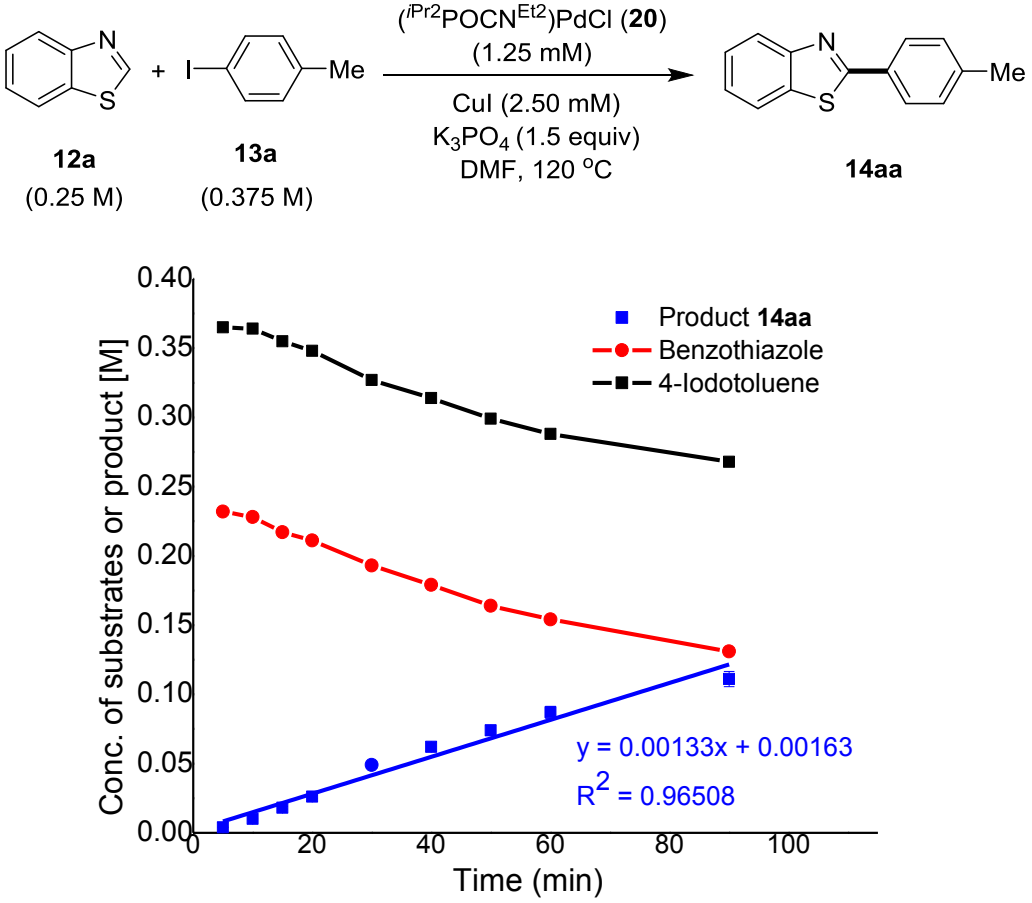

Figure 4.2 Reaction profile for arylation of benzothiazole with 4-iodotoluene.

4.2.3 Rate order determination with various reaction components

The order of the arylation reaction with various reaction components was determined by the initial rate method. The data of the concentration of the product *vs* time (min) plot was fitted linear with Origin Pro 8. The slope of the linear fitting represents the reaction rate. The order of the reaction was then determined by plotting the log(rate) *vs* log(conc. of component) for a particular component.

Rate order of arylation with benzothiazole: To determine the order of the arylation reaction on benzothiazole, the initial rates at different initial concentrations of benzothiazole (**12a**) were recorded. The final data was obtained by averaging the results of three independent runs for each experiment. The initial rates for the formation of arylated product **14aa** with different concentration of benzothiazole are shown in Table 4.2. The initial rates for formation of arylated product **14aa** were almost similar with the different initial concentration of benzothiazole (Figure 4.3 A). The plot of log(rate) *vs* log(conc. of benzothiazole) shows that the reaction is zeroth-order in the concentration of benzothiazole (Figure 4.3 B).

Table 4.2 Rate of arylation reaction with varying concentration of benzothiazole

Experiment	Amount of (**12a**) (g)	Initial conc. of (**12a**) [M]	Initial rate [$Mmin^{-1}$] x 10^{-3}
1	0.067	0.250	1.33
2	0.101	0.375	1.41
3	0.135	0.500	1.35
4	0.202	0.750	1.43

Rate order of arylation with 4-iodotoluene: To determine the order of the arylation reaction on 4-iodotoluene, the initial rates at different initial concentrations of 4-iodotoluene (**13a**) were recorded. The final data was obtained by averaging the result of three independent runs for each experiment. The initial rates for the formation of arylated product **14aa** with different concentration of 4-iodotoluene are shown in Table 4.3. The initial rates for formation of arylated product **14aa** were almost similar with the different initial concentration of 4-iodotoluene (Figure 4.4 A). The plot of log(rate) *vs* log(conc. of 4-iodotoluene) shows that the reaction is independent in the concentration of 4-iodotoluene (Figure 4.4 B).

Table 4.3 Rate of arylation reaction with varying concentration of 4-iodotoluene

Experiment	Amount of **13a** (g)	Initial conc. of **13a** [M]	Initial rate [$Mmin^{-1}$] x 10^{-3}
1	0.163	0.375	1.33
2	0.327	0.750	1.26
3	0.490	1.125	1.36
4	0.654	1.500	1.27

Rate order of arylation with (^{iPr2}POCN^{Et2})PdCl: To determine the order of the arylation reaction on the catalyst (**20**), the initial rates at the different initial concentration of **20** were recorded. The final data was obtained by averaging the result of three independent runs for each experiment. The initial rates for the formation of arylated product **14aa** with different concentration of **20** are shown in Table 4.4. The initial rates for formation of arylated product **14aa** were almost similar with the different initial concentration of **20** (Figure 4.5 A). A slope of 0.067 was obtained from the plot of log(rate) *vs* log(conc. **20**), suggesting the order of reaction independent on different loading of (^{iPr2}POCN^{Et2})PdCl (Figure 4.5 B).

Table 4.4 Rate of arylation reaction with varying concentration of (^{iPr2}POCN^{Et2})PdCl

Experiment	Amount of **20** (g)	Initial conc. of **20** [M]	Initial rate [Mmin^{-1}] x 10^{-3}
1	0.00109	0.00125	1.33
2	0.00218	0.0025	1.41
3	0.00436	0.0050	1.46
4	0.00654	0.0075	1.48

Rate order of arylation with CuI: To determine the order of the arylation reaction on CuI, the initial rates at different initial concentration of CuI were recorded. The final data was obtained by averaging the results of three independent runs for each experiment. The initial rates for the formation of arylated product **14aa** with different concentration of CuI have shown in Table 4.5. The rates of arylation reaction slightly decelerate with the increase in the initial concentration of the CuI with a negative order of –0.15 (Figure 4.6). The fractional order of –0.15 indicates that the high concentration of CuI actually retards the rate of the arylation reaction, which might be due to the degradation of an active palladium catalyst in the higher concentration of CuI. A plausible decoordination of the *N*-arm of the pincer palladium and coordination of the same to CuI can be assumed in the presence of an excess of CuI, which will reduce the activity of pincer Pd-catalyst.

Table 4.5 Rate of arylation reaction with varying concentration of CuI

Experiment	Amount of CuI (g)	Initial conc. of CuI [M]	Initial rate [Mmin^{-1}] x 10^{-3}
1	0.0009	0.00249	1.33
2	0.0028	0.00747	1.31
3	0.0047	0.01245	0.93
4	0.0095	0.02490	1.02

Rate order of arylation with K_3PO_4: To determine the order of the arylation reaction on K_3PO_4, the initial rates at different equiv of K_3PO_4 were recorded. The final data was obtained by averaging the result of three independent runs for each experiment. The initial rates for the formation of arylated product **14aa** with the different equivalence of K_3PO_4 have shown in Table 4.6. The rate of arylation reaction increases upon the higher loadings of K_3PO_4 (Figure 4.7 A). A slope of 0.74 was obtained from the plot of log(rate) *vs* log(equiv K_3PO_4) indicating a fractional order of arylation reaction in K_3PO_4 (Figure 4.7 B). The partial order in base indicates that more than one pathway is operative for the deprotonation of

benzothiazole involving K_3PO_4 (most likely *via* direct electrophilic C–H deprotonation of benzothiazole as well as from the CuI coordinated benzothiazole).

Table 4.6 Rate of arylation reaction with varying concentration of K_3PO_4

Experiment	Amount of K_3PO_4 (g)	Conc. of K_3PO_4 [equiv]	Initial rate [$Mmin^{-1}$] x 10^{-3}
1	0.106	1.0	0.90
2	0.159	1.5	1.33
3	0.212	2.0	1.47
4	0.318	3.0	2.09

Overall order of arylation reaction: The kinetic analysis data shows that the order of reaction is 0.74 fractional with K_3PO_4 and –0.15 with a concentration of CuI. Hence, the rate equation can be drawn as a shown in eq 1. The overall order for the reaction is 0.6.

$$\text{rate} = k\,[K_3PO_4]^{0.74}\,[CuI]^{-0.15}$$

Over all reaction order = 0.6 (1)

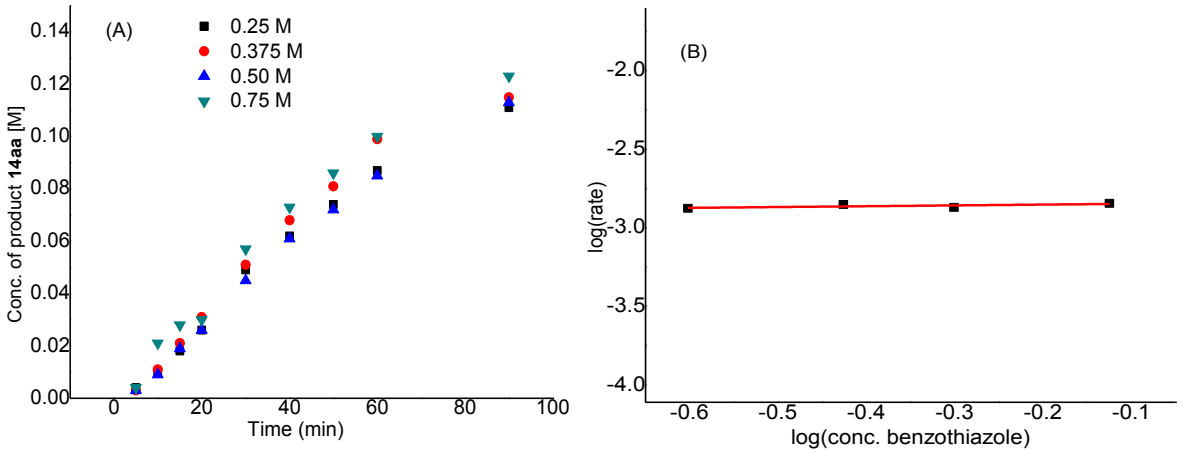

Figure 4.3 (A) Formation of **14aa** with varying concentration of benzothiazole. (B) Plot of log(rate) *vs* log(conc. benzothiazole).

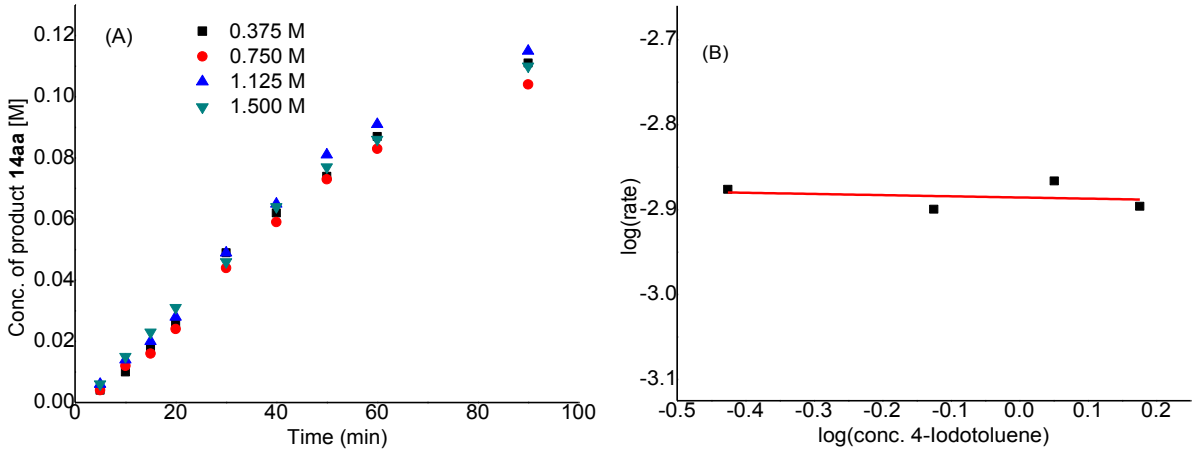

Figure 4.4 (A) Formation of **14aa** with varying concentration of 4-iodotoluene. (B) Plot of log(rate) *vs* log(conc. 4-iodotoluene).

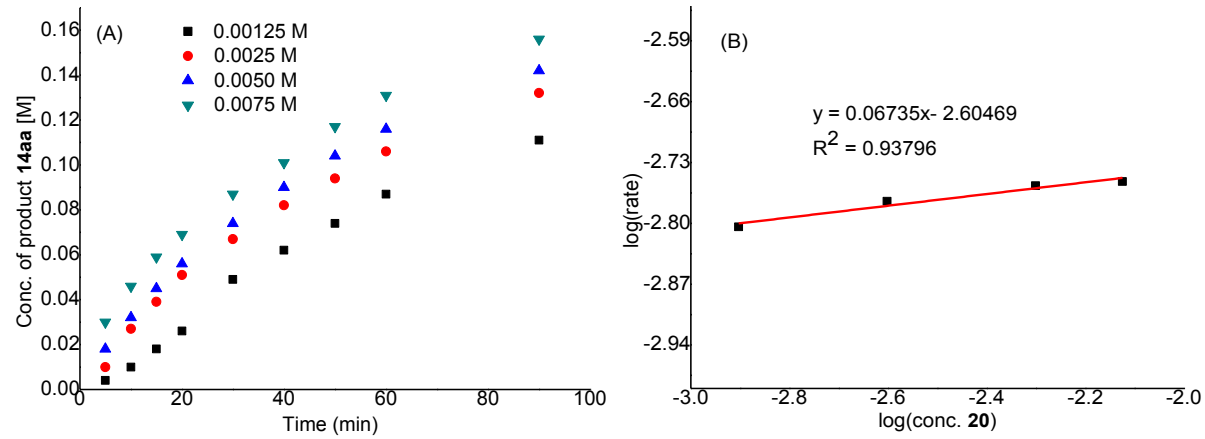

Figure 4.5 (A) Formation of **14aa** at different concentration of **20**. (B) Plot of log(rate) *vs* log(conc. **20**).

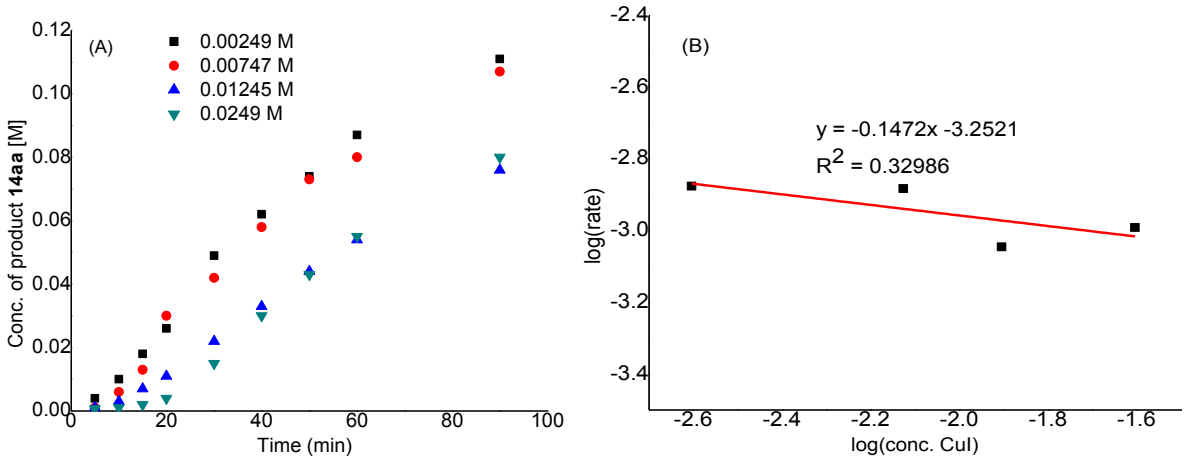

Figure 4.6 (A) Formation of **14aa** at varying concentration of CuI. (B) Plot of log(rate) *vs* log(conc. CuI).

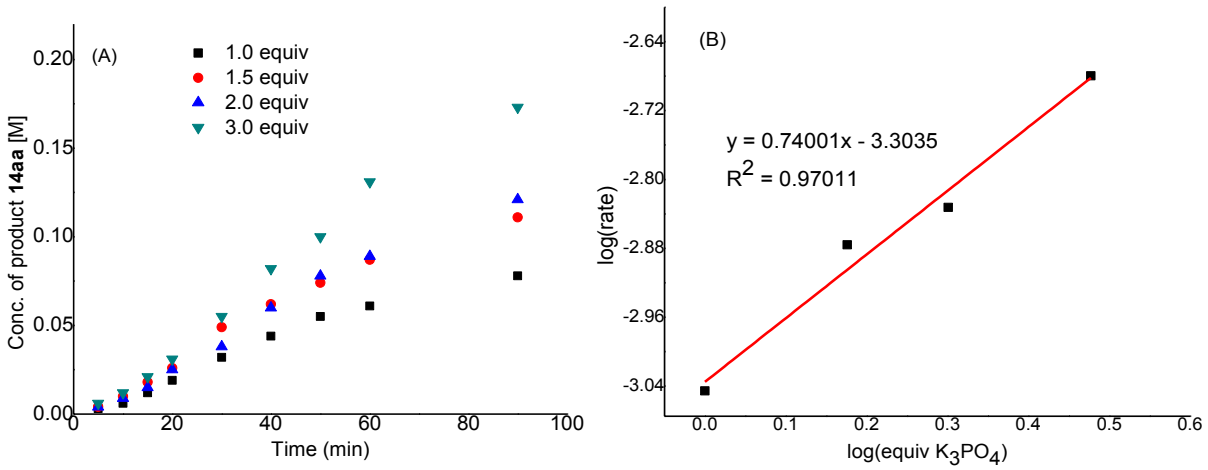

Figure 4.7 (A) Formation of **14aa** at different loading of K_3PO_4. (B) Plot of log(rate) *vs* log(equiv K_3PO_4).

4.2.4 Catalyst stability and product inhibition study

Catalyst recycling experiment: In order to investigate the possible catalyst deactivation, the recycling experiment of the catalytic reaction system was conducted (Scheme 4.1). After the first catalytic run between the benzothiazole and 4-iodotoluene, the yield of the coupled product observed was 98% (GC yield). To the same reaction vessel, fresh benzothiazole, 4-iodotoluene, and K_3PO_4 were added, and the reaction was continued further without the addition of catalyst (^{iPr2}POCN^{Et2})PdCl and CuI. After 16 h, the yield determined for the second cycle was 90%. After two catalytic cycles, the formation of arylated product is almost same, which indicates that catalyst deactivation or product inhibition is less likely during catalysis.

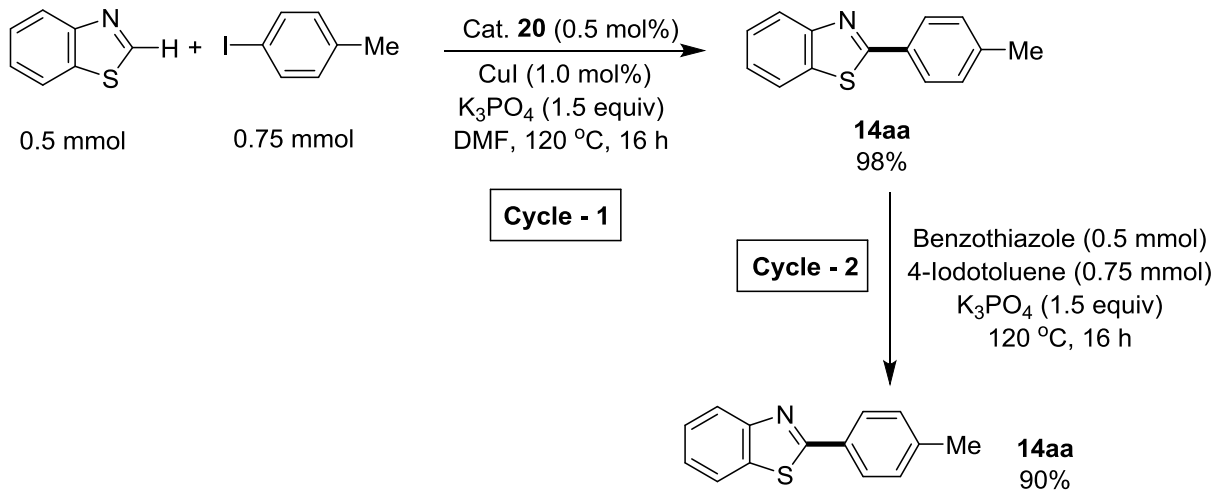

Scheme 4.1 Recycling experiments of the catalyst **20**

Same [excess] experiment for catalyst: In order to determine the possible catalyst deactivation and/or product inhibition along the reaction, the reaction progress analysis was investigated by carrying out four arylation reactions at the same [excess] but different initial concentrations of the benzothiazole and 4-iodotoluene (See Table 4.7). As shown in Figure 4.8, the rates of the reactions are identical with different starting concentrations of the benzothiazole and 4-iodotoluene, with identical values of the [excess].[338] All these rates are almost similar, which suggest that there was no significant catalyst deactivation or product inhibition during the arylation reaction of benzothiazole.

Table 4.7 Rate of arylation reaction at same [excess] concentration of substrate

Experiment	Conc. of **12a** [M]	Conc. of **13a** [M]	Initial rate $[Mmin^{-1}] \times 10^{-3}$	Excess [M]
1	0.25	0.375	0.887	0.125
2	0.30	0.425	0.945	0.125
3	0.40	0.525	0.860	0.125
4	0.50	0.625	0.883	0.125

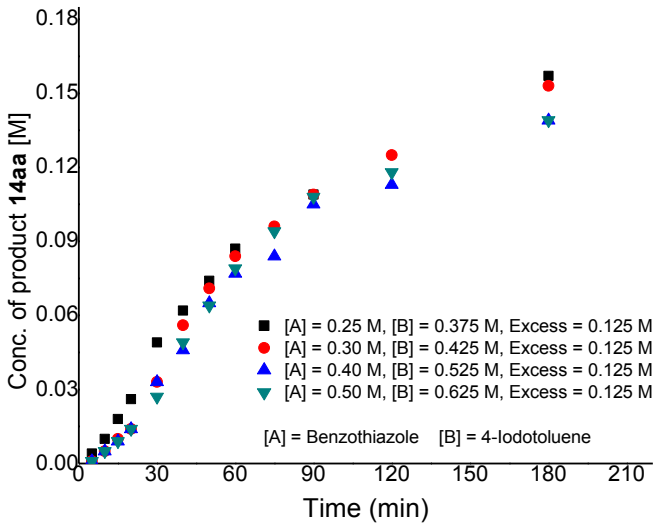

Figure 4.8 Formation of **14aa** at same [excess] concentrations of benzothiazole and 4-iodotoluene.

4.2.5 Isotope labelling experiments

Kinetic isotope effect (KIE) experiment: The kinetic analyses of the arylation reaction reveal that the reaction is zeroth-order in benzothiazole, 4-iodotoluene and in the catalyst concentration, whereas a fractional order was observed in K_3PO_4. Since the arylation reaction is of fractional order in K_3PO_4, it assumed that the C–H bond cleavage is the

probable turnover-limiting step. To probe this possibility, the kinetic isotope effect (KIE) study was carried out. The rates of the arylation reactions employing 2-*H*-benzothiazole and 2-*D*-benzothiazole with 4-iodotoluene were found to be almost similar and the observed isotope effect (k_H/k_D) was approximately 1.0 (Figure 4.9), which indicates that the C–H bond cleavage is less likely involved in the turnover-determining step during the catalysis.

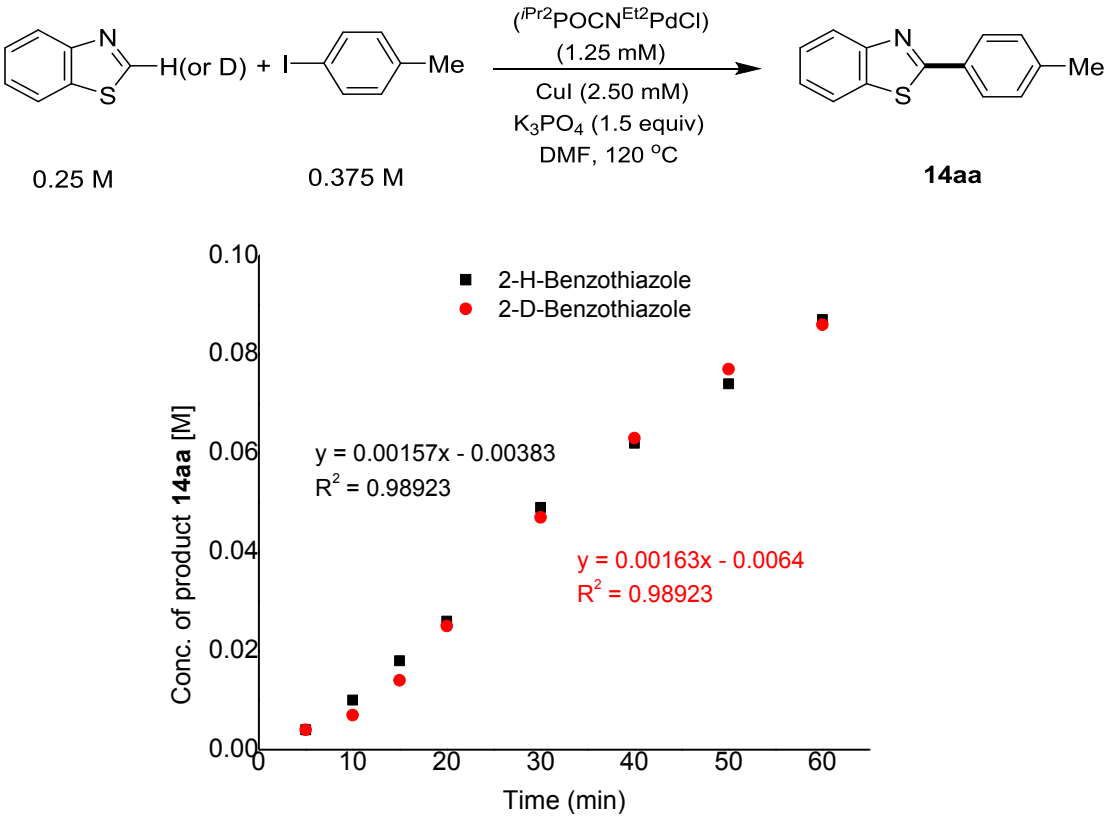

Figure 4.9 Formation of **14aa** using 2-*H/D*-benzothiazole with 4-iodotoluene.

H/D scrambling experiment: The deuterium scrambling experiment was carried out to check the nature of C–H bond cleavage on benzothiazole. The mixture of 2-*D*-benzothiazole and 2-*H*-6-ethoxy-benzothiazole were treated with the optimized catalytic reaction condition in the absence of aryl iodide (Scheme 4.2). It was observed that the H incorporation at the C(2) position of 2-*D*-benzothiazole; while D incorporation at the C(2) position of 2-*H*-6-ethoxy-benzothiazole was occurred in the presence of catalyst **20**. Also, this deuterium scrambling was observed solely in the presence of a K_3PO_4 base (Scheme 4.2). This indicates that the C–H bond deprotonation to be reversible in nature and hence, it may not be involved in the turnover-limiting step.

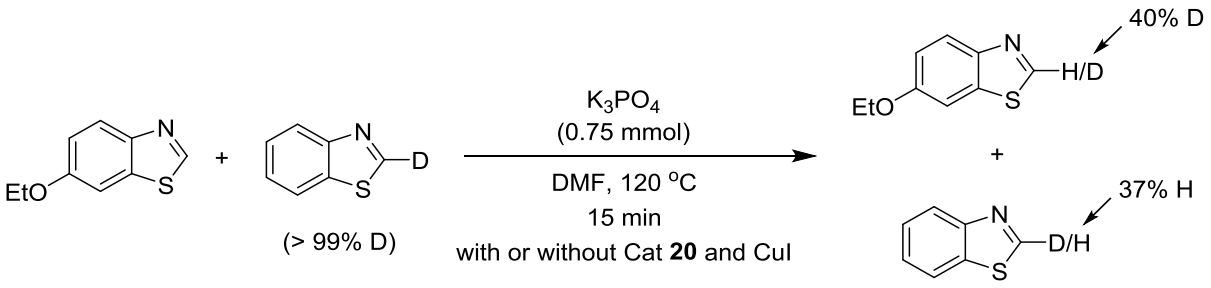

Scheme 4.2 H/D scrambling experiment

4.2.6 Electronic effect on arylation

Effect of benzothiazole substitutions on arylation: The rates of the coupling of benzothiazole, 6-ethoxy-benzothiazole, and 6-fluoro-benzothiazole with 4-iodotoluene were determined in order to understand the electronic influence of the substrates on arylation reaction (Figure 4.10). The rates of the coupling reaction were found to be similar, though the substrates are electronically different. Furthermore, the intermolecular competition experiments between the differently substituted benzothiazoles with 4-iodotoluene concurrently furnished the arylation products from both the electron-rich and electron-deficient substrates (Scheme 4.3). These findings indicate that the electronic property of the substituted-benzothiazole has negligible influence on the arylation reaction and hence, the probability of the transmetalation between (benzothiazolyl)-K and CuX or (benzothiazolyl)CuL_n and (^{iPr2}POCN^{Et2})PdX being a turnover-limiting step is less likely; because the more electron-rich substrates with high nucleophilicity would favor transmetalation process. Further, these experimental findings do not support the reductive elimination as a turnover-limiting step, as the reductive elimination tends to be more favorable from electron-poor metal centers.[339] The interpretation of the reductive elimination being not a turnover-limiting step was further supported by the DFT calculations (discussed *vide infra*), which show a lower energy barrier for this step.

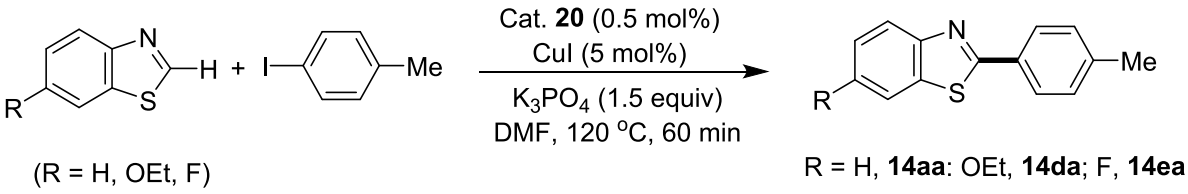

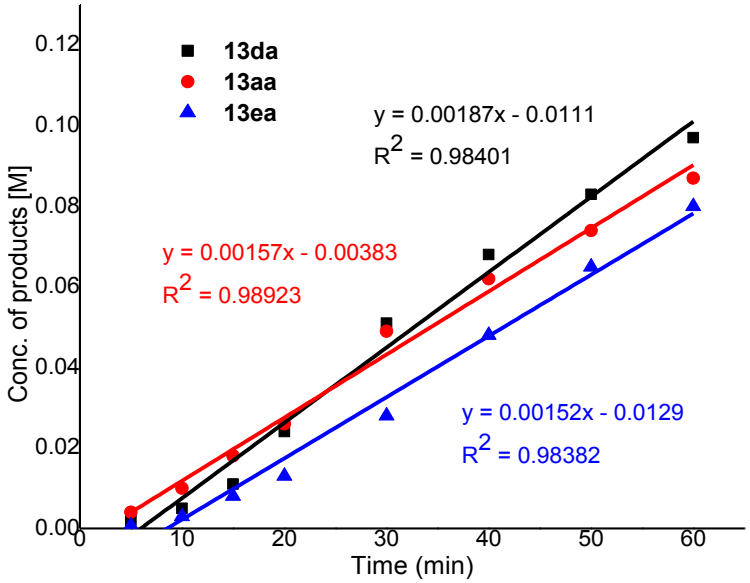

Figure 4.10 The kinetics for reactions of 6-ethoxy-benzothiazole, benzothiazole, and 6-fluorobenzothiazole with 4-iodotoluene.

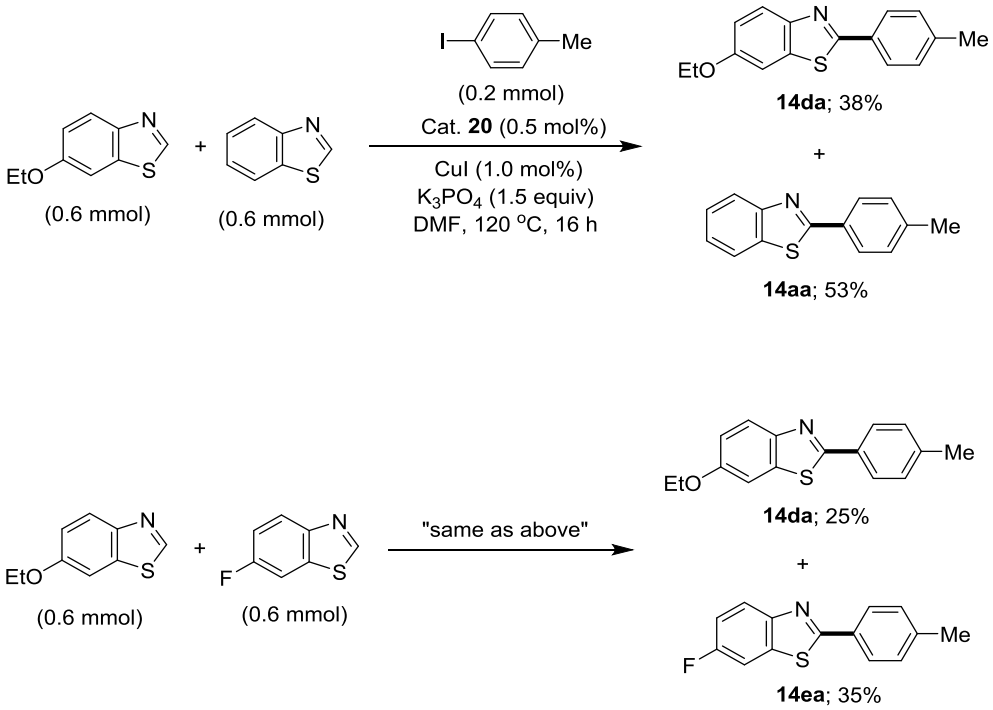

Scheme 4.3 Intermolecular competition experiments

Effect of substitutions of aryl iodides on arylation (Hammett plot analysis): In order to know the electronic effect of aryl iodides on the arylation reaction, the rates of the reaction with electronically different aryl iodides were calculated. The initial rates for the formation of product with aryl iodides having –OMe, –Me, –H, –Cl and –COOMe group at *para*-position were determined (Figure 4.11). The Hammett plot was drawn from the correlation between the initial rates and the σ_p values, which shows linear fit with a slope of –0.777. The negative ρ value suggests that a positive charge is being produced in the activated complex and that electron-donating substituents on the aryl iodide will enhance the rate of the arylation reaction. This is in support of the oxidative addition of aryl iodides to a Pd(II) species rather than to a Pd(0) species, as in the former an electron-donating substituent would be expected to stabilize the resulting Pd(IV)-intermediate, and hence lower the energy of the process.

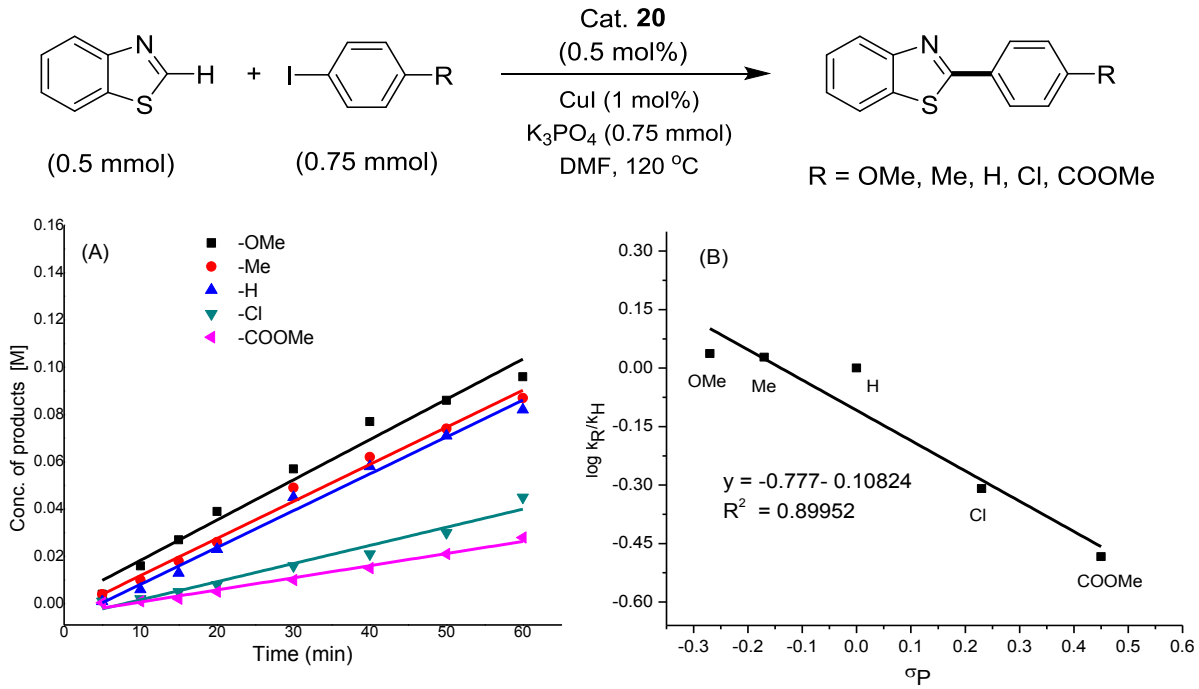

Figure 4.11 (A) Arylations using different *para*-substituted aryl iodides with benzothiazole. (B) Hammett plot correlation.

4.2.7 Role of CuI and (POCN)Pd-catalyst in arylation reaction

To understand the respective roles of the palladium catalyst **4** and CuI, a number of experiments were carried out, which involved decreased catalyst **4** loading and increased CuI loading. Hence, the catalytic reactions using 0.5% of **4** + 5% of CuI, 0.25% of **4** + 10% of CuI and 0.125% of **4** + 20% of CuI under standard catalytic conditions afforded the coupled product **14aa** as yields (TONs): 97% (194), 76% (304) and 67% (536), respectively. Even large amount of CuI could not replace **4** under the present catalytic conditions. For example, when the standard catalytic reaction was carried out employing 20 mol% of CuI in the absence of **4**, only 8% (^{1}HNMR yield) of coupled product was formed. This suggests that the complex **4** acts as a catalyst and CuI as a co-catalyst.

Most likely, the CuI facilitates the transmetalation of the benzothiazolyl moiety to the palladium catalyst in the presence of a base. Furthermore, in order to check the role of CuI, the benzothiazole was treated with CuI in acetonitrile, which gave a white crystalline compound. The proton NMR spectrum of the resulted compound displayed a peak at 9.59 ppm corresponding to the C(2)–H proton of the *N*-coordinated (benzothiazole)CuI moiety (0.18 ppm more deshielded than the free benzothiazole). This coordination could enhance the acidity of the C(2)–H proton, which facilitates the deprotonation/carbo-metalation of the benzothiazole with the Cu-metal followed by transmetalation with the palladium catalyst. This experiment further supports that the (POCN)-palladium acts as a catalyst and CuI acts as a co-catalyst for the arylation reaction. Similar role of the organo-copper intermediate has been reported for the arylation of azoles as well as for other coupling reactions.[180,340-343]

4.2.8 Controlled reactivity of ($^{i\mathrm{Pr2}}$POCN$^{\mathrm{Et2}}$)PdCl (**20**)

The status of the catalyst **20** under the catalytic conditions was monitored by ^{31}P NMR spectroscopy to know the resting state of the catalyst as well as to detect the probable intermediate species during the reaction. The ^{31}P NMR experiments were carried out in J-Young NMR tubes and the yields of different (POCN)Pd-species were determined with reference to the external standard (PMe_3 capillary). Initially, the catalyst **20** (0.025 mmol), CuI (0.0025 mmol), benzothiazole (0.25 mmol), 4-iodotoluene (0.375 mmol) and K_3PO_4 (0.375 mmol) in DMF (0.5 mL) were heated at 100 ^{o}C in an oil bath and the reaction was monitored at regular intervals (Scheme 4.4a). After 3 h, the reaction mixture showed 5% of **20** and 95% of ($^{i\mathrm{Pr2}}$POCN$^{\mathrm{Et2}}$)PdI (**22**) complex as the ^{31}P NMR-detectable species. Further, the reaction mixture was heated for 40 h, wherein complex **22** observed as the major species (91%) and complex **20** (3%) as minor species by ^{31}P NMR. This observation indicates that

the catalyst decomposition was not significant and further it demonstrates that the ($^{i\text{Pr}2}$POCN$^{\text{Et}2}$)PdI (**22**) species could be the resting state of the catalyst.

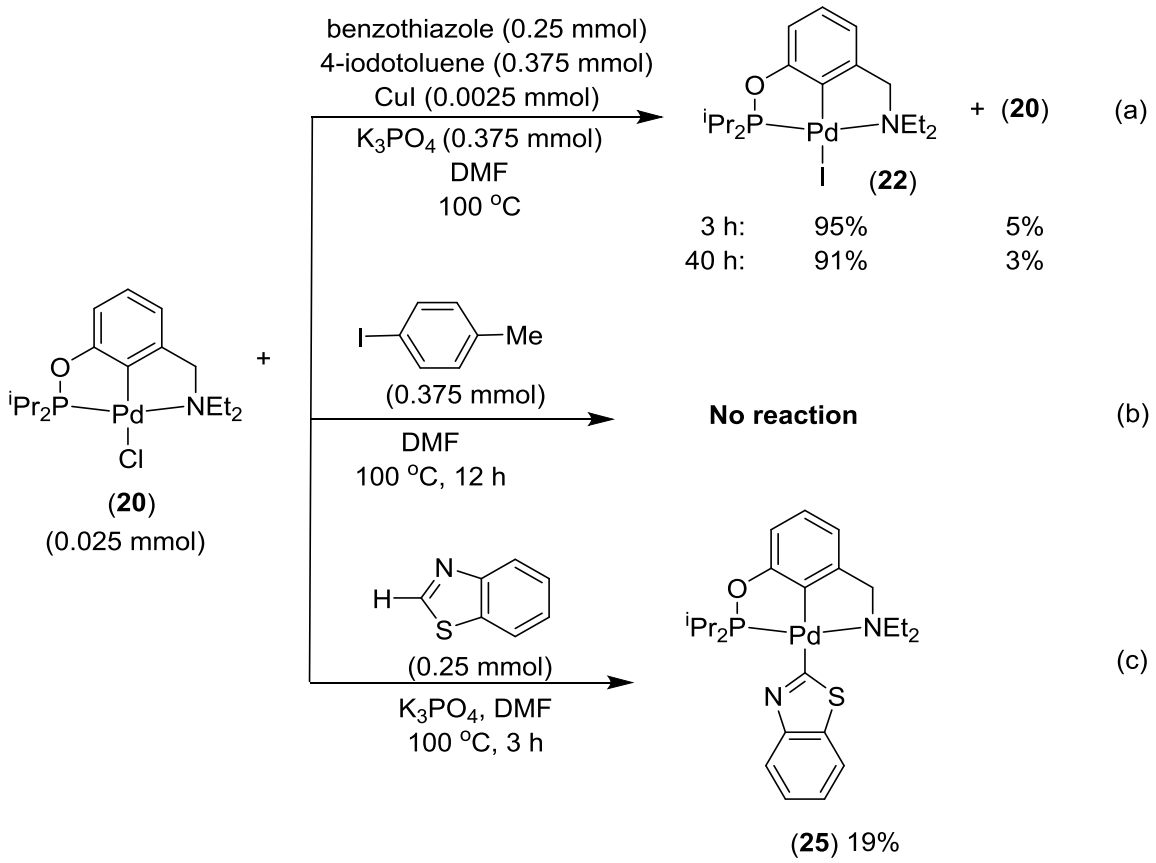

Scheme 4.4 Stoichiometric reaction and resting state of catalyst **20**

Further, to detect any catalytic intermediate species the control experiments were performed. Hence, the complex **20** was treated with 4-iodotoluene (15 equiv) in DMF for 12 h (Scheme 4.4b). The ^{31}P NMR spectrum of the reaction mixture shows only the starting complex **20** without any decomposition or the formation of iodide-derivative **22**, which suggests that the oxidative addition of 4-iodotoluene to the 16e$^-$ species **20** might not be a feasible process, and such a reaction may not involved in the first step of the catalytic reaction. In another experiment, complex **20** was treated with benzothiazole (10 equiv) in the presence of K_3PO_4 (Scheme 4.4c). After heating the reaction mixture at 100 ^{o}C for 3 h, the formation of a new complex ($^{i\text{Pr}2}$POCN$^{\text{Et}2}$)Pd-benzothiazolyl (**25**) was observed in 19% yield. The authenticity of **25** was established by it's independent synthesis and characterization which is discussed in next section. Though the species ($^{i\text{Pr}2}$POCN$^{\text{Et}2}$)PdX is significantly stable under standard catalytic conditions; in the above mentioned non-catalytic condition, the

palladium-species decomposed significantly. The observed complex **25** could be a crucial intermediate for the arylation of benzothiazole. This observation further indicated that the reaction of **20** with the benzothiazole is most likely the early step of the catalytic reaction than the reaction of **20** with the 4-iodotoluene.

4.2.9 Synthesis and reactivity of intermediate (^{iPr2}POCN^{Et2})Pd-benzothiazolyl (25)

Synthesis of (^{iPr2}POCN^{Et2})Pd-benzothiazolyl (25): The complex (^{iPr2}POCN^{Et2})Pd(benzothiazolyl) (**25**) was synthesized by the treatment of (^{iPr2}POCN^{Et2})PdCl (**20**) with 5 equiv of benzothiazolyl-lithium compound at –78 ^{o}C (Scheme 4.5). The ^{31}P NMR spectrum of the complex **25** showed a singlet at 196.0 ppm. The complex (^{iPr2}POCN^{Et2})Pd(benzothiazolyl) (**25**) was characterized by ^{1}H, ^{13}C NMR spectroscopy as well as by single crystal X-ray diffraction study.

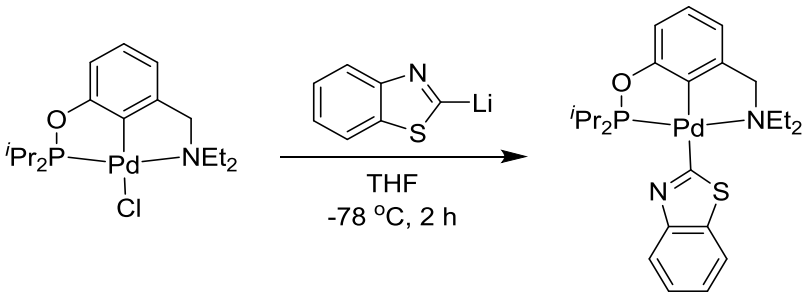

20 **25**

Scheme 4.5 Synthesis of catalyst (^{iPr2}POCN^{Et2})Pd-benzothiazolyl **25**

The ORTEP diagram of **25** is shown in Figure 4.12 and selected bond lengths and bond angles are listed in Table 4.8. In the (^{iPr2}POCN^{Et2})Pd-benzothiazolyl (**25**) complex, the geometry around Pd atom is distorted square planar. The Pd–C(*ipso*) bond length (1.985(2) Å) is similar to the Pd–C bond length 1.955(4) Å of (^{iPr2}POCN^{Et2})PdCl (**20**). The bond length of Pd–C(benzothiazolyl) is 2.072(2) Å. The P–Pd–N bond angle 161.60(6)° of (^{iPr2}POCN^{Et2})Pd(benzothiazolyl) is similar to that observed in the palladium complex (^{iPr}POCN^{Et})PdCl (P–Pd–N, 162.53(11)°). The bond angle between C(*ipso*)–Pd–C(heterocycle ring) is 174.46(10)^{o}. In the complex **25**, the benzothiazolyl moiety is almost perpendicular to the POCN-pincer ring, having both the N(1)–Pd(1)–C(18)–N(2) and P(1)–Pd(1)–C(18)–S(1) torsion angles around 70^{o}.

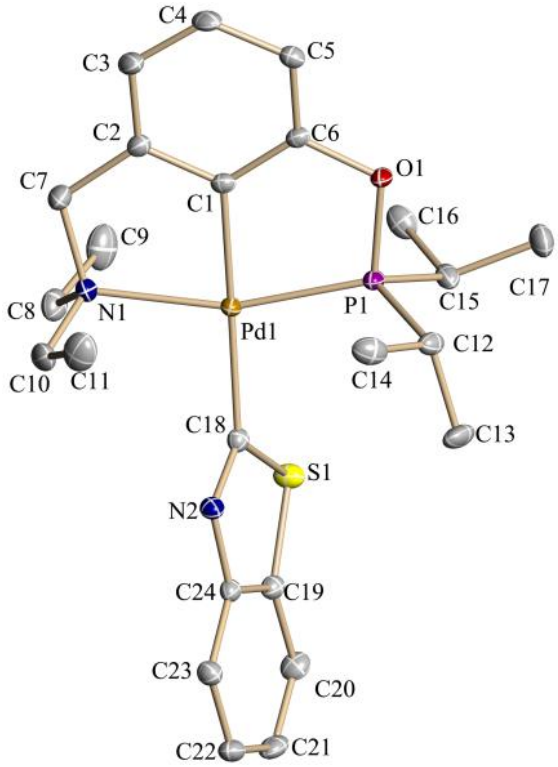

Figure 4.12 ORTEP diagram of (^{iPr2}POCN^{Et2})Pd(benzothiazolyl) (**25**).

Table 4.8 Selected bond lengths(Å) and bond angles (^{o}) for **25**

Bond length (Å)		**Bond angles (^{o})**	
Complex 25			
Pd(1)–C(1)	1.985(2)	C(1)–Pd(1)–P(1)	80.30(7)
Pd(1)–P(1)	2.195(6)	C(1)–Pd(1)–N(1)	81.31(9)
Pd(1)–N(1)	2.181(2)	P(1)–Pd(1)–N(1)	161.60(6)
Pd(1)–C(18)	2.072(2)	C(1)–Pd(1)–C(18)	174.46(10)
C(7)–N(1)	1.512(3)	P(1)–Pd(1)– C(18)	99.70(7)
C(18)–N(2)	1.312(3)	N(1)–Pd(1)– C(18)	98.58(8)

Reactivity of (^{iPr2}POCN^{Et2})Pd-benzothiazolyl (**25**): The control reactivity study of (^{iPr2}POCN^{Et2})PdCl (**20**) suggests that the (^{iPr2}POCN^{Et2})Pd-benzothiazolyl (**25**) is an active intermediate during arylation. In order to understand the progress of the arylation reaction originating from the intermediate species (^{iPr2}POCN^{Et2})Pd-benzothiazolyl (**25**), the reactivity of **25** with various electrophiles was investigated (Scheme 4.6). Complex yields are measured from the ^{31}P NMR spectrum (PMe_3 capillary as external standard) and coupled products yields are from GC or ^{1}H NMR analysis. The reaction of **25** (0.010 g, 0.019 mmol) with one equiv of 4-iodotoluene in DMF at elevated temperature exclusively produced the complex

($^{i\text{Pr2}}$POCN$^{\text{Et2}}$)PdI (**22**) and the coupled product 2-(*p*-tolyl)benzo[*d*]thiazole (**14aa**). This observation again confirmed the intermediacy of **25** during the arylation of benzothiazole with 4-iodotoluene. Further, in order to know the possible pathway in which **25** reacts with 4-iodotoluene, the complex **25** was treated with other strong oxidants, like I_2. Hence, the treatment of **25** with molecular I_2 solely produced the complex **22** and 2-iodo-benzo[*d*]thiazole at room temperature.

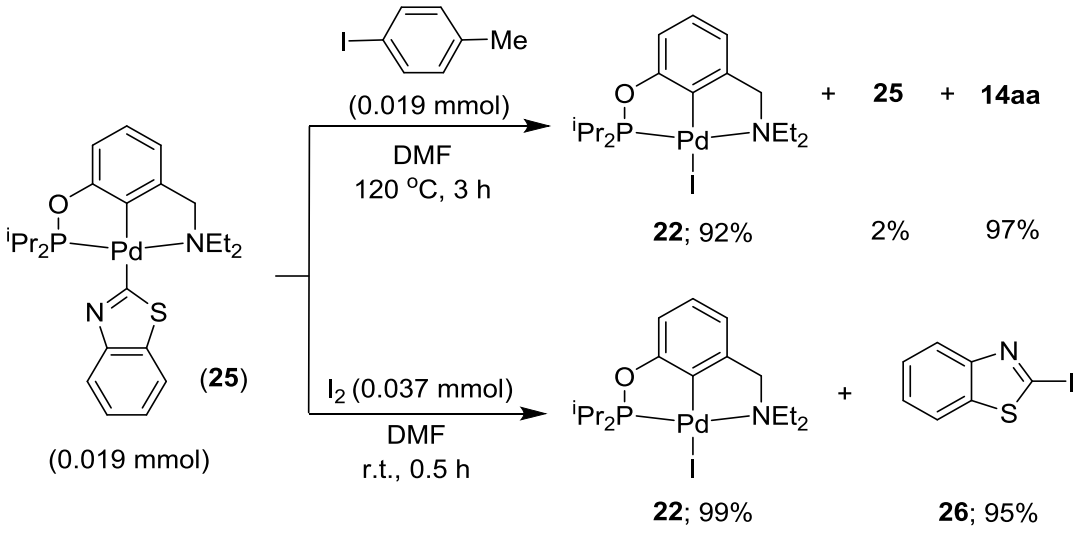

Scheme 4.6 Reactivity of ($^{i\text{Pr2}}$POCN$^{\text{Et2}}$)Pd-benzothiazolyl (**25**) with electrophiles

Further, the rates of the reaction of ($^{i\text{Pr2}}$POCN$^{\text{Et2}}$)Pd(benzothiazolyl) **25** with 4-methoxy-iodobenzene and 4-acetyl-iodobenzene were determined by calculating the rate of the formation of ($^{i\text{Pr2}}$POCN$^{\text{Et2}}$)PdI (**22**) species at 100 °C. As shown in Figure 4.13, the rate of formation of ($^{i\text{Pr2}}$POCN$^{\text{Et2}}$)PdI (**22**) is almost double while employing the electron-rich 4-methoxy-iodobenzene than with the electron-deficient electrophile 4-acetyl-iodobenzene.

All these experimental findings suggest that the involvement of a transient Pd(IV) intermediate during the reaction of **25** with 4-iodotoluene or molecular iodine, before reductively eliminating the coupled products and generating the active palladium (II) catalyst. This represents a unique experimental evidence, where the oxidative addition of C(sp^2)–X electrophile to a Pd(II) center is unequivocally shown. This further suggests that the oxidative addition step is most likely the turnover-limiting step, as an electron-rich aryl iodide would favor oxidative addition to a Pd(II) species. Though the formation of such Pd(IV) species involving C(sp^3)–X electrophiles are well documented both experimentally and theoretically,[311,344-347] similar oxidative addition of the C(sp^2)–X electrophiles to Pd(II)

complexes is rare.[151,324-326] Further, DFT calculations were carried out to validate the experimental observations on the probable transient species, which is discussed below.

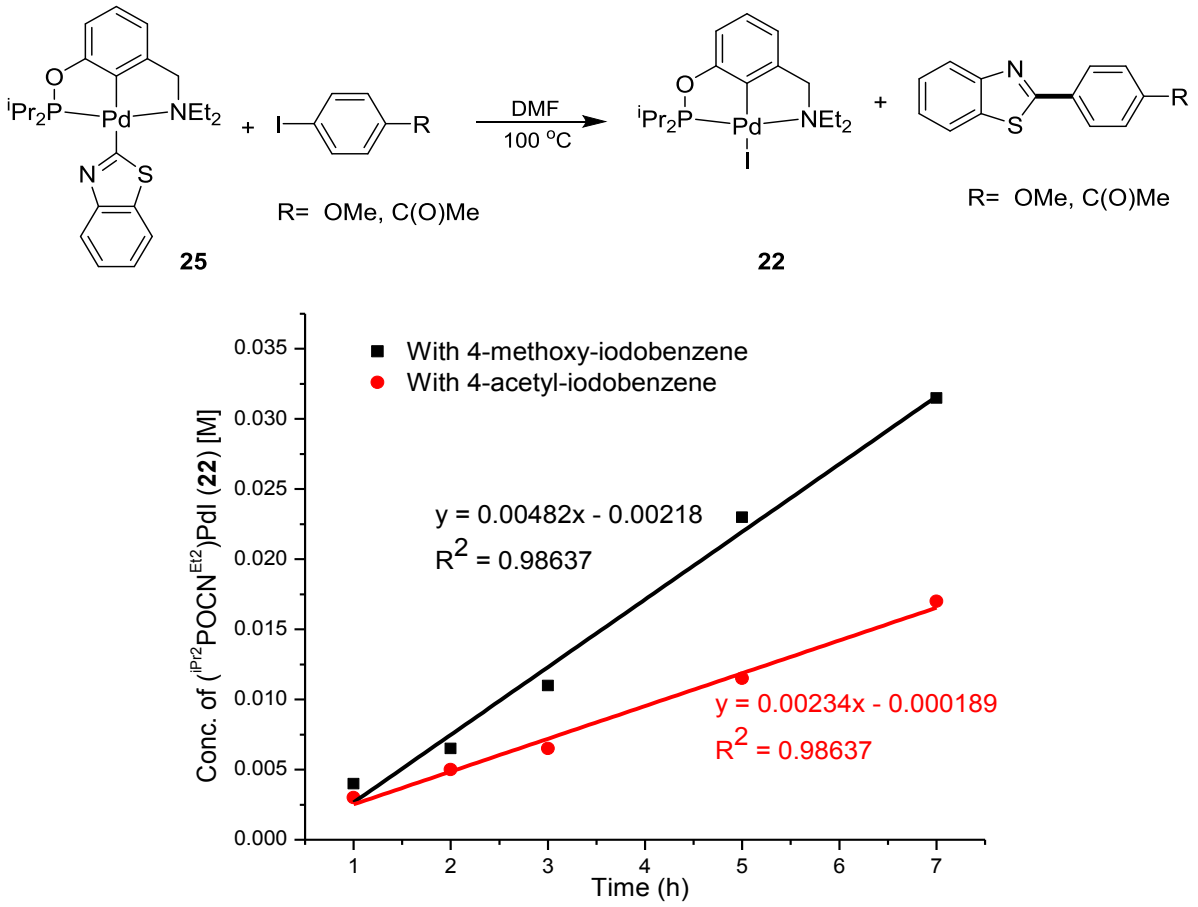

Figure 4.13 Formation of (^{iPr2}POCN^{Et2})PdI (**22**) from **25** and aryl iodides.

4.2.10 DFT study and energy profile diagram

In order to get more insight into the reactivity pattern of aryl iodide with the intermediate (^{iPr2}POCN^{Et2})Pd(benzothiazolyl) (**25**), the reaction of iodobenzene (**RC1**) with the square planar palladium complex **25** has been investigated through density functional theory (DFT). The two steps (i) oxidative addition and (ii) reductive elimination have been considered.

(i) Oxidative addition: The oxidative addition of aryl iodide (**RC1**) can occur through four different possibilities. The transition states for these different possibilities have been explored. As shown in Figure 4.14, out of the four different transition states the transition state **TS1** is lower in energy than the **TS1a**, **TS1b** and **TS1c** transition states by 3.1 kcal/mol, 10.7 kcal/mol and 15.6 kcal/mol, respectively. Thus, the addition of aryl iodide (**RC1**) to **25**

proceeds *via* **TS1** leading to the octahedral intermediate **IM**, which is endergonic by 20.0 kcal/mol, as shown in Figure 4.15.

ii) Reductive elimination: The octahedral intermediate (**IM**) is an unstable species (20.0 kcal/mol endergonic). The formation of the C–C bond is feasible through a transition state **TS2** *via* a barrier of 12.9 kcal/mol. This reductive elimination process yields the iodated Pd-complex ($^{i\text{Pr}2}$POCN$^{\text{Et}2}$)PdI (**22**) and the C–C coupled product **14ab**, with the reaction being exergonic by 45.8 kcal/mol with respect to the starting reactant, as shown in Figure 4.15. It is also clear from the figure that the barrier for the key step of the overall reaction of **RC1** with **25** is 32.9 kcal/mol. Therefore, at the given experimental conditions of elevated temperature (120 °C), this process would be expected to be feasible.

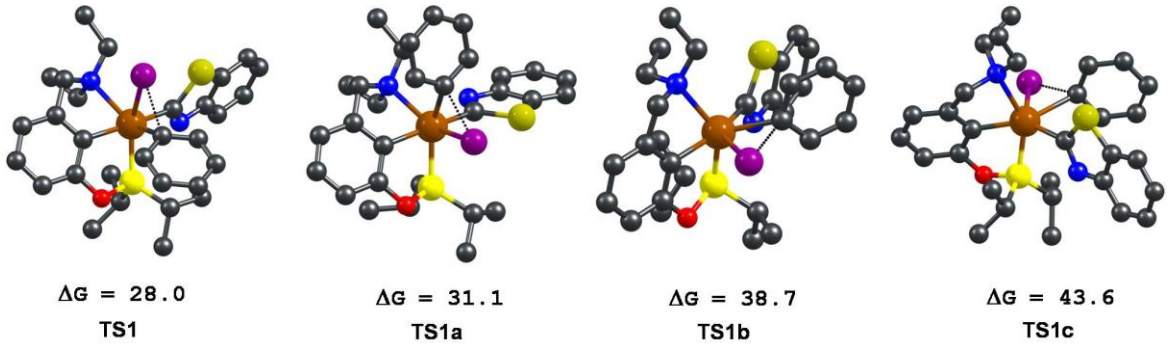

Figure 4.14 Possible transition states for the oxidative addition of RC1 to **25**; all values are in kcal/mol and with respect to (**RC1**+**25**). Hydrogen atoms are omitted for the purpose of clarity. The color scheme is as follow palladium: brown, iodide: maroon, sulfur: dark yellow, phosphorus: light yellow, nitrogen: blue, oxygen: red and carbon: black.

The possibility of a concerted pathway for the formation of **22** and **14ab** from the reaction of phenyl iodide (**RC1**) with **25** has also been investigated. All attempts to find the concerted transition state either lead to the formation of **IM** or back to the reactants. The concerted pathway is likely to be an energetically unfavorable process, due to steric hindrance. Hence, our calculations suggest a stepwise pathway.

Therefore, the corroboration with experimental results suggest that the palladium complex is able to go through oxidative addition and reductive elimination reactions, with the formation of a stable octahedral Pd-complex (**IM**), where the palladium exists in the +4 oxidation state. Similar observation of the palladium being in +4 oxidation state *via* the C(sp^2)–X electrophilic oxidative addition to a Pd(II) center has rarely been documented.[151, 324-326]

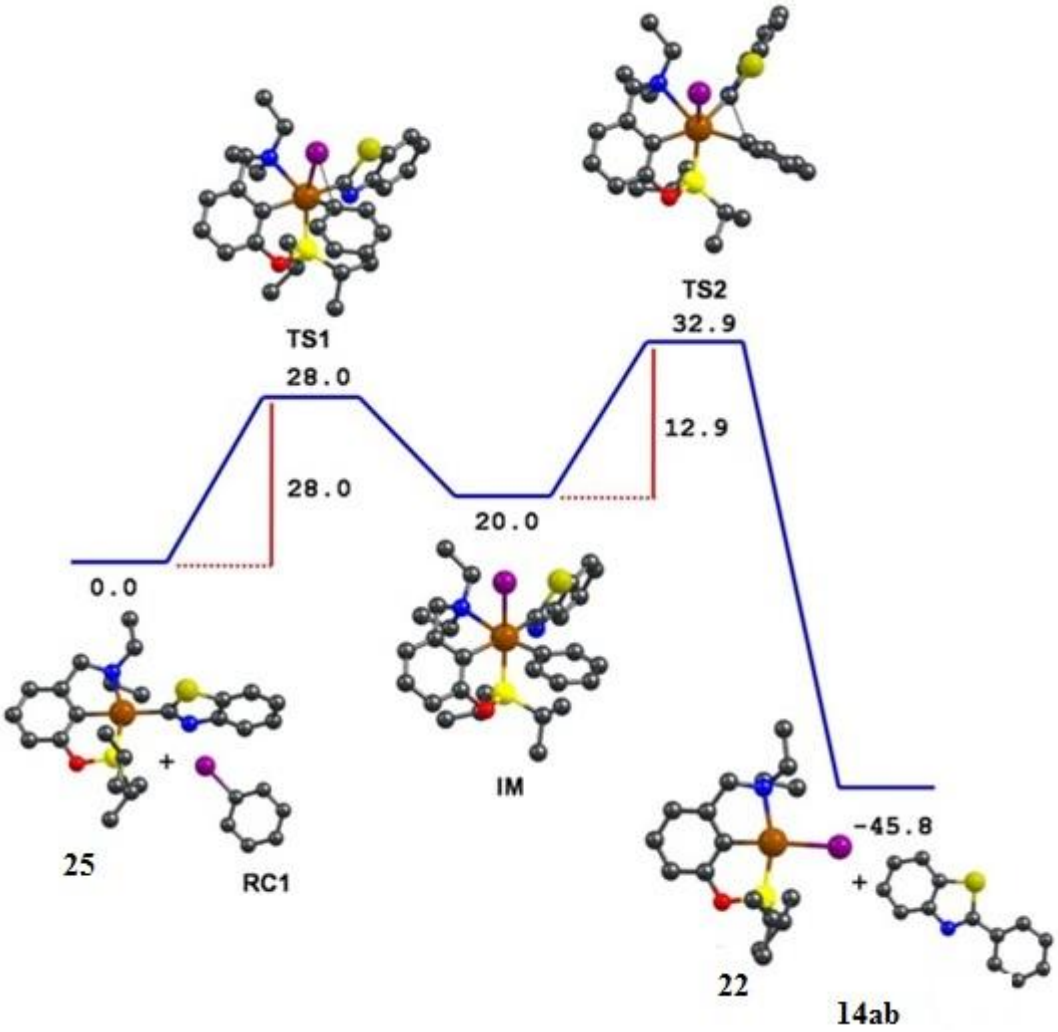

Figure 4.15 The free energy profile for the reaction of phenyl iodide (**RC1**) with **25**.

4.2.11 Probable catalytic cycle

On the basis of the experimental results a probable catalytic cycle can be drawn for the (^{iPr2}POCN^{Et2})PdCl (**20**) catalyzed arylation of azoles with aryl iodides (Figure 4.16). First, the benzothiazole coordinates to CuI to form a copper complex **A**, followed by the deprotonation and rearrangement to generate the species **B**. The K_3PO_4 most likely deprotonates the free-benzothiazole, in addition to the benzothiazole coordinated to CuI, because the reaction is of fractional-order with respect to the concentration of K_3PO_4. This is also evident from the deuterium scrambling between 2-*D*-benzothiazole and 2-*H*-6-ethoxybenzothiazole, which occurs even in the absence of CuI. The copper-benzothiazolyl species **B** then undergoes transmetalation with the (^{iPr2}POCN^{Et2})PdX complex leading to the complex **25**. The possibility of the reaction of (^{iPr2}POCN^{Et2})PdX complex with aryl iodide rather than with the species **B** can be ruled out because the former reaction will generate a

saturated 18e$^-$ complex, which may not react further. The generated palladium-benzothiazolyl complex **25** then oxidatively reacts with the aryl iodide in the turnover-limiting step to produce an octahedral (^{iPr2}POCN^{Et2})Pd(IV)(benzothiazolyl)(Ar)I species **C**. The reductive elimination of the coupled product from species **C** will regenerate the catalyst (^{iPr2}POCN^{Et2})PdX. Though there exist a number of reports on the arylation of azoles by palladium catalysts, all of them have shown a conventional Pd(0)/Pd(II) redox process with little experimental input. Herein, we have demonstrated a new mechanistic avenue for the arylation of azoles by installing a suitable ligand on the palladium. The reactions occur *via* a Pd(II)-Pd(IV)-Pd(II) pathway with C(sp^2)–X aryl iodide oxidative addition to the Pd(II)-species.

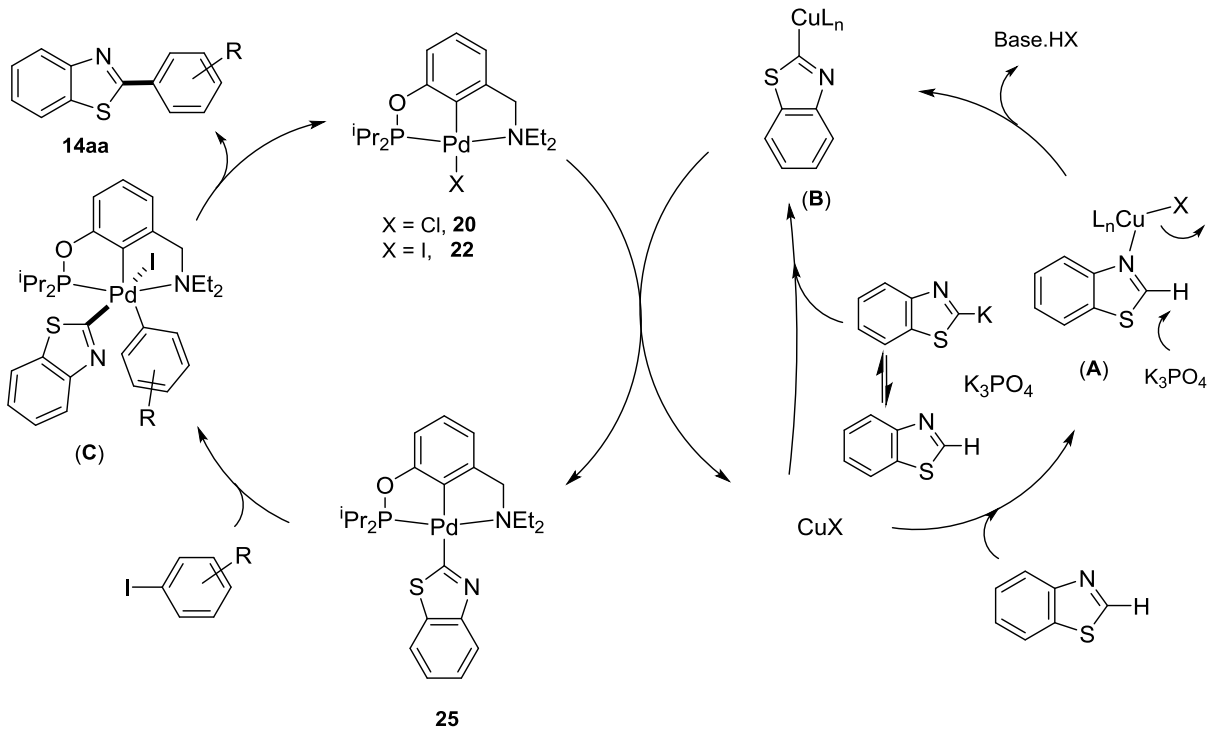

Figure 4.16 Proposed arylation pathway using (POCN)PdX.

4.3 Conclusion

This chapter demonstrated the detailed mechanistic study for the arylation of azoles using newly synthesized hybrid pincer palladium complex. Kinetic measurements, reactivity studies and DFT calculations on the arylation reaction strongly support a Pd(II)/Pd(IV)/Pd(II) redox process for the reaction, which occurs *via* the oxidative addition of the C(sp^2)–X electrophile, aryl iodide, to the (POCN)Pd(II)-species. Intermolecular competition experiments between the electronically distinct azoles and their comparative kinetic studies

for the arylation reaction establish that the electronic properties on azoles are kinetically not relevant. The isolation and characterization of a catalytically active intermediate ($^{i\text{Pr}2}$POCN$^{\text{Et}2}$)Pd(benzothiazolyl) complex allowed the precise demonstration of the mechanistic pathway. Kinetic and reactivity studies of ($^{i\text{Pr}2}$POCN$^{\text{Et}2}$)Pd(benzothiazolyl) species are consistent with the oxidative addition of aryl iodide electrophile to the Pd(II)-species being a kinetically important step for the arylation reaction. All these studies provided a significant mechanistic insight into the direct arylation of azoles with aryl iodides, which could shed light into the palladium-catalyzed C–H bond arylation of other arenes and heteroarenes.

4.4 Experimental section

4.4.1 General procedure for added ligand experiments: To a flame-dried screw-capped Schlenk tube equipped with magnetic stir bar was introduced 4-iodotoluene **13a** (0.164 g, 0.75 mmol), Cs_2CO_3 (0.244 g, 0.75 mmol) and CuI (0.005 g, 0.025 mmol, 5.0 mol%) under argon. The screw-capped Schlenk tube with mixture was then evacuated and refilled with argon. To the above mixture was added benzothiazole **12a** (0.068 g, 0.50 mmol) and ($^{i\text{Pr}2}$POCN$^{i\text{Pr}2}$)PdCl (0.0025 mmol, 0.5 mol%, 1.0 mL of 0.0025 M stock solution in DMF) and appropriate amount of external ligand Bu_4NBr (0.016 g, 0.05 mmol) in DMF under argon. The resultant reaction mixture was then degassed, refilled with argon and was stirred at 120 ^{o}C in a pre-heated oil bath for 16 h. After stirring the reaction mixture at 120 ^{o}C for 16 h, the products were isolated by column chromatography. A similar protocol was followed for other additives, such as Hg (0.1 g, 0.5 mmol), PPh_3 (0.0013 g, 0.005 mmol), Py (0.03 g, 0.375 mmol) or PVPy (0.04 g, 0.375 mmol) and products were isolated by column chromatography.

The isolated yields of **14aa** obtained employing Bu_4NBr, Hg, PPh_3, Py and PVPy in the reactions are 40%, 42%, 94%, 76% and 80%, respectively.

4.4.2 Kinetic measurements for arylation reaction

Representative procedure for rate of arylation reaction using ($^{i\text{Pr}2}$POCN$^{\text{Et}2}$)PdCl: To the teflon-screw capped tube equipped with magnetic stir bar was introduced ($^{i\text{Pr}2}$POCN$^{\text{Et}2}$)PdCl (0.0011 g, 0.0025 mmol, from a stock solution), CuI (0.0009 g, 0.005 mmol, from a stock solution), K_3PO_4 (0.159 g, 0.75 mmol), 4-iodotoluene (0.163 g, 0.75 mmol) and benzothiazole (0.0675 g, 0.5 mmol), and DMF (required amount) was added to make the total volume 2.0 mL. To the reaction mixture mesitylene (0.030 mL, 0.2154 mmol) was added as an internal standard. The reaction mixture was then stirred at 120 ^{o}C in a pre-

heated oil bath. At regular intervals, the reaction vessel was cooled to ambient temperature and an aliquot of the sample was withdrawn to the GC vial. The sample was diluted with acetone and subjected to GC analysis. The concentration of the product **14aa** obtained in each sample was determined with respect to the internal standard mesitylene. The data of the concentration of the product *vs* time (min) plot was drawn (Figure 4.4).

Representative procedure for order determination: *Rate order determination for benzothiazole***:** To the teflon-screw capped tube equipped with magnetic stir bar was introduced catalyst ($^{i\text{Pr}2}$POCN$^{\text{Et}2}$)PdCl **20** (0.0011 g, 0.0025 mmol), CuI (0.0009 g, 0.005 mmol), K_3PO_4 (0.159 g, 0.75 mmol), 4-iodotoluene (0.163 g, 0.75 mmol) and specific amount of benzothiazole (as shown in Table 4.2), and DMF (required amount) was added to make the total volume 2.0 mL. To the reaction mixture mesitylene (0.030 mL, 0.2154 mmol) was added as an internal standard. The reaction mixture was then stirred at 120 ^{o}C in a pre-heated oil bath. At regular intervals, the reaction vessel was cooled to ambient temperature and an aliquot of the sample was withdrawn to the GC vial. The sample was diluted with acetone and subjected to GC analysis. The concentration of the product **14aa** obtained in each sample was determined with respect to the internal standard mesitylene.

4.4.3 Catalyst stability and product inhibition study

Procedure for catalyst recycling experiment: To the teflon-screw capped tube equipped with magnetic stir bar was introduced catalyst **20** (0.0011 g, 0.0025 mmol), CuI (0.0009 g, 0.005 mmol), K_3PO_4 (0.159 g, 0.75 mmol), 4-iodotoluene (0.163 g, 0.75 mmol) and benzothiazole (0.068 g, 0.5 mmol). To the reaction mixture, DMF (2.0 mL) and mesitylene (0.030 mL, 0.2154 mmol) were added, and the reaction mixture was stirred at 120 ^{o}C in a pre-heated oil bath for 16 h. The reaction vessel was then cooled to ambient temperature and an aliquot of the sample was withdrawn, whose GC analysis shown 98% yield of coupled product. To the same reaction mixture fresh benzothiazole (0.068 g, 0.5 mmol), 4-iodotoluene (0.163 g, 0.75 mmol) and K_3PO_4 (0.159 g, 0.75 mmol) were added and the reaction was further continued for 16 h. GC analysis of the reaction mixture after the second cycle showed 90% product.

Procedure for same [excess] experiment: The representative procedure of rate measurement was followed (sec 4.4.2), employing **20** (0.0011 g, 0.0025 mmol), CuI (0.0009 g, 0.005 mmol), K_3PO_4 (0.159 g, 0.75 mmol), benzothiazole (as shown in Table 4.7), 4-iodootoluene (as shown in Table 4.7) and required amount of DMF. The data were collected

till 180 min. The final data was obtained by averaging the result of two independent runs for each experiment.

4.4.4 Isotope labelling experiments

Procedure for determination of kinetic isotope effects: Representative procedure of rate measurement was followed (sec 4.4.2), employing **20** (0.0011 g, 0.0025 mmol), CuI (0.0009 g, 0.005 mmol), K_3PO_4 (0.159 g, 0.75 mmol), 2-*H*-benzothiazole (0.0675 g, 0.5 mmol) or 2-*D*-benzothiazole (0.0685 g, 0.5 mmol), 4-iodootoluene (0.163 g, 0.75 mmol) and DMF (~ 2.0 mL). The final data was obtained by averaging the result of two independent runs for each experiment. The data were collected till 60 min. The initial rate obtained for the coupling of 2-*H*-benzothiazole with 4-iodotoluene is 1.57×10^{-3} $Mmin^{-1}$, whereas the rate for the coupling of 2-*D*-benzothiazole with 4-iodotoluene is 1.63×10^{-3} $Mmin^{-1}$ (Figure 4.9). Therefore, the $k_H/k_D = 1.57 \times 10^{-3}/1.63 \times 10^{-3} = 0.96$.

Procedure for deuterium scrambling experiments: To a flame-dried screw-capped Schlenk tube equipped with magnetic stir bar was introduced 6-ethoxy benzothiazole (0.088 g, 0.5 mmol), 2-*D*-benzothiazole (0.068 g, 0.5 mmol) and K_3PO_4 (0.159 g, 0.75 mmol) under argon. To the reaction mixture, DMF (1.0 mL) was added and the reaction mixture was heated at 120 ^oC for 15 min. At ambient temperature, the reaction mixture was diluted with H_2O (15 mL) and extracted with ethyl acetate (20 mL x 3). The combined organic layers were dried over $MgSO_4$ and the solvent was evaporated *in vacuo*. The remaining residue was purified by column chromatography on silica gel (petroleum ether/EtOAc: 40/1→ 5/1) to obtained 6-ethoxy-2-*H/D*-benzothiazole (0.084 g, 95% with 40% D) and 2-*H/D*-benzothiazole (0.052 g, 75% with 37% H). The deuterium incorporations were around similar even in the presence of catalyst **20** and co-catalyst CuI.

4.4.5 Procedure for electronic effect study

Rate of arylation for substituted benzothiazole: Representative procedure of rate measurement was followed (sec 4.4.2), employing **20** (0.0011 g, 0.0025 mmol), CuI (0.0009 g, 0.005 mmol), K_3PO_4 (0.159 g, 0.75 mmol), 4-iodootoluene (0.163 g, 0.75 mmol), benzothiazoles **12a** (0.675 g) (or **12d**: 0.0896 g; **12e**: 0.0765 g) (0.5 mmol) and required amount of DMF. The data were collected till 60 min. The final data was obtained by averaging the result of two independent runs for each experiment. The initial rates for the coupling reactions are shown in Figure 4.10.

Procedure for intermolecular competition experiment: Representative procedure of the catalysis experiment was followed, employing **20** (0.0011 g, 0.0025 mmol), CuI (0.0009 g, 0.005 mmol), K_3PO_4 (0.159 g, 0.75 mmol), 4-iodootoluene (0.043 g, 0.2 mmol) and 6-ethoxy-benzothiazole (0.107 g, 0.6 mmol), benzothiazole (0.081 g, 0.6 mmol) [or 6-ethoxy-benzothiazole (0.107 g, 0.6 mmol) and 6-flouro-benzothiazole (0.092 g, 0.6 mmol)] and DMF (2.0 mL), and the reaction mixture was heated at 120 ^oC for 16 h. The reaction mixture was then cooled to ambient temperature and was diluted with H_2O (15 mL). The reaction mixture was extracted with ethyl acetate (20 mL x 3), the combined organic layers were dried over $MgSO_4$ and the solvent was evaporated *in vacuo*. The remaining residue was purified by column chromatography on silica gel (petroleum ether/EtOAc: 40/1→ 20/1) to yield the coupled products in different yields. The ratio of **14aa**: **14da** = 1.39 and **14ea**: **14da** = 1.4.

Rate of arylation for different *para*-substituted aryl iodide: Representative procedure of rate measurement was followed (sec 4.4.2), employing **12a** (0.0011 g, 0.0025 mmol), CuI (0.0009 g, 0.005 mmol), K_3PO_4 (0.159 g, 0.75 mmol), benzothiazole **5a** (0.068 g, 0.5 mmol) and 4-iodootoluene (0.163 g, 0.75 mmol) or [4-iodoanisole (0.175 g, 0.75 mmol); iodobenzene (0.153 g, 0.75 mmol); 4-chloroiodobenzene (0.178 g, 0.75 mmol); methy-4-iodobenzoate (0.196 g, 0.75 mmol)] and required amount of DMF to make total volume 2.0 mL. The data were collected till 60 min. The final data was obtained by averaging the result of three independent runs for each experiment.

4.4.6 Catalyst reactivity study

Representative procedure: *Reaction of ($^{iPr2}POCN^{Et2}$)PdCl with **12a**, **13a**, CuI and K_3PO_4:* To a J-Young NMR tube with PMe_3 capillary (as standard) was introduced (^{iPr2}POCN^{Et2})PdCl (**20**) (0.0109 g, 0.025 mmol), benzothiazole (0.0337 g, 0.25 mmol), 4-iodotoluene (0.0817 g, 0.375 mmol), CuI (0.0005 g, 0.0025 mmol), K_3PO_4 (0.0795 g, 0.375 mmol), and DMF (0.5 mL) was added in-side the Glove-box. The J-Young NMR tube with the reaction mixture was then heated in a pre-heated oil-bath at 100 ^oC, and the reaction mixture was analyzed by NMR at regular intervals.

*Reaction ($^{iPr2}POCN^{Et2}$)PdCl with 4-iodotoluene (**13a**):* The representative procedure was followed, using (^{iPr2}POCN^{Et2})PdCl (**20**) (0.0109 g, 0.025 mmol), 4-iodotoluene (0.0817 g, 0.375 mmol) and DMF (0.5 mL).

*Reaction ($^{iPr2}POCN^{Et2}$)PdCl with benzothiazole (**12a**) and K_3PO_4:* The representative procedure was followed,, using (^{iPr2}POCN^{Et2})PdCl (**20**) (0.0109 g, 0.025 mmol), benzothiazole (0.0337 g, 0.25 mmol), K_3PO_4 (0.0795 g, 0.375 mmol), and DMF (0.5 mL).

4.4.7 Procedure for synthesis of (^{iPr2}POCN^{Et2})Pd-benzothiazolyl (25): To a stirred solution of benzothiazole (0.310 g, 2.293 mmol) in THF (10 mL) was added *n*-BuLi (1.58 mL, 1.6 M in hexane, 2.520 mmol) at –78 ^{o}C. After stirring the resultant reaction mixture at -78 ^{o}C for 20 min, a cold (-78 ^{o}C) solution of (^{iPr2}POCN^{Et2})PdCl (0.2 g, 0.458 mmol) in THF (10 mL) was added *via* cannula. The reaction mixture was stirred at –78 ^{o}C for 2 h and the volatiles were evaporated under reduced pressure. The crude product was extracted with ethyl acetate (40 mL) and purified by column chromatography on neutral alumina (petroleum ether/EtOAc: 20/1→5/1→2/1) to obtain compound **25**. Yield: 0.194 g, 79%. M.p. = 142–144 ^{o}C. ^{1}H-NMR (500 MHz, $CDCl_3$): δ = 8.01 (d, *J* = 7.9 Hz, 1H, Ar–H), 7.84 (d, *J* = 7.9 Hz, 1H, Ar–H), 7.30 (dd, *J* = 7.9, 7.0 Hz, 1H, Ar–H), 7.17 (dd, *J* = 7.6, 7.3 Hz, 1H, Ar–H), 6.97 (dd, *J* = 7.9, 7.6 Hz, 1H, Ar–H), 6.71 (d, *J* = 7.3 Hz, 1H, Ar–H), 6.66 (d, *J* = 7.9 Hz, 1H, Ar–H), 4.26 (s, 2H, CH_2), 3.21 (app sextet, *J* = 7.3 Hz, 2H, C*H*$_2$CH$_3$), 2.77 (app septet, *J* = 6.1 Hz, 2H, C*H*$_2$CH$_3$), 2.36-2.45 (m, 2H, C*H*(CH$_3$)$_2$), 1.50 (t, *J* = 7.0 Hz, 6H, CH$_2$C*H*$_3$), 1.29 (dd, *J* = 15.6 Hz, *J* = 7.0 Hz, 6H, CH(C*H*$_3$)$_2$), 1.18 (dd, *J* = 19.2 Hz, *J* = 7.3 Hz, 6H, CH(C*H*$_3$)$_2$). ^{13}C{^{1}H}-NMR (125 MHz, $CDCl_3$): δ = 205.2 (d, J_{P-C} = 13.4 Hz, C_q), 163.1 (d, J_{P-C} = 6.7 Hz, C_q), 157.1 (C_q), 152.7 (C_q), 152.6 (C_q), 137.8 (C_q), 126.6 (CH), 123.9 (CH), 121.8 (CH), 120.8 (CH), 120.7 (CH), 114.8 (CH), 107.8 (d, J_{P-C} = 16.2 Hz, CH), 68.1 (CH_2), 56.8 (2C, *C*H$_2$CH$_3$), 29.0 (d, J_{P-C} = 26.7 Hz, 2C, *C*H(CH$_3$)$_2$), 17.8 (d, J_{P-C} = 5.7 Hz, 2C, CH(*C*H$_3$)$_2$), 16.9 (2C, CH(*C*H$_3$)$_2$), 13.9 (2C, CH$_2$(*C*H$_3$)$_2$). ^{31}P{^{1}H}-NMR (202 MHz, $CDCl_3$): δ = 196.0 (s). HRMS (ESI): *m/z* calcd for $C_{24}H_{33}N_2OPPdS+H^+$ $[M+H]^+$ 535.1164, found 535.1169. Anal. calcd for $C_{24}H_{33}N_2OPPdS$: C, 53.88; H, 6.22; N, 5.24. Found: C, 54.25; H, 7.16; N, 4.59.[291]

4.4.8 Reactivity of (^{iPr2}POCN^{Et2})Pd-benzothiazolyl (25)

Representative procedure: *Reaction (^{iPr2}POCN^{Et2})Pd-benzothiazolyl (**25**) with 4-iodotolune:* To a J-Young NMR tube with PMe_3 capillary (as standard) was introduced (^{iPr2}POCN^{Et2})Pd-benzothiazolyl (**25**) (0.010 g, 0.019 mmol) and 4-iodotoluene (0.0041 g, 0.019 mmol), and DMF (0.5 mL) was added in-side the Glove-box. The J-Young NMR tube with the reaction mixture was then heated in a pre-heated oil-bath at 100 ^{o}C and the reaction mixture was analyzed by ^{31}P NMR as well as by GC analysis.

*Reaction of (^{iPr2}POCN^{Et2})Pd-benzothiazolyl (**25**) with I_2***:** The representative procedure was followed, using (^{iPr2}POCN^{Et2})Pd-benzothiazolyl (**25**) (0.010 g, 0.019 mmol) and I_2 (0.0093 g, 0.037 mmol), the reaction mixture shaken at room temperature for 30 min

Procedure for reaction of (^{iPr2}POCN^{Et2})Pd-benzothiazolyl (25) with different aryl iodides: To a J-Young NMR tube with PMe_3 capillary (as standard) was introduced (^{iPr2}POCN^{Et2})Pd-benzothiazolyl (**25**) (0.013 g, 0.025 mmol, 0.05 M), 4–methoxy-iodobenzene (0.0058 g, 0.025mmol) or 4-acetyl-iodobenzene (0.062 g, 0.025 mmol), and DMF (0.5 mL) was added in-side the Glove-box. The J-Young NMR tube with the reaction mixture was then heated in a pre-heated oil-bath at 100 ^{o}C and the formation of product (^{iPr2}POCN^{Et2})PdI (**22**) was monitored by ^{31}P NMR at different time intervals (1 h, 2 h, 3 h, 5 h, 7 h). The conversion percentage of **25** to **22** and concentrations thereof were calculated w.r.t standard PMe_3 capillary. The plot was drawn between conc. of **22** *verses* time (h) (Figure 4.13).

NB: The conversion of (^{iPr2}POCN^{Et2})Pd-benzothiazolyl (**25**) to (^{iPr2}POCN^{Et2})PdI (**22**) was faster at 120 ^{o}C, hence this kinetic was performed at 100 ^{o}C.

Chapter 5

Nickel(II)-catalyzed selective C(2)–H alkynylation of heteroarenes with alkynyl bromide

5.1 Introduction

Nitrogen-containing heteroarenes are the key structural motif of many natural products, biologically active compounds, agrochemicals and functional materials.[348-358] As a consequence, efficient functionalization of such heteroaromatic scaffolds is very crucial, particularly, by the transition-metal-catalyzed direct C–H bond activation strategy.[191,196,198, 200-205,271,274,359-365] Though, numerous methods for the C–H bond arylations, alkenylations and alkylations of heteroarenes have established and utilized in organic synthesis,[269-273,366-368] the alkynylation reaction is of particular interest due to the versatile alkynyl-functionality for late-stage modification and diversification.[369-371] Till date, direct alkynylation of heteroarenes has mostly been executed by the use of noble and expensive 4d and 5d transition-metal-catalysts, typically with high loadings, which clog the practical applications.[372-390] However, in recent years, the earth-abundant 3d transition metals for C–H bond functionalization have attracted considerable attention because of their beneficial features and low-cost.[278,391-397] In that direction, Cu-catalyzed alkynylation of heteroarenes, such as activated azoles[398-400] as well as heterocycle-amides bearing a bidentate-chelate auxiliary[401] has been reported. In 2015, Shi group has introduced the cobalt metal for alkynylation of indole with alkynylated hypervalent iodine under simple and redox-neutral condition.[402] Recently, Ackerman and co-workers reported alkynylation of indole with the readily available 1-alkynyl bromides under mild reaction condition.[403]

Recently, nickel-catalyzed C–H functionalization has given particular attention because of the wide availability and versatile reactivity of nickel, and found beneficial for many crucial transformations.[278,395,396,404] In that regard, Miura and co-workers reported the Ni-catalyzed alkynylation of azoles, however, this method is mostly limited to the activated heteroarenes.[242,243] Particularly, for the most part, Ni-catalyzed direct alkynylation of (hetero)arenes has been described for the electron-deficient carboxamides involving *N*, *N*-bidentate-chelate auxiliary, 8-quinolinyl or isopropyl-2-pyridinyl; wherein the installation of expensive bidentate auxiliary on each substrate stages the major disadvantage.[244,245,405,406] Nevertheless, recently, Ackermann and co-worker developed a novel strategy for the nickel-catalyzed alkynylation of anilines with the help of a monodentate-chelate auxiliary,[230] however, with limited success for heteroarenes. In this chapter, the regioselective C-2 alkynylation of indoles and similar heteroarenes with bromoalkyne by nickel-catalysis has been discussed *via* mono-chelate assistance.[407]

5.2 Result and discussion

5.2.1 Optimization of catalytic condition

The optimization of the reaction conditions for C–H alkynylation was investigated using indole **27a** as a model substrate (bearing monodentate *N*-2-pyridinyl substituent) with the alkynyl bromide **28** (Table 5.1). Various nickel(II) precursors were tested as a catalyst for the alkynylation reaction employing bidentate ligand, 1,10-phenanthroline (Phen) and LiO^tBu base. Interestingly, all the Ni(II)-precursors efficiently catalyze the alkynylation reaction, and excellent yield of alkynylation product **29a** (96%) was obtained using $(THF)_2NiBr_2$/Phen system in the presence of LiO^tBu in toluene (Table 5.1, entries 2-5); however, alkynylation was not observed in the absence of Ni-catalyst (Table 5.1, entry 1). The use of other nitrogen-containing bidentate ligand, such as 2,2'-bipyridine (Bipy) gave slightly lower yield, whereas neocuproine, bathocuproine, and monodentate ligands (pyridine, lutidine, 4-*N*,*N*-dimethyl amino pyridine (DMAP)) were less effective and resulted in poor yield of **29a** (Table 5.1, entries 6-11). A catalyst stabilizing ligand is essential to achieve a good yield of the alkynylation product, without that only 10% yield of **29a** was observed (Entry 12). Alkynylation reaction in the presence of other inorganic mild bases, like K_3PO_4, Li_2CO_3, Na_2CO_3, and $NaHCO_3$ produces diminish yield of **29a** (Entries 13-16). The reaction was also efficient in solvents like 1,4-dioxane, *o*-xylene, *p*-xylene, and mesitylene (Table 5.1, entries 18-21). When the reaction temperature was lowered to 130 ^oC, desired coupled product was obtained in 78% yield (Entry 22). Employing the low loading of catalyst 0.1% and 0.01%, the coupled product **29a** was produced in 56% and 45% yield, respectively (Entries 23, 24). Thus, all the alkynylation reactions of heteroarenes were performed using $(THF)_2NiBr_2$/Phen (3 mol%) in toluene at 150 ^oC and the reactions were carried out for 12 h, except as noted otherwise. Unfortunately, the phenyl acetylene bromide and octyl acetylene bromide did not react to give the desired alkynylated products.

Table 5.1 Optimization of reaction conditions for alkynylation[a]

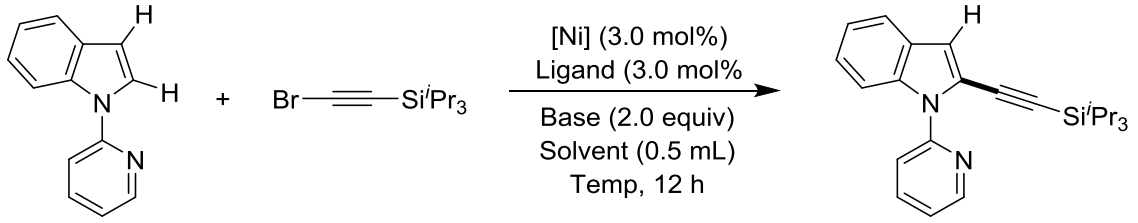

27a **28** **29a**

Entry	[Ni]	Ligand	Base	Solvent	Temp (^{o}C)	Yield (%)[b]
1	-	Phen	LiO^{t}Bu	toluene	150	0
2	Ni(OAc)$_2$	Phen	LiO^{t}Bu	toluene	150	72
3	Ni(OTf)$_2$	Phen	LiO^{t}Bu	toluene	150	93
4	(DME)NiCl$_2$	Phen	LiO^{t}Bu	toluene	150	73
5	**(THF)$_2$NiBr$_2$**	**Phen**	**LiO^{t}Bu**	toluene	**150**	**96**
6	(THF)$_2$NiBr$_2$	Bipy	LiO^{t}Bu	toluene	150	79
7	(THF)$_2$NiBr$_2$	Neocuproine	LiO^{t}Bu	toluene	150	27[c]
8	(THF)$_2$NiBr$_2$	Bathocuproine	LiO^{t}Bu	toluene	150	15[c]
9	(THF)$_2$NiBr$_2$	Pyridine	LiO^{t}Bu	toluene	150	55[c]
10	(THF)$_2$NiBr$_2$	Lutidine	LiO^{t}Bu	toluene	150	26[c]
11	(THF)$_2$NiBr$_2$	DMAP	LiO^{t}Bu	toluene	150	27[c]
12	(THF)$_2$NiBr$_2$	-	LiO^{t}Bu	toluene	150	10[c]
13	(THF)$_2$NiBr$_2$	Phen	K_3PO_4	toluene	150	5[c]
14	(THF)$_2$NiBr$_2$	Phen	Li_2CO_3	toluene	150	trace
15	(THF)$_2$NiBr$_2$	Phen	Na_2CO_3	toluene	150	2[c]
16	(THF)$_2$NiBr$_2$	Phen	$NaHCO_3$	toluene	150	trace
18	(THF)$_2$NiBr$_2$	Phen	LiO^{t}Bu	1,4-dioxane	150	75[c]
19	(THF)$_2$NiBr$_2$	Phen	LiO^{t}Bu	*o*-xylene	150	93
20	(THF)$_2$NiBr$_2$	Phen	LiO^{t}Bu	*p*-xylene	150	90
21	(THF)$_2$NiBr$_2$	Phen	LiO^{t}Bu	mesitylene	150	90
22	(THF)$_2$NiBr$_2$	Phen	LiO^{t}Bu	toluene	130	78
23	(THF)$_2$NiBr$_2$	Phen	LiO^{t}Bu	toluene	150	56[d]
24	(THF)$_2$NiBr$_2$	Phen	LiO^{t}Bu	toluene	150	45[e]

[a] Reaction conditions: **27a** (0.059 g, 0.304 mmol), **28** (0.117 g, 0.45 mmol), [Ni]-source (0.009 mmol, 3 mol%), ligand (0.009 mmol, 3 mol%), base (0.6 mmol), solvent (0.5 mL), 12 h. [b] Isolated yield. [c] GC yield using mesitylene as internal standard. [d] Using 0.1 mol% of [Ni]-catalyst and heated for 40 h. [e] Using 0.01 mol% of [Ni]-catalyst and heated for 48 h.

5.2.2 Screening of *N*-substituent at indole

Indole **27a** bearing 2-pyridinyl as the *N*-substituent efficiently coupled with alkynyl bromide **28** and afforded 96% of **29a** under the optimized catalytic conditions. Hence, the possibility of other *N*-substituents was explored by installing 2-pyrimidinyl and 2-pyrazinyl at the nitrogen of indole, wherein the yields of the desired coupled products obtained were 85% and 66%, respectively (Scheme 5.1). Further, to understand the coordinating ability *verses* the electronic impact of *N*-substituents, the 3-pyridinyl and 4-pyridinyl-substituted indoles were employed for the reaction, wherein the alkynylation was not observed. This clearly suggests that the coordinating functionality, not the electronically similar substituent, is mandatory at the *N*-center of indole. On the other hand, indoles containing different coordinating groups, such as –C(O)Ph, –C(O)O^{t}Bu and 2-thiophenyl at the *N*-center did not produce the desired alkynylation products. These results indicate that a nitrogen coordinating group at the 2-position of the *N*-substituent is essential for the alkynylation of indole derivatives.

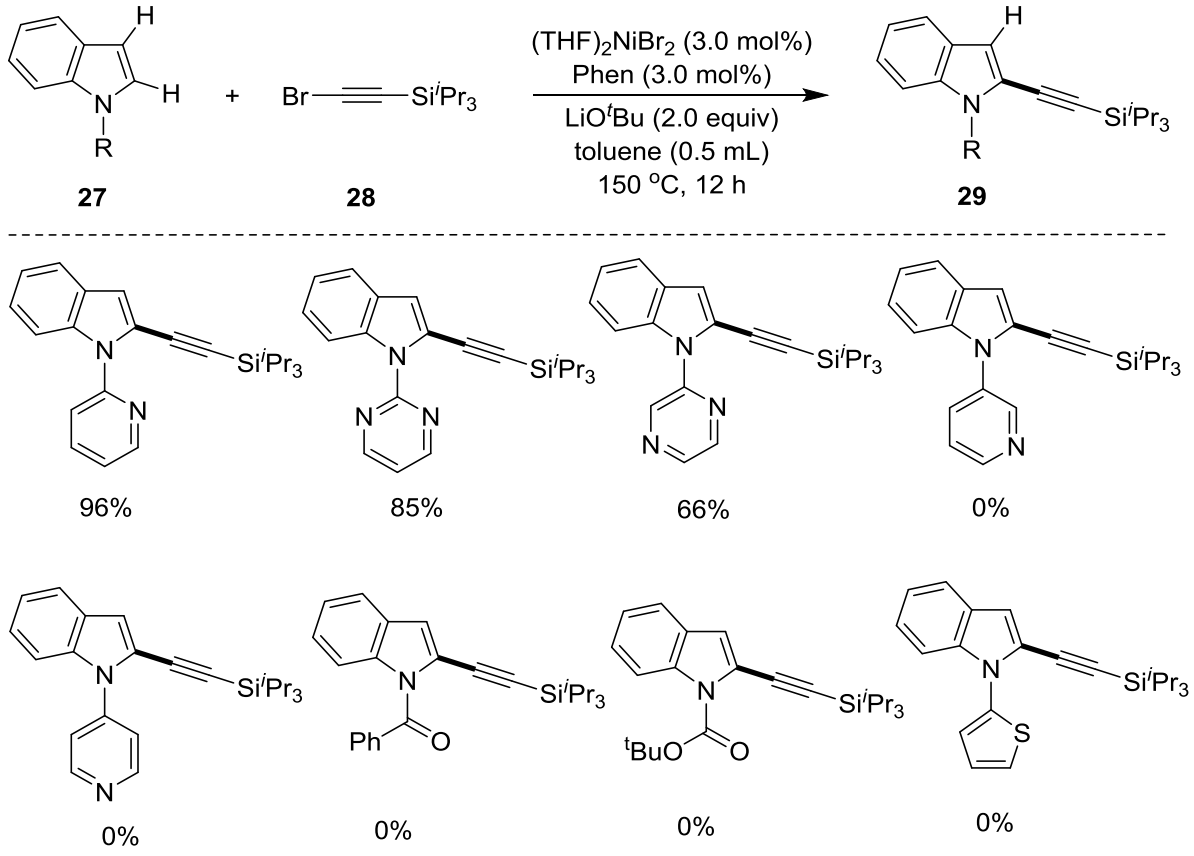

Scheme 5.1 Screening of *N*-substituent at indole

5.2.3 Scope of nickel-catalyzed alkynylation

5.2.3.1 Scope of indoles and pyrroles

With the optimized reaction conditions in hand, the method was employed for the C–H alkynylation of diversely substituted indoles **27** using $(THF)_2NiBr_2$/Phen (3.0 mol%) in toluene (Scheme 5.2). Numerous functional groups, such as ether, halides, nitrile, and nitro were tolerated in the indole backbone and afforded good to excellent yields of desired C(2) alkynylation products **29a**-**g**. The alkynylation reaction progressed conveniently for indoles bearing both the electron-donating and electron-withdrawing substituents. Notably, the alkynylation occurred only at the C(2)–H position of indoles, and the C(3)–H remained intact. To our surprise, the C(3) substituted indoles also afforded excellent yields of alkynylation products **29h** (91%) and **29i** (94%). As discussed earlier, this protocol is not only restricted to *N*-2-pyridinyl substituted indoles, the 2-pyrimidinyl and 2-pyrazinyl substituted indoles also reacted smoothly with the alkynyl bromide **28** to produce the C(2) alkynylation products **29j**-**29r** in good yields, with the exceptional functional group tolerability.

This Ni-catalyzed protocol was applied to the C–H alkynylation of pyrrole. Thus, the treatment of 3.0 equiv *N*-2-pyrimidinyl-pyrrole **27s** with alkynyl bromide **28** as limiting substrate afforded the mono-alkynylation product **29s** in 50% yield and 2,5-bis-alkynylation pyrrole **29t** in 20% yield; whereas the reaction of **27s** with an excess of **28** (2.5 equiv) gave selectively 2,5-bis-alkynylation pyrrole **29t** in 56% yield (Scheme 5.2). In both the alkynylation reactions, quantitative conversion of pyrrole substrate was observed, though the isolated yields were moderate. In particular, previously reported Co-catalyzed alkynylations were mainly demonstrated for the 2-pyrimidinyl-substituted indoles and pyrroles, while low yield was reported for a 2-pyridinyl substituted indole substrate.[402,403] This methodology provides easy alkynylation of indole bearing 2-pyridinyl, 2-pyrimidinyl, and 2-pyrazinyl as the *N*-substituents, as well as tolerate essential functional groups, such as –CN and $–NO_2$ in the indole backbone. Previous Co-catalyzed alkynylation method did not show tolerance of such functional groups.[402] These features of the present Ni-catalyzed alkynylation protocol makes it unique, compared to the previously reported 3d transition-metal-catalyzed indole alkynylation processes.

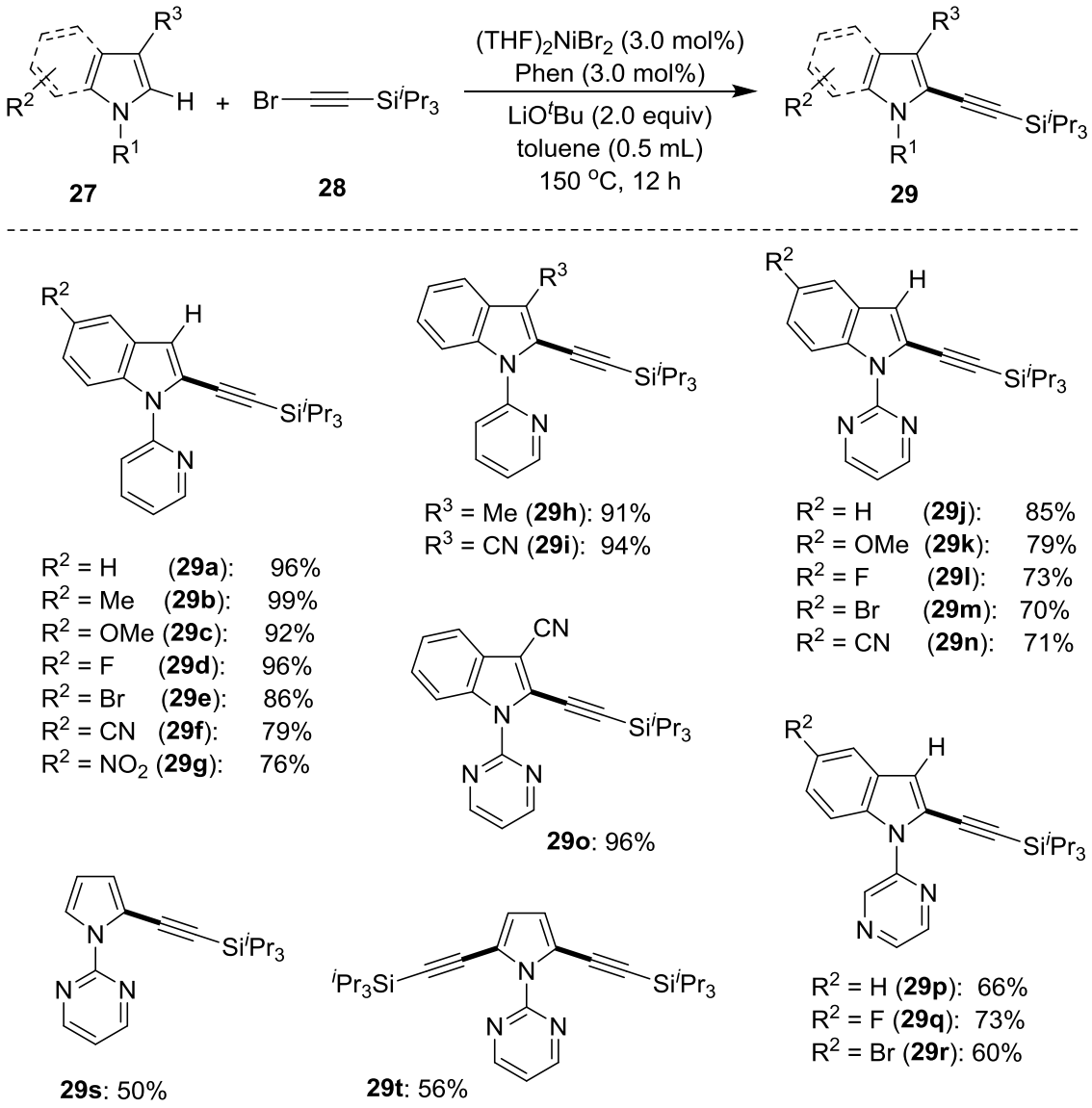

Scheme 5.2 Scope of nickel-catalyzed alkynylation of indoles and pyrroles

5.2.3.2 Scope of benzimidazoles, imidazoles, and pyrazoles

The Ni-catalyzed C–H alkynylation protocol is extended to other heteroarenes, such as imidazoles, benzimidazoles, and pyrazole (Scheme 5.3). The *N*-2-pyridinyl and *N*-2-pyrimidinyl substituted benzimidazoles (**30a**, **30b**) afforded moderate to good yields of C-2 alkynylation products **31a** and **31b**. The mixture of 5-methyl-1-(pyridin-2-yl)-1*H*-benzo[*d*]imidazole (**30c**) and 6-methyl-1-(pyridin-2-yl)-1*H*-benzo[*d*]imidazole (**30c'**) upon alkynylation gave good yield of the alkynylation products **31c** and **31c'** as mixture. These two isomers were not separable by column chromatography and hence, characterized as a mixture. The 2-(2-methyl-1*H*-imidazol-1-yl)pyridine (**30d**) exclusively produced the C-5 alkynylation product **31d** at 130 °C in moderate yield, whereas the *N*-2-pyridinyl-imidazole **30e** gave the

mixture of mono-alkynylation imidazole **31e** and bis-alkynylation imidazole **31f**. Additionally, a pyrazole-derivative **30g** on alkynylation at 130 ^{o}C affords particularly C-5 alkynylation product **31g** in 48% yield. Similar to the alkynylation of pyrrole, the reactions of imidazole and benzimidazole derivatives resulted in the complete conversions, although the isolated yields of the products were moderate. This might be due to the partial decomposition of substrates and/or the products during the reaction under the optimized conditions.

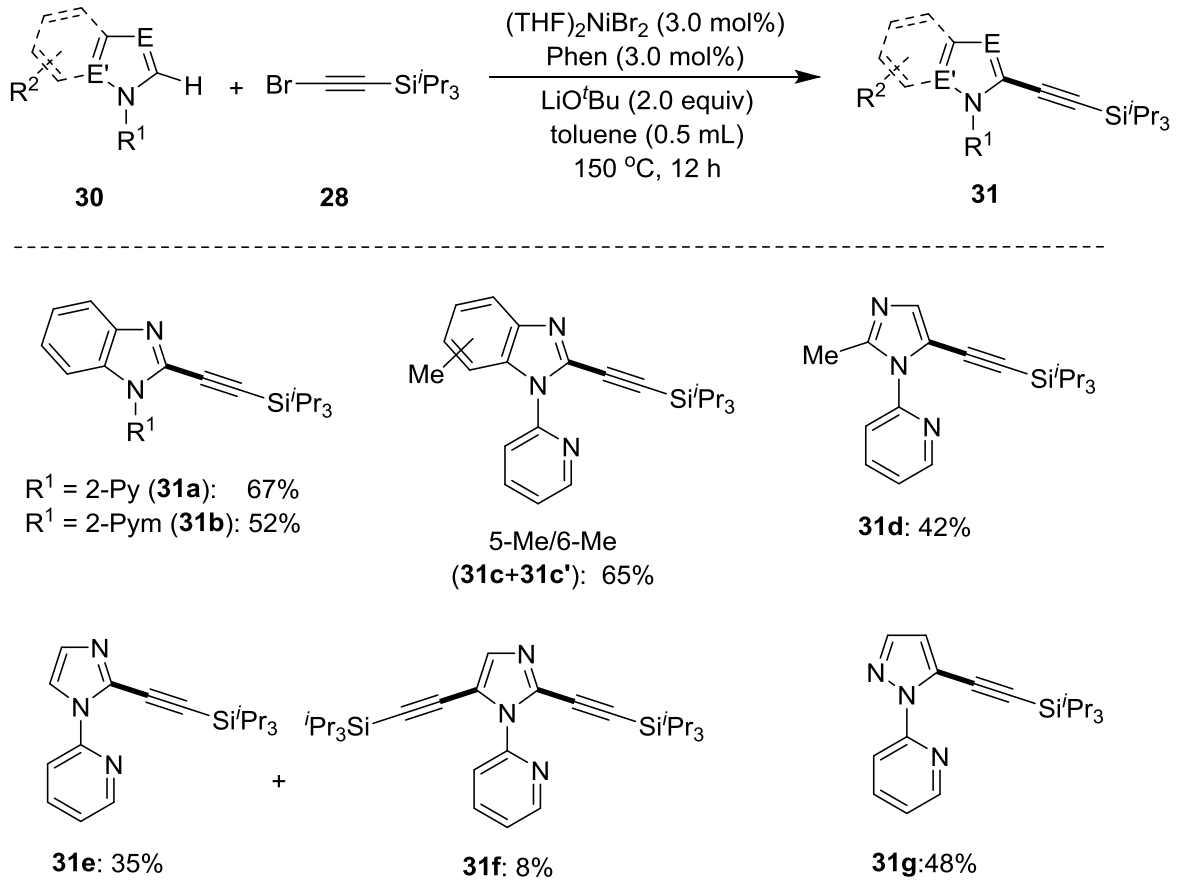

Scheme 5.3 Scope of nickel-catalyzed alkynylation of benzimidazole, imidazole, and pyrazole

5.2.4 Synthetic utility of Ni-catalyzed alkynylation reaction

The synthetic utility of Ni-catalyzed alkylation reaction was demonstrated by the deprotection of silyl group and further functionalization into triazole, alkynyl arenes and benzofuran derivatives. The deprotection of silyl group of **29a** was carried out using tetrabutyl ammonium fluoride in THF, which produces free alkyne **32a** in excellent yield (Scheme 5.4). Similarly, deprotection of **29b**, **29f**, and **29g** achieved using TBAF in THF to provide free alkynyl **32b**, **32f**, and **32g**, respectively. Further, these compounds, **32a**, **32b**, **32f**

and **32g** on treatments with benzyl azide in the presence of CuI produced cyclized products **33a**, **33b**, **33f**, and **33g**, respectively in excellent yields (Scheme 5.5). These compounds are essential building blocks of many pharmaceutical and biologically active compounds.[408-410]

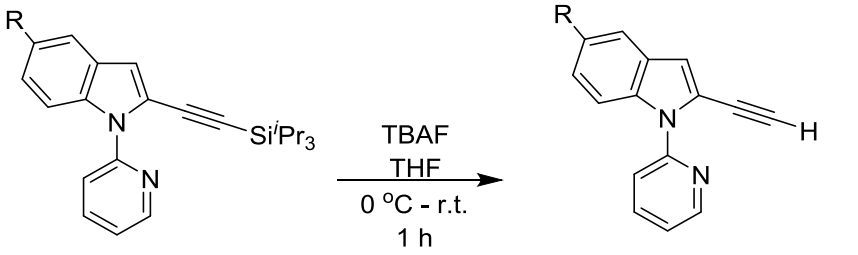

R = H, (**29a**)
R = Me, (**29b**)
R = CN, (**29f**)
R = NO_2, (**29g**)

R = H, (**32a**): 94%
R = Me, (**32b**): 87%
R = CN, (**32f**): 91%
R = NO_2, (**32g**): 97%

Scheme 5.4 Deprotection silyl group

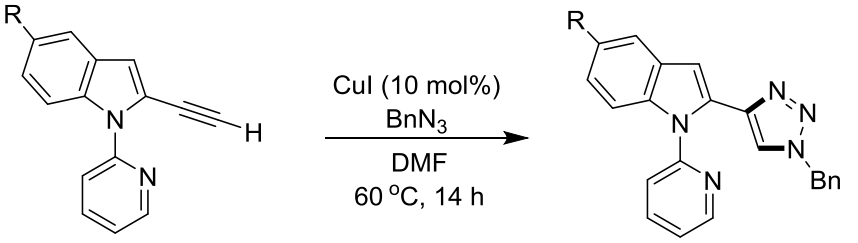

R = H, (**32a**)
R = Me, (**32b**)
R = CN, (**32f**)
R = NO_2, (**32g**)

R = H, (**33a**): 79%
R = Me, (**33b**): 93%
R = CN, (**33f**): 68%
R = NO_2, (**33g**): 50%

Scheme 5.5 Synthesis of triazole derivatives

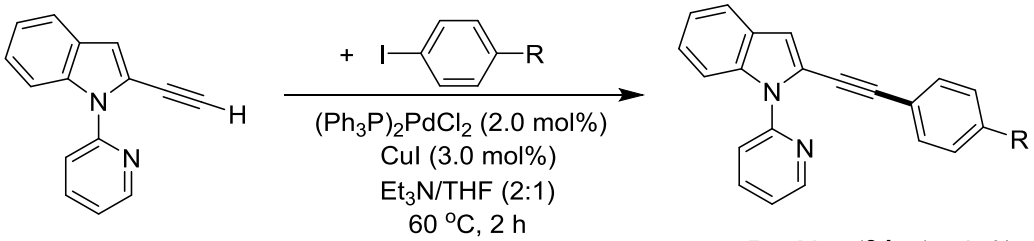

32a

R = Me, (**34aa**): 87%
R = OMe, (**34ab**): 77%

Scheme 5.6 Synthesis of alkynyl arenes

The efficient synthesis of alkynyl arenes **34aa** and **34ab** were achieved by the coupling of deprotected alkynyl derivatives **32a** with different aryl iodide using $(Ph_3P)_2PdCl_2$, CuI, and Et_3N in THF at 60 ^oC (Scheme 5.6). Similarly, the coupling of **32a** with 2-hydroxy iodobenzene in the presence of $(Ph_3P)_2PdCl_2$ provides benzofuranyl derivatives **35a** in moderate yield (Scheme 5.7).

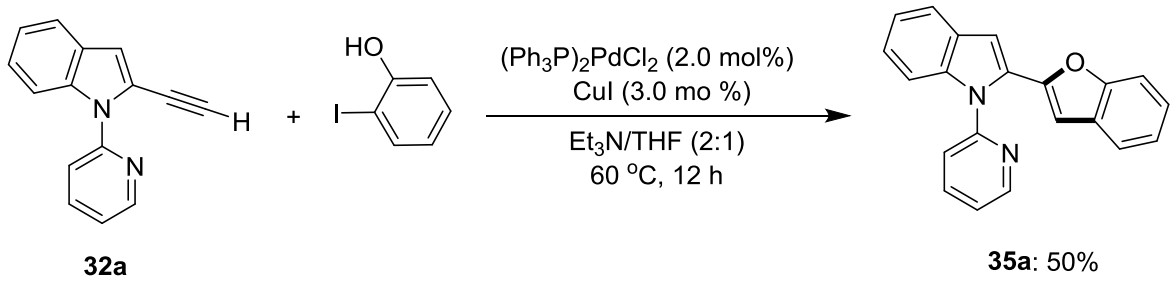

Scheme 5.7 Synthesis of benzofuranyl derivative

5.3 Conclusion

This chapter describes the Ni(II)-catalyzed regioselective C(2)–H alkynylation of heteroarenes with alkynyl bromide. This is the first example of Ni^{II}-catalyzed C–H alkynylation of diverse nitrogen-containing heteroarenes, such as indoles, pyrroles, benzimidazoles, imidazoles, and pyrazole, through monodentate chelation assistance. This method promotes extensive substrates scope with remarkable functional groups (–OMe, –CN, $–NO_2$ and halides) tolerance. Synthetic utility of this Ni-catalyzed process has been demonstrated by the deprotection of silyl-moiety, and by synthesizing pharmaceutically relevant triazolyl-2-pyridinyl-1*H*-indole and benzofuranyl-2-pyridinyl-1*H*-indole derivatives.

5.4 Experimental section

All manipulations were conducted under an argon atmosphere in a glove box or by using standard Schlenk techniques in predried glassware. The catalytic reactions were performed in flame-dried reaction vessels with Teflon screw caps. Solvents were dried over Na/benzophenone or CaH_2 and distilled prier to use. Liquid reagents were flushed with argon prior to use. $(THF)_2NiBr_2$,[411] 2-pyridinyl-substituted indoles (**27a**–**27i**),[412-414] 2-pyrimidinyl-substituted indoles (**27j**–**27o**),[415,416] 2-pyrazinyl-substituted indoles (**27p**–**27r**),[417] N-(2-pyrimidinyl)pyrrole (**27s**),[412,415] *N*-(2-pyridinyl)benzimidazole (**30a**),[418] and N-(2-pyridinyl)imidazole (**30e**)[418] were synthesized according to previously described procedures. Alkynyl bromide **28**, phenylacetylene bromide and octylacetylene bromide were synthesized

according to literature procedures.[419] All other chemicals were obtained from commercial sources and were used without further purification.

5.4.1 Synthesis and characterization of starting precursors

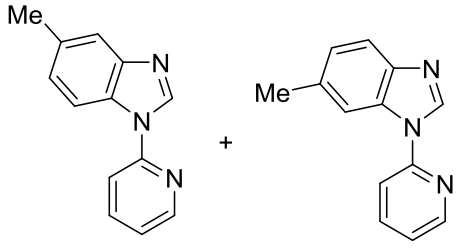

(**30c**) (**30c'**)

5-Methyl-1-(pyridin-2-yl)-1*H*-indole and 6-Methyl-1-(pyridin-2-yl)-1*H*-indole (30c and 30c'): These two compounds were synthesized as a mixture following the procedure similar to the synthesis of 1-(pyridin-2-yl)-1*H*-benzo[*d*]imidazole,[412] using 5-methyl-1*H*-benzo[*d*]imidazole (0.25 g, 1.891 mmol), 2-bromopyridine (0.198 ml, 2.08 mmol) and KOH (0.265 g, 4.725 mmol). Purification by column chromatography on basic alumina (Petroleum ether/EtOAc: 30/1→5/1) yielded mixture of **30c** and **30c'** as oily liquids (Note: *Though the reaction was conducted with 5-methyl-1H-benzo[d]imidazole, gave mixture of **30c** and **30c'**. It is assumed that the deprotonated benzoimidazole i.e.5-methyl amido species isomerized to 6-methyl amido species, which leads to the product* **30c'** *in addition to* **30c**). Yield: 0.225 g, 57%. ^{1}H-NMR (500 MHz, $CDCl_3$): δ 8.61-8.59 (m, 2H, Ar–H), 8.54 (s, 1H, Ar–H), 8.49 (s, 1H, Ar–H), 7.93 (d, J = 8.3 Hz, 1H, Ar–H), 7.89 (td, J = 7.6, 1.9 Hz, 1H, Ar–H), 7.86 (d, J = 1.5, Hz, 1H, Ar–H), 7.85 (br s, 1H, Ar–H), 7.73 (d, J = 8.3 Hz, 1H, Ar–H), 7.64 (s, 1H, Ar–H), 7.56-7.54 (m, 2H, Ar–H), 7.30-7.26 (m, 2H, Ar–H), 7.21-7.17 (m, 2H, Ar–H), 2.52 (s, 3H, CH_3), 2.50 (s, 3H, CH_3). ^{13}C{^{1}H}-NMR (125 MHz, $CDCl_3$): δ 150.1 (C_q), 150.1 (C_q), 149.6 (CH), 149.5 (CH), 145.1 (C_q), 142.9 (C_q), 141.4 (CH), 141.0 (CH), 139.1 (CH), 139.0 (CH), 134.4 (C_q), 133.2 (C_q), 132.5 (C_q), 130.3 (C_q), 125.8 (CH), 124.9 (CH), 121.9 (CH), 121.8 (CH), 120.6 (CH), 120.2 (CH), 114.6 (CH), 114.2 (CH), 112.7 (CH), 112.3 (CH), 22.1 (CH_3), 21.6 (CH_3). HRMS (ESI): *m/z* calcd for $C_{13}H_{11}N_3+H^+$ $[M+H]^+$ 210.1028; found 210.1026.

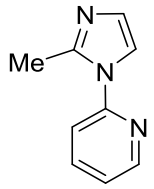

2-(2-Methyl-1*H*-imidazol-1-yl)pyridine (30d): This compound was synthesized following the procedure similar to the synthesis of 2-(1*H*-imidazol-1-yl)pyridine,[412] using 2-methylimidazole (1.0 g, 12.18 mmol), 2-bromopyridine (1.27 mL, 13.39 mmol) and KOH (1.71 g, 30.45 mmol). Purification by column chromatography on basic alumina (Petroleum ether/EtOAc: 10/1→1/3) yielded **30d** as a brown oil. Yield: 0.78 g, 40%. ^{1}H-NMR (500 MHz, $CDCl_3$): δ 8.51 (d, J = 3.8 Hz, 1H, Ar–H), 7.81 (td, J = 8.0, 1.5 Hz, 1H, Ar–H), 7.29-7.27 (m, 2H, Ar–H), 7.23 (d, J = 1.1, Hz, 1H, Ar–H), 6.99 (d, J = 1.5 Hz, 1H, Ar–H), 2.55 (s, 3H, CH_3). ^{13}C^{401}-NMR (125 MHz, $CDCl_3$): δ 150.5 (C_q), 149.2 (CH), 145.0 (C_q), 138.9 (CH), 127.1 (CH), 122.7 (CH), 119.1 (CH), 117.4 (CH), 15.0 (CH_3). HRMS (ESI): *m/z* calcd for $C_9H_9N_3$+H^+ $[M+H]^+$ 160.0869; found 160.0869.

5.4.2 Representative procedure for alkynylation and characterization data

Synthesis of 1-(pyridin-2-yl)-2-((triisopropylsilyl)ethynyl)-1*H*-indole (29a): To a flame dried screw-capped tube equipped with magnetic stir bar was introduced 1-(pyridin-2-yl)-1*H*-indole **27a** (0.059 g, 0.304 mmol), alkynyl bromide **28** (0.117 g, 0.45 mmol), $(THF)_2NiBr_2$ (0.0032 g, 0.009 mmol, 3 mol%), 1,10-phenanthroline (0.0016 g, 0.009 mmol, 3 mol%) and LiO^tBu (0.048 g, 0.6 mmol), and toluene (0.5 mL) was added inside the glove box. The resultant reaction mixture was stirred at 150 ^{o}C in a pre-heated oil bath for 12 h. At ambient temperature, H_2O (15 mL) was added and the compound was extracted with EtOAc (20 mL × 3). The combined organic extract was dried over Na_2SO_4 and the volatiles were evaporated *in vacuo*. The remaining residue was purified by column chromatography on basic alumina (petroleum ether/EtOAc: 100/1→50/1) to yield **29a** as light yellow solid.

Characterization data for compounds 29

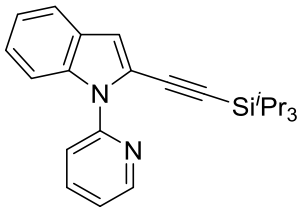

1-(Pyridin-2-yl)-2-((triisopropylsilyl)ethynyl)-1*H*-indole (**29a):** Yield: 0.108 g, 96%. M.p. = 44–46 ^{o}C. ^{1}H-NMR (400 MHz, $CDCl_3$): δ 8.61 (d, J = 4.4 Hz, 1H, Ar–H), 7.78-7.72 (m,

2H, Ar–H), 7.65 (d, *J* = 7.8 Hz, 1H, Ar–H), 7.57 (d, *J* = 7.8 Hz, 1H, Ar–H), 7.24-7.21 (m, 2H, Ar–H), 7.15 (vt, *J* = 7.3 Hz, 1H, Ar–H), 6.99 (s, 1H, Ar–H), 1.04-1.01 (m, 21H). $^{13}C\{^{1}H\}$-NMR (100 MHz, $CDCl_3$): δ 151.3 (C_q), 149.0 (CH), 137.9 (CH), 136.8 (C_q), 127.8 (C_q), 124.5 (CH), 121.8 (CH), 121.7 (CH), 121.0 (CH), 120.8 (C_q), 120.7 (CH), 112.6 (CH), 112.3 (CH), 98.6 (C_q), 98.4 (C_q), 18.7 (6C, CH_3), 11.4 (3C, CH). HRMS (ESI): *m/z* calcd for $C_{24}H_{30}N_2Si+H^+$ $[M+H]^+$ 375.2251; found 375.2256. The analytical data are in accordance with those reported in the literature.[402]

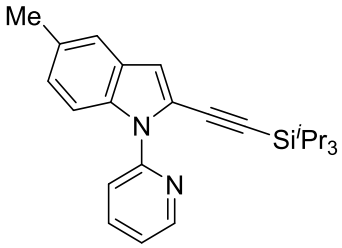

5-Methyl-1-(pyridin-2-yl)-2-((triisopropylsilyl)ethynyl)-1*H*-indole (29b): The representative procedure was followed, using **27b** (0.063 g, 0.302 mmol) and alkyne **28** (0.117 g, 0.45 mmol). Purification by column chromatography on basic alumina (petroleum ether/EtOAc: 100/1→30/1) yielded **29b** as a yellow liquid. Yield: 0.116 g, 99%. ^{1}H-NMR (500 MHz, $CDCl_3$): δ 8.66 (d, *J* = 4.5 Hz, 1H, Ar–H), 7.80 (td, *J* = 7.6, 1.9 Hz, 1H, Ar–H), 7.72-7.70 (m, 2H, Ar–H), 7.41 (s, 1H, Ar–H), 7.27 (dd, *J* = 7.2, 4.9 Hz, 1H, Ar–H), 7.14 (d, *J* = 8.4 Hz, 1H, Ar–H), 6.98 (s, 1H, Ar–H), 2.48 (s, 3H, CH_3), 1.12-1.09 (m, 21H). $^{13}C\{^{1}H\}$-NMR (100 MHz, $CDCl_3$): δ 151.4 (C_q), 148.9 (CH), 137.8 (CH), 135.2 (C_q), 131.0 (C_q), 128.1 (C_q), 126.2 (CH), 121.6 (CH), 120.7 (C_q), 120.5 (2C, CH), 112.4 (CH), 112.0 (CH), 98.6 (C_q), 98.3 (C_q), 21.5 (CH_3), 18.7 (6C, CH_3), 11.4 (3C, CH). HRMS (ESI): *m/z* calcd for $C_{25}H_{32}N_2Si+H^+$ $[M+H]^+$ 389.2408; found 389.2413.

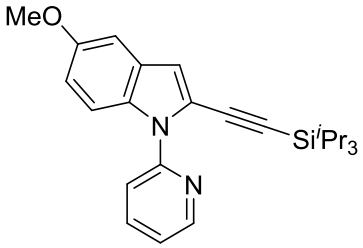

5-Methoxy-1-(pyridin-2-yl)-2-((triisopropylsilyl)ethynyl)-1*H*-indole (29c): The representative procedure was followed, using **27c** (0.068 g, 0.303 mmol) and alkyne **28** (0.117 g, 0.45 mmol). Purification by column chromatography on basic alumina (petroleum ether/EtOAc: 100/1→30/1) yielded **29c** as a yellow liquid. Yield: 0.113 g, 92% ^{1}H-NMR

(500 MHz, $CDCl_3$): δ 8.65 (s, 1H, Ar–H), 7.81-7.79 (m, 1H, Ar–H), 7.76-7.73 (m, 2H, Ar–H), 7.28-7.24 (m, 1H, Ar–H), 7.05 (br s, 1H, Ar–H), 6.98-6.96 (m, 2H, Ar–H), 3.87 (s, 3H, CH_3), 1.11 (br s, 21H). $^{13}C\{^1H\}$-NMR (100 MHz, $CDCl_3$): δ 155.5 (C_q), 151.4 (C_q), 148.9 (CH), 137.8 (CH), 132.0 (C_q), 128.4 (C_q), 121.6 (CH), 121.0 (C_q), 120.3 (CH), 114.8 (CH), 113.4 (CH), 112.5 (CH), 102.0 (CH), 98.6 (C_q), 98.4 (C_q), 55.7 (CH_3), 18.7 (6C, CH_3), 11.4 (3C, CH). HRMS (ESI): *m/z* calcd for $C_{25}H_{32}N_2OSi+H^+$ $[M+H]^+$ 405.2357; found 405.2361.

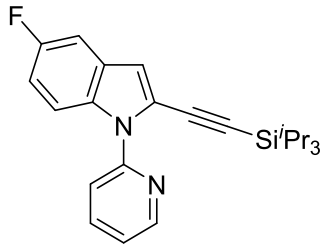

5-Fluoro-1-(pyridin-2-yl)-2-((triisopropylsilyl)ethynyl)-1*H*-indole (29d): The representative procedure was followed, using **27d** (0.064 g, 0.301 mmol) and alkyne **28** (0.117 g, 0.45 mmol). Purification by column chromatography on basic alumina (petroleum ether/EtOAc: 100/1→20/1) yielded **29d** as a yellow liquid. Yield: 0.113 g, 96%. ^{1}H-NMR (500 MHz, $CDCl_3$): δ 8.66 (d, J = 3.8 Hz, 1H, Ar–H), 7.85-7.82 (m, 1H, Ar–H), 7.77-7.72 (m, 2H, Ar–H), 7.32-7.30 (m, 1H, Ar–H), 7.27 (dd, J = 9.1, 1.9 Hz, 1H, Ar–H), 7.05 (td, J = 9.1, 2.3 Hz, 1H, Ar–H), 6.99 (s, 1H, Ar–H), 1.14-1.09 (m, 21H). $^{13}C\{^1H\}$-NMR (125 MHz, $CDCl_3$): δ 158.9 (d, $^1J_{C–F}$ = 237.5 Hz, C_q), 151.0 (C_q), 149.0 (CH), 138.0 (CH), 133.3 (C_q), 128.3 (d, $J_{C–F}$ = 10.5 Hz, C_q), 122.2 (C_q), 122.0 (CH), 120.6 (CH), 113.4 (d, $^3J_{C–F}$ = 9.5 Hz, CH), 112.8 (d, $^2J_{C–F}$ = 25.7 Hz, CH), 112.3 (d, $^4J_{C–F}$ = 4.7 Hz, CH), 105.5 (d, $^2J_{C–F}$ = 22.9 Hz, CH), 99.3 (C_q), 98.0 (C_q), 18.7 (6C, CH_3), 11.4 (3C, CH). ^{19}F-NMR (376 MHz, $CDCl_3$): δ –122.4. HRMS (ESI): *m/z* calcd for $C_{24}H_{29}FN_2Si$ $+H^+$ $[M+H]^+$ 393.2157; found 393.2164.

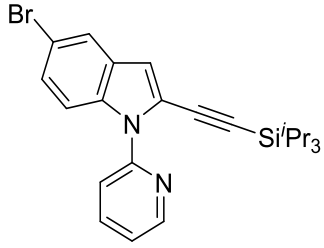

5-Bromo-1-(pyridin-2-yl)-2-((triisopropylsilyl)ethynyl)-1*H*-indole (29e): The representative procedure was followed, using **27e** (0.082 g, 0.30 mmol) and alkyne **28** (0.117

g, 0.45 mmol). Purification by column chromatography on basic alumina (petroleum ether/EtOAc: 100/1→30/1) yielded **29e** as a yellow liquid. Yield: 0.117 g, 86%. ^{1}H-NMR (500 MHz, $CDCl_3$): δ 8.62 (d, J = 4.4 Hz, 1H, Ar–H), 7.80 (t, J = 7.8 Hz, 1H, Ar–H), 7.71 (s, 1H, Ar–H), 7.68-7.62 (m, 2H, Ar–H), 7.33 (d, J = 8.8, 1H, Ar–H), 7.27 (t, J = 5.8 Hz, 1H, Ar–H), 6.92 (s, 1H, Ar–H), 1.09-1.06 (m, 21H). ^{13}C{^{1}H}-NMR (100 MHz, $CDCl_3$): δ 150.8 (C_q), 149.1 (CH), 138.0 (CH), 135.3 (C_q), 129.5 (C_q), 127.2 (CH), 123.2 (CH), 122.1 (CH), 121.9 (C_q), 120.6 (CH), 114.9 (C_q), 113.9 (CH), 111.6 (CH), 99.5 (C_q), 97.7 (C_q), 18.7 (6C, CH_3), 11.3 (3C, CH). HRMS (ESI): *m/z* calcd for $C_{24}H_{29}BrN_2Si+H^+$ $[M+H]^+$ 453.1356, 455.1336; found 453.1364, 455.1334.

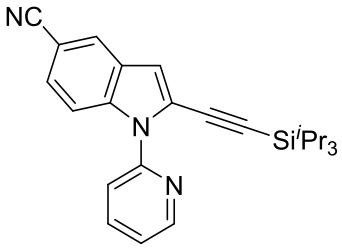

1-(Pyridine-2-yl)-2-((triisopropylsilyl)ethyl)-1*H*-indole-5-carbonitrile (29f): The representative procedure was followed, using **27f** (0.066 g, 0.301 mmol) and alkyne **28** (0.117 g, 0.45 mmol). Purification by column chromatography on basic alumina (petroleum ether/EtOAc: 100/1→30/1) yielded **29f** as an off-white solid. Yield: 0.095 g, 79%. M.p. = 84–86 ^{o}C. ^{1}H-NMR (500 MHz, $CDCl_3$): δ 8.65 (d, J = 4.4 Hz, 1H, Ar–H), 7.92 (s, 1H, Ar–H), 7.87-7.83 (m, 1H, Ar–H), 7.75 (d, J = 8.8 Hz, 1H, Ar–H), 7.67 (d, J = 8.3, 1H, Ar–H), 7.45 (d, J = 8.8 Hz, 1H, Ar–H), 7.37-7.34 (m, 1H, Ar–H), 7.02 (s, 1H, Ar–H), 1.09-1.02 (m, 21H). ^{13}C{^{1}H}-NMR (100 MHz, $CDCl_3$): δ 150.2 (C_q), 149.2 (CH), 138.3 (CH), 138.1 (C_q), 127.5 (C_q), 126.9 (CH), 126.3 (CH), 123.4 (C_q), 122.8 (CH), 120.9 (CH), 120.3 (C_q), 113.3 (CH), 112.1 (CH), 104.9 (C_q), 100.8 (C_q), 96.9 (C_q), 18.6 (6C, CH_3), 11.3 (3C, CH). HRMS (ESI): *m/z* calcd for $C_{25}H_{29}N_3Si+H^+$ $[M+H]^+$ 400.2204; found 400.2206.

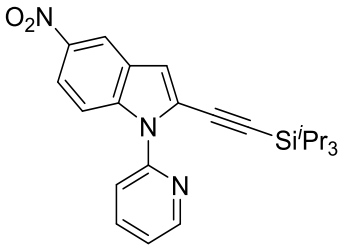

5-Nitro-1-(pyridin-2-yl)-2-((triisopropylsilyl)ethynyl)-1*H*-indole (29g): The representative procedure was followed, using **27g** (0.072 g, 0.301 mmol) and alkyne **28** (0.117 g, 0.45

mmol). Purification by column chromatography on basic alumina (petroleum ether/EtOAc: 100/1→30/1) yielded **29g** as a yellow solid. Yield: 0.096 g, 76%. M.p. = 66–68 ^{o}C. ^{1}H-NMR (500 MHz, $CDCl_3$): δ 8.66 (d, J = 4.2 Hz, 1H, Ar–H), 8.52 (s, 1H, Ar–H), 8.11 (d, J = 9.1 Hz, 1H, Ar–H), 7.87 (t, J = 7.6 Hz 1H, Ar–H), 7.73 (d, J = 9.1 Hz, 1H, Ar–H), 7.69 (d, J = 8.0 Hz, 1H, Ar–H), 7.37 (vt, J = 6.1 Hz, 1H, Ar–H), 7.10 (s, 1H, Ar–H), 1.07-1.03 (m, 21H). ^{13}C{^{1}H}-NMR (125 MHz, $CDCl_3$): δ 150.1 (C_q), 149.3 (CH), 143.1 (C_q), 139.3 (C_q), 138.4 (CH), 127.1 (C_q), 124.3 (C_q), 123.0 (CH), 121.0 (CH), 119.5 (CH), 117.8 (CH), 113.2 (CH), 112.5 (CH), 101.2 (C_q), 96.7 (C_q), 18.6 (6C, CH_3), 11.3 (3C, CH). HRMS (ESI): *m/z* calcd for $C_{24}H_{29}O_2N_3Si+H^+$ $[M+H]^+$ 420.2102; found 420.2109.

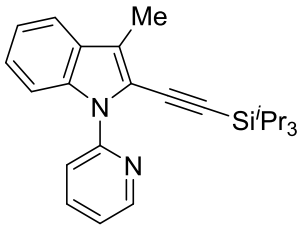

3-Methyl-1-(pyridin-2-yl)-2-((triisopropylsilyl)ethynyl)-1*H*-indole (29h): The representative procedure was followed, using **27h** (0.063 g, 0.30 mmol) and alkyne **28** (0.117 g, 0.45 mmol). Purification by column chromatography on basic alumina (petroleum ether/EtOAc: 100/1→50/1) yielded **29h** as a yellow liquid. Yield: 0.107 g, 91%. ^{1}H-NMR (500 MHz, $CDCl_3$): δ 8.67 (s, 1H, Ar–H), 7.92 (d, J = 8.4 Hz, 1H, Ar–H), 7.83-7.78 (m, 2H, Ar–H), 7.64 (d, J = 8.4 Hz, 1H, Ar–H), 7.35 (vt, J = 7.2, 1H, Ar–H), 7.27-7.26 (m, 2H, Ar–H), 2.56 (s, 3H, CH_3), 1.17 (s, 21H). ^{13}C{^{1}H}-NMR (125 MHz, $CDCl_3$): δ 151.6 (C_q), 148.8 (CH), 137.7 (CH), 136.4 (C_q), 128.5 (C_q), 124.8 (CH), 122.5 (C_q), 121.2 (2 x CH), 120.0 (CH), 119.3 (CH), 118.9 (C_q), 112.4 (CH), 101.4 (C_q), 98.1 (C_q), 18.8 (6C, CH_3), 11.4 (3C, CH), 10.0 (CH_3). HRMS (ESI): *m/z* calcd for $C_{25}H_{32}N_2Si+H^+$ $[M+H]^+$ 389.2309; found 389.2314.

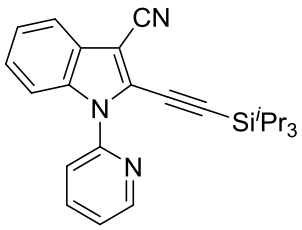

1-(Pyridine-2-yl)-2-((triisopropylsilyl)ethyl)-1*H*-indole-3-carbonitrile (29i): The representative procedure was followed, using **27i** (0.066 g, 0.30 mmol) and alkyne **28** (0.117

g, 0.45 mmol). Purification by column chromatography on basic alumina (petroleum ether/EtOAc: 100/1→10/1) yielded **29i** as a yellow liquid. Yield: 0.113 g, 94%. ^{1}H-NMR (500 MHz, $CDCl_3$): δ 8.67 (d, J = 3.8 Hz, 1H, Ar–H), 7.89 (vt, J = 7.2 Hz, 1H, Ar–H), 7.72 (d, J = 7.6 Hz, 1H, Ar–H), 7.67-7.66 (m, 2H, Ar–H), 7.41-7.39 (m, 1H, Ar–H), 7.36-7.30 (m, 2H, Ar–H), 1.10-1.06 (m, 21H). ^{13}C{^{1}H}-NMR (125 MHz, $CDCl_3$): δ 149.7 (C_q), 149.6 (CH), 138.5 (CH), 135.7 (C_q), 127.6 (C_q), 126.7 (C_q), 126.1 (CH), 123.7 (CH), 123.4 (CH), 120.9 (CH), 119.6 (CH), 114.7 (C_q), 112.9 (CH), 106.5 (C_q), 95.4 (C_q), 94.2 (C_q), 18.6 (6C, CH_3), 11.2 (3C, CH). HRMS (ESI): *m/z* calcd for $C_{25}H_{29}N_3Si+H^+$ $[M+H]^+$ 400.2204; found 400.2206.

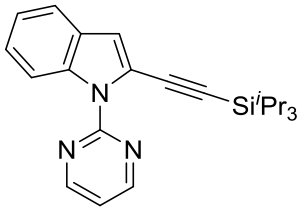

1-(Pyrimidin-2-yl)-2-((triisopropylsilyl)ethynyl)-1*H*-indole (**29j):** The representative procedure was followed, using **27j** (0.059 g, 0.302 mmol) and alkyne **28** (0.117 g, 0.45 mmol). Purification by column chromatography on basic alumina (petroleum ether/EtOAc: 100/1→50/1) yielded **29j** as a yellow liquid. Yield: 0.096 g, 85%. ^{1}H-NMR (400 MHz, $CDCl_3$): δ 8.80 (d, J = 4.9 Hz, 2H, Ar–H), 8.33 (d, J = 8.3 Hz, 1H, Ar–H), 7.62 (d, J = 7.8 Hz, 1H, Ar–H), 7.39-7.35 (m, 1H, Ar–H), 7.26 (t, J = 7.3 Hz, 1H, Ar–H), 7.17 (t, J = 4.8 Hz, 1H, Ar–H), 7.13 (s, 1H, Ar–H), 1.18 (s, 21H). ^{13}C{^{1}H}-NMR (100 MHz, $CDCl_3$): δ 158.2 (2C, CH), 157.4 (C_q), 136.3 (C_q), 128.7 (C_q), 124.9 (CH), 122.5 (CH), 121.1 (C_q), 120.8 (CH), 117.7 (CH), 115.8 (CH), 114.2 (CH), 98.9 (C_q), 98.0 (C_q), 18.8 (6C, CH_3), 11.5 (3C, CH). HRMS (ESI): *m/z* calcd for $C_{23}H_{29}N_3Si+H^+$ $[M+H]^+$ 376.2204; found 376.2208. The analytical data are in accordance with those reported in the literature.[420]

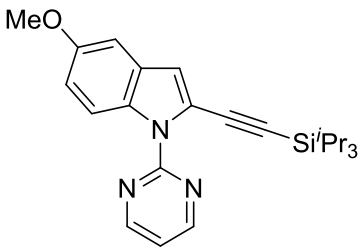

5-Methoxy-1-(pyrimidin-2-yl)-2-((triisopropylsilyl)ethynyl)-1*H*-indole (**29k):** The representative procedure was followed, using **27k** (0.068 g, 0.301 mmol) and alkyne **28**

(0.117 g, 0.45 mmol). Purification by column chromatography on basic alumina (petroleum ether/EtOAc: 100/1→20/1) yielded **29k** as a light-yellow solid. Yield: 0.096 g, 79%. M.p. = 108–110 ^{o}C. ^{1}H-NMR (400 MHz, $CDCl_3$): δ 8.76 (d, J = 4.4 Hz, 2H, Ar–H), 8.23 (d, J = 9.2 Hz, 1H, Ar–H), 7.14 (t, J = 4.6 Hz, 1H, Ar–H), 6.99-6.97 (m, 2H, Ar–H), 6.96 (dd, J = 9.2, 2.4 Hz, 1H, Ar–H), 3.86 (s, 3H, OCH_3), 1.14 (s, 21H). ^{13}C{^{1}H}-NMR (100 MHz, $CDCl_3$): δ 158.2 (2C, CH), 157.5 (C_q), 155.9 (C_q), 131.3 (C_q), 129.4 (C_q), 121.4 (C_q), 117.5 (CH), 115.8 (CH), 115.5 (CH), 114.6 (CH), 102.3 (CH), 99.1 (C_q), 98.0 (C_q), 55.8 (OCH_3), 18.8 (6C, CH_3), 11.6 (3C, CH). HRMS (ESI): *m/z* calcd for $C_{24}H_{31}ON_3Si+H^+$ $[M+H]^+$ 406.2309; found 406.2314. The analytical data are in accordance with those reported in the literature.[420]

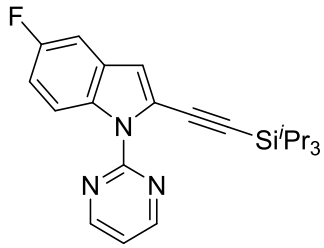

5-Fluoro-1-(pyrimidin-2-yl)-2-((triisopropylsilyl)ethynyl)-1*H*-indole (**29l):** The representative procedure was followed, using **27l** (0.064 g, 0.30 mmol) and alkyne **28** (0.117 g, 0.45 mmol). Purification by column chromatography on basic alumina (petroleum ether/EtOAc: 100/1→30/1) yielded **29l** as a yellow solid. Yield: 0.086 g, 73%. M.p. = 58–60 ^{o}C. ^{1}H-NMR (400 MHz, $CDCl_3$): δ 8.76 (d, J = 4.9 Hz, 2H, Ar–H), 8.27 (dd, J = 9.2, 4.9 Hz, 1H, Ar–H), 7.21 (dd, J = 8.8, 1.9 Hz, 1H, Ar–H), 7.16 (t, J = 4.6 Hz, 1H, Ar–H), 7.08-7.02 (m, 2H, Ar–H), 1.14 (br s, 21H). ^{13}C{^{1}H}-NMR (100 MHz, $CDCl_3$): δ 159.2 (d, $^{1}J_{C–F}$ = 238.1 Hz, C_q), 158.2 (2C, CH), 157.3 (C_q), 132.7 (C_q), 129.3 (d, $^{3}J_{C–F}$ = 10.8 Hz, C_q), 122.5 (C_q), 117.8 (CH), 115.5 (d, $^{3}J_{C–F}$ = 9.2 Hz, CH), 115.4 (d, $^{4}J_{C–F}$ = 4.6 Hz, CH), 112.9 (d, $^{2}J_{C–F}$ = 24.6 Hz, CH), 105.6 (d, $^{2}J_{C–F}$ = 23.1 Hz, CH), 98.8 (C_q), 98.5 (C_q), 18.8 (6C, CH_3), 11.5 (3C, CH). ^{19}F-NMR (376 MHz, $CDCl_3$): δ –121.5. HRMS (ESI): *m/z* calcd for $C_{23}H_{28}FN_3Si+H^+$ $[M+H]^+$ 394.2109; found 394.2116. The analytical data are in accordance with those reported in the literature.[420]

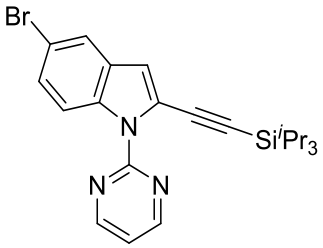

5-Bromo-1-(pyrimidin-2-yl)-2-((triisopropylsilyl)ethynyl)-1*H*-indole (29m): The representative procedure was followed, using **27m** (0.082 g, 0.30 mmol) and alkyne **28** (0.117 g, 0.45 mmol). Purification by column chromatography on basic alumina (petroleum ether/EtOAc: 100/1→30/1) yielded **29m** as a brown solid. Yield: 0.095 g, 70%. M.p. = 86–88 ^{o}C. ^{1}H-NMR (400 MHz, $CDCl_3$): δ 8.78 (d, J = 4.4 Hz, 2H, Ar–H), 8.17 (d, J = 8.8 Hz, 1H, Ar–H), 7.69 (d, J = 1.4 Hz, 1H, Ar–H), 7.38 (dd, J = 8.8, 1.4 Hz, 1H, Ar–H), 7.20 (t, J = 8.9 Hz, 1H, Ar–H), 6.98 (s, 1H, Ar–H), 1.13 (br s, 21H). ^{13}C{^{1}H}-NMR (100 MHz, $CDCl_3$): δ 158.3 (2C, CH), 157.2 (C_q), 134.9 (C_q), 130.4 (C_q), 127.7 (CH), 123.2 (CH), 122.3 (C_q), 118.1 (CH), 115.9 (CH), 115.8 (C_q), 114.8 (CH), 99.1 (C_q), 98.3 (C_q), 18.8 (6C, CH_3), 11.5 (3C, CH). HRMS (ESI): *m/z* calcd for $C_{23}H_{28}BrN_3Si+H^+$ $[M+H]^+$ 454.1309, 456.1288; found 454.1313, 456.1288. The analytical data are in accordance with those reported in the literature.[420]

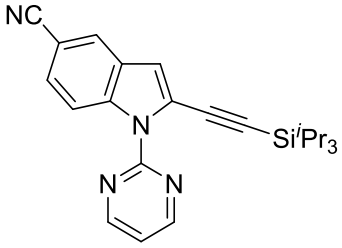

1-(Pyrimidin-2-yl)-2-((triisopropylsilyl)ethynyl)-1*H*-indole-5-carbonitrile (29n): The representative procedure was followed, using **27n** (0.066 g, 0.30 mmol) and alkyne **28** (0.117 g, 0.45 mmol). Purification by column chromatography on basic alumina (petroleum ether/EtOAc: 100/1→5/1) yielded **29n** as an off-white solid. Yield: 0.085 g, 71%. M.p. = 108–110 ^{o}C. ^{1}H-NMR (500 MHz, $CDCl_3$): δ 8.82 (d, J = 4.6 Hz, 2H, Ar–H), 8.30 (d, J = 8.7 Hz, 1H, Ar–H), 7.90 (s, 1H, Ar–H), 7.52 (d, J = 8.7 Hz, 1H, Ar–H), 7.29-7.27 (m, 1H, Ar–H), 7.07 (s, 1H, Ar–H), 1.13-1.11 (m, 21H). ^{13}C{^{1}H}-NMR (125 MHz, $CDCl_3$): δ 158.5 (2C, CH), 156.9 (C_q), 137.7 (C_q), 128.5 (C_q), 127.5 (CH), 125.9 (CH), 123.6 (C_q), 120.1 (C_q), 118.7 (CH), 115.1 (CH), 114.8 (CH), 105.8 (C_q), 100.3 (C_q), 97.5 (C_q), 18.8 (6C, CH_3), 11.5 (3C, CH). HRMS (ESI): *m/z* calcd for $C_{24}H_{28}N_4Si+H^+$ $[M+H]^+$ 401.2156; found 401.2159.

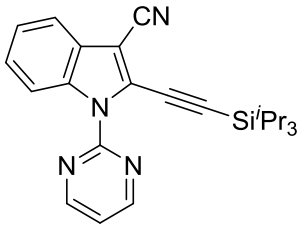

1-(Pyrimidin-2-yl)-2-((triisopropylsilyl)ethyl)-1*H*-indole-3-carbonitrile (29o): The representative procedure was followed, using **27o** (0.066 g, 0.30 mmol) and alkyne **28** (0.117 g, 0.45 mmol). Purification by column chromatography on basic alumina (petroleum ether/EtOAc: 100/1→5/1) yielded **29o** as a yellow solid. Yield: 0.115 g, 96%. M.p. = 72–74 ^{o}C. ^{1}H-NMR (500 MHz, $CDCl_3$): δ 8.83 (d, J = 4.6 Hz, 2H, Ar–H), 8.26 (d, J = 8.3Hz, 1H, Ar–H), 7.71 (d, J = 7.6 Hz, 1H, Ar–H), 7.42-7.39 (m, 1H, Ar–H), 7.35 (d, J = 7.2 Hz, 1H, Ar–H), 7.33 (d, J = 4.9 Hz, 1H, Ar–H), 1.16 (br s, 21H). ^{13}C{^{1}H}-NMR (125 MHz, $CDCl_3$): δ 158.5 (2C, CH), 156.5 (C_q), 135.0 (C_q), 128.0 (C_q), 127.1 (C_q), 126.5 (CH), 124.3 (CH), 119.5 (CH), 119.3 (CH), 115.0 (CH), 114.5 (C_q), 106.9 (C_q), 98.6 (C_q), 95.0 (C_q), 18.7 (6C, CH_3), 11.3 (3C, CH). HRMS (ESI): *m/z* calcd for $C_{24}H_{28}N_4Si+H^+$ $[M+H]^+$ 401.2156; found 401.2159. The analytical data are in accordance with those reported in the literature.[402]

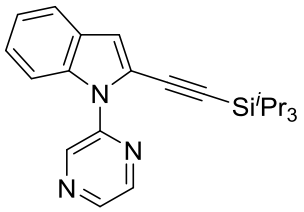

1-(Pyrazin-2-yl) -2-((triisopropylsilyl)ethynyl)-1*H*-indole (29p): The representative procedure was followed, using **27p** (0.059 g, 0.302 mmol) and alkyne **28** (0.117 g, 0.45 mmol). Purification by column chromatography on basic alumina (petroleum ether/EtOAc: 100/1→50/1) yielded **29p** as a yellow liquid. Yield: 0.075 g, 66%. ^{1}H-NMR (500 MHz, $CDCl_3$): δ 9.10 (d, J = 1.1 Hz, 1H, Ar–H), 8.60 (dd, J = 2.3, 1.5 Hz, 1H, Ar–H), 8.55 (d, J = 2.6 Hz, 1H, Ar–H), 7.78 (d, J = 8.4 Hz, 1H, Ar–H), 7.62 (d, J = 8.4 Hz, 1H, Ar–H), 7.31 (td, J = 8.4 Hz, 1H, Ar–H), 7.24-7.21 (m, 1H, Ar–H), 7.01 (s, 1H, Ar–H), 1.11-1.08 (m, 21H). ^{13}C{^{1}H}-NMR (100 MHz, $CDCl_3$): δ 148.0 (C_q), 142.9 (CH), 142.1 (CH), 141.9 (CH), 136.6 (C_q), 128.2 (C_q), 125.0 (CH), 122.4 (CH), 121.2 (CH), 120.5 (C_q), 113.7 (CH), 112.1 (CH), 99.9 (C_q), 97.6 (C_q), 18.7 (6C, CH_3), 11.3 (3C, CH). HRMS (ESI): *m/z* calcd for $C_{23}H_{29}N_3Si+H^+$ $[M+H]^+$ 376.2204; found 376.2207.

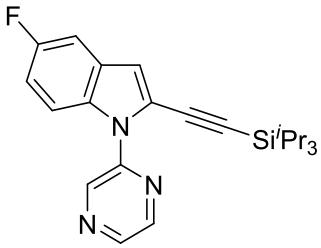

5-Fluoro-1-(pyrazin-2-yl)-2-((triisopropylsilyl)ethynyl)-1*H*-indole (29q): The representative procedure was followed, using **27q** (0.064 g, 0.30 mmol) and alkyne **28** (0.117 g, 0.45 mmol). Purification by column chromatography on basic alumina (petroleum ether/EtOAc: 100/1→5/1) yielded **29q** as a yellow solid. Yield: 0.086 g, 73%. M.p. = 58–60 ^{o}C. ^{1}H-NMR (500 MHz, $CDCl_3$): δ 9.13 (s, 1H, Ar–H), 8.60 (br s, 1H, Ar–H), 8.58 (d, J = 2.4, 1H, Ar–H), 7.75 (dd, J = 9.1, 4.3 Hz, 1H, Ar–H), 7.27 (dd, J = 8.9, 2.2 Hz, 1H, Ar–H), 7.05 (td, J = 9.1, 2.4 Hz, 1H, Ar–H), 7.01 (s, 1H, Ar–H), 1.14-1.09 (m, 21H). ^{13}C{^{1}H}-NMR (125 MHz, $CDCl_3$): δ 159.2 (d, $^{1}J_{C–F}$ = 238.4 Hz, C_q), 147.8 (C_q), 142.8 (CH), 142.0 (CH), 141.9 (CH), 133.0 (C_q), 128.8 (d, $^{3}J_{C–F}$ = 10.4 Hz, C_q), 121.9 (C_q), 113.4 (d, $^{4}J_{C–F}$ = 3.8 Hz, CH), 113.3 (CH), 113.2 (d, $^{2}J_{C–F}$ = 19.1 Hz, CH), 105.9 (d, $^{2}J_{C–F}$ = 23.8 Hz, CH), 100.7 (C_q), 97.2 (C_q), 18.7 (6C, CH_3), 11.3 (3C, CH). ^{19}F-NMR (376 MHz, $CDCl_3$): δ –121.23. HRMS (ESI): *m/z* calcd for $C_{23}H_{28}FN_3Si+H^+$ $[M+H]^+$ 394.2112; found 394.2112.

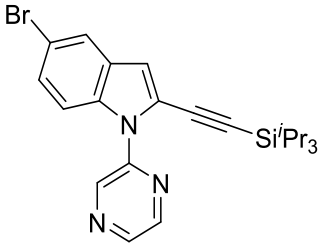

5-Bromo-1-(pyrazin-2-yl)-2-((triisopropylsilyl)ethynyl)-1*H*-indole (29r): The representative procedure was followed, using **27r** (0.082 g, 0.30 mmol) and alkyne **28** (0.117 g, 0.45 mmol). Purification by column chromatography on basic alumina (petroleum ether/EtOAc: 100/1→20/1) yielded **29r** as a light-yellow solid. Yield: 0.082 g, 60%. M.p. = 42–44 ^{o}C. ^{1}H-NMR (500 MHz, $CDCl_3$): δ 9.09 (s, 1H, Ar–H), 8.58 (d, J = 1.2 Hz, 1H, Ar–H), 8.56 (d, J = 1.2 Hz, 1H, Ar–H), 7.73 (d, J = 1.8 Hz, 1H, Ar–H), 7.65 (d, J = 8.9 Hz, 1H, Ar–H), 7.36 (dd, J = 8.9, 1.8 Hz, 1H, Ar–H), 6.96 (s, 1H, Ar–H), 1.10-1.05 (m, 21H). ^{13}C NMR (100 MHz, $CDCl_3$): δ 147.6 (C_q), 142.9 (CH), 142.2 (CH), 141.9 (CH), 135.2 (C_q), 129.9 (C_q), 127.8 (CH), 123.6 (CH), 121.6 (C_q), 115.6 (C_q), 113.8 (CH), 112.7 (CH), 100.9 (C_q), 97.0 (C_q), 18.7 (6C, CH_3), 11.3 (3C, CH,). HRMS (ESI): *m/z* calcd for $C_{23}H_{28}BrN_3Si+H^+$ $[M+H]^+$ 454.1309, 456.1288; found 454.1313, 456.1288.

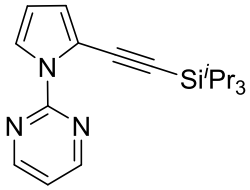

2-(2-((Triisopropylsilyl)ethynyl)-1*H*-pyrrol-1-yl)pyrimidine (29s): The representative procedure was followed, using **27s** (0.044 g, 0.303 mmol) and alkyne **28** (0.026 g, 0.1 mmol), and the reaction mixture was stirred at 150 ^{o}C for 3 h. Purification by column chromatography on basic alumina (petroleum ether/EtOAc: 20/1→ 1/1) yielded **29s** as an oil. Yield: 0.016 g, 50%. ^{1}H-NMR (500 MHz, $CDCl_3$): δ 8.65 (d, J = 4.9 Hz, 2H, Ar–H), 7.70 (dd, J = 2.6, 1.1 Hz, 1H, Ar–H), 7.13-7.11 (m, 1H, Ar–H), 6.70 (dd, J = 3.0, 1.5 Hz, 1H, Ar–H), 6.25 (t, J = 3.4 Hz, 1H, Ar–H), 1.14 (br s, 21H). ^{13}C{^{1}H}-NMR (125 MHz, $CDCl_3$): δ 158.3 (2C, CH), 156.8 (C_q), 122.3 (CH), 122.1 (CH), 118.1 (CH), 115.2 (C_q), 111.0 (CH), 99.3 (C_q), 94.9 (C_q), 18.9 (6C, CH_3), 11.7 (3C, CH). HRMS (ESI): *m/z* calcd for $C_{19}H_{27}N_3Si+H^+$ $[M+H]^+$ 326.2047; found 326.2052.

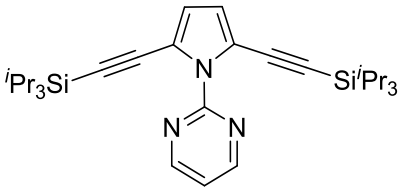

2-(2,5-Bis((triisopropylsilyl)ethynyl)-1*H*-pyrrol-1-yl)pyrimidine (29t): The representative procedure was followed, using **27s** (0.044 g, 0.303 mmol) and alkyne **28** (0.195 g, 0.75 mmol). Purification by column chromatography on basic alumina (petroleum ether /EtOAc: 100/1→ 30/1) yielded **29t** as a green solid. Yield: 0.086 g, 56%. M.p. = 60–63 ^{o}C. ^{1}H-NMR (500 MHz, $CDCl_3$): δ 8.78 (d, J = 4.6 Hz, 2H, Ar–H), 7.27 (t, J = 4.9, Hz, 1H, Ar–H), 6.53 (s, 2H, Ar–H), 1.00 (br s, 42H). ^{13}C{^{1}H}-NMR (125 MHz, $CDCl_3$): δ 158.5 (2C, CH), 156.7 (C_q), 119.6 (CH), 117.8 (2C, CH), 117.5 (2C, C_q), 97.9 (2C, C_q), 95.4 (2C, C_q), 18.7 (12C, CH_3), 11.4 (6C, CH). HRMS (ESI): *m/z* calcd for $C_{30}H_{47}N_3Si_2+H^+$ $[M+H]^+$ 506.3381; found 506.3377. The analytical data are in accordance with those reported in the literature.[403]

Characterization data for compounds 31

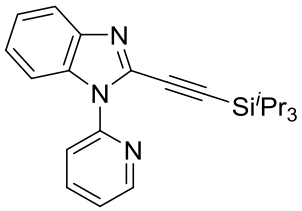

1-(Pyridin-2-yl)-2-((triisopropylsilyl)ethynyl)-1*H*-benzo[*d*]imidazole (31a): The representative procedure was followed, using **30a** (0.059 g, 0.302 mmol) and alkyne **28** (0.117 g, 0.45 mmol). Purification by column chromatography on basic alumina (petroleum ether/EtOAc: 100/1→5/1) yielded **31a** as a light brown solid. Yield: 0.076 g, 67%. M.p. = 66–68 ^{o}C. ^{1}H-NMR (500 MHz, $CDCl_3$): δ 8.67 (d, J = 3.8 Hz, 1H, Ar–H), 7.89 (t, J = 7.2 Hz, 1H, Ar–H), 7.72 (d, J = 7.6 Hz, 1H, Ar–H), 7.67-7.65 (m, 2H, Ar–H), 7.41-7.39 (m, 1H, Ar–H), 7.36-7.30 (m, 2H, Ar–H), 1.14-1.06 (m, 21H). ^{13}C{^{1}H}-NMR (125 MHz, $CDCl_3$): δ 149.6 (C_q, CH), 142.9 (C_q), 138.5 (CH), 134.4 (C_q), 133.9 (C_q), 125.2 (CH), 124.0 (CH), 123.1 (CH), 120.4 (CH), 120.3 (CH), 112.2 (CH), 99.5 (C_q), 96.0 (C_q), 18.7 (6C, CH_3), 11.3 (3C, CH). HRMS (ESI): *m/z* calcd for $C_{23}H_{29}N_3Si+H^+$ $[M+H]^+$ 376.2204; found 376.2208.

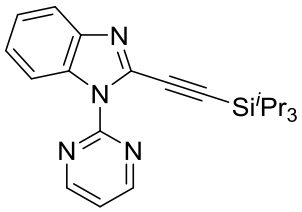

1-(Pyrimidin-2-yl)-2-((triisopropylsilyl)ethynyl)-1*H*-benzo[*d*]imidazole (31b): The representative procedure was followed, using **30b** (0.059 g, 0.30 mmol) and alkyne **28** (0.117 g, 0.45 mmol). Purification by column chromatography on basic alumina (Petroleum ether /EtOAc: 50/1→ 10/1) yielded **31b** as a yellow solid. Yield: 0.059 g, 52%. M.p. = 78–80 ^{o}C. ^{1}H-NMR (500 MHz, $CDCl_3$): δ 8.85 (d, J = 4.9 Hz, 2H, Ar–H), 8.20 (d, J = 7.2 Hz, 1H, Ar–H), 7.81 (d, J = 7.2 Hz, 1H, Ar–H), 7.41-7.35 (m, 2H, Ar–H), 7.32-7.30 (m, 1H, Ar–H), 1.15-1.14 (m, 21H). ^{13}C{^{1}H}-NMR (125 MHz, $CDCl_3$): δ 158.7 (2C, CH), 156.4 (C_q), 143.2 (C_q), 135.7 (C_q), 132.9 (C_q), 125.5 (CH), 124.5 (CH), 120.5 (CH), 119.1 (CH), 114.3 (CH), 99.3 (C_q), 96.9 (C_q), 18.8 (6C, CH_3), 11.4 (3C, CH). HRMS (ESI): *m/z* calcd for $C_{22}H_{28}N_4Si+H^+$ $[M+H]^+$ 377.2156; found 377.2152.

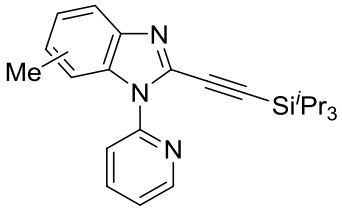

[5-Me(**31c**)+6-Me(**31c'**)]

5-Methyl-1-(pyridin-2-yl)-2-((triisopropylsilyl)ethynyl)-1*H*-benzo[*d*]imidazole (31c) and 6-Methyl-1-(pyridin-2-yl)-2-((triisopropylsilyl)ethynyl)-1*H*-benzo[*d*]imidazole (31c'): The representative procedure was followed, using the mixture of **30c** and **30c'** (0.063 g, 0.301 mmol) and alkyne **28** (0.117 g, 0.45 mmol). Purification by column chromatography on basic alumina (petroleum ether/EtOAc: 20/1→5/1) yielded mixture of **31c** and **31c'** as oily liquids. Yield: 0.075 g, 65%. ^{1}H-NMR (500 MHz, $CDCl_3$): δ 8.67-8.64 (m, 2H, Ar–H), 7.87-7.83 (m, 2H, Ar–H), 7.76-7.33 (m, 2H, Ar–H), 7.67 (d, J = 8.0, 1H, Ar–H), 7.57-7.55 (m, 2H, Ar–H), 7.46 (s, 1H, Ar–H), 7.37-7.33 (m, 2H, Ar–H), 7.15-7.14 (m, 2H, Ar–H), 2.46 (s, 3H, CH_3), 2.45 (s, 3H, CH_3), 1.05-1.04 (m, 42H). ^{13}C{^{1}H}-NMR (125 MHz, $CDCl_3$): δ 149.8 (C_q), 149.7 (C_q), 149.5 (CH), 149.4 (CH), 143.2 (C_q), 141.0 (C_q), 138.4 (CH), 138.3 (CH), 135.4 (C_q), 135.2 (C_q), 134.9 (C_q), 134.1 (C_q), 133.7 (C_q), 132.0 (C_q), 126.8 (CH), 125.7 (CH), 123.0 (CH), 122.9 (CH), 120.4 (CH), 120.1 (CH), 119.9 (CH), 119.8 (CH), 111.8 (CH), 111.7 (CH), 99.1 (C_q), 99.0 (C_q), 96.2 (C_q), 96.1 (C_q), 22.0 (CH_3), 21.8 (CH_3), 18.6 (12C, CH_3), 11.2 (6C, CH). GC-MS showed two peaks with *m/z* = 389.2 each, which indicates that two isomers are exist.

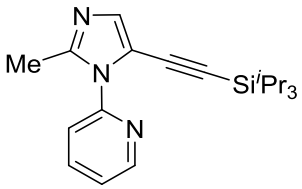

2-(2-Methyl-5-((triisopropylsilyl)ethynyl)-1*H*-imidazol-1-yl)pyridine (31d): The representative procedure was followed, using **30d** (0.048 g, 0.301 mmol) and alkyne **28** (0.117 g, 0.45 mmol), and reaction mixture was heated at 130 ^{o}C for 12 h. Purification by column chromatography on basic alumina (petroleum ether /EtOAc: 20/1→1/1) yielded **31d** as an oil. Yield: 0.043 g, 42%. ^{1}H-NMR (500 MHz, $CDCl_3$): δ 8.61 (d, J = 3.8 Hz, 1H, Ar–H), 7.83 (td, J = 7.6, 1.9 Hz, 1H, Ar–H), 7.48 (d, J = 8.0 Hz, 1H, Ar–H), 7.36 (dd, J = 4.9, 1.9 Hz, 1H, Ar–H), 7.28 (s, 1H, Ar–H), 2.42 (s, 3H, CH_3), 0.97-0.96 (m, 21H). ^{13}C{^{1}H}-NMR (125 MHz, $CDCl_3$): δ 149.5 (CH), 149.4 (C_q), 146.6 (C_q), 138.3 (CH), 134.2 (CH),

123.6 (CH),121.6 (CH), 116.1 (C_q), 98.6 (C_q), 95.0 (C_q), 18.7 (6C, CH_3), 14.9 (CH_3), 11.3 (3C, CH). HRMS (ESI): *m/z* calcd for $C_{20}H_{29}N_3Si+H^+$ $[M+H]^+$ 340.2204; found 340.2204.

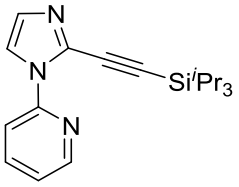

31e

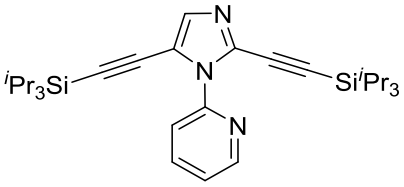

31f

2-(2-((Triisopropylsilyl)ethynyl)-1*H*-imidazol-1-yl)pyridine (31e) and 2-(2,5-Bis((Triisopropylsilyl)ethynyl)-1*H*-imidazol-1-yl)pyridine (31f): The representative procedure was followed, using **30e** (0.044 g, 0.303 mmol) and alkyne **28** (0.117 g, 0.45 mmol). Purification by column chromatography on basic alumina (petroleum ether/EtOAc: 100/1→ 5/1) yielded **31e** and **31f** as yellow liquids. **31e**: 0.035 g, 35%. ^{1}H-NMR (500 MHz, $CDCl_3$): δ 8.54 (d, *J* = 4.6 Hz, 1H, Ar–H), 8.07 (d, *J* = 8.4 Hz, 1H, Ar–H), 7.78 (td, *J* = 8.0, 1.5 Hz, 1H, Ar–H), 7.68 (d, *J* = 1.1 Hz, 1H, Ar–H), 7.29 (dd, *J* = 4.9, 2.2 Hz, 1H, Ar–H), 7.15 (d, *J* = 1.1 Hz, 1H, Ar–H), 1.09-1.08 (m, 21H). ^{13}C{^{1}H}-NMR (125 MHz, $CDCl_3$): δ 149.5 (C_q), 149.3 (CH), 138.4 (CH), 130.0 (C_q), 129.9 (CH), 122.9 (CH), 119.8 (CH), 117.2 (CH), 96.9 (C_q), 96.5 (C_q), 18.7 (6C, CH_3), 11.4 (3C, CH). HRMS (ESI): *m/z* calcd for $C_{19}H_{27}N_3Si+H^+$ $[M+H]^+$ 326.2047; found 326.2045.

31f: 0.012 g, 8%. ^{1}H-NMR (500 MHz, $CDCl_3$): δ 8.60 (d, *J* = 4.6 Hz, 1H, Ar–H), 7.83 (td, *J* = 6.1, 1.5 Hz, 1H, Ar–H), 7.51 (d, *J* = 7.6 Hz, 1H, Ar–H), 7.37 (dd, *J* = 7.6, 2.7 Hz, 1H, Ar–H), 7.35 (s, 1H, Ar–H), 0.97-0.96 (m, 42H). ^{13}C{^{1}H}-NMR (125 MHz, $CDCl_3$): δ 149.5 (CH), 148.9 (C_q), 138.2 (CH), 135.2 (CH), 131.9 (C_q), 124.1 (CH), 121.9 (CH), 117.2 (C_q), 99.6 (C_q), 99.5 (C_q), 95.4 (C_q), 94.0 (C_q), 18.6 (12C, CH_3), 11.3 (6C, CH). HRMS (ESI): *m/z* calcd for $C_{30}H_{47}N_3Si_2+H^+$ $[M+H]^+$ 506.3381; found 506.3378.

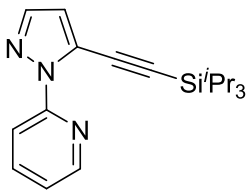

2-(5-((Triisopropylsilyl)ethynyl)-1*H*-pyrazol-1-yl)pyridine (31g): The representative procedure was followed, using **30g** (0.044 g, 0.303 mmol) and alkyne **28** (0.117 g, 0.45 mmol), and the reaction mixture was heated at 130 ^{o}C for 12 h. Purification by column

chromatography on basic alumina (petroleum ether/EtOAc: 100/1→20/1) yielded **31g** as an oil. Yield: 0.047 g, 48%. ^{1}H-NMR (500 MHz, $CDCl_3$): δ 8.52 (d, J = 4.2 Hz, 1H, Ar–H), 7.86 (d, J = 8.0 Hz, 1H, Ar–H), 7.81 (td, J = 8.0, 1.1 Hz, 1H, Ar–H), 7.68 (d, J = 1.5 Hz, 1H, Ar–H), 7.28-7.26 (m, 1H, Ar–H), 6.69 (d, J = 1.5 Hz, 1H, Ar–H), 1.12-1.11 (m, 21H). ^{13}C{^{1}H}-NMR (125 MHz, $CDCl_3$): δ 152.0 (C_q), 148.6 (CH), 140.8 (CH), 138.2 (CH), 125.1 (C_q), 122.6 (CH), 116.8 (CH), 114.5 (CH), 100.4 (C_q), 95.3 (C_q), 18.7 (6C, CH_3), 11.4 (3C, CH). HRMS (ESI): *m/z* calcd for $C_{19}H_{27}N_3Si+H^+$ $[M+H]^+$ 326.2047; found 326.2045.

5.4.3 Deprotection and functionalization

Representative procedure for deprotection:[403] **Synthesis of 32a:** The compound **29a** (0.2 g, 0.534 mmol) was introduced into a 100 mL Schlenk flask and THF (10 mL) was added into it. The reaction flask was cooled to 0 ^{o}C and TBAF solution (0.64 mL, 1 M solution in THF) was added *via* a syringe. The reaction mixture was warmed up to ambient temperature and stirred for additional 1 h. Then, the reaction mixture was quenched with H_2O (15 mL), and the compound was extracted with EtOAc (30 mL × 3). The combined organic extract was dried over Na_2SO_4 and the volatiles were evaporated *in vacuo*. The remaining residue was purified by column chromatography on basic alumina (petroleum ether/EtOAc: 20/1→10/1) to yield **32a** as an oil.

Characterization data of compounds 32

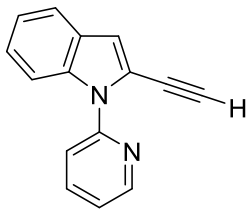

Data of 32a: Yield: 0.11 g, 94%. ^{1}H-NMR (500 MHz, $CDCl_3$): δ 8.67 (dd, J = 4.9, 1.1 Hz, 1H, Ar–H), 7.88 (td, J = 7.6, 5.7 Hz, 1H, Ar–H), 7.73 (d, J = 8.3 Hz, 1H, Ar–H), 7.64-7.62 (m, 2H, Ar–H), 7.33-7.28 (m, 2H, Ar–H), 7.20 (t, J = 8.0 Hz, 1H, Ar–H), 7.06 (s, 1H, Ar–H), 3.37 (s, 1H). ^{13}C{^{1}H}-NMR (125 MHz, $CDCl_3$): δ 151.1 (C_q), 149.2 (CH), 138.2 (CH), 136.9 (C_q), 127.7 (C_q), 124.8 (CH), 122.1 (CH), 121.9 (CH), 121.2 (CH), 120.5 (CH), 119.5 (C_q), 113.3 (CH), 112.2 (CH), 84.0 (CH), 76.0 (C_q). HRMS (ESI): *m/z* calcd for $C_{15}H_{10}N_2+H^+$ $[M+H]^+$ 219.0917; found 219.0919.

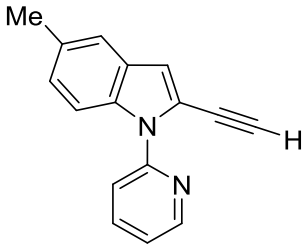

2-Ethynyl-5-methyl-1-(pyridin-2-yl)-1*H*-indole (32b): The representative procedure was followed, using **29b** (0.094 g, 0.241 mmol) and TBAF (0.29 mL, 1.0 M in THF). The compound was purified by column chromatography on basic alumina (petroleum ether/ EtOAc: 10/1→2/1) to yield **32b** as an oily liquid. Yield: 0.049 g, 87%. ^{1}H-NMR (500 MHz, $CDCl_3$): δ 8.65 (d, J = 3.4 Hz, 1H, Ar–H), 7.83 (td, J = 7.6, 1.5 Hz, 1H, Ar–H), 7.65 (d, J = 8.7 Hz, 1H, Ar–H), 7.62 (d, J = 8.3 Hz, 1H, Ar–H), 7.40 (s, 1H, Ar–H), 7.27 (dd, J = 7.2, 1.9 Hz, 1H, Ar–H), 7.13 (d, J = 8.8 Hz, 1H, Ar–H), 6.98 (s, 1H, Ar–H), 3.37 (s, 1H, CH), 2.45 (s, 3H, CH_3). ^{13}C{^{1}H}-NMR (125 MHz, $CDCl_3$): δ 151.2 (C_q), 149.1 (CH), 138.1 (CH), 135.3 (C_q), 131.2 (C_q), 127.9 (C_q), 126.5 (CH), 121.9 (CH), 120.6 (CH), 120.2 (CH), 119.3 (C_q), 113.0 (CH), 111.9 (CH), 83.8 (CH), 76.2 (C_q), 21.5 (CH_3). HRMS (ESI): *m/z* calcd for $C_{16}H_{12}N_2$+H^+ $[M+H]^+$ 233.1073; found 233.1073.

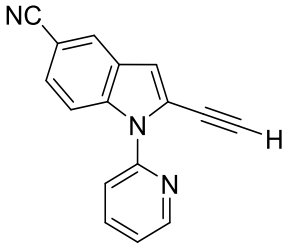

2-Ethynyl-1-(pyridin-2-yl)-1*H*-indole-5-carbonitrile (32f): The representative procedure was followed, using **29f** (0.058 g, 0.145 mmol) and TBAF (0.17 mL, 1.0 M in THF). The compound was purified by column chromatography on basic alumina (petroleum ether/ EtOAc: 5/1→1/1) to yield **32f** as an oily liquid. Yield: 0.032 g, 91%. ^{1}H-NMR (500 MHz, $CDCl_3$): δ = 8.68 (d, J = 2.3 Hz, 1H, Ar–H), 7.97-7.93 (m, 2H, Ar–H), 7.77 (d, J = 8.4 Hz, 1H, Ar–H), 7.65 (d, J = 7.6 Hz, 1H, Ar–H), 7.49 (d, J = 8.4 Hz, 1H, Ar–H), 7.40-7.38 (m, 1H, Ar–H), 7.08 (s, 1H, Ar–H), 3.42 (s, 1H, CH). ^{13}C{^{1}H}-NMR (125 MHz, $CDCl_3$): δ = 150.2 (CN), 149.4 (CH), 138.6 (CH), 138.3 (C_q), 127.5 (C_q), 127.3 (CH), 126.6 (CH), 123.1 (CH), 122.1 (C_q), 120.7 (CH), 120.2 (C_q), 113.4 (CH), 112.9 (CH), 105.2 (C_q), 85.5 (CH), 74.8 (C_q). HRMS (ESI): *m/z* calcd for $C_{16}H_9N_3$+H^+ $[M+H]^+$ 244.0869; found 244.0870.

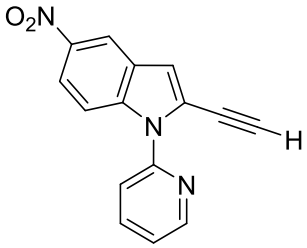

2-Ethynyl-5-nitro-1-(pyridin-2-yl)-1*H*-indole (32g): The representative procedure was followed using, **29g** (0.058 g, 0.138 mmol) and TBAF (0.16 mL, 1.0 M in THF). The compound was purified by column chromatography on basic alumina (petroleum ether/ EtOAc: 10/1→2/1) to yield **32g** as a yellow solid. Yield: 0.035 g, 97%. M.p. = 125–127 ^{o}C. ^{1}H-NMR (500 MHz, $CDCl_3$): δ 8.70 (d, J = 3.8 Hz, 1H, Ar–H), 8.57 (d, J = 1.5 Hz, 1H, Ar–H), 8.16 (dd, J = 9.1, 2.2 Hz, 1H, Ar–H), 7.94 (td, J = 7.6, 1.5 Hz, 1H, Ar–H), 7.76 (d, J = 9.5 Hz, 1H, Ar–H), 7.67 (d, J = 8.0 Hz, 1H, Ar–H), 7.41 (dd, J = 7.2, 5.3 Hz, 1H, Ar–H), 7.17 (s, 1H, Ar–H), 3.44 (s, 1H, CH). ^{13}C{^{1}H}-NMR (125 MHz, $CDCl_3$): δ 150.1 (C_q), 149.5 (CH), 143.3 (C_q), 139.5 (C_q), 138.6 (CH), 127.0 (C_q), 123.2 (CH), 123.0 (C_q), 120.7 (CH), 119.9 (CH), 118.1 (CH), 114.1 (CH), 112.6 (CH), 85.8 (CH), 74.6 (C_q). HRMS (ESI): *m/z* calcd for $C_{15}H_9N_3O_2$+H^+ $[M+H]^+$ 264.0768; found 264.0768.

Representative procedure for functionalizations

Synthesis of 2-(1-Benzyl-1*H*-1,2,3-triazol-4-yl)-1-(pyridin-2-yl)-1*H*-indole (33a):[403] Compound **32a** (0.036 g, 0.165 mmol), BnN_3 (0.022 g, 0.165 mmol) and CuI (0.0031 g, 10 mol%, 0.0165 mmol) were charged into a Schlenk tube, and DMF (2 mL) was added under argon. The reaction mixture was stirred at 60 ^{o}C in a pre-heated oil bath for 14 h. At ambient temperature, H_2O (5 mL) was added and the compound was extracted with EtOAc (30 mL × 3). The combined organic extract was washed with water (10 mL × 3) and dried over Na_2SO_4, and the volatiles were evaporated *in vacuo*. The remaining residue was purified by column chromatography on basic alumina (petroleum ether/EtOAc: 5/1→1/1) to yield **33a** as a white solid.

Characterization data of compound 33

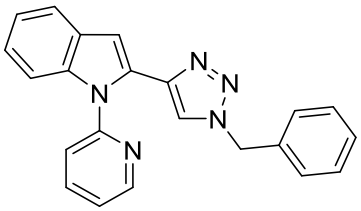

2-(1-Benzyl-1*H*-1,2,3-triazol-4-yl)-1-(pyridin-2-yl)-1*H*-indole (33a): Yield: 0.046 g, 79%. ^{1}H-NMR (500 MHz, $CDCl_3$): δ 8.67 (dd, J = 3.4, 1.1 Hz, 1H, Ar–H), 7.75 (td, J = 8.0, 6.1 Hz, 1H, Ar–H), 7.70-7.69 (m, 1H, Ar–H), 7.44 (d, J = 7.6 Hz, 1H, Ar–H), 7.38-7.36 (m, 3H, Ar–H), 7.30-7.28 (m, 1H, Ar–H), 7.26-7.19 (m, 5H, Ar–H), 7.11 (s, 1H, Ar–H), 7.07 (s, 1H, Ar–H), 5.47 (s, 2H, CH_2). ^{13}C{^{1}H}-NMR (125 MHz, $CDCl_3$): δ 151.5 (C_q), 149.4 (CH), 140.9 (C_q), 138.5 (C_q), 138.3 (CH), 134.6 (C_q), 130.1 (C_q), 129.2 (2C, CH), 128.9 (CH), 128.5 (C_q), 128.1 (2C, CH), 123.4 (CH), 122.7 (CH), 122.4 (CH), 121.8 (CH), 121.4 (CH), 121.1 (CH), 111.0 (CH), 105.6 (CH), 54.2 (CH_2). HRMS (ESI): *m/z* calcd for $C_{22}H_{17}N_5$+H^+ $[M+H]^+$ 352.1557; found 352.1573.

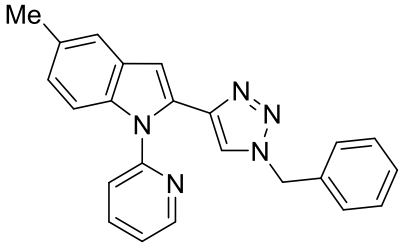

2-(1-Benzyl-1*H*-1,2,3-triazol-4-yl)-5-methyl-1-(pyridin-2-yl)-1*H*-indole (33b): The representative procedure was followed using **32b** (0.045 g, 0.193 mmol), BnN_3 (0.026 g, 0.195 mmol), CuI (0.0037 g, 10 mol%, 0.0193 mmol). The compound was purified by column chromatography on basic alumina (petroleum ether/EtOAc: 5/1→1/4) to yield **32b** as an off-white solid. Yield: 0.066 g, 93%. M.p. = 99–103 ^{o}C. ^{1}H-NMR (500 MHz, $CDCl_3$): δ 8.58 (br s, 1H, Ar–H), 7.70 (br s, 1H, Ar–H), 7.52 (s, 1H, Ar–H), 7.40 (br s, 4H, Ar–H), 7.31 (s, 1H, Ar–H), 7.26-7.24 (m, 3H, Ar–H), 7.11-7.10 (m, 3H, Ar–H), 5.49 (s, 2H, CH_2), 2.52 (s, 3H, CH_3). ^{13}C{^{1}H}-NMR (125 MHz, $CDCl_3$): δ 162.7 (C_q), 151.5 (C_q), 149.2 (CH), 140.9 (C_q), 138.2 (CH), 136.8 (C_q), 134.6 (C_q), 130.6 (C_q), 130.0 (C_q), 129.1 (2C, CH), 128.7 (CH), 128.0 (2C, CH), 124.9 (CH), 122.4 (CH), 122.1 (CH), 121.7 (CH), 120.7 (CH), 110.6 (CH), 105.1 (CH), 54.0 (CH_2), 21.4 (CH_3). HRMS (ESI): *m/z* calcd for $C_{23}H_{19}N_5$+H^+ $[M+H]^+$ 366.1713; found 366.1711.

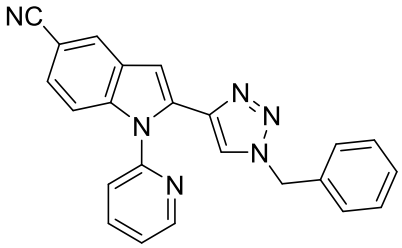

2-(1-Benzyl-1*H*-1,2,3-triazol-4-yl)-1-(pyridin-2-yl)-1*H*-indole-5-carbonitrile (33f): The representative procedure was followed, using **32f** (0.020 g, 0.082 mmol), BnN_3 (0.011 g, 0.082 mmol) and CuI (0.0016 g, 10 mol%, 0.0082 mmol). The compound was purified by column chromatography on basic alumina (petroleum ether/EtOAc: 10/1→1/1) to yield **33f** as an oily liquid. Yield: 0.021 g, 68%. ^{1}H-NMR (500 MHz, $CDCl_3$): δ 8.64 (br s, 1H, Ar–H), 8.07 (s, 1H, Ar–H), 7.85 (br s, 1H, Ar–H), 7.48-7.43 (m, 6H, Ar–H), 7.33-7.26 (m, 3H, Ar–H), 7.16 (br s, 2H, Ar–H), 5.53 (s, 2H, CH_2). ^{13}C{^{1}H}-NMR (125 MHz, $CDCl_3$): δ 150.6 (2C, C_q), 149.7 (CH), 139.9 (C_q), 139.9 (C_q), 138.7 (CH), 134.4 (C_q), 132.6 (C_q), 129.3 (2C, CH), 129.0 (CH), 128.2 (2C, CH), 126.4 (CH), 126.1 (CH), 123.6 (CH), 122.6 (CH), 122.2 (CH), 120.5 (C_q), 112.1 (CH), 105.2 (CH), 104.6 (C_q), 54.3 (CH_2). HRMS (ESI): *m/z* calcd for $C_{23}H_{16}N_6$+H^+ $[M+H]^+$ 377.1509; found 377.1509.

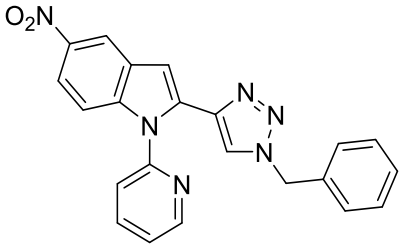

2-(1-Benzyl-1*H*-1,2,3-triazol-4-yl)-5-nitro-1-(pyridin-2-yl)-1*H*-indole (33g): The representative procedure was followed using **32g** (0.020 g, 0.075 mmol), BnN_3 (0.010 g, 0.075 mmol) and CuI (0.0014 g, 10 mol%, 0.0075 mmol). The compound was purified by column chromatography on basic alumina (petroleum ether/EtOAc: 5/1→1/4) to yield **33g** as a yellow solid. Yield: 0.015 g, 50%. M.p. = 140–143 ^{o}C. ^{1}H-NMR (500 MHz, $CDCl_3$): δ 8.58 (d, *J* = 12.2 Hz, 2H, Ar–H), 8.08 (d, *J* = 8.3 Hz, 1H, Ar–H), 7.79 (br s, 1H, Ar–H), 7.39-7.35 (m, 5H, Ar–H), 7.24 (s, 1H, Ar–H), 7.18 (br s, 3H, Ar–H), 7.10 (s, 1H, Ar–H), 5.46 (s, 2H, CH_2). ^{13}C{^{1}H}-NMR (125 MHz, $CDCl_3$): δ 150.6 (C_q), 149.8 (CH), 143.1 (C_q), 141.1 (C_q), 139.8 (C_q), 138.8 (CH), 134.4 (C_q), 133.5 (C_q), 129.4 (2C, CH), 129.1 (CH), 128.3 (2C, CH), 127.8 (C_q), 123.8 (CH), 122.6 (CH), 122.3 (CH), 118.8 (CH), 118.0 (CH), 111.3 (CH), 106.5 (CH), 54.4 (CH_2). HRMS (ESI): *m/z* calcd for $C_{22}H_{16}N_6O_2$+H^+ $[M+H]^+$ 397.1408; found 397.1405.

Synthesis and characterization data of compounds 34

Representative procedure for synthesis of 1-(Pyridin-2-yl)-2-(*p*-tolylethynyl)-1*H*-indole (**34aa**)**:** To a flame dried screw-capped Schlenk tube equipped with magnetic stir bar was introduced 4-iodotoluene (0.033 g, 0.151 mmol), $(PPh_3)_2PdCl_2$ (0.002 g, 0.003 mmol, 2.0 mol%), CuI (0.0008 g, 0.0045 mmol, 3.0 mol%) and Et_3N (1.5 mL, 10.7 mmol). To this mixture, a solution of **32a** (0.033 g, 0.151 mmol) in THF/Et_3N (1/0.5 mL) was added dropwise at room temperature. Then, the reaction mixture was stirred at 60 ^oC in a pre-heated oil bath for 2 h. At ambient temperature, H_2O (5 mL) was added and the compound was extracted with EtOAc (30 mL × 3). The combined organic extract was dried over Na_2SO_4 and the volatiles were evaporated *in vacuo*. The remaining residue was purified by column chromatography on basic alumina (petroleum ether/EtOAc: 5/1→1/1) to yield **34aa** as a brown solid.

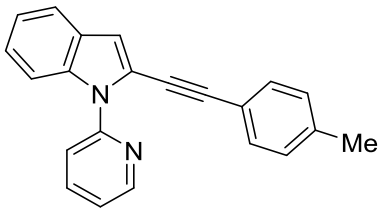

Data of 1-(Pyridin-2-yl)-2-(p-tolylethynyl)-1*H*-indole (34aa): Yield: 0.040 g, 87%. M.p. = 103–105 ^oC. ^1H-NMR (400 MHz, $CDCl_3$): δ 8.70 (d, J = 4.2 Hz, 1H, Ar–H), 7.91-7.87 (m, 1H, Ar–H), 7.81 (d, J = 8.5 Hz, 1H, Ar–H), 7.74 (d, J = 7.9 Hz, 1H, Ar–H), 7.65 (d, J = 7.9 Hz, 1H, Ar–H), 7.32-7.31 (m, 4H, Ar–H), 7.23-7.19 (m, 1H, Ar–H), 7.14 (d, J = 7.9 Hz, 2H, Ar–H), 7.04 (s, 1H, Ar–H), 2.37 (s, 3H, CH_3). $^{13}C\{^1H\}$-NMR (100 MHz, $CDCl_3$): δ 151.4 (C_q), 149.1 (CH), 139.0 (C_q), 137.9 (CH), 137.0 (C_q), 131.2 (2C, CH), 129.3 (2C, CH), 128.2 (C_q), 124.4 (CH), 121.9 (CH), 121.8 (CH), 121.0 (CH), 120.9 (C_q), 120.5 (CH), 119.8 (C_q), 112.3 (CH), 111.7 (CH), 95.8 (C_q), 81.3 (C_q), 21.7 (CH_3). HRMS (ESI): *m/z* calcd for $C_{22}H_{16}N_2+H^+$ $[M+H]^+$ 309.1386; found 309.1384.

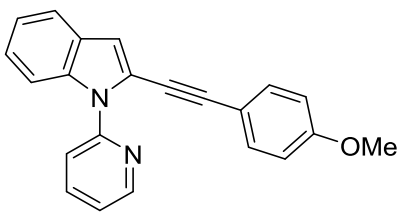

2-((4-Methoxyphenyl)ethynyl)-1-(pyridin-2-yl)-1*H*-indole (34ab): The representative procedure was followed using, 4-iodoanisole (0.035 g, 0.151 mmol), $(PPh_3)_2PdCl_2$ (0.002 g, 2

mol%, 0.003 mmol), CuI (0.0009 g, 3 mol%, 0.0045) and **32a** (0.033 g, 0.151 mmol). The compound was purified by column chromatography on basic alumina (petroleum ether/EtOAc: 5/1→1/1) to yield **34ab** as a brown solid. Yield: 0.038 g, 77%. M.p. = 108–110 ^{o}C. ^{1}H-NMR (400 MHz, $CDCl_3$): δ 8.69 (d, J = 3.4 Hz, 1H, Ar–H), 7.88 (td, J = 7.6, 1.1 Hz, 1H, Ar–H), 7.80 (d, J = 8.3 Hz, 1H, Ar–H), 7.74 (d, J = 8.0 Hz, 1H, Ar–H), 7.64 (d, J = 8.0 Hz, 1H, Ar–H), 7.35 (d, J = 8.8 Hz, 2H, Ar–H), 7.33-7.27 (m, 2H, Ar–H), 7.21 (t, J = 7.2 Hz, 1H, Ar–H), 7.02 (s, 1H, Ar–H), 6.86 (d, J = 8.8 Hz, 2H, Ar–H), 3.81 (s, 3H, OCH_3). ^{13}C{^{1}H}-NMR (100 MHz, $CDCl_3$): δ 160.0 (C_q), 151.5 (C_q), 149.1 (CH), 137.9 (CH), 136.9 (C_q), 132.9 (2C, CH), 128.3 (C_q), 124.3 (CH), 121.9 (CH), 121.8 (CH), 121.0 (C_q), 120.9 (CH), 120.5 (CH), 114.9 (C_q), 114.3 (2C, CH), 112.2 (CH), 111.4 (CH), 95.7 (C_q), 80.6 (C_q), 55.5 (CH_3). HRMS (ESI): *m/z* calcd for $C_{22}H_{16}N_2O+H^+$ $[M+H]^+$ 325.1335; found 325.1331.

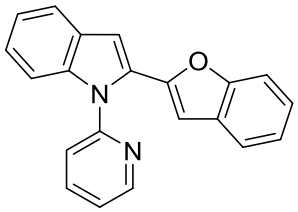

Synthesis of 2-(Benzofuran-2-yl)-1-(pyridin-2-yl)-1*H*-indole (35a):[421] To a flame dried screw-capped Schlenk tube equipped with magnetic stir bar was introduced 2-iodophenol (0.047 g, 0.213 mmol), $(PPh_3)_2PdCl_2$ (0.003 g, 0.0043 mmol, 2.0 mol%), CuI (0.0012 g, 0.0063 mmol, 3.0 mol %) and Et_3N (1.5 mL). To this mixture, a solution of **32a** (0.046 g, 0.213 mmol) in THF/Et_3N (1/0.5 mL) was added dropwise at room temperature. Then, the reaction mixture was stirred at 60 ^{o}C in a pre-heated oil bath for 12 h. At ambient temperature, H_2O (5 mL) was added and the compound was extracted with EtOAc (30 mL × 3). The combined organic extract was washed dried over Na_2SO_4, and the volatiles were evaporated *in vacuo*. The remaining residue was purified by column chromatography on basic alumina (petroleum ether/EtOAc: 50/1→1/1) to yield **35a** as a brown liquid. Yield: 0.033 g, 50%. ^{1}H-NMR (500 MHz, $CDCl_3$): δ 8.76 (d, J = 3.4 Hz, 1H, Ar–H), 7.89 (td, J = 9.5, 1.9 Hz, 1H, Ar–H), 7.75 (d, J = 7.2 Hz, 1H, Ar–H), 7.49-7.43 (m, 4H, Ar–H), 7.38 (d, J = 8.0 Hz, 1H, Ar–H), 7.30-7.20 (m, 5H, Ar–H), 6.25 (s, 1H, Ar–H). ^{13}C{^{1}H}-NMR (125 MHz, $CDCl_3$): δ 154.7 (C_q), 151.9 (C_q), 149.8 (CH), 148.9 (C_q), 139.4 (C_q), 138.6 (CH), 130.3 (C_q), 128.9 (C_q), 128.4 (C_q), 124.6 (CH), 124.1 (CH), 123.1 (CH), 123.1 (CH), 122.4 (CH), 121.7 (CH), 121.4 (CH), 121.1 (CH), 111.2 (CH), 111.2 (CH), 106.4 (CH), 104.3 (CH). HRMS (ESI): *m/z* calcd for $C_{21}H_{14}N_2O+H^+$ $[M+H]^+$ 311.1179; found 311.1178.

Chapter 6

Mechanistic aspects of nickel-catalyzed C(2)–H alkynylation of indoles

6.1 Introduction

Transition-metal-catalyzed direct C–H bond alkynylation of arenes and heteroarenes is of significant importance because of the late-stage diversification of the alkynylated compounds. Various transition-metal catalysts have been known for the alkynylation of diverse (hetero)arenes.[230,243, 245,372,390,405] Among them the nickel catalyst is particularly used for the alkynylation of azoles and benzamide derivatives. However, the detailed mechanistic study for the Ni-catalyzed alkynylation is not well understood.[243,245] In chapter 5, the Ni(II)-catalyzed regioselective C(2)-alkynylation is described using monodentate directing group, wherein the in-situ generated nickel catalyst $(THF)_2NiBr_2$/Phen efficiently catalyzes the alkynylation of diverse heteroarenes. This chapter focuses on the synthesis and isolation of nickel complexes based on [Ni]/Phen system, such as $[(Phen)_3Ni\cdot NiBr_4]$, $[(Phen)_2NiCl_2]$ and $[(Phen)_3Ni]\cdot NiCl_4$. Detailed mechanistic study of the alkynylation of indole by the well-defined nickel complex is described. Various controlled studies, kinetic experiments, isotope labelling studies and DFT calculations were performed to get more mechanistic insights. An improved mechanistic cycle has been proposed considering all the experimental findings.

6.2 Results and discussion

6.2.1 Synthesis and characterization of $(Phen)_nNiX_n$ complexes

Synthesis of $[(Phen)_3Ni]\cdot NiBr_4$ (36): The treatment of 1,10-phenanthroline (Phen) with $(THF)_2NiBr_2$ in acetonitrile at room temperature for 1 h afforded the $[(Phen)_3Ni]\cdot NiBr_4$ complex (**36**) as light green solid (Scheme 6.1). The complex **36** is NMR silent and characterized by elemental analysis. Further, the molecular structure of complex **36** was confirmed by the single crystal X-ray diffraction study. The complex **36** is most likely generated by the disproportion reaction between the initially formed complexes, $(Phen)_2NiBr_2$ and $(Phen)NiBr_2$. Though the different stoichiometry of Phen and $(THF)_2NiBr_2$ used for the isolation of $(Phen)_2NiBr_2$ or $(Phen)NiBr_2$, the reaction always produced complex $[(Phen)_3Ni]\cdot NiBr_4$.

The ORTEP diagram of complex **36** is shown in Figure 6.1. The selected bond lengths and bond angles are given in Table 6.1. The ORTEP diagram shows that the complex **36** has two different Ni-centers, one is coordinated by three phenanthroline ligands with distorted octahedral geometry, whereas the other is $NiBr_4$ with tetrahedral geometry around the nickel. The six Ni(1)–N bond lengths are in the range of 2.051(6) Å to 2.085(6) Å, and the N–Ni–N bite angles of three phenanthroline ligands are around 80^o. The different N–Ni–N bond angles around the Ni(1) center suggest that the three phenanthroline moieties are almost

perpendicular to each other. The Br–Ni–Br bond angles around Ni(2) are in the range of 100.61(7)^{o} to 113.57(7)^{o}, which indicate the distorted tetrahedral geometry around the nickel.

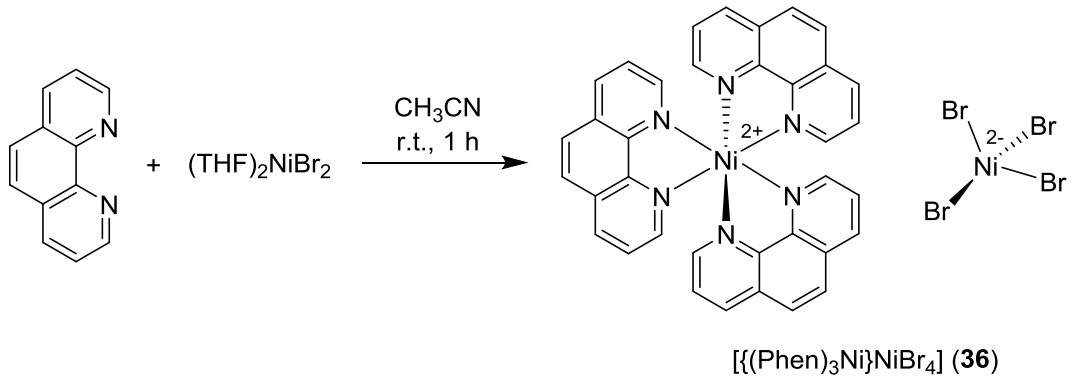

Scheme 6.1 Synthesis of $[(Phen)_3Ni]\cdot NiBr_4$ (**36**) complex

Synthesis of $[(Phen)_3Ni]\cdot NiCl_4$ (37): Treatment of an excess of phenanthroline with $(DME)NiCl_2$ metal precursor in THF at room temperature afforded the complex $[(Phen)_3Ni]\cdot NiCl_4$ (**37**) (Scheme 6.2). The complex **37** obtained as blue solid after washing with acetonitrile. This complex is also NMR silent and characterized by the elemental analysis. Further, complex **37** was characterized by X-ray diffraction study (Figure 6.2). The selected bond lengths and bond angles are shown in Table 6.1. The ORTEP diagram of **37** shows two different nickel centers: one is coordinated through the three phenanthroline ring in octahedral fashion and other nickel center is $NiCl_4$ with tetrahedral geometry, similar to the complex **36**. All the three rings are perpendicular to each other and all six Ni–N bonds are in the range of 2.06(6) Å to 2.09(6) Å around the Ni(1) center. The N–Ni–N bite angles of three phenanthroline ligands are around 80^{o}. The Cl–Ni–Cl bond angles around Ni(2) are in the range of 106.28(7)^{o} to 114.54(7)^{o}, which indicate the distorted tetrahedral geometry around the nickel.

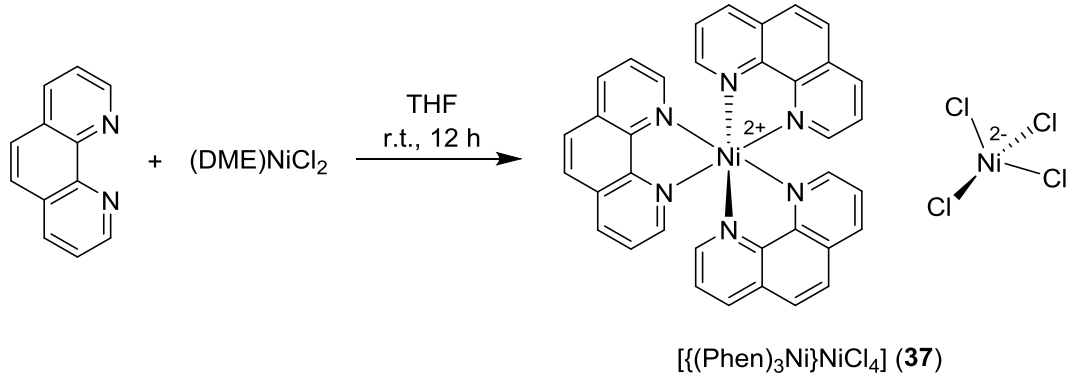

Scheme 6.2 Synthesis of $[(Phen)_3Ni]\cdot NiCl_4$ (**37**) complex

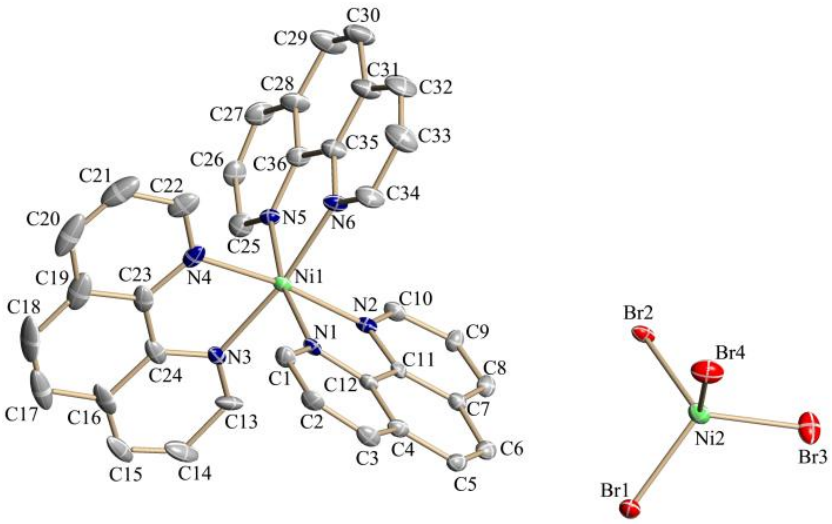

Figure 6.1 ORTEP diagram of $[(Phen)_3Ni]\cdot NiBr_4$ (**36**)

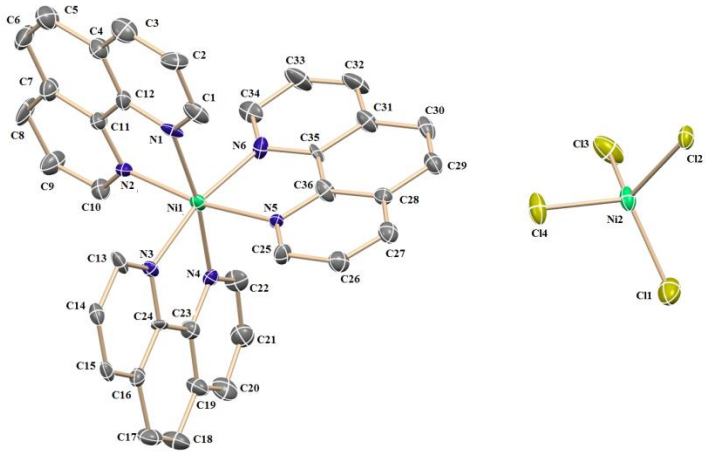

Figure 6.2 ORTEP diagram of $[(Phen)_3Ni]\cdot NiCl_4$ (**37**).

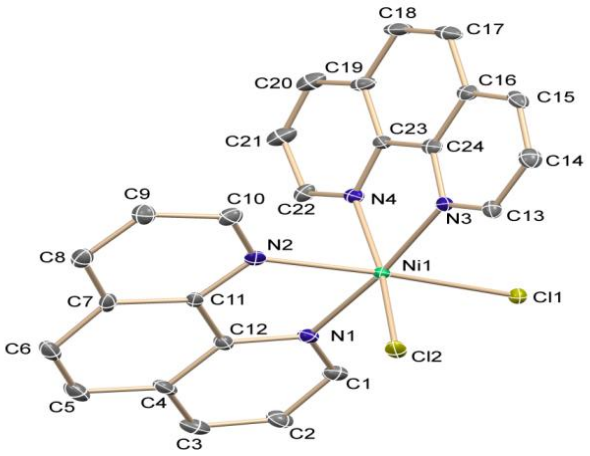

Figure 6.3 ORTEP diagram of $(Phen)_2NiCl_2$ (**38**).

Table 6.1 Selected bond lengths (Å) and bond angles (^{o}) for complexes **36**, **37** and **38**

Bond length (Å)		**Bond angles (^{o})**	
Complex 36			
Ni(1)–N(1)	2.073(6)	N(2)–Ni(1)–N(1)	80.0(2)
Ni(1)–N(2)	2.051(6)	N(4)–Ni(1)–N(3)	79.5(3)
Ni(1)–N(4)	2.071(6)	N(2)–Ni(1)–N(4)	172.0(2)
Ni(1)–N(6)	2.076(6)	Br(3)–Ni(2)–Br(4)	108.08(6)
Complex 37			
Ni(2)–Cl(1)	2.2678(6)	N(2)–Ni(1)–N(1)	80.24(2)
Ni(1)–N(2)	2.0658(6)	N(4)–Ni(1)–N(3)	78.78(3)
Ni(1)–N(4)	2.0739(6)	N(2)–Ni(1)–N(4)	171.75(2)
Ni(1)–N(1)	2.0978(6)	Cl(1)–Ni(2)–Cl(4)	108.81(6)
Complex 38			
Ni(1)–Cl(1)	2.418(6)	N(2)–Ni(1)–Cl(1)	172.5(2)
Ni(1)–N(2)	2.10(6)	N(4)–Ni(1)–Cl(2)	79.5(3)
Ni(1)–N(4)	2.07 (6)	N(2)–Ni(1)–N(4)	85.2(2)
Ni(1)–N(6)	2.09(6)	Cl(1)–Ni(1)–Cl(2)	98.11(6)

Synthesis of $(Phen)_2NiCl_2$ (38) complex: In order to synthesize a mono ligand coordinated nickel complex *i.e.* $(Phen)NiCl_2$, a stoichiometric reaction of 1,10-phenanthroline and $(DME)NiCl_2$ (1:1) was performed in THF at room temperature. However, the reaction led to the formation of complex $(Phen)_2NiCl_2$ (**38**) (Scheme 6.3). The complex **38** is NMR inactive and characterized by the elemental analysis as well as by the X-ray diffraction study. The ORTEP diagram of **38** is shown in Figure 6.3. Selected bond lengths and bond angles are shown in Table 6.1. The geometry around the nickel center is distorted octahedral in complex **38**, and two phenanthroline rings are perpendicular to each other. The Ni(1)–Cl(1) bond length is 2.418(6) Å, whereas all four Ni(1)–N bond lengths are around 2.10 Å. This indicates that both the Phen rings are around the same distance from nickel center.

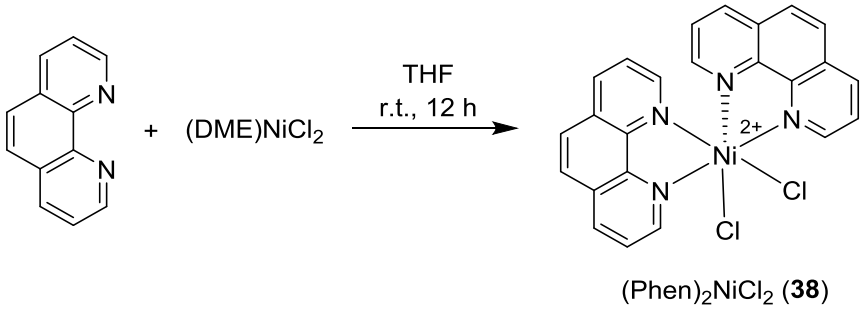

Scheme 6.3 Synthesis of $(Phen)_2NiCl_2$ (**38**) complex

6.2.2 Catalytic competency of isolated nickel complexes

Chapter 5 described the alkynylation of indole with alkynyl bromide using in situ generated catalyst system from $(THF)_2NiBr_2$ and Phen. This catalytic system efficiently gives the alkynylation products of various heteroarenes with the tolerance of sensitive functional groups. In order to know the competencies of isolated nickel catalysts for the alkynylation of indoles, the complexes $[(Phen)_3Ni]\cdot NiBr_4$ (**36**), $[(Phen)_3Ni]\cdot NiCl_4$ (**37**) and $(Phen)_2NiCl_2$ (**38**) were employed for the alkynylation of indoles with alkynyl bromide under the standard catalytic conditions. All the three complexes were as competent as in situ generated catalyst for the alkynylation reaction (Scheme 6.4). Hence, the catalyst **36** or $(THF)_2NiBr_2$/Phen was employed for further mechanistic studies for the alkynylation reaction.

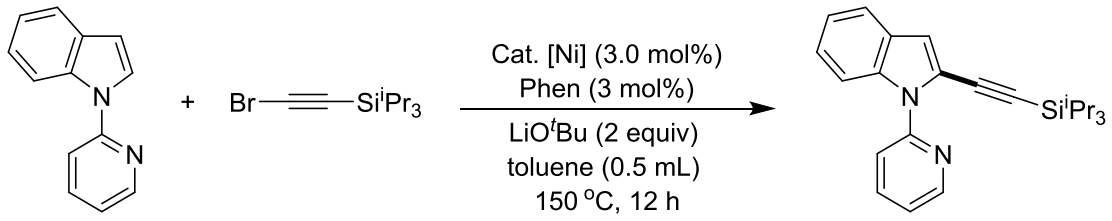

27a **28** **29a**

Cat. [Ni]	Yield(%)
36	94
37	91
38	90

Scheme 6.4 Alkynylation with the isolated nickel-catalysts

6.2.3 External additive experiments

The alkynylation reaction of indole **27a** with alkynyl bromide **28** in the presence of 1800 mol% of Hg under the standard catalytic conditions afforded the product **29a** in 90% yield (Scheme 6.5). The addition of Hg did not affect the alkynylation reaction significantly.

This clearly suggests that the reaction is homogeneous in nature, and may not be proceeding *via* the active nickel nanoparticles.

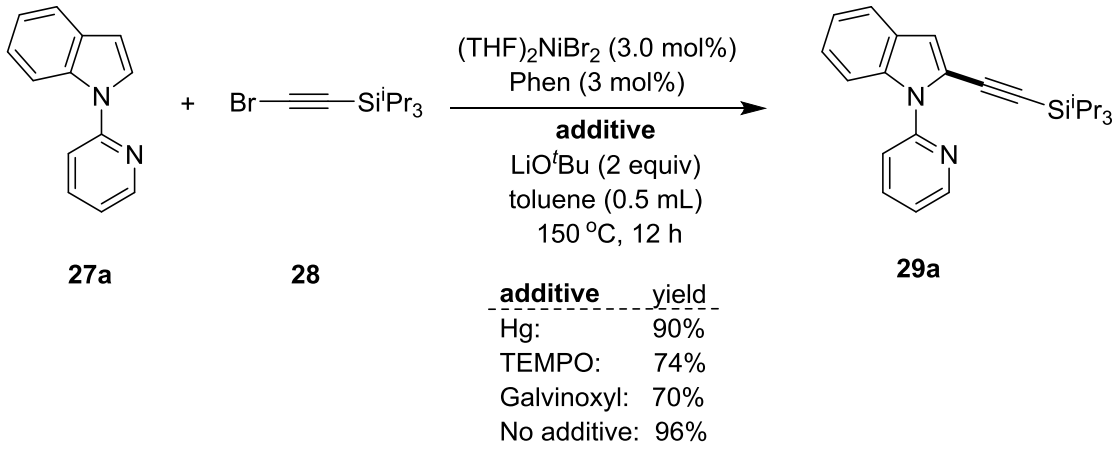

Scheme 6.5 Reaction in presence of external additive

Similarly, the standard alkynylation reaction was performed in the presence of a stoichiometric amount of 2,2,6,6-tetramethylpiperidin-1-yl)oxyl (TEMPO) (1.0 equiv) or galvinoxyl (1 equiv) in order to understand the two electrons or single electron pathway for the nickel-catalyzed alkynylation. Hence, the alkynylation of indole **27a** in the presence of TEMPO or galvinoxyl afforded 74% and 70% of **29a**, respectively (Scheme 6.5). There is no significant decrease in the yield of alkynylated product compared to the same reaction without the additive. In addition, no coupled product of TEMPO with any other organic radical species was observed. This finding ruled out the probable involvement of a free-radical intermediate (*i.e*. one electron path) during the present Ni-catalyzed indole alkynylation.

6.2.4 Kinetic analysis of alkynylation reaction

Kinetic analysis using $(THF)_2NiBr_2$/Phen: The kinetic analysis of the alkynylation reaction was performed to understand the rate of reaction as well as the reactivity of nickel catalyst. In a standard kinetic experiment, a teflon-screw capped tube equipped with magnetic stir bar was introduced $(THF)_2NiBr_2$ (0.0032 g, 0.009 mmol), 1,10-phenanthroline (0.0016 g, 0.009 mmol), LiO^tBu (0.048 g, 0.6 mmol), alkynyl bromide **28** (0.117 g, 0.45 mmol, 0.45 M) and 1-(pyridin-2-yl)-1*H*-indole **27a** (0.059 g, 0.304 mmol, 0.30 M) and toluene (required amount) was added to make the total volume 1.0 mL. To the reaction mixture mesitylene (0.030 mL, 0.2154 mmol) was added as an internal standard. The reaction mixture was then stirred at 150 ^oC in a pre-heated oil bath, and at regular intervals (10, 20, 30, 40, 50, 60, 90,

120 and 180 min), the progress of the reaction was monitored by the GC analysis. The data of the concentration of the product *vs* time (min) plot was drawn with Origin Pro 8. For the reaction rate, the data were fitted linear (excluding induction period) with Origin Pro 8 and the rate was determined by initial rate method. The reaction profile of the nickel-catalyzed alkynylation of indole with alkynyl bromide over a period of 180 min has shown in Figure 6.4. The reaction profile shows that the reaction needs an induction period of about 50 min, and after that alkynylation product **29a** formed. This suggests that $(THF)_2NiBr_2$ is not the active catalyst species and the actual catalytic species is formed during the initial 50 minutes.

Kinetic analysis using $Ni(COD)_2$/Phen: The kinetic analysis of the standard alkynylation reaction was performed using $Ni(COD)_2$/Phen, assuming that the Ni(0) could be the active catalyst during the reaction as the catalyst $(THF)_2NiBr_2$/Phen has an induction period of 50 min. The alkynylation reaction with $Ni(COD)_2$/Phen also shows an induction period of 40 min. This study indicates that Ni(0) is not the actual catalytic species. Hence, the probability of generation of Ni(0) active species during $(THF)_2NiBr_2$/Phen catalyzed alkynylation is unlikely.

Kinetic analysis using $(THF)_2NiBr_2$/Phen upon preheating: The kinetic analysis for the alkynylation reaction with $Ni(COD)_2$/Phen as well as with in situ generated $(THF)_2NiBr_2$/Phen catalyst suggests that Ni(0) or $(THF)_2NiBr_2$ is not the active catalytic species during the reaction. To know whether the preformed complex from $(THF)_2NiBr_2$ and Phen could be the active species, the kinetic analyses of the standard alkynylation reaction was performed after preheating the mixture of $(THF)_2NiBr_2$ and Phen in toluene at 150 ^oC for 1 h. Hence, after heating the mixture of $(THF)_2NiBr_2$ and Phen, the substrate **27a**, alkynyl bromide and LiO^tBu were added and the reaction mixture was further heated at 150 ^oC. At regular interval the sample was analyzed and the data were collected over 300 min. The kinetic analysis of this reaction also shows an induction period of 40 min for the formation of product **29a**. This experiment suggests that the formation of complex from $(THF)_2NiBr_2$ and Phen, *i.e.* $[(Phen)_3Ni]\cdot NiBr_4$ is not the active catalyst during the reaction.

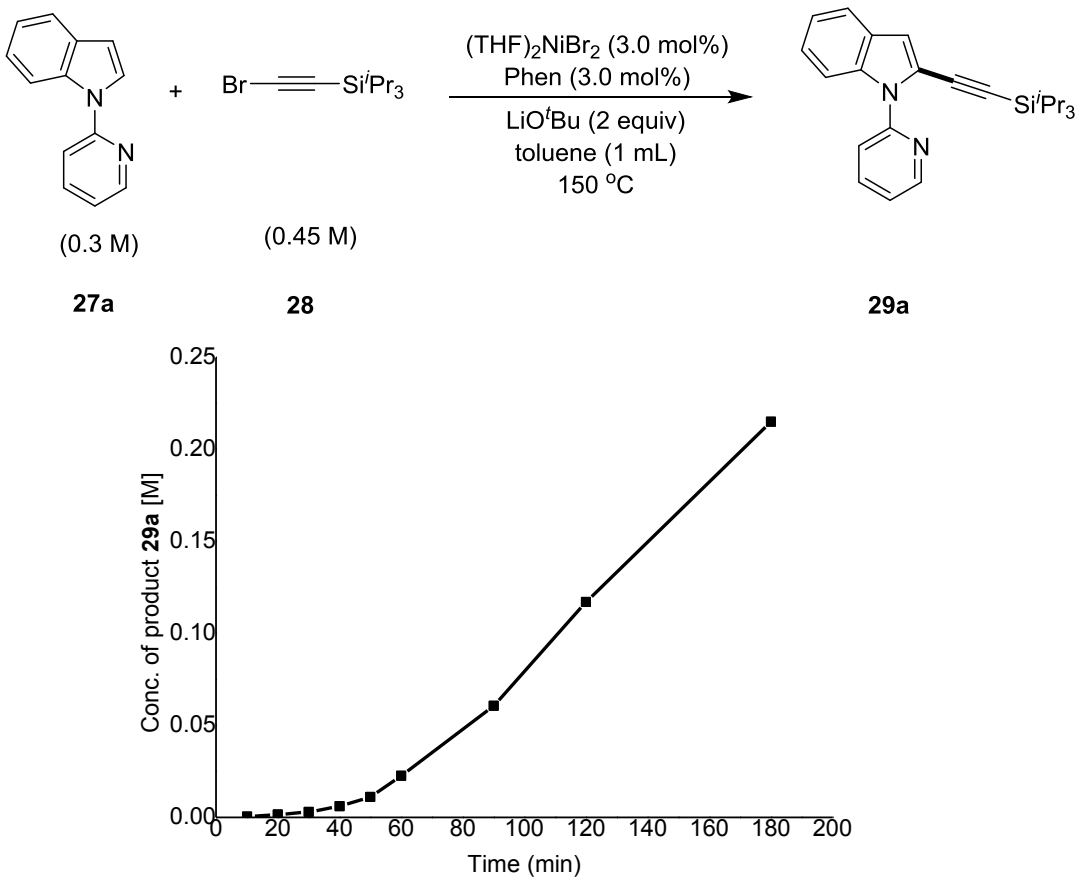

Figure 6.4 Formation of **29a** using 1-(pyridin-2- yl)-1*H*-indole (**27a**) and **28**.

Kinetic analysis using $(THF)_2NiBr_2$/Phen, 27a and LiO^{t}Bu upon preheating: Assuming that the substrate **27a**-ligated nickel complex might be the active catalyst during the reaction, the combination of $(THF)_2NiBr_2$/Phen, indolepyridine (**27a**) and LiO^{t}Bu were heated in toluene for 1 h before the actual catalytic kinetic analysis. After 1 h, alkynyl bromide **28** (0.117 g, 0.45 mmol) was added and the reaction mixture was heated at 150 ^{o}C, and the formation of product was analyzed at different time intervals (up to 90 min) (Figure 6.5). At 10 and 20 min, the product **29a** formed was 0.017 mM and 0.0257 mM, which correspond to 2 and 3 TON's, respectively. The plot of product *vs* time shows the absence of induction period for the formation of a product, which suggests that the combination of $(THF)_2NiBr_2$/Phen, **27a** and LiO^{t}Bu formed an active species that catalyzes alkynylation of indole. The formation of a nickelacycle by the C(2)–H activation of substrate **27a** could be assumed as the active nickel catalyst during the reaction, which is discussed below.

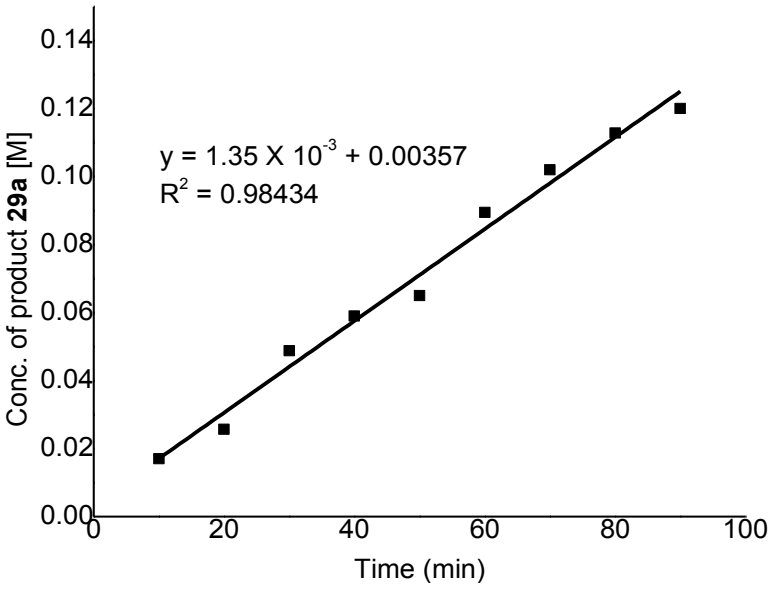

Figure 6.5 Formation of **29a** from the reaction of **27a** with **28**.

6.2.5 Rate order determination

In order to know the order of reaction, the rate of the alkynylation reaction with various reaction components was determined by the initial rate method. The data of the concentration of the product *vs* time (min) plot was fitted linear with Origin Pro 8. The slope of the linear fitting represents the reaction rate. The order of the reaction was then determined by plotting the log(rate) *vs* log(conc. component) for a particular component.

Rate order of alkynylation with (pyridin-2-yl)-1*H*-indole: To determine the order of the alkynylation reaction on (pyridin-2-yl)-1*H*-indole (**27a**), the initial rates at different initial concentrations of **27a** were recorded. The final data was obtained by averaging the results of two independent runs for each experiment. The initial rates for the formation of alkynylated product **29a** with different concentrations of **27a** have been shown in Table 6.2. The initial rates for the formation of alkynylated product **29a** increases with the increase in the initial concentration of **27a** (Figure 6.6 A). A slope of 1.146 was obtained from the plot of log(rate) *vs* log(conc. **27a**) suggesting the reaction is first-order with respect to substrate **27a** (Figure 6.6 B). This finding indicates the probable involvement of (pyridin-2-yl)-1*H*-indole in more than one way during the catalytic cycle.

Table 6.2 Rate of alkynylation reaction with varying concentration of **27a**

Experiment	Amount of **27a** (g)	Initial conc. of **27a** [M]	Initial rate [$Mmin^{-1}$] x 10^{-3}
1	0.0583	0.3	1.9
2	0.117	0.6	4.3
3	0.175	0.9	5.7
4	0.233	1.2	10

Rate order of alkynylation with alkynyl bromide (28): To determine the order of the alkynylation reaction on alkynyl bromide **(28)**, the initial rates at different initial concentrations of **28** were recorded. The initial rates for the formation of alkynylated product **29a** with different concentrations of **28** are shown in Table 6.3. The initial rates for formation of alkynylated product **29a** were almost similar with the different initial concentration of **28** (Figure 6.7 A). The plot of log(rate) *vs* log(conc. **28**) suggests the reaction is independent of the concentration of alkynyl bromide (**28**) (Figure 6.7 B).

Table 6.3 Rate of alkynylation reaction with varying concentration alkynyl bromide (**28**)

Experiment	Amount of **28** (g)	Initial conc. of **28** [M]	Initial rate [$Mmin^{-1}$] x 10^{-4}
1	0.078	0.3	8.68
2	0.117	0.45	5.55
3	0.235	0.9	8.7
4	0.470	1.8	6.99

Rate order of alkynylation with LiO^tBu: The order of the alkynylation reaction on concentration of LiO^tBu was determined. Hence, the rates of alkynylation were calculated with various LiO^tBu concentrations. The initial rates for the formation of alkynylated product **29a** with different concentration of LiO^tBu have shown in Table 6.4. It was observed that rate of formation **29a** is does not change with varing LiO^tBu concentrations (Figure 6.8 A). The plot of log(rate) *vs* log(equiv. LiO^tBu) which indicates the reaction is zeroth order with LiO^tBu (Figure 6.8 B).

Table 6.4 Rate of alkynylation reaction at different loading of LiO^tBu

Experiment	Amount of LiO^tBu (g)	Equiv. of LiO^tBu	Initial rate [$Mmin^{-1}$] x 10^{-3}
1	0.048	2	1.86
2	0.096	4	1.73
3	0.144	6	1.80
4	0.194	8	2.2

Rate order for alkynylation with ((Phen)$_3$Ni)·NiBr$_4$ (36): To determine the order of the alkynylation reaction on ((Phen)$_3$Ni)·NiBr$_4$ (**36**), the initial rates at different loading of **36** were recorded. The initial rates for the formation of alkynylated product **29a** with different loading of **36** are shown in Table 6.5. The initial rates for formation of alkynylated product **29a** were slightly increased with the varing concentration of **36** (Figure 6.9 A). The plot of log(rate) *vs* log(conc. **36**) shows a slope of 0.4578, which indicates the alkynylation is fractional order with respect to catalyst loading (Figure 6.9 B).

Table 6.5 Rate of alkynylation reaction at different loading of **36**

Experiment	Amount of **36** (g)	Conc. of **36**	Initial rate [Mmin^{-1}] x 10^{-3}
1	0.0044	0.009	1.81
2	0.0087	0.018	2.2
3	0.0131	0.027	2.99
4	0.0175	0.036	3.47

Overall order of alkynylation reaction

The kinetic analysis data shows that the order of reaction is 1.146 with indole **27a** and 0.4578 with the concentration of (Phen)$_{1.5}$NiBr$_2$ (**36**). Hence, the rate equation can be drawn as a shown in eq 2. The overall order for the reaction is 1.6.

rate = k [**27a**]$^{1.15}$ [**36**]$^{0.46}$

Over all reaction order = 1.6 (2)

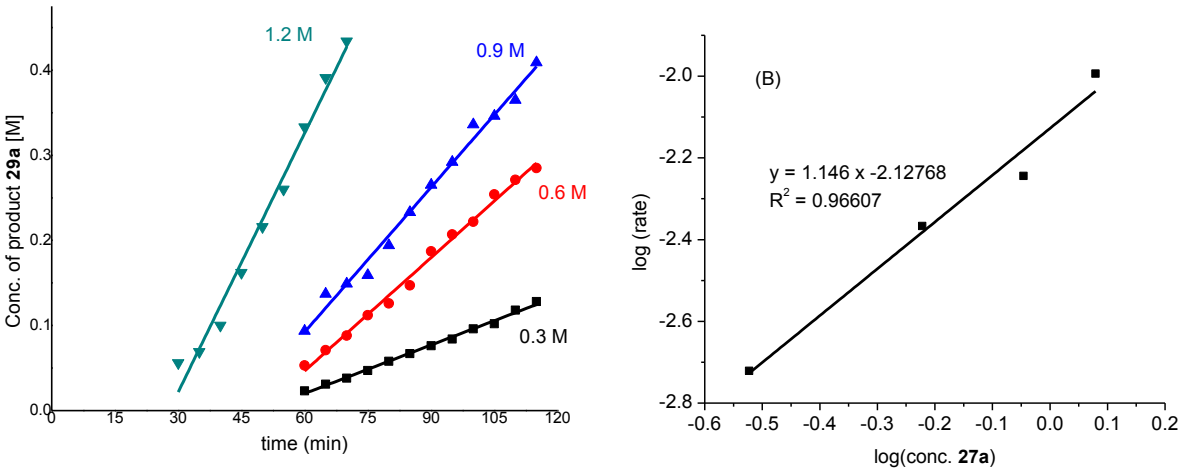

Figure 6.6 (A) Product **29a** at different initial concentration of **27a**. (B) Plot of log(rate) *vs* log(conc. **27a**).

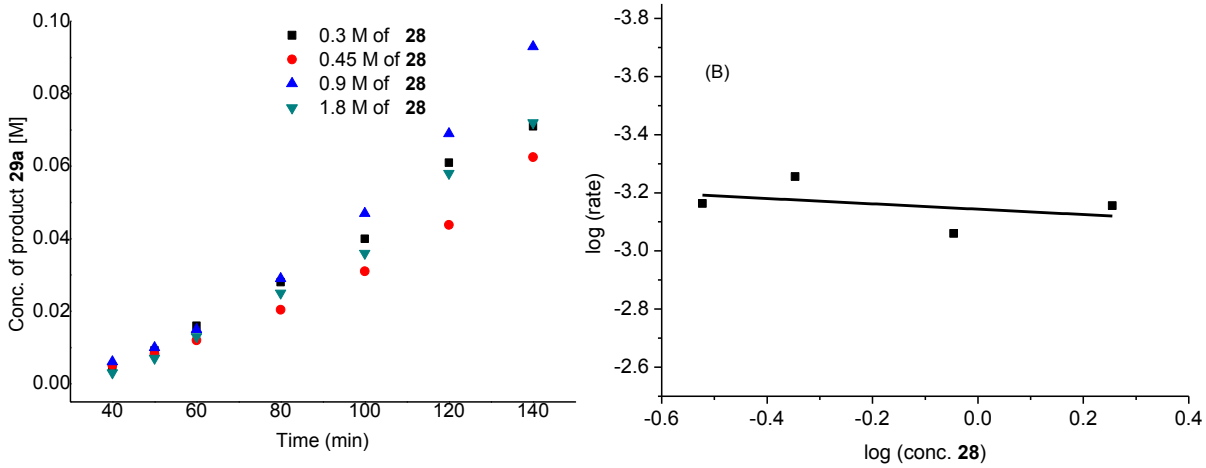

Figure 6.7 (A) Formation of **29a** with varying concentration of **28**. (B) Plot of log(rate) *vs* log(conc. **28**).

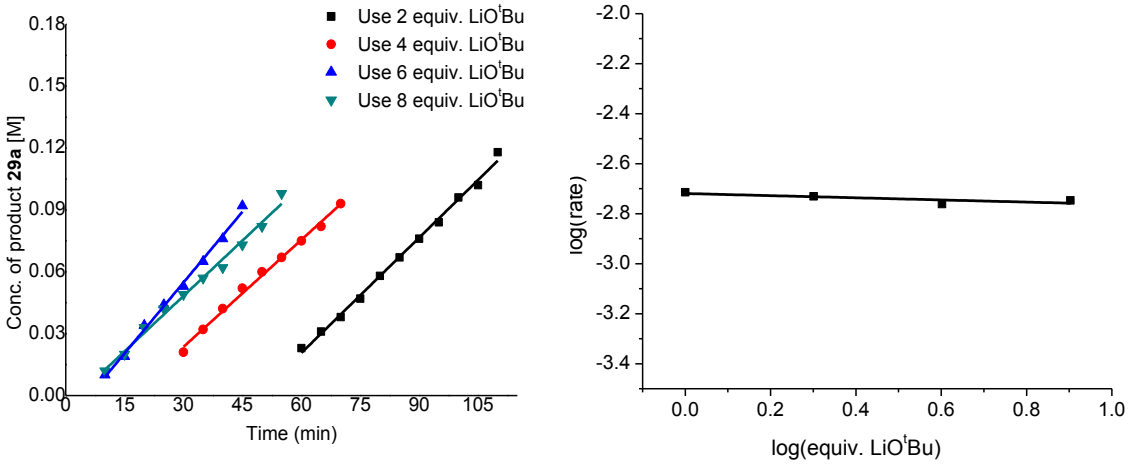

Figure 6.8 (A) Formation of **29a** at a different loading of LiO^{t}Bu. (B) Plot of log(rate) *vs* log(equiv. LiO^{t}Bu).

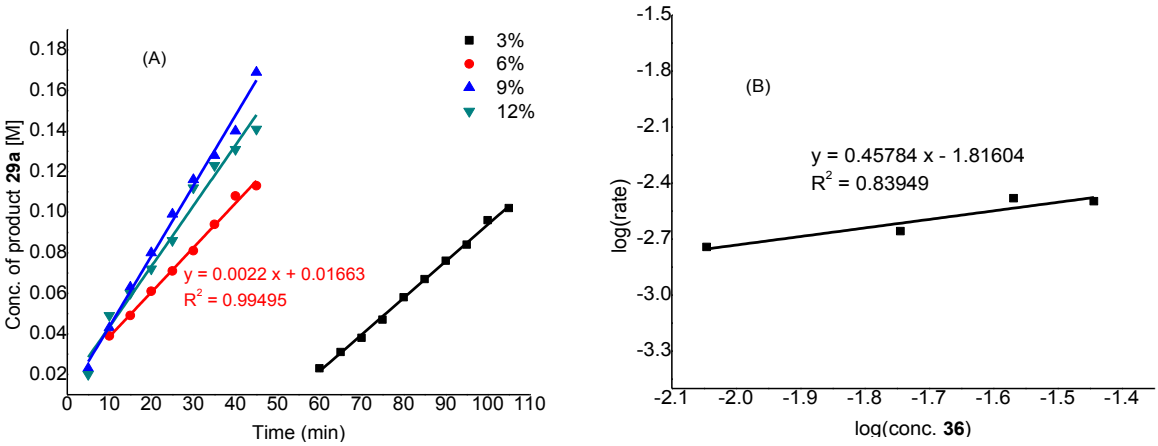

Figure 6.9 (A) Formation of **29a** at a different loading of **36**. (B) Plot of log(rate) *vs* log(conc. **36**).

6.2.6 Isotope labelling experiments

Kinetic isotope effect experiment (KIE): To know whether the C–H bond breaking is involved in the rate determining step, the kinetic isotope effect (KIE) study was carried out using 1-(pyridin-2-yl)-1*H*-indole (**27a**) and 1-(pyridin-2-yl)-1*H*-indole-2-*d* [2-D]-**27a**. The rate of alkynylation of **27a** with alkynyl bromide **28** was calculated as 1.59 x 10^{-3} Mmin^{-1}. Similarly, the rate of alkynylation reaction of [2-D]-**27a** was found to be 0.4 x 10^{-3} Mmin^{-1}. From these two reaction rates, the kinetic isotope effect (KIE) calculated as k_H/k_D = 3.6 (Figure 6.10). The high kinetic isotope effect (k_H/k_D) value suggest that the C–H bond cleavage of indole is most likely the rate-limiting step during the alkynylation reaction.

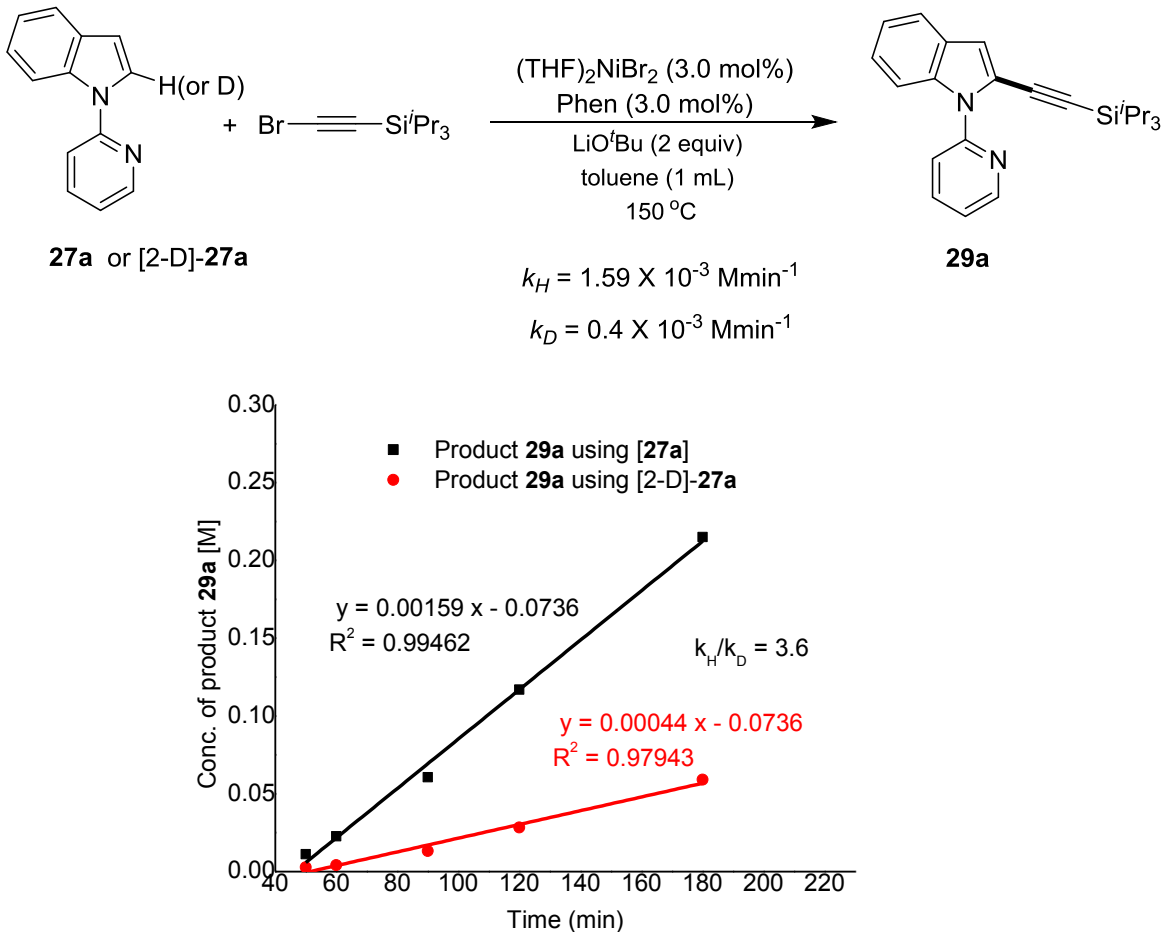

Figure 6.10 Formation of the product **29a** from the reactions of **27a** or [2-D]-**27a** with **28**.

H/D scrambling experiment: The deuterium scrambling experiment was carried out to understand the nature of C–H bond metalation process. Hence, the compounds 1-(pyridin-2-yl)-1*H*-indole-2-*d* (0.4 mmol) and 5-methoxy-1-(pyridin-2-yl)-1*H*-indole (0.4 mmol) were treated with alkynyl bromide (0.2 mmol) under the optimized reaction condition for 2 h

(Scheme 6.6). The starting substrates 1-(pyridin-2-yl)-1*H*-indole-2-*d* and 5-methoxy-1-(pyridin-2-yl)-1*H*-indole were recovered as well as the alkynylated products **29a** and **29c** were isolated. The ^{1}H NMR analysis of the recovered substrates suggest that the H/D has not occurred at the C(2) positions. This H/D scrambling experiment indicates that the C–H bond metalation is the irreversible process during the reaction.

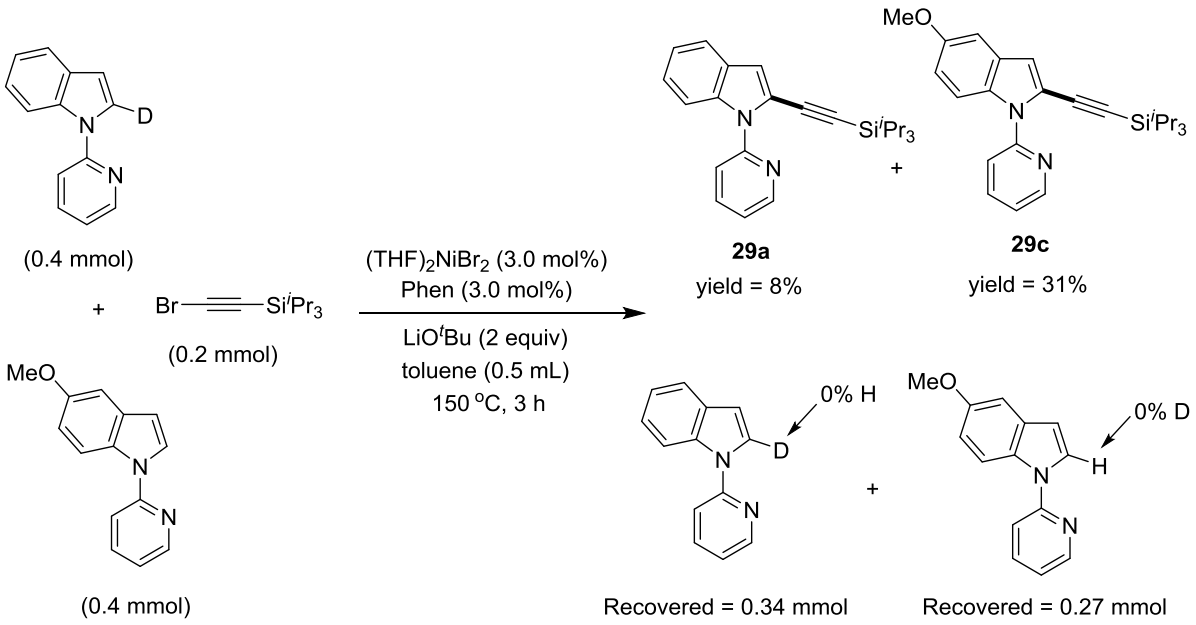

Scheme 6.6 H/D scrambling experiment

6.2.7 Electronic effect on alkynylation of indole

The intermolecular competition experiment was performed between the electronically distinct indoles, such as 5-methoxy-1-(pyridin-2-yl)-1*H*-indole (**27c**) and 5-fluoro-1-(pyridin-2-yl)-1*H*-indole (**27d**) with alkyne **28**. This reaction afforded the compounds **29c** and **29d** in 31% and 38%, respectively (Scheme 6.7). The formation of both the products **29c** and **29d** occurs concurrently, which indicates that the electrophilic-type C–H activation of indole is less likely.

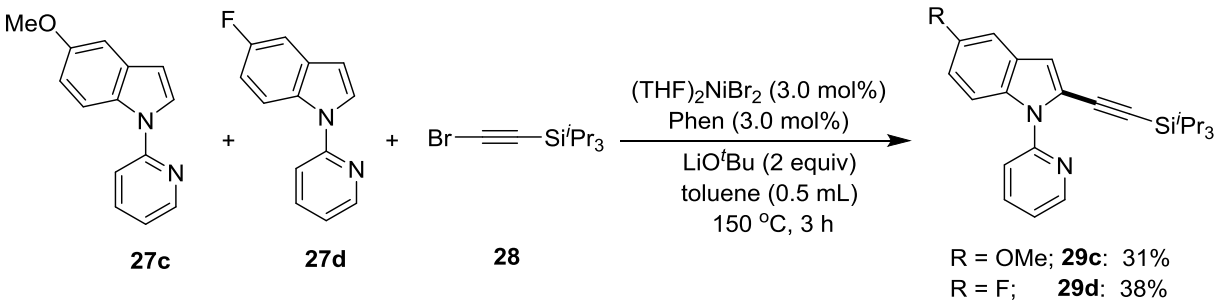

Scheme 6.7 Intermolecular competition experiment

6.2.8 Controlled reactivity study

Experimental observation shows that the catalysis does not follow a radical pathway, and the catalysis is homogeneous in nature. Further, the combination of $(THF)_2NiBr_2$/Phen, (pyridin-2-yl)-1*H*-indole (**27a**) and LiO^{t}Bu forms an active species, which catalyzes the alkynylation reaction. Looking at the reaction component, a nickelcycle from $(THF)_2NiBr_2$ and indole **27a** could be presumed. In this regard, to isolate the presumed active nickelacycle species, a stoichiometric reaction of $(THF)_2NiBr_2$/Phen and **27a** in the presence of LiO^{t}Bu was carried out in toluene at 150 °C, which resulted in the formation of indole dimer **41**. The self coupled product of indole **41** might form *via* the intermediacy of the nickelacycle **39** (Scheme 6.8). Several attempts to isolate nickelacycle species **39** were unsuccessful and the reaction always ends up with the dimerized product **41**. The formation of dimerized indole **41** most likely occurs through intermediate **40**. Interestingly, the same reaction in the presence of added alkynyl bromide failed to produce **41**. This study clearly indicates the nickelacycle **39** is the crucial intermediate during reaction.

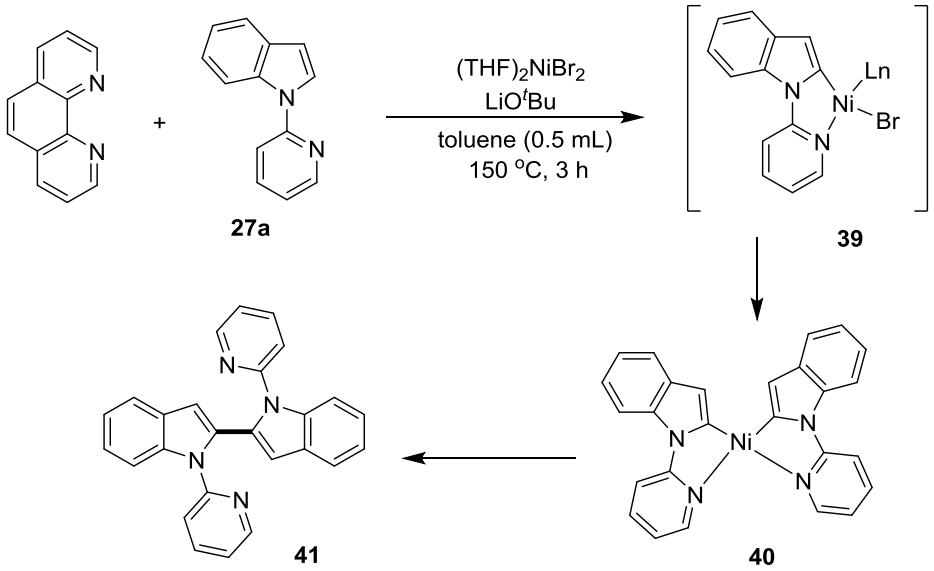

Scheme 6.8 Reactivity study of $(THF)_2NiBr_2$/Phen with (pyridin-2-yl)-1*H*-indole (**27a**)

6.2.9 DFT calculation

Full quantum chemical calculations were done with density functional theory (DFT) at the PBE/TZVP level of theory in order to understand the mechanism of Ni(II)-catalyzed C–H bond alkynylation on indole. The reaction first proceeds through the six membered transition state **TS-1** in which C–H bond of **27a** is activated and leads to the formation of intermediate **A** after the surmounting of a barrier of 22.2 kcal/mol (Figure 6.11).

Calculations further show that the approach of the substrate **28** to **A** leading to the formation of **B** by the coordination of π bond on **28** to Ni(II). The barrier for this is 17.1 kcal/mol. Now **B** has two possibilities, either it can convert into intermediate **C** or into intermediate **E** by the oxidative addition. DFT calculations suggest that formation of **C** (10.0 kcal/mol) has lower barrier than formation of **E** (20.8 kcal/mol) (Figure 6.11). The formation of final product **29a** takes place *via* **TS-4** (Figure 6.11).

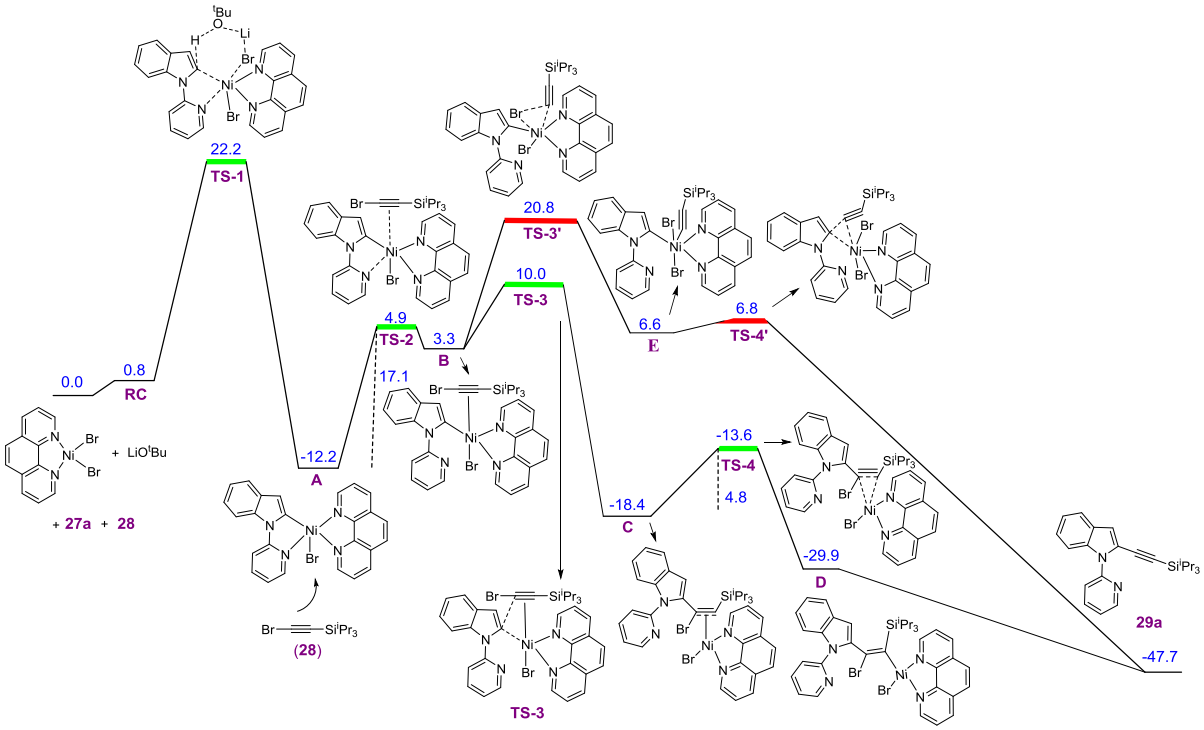

Figure 6.11 Free energy profile for the Ni(II)-catalyzed alkynylation of indoles. The free energy values are in kcal/mol. **27a** = *N*-pyridinyl-indole, **28** = alkynyl bromide.

6.2.10 Probable catalytic cycle

The Hg drop experiment suggests that the catalyst does not have heterogeneous nature. The reaction in the presence of TEMPO and galvinoxyl radical scavengers highlighted that the catalysis does not follow the free radical pathway. The kinetic analysis indicates that neither the isolated complex, $[(Phen)_3Ni.NiBr_4]$ (**36**) nor the Ni(0) species is the active

catalyst during the alkynylation reaction. Further, it was observed that the active Ni-catalyst most likely involves the substrate **27a**. Considering the structure of substrate **27a**, it is assumed that a pyridinyl-coordinated nickelacycle species, upon C(2)–H activation could be the active catalyst during alkynylation.

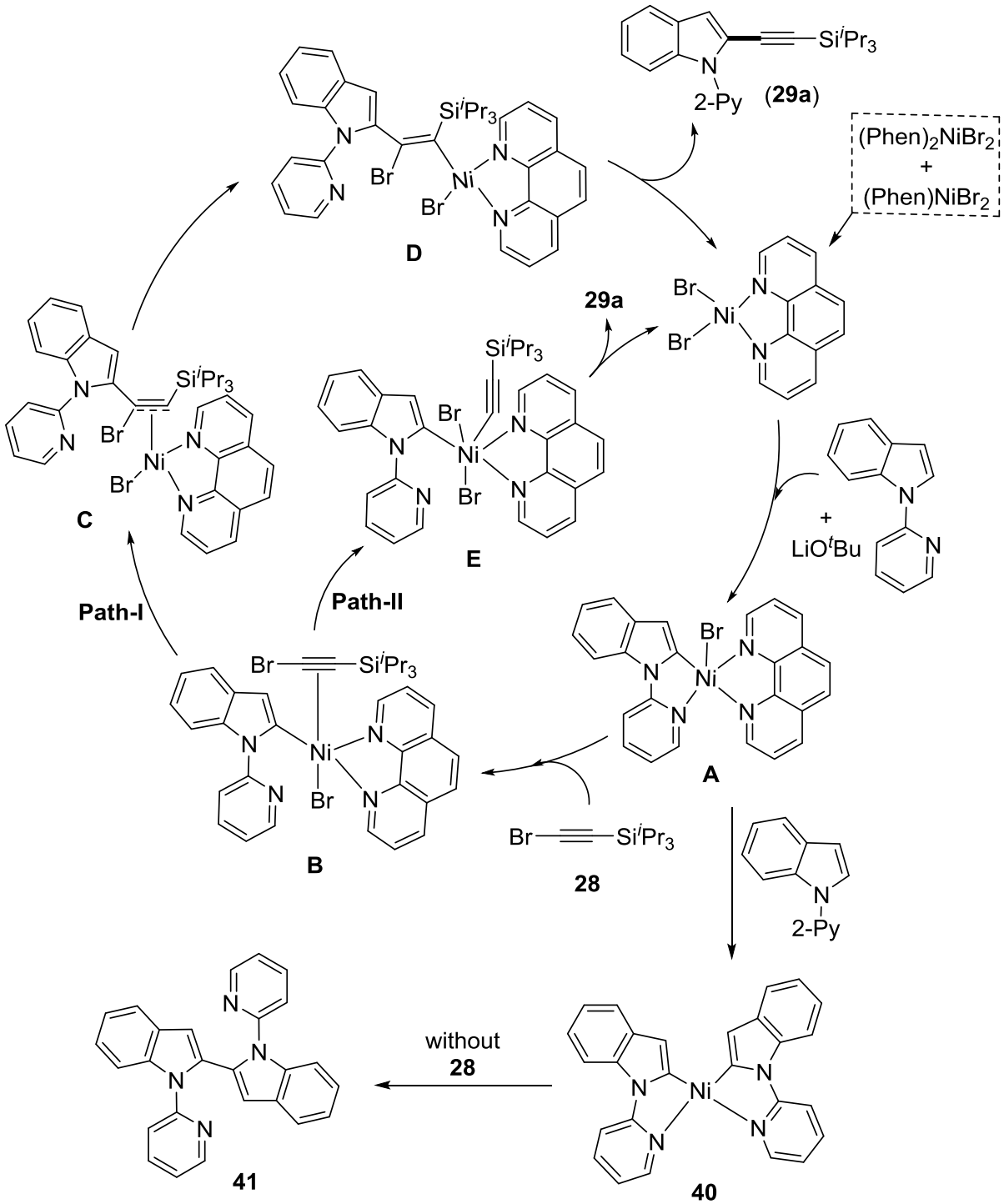

Figure 6.12 Probable catalytic cycle for alkynylation reaction

On the basis of the experimental results and DFT calculations, a more authentic catalytic cycle is proposed. It is assumed that the complex [$(Phen)_3Ni.NiBr_4$] (**36**) remains in equilibrium with various phenanthroline coordinated Ni-species, *i.e.* $(Phen)_nNiBr_2$ [$(Phen)_2NiBr_2$ and $(Phen)NiBr_2$]. The $(Phen)NiBr_2$ species enters the catalytic cycle and reacts with **27a** in the turnover-limiting step to form the active nickelacylce species **A**. The reaction of **A** with alkynyl bromide **28** will generate the nickel complex **B** through π-coordination of alkyne moiety. The migratory insertion of alkynyl bromide occurs in Ni(II)–C(2) bond to form complex **D** *via* the intermediate **C** (Path-I; Figure 6.12). The formation of complex **D** is supported by DFT study. The complex **D** upon *β*-bromide elimination generates alkynylated product **29a** and Ni(II) catalyst. Another possibility is that the complex **B** upon oxidative addition with alkynyl bromide will generate complex **E**, which upon reductive elimination would afford the alkynylated product **29a** (Path-II; Figure 6.12).[422,423] The DFT study shows that the energy barrier for the conversion complex **B** to complex **C** is lower than the conversion of complex **B** to complex **E**. Most likely, this catalytic cycle follows insertion pathway (Path-I) rather than the oxidative addition pathway (Path-II) of alkynyl bromide to complex **B**. Since the reaction is first-order with 2-pyridinyl indole (**27a**), we assume that an intermediate of the type **40** also can enter into the catalytic cycle in addition to **A**. However, the complex **40** without alkynyl bromide generates the indole dimer **41**.

6.3 Conclusion

The detailed mechanism for the nickel-catalyzed alkynylation of indole with alkyl bromide is described. The catalytically competent nickel-complexes were isolated and structurally characterized. The external additive experiments ruled out the involvement of heterogeneous catalytic species or a free-radical intermediate. The kinetics of the alkynylation reaction suggest that an induction period for the alkynylation reaction in the absence of indole. Hence, the active nickel catalyst involves the indole substrate. Mechanistic findings demonstrate that the C–H bond nickelation is a kinetically relevant process and most likely involves in the turnover limiting step. Considering all these experimental findings and DFT calculations, an authentic catalytic cycle for the nickel-catalyzed alkynylation of indole with alkynyl bromide is drawn that occurs through coordinative insertion of alkynyl bromide into the Ni(II)–C bond, and does not involve the Ni(IV) intermediate.

6.4 Experimental section

6.4.1 Synthesis of $NiBr_2(Phen)_n$ complexes

[{(Phen)$_3$Ni}NiBr$_4$] (36): A solution of 1,10-phenanthroline (0.05 g, 0.277 mmol) in CH_3CN (10 mL) was added dropwise to the suspension of $(THF)_2NiBr_2$ (0.1 g, 0.277 mmol) in CH_3CN (15 mL), and the reaction mixture was stirred at room temperature for 1 h. The reaction mixture was then filtered to remove the insoluble materials and the filtrate was concentrated under vacuum, wherein the light green crystalline compound, [{(Phen)$_3$Ni}NiBr$_4$] (**36**) was obtained. The compound was separated from the mother liquor and dried under vacuum. Yield: 0.061 g, 67% (w.r.t [Ni]). Anal. calcd for $C_{36}H_{24}Br_4N_6Ni_2$: C, 44.23; H, 2.47; N, 8.60. Found: C, 44.85; H, 2.67; N, 8.23.

[{(Phen)$_3$Ni}NiCl$_4$] (37): In a Schlenk flask, $(DME)NiCl_2$ (0.5 g, 2.275 mmol) and 1,10-phenanthroline (1.025 g, 5.689 mmol) were taken and THF (15 mL) was added into it. The reaction mixture was stirred at room temperature for 12 h, during which a blue coloured precipitate was formed. The reaction mixture was filtered, and the blue solid was washed with THF (30 mL) and dried under vacuum. The compound was then recrystallized in CH_3CN to obtain blue crystals suitable for X-ray analysis. Yield: 0.8 g, 88% (w.r.t [Ni]). Anal. calcd for $C_{36}H_{24}Cl_4N_6Ni_2$: C, 54.06; H, 3.06; N, 10.51. Found: C, 47.31; H, 3.09; N, 9.47.

(Phen)$_2$NiCl$_2$ (38): Compound **38** was synthesized following the procedure similar to the synthesis of **37**, using $(DME)NiCl_2$ (0.070 g, 0.318 mmol) and 1,10-phenanthroline (0.056 g, 0.318 mmol). The compound was then recrystallized in CH_3CN to obtain analytically pure product of **38**. Yield: 0.081 g, 54%. Anal. calcd for $C_{24}H_{16}Cl_2N_4Ni$: C, 58.83; H, 3.29; N, 11.43. Found: C, 44.3; H, 6.6; N, 8.68.

6.4.2 Procedure for external additive experiments

Hg addition experiment: To a flame-dried screw-capped Schlenk tube equipped with magnetic stir bar was introduced 1-(pyridin-2-yl)-1*H*-indole, **27a** (0.059 g, 0.304 mmol), alkyne **28** (0.117 g, 0.45 mmol), $(THF)_2NiBr_2$ (0.0032 g, 3 mol%, 0.009 mmol), 1,10-phenanthroline (0.0016 g, 3 mol%, 0.009 mmol), LiO^tBu (0.048 g, 0.6 mmol) and Hg (1.083 g, 5.4 mmol, 600 equivalent w.r.t [Ni]), and toluene (0.5 mL) was added under argon. The reaction mixture was stirred at 150 ^oC in a pre-heated oil bath for 12 h. At ambient temperature, H_2O (15 mL) was added and the reaction mixture was extracted with EtOAc (20 mL × 3). The combined organic extract was dried over Na_2SO_4 and the volatiles were evaporated *in vacuo*. The remaining residue was purified by column chromatography on basic

alumina (petroleum ether/EtOAc: 100/1→30/1) to yield **29a** (0.101 g, 90%) as a light yellow solid.

TEMPO addition experiment: To a flame-dried screw-capped Schlenk tube equipped with magnetic stir bar was introduced 1-(pyridin-2-yl)-1*H*-indole, **27a** (0.059 g, 0.304 mmol), alkyne bromide **28** (0.117 g, 0.45 mmol), $(THF)_2NiBr_2$ (0.0032 g, 3 mol%, 0.009 mmol), 1,10-phenanthroline (0.0016 g, 3 mol%, 0.009 mmol), LiO^tBu (0.048 g, 0.6 mmol) and TEMPO (0.047 g, 0.30 mmol), and toluene (0.5 mL) was added under argon. The reaction mixture was stirred at 150 ^oC in a pre-heated oil bath for 12 h. The reaction mixture was quenched at ambient temperature and subjected to GC analysis, which showed 74% (GC yield) of **29a**.

Galvinoxyl addition experiment: To a flame-dried screw-capped Schlenk tube equipped with magnetic stir bar was introduced 1-(pyridin-2-yl)-1*H*-indole, **27a** (0.059 g, 0.304 mmol), alkyne bromide **28** (0.117 g, 0.45 mmol), $(THF)_2NiBr_2$ (0.0032 g, 3 mol%, 0.009 mmol), 1,10-phenanthroline (0.0016 g, 3 mol%, 0.009 mmol), LiO^tBu (0.048 g, 0.6 mmol) and Galvinoxyl (0.126 g, 0.30 mmol), and toluene (0.5 mL) was added under argon. The reaction mixture was stirred at 150 ^oC in a pre-heated oil bath for 12 h. At ambient temperature, H_2O (15 mL) was added and the reaction mixture was extracted with EtOAc (20 mL × 3). The combined organic extract was dried over Na_2SO_4 and the volatiles were evaporated *in vacuo*. The remaining residue was purified by column chromatography on basic alumina (petroleum ether/EtOAc: 100/1→30/1) to yield **29a** (0.079 g, 70%) as a light yellow solid.

6.4.3 Kinetics of alkynylation reaction

Representative procedure: Standard alkynylation reaction: To the teflon-screw capped tube equipped with magnetic stir bar was introduced $(THF)_2NiBr_2$ (0.0032 g, 0.009 mmol), 1,10-phenanthroline (0.0016 g, 0.009 mmol), LiO^tBu (0.048 g, 0.6 mmol), alkynyl bromide **28** (0.117 g, 0.45 mmol, 0.45 M) and 1-(pyridin-2-yl)-1*H*-indole **27a** (0.059 g, 0.304 mmol, 0.30 M) and toluene (required amount) was added to make the total volume 1.0 mL. To the reaction mixture mesitylene (0.030 mL, 0.2154 mmol) was added as an internal standard. The reaction mixture was then stirred at 150 ^oC in a pre-heated oil bath. At regular intervals (10, 20, 30, 40, 50, 60, 90, 120 and 180 min), the reaction vessel was cooled to ambient temperature, introduced to the glove box and an aliquot of the sample was withdrawn to the GC vial. The sample was diluted with toluene/acetone and subjected to GC analysis.

The data of the concentration of the product *vs* time (min) plot was drawn with Origin Pro 8. The reaction rate was determined by initial rate method.

Kinetics using $Ni(COD)_2$/Phen: Representative procedure was followed, using $Ni(COD)_2$ (0.0024 g, 0.009 mmol) and 1,10-phenanthroline (0.0016 g, 0.009 mmol), LiO^tBu (0.048 g, 0.6 mmol), alkynyl bromide **28** (0.117 g, 0.45 mmol, 0.45 M) and 1-(pyridin-2-yl)-1*H*-indole **27a** (0.059 g, 0.304 mmol, 0.30 M). The concentration of product was determined at regular intervals (10, 20, 30, 40, 50, 60, 90, 120 and 180 min).

Kinetics using $(THF)_2NiBr_2$/Phen (upon preheating): To the teflon-screw capped tube equipped with magnetic stir bar was introduced $(THF)_2NiBr_2$ (0.0032 g, 0.009 mmol) and 1,10-phenanthroline (0.0016 g, 0.009 mmol). In that, 0.5 mL of toluene was added and the reaction mixture was heated at 150 ^oC for 1 h. After 1 h, the reaction vessel was cooled to room temperature and transferred to the glove box. To the reaction vessel, LiO^tBu (0.048 g, 0.6 mmol), alkynyl bromide **28** (0.117 g, 0.45 mmol, 0.45 M) and 1-(pyridin-2-yl)-1*H*-indole **27a** (0.059 g, 0.304 mmol, 0.30 M) and toluene (remaining amount) was added to make the total volume 1.0 mL. Mesitylene (0.030 mL, 0.2154 mmol) was added as an internal standard. The reaction mixture was then stirred at 150 ^oC in a pre-heated oil bath and formation of product was determined by GC analysis.

Kinetics using $(THF)_2NiBr_2$/Phen, 27a and LiO^tBu (upon preheating): To the teflon-screw capped tube equipped with magnetic stir bar was introduced $(THF)_2NiBr_2$ (0.0032 g, 0.009 mmol) 1,10-phenanthroline (0.0016 g, 0.009 mmol), 1-(pyridin-2-yl)-1*H*-indole **27a** (0.059 g, 0.304 mmol) and LiO^tBu (0.048 g, 0.6 mmol). In that, 0.5 mL of toluene was added and the reaction mixture was heated at 150 ^oC for 1 h. After 1h, the reaction vessel was cooled to room temperature and transferred to the glove box. To the reaction vessel, alkynyl bromide (**28**; 0.117 g, 0.45 mmol, 0.45 M) and toluene (required amount) were added to make the total volume 1.0 mL. Mesitylene (0.030 mL, 0.2154 mmol) was added as an internal standard. The reaction mixture was then stirred at 150 ^oC in a pre-heated oil bath and the formation of product was determined by GC analysis.

6.4.4 Procedure for rate order determination

The rate order of the alkynylation reaction with various reaction components was determined by the initial rate method. All these order determination reactions were carried out using isolated $(Phen)_{1.5}NiBr_2$ (**36**) complex. The data of the concentration of the product *vs* time (min) plot was fitted linear with Origin Pro 8 (excluding the induction period). The slope

of the linear fitting represents the reaction rate. The order of the reaction was then determined by plotting the log(rate) *vs* log(conc. component) for a particular component.

Representative procedure: **Rate order determination on 1-(pyridin-2-yl)-1*H*-indole 27a:** To the teflon-screw capped tube equipped with magnetic stir bar was introduced $(Phen)_{1.5}NiBr_2$ (0.0044 g, 0.009 mmol), alkynyl bromide **28** (0.117 g, 0.45 mmol, 0.45 M), LiO^tBu (0.048 g, 0.6 mmol) and specific amount of 1-(pyridin-2-yl)-1*H*-indole **27a** (shown in Table 6.2), and toluene (required amount) was added to make the total volume 1.0 mL. To the reaction mixture mesitylene (0.030 mL, 0.2154 mmol) was added as an internal standard. The reaction mixture was then stirred at 150 ^oC in a pre-heated oil bath. At regular intervals, the reaction vessel was cooled to ambient temperature and an aliquot of the sample was withdrawn to the GC vial. The sample was diluted with acetone and subjected to the GC analysis. The concentration of the product **29a** obtained in each sample was determined with respect to the internal standard mesitylene. The data of the concentration of the **29a** *vs* time (min) plot was fitted linear with Origin Pro 8 (excluding the induction period). The order of the reaction was then determined by plotting the log(rate) *vs* log(conc. **27a**) for component **27a**.

Rate order determination on alkynyl bromide 28: The representative procedure was followed using $(Phen)_{1.5}NiBr_2$ (0.0044 g, 0.009 mmol), 1-(pyridin-2-yl)-1*H*-indole **27a** (0.585 g, 0.3 mmol, 0.3 M), LiO^tBu (0.048 g, 0.6 mmol) and specific amount of alkynyl bromide **28** (shown in Table 6.3) in toluene. The data of the concentration of the **29a** *vs* time (min) plot was fitted linear with Origin Pro 8 (excluding the induction period). The order of the reaction was then determined by plotting the log(rate) *vs* log(conc. **28**) for component **28**.

Rate order determination on LiO^tBu: The representative procedure was followed using 1-(pyridin-2-yl)-1*H*-indole **27a** (0.585 g, 0.3 mmol, 0.3 M), alkynyl bromide **28** (0.117 g, 0.45 mmol, 0.45 M), $(Phen)_{1.5}NiBr_2$ **36** (0.0044 g, 0.009 mmol) and specific amount of LiO^tBu (shown in Table 6.4) in toluene. The data of the concentration of the **29a** *vs* time (min) plot was fitted linear with Origin Pro 8 (excluding the induction period). The order of the reaction was then determined by plotting the log(rate) *vs* log(conc. LiO^tBu) for LiO^tBu.

Rate order determination on $(Phen)_{1.5}NiBr_2$: The representative procedure was followed using 1-(pyridin-2-yl)-1*H*-indole **27a** (0.585 g, 0.3 mmol, 0.3 M), alkynyl bromide **28** (0.117 g, 0.45 mmol, 0.45 M), LiO^tBu (0.048 g, 0.6 mmol) and specific amount of $(Phen)_{1.5}NiBr_2$ (**36**) (shown in Table 6.5) in toluene. The data of the concentration of the **29a** *vs* time (min) plot was fitted linear with Origin Pro 8 (excluding the induction period). The

order of the reaction was then determined by plotting the log(rate) *vs* log(conc. **36**) for catalyst **36**.

6.4.5 Isotope labelling experiments

Procedure for kinetic isotope effect (KIE) experiment: To the teflon-screw capped tube equipped with magnetic stir bar was introduced $(THF)_2NiBr_2$ (0.0032 g, 0.009 mmol), 1,10-phenanthroline (0.0016 g, 0.009 mmol), LiO^tBu (0.048 g, 0.6 mmol), alkynyl bromide **28** (0.117 g, 0.45 mmol) and 1-(pyridin-2-yl)-1*H*-indole **27a** (0.059 g, 0.304 mmol, 0.30 M) or 1-(pyridin-2-yl)-1*D*-indole ([2-D]-**27a**; 0.059 g, 0.302 mmol), and toluene (required amount) was added to make the total volume 1.0 mL. To the reaction mixture mesitylene (0.030 mL, 0.2154 mmol) was added as an internal standard. The reaction mixture was heated at 150 ^oC in an oil bath. At regular intervals (10, 20, 30, 40, 50, 60, 90, 120 and 180 min), the reaction vessel was cooled to ambient temperature, introduced to the glove box and an aliquot of the sample was withdrawn to the GC vial. The sample was diluted with toluene/acetone and subjected to GC analysis.

Procedure for H/D scrambling experiment: To a flame-dried screw-capped Schlenk tube equipped with magnetic stir bar was introduced 1-(pyridin-2-yl)-1*D*-indole, [2-D]-**27a** (0.078 g, 0.4 mmol), 5-methoxy-1-(pyridin-2-yl)-1*H*-indole (**27c**; 0.090 g, 0.4 mmol), alkynyl bromide (**28**; 0.052 g, 0.2 mmol), $(THF)_2NiBr_2$ (0.0021 g, 3 mol%, 0.006 mmol), 1,10-phenanthroline (0.0011 g, 3 mol%, 0.006 mmol) and LiO^tBu (0.032 g, 0.4 mmol), and toluene (0.5 mL) was added under argon. The reaction mixture was stirred at 150 ^oC in a pre-heated oil bath for 2 h. At ambient temperature, H_2O (15 mL) was added and the reaction mixture was extracted with EtOAc (20 mL × 3). The combined organic extract was dried over Na_2SO_4 and the volatiles were evaporated *in vacuo*. The remaining residue was purified by column chromatography on basic alumina (petroleum/ EtOAc: 100/1→10/1) to yield **29a** (0.009 g, 12%) and **29c** (0.025 g, 30%) as light yellow solids, and starting compound [2-D]-**27a** (85%) and **27c** (68%) were recovered. There was no H/D exchange between the [2-D]-**27a** and **27c** (Scheme 6.5).

6.4.6 Procedure for intermolecular competition experiment

To a flame-dried screw-capped Schlenk tube equipped with magnetic stir bar was introduced 5-methoxy-1-(pyridin-2-yl)-1*H*-indole, **27c** (0.090 g, 0.4 mmol), 5-fluoro-1-(pyridin-2-yl)-1*H*-indole, **27d** (0.085 g, 0.4 mmol), alkyne **28** (0.052 g, 0.2 mmol), $(THF)_2NiBr_2$ (0.0021 g, 3 mol%, 0.006 mmol), 1,10-phenanthroline (0.0011 g, 3 mol%, 0.006

mmol) and LiO^{t}Bu (0.032 g, 0.4 mmol), and toluene (0.5 mL) was added under argon. The reaction mixture was stirred at 150 ^{o}C in a pre-heated oil bath for 3 h. At ambient temperature, H_2O (15 mL) was added and the reaction mixture was extracted with EtOAc (20 mL × 3). The combined organic extract was dried over Na_2SO_4 and the volatiles were evaporated *in vacuo*. The remaining residue was purified by column chromatography on basic alumina (petroleum ether/EtOAc: 100/1→10/1) to yield **29c** (0.025g, 31%) and **29d** (0.030 g, 38%) as light yellow solids.

6.4.7 Procedure for control reaction

To a flame-dried screw-capped Schlenk tube equipped with magnetic stir bar was introduced 1-(pyridin-2-yl)-1*H*-indole, **27a** (0.0483 g, 0.248 mmol), $(THF)_2NiBr_2$ (0.178 g, 0.248 mmol), 1,10-phenanthroline (0.045 g, 0.248 mmol) and LiO^{t}Bu (0.0198 g, 0.248 mmol), and toluene (2 mL) was added under argon. The reaction mixture was stirred at 150 ^{o}C in a pre-heated oil bath for 3 h. The reaction mixture was then filtered and mother liquor was evaporated under vacuum. The remaining residue was purified by column chromatography on basic alumina (petroleum ether/EtOAc: 100/1→3/1) to yield **41**as light yellow solid. Yield: 0.015 g, 62%. ^{1}H-NMR (500 MHz, DMSO-d_6): δ 8.31 (br s, 2H, Ar–H), 7.72-7.69 (m, 2H, Ar–H), 7.64 (d, J = 7.6 Hz, 2H, Ar–H), 7.47 (d, J = 7.6 Hz, 2H, Ar–H), 7.27-7.24 (m, 2H, Ar–H), 7.18-7.13 (m, 4H, Ar–H), 6.93 (s, 2H, Ar–H). ^{13}C{^{1}H}-NMR (125 MHz, DMSO-d_6): δ 150.6 (2C, C_q), 148.7 (2CH), 138.4 (2 CH), 136.8 (2C, C_q), 130.8 (2C, C_q), 127.8 (2C, C_q), 123.0 (2CH), 121.9 (2CH), 121.1 (2CH), 120.6 (2CH), 119.5 (2CH), 111.3 (2CH), 107.0 (2CH). HRMS (ESI): *m/z* calcd for $C_{26}H_{18}N_4$+H^+ $[M+H]^+$ 387.1604; found 387.1603.

X-ray structure determination

X-ray intensity data measurements of all complexes were carried out on a Bruker SMART APEX II CCD diffractometer with graphite-monochromatized (MoK_{α}= 0.71073 Å) radiation range 90(2) - 297 (2) K, respectively. The X-ray generator was operated at 50 kV and 30 mA. A preliminary set of cell constants and an orientation matrix were calculated from three sets of 12 frames (total 36 frames). Data were collected with ω scan width of 0.5° at eight different settings of φ and 2θ with a frame time of 10 sec keeping the sample-to-detector distance fixed at 5.00 cm for both compounds. The X-ray data collection was monitored by the APEX2 program (Bruker, 2006).[424] All the data were corrected for Lorentzian, polarization and absorption effects using SAINT and SADABS programs (Bruker, 2006). SHELX-97 was used for structure solution and full matrix least-squares refinement on F^2.[425] Hydrogen atoms were placed in geometrically idealized position and constrained to ride on their parent atoms.

Crystal data and structure refinement for complexes **4**, **5** and **20**

	4	**5**	**20**
Empirical formula	$C_{19}H_{33}ClNOPPd$	$C_{21}H_{37}ClNOPPd$	$C_{17}H_{29}ClNOPPd$
Formula weight	464.28	492.34	436.23
Temperature, K	297(2) K	90(2) K	296(2)
Cryst. Syst.	Orthorhombic	Monoclinic	Orthorhombic
Space group	P2(1)2(1)2(1)	P2(1)/c	Pna2(1)
a (Å)	8.2182(2)	13.4029(16)	20.8926(8)
b (Å)	12.987(3)	8.1183(10)	8.1610(3)
c (Å)	20.2391(5)	21.221(3)	11.7355(4)
α (°)	90	90	90
β (°)	90	103.850(8)	90
γ (°)	90	90	90
V ($Å^3$)	2160.23(9)	2241.9(5)	2000.96(13)
Z	4	4	4
$\rho_{cald.}$ g/cm^3	1.428	1.459	1.448
ε (mm^{-1})	1.063	1.029	1.142
F (000)	960	1040	896
Crystal size (mm)	0.24 x 0.19 x 0.15	0.35 x 0.22 x 0.15	0.35 x 0.30 x 0.24
θ (min, max) (°)	1.86, 30.00	1.98, 27.00	1.95, 24.99
R(int)	0.0263	0.0837	0.0304
Independent reflections	6257	4822	3422
Completeness to θ	99.6 %	98.6 %	99.9 %
Max. and min. transmission	0.8569, 0.7845	0.8610, 0.7148	0.7711, 0.6906
Data / restraints / parameters	6257 / 0 / 225	4822 / 92 / 285	3422 / 1 / 205
GOF on F^2	1.010	1.040	1.015
R_1, wR_2 ($I>2\sigma(I)$)	0.0260, 0.0601	0.0465, 0.0989	0.0303, 0.0562
R_1, wR_2 (all data)	0.0303, 0.0623	0.0672, 0.1079	0.0394, 0.0597

Crystal data and structure refinement for complexes **22**, **23** and **24**

	22	**23**	**24**
Empirical formula	$C_{17}H_{29}INOPPd$	$C_{19}H_{32}NO_3PPd$	$C_{18}H_{29}F_3NO_4PPdS$
Formula weight	527.68	459.83	549.85
Temperature, K	150(2)	296(2) K	296(2) K
Cryst. Syst.	Orthorhombic	Monoclinic	Triclinic
Space group	Pna2(1)	P2(1)/n	P-1
a (Å)	20.6345(10)	8.19220(10)	9.4040(7)
b (Å)	8.0577(4)	20.7949(3)	10.2955(7)
c (Å)	12.4254(6)	12.7830(2)	12.8638(9)
α (°)	90	90	93.050(4)
β (°)	90	104.2930(10)	104.023(4)
γ (°)	90	90	100.157(4)
V ($Å^3$)	2065.93(17)	2110.25(5)	1183.39(15)
Z	4	4	2
$\rho_{cald.}$ g/cm^3	1.697	1.447	1.543
ε (mm^{-1})	2.472	0.972	0.986
F (000)	1040	952	560
Crystal size (mm)	0.42 x 0.21 x 0.13	0.35 x 0.25 x 0.20	0.39 x 0.14 x 0.10
θ (min, max) (°)	1.97, 30.00	1.91, 24.99	1.64, 25.00
R(int)	0.0337	0.0191	0.0265
Independent reflections	5574	3687	3868
Completeness to θ	100.0 %	99.1 %	92.9 %
Max. and min. transmission	0.7394, 0.4233	0.8294, 0.7273	0.9079, 0.6998
Data / restraints / parameters	5574 / 1 / 205	3687 / 0 / 233	3868 / 0 / 268
GOF on F^2	1.056	1.108	1.012
R_1, wR_2 ($I>2\sigma(I)$)	0.0210, 0.0529	0.0229, 0.0505	0.0467, 0.0790
R_1, wR_2 (all data)	0.0213, 0.0530	0.0256, 0.0515	0.0604, 0.0843

Crystal data and structure refinement for complexes **25** and **36**

	25	**36**
Empirical formula	$C_{24}H_{33}N_2OPPdS$	$C_{36}H_{24}N_6Ni_1$, Ni_1 Br_4
Formula weight	534.95	977.6328
Temperature, K	150(2)	100(2) K
Cryst. Syst.	Monoclinic	Triclinic
Space group	P2(1)/n	P-1
a (Å)	16.2191(7)	9.7661(14)
b (Å)	12.0992(6)	11.9843(17)
c (Å)	25.0235(11)	17.090(3)
α (°)	90	75.919(6)
β (°)	98.253(2)	87.535(6)
γ (°)	90	82.999(6)
V ($Å^3$)	4859.7(4)	1925.4(5)
Z	8	2
$\rho_{cald.}$ g/cm^3	1.462	1.828
ε (mm^{-1})	0.933	5.170
F (000)	2208	1044
Crystal size (mm)	0.45 x 0.32 x 0.22	0.42 x 0.31 x 0.20
θ (min, max) (°)	1.41, 26.00	
R(int)	0.0305	0.0573
Independent reflections	9527	6763
Completeness to θ	100.0 %	99.5 %
Max. and min. transmission	0.8210, 0.6788	0.220, 0.424
Data / restraints / parameters	9527 / 12 / 571	
GOF on F^2	1.062	1.084
R_1, wR_2 ($I>2\sigma(I)$)	0.0284, 0.0578	0.0592, 0.1458
R_1, wR_2 (all data)	0.0359, 0.0607	0.0933, 0.1623

Crystal data and structure refinement for complexes **37** and **38**

	37	**38**
Empirical formula	$C_{36}H_{24}N_6Ni_1$, Ni_1 Cl_4	$C_{24}H_{16}Cl_2N_4Ni$
Formula weight	741.1234	488.0105
Temperature, K	296(2) K	100(2) K
Cryst. Syst.	Monoclinic	Monoclinic
Space group	P 1 21/n 1	$P2_1/n$
a (Å)	18.6673(11)	10.8941(9)
b (Å)	12.6136(7)	20.1321(17)
c (Å)	34.3763(18)	11.4847(10)
α (°)	90	90
β (°)	91.788(3)	98.843(5)
γ (°)	90	90
V ($Å^3$)	8090.4(8)	2488.9(4)
Z	8	4
$\rho_{cald.}$ g/cm^3	1.520	1.527
ε (mm^{-1})	1.245	1.025
F (000)	3768	1176
Crystal size (mm)	0.29 x 0.26 x 0.18	0.420 x 0.310 x 0.23
θ (min, max) (°)	1.19, 28.86°	2.023, 26.997
R(int)	0.1943	0.0538
Independent reflections	21078	5434
Completeness to θ	99.9 %	100 %
Max. and min. transmission	0.637,0.752	0.798, 0.673
Data / restraints / parameters	21078 / 0 / 949	5434 / 60 / 336
GOF on F^2	1.079	1.111
R_1, wR_2 ($I>2\sigma(I)$)	0.1374, 0.2903	0.0603, 0.1549
R_1, wR_2 (all data)	0.1854, 0.3164	0.0678, 0.1596

References

(1) Moulton, C. J.; Shaw, B. L. *J. Chem. Soc., Dalton Trans.* **1976**, 1020-1024.

(2) van Koten, G.; Timmer, K.; Noltes, J. G.; Spek, A. L. *J. Chem. Soc., Chem. Comm.* **1978**, 250-252.

(3) Fryzuk, M. D.; MacNeil, P. A.; Rettig, S. J.; Secco, A. S.; Trotter, J. *Organometallics* **1982**, *1*, 918-930.

(4) Grove, D. M.; Van Koten, G.; Ubbels, H. J. C.; Zoet, R.; Spek, A. L. *Organometallics* **1984**, *3*, 1003-1009.

(5) Grove, D. M.; Van Koten, G.; Verschuuren, A. H. M. *J. Mol. Cat.* **1988**, *45*,169-174.

(6) Morales-Morales, D.; Redon, R.; Yung, C.; Jensen, C. M. *Chem. Comm.* **2000**, 1619-1620.

(7) Morales-Morales, D.; Grause, C.; Kasaoka, K.; Redón, R.; Cramer, R. E.; Jensen, C. M. *Inorg. Chim. Acta.* **2000**, *300-302*, 958-963.

(8) Morales-Morales, D.; Lee, D. W.; Wang, Z.; Jensen, C. M. *Organometallics* **2001**, *20*, 1144-1147.

(9) Salem, H.; Ben-David, Y.; Shimon, L. J. W.; Milstein, D. *Organometallics* **2006**, *25*, 2292-2300.

(10) Sykes, A. C.; White, P.; Brookhart, M. *Organometallics* **2006**, *25*, 1664-1675.

(11) Benito-Garagorri, D.; Bocokić, V.; Mereiter, K.; Kirchner, K. *Organometallics* **2006**, *25*, 3817-3823.

(12) Gründemann, S.; Albrecht, M.; Loch, J. A.; Faller, J. W.; Crabtree, R. H. *Organometallics* **2001**, *20*, 5485-5488.

(13) Lee, D. W.; Kaska, W. C.; Jensen, C. M. *Organometallics* **1998**, *17*, 1-3.

(14) Göttker-Schnetmann, I.; White, P.; Brookhart, M. *J. Am. Chem. Soc.* **2004**, *126*, 1804-1811.

(15) Zhu, K.; Achord, P. D.; Zhang, X.; Krogh-Jespersen, K.; Goldman, A. S. *J. Am. Chem. Soc.* **2004**, *126*, 13044-13053.

(16) Ray, A.; Zhu, K.; Kissin, Y. V.; Cherian, A. E.; Coates, G. W.; Goldman, A. S. *Chem. Commun.* **2005**, 3388-3390.

(17) Poverenov, E.; Gandelman, M.; Shimon, L. J. W.; Rozenberg, H.; Ben-David, Y.; Milstein, D. *Chem. Eur. J.* **2004**, *10*, 4673-4684.

(18) Gagliardo, M.; Selander, N.; Mehendale, N. C.; van Koten, G.; Klein Gebbink, R. J. M.; Szabó, K. J. *Chem. Eur. J.* **2008**, *14*, 4800-4809.

(19) Poverenov, E.; Gandelman, M.; Shimon, L. J. W.; Rozenberg, H.; Ben-David, Y.; Milstein, D. *Organometallics* **2005**, *24*, 1082-1090.

(20) Bedford, R. B. *Chem. Comm.* **2003**, 1787-1796.

(21) Herrmann, W. A.; Böhm, V. P. W.; Reisinger, C.-P. *J. Organomet. Chem.* **1999**, *576*, 23-41.

(22) Dupont, J.; Pfeffer, M.; Spencer, J. *Eur. J. Inorg. Chem.* **2001**, *2001*, 1917-1927

(23) Dupont, J.; Consorti, C. S.; Spencer, J. *Chem.Rev.* **2005**, *105*, 2527-2572.

(24) Mazzeo, M.; Lamberti, M.; Massa, A.; Scettri, A.; Pellecchia, C.; Peters, J. C. *Organometallics* **2008**, *27*, 5741-5743.

(25) Takaya, J.; Iwasawa, N. *J. Am. Chem. Soc.* **2008**, *130*, 15254-15255.

(26) Takaya, J.; Iwasawa, N. *Organometallics* **2009**, *28*, 6636-6638.

(27) Begum, R. A.; Powell, D.; Bowman-James, K. *Inorg. Chem.* **2006**, *45*, 964-966.

(28) Liu, J.; Wang, H.; Zhang, H.; Wu, X.; Zhang, H.; Deng, Y.; Yang, Z.; Lei, A. *Chem. Eur. J.* **2009**, *15*, 4437-4445.

(29) Inés, B.; SanMartin, R.; Moure, M. J.; Domínguez, E. *Adv. Synth. Catal.* **2009**, 351, 2124-2132.

(30) Longmire, J. M.; Zhang, X.; Shang, M. *Organometallics* **1998**, *17*, 4374-4379.

(31) Albrecht, M.; van Koten, G. *Angew. Chem. Int. Ed.* **2001**, *40*, 3750-3781.

(32) van der Boom, M. E.; Milstein, D. *Chem. Rev.* **2003**, *103*, 1759-1792.

(33) Singleton, J. T. *Tetrahedron* **2003**, *59*, 1837-1857.

(34) Szabó, K. J. *Synlett* **2006**, *2006*, 811-824.

(35) Benito-Garagorri, D.; Kirchner, K. *Acc. Chem. Res.* **2008**, *41*, 201-213.

(36) Selander, N.; Szabo, K. J. *Dalton Trans.* **2009**, 6267-6279.

(37) Selander, N.; J. Szabó, K. *Chem.Rev.* **2011**, *111*, 2048-2076.

(38) Eberhard, M. R. *Org. Lett.* **2004**, *6*, 2125-2128.

(39) Sommer, W. J.; Yu, K.; Sears, J. S.; Ji, Y.; Zheng, X.; Davis, R. J.; Sherrill, C. D.; Jones, C. W.; Weck, M. *Organometallics* **2005**, *24*, 4351-4361.

(40) Lagunas, M. C.; Gossage, R. A.; Spek, A. L.; van Koten, G. *Organometallics* **1998**, *17*, 731-741.

(41) Canty, A. J.; Rodemann, T.; Skelton, B. W.; White, A. H. *Organometallics***2006**, *25* 3996-4001.

(42) Pilarski, L. T.; Selander, N.; Böse, D.; Szabó, K. J. *Org.Lett.* **2009**, *11*, 5518-5521.

(43) Vicente, J.; Arcas, A.; Julia-Hernandez, F.; Bautista, D. *Chem. Comm.* **2010**, 46, 7253-7255.

(44) Alsters, P. L.; Baesjou, P. J.; Janssen, M. D.; Kooijman, H.; Sicherer- Roetman, A.; Spek, A. L.; Van Koten, G. *Organometallics* **1992**, *11*, 4124-4135.

(45) Aydin, J.; Kumar, K. S.; Eriksson, L.; Szabó, K. J. *Adv. Synth. Catal.* **2007**, *349*, 2585-2594.

(46) Wallner, O. A.; Olsson, V. J.; Eriksson, L.; Szabó, K. J. *Inorg. Chim. Acta* **2006**, *359*, 1767-1772.

(47) Aydin, J.; Kumar, K. S.; Sayah, M. J.; Wallner, O. A.; Szabó, K. J. *J. Org. Chem* **2007**, *72*, 4689-4697.

(48) Aydin, J.; Conrad, C. S.; Szabó, K. J. *Org. Lett.* **2008**, *10*, 5175-5178.

(49) Rimml, H.; Venanzi, L. M. *J. Organomet. Chem.* **1983**, *259*, C6-C7.

(50) Baber, R. A.; Bedford, R. B.; Betham, M.; Blake, M. E.; Coles, S. J.; Haddow, M. F.; Hursthouse, M. B.; Orpen, A. G.; Pilarski, L. T.; Pringle, P. l. G.; Wingad, R. L. *Chem. Commun.* **2006**, 3880-3882.

(51) Ohff, M.; Ohff, A.; van der Boom, M. E.; Milstein, D. *J. Am. Chem. Soc.* **1997**, *119*, 11687-11688.

(52) Bedford, R. B.; Draper, S. M.; Noelle Scully, P.; Welch, S. L. *N. J. Chem.* **2000**, *24*, 745-747.

(53) Aydin, J.; Szabó, K. J. *Org. Lett.* **2008**, *10*, 2881-2884.

(54) Albrecht, M.; Dani, P.; Lutz, M.; Spek, A. L.; van Koten, G. *J. Am. Chem. Soc.* **2000**, *122*, 1822-11833.

(55) Wallner, O. A.; Szabó, K. J. *Org. Lett.* **2004**, *6*, 1829-1831.

(56) Cope, A. C.; Friedrich, E. C. *J. Am. Chem. Soc.* **1968**, *90*, 909-913.

(57) Takenaka, K.; Uozumi, Y. *Org. Lett.* **2004**, *6*, 1833-1835.

(58) Takenaka, K.; Minakawa, M.; Uozumi, Y. *J. Am. Chem. Soc.* **2005**, *127*, 12273-12281.

(59) Kimura, T.; Uozumi, Y. *Organometallics* **2006**, *25*, 4883-4887.

(60) Kimura, T.; Uozumi, Y. *Organometallics* **2008**, *27*, 5159-5162.

(61) Bolliger, J. L.; Blacque, O.; Frech, C. M. *Angew. Chem. Int. Ed.* **2007**, *46*, 6514-6517.

(62) Anastasia, L.; Negishi, E. In *Handbook of Organopalladium Chemistry for Organic Synthesis*; John Wiley & Sons, Inc.: 2003, p 311-334.

(63) Phan, N. T. S.; Van Der Sluys, M.; Jones, C. W. *Adv. Synth. Catal.* **2006**, *348*, 609-679.

(64) Yao, Q.; Kinney, E. P.; Zheng, C. *Org. Lett.* **2004**, *6*, 2997-2999.

(65) Hahn, F. E.; Jahnke, M. C.; Gomez-Benitez, V.; Morales-Morales, D.; Pape, T. *Organometallics* **2005**, *24*, 6458-6463.

(66) Yoon, M. S.; Ryu, D.; Kim, J.; Ahn, K. H. *Organometallics* **2006**, *25*, 2409-2411.

(67) Naghipour, A.; Sabounchei, S. J.; Morales-Morales, D.; Canseco-González, D.; Jensen, C. M. *Polyhedron* **2007**, *26*, 1445-1448.

(68) da Costa, R. C.; Jurisch, M.; Gladysz, J. A. *Inorg. Chim. Acta* **2008**, *361*, 3205-3214.

(69) Schuster, E. M.; Botoshansky, M.; Gandelman, M. *Angew. Chem. Int. Ed.* **2008**, *47*, 4555-4558.

(70) Bröring, M.; Kleeberg, C.; Köhler, S. *Inorg. Chem.* **2008**, *47*, 6404-6412.

(71) Aydin, J.; Larsson, J. M.; Selander, N.; Szabó, K. J. *Org. Lett.* **2009**, *11*, 2852-2854.

(72) Kumar, A.; Agarwal, M.; Singh, A. K.; Butcher, R. J. *Inorg. Chim. Acta* **2009**, *362*, 3208-3218.

(73) Solano-Prado, M. A.; Estudiante-Negrete, F.; Morales-Morales, D. *Polyhedron* **2010**, *29*, 592-600.

(74) Yoo, K. S.; O′Neill, J.; Sakaguchi, S.; Giles, R.; Lee, J. H.; Jung, K. W. *J. Org. Chem.* **2010**, *75*, 95-101.

(75) Blacque, O.; Frech, C. M. *Chem. Eur. J.* **2010**, *16*, 1521-1531.

(76) Duncan, D.; Hope, E. G.; Singh, K.; Stuart, A. M. *Dalton Trans.* **2011**, *40*, 1998-2005.

(77) Luo, Q.-L.; Tan, J.-P.; Li, Z.-F.; Qin, Y.; Ma, L.; Xiao, D.-R. *Dalton Trans.* **2011**, *40*, 3601-3609.

(78) Wang, Z.; Feng, X.; Fang, W.; Tu, T. *Synlett* **2011**, *2011*, 951-954.

(79) SanMartin, R.; Inés, B.; Moure, M. J.; Herrero, M. T.; Domínguez, E. *Helvetica Chim. Acta* **2012**, *95*, 955-962.

(80) Feng, J.; Cai, C. *J. Fluorine Chem.* **2013**, *146*, 6-10.

(81) Leigh, V.; Ghattas, W.; Mueller-Bunz, H.; Albrecht, M. *J. Organom. Chem.***2014**, *771*, 33-39.

(82) Yang, L.; Zhang, X.; Mao, P.; Xiao, Y.; Bian, H.; Yuan, J.; Mai, W.; Qu, L. *RSC Adv.* **2015**, *5*, 25723-25729.

(83) Sobhani, S.; Zeraatkar, Z.; Zarifi, F. *New J. Chem.* **2015**, *39*, 7076-7085.

(84) Sobhani, S.; Zeraatkar, Z.; Zarifi, F. *New J. Chem.* **2016**, *40*, 8969-8969.

(85) Lee, H. M.; Zeng, J. Y.; Hu, C.-H.; Lee, M.-T. *Inorg. Chem.* **2004**, *43*, 6822-6829.

(86) Kjellgren, J.; Aydin, J.; Wallner, O. A.; Saltanova, I. V.; Szabó, K. J. *Chem. Eur. J.*

2005, *11*, 5260-5268.

(87) Churruca, F.; SanMartin, R.; Tellitu, I.; Domínguez, E. *Synlett* **2005**, *2005*, 3116-3120.

(88) Hahn, F. E.; Jahnke, M. C.; Pape, T. *Organometallics* **2007**, *26*, 150-154.

(89) Wei, W.; Qin, Y.; Luo, M.; Xia, P.; Wong, M. S. *Organometallics* **2008**, *27*, 2268-2272.

(90) Bonnet, S.; van Lenthe, J. H.; Siegler, M. A.; Spek, A. L.; van Koten, G.; Gebbink, R. J. M. K. *Organometallics* **2009**, *28*, 2325-2333.

(91) Olsson, D.; Wendt, O. F. *J. Organomet. Chem.* **2009**, *694*, 3112-3115.

(92) Bonnet, S.; Lutz, M.; Spek, A. L.; van Koten, G.; Klein Gebbink, R. J. M. *Organometallics* **2010**, *29*, 1157-1167.

(93) Tu, T.; Feng, X.; Wang, Z.; Liu, X. *Dalton Trans.* **2010**, *39*, 10598-10600.

(94) Kozlov, V. A.; Aleksanyan, D. V.; Nelyubina, Y. V.; Lyssenko, K. A.; Petrovskii, P. V.; Vasil'ev, A. A.; Odinets, I. L. *Organometallics* **2011**, *30*, 2920-2932.

(95) Luo, Q.-L.; Tan, J.-P.; Li, Z.-F.; Nan, W.-H.; Xiao, D.-R. *J. Org. Chem.* **2012**, *77*, 8332-8337.

(96) Li, P.; Zhou, H.-F.; Liu, F.; Hu, Z.-X.; Wang, H.-X. *Inorg. Chem. Commun.* **2013**, *32*, 78-81.

(97) Kumar, S.; Rao, G. K.; Kumar, A.; Singh, M. P.; Singh, A. K. *Dalton Trans.* **2013**, *42*, 16939-16948.

(98) Rao, G. K.; Kumar, A.; Kumar, S.; Dupare, U. B.; Singh, A. K. *Organometallics* **2013**, *32*, 2452-2458.

(99) RamÍrez-Rave, S.; Estudiante-Negrete, F.; Toscano, R. A.; Hernández-Ortega, S.; Morales-Morales, D.; Grévy, J.-M. *J. Organomet. Chem.* **2014**, *749*, 287-295.

(100) Tamizmani, M.; Kankanala, R.; Sivasankar, C. *J. Organomet. Chem.* **2014**, *763*, 6-13.

(101) Imanaka, Y.; Hashimoto, H.; Kinoshita, I.; Nishioka, T. *Chem. Lett.* **2014**, *43*, 687-689.

(102) Arumugam, V.; Kaminsky, W.; Bhuvanesh, N. S. P.; Nallasamy, D. *RSC Adv.* **2015**, *5*, 59428-59436.

(103) Liang, L.-C.; Chien, P.-S.; Song, L.-H. *J. Organomet. Chem.* **2016**, *804*, 30-34.

(104) Baran, T.; Menteş, A. *J. Mol. Str.* **2017**, *1134*, 591-598.

(105) Vignesh, A.; Kaminsky, W.; Dharmaraj, N. *ChemCatChem* **2017**, *9*, 910-914.

(106) Inés, B.; SanMartin, R.; Churruca, F.; Domínguez, E.; Urtiaga, M. K.; Arriortua, M. I. *Organometallics* **2008**, *27*, 2833-2839.

(107) Bolliger, J. L.; Frech, C. M. *Adv. Synth. Catal.* **2009**, *351*, 891-902.

(108) Gu, S.; Chen, W. *Organometallics* **2009**, *28*, 909-914.

(109) Huynh, H. V.; Lee, C.-S. *Dalton Trans.* **2013**, *42*, 6803-6809.

(110) Scharf, A.; Goldberg, I.; Vigalok, A. *J. Am. Chem. Soc.* **2013**, *135*, 967-970.

(111) Hung, Y.-T.; Chen, M.-T.; Huang, M.-H.; Kao, T.-Y.; Liu, Y.-S.; Liang, L.-C. *Inorg. Chem. Front.***2014**, *1*, 405-413.

(112) Zhang, J.-H.; Li, P.; Hu, W.-P.; Wang, H.-X. *Polyhedron* **2015**, *96*, 107-112.

(113) Bagherzadeh, M.; Mousavi, N.; Zare, M.; Jamali, S.; Ellern, A.; Woo, L. K. *Inorg. Chim. Acta* **2016**, *451*, 227-232.

(114) Kumar, S.; Saleem, F.; Mishra, M.; Singh, A. K. *New. J. Chem.* **2017**, *41*, 2745-2755.

(115) Olsson, D.; Nilsson, P.; El Masnaouy, M.; Wendt, O. F. *Dalton Trans.* **2005**, 1924-1929.

(116) Wang, H.; Liu, J.; Deng, Y.; Min, T.; Yu, G.; Wu, X.; Yang, Z.; Lei, A. *Chem. Eur. J.* **2009**, *15*, 1499-1507.

(117) Gerber, R.; Blacque, O.; Frech, C. M. *Dalton Trans.* **2011**, *40*, 8996-9003.

(118) Van der Ploeg, A. F. M. J.; Van Koten, G.; Brevard, C. *Inorg. Chem.* **1982**, *21*, 2878-2881.

(119) Albrecht, M.; Gossage, R. A.; Lutz, M.; Spek, A. L.; van Koten, G. *Chem. Eur. J.* **2000**, *6*, 1431-1445.

(120) Albrecht, M.; Schlupp, M.; Bargon, J.; van Koten, G. *Chem. Commun.* **2001**, 1874-1875.

(121) Bolliger, J. L.; Blacque, O.; Frech, C. M. *Chem. Eur. J.* **2008**, *14*, 7969-7977.

(122) Luquin, A.; Castillo, N.; Cerrada, E.; Merchan, F. L.; Garrido, J.; Laguna, M. *Eur. J. Org.Chem.* **2016**, *2016*, 789-798.

(123) Miyaura, N.; Suzuki, A. *Chem.Rev.* **1995**, *95*, 2457-2483.

(124) Takemoto, T.; Iwasa, S.; Hamada, H.; Shibatomi, K.; Kameyama, M.; Motoyama, Y.; Nishiyama, H. *Tetrahedron Lett.* **2007**, *48*, 3397-3401.

(125) Gelman, D.; Buchwald, S. L. *Angew. Chem. Int. Ed.* **2003**, *42*, 5993-5996.

(126) Lipshutz, B. H.; Chung, D. W.; Rich, B. *Org. Lett.* **2008**, *10*, 3793-3796.

(127) Stark, M. A.; Richards, C. J. *Tetrahedron Lett.* **1997**, *38*, 5881-5884.

(128) Stark, M. A.; Jones, G.; Richards, C. J. *Organometallics* **2000**, *19*, 1282-1291.

(129) McDonald, A. R.; Dijkstra, H. P.; Suijkerbuijk, B. M. J. M.; van Klink, G. P. M.; van Koten, G. *Organometallics* **2009**, *28*, 4689-4699.

(130) Giménez, R.; Swager, T. M. *J. Mol. Catal. A* **2001**, *166*, 265-273.

(131) Soro, B.; Stoccoro, S.; Minghetti, G.; Zucca, A.; Cinellu, M. A.; Manassero, M.; Gladiali, S. *Inorg. Chim. Acta* **2006**, *359*, 1879-1888.

(132) Gosiewska, S.; Martinez Herreras, S.; Lutz, M.; Spek, A. L.; Havenith, R. W. A.; van Klink, G. P. M.; van Koten, G.; Gebbink, R. J. M. K. *Organometallics* **2008**, *27*, 2549-2559.

(133) Yamamoto, Y.; Asao, N. *Chem. Rev.* **1993**, *93*, 2207-2293.

(134) Bloch, R. *Chem. Rev.* **1998**, *98*, 1407-1438.

(135) Denmark, S. E.; Fu, J. *Chem.Rev.* **2003**, *103*, 2763-2794.

(136) Zanoni, G.; Pontiroli, A.; Marchetti, A.; Vidari, G. *Eur. J. Org. Chem.* **2007**, *2007*, 3599-3611.

(137) Fujimoto, K.; Yoneda, T.; Yorimitsu, H.; Osuka, A. *Angew. Chem. Int. Ed.* **2014**, *53*, 1127-1130.

(138) Nakamura, H.; Iwama, H.; Yamamoto, Y. *J. Am. Chem. Soc.* **1996**, *118*, 6641-6647.

(139) Nakamura, H.; Nakamura, K.; Yamamoto, Y. *J. Am. Chem. Soc.* **1998**, *120*, 4242-4243.

(140) Nakamura, H.; Aoyagi, K.; Shim, J.-G.; Yamamoto, Y. *J. Am. Chem. Soc.* **2001**, *123*, 372-377.

(141) Nakamura, H.; Bao, M.; Yamamoto, Y. *Angew. Chem. Int. Ed.* **2001**, *40*, 3208-3210.

(142) Fernandes, R. A.; Stimac, A.; Yamamoto, Y. *J. Am. Chem. Soc.* **2003**, *125*, 14133-14139.

(143) Solin, N.; Narayan, S.; Szabó, K. J. *J. Org. Chem.* **2001**, *66*, 1686-1693.

(144) Szabó, K. J. *Chem. Eur. J.* **2000**, *6*, 4413-4421.

(145) Wallner, O. A.; Szabó, K. J. *Chem. Eur. J.* **2003**, *9*, 4025-4030.

(146) Pichierri, F.; Yamamoto, Y. *J. Org. Chem.* **2007**, *72*, 861-869.

(147) Solin, N.; Kjellgren, J.; Szabó, K. J. *J. Am. Chem. Soc.* **2004**, *126*, 7026-7033.

(148) Wallner, O. A.; Szabó, K. J. *Chem. Eur. J.* **2006**, *12*, 6976-6983.

(149) Szabó, K. J. *Chem. Eur. J.* **2004**, *10*, 5268-5275.

(150) Yao, Q.; Sheets, M. *J. Org. Chem.* **2006**, *71*, 5384-5387.

(151) Vicente, J.; Arcas, A.; Juliá-Hernández, F.; Bautista, D. *Angew. Chem. Int. Ed.* **2011**, *50*, 6896–6899.

(152) Yu, K.; Sommer, W. J.; Richardson, J. M.; Weck, M.; Jones, C. W. *Adv. Synth. Catal.* **2005**, *347*, 161-171.

(153) Weck, M.; Jones, C. W. *Inorg. Chem.* **2007**, *46*, 1865-1875.

(154) Suijkerbuijk, B. M. J. M.; Herreras Martínez, S. D.; van Koten, G.; Klein Gebbink,

R. J. M. *Organometallics* **2008**, *27*, 534-542.

(155) Frech, C. M.; Shimon, L. J. W.; Milstein, D. *Angew. Chem. Int. Ed.* **2005**, *44*, 1709 -1711.

(156) Canty, A. J.; Denney, M. C.; van Koten, G.; Skelton, B. W.; White, A. H. *Organometallics* **2004**, *23*, 5432-5439.

(157) Gerber, R.; Blacque, O.; Frech, C. M. *ChemCatChem* **2009**, *1*, 393-400.

(158) Bolliger, J. L.; Frech, C. M. *Adv. Synth. Catal.* **2010**, *352*, 1075-1080.

(159) Lipke, M. C.; Woloszynek, R. A.; Ma, L.; Protasiewicz, J. D. *Organometallics* **2009**, *28*, 188-196.

(160) Razavi, H.; Palaninathan, S. K.; Powers, E. T.; Wiseman, R. L.; Purkey, H. E.; Mohamedmohaideen, N. N.; Deechongkit, S.; Chiang, K. P.; Dendle, M. T. A.; Sacchettini, J. C.; Kelly, J. W. *Angew. Chem. Int. Ed.* **2003**, *42*, 2758-2761.

(161) Okamoto, K.; Eger, B. T.; Nishino, T.; Kondo, S.; Pai, E. F.; Nishino, T. *J. Bio. Chem.* **2003**, *278*, 1848-1855.

(162) Coqueron, P.-Y.; Didier, C.; Ciufolini, M. A. *Angew. Chem. Int. Ed.* **2003**, *42*, 1411-1414.

(163) Giddens, A. C.; Boshoff, H. I. M.; Franzblau, S. G.; Barry Iii, C. E.; Copp, B. R. *Tetrahedron Lett.* **2005**, *46*, 7355-7357.

(164) Do, H.-Q.; Daugulis, O. *J. Am. Chem. Soc.* **2007**, *129*, 12404-12405.

(165) Verrier, C.; Lassalas, P.; Théveau, L.; Quéguiner, G.; Trécourt, F.; Marsais, F.; Hoarau, C. *Beilstein J. Org. Chem.* **2011**, *7*, 1584-1601.

(166) Yang, F.; Xu, Z.; Wang, Z.; Yu, Z.; Wang, R. *Chem. Eur. J.* **2011**, *17*, 6321-6325.

(167) Han, Y.; Wang, X.; Wang, X.; Lv, L.; Diao, G.; Yuan, Y. *Synthesis* **2012**, *44*, 3027-3032.

(168) Zhang, W.; Tian, Y.; Zhao, N.; Wang, Y.; Li, J.; Wang, Z. *Tetrahedron* **2014**, *70*, 6120-6126.

(169) Kim, D.; Yoo, K. S.; Kim, S. E.; Cho, H. J.; Lee, J. H.; Kim, Y.; Kim, M. *J.Org. Chem.***2015**, *80*, 3670-3676.

(170) Yang, F.; Koeller, J.; Ackermann, L. *Angew. Chem. Int. Ed.* **2016**, *55*, 4759-4762.

(171) Mori, A.; Sekiguchi, A.; Masui, K.; Shimada, T.; Horie, M.; Osakada, K.; Kawamoto, M.; Ikeda, T. *J. Am. Chem. Soc.* **2003**, *125*, 1700-1701.

(172) Bellina, F.; Cauteruccio, S.; Rossi, R. *Eur. J. Org. Chem.* **2006**, *2006*, 1379-1382.

(173) Turner, G. L.; Morris, J. A.; Greaney, M. F. *Angew. Chem. Int. Ed.* **2007**, *46*, 7996-8000.

(174) Bellina, F.; Calandri, C.; Cauteruccio, S.; Rossi, R. *Tetrahedron* **2007**, *63*, 1970-1980.

(175) Chiong, H. A.; Daugulis, O. *Org. Lett.* **2007**, *9*, 1449-1451.

(176) Ackermann, L.; Althammer, A.; Fenner, S. *Angew. Chem. Int. Ed.* **2009**, *48*, 201-204.

(177) Doğan, Ö.; Gürbüz, N.; Özdemir, I.; Çetinkaya, B.; Şahin, O.; Büyükgüngör, O. *Dalton Trans.* **2009**, 7087-7093.

(178) Campeau, L.-C.; Stuart, D. R.; Leclerc, J.-P.; Bertrand-Laperle, M.; Villemure, E.; Sun, H.-Y.; Lasserre, S.; Guimond, N.; Lecavallier, M.; Fagnou, K. *J. Am. Chem.Soc.* **2009**, *131*, 3291-3306.

(179) Ackermann, L.; Barfüsser, S.; Pospech, J. *Org. Lett.* **2010**, *12*, 724-726.

(180) Huang, J.; Chan, J.; Chen, Y.; Borths, C. J.; Baucom, K. D.; Larsen, R. D.; Faul, M. M. *J. Am. Chem. Soc.* **2010**, *132*, 3674-3675.

(181) Shibahara, F.; Yamaguchi, E.; Murai, T. *Chem. Commun.* **2010**, *46*, 2471- 2473.

(182) Saha, D.; Adak, L.; Ranu, B. C. *Tetrahedron Lett.* **2010**, *51*, 5624-5627.

(183) Demir, S.; Özdemir, I.; Arslan, H.; VanDerveer, D. *J. Organomet. Chem.* **2011**, *696*, 2589-2593.

(184) Ödemir, I.; Arslan, H.; Demir, S.; VanDerveer, D.; Şetinkaya, B. *Inorg.Chem. Commun.* **2011**, *14*, 672-675.

(185) Zhang, G.; Zhao, X.-M.; Yan, Y.; Ding, C. *Eur. J. Org. Chem.* **2012**, *2012*, 669-672.

(186) Shen, X.-B.; Zhang, Y.-F.; Chen, W.-X.; Xiao, Z.-K.; Hu, T.-T.; Shao, L.-X. *Org. Lett.* **2014**, *16*, 1984-1987.

(187) Gu, J.; Cai, C. *RSC Adv.* **2015**, *5*, 56311-56315.

(188) Canivet, J.; Yamaguchi, J.; Ban, I.; Itami, K. *Org. Lett.* **2009**, *11*, 1733-1736.

(189) Hachiya, H.; Hirano, K.; Satoh, T.; Miura, M. *Org. Lett.* **2009**, *11*, 1737-1740.

(190) Yamamoto, T.; Muto, K.; Komiyama, M.; Canivet, J.; Yamaguchi, J.; Itami, K. *Chem. Eur. J.* **2011**, *17*, 10113-10122.

(191) Arockiam, P. B.; Bruneau, C.; Dixneuf, P. H. *Chem. Rev.* **2012**, *112*, 5879- 5918.

(192) Lewis, J. C.; Wiedemann, S. H.; Bergman, R. G.; Ellman, J. A. *Org.Lett.* **2004**, *6*, 35-38.

(193) Lewis, J. C.; Wu, J. Y.; Bergman, R. G.; Ellman, J. A. *Angew. Chem. Int. Ed.* **2006**, *45*, 589-1591.

(194) Lewis, J. C.; Bergman, R. G.; Ellman, J. A. *Acc. Chem. Res.* **2008**, *41*, 1013-1025.

(195) Lewis, J. C.; Berman, A. M.; Bergman, R. G.; Ellman, J. A. *J. Am. Chem. Soc.* **2008**, *130*, 2493-2500.

(196) Colby, D. A.; Bergman, R. t. G.; Ellman, J. A. *Chem. Rev.* **2010**, *110*, 624-655.

(197) Ohta, A.; Akita, Y.; Ohkwa, T.; Chiba, M.; Fukunaga, R.; Miyafuji, A.; Nakata, T.; Tani, N.; Aoyagi, Y. *Heterocycles* **1990**, *31*, 1951-1958.

(198) Alberico, D.; Scott, M. E.; Lautens, M. *Chem. Rev.* **2007**, *107*, 174-238.

(199) Quasdorf, K. W.; Tian, X.; Garg, N. K. *J. Am. Chem. Soc.* **2008**, *130*, 14422-14423.

(200) Kakiuchi, F.; Kochi, T. *Synthesis* **2008**, *2008*, 3013-3039.

(201) Li, C.-J. *Acc. Chem. Res.* **2009**, *42*, 335-344.

(202) Quasdorf, K. W.; Riener, M.; Petrova, K. V.; Garg, N. K. *J. Am. Chem. Soc.* **2009**, *131*, 17748-17749.

(203) Ackermann, L.; Vicente, R.; Kapdi, A. R. *Angew. Chem. Int. Ed.* **2009**, *48*, 9792-9826.

(204) Chen, X.; Engle, K. M.; Wang, D.-H.; Yu, J.-Q. *Angew. Chem. Int. Ed.* **2009**, *48*, 5094-5115.

(205) Messaoudi, S.; Brion, J.-D.; Alami, M. *Eur. J. Org. Chem.* **2010**, *2010*, 6495-6516.

(206) Sun, C.-L.; Li, B.-J.; Shi, Z.-J. *Chem. Rev.* **2011**, *111*, 1293-1314.

(207) Yamaguchi, J.; Yamaguchi, A. D.; Itami, K. *Angew. Chem. Int. Ed.* **2012**, *51*, 8960-9009.

(208) Mesganaw, T.; Garg, N. K. *Org. Process Res. Dev.* **2012**, *17*, 29-39.

(209) Yu, D.-G.; Wang, X.; Zhu, R.-Y.; Luo, S.; Zhang, X.-B.; Wang, B.-Q.; Wang, L.; Shi, Z.-J. *J. Am. Chem. Soc.* **2012**, *134*, 14638-14641.

(210) Keim, W. *Angew. Chem. Int.Ed. Engl.* **1990**, *29*, 235-244.

(211) Wilke, G. *Angew. Chem. Int. Ed.*. **1988**, *27*, 185-206.

(212) Trotuş, I.-T.; Zimmermann, T.; Schüth, F. *Chem. Rev.* **2014**, *114*, 1761-1782.

(213) Tasker, S. Z.; Standley, E. A.; Jamison, T. F. *Nature* **2014**, *509*, 299-309.

(214) Henrion, M.; Ritleng, V.; Chetcuti, M. J. *ACS Catal.* **2015**, *5*, 1283-1302.

(215) Prakasham, A. P.; Ghosh, P. *Inorg. Chim. Acta* **2015**, *431*, 61-100.

(216) Montgomery, J. *Angew. Chem. Int. Ed.* **2004**, *43*, 3890-3908.

(217) Netherton, M. R.; Fu, G. C. *Adv. Synth. Catal.* **2004**, *346*, 1525-1532.

(218) Terao, J.; Kambe, N. *Acc. Chem. Res.* **2008**, *41*, 1545-1554.

(219) Denmark, S. E.; Butler, C. R. *Chem. Commun.* **2009**, 20-33.

(220) Jacobsen, E. N.; Breinbauer, R. *Science* **2000**, *287*, 437-438.

(221) Kleiman, J. P.; Dubeck, M. *J. Am. Chem. Soc.* **1963**, *85*, 1544-1545.

(222) Mukai, T.; Hirano, K.; Satoh, T.; Miura, M. *J. Org. Chem.* **2009**, *74*, 6410-6413.

(223) Vechorkin, O.; Proust, V.; Hu, X. *Angew. Chem. Int. Ed.* **2010**, *49*, 3061-3064.

(224) Yao, T.; Hirano, K.; Satoh, T.; Miura, M. *Chem. Eur. J.* **2010**, *16*, 12307-12311.

(225) Nakatani, A.; Hirano, K.; Satoh, T.; Miura, M. *Chem. Eur. J.* **2013**, *19*, 7691-7695.

(226) Aihara, Y.; Chatani, N. *J. Am. Chem. Soc.* **2013**, *135*, 5308-5311.

(227) Gartia, Y.; Ramidi, P.; Jones, D. E.; Pulla, S.; Ghosh, A. *Catalysis. Lett.* **2014**, *144*, 507-515.

(228) Wu, X.; Zhao, Y.; Ge, H. *J. Am. Chem. Soc.* **2014**, *136*, 1789-1792.

(229) Song, W.; Lackner, S.; Ackermann, L. *Angew. Chem. Int. Ed.* **2014**, *53*, 2477-2480.

(230) Ruan, Z.; Lackner, S.; Ackermann, L. *Angew. Chem. Int. Ed.* **2016**, *55*, 3153-3157.

(231) Chen, H.; Li, P.; Wang, M.; Wang, L. *Org. Lett.* **2016**, *18*, 4794-4797.

(232) Patel, U. N.; Pandey, D. K.; Gonnade, R. G.; Punji, B. *Organometallics* **2016**, *35*, 1785-1793.

(233) Soni, V.; Jagtap, R. A.; Gonnade, R. G.; Punji, B. *ACS Catal.* **2016**, *6*, 5666-5672.

(234) Kanyiva, K. S.; Nakao, Y.; Hiyama, T. *Angew. Chem. Int. Ed.* **2007**, *46*, 8872-8874.

(235) Nakao, Y.; Kashihara, N.; Kanyiva, K. S.; Hiyama, T. *J. Am. Chem. Soc.* **2008**, *130*, 16170-16171.

(236) Nakao, Y.; Kanyiva, K. S.; Hiyama, T. *J. Am. Chem. Soc.* **2008**, *130*, 2448-2449.

(237) Aihara, Y.; Chatani, N. *J. Am. Chem. Soc.* **2014**, *136*, 898-901.

(238) Muto, K.; Yamaguchi, J.; Itami, K. *J. Am. Chem. Soc.* **2012**, *134*, 169-172.

(239) Hachiya, H.; Hirano, K.; Satoh, T.; Miura, M. *Angew. Chem. Int. Ed.* **2010**, *49*, 2202-2205.

(240) Hachiya, H.; Hirano, K.; Satoh, T.; Miura, M. *ChemCatChem* **2010**, *2*, 1403-1406.

(241) Qu, G.-R.; Xin, P.-Y.; Niu, H.-Y.; Wang, D.-C.; Ding, R.-F.; Guo, H.-M. *Chem. Commun.* **2011**, *47*, 11140-11142.

(242) Matsuyama, N.; Hirano, K.; Satoh, T.; Miura, M. *Org. Lett.* **2009**, *11*, 4156-4159.

(243) Matsuyama, N.; Kitahara, M.; Hirano, K.; Satoh, T.; Miura, M. *Org. Lett.* **2010**, *12*, 2358-2361.

(244) Yi, J.; Yang, L.; Xia, C.; Li, F. *J. Org. Chem.* **2015**, *80*, 6213-6221.

(245) Landge, V. G.; Shewale, C. H.; Jaiswal, G.; Sahoo, M. K.; Midya, S. P.; Balaraman, E. *Catal. Sci. Tech.* **2015**, *6*, 1946-1951.

(246) Luo, F.-X.; Cao, Z.-C.; Zhao, H.-W.; Wang, D.-C.; Zhang, Y.-F.; Xu, X.; Shi, Z.-J. *Organometallics* **2017**, *36*, 18-21.

(247) Carey, J. S.; Laffan, D.; Thomson, C.; Williams, M. T. *Org. Biomol. Chem.* **2006**, *4*,

2337-2347.

(248) Godula, K.; Sames, D. *Science* **2006**, *312*, 67-72.

(249) Kraft, A.; Grimsdale, A. C.; Holmes, A. B. *Angew. Chem. Int. Ed.* **1998**, *37*, 402-428.

(250) Shimizu, M.; Hiyama, T. *Angew. Chem. Int. Ed.* **2005**, *44*, 214-231.

(251) Harper, R. J.; Soloski, E. J.; Tamborski, C. *J. Org. Chem.* **1964**, *29*, 2385-2389.

(252) Lafrance, M.; Rowley, C. N.; Woo, T. K.; Fagnou, K. *J. Am. Chem. Soc.* **2006**, *128*, 8754-8756.

(253) Do, H.-Q.; Daugulis, O. *J. Am. Chem. Soc.* **2008**, *130*, 1128-1129.

(254) Jagtap, R. A.; Soni, V.; Punji, B. *ChemSusChem* **2017**, DOI: 10.1002/cssc.201700321.

(255) Kumar, D.; David, W. M.; Kerwin, S. M. *Bioorg. Med. Chem. Lett.* **2001**, *11*, 2971-2974.

(256) Callstrom, M. R.; Neenan, T. X.; McCreery, R. L.; Alsmeyer, D. C. *J. Am. Chem. Soc.* **1990**, *112*, 4954-4956.

(257) Kondo, T.; Mitsudo, T. *Chem. Rev.* **2000**, *100*, 3205-3220.

(258) Hartwig, J. F. *Acc. Chem. Res.* **2008**, *41*, 1534-1544.

(259) Beletskaya, I. P.; Ananikov, V. P. *Chem. Rev.*, *111*, 1596-1636.

(260) Reddy, V. P.; Qiu, R.; Iwasaki, T.; Kambe, N. *Org. Biomol. Chem.* **2015**, *13*, 6803-6813.

(261) Ye, X.; Petersen, J. L.; Shi, X. *Chem. Commun.* **2015**, *51*, 7863-7866.

(262) Yan, S.-Y.; Liu, Y.-J.; Liu, B.; Liu, Y.-H.; Shi, B.-F. *Chem. Commun.* **2015**, *51*, 4069-4072.

(263) Macgregor, S. A.; Neave, G. W.; Smith, C. *Faraday Discuss.* **2003**, *124*, 111-127.

(264) Ananikov, V. P.; Musaev, D. G.; Morokuma, K. *Organometallics* **2005**, *24*, 715-723.

(265) Cong, X.; Li, Y.; Wei, Y.; Zeng, X. *Org. Lett.* **2014**, *16*, 3926-3929.

(266) Gorelsky, S. I.; Lapointe, D.; Fagnou, K. *J. Am. Chem. Soc.* **2008**, *130*, 10848-10849.

(267) Diederich, F.; Stang, P. J. *Metal-Catalyzed Cross-Coupling Reactions; Eds.; Wiley-VCH: Weinheim, Germany* **1998**.

(268) Ackermann, L. *Modern Arylation Methods; Ed.; Wiley-VCH: Weinheim, Germany* **2009**.

(269) Satoh, T.; Miura, M. *Chem. Lett.* **2007**, *36*, 200-205.

(270) Seregin, I. V.; Gevorgyan, V. *Chem. Soc. Rev.* **2007**, *36*, 1173-1193.

(271) McGlacken, G. P.; Bateman, L. M. *Chem. Soc. Rev.* **2009**, *38*, 2447-2464.

(272) Ackermann, L. *Chem. Commun.* **2010**, *46*, 4866-4877.

(273) Hirano, K.; Miura, M. *Synlett* **2011**, 294-307.

(274) Kuhl, N.; Hopkinson, M. N.; Wencel-Delord, J.; Glorius, F. *Angew. Chem. Int. Ed.* **2012**, *51*, 10236-10254.

(275) Kozhushkov, S. I.; Potukuchi, H. K.; Ackermann, L. *Catal. Sci. Technol.* **2013**, *3*, 562-571.

(276) Verrier, C.; Lassalas, P.; Théveau, L.; Quéguiner, G.; Trécourt, F.; Marsais, F.; Hoarau, C. *Beilstein J. Org. Chem.* **2011**, *7*, 1584-1601.

(277) Yamaguchi, J.; Muto, K.; Itami, K. *Eur. J. Org. Chem.* **2013**, *2013*, 19-30.

(278) Kulkarni, A. A.; Daugulis, O. *Synthesis* **2009**, *2009*, 4087-4109.

(279) Han, Y.; Wang, X.; Wang, X.; Lv, L.; Diao, G.; Yuan, Y. *Synthesis* **2012**, *44*, 3027-3032.

(280) Pivsa-Art, S.; Satoh, T.; Kawamura, Y.; Miura, M.; Nomura, M. *Bull. Chem. Soc. Jpn.* **1998**, *71*, 467-473.

(281) Derridj, F.; Gottumukkala, A. L.; Djebbar, S.; Doucet, H. *Eur. J. Inorg. Chem.* **2008**, 2550-2559.

(282) Zhang, G.; Zhao, X.; Yan, Y.; Ding, C. *Eur. J. Org. Chem.* **2012**, 669-672.

(283) Selander, N.; Szabó, K. J. *Chem. Rev.* **2011**, *111*, 2048-2076.

(284) Szabó, K. J. *Top Organomet. Chem.* **2013**, *40*, 203-242.

(285) Tabares-Mendoza, C.; Guadarrama, P. *J. Organomet. Chem.* **2006**, *691*, 2978-2986.

(286) Khake, S. M.; Soni, V.; Gonnade, R. G.; Punji, B., *Dalton Trans*., **2014,** *43*, 16084-16096.

(287) Polukeev, A. V.; Kuklin, S. A.; Petrovskii, P. V.; Peregudova, S. M.; Smolyakov, A. F.; Dolgushin, F. M.; Koridze, A. A. *Dalton Trans.* **2011**, *40*, 7201-7209.

(288) Przybilla, K. J.; Vögtle, F. *Chem. Ber.* **1989**, *122*, 347-355.

(289) Kunz, K. R.; Taylor, E. W.; Hutton, H. M.; Blackburn, B. J. *Org. Prep. Proce. Int.* **1990**, *22*, 613-618.

(290) van Leusen, A. M.; Hoogenboom, B. E.; Siderius, H. *Tetrahedron Lett.* **1972**, *13*, 2369-2372.

(291) In principle, CH of -N{CH(CH_3)$_2$}$_2$ should show a septet (if both CH are equivalents) or two separate septet (if CH are non-equivalent); however, an apparent octet is observed most likely due to partial overlapping of two septet for each CH of -N{CH(CH_3)$_2$}$_2$.

(292) A satisfactory elemental analysis is not observed for this compound, which might be due to the presence of a trace amount of unknown impurity. However, this compound is > 95% pure by NMR analysis.

(293) Khake, S. M.; Jagtap, R. A.; Dangat, Y. B.; Gonnade, R. G.; Vanka, K.; Punji., B., *Organometallics.*, **2016**, *35*, 875-886

(294) Spasyuk, D. M.; Zargarian, D.; van der Est, A. *Organometallics* **2009**, *28*, 6531-6540.

(295) Gong, J.-F.; Zhang, Y.-H.; Song, M.-P.; Xu, C. *Organometallics* **2007**, *26*, 6487-6492.

(296) Salah, A. B.; Zargarian, D. *Dalton Trans.* **2011**, *40*, 8977-8985.

(297) Besselièvre, F.; Mahuteau-Betzer, F.; Grierson, D. S.; Piguel, S. *J. Org. Chem.* **2008**, *73*, 3278-3280.

(298) Campeau, L.-C.; Bertrand-Laperle, M.; Leclerc, J.-P.; Villemure, E.; Gorelsky, S. I.; Fagnou, K. *J. Am. Chem. Soc.* **2008**, *130*, 3276-3277.

(299) Bellina, F.; Rossi, R. *Tetrahedron* **2009**, *65*, 10269-10310.

(300) Yu, D.; Lu, L.; Shen, Q. *Org. Lett.* **2013**, *15*, 940-943.

(301) Shen, X.-B.; Zhang, Y.; Chen, W.-X.; Xiao, Z.-K.; Hu, T.-T.; Shao, L.-X. *Org. Lett.* **2014**, *16*, 1984-1987.

(302) Gao, F.; Kim, B.-S.; Walsh, P. J. *Chem. Commun.* **2014**, *50*, 10661-10664.

(303) Ferguson, D. M.; Rudolph, S. R.; Kalyani, D. *ACS Catal.* **2014**, *4*, 2395-2401.

(304) Tani, S.; Uehara, T. N.; Yamaguchi, J.; Itami, K. *Chem. Sci.* **2014**, *5*, 123-135.

(305) Pandey, D. K.; Khake, S. M.; Gonnade, R. G.; Punji, B. *RSC Adv.* **2015**, *5*, 81502-81514.

(306) Zhu, F.; Wang, Z.-X. *Org. Lett.* **2015**, *17*, 1601-1604.

(307) Bellina, F.; Cauteruccio, S.; Rossi, R. *Curr. Org. Chem.* **2008**, *12*, 774–790.

(308) Wakioka, M.; Nakamura, Y.; Hihara, Y.; Ozawa, F.; Sakaki, S. *Organometallics* **2013**, *32*, 4423-4430.

(309) Wakioka, M.; Nakamura, Y.; Hihara, Y.; Ozawa, F.; Sakaki, S. *Organometallics* **2014**, *33*, 6247-6252.

(310) Sánchez, R. S.; Zhuravlev, F. A. *J. Am. Chem. Soc.* **2007**, *129*, 5824-5825.

(311) Xu, L.-M.; Li, B.-J.; Yang, Z.; Shi, Z.-J. *Chem. Soc. Rev.* **2010**, *39*, 712-733.

(312) Kalyani, D.; Deprez, N. R.; Desai, L. V.; Sanford, M. S. *J. Am. Chem. Soc.* **2005**, *127*, 7330-7331.

(313) Deprez, N. R.; Kalyani, D.; Krause, A.; Sanford, M. S. *J. Am. Chem. Soc.* **2006**, *128*, 4972-4973.

(314) Deprez, N. R.; Sanford, M. S. *Inorg. Chem.* **2007**, *46*, 1924-1935.

(315) Deprez, N. R.; Sanford, M. S. *J. Am. Chem. Soc.* **2009**, *131*, 11234-11241.

(316) Szabó, K. J. *J. Mol. Catal. A: Chem.* **2010**, *324*, 56–63.

(317) Hickman, A. J.; Sanford, M. S. *ACS Catal.* **2011**, *1*, 170-174.

(318) Daugulis, O.; Zaitsev, V. G. *Angew. Chem. Int. Ed.* **2005**, *44*, 4046-4048.

(319) Zaitsev, V. G.; Shabashov, D.; Daugulis, O. *J. Am. Chem. Soc.* **2005**, *127*, 13154-13155.

(320) Zhang, Q.; Chen, K.; Rao, W.; Zhang, Y.; Chen, F.-J.; Shi, B.-F. *Angew. Chem. Int. Ed.* **2013**, *52*, 13588-13592.

(321) Gong, W.; Zhang, G.; Liu, T.; Giri, R.; Yu, J.-Q. *J. Am. Chem. Soc.* **2014**, *136*, 16940-16946.

(322) Arroniz, C.; Denis, J. G.; Ironmonger, A.; Rassias, G.; Larrosa, I. *Chem. Sci.* **2014**, *5*, 3509-3514.

(323) Dastbaravardeh, N.; Toba, T.; Farmer, M. E.; Yu, J.-Q. *J. Am. Chem. Soc.* **2015**, *137*, 9877-9884.

(324) Vicente-Hernandez, I.; Chicote, M.-T.; Vicente, J.; Bautista, D. *Chem. Commun.* **2016**, *52*, 594-596.

(325) Shabashov, D.; Daugulis, O. *J. Am. Chem. Soc.* **2010**, *132*, 3965-3972.

(326) Maestri, G.; Motti, E.; Della Ca', N.; Malacria, M.; Derat, E.; Catellani, M. *J. Am. Chem.Soc.* **2011**, *133*, 8574-8585.

(327) Sundermann, A.; Uzan, O.; Martin, J. M. L. *Chem. Eur. J.* **2001**, *7*, 1703-1711.

(328) Yu, K.; Sommer, W. J.; Weck, M.; Jones, C. W. *J.Cataly.* **2004**, *226*, 101-110.

(329) Reetz, M. T.; Westermann, E. *Angew. Chem. Int. Ed.* **2000**, *39*, 165-168.

(330) Zapf, A.; Beller, M. *Chem. Eur. J.* **2001**, *7*, 2908-2915.

(331) Widegren, J. A.; Finke, R. G. *J. Mol. Catal. A: Chem.* **2003**, *198*, 317-341.

(332) Lin, Y.; Finke, R. G. *Inorg. Chem.* **1994**, *33*, 4891-4910.

(333) Weddle, K. S.; Aiken, J. D.; Finke, R. G. *J. Am. Chem. Soc.* **1998**, *120*, 5653-5666.

(334) Yu, K.; Sommer, W.; Weck, M.; Jones, C. W. *J. Catal.* **2004**, *226*, 101-110.

(335) Yu, K.; Sommer, W.; Richardson, J. M.; Weck, M.; Jones, C. W. *Adv. Synth. Catal.* **2005**, *347*, 161-171.

(336) Foley, P.; DiCosimo, R.; Whitesides, G. M. *J. Am. Chem. Soc.* **1980**, *102*, 6713-6725.

(337) Anton, D. R.; Crabtree, R. H. *Organometallics* **1983**, *2*, 855-859.

(338) Blackmond, D. G. *Angew. Chem. Int. Ed.* **2005**, *44*, 4302-4320.

(339) Hartwig, J. F. *Organotransition Metal Chemistry - From Bonding to Catalysis; University Science Books: Mill Valley, California, USA* **2010**.

(340) Osakada, K.; Sakata, R.; Yamamoto, T. *Organometallics* **1997**, *16*, 5354-5364.

(341) Deng, J. Z.; Paone, D. V.; Ginnetti, A. T.; Kurihara, H.; Dreher, S. D.; Weissman, S. A.; Stauffer, S. R.; Burgey, C. S. *Org. Lett.* **2009**, *11*, 345-347.

(342) Gorelsky, S. I. *Organometallics* **2012**, *31*, 794-797.

(343) Hu, W.-Y.; Wang, P.-P.; Zhang, S.-L. *Synthesis* **2015**, *47*, 42-48.

(344) Canty, A. J. *Acc. Chem. Res.* **1992**, *25*, 83-90.

(345) Catellani, M.; Chiusoli, G. P.; Costa, M. *J. Organomet. Chem.* **1995**, *500*, 69-80.

(346) Kruis, D.; Markies, B. A.; Canty, A. J.; Boersma, J.; van Koten, G. *J. Organomet. Chem.***1997**, *532*, 235-242.

(347) Mateo, C.; Fernández-Rivas, C.; Cárdenas, D. J.; Echavarren, A. M. *Organometallics* **1998**, *17*, 3661-3669.

(348) Sundberg, R. J. *In Comprehensive Heterocyclic Chemistry, 2nd ed.; Katritzky, A. R., Rees, C. W., Eds.; Pergamon Press: Oxford,* **1996**, *2*, 119-206.

(349) Horton, D. A.; Bourne, G. T.; Smythe, M. L. *Chem. Rev.* **2003**, *103*, 893-930.

(350) Carey, J. S.; Laffan, D.; Thomson, C.; Williams, M. T. *Org. Bio. Chem.* **2006**, *4*, 2337-2347.

(351) Walker, S. R.; Carter, E. J.; Huff, B. C.; Morris, J. C. *Chem. Rev.* **2009**, *109*, 3080-3098.

(352) Kochanowska-Karamyan, A. J.; Hamann, M. T. *Chem. Rev.* **2010**, *110*, 4489-4497.

(353) Campbell, J. A.; Bordunov, V.; Broka, C. A.; Browner, M. F.; Kress, J. M.; Mirzadegan, T.; Ramesha, C.; Sanpablo, B. F.; Stabler, R.; Takahara, P.; Villasenor, A.; Walker, K. A. M.; Wang, J.-H.; Welch, M.; Weller, P. *Bioorg. Med. Chem. Lett.* **2004**, *14*, 4741-4745.

(354) Smart, B. P.; Oslund, R. C.; Walsh, L. A.; Gelb, M. H. *J. Med. Chem.* **2006**, *49*, 2858-2860.

(355) Alex, K.; Schwarz, N.; Khedkar, V.; Sayyed, I. A.; Tillack, A.; Michalik, D.; Holenz, J.; Diaz, J. L.; Beller, M. *Org. Biomol. Chem.* **2008**, *6*, 1802-1807.

(356) Zhou, G.; Wu, D.; Snyder, B.; Ptak, R. G.; Kaur, H.; Gochin, M. *J. Med. Chem.* **2011**, *54*, 7220-7231.

(357) Chu, U. B.; Vorperian, S. K.; Satyshur, K.; Eickstaedt, K.; Cozzi, N. V.; Mavlyutov, T.; Hajipour, A. R.; Ruoho, A. E. *Biochemistry* **2014**, *53*, 2956−2965.

(358) Melander, R. J.; Minvielle, M. J.; Melander, C. *Tetrahedron* **2014**, *70*, 6363-6372.

(359) Lyons, T. W.; Sanford, M. S. *Chem. Rev.* **2010**, *110*, 1147-1169.

(360) Ackermann, L. *Chem. Rev.* **2011**, *111*, 1315-1345.

(361) Neufeldt, S. R.; Sanford, M. S. *Acc. Chem. Res.* **2012**, *45*, 936-946.

(362) Li, B.-J.; Shi, Z.-J. *Chem. Soc. Rev.* **2012**, *41*, 5588-5598.

(363) Zhang, F.; Spring, D. R. *Chem. Soc. Rev.* **2014**, *43*, 6906-6919.

(364) Zhang, M.; Zhang, Y.; Jie, X.; Zhao, H.; Li, G.; Su, W. *Org. Chem. Front.* **2014**, *1*, 843-895.

(365) Chen, Z.; Wang, B.; Zhang, J.; Yu, W.; Liu, Z.; Zhang, Y. *Org. Chem. Front.* **2015**, *2*, 1107-1295.

(366) Han, W.; Ofial, A. R. *Synlett* **2011**, 1951–1955.

(367) Cho, S. H.; Kim, J. Y.; Kwak, J.; Chang, S. *Chem. Soc. Rev.* **2011**, *40*, 5068-5083.

(368) Mercier, L. G.; Leclerc, M. *Acc. Chem. Res.* **2013**, *46*, 1597-1605.

(369) Chinchilla, R.; Nájera, C. *Chem. Rev.* **2014**, *114*, 1783-1826.

(370) Boyarskiy, V. P.; Ryabukhin, D. S.; Bokach, N. A.; Vasilyev, A. V. *Chem. Rev.* **2016**, *116*, 5894-5986.

(371) Wu, W.; Jiang, H. *Acc. Chem. Res.* **2014**, *47*, 2483-2504.

(372) Seregin, I. V.; Ryabova, V.; Gevorgyan, V. *J. Am. Chem. Soc.* **2007**, *129*, 7742-7743.

(373) Brand, J. P.; Charpentier, J.; Waser, J. *Angew. Chem. Int. Ed.* **2009**, *48*, 9346-9349.

(374) Gu, Y.; Wang, X. *Tetrahedron Lett.* **2009**, *50*, 763-766.

(375) Dudnik, A. S.; Gevorgyan, V. *Angew. Chem. Int. Ed.* **2010**, *49*, 2096-2098.

(376) Kim, S. H.; Chang, S. *Org. Lett.* **2010**, *12*, 1868-1871.

(377) Ackermann, L.; Lygin, A. V. *Org. Lett.* **2012**, *14*, 764-767.

(378) Ackermann, L.; Pospech, J.; Graczyk, K.; Rauch, K. *Org. Lett.* **2012**, *14*, 930-933.

(379) Shibahara, F.; Dohke, Y.; Murai, T. *J. Org. Chem.* **2012**, *77*, 5381-5388.

(380) Ano, Y.; Tobisu, M.; Chatani, N. *Org. Lett.* **2012**, *14*, 354-357.

(381) Brand, J. P.; Waser, J. *Synthesis* **2012**, *44*, 1155-1158.

(382) Li, Y.; Brand, J. P.; Waser, J. *Angew. Chem. Int. Ed.* **2013**, *52*, 6743-6747.

(383) Tolnai, G. L.; Ganss, S.; Brand, J. P.; Waser, J. *Org. Lett.* **2013**, *15*, 112-115.

(384) Wang, L.; Ackermann, L. *Org. Lett.* **2013**, *15*, 176-179.

(385) Feng, C.; Loh, T.-P. *Angew. Chem. Int. Ed.* **2014**, *53*, 2722-2726.

(386) Brachet, E.; Belmont, P. *J. Org. Chem.* **2015**, *80*, 7519-7529.

(387) Parsharamulu, T.; Vishnuvardhan Reddy, P.; Likhar, P. R.; Lakshmi Kantam, M. *Tetrahedron* **2015**, *71*, 1975-1981.

(388) Wu, Y.; Yang, Y.; Zhou, B.; Li, Y. *J. Org. Chem.* **2015**, *80*, 1946-1951.

(389) Li, Y.; Xie, F.; Li, X. *J. Org. Chem.* **2016**, *81*, 715-722.

(390) Shaikh, A. C.; Shinde, D. R.; Patil, N. T. *Org. Lett.* **2016**, *18*, 1056-1059.

(391) Nakamura, E.; Yoshikai, N. *J. Org. Chem.* **2010**, *75*, 6061-6067.

(392) Yoshikai, N. *Synlett* **2011**, *2011*, 1047-1051.

(393) Ackermann, L. *J. Org. Chem.* **2014**, *79*, 8948-8954.

(394) Gao, K.; Yoshikai, N. *Acc. Chem. Res.* **2014**, *47*, 1208-1219.

(395) Su, B.; Cao, Z.-C.; Shi, Z.-J. *Acc. Chem. Res.* **2015**, *48*, 886-896.

(396) Miao, J.; Ge, H. *Eur. J. Org. Chem.* **2015**, *2015*, 7859-7868.

(397) Moselage, M.; Li, J.; Ackermann, L. *ACS Catal.* **2016**, *6*, 498-525.

(398) Besselièvre, F.; Piguel, S. *Angew.Chem. Int. Ed.* **2009**, *48*, 9553-9556.

(399) Kawano, T.; Matsuyama, N.; Hirano, K.; Satoh, T.; Miura, M. *J. Org. Chem.* **2010**, *75*, 1764-1766.

(400) Aziz, J.; Baladi, T.; Piguel, S. *J. Org. Chem.* **2016**, *81*, 4122-4133.

(401) Shang, M.; Wang, H.-L.; Sun, S.-Z.; Dai, H.-X.; Yu, J.-Q. *J. Am. Chem. Soc.* **2014**, *136*, 11590-11593.

(402) Zhang, Z.-Z.; Liu, B.; Wang, C.-Y.; Shi, B.-F. *Org. Lett.* **2015**, *17*, 4094-4097.

(403) Sauermann, N.; Gonza′lez, M. J.; Ackermann, L. *Org. Lett.* **2015**, *17*, 5316-5319.

(404) Ananikov, V. P. *ACS Catal.* **2015**, *5*, 1964-1971.

(405) Liu, Y.-J.; Liu, Y.-H.; Yan, S.-Y.; Shi, B.-F. *Chem. Commun.* **2015**, *51*, 6388-6391.

(406) Liu, Y.-H.; Liu, Y.-J.; Yan, S.-Y.; Shi, B.-F. *Chem. Commun.* **2015**, *51*, 11650-11653.

(407) Khake, S. M.; Soni, V.; Gonnade, R. G.; Punji, B., *Chem. Eur. J.* **2017**, *23*, 2907-2914.

(408) Buckle, D. R.; Outred, D. J.; Rockell, C. J. M.; Smith, H.; Spicer, B. A. *J. Med.Chem.* **1983**, *26*, 251-254.

(409) Genin, M. J.; Allwine, D. A.; Anderson, D. J.; Barbachyn, M. R.; Emmert, D. E.; Garmon, S. A.; Graber, D. R.; Grega, K. C.; Hester, J. B.; Hutchinson, D. K.; Morris, J.; Reischer, R. J.; Ford, C. W.; Zurenko, G. E.; Hamel, J. C.; Schaadt, R. D.; Stapert, D.; Yagi, B. H. *J. Med. Chem.* **2000**, *43*, 953-970.

(410) Giffin, M. J.; Heaslet, H.; Brik, A.; Lin, Y.-C.; Cauvi, G.; Wong, C.-H.; McRee, D. E.; Elder, J. H.; Stout, C. D.; Torbett, B. E. *J. Med. Chem.* **2008**, *51*, 6263-6270.

(411) Pandarus, V.; Zargarian, D. *Organometallics* **2007**, *26*, 4321-4334.

(412) Ackermann, L.; Lygin, A. V. *Org.Lett.* **2011**, *13*, 3332-3335.

(413) Teo, Y.-C.; Yong, F.-F.; Sim, S. *Tetrahedron* **2013**, *69*, 7279-7284.

(414) Tiwari, V. K.; Kamal, N.; Kapur, M. *Org. Lett.* **2015**, *17*, 1766-1769.

(415) Xu, S.; Huang, X.; Hong, X.; Xu, B. *Org.Lett.* **2012**, *14*, 4614-4617.

(416) Shi, J.; Zhou, B.; Yang, Y.; Li, Y. *Org. Biomol. Chem.* **2012**, *10*, 8953-8955.

(417) Soni, V.; Patel, U. N.; Punji, B. *RSC Adv.* **2015**, *5*, 57472-57481.

(418) Cano, R.; Ramón, D. J.; Yus, M. *J. Org. Chem.* **2011**, *76*, 654-660.

(419) Orcel, U.; Waser, J. *Angew. Chem. Int. Ed.* **2015**, *54*, 5250-5254.

(420) Sauermann, N.; González, M. J.; Ackermann, L. *Org. Lett.* **2015**, *17*, 5316-5319.

(421) Fiandanese, V.; Bottalico, D.; Marchese, G.; Punzi, A. *Tetrahedron* **2008**, *64*, 53-60.

(422) Cheng, Y.; Wu, Y.; Tan, G.; You, J. *Angew. Chem. Int. Ed.* **2016**, *55*, 12275.

(423) Yan, Q.; Chen, Z.; Yu, W.; Yin, H.; Liu, Z.; Zhang, Y. *Org. Lett.* **2015**, *17*, 2482-2485.

(424) APEX2, SAINT and SADABS, *Bruker AXS Inc.*, Madison, Wisconsin, USA **2006**.

(425) Sheldrick, G. M. *Acta Crystallogr.* **2008**, *A64*, 112-122.

NMR and HRMS spectra of complexes

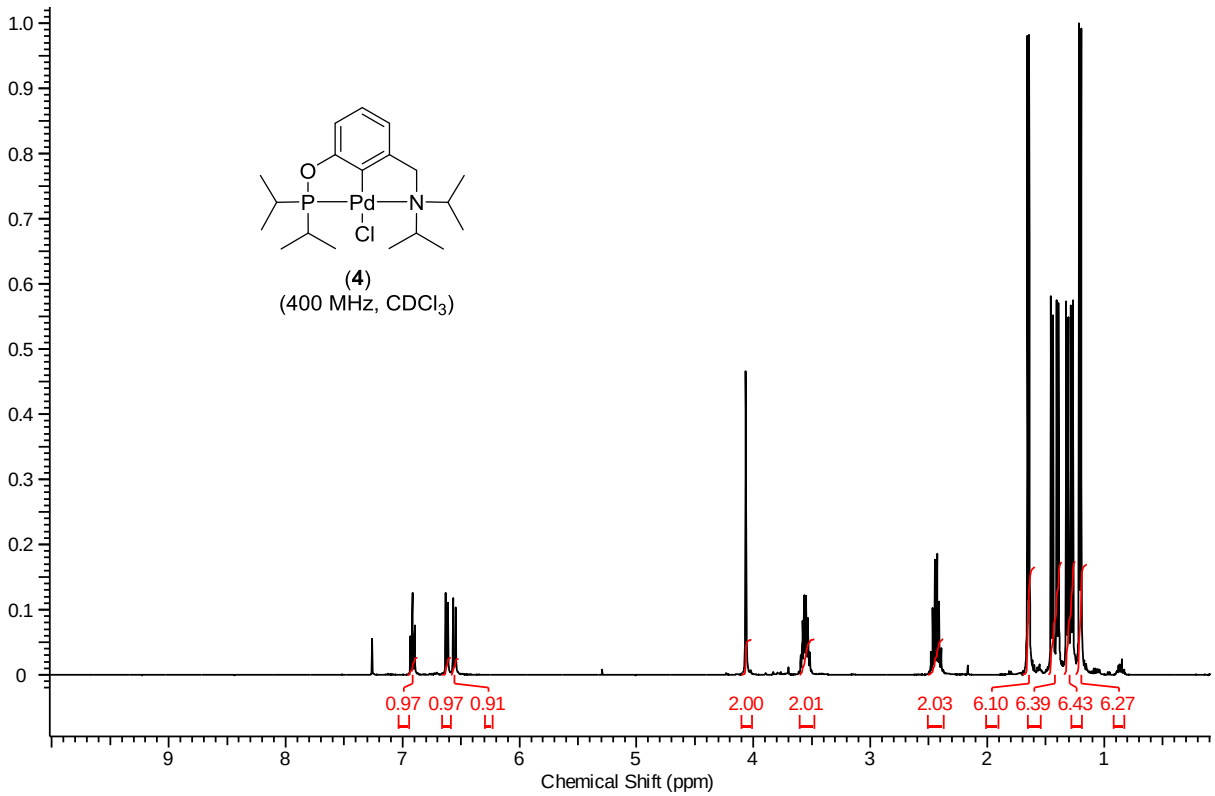

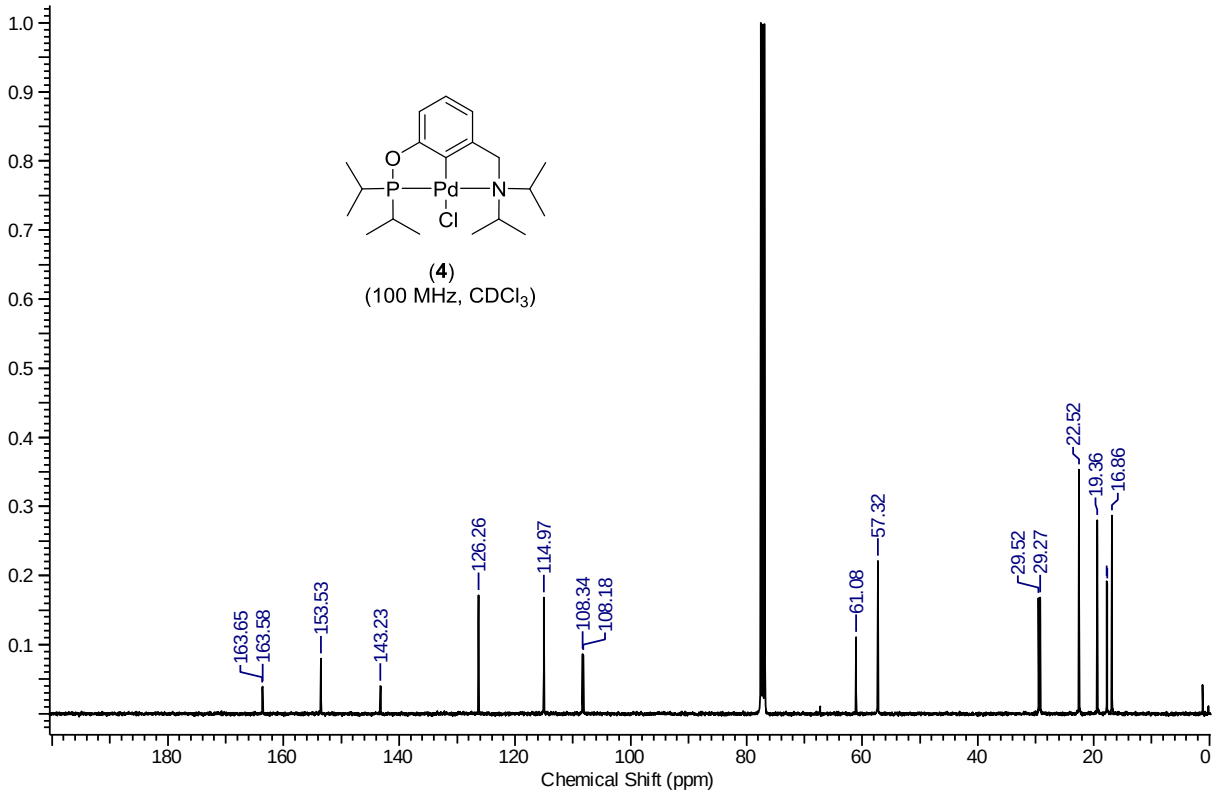

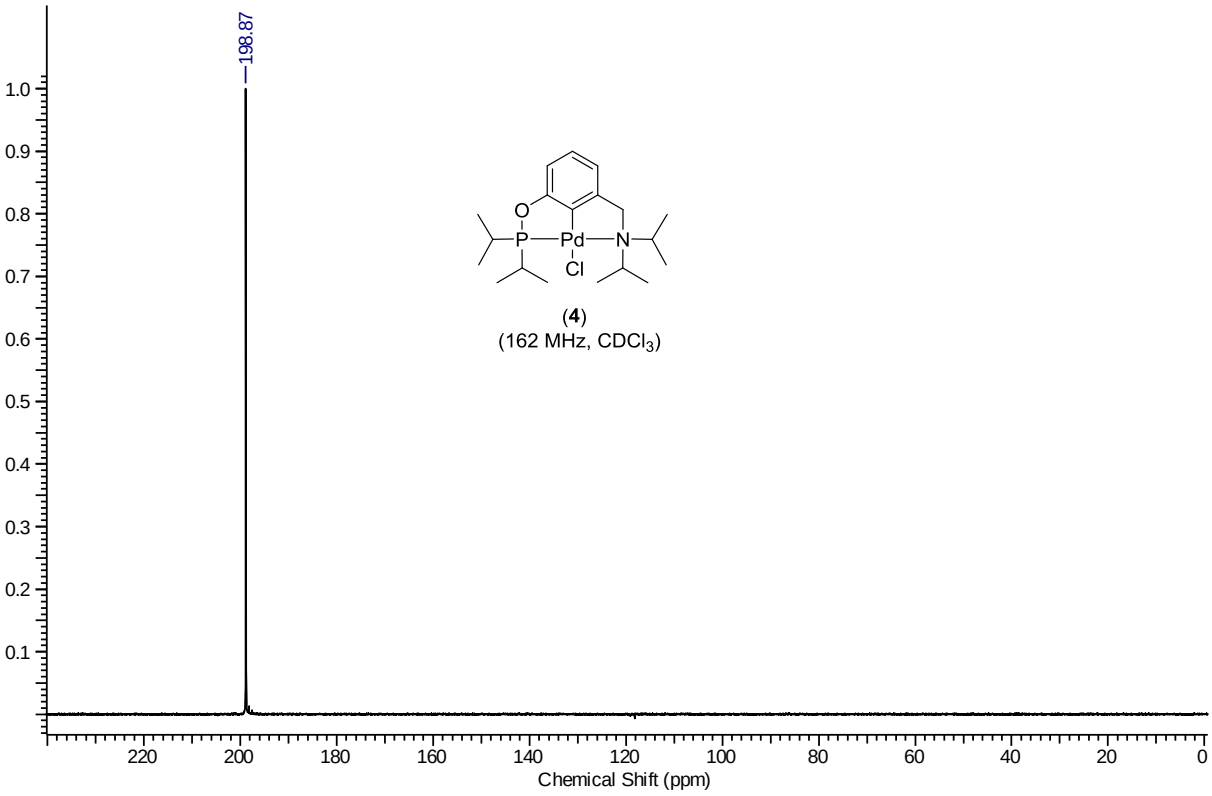

(**4**)
(162 MHz, $CDCl_3$)

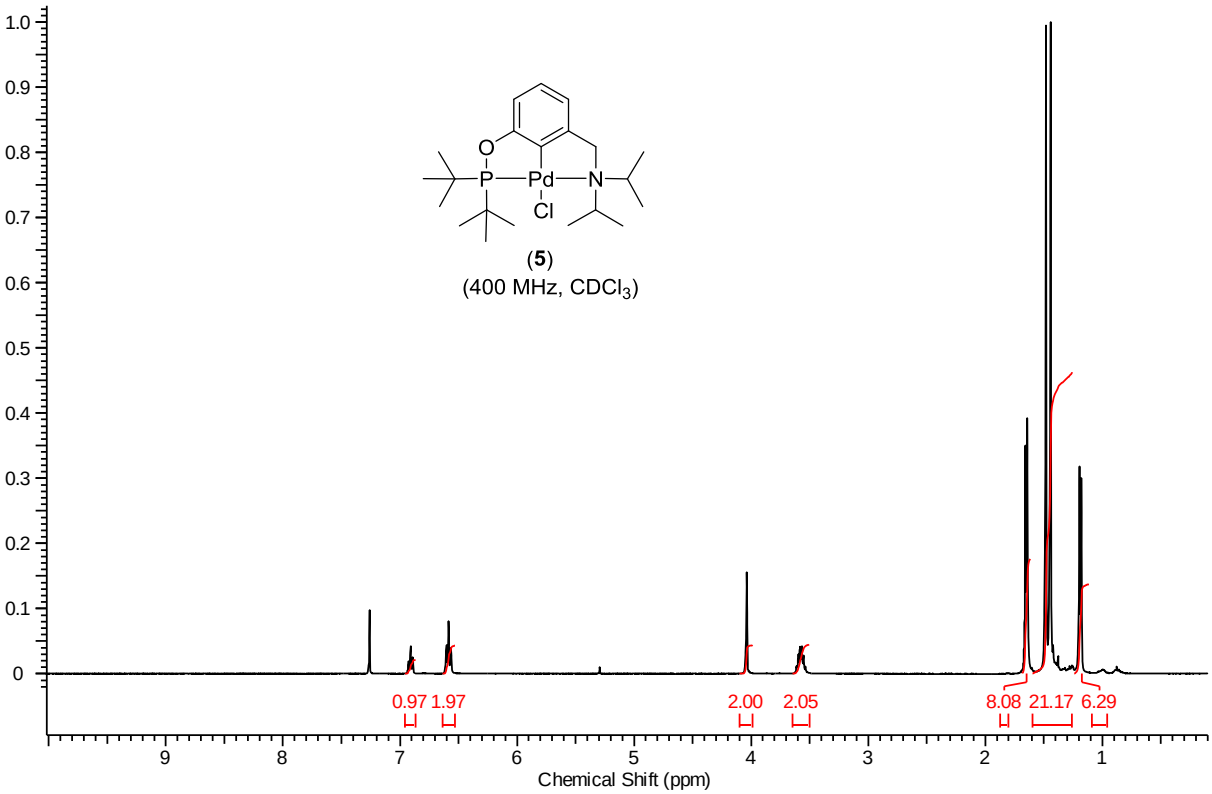

(**5**)
(400 MHz, $CDCl_3$)

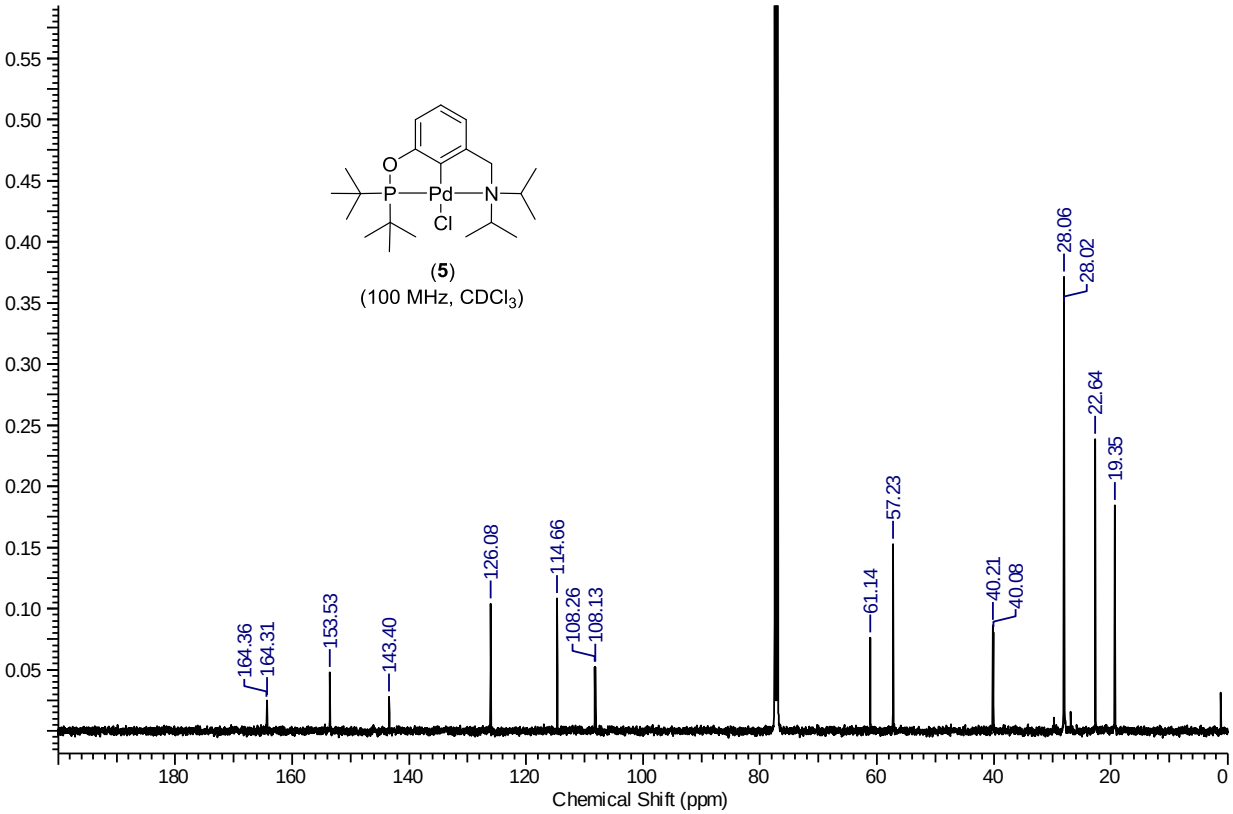
(5)
(100 MHz, CDCl3)
164.36
164.31
153.53
143.40
126.08
114.66
108.26
108.13
61.14
57.23
40.21
40.08
28.06
28.02
22.64
19.35
Chemical Shift (ppm)

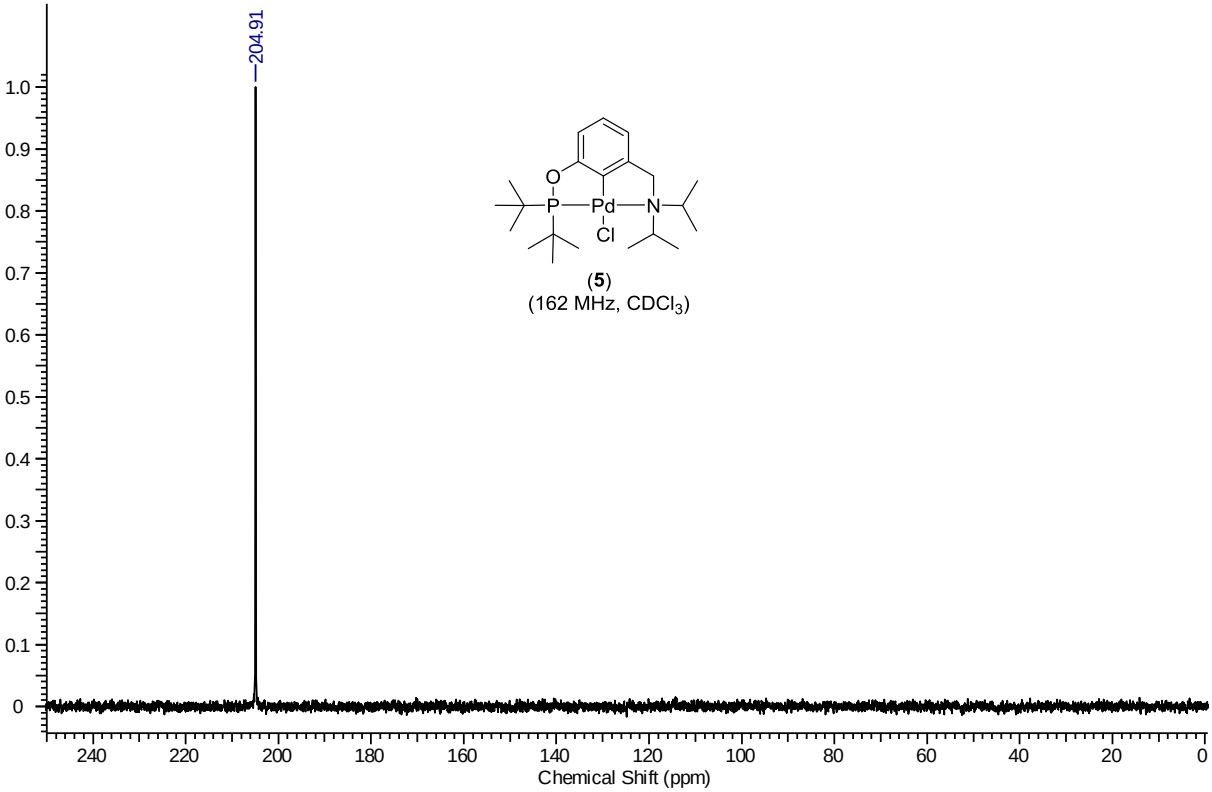
204.91
(5)
(162 MHz, CDCl3)
Chemical Shift (ppm)

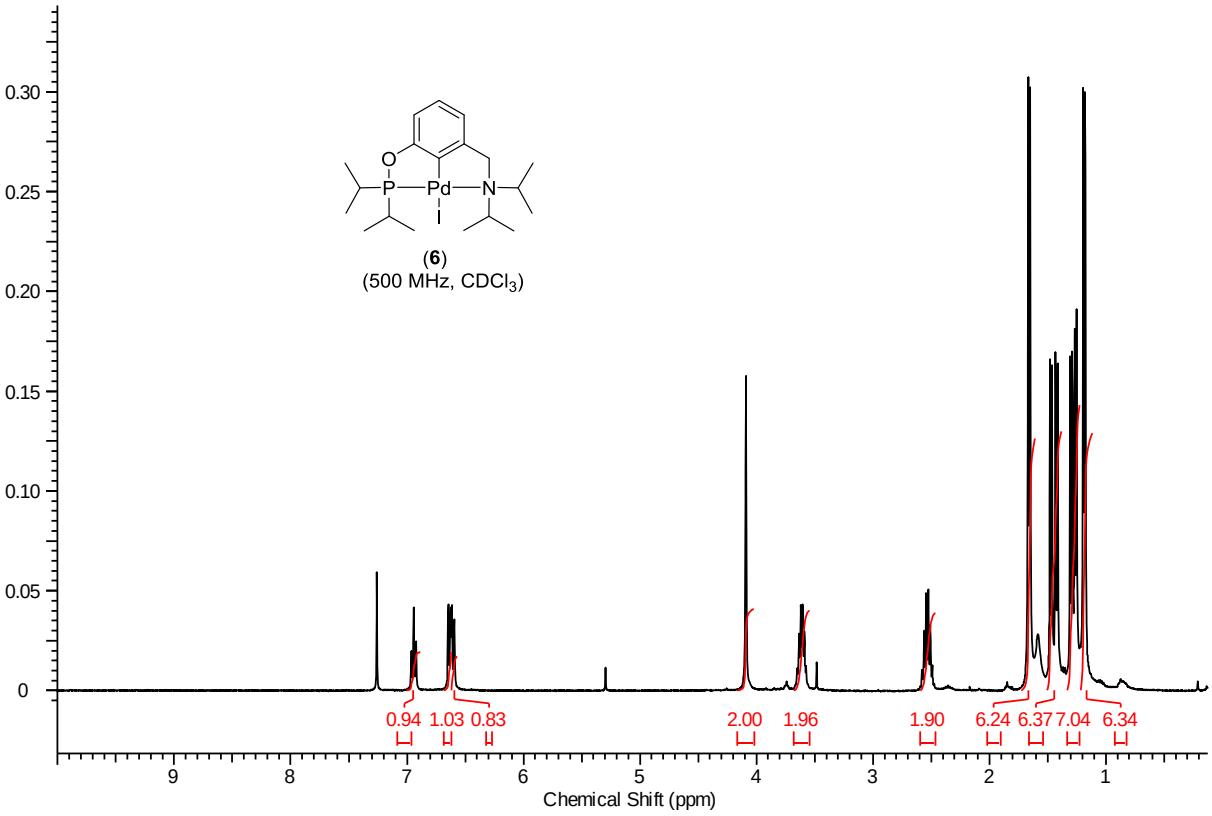
(6)
(500 MHz, CDCl3)
0.94 1.03 0.83
2.00 1.96
1.90
6.24 6.37 7.04 6.34
Chemical Shift (ppm)

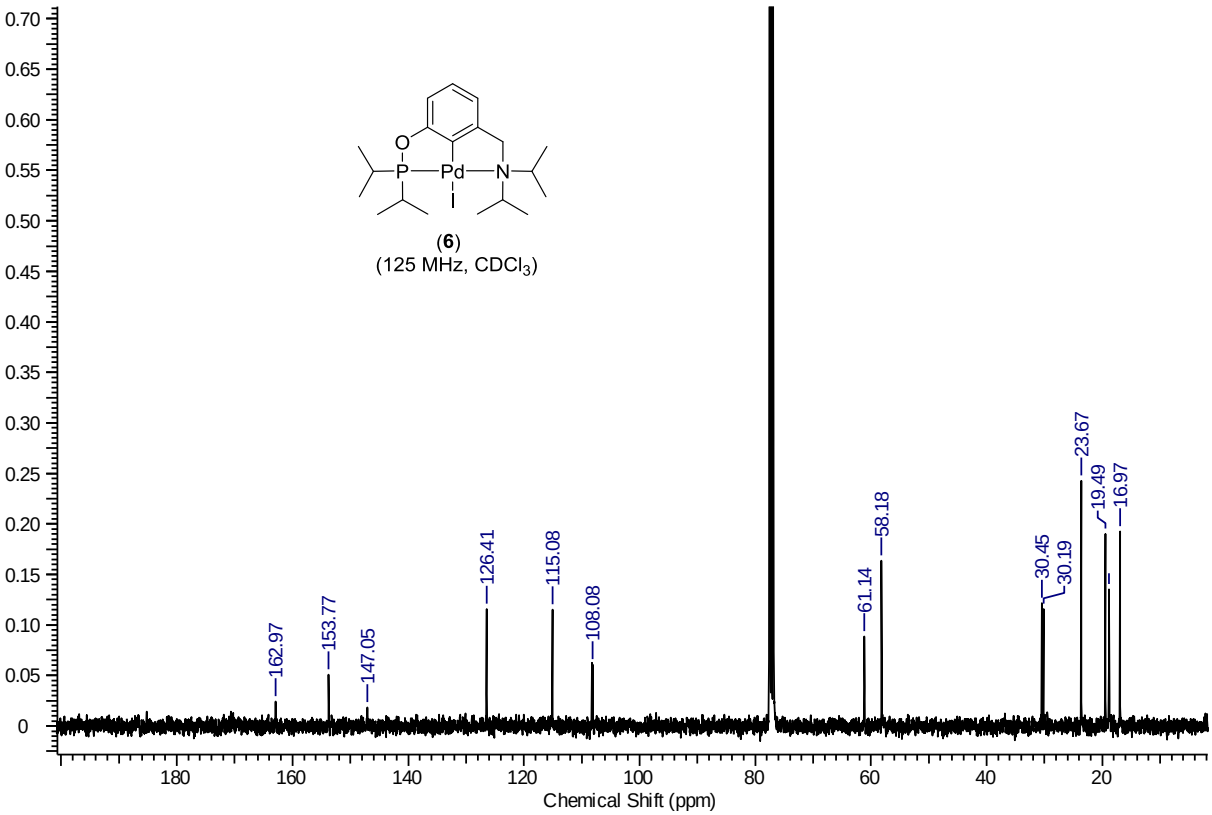
(6)
(125 MHz, CDCl3)
162.97
153.77
147.05
126.41
115.08
108.08
61.14
58.18
30.45
30.19
23.67
19.49
16.97
Chemical Shift (ppm)

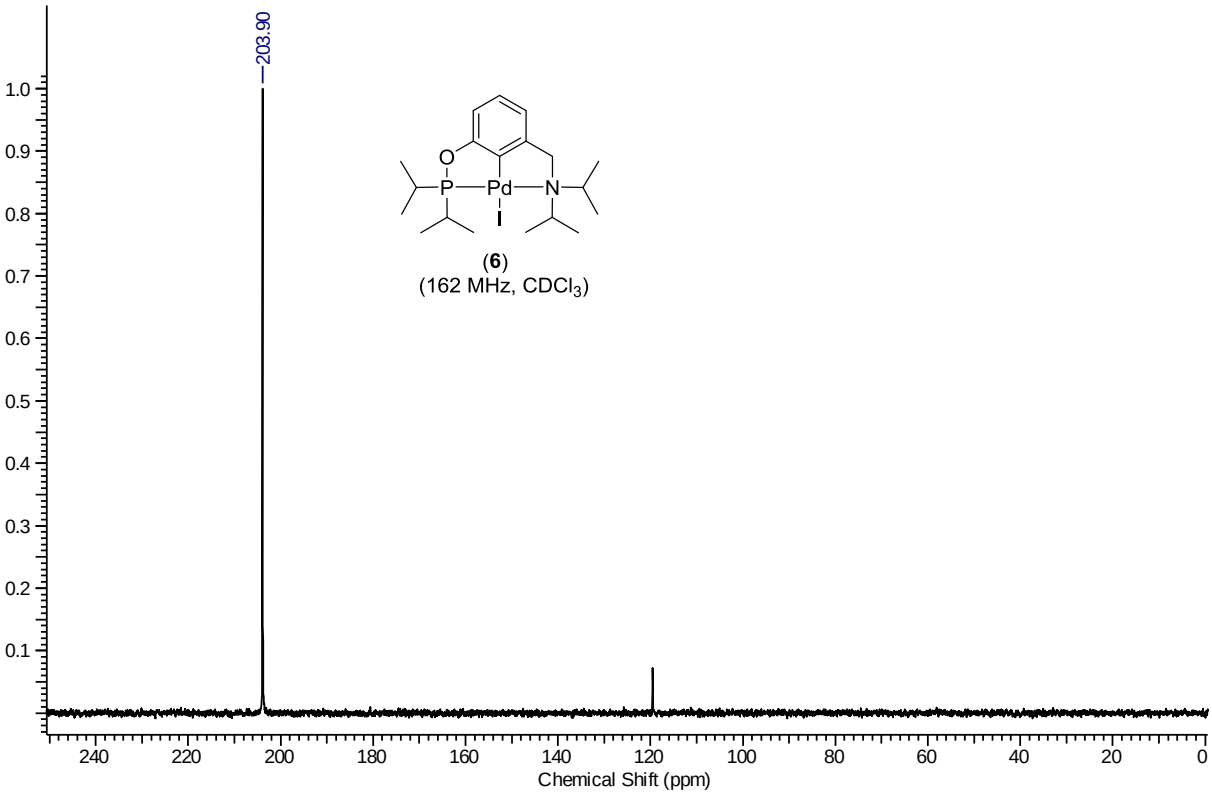
203.90
O
P
Pd
N
I
(6)
(162 MHz, CDCl3)
Chemical Shift (ppm)

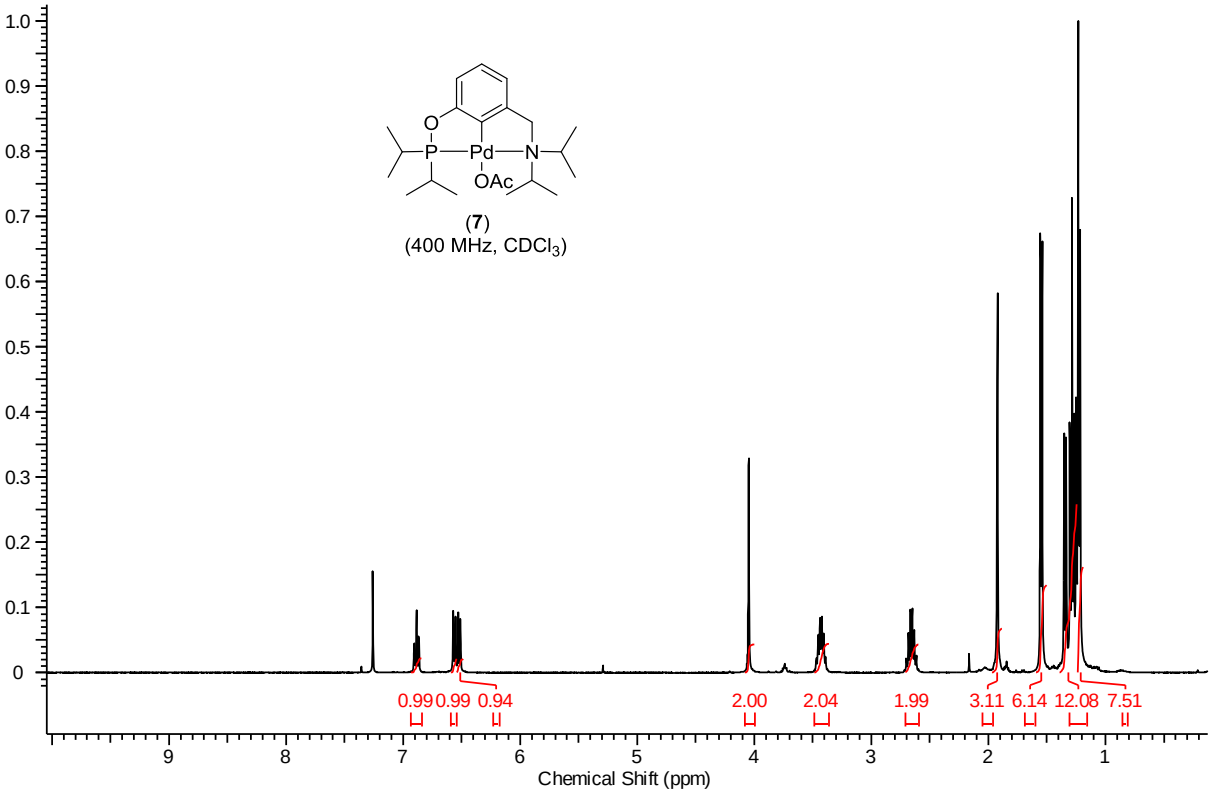
O
P
Pd
N
OAc
(7)
(400 MHz, CDCl3)
0.99 0.99 0.94
2.00
2.04
1.99
3.11
6.14
12.08
7.51
Chemical Shift (ppm)

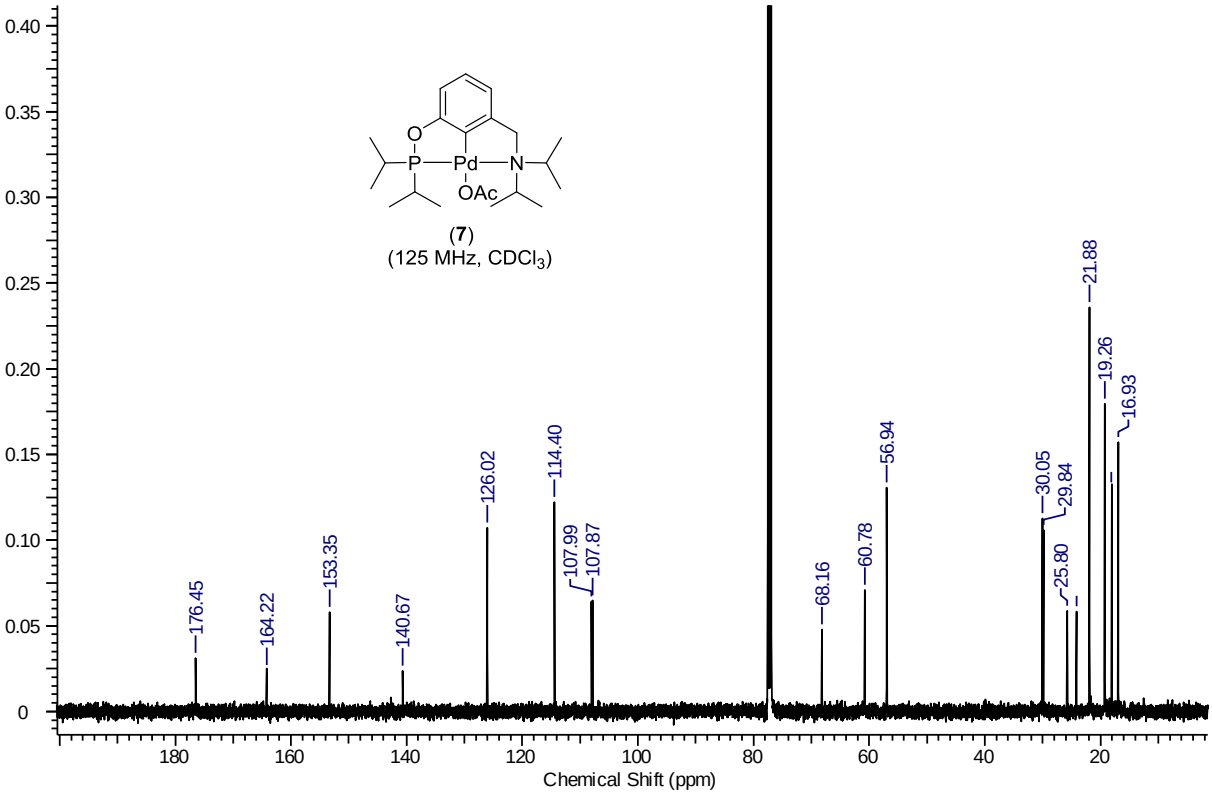
(7)
(125 MHz, CDCl3)
176.45
164.22
153.35
140.67
126.02
114.40
107.99
107.87
68.16
60.78
56.94
30.05
29.84
25.80
21.88
19.26
16.93
Chemical Shift (ppm)

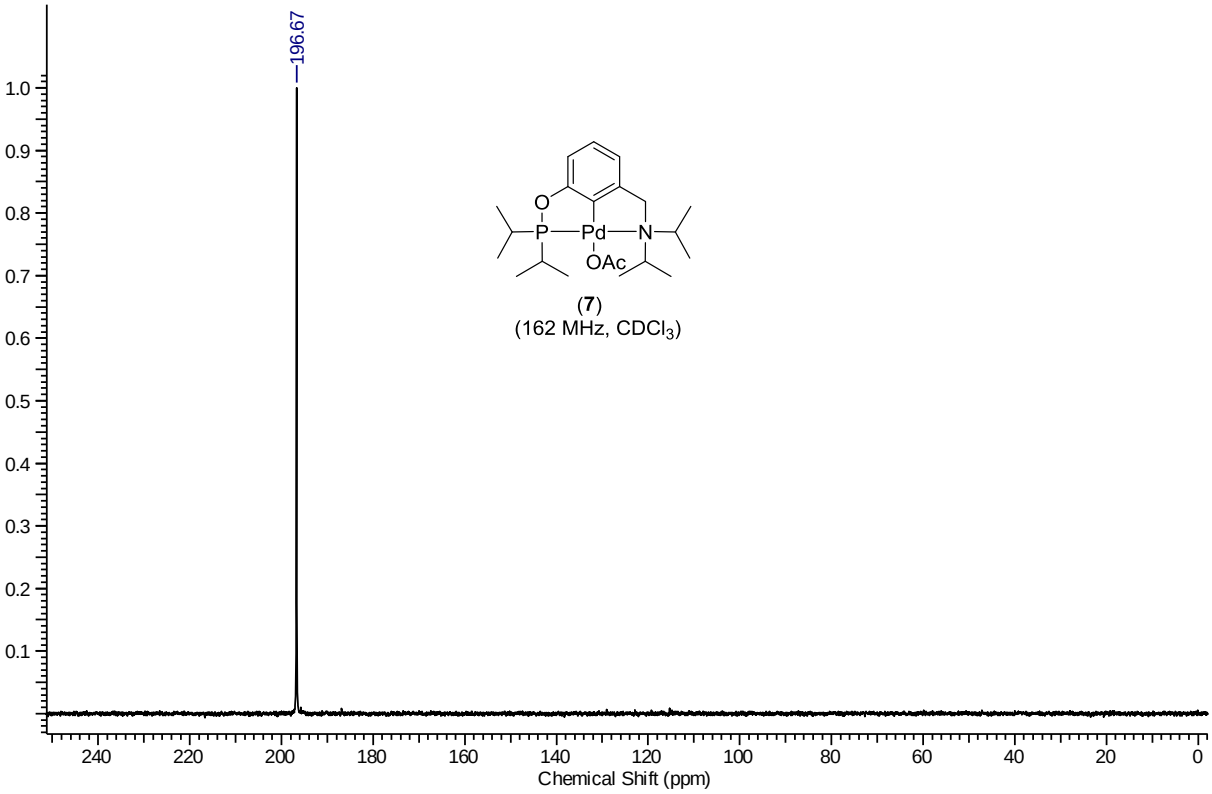
196.67
(7)
(162 MHz, CDCl3)
Chemical Shift (ppm)

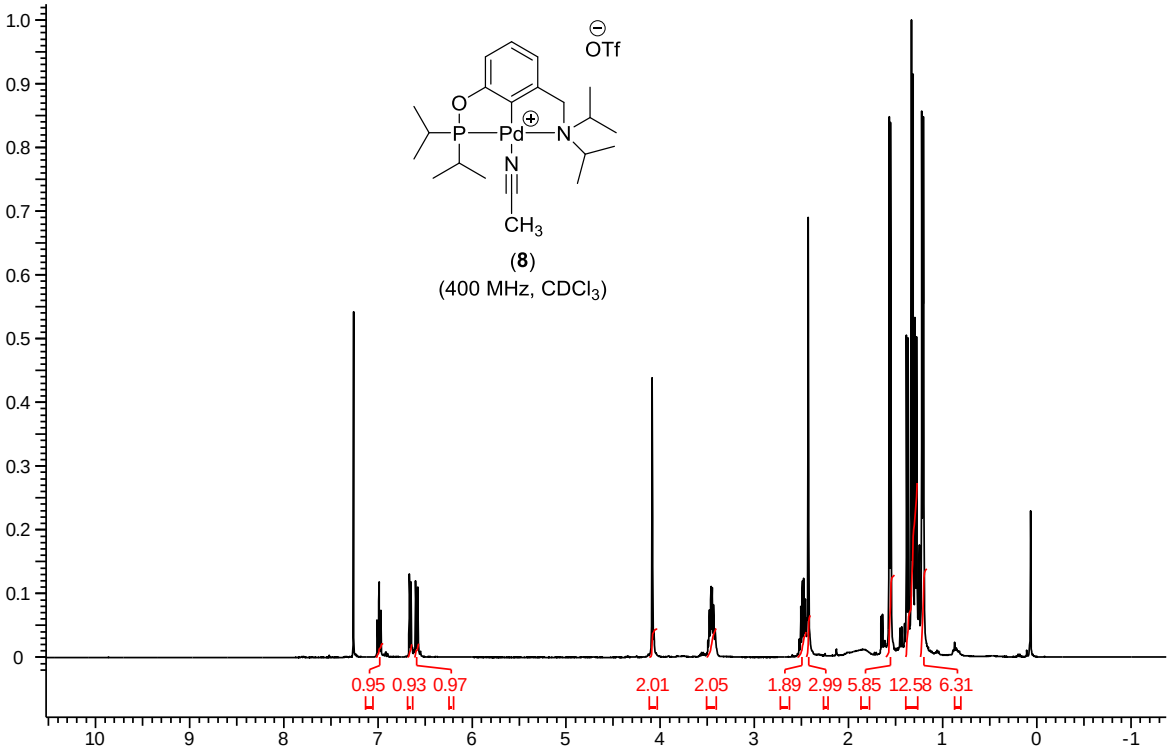
OTf
(8)
(400 MHz, CDCl3)
0.95 0.93 0.97
2.01 2.05
1.89 2.99 5.85 12.58 6.31

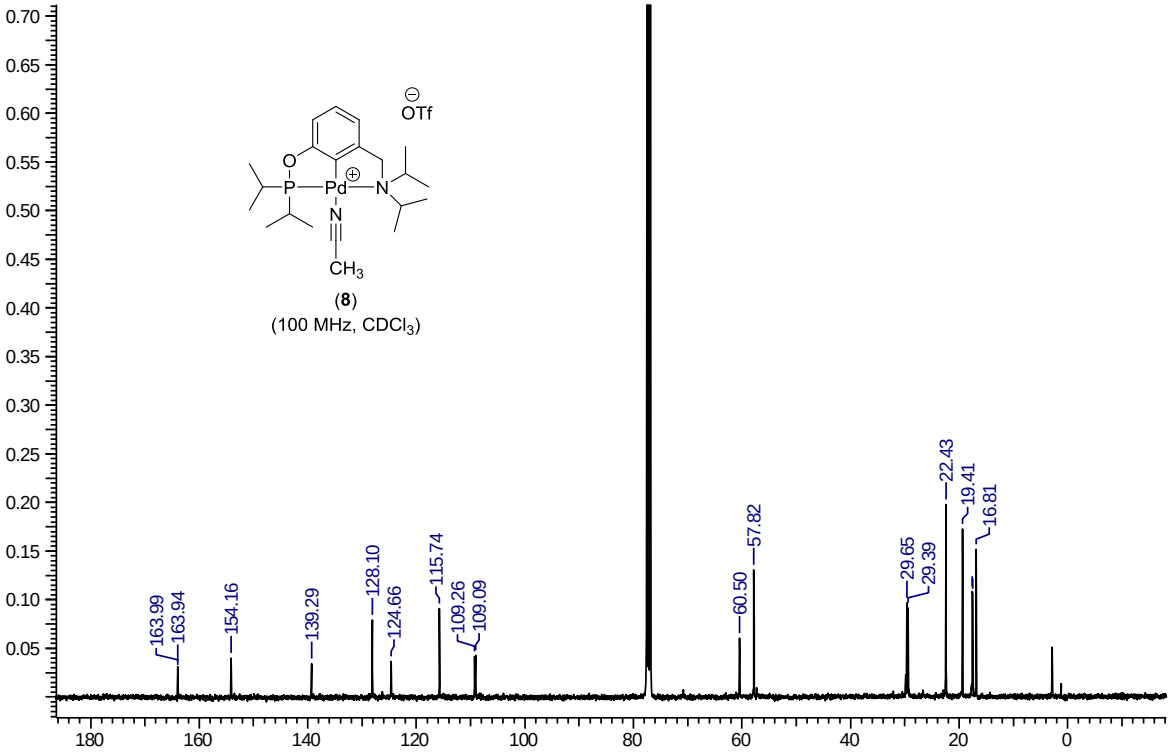
OTf
(8)
(100 MHz, CDCl3)
163.99
163.94
154.16
139.29
128.10
124.66
115.74
109.26
109.09
60.50
57.82
29.65
29.39
22.43
19.41
16.81

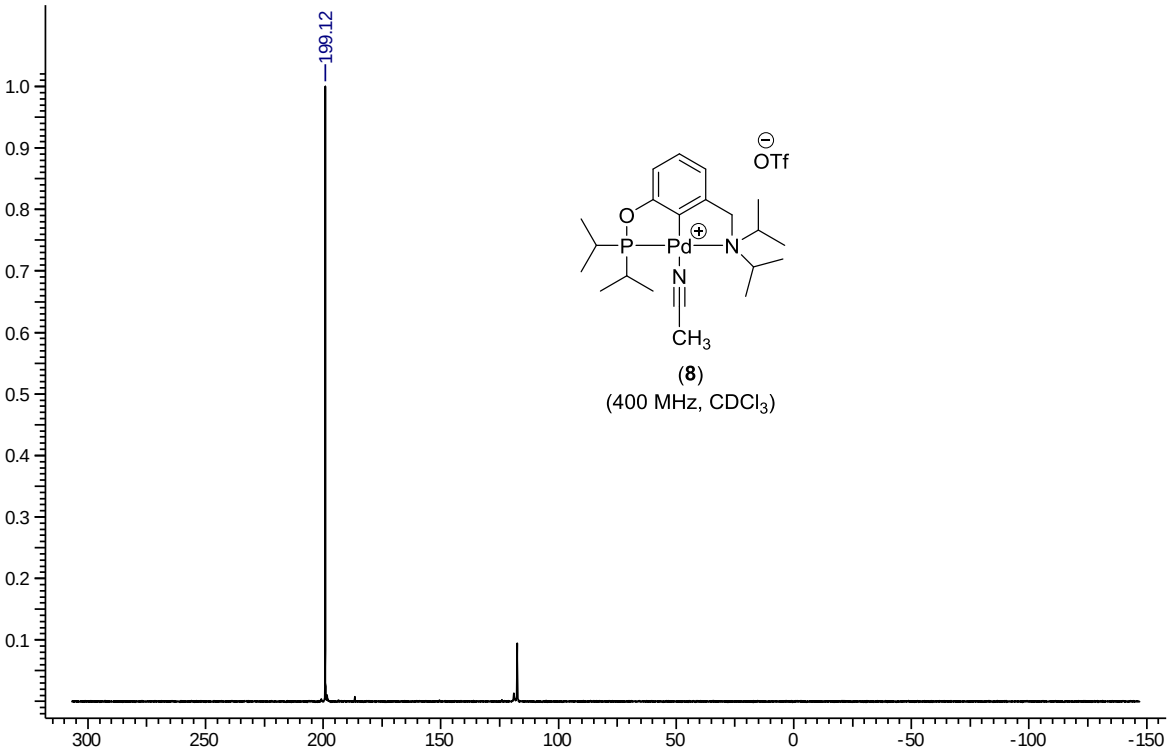

(**8**)
(400 MHz, $CDCl_3$)

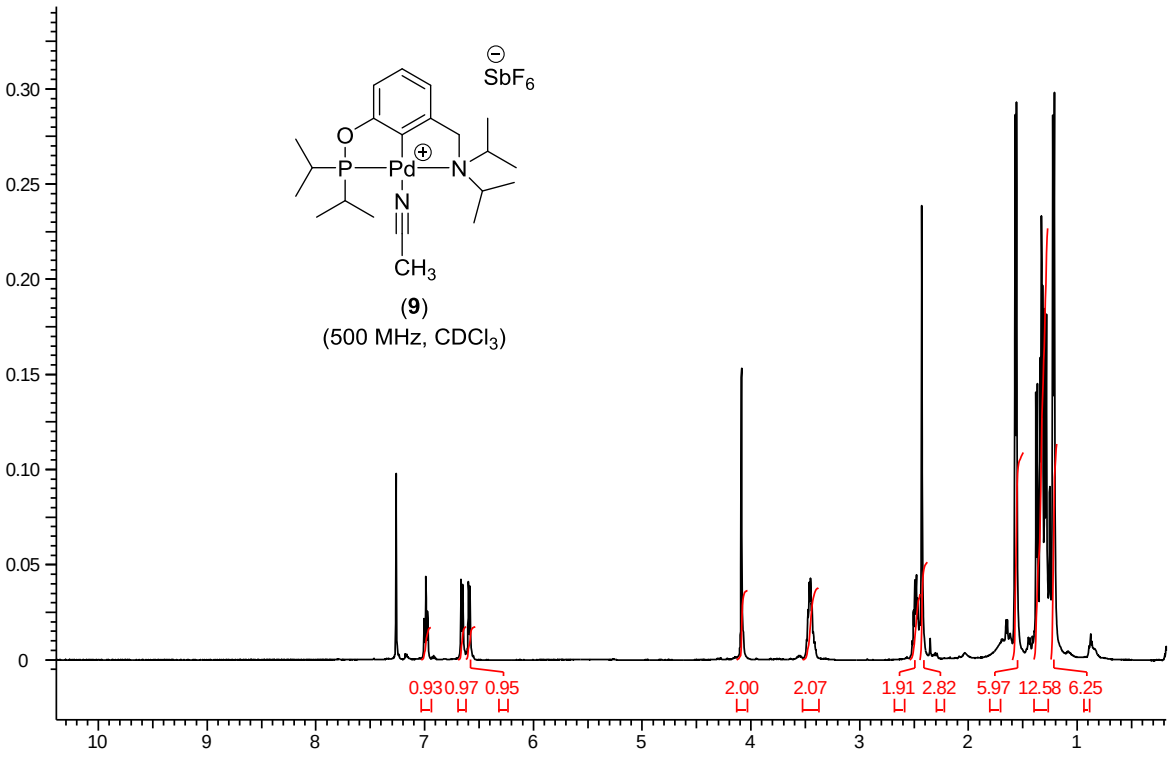

(**9**)
(500 MHz, $CDCl_3$)

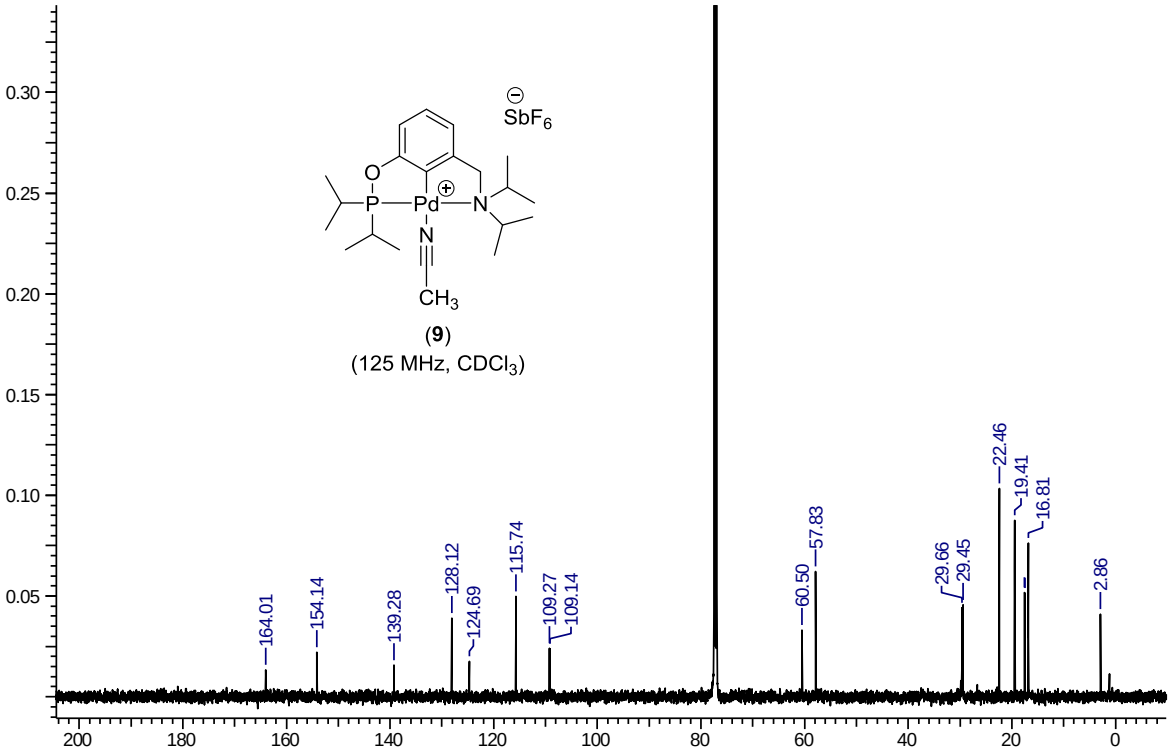
SbF6
O
P
Pd
N
N
CH3
(9)
(125 MHz, CDCl3)
164.01
154.14
139.28
128.12
124.69
115.74
109.27
109.14
60.50
57.83
29.66
29.45
22.46
19.41
16.81
2.86

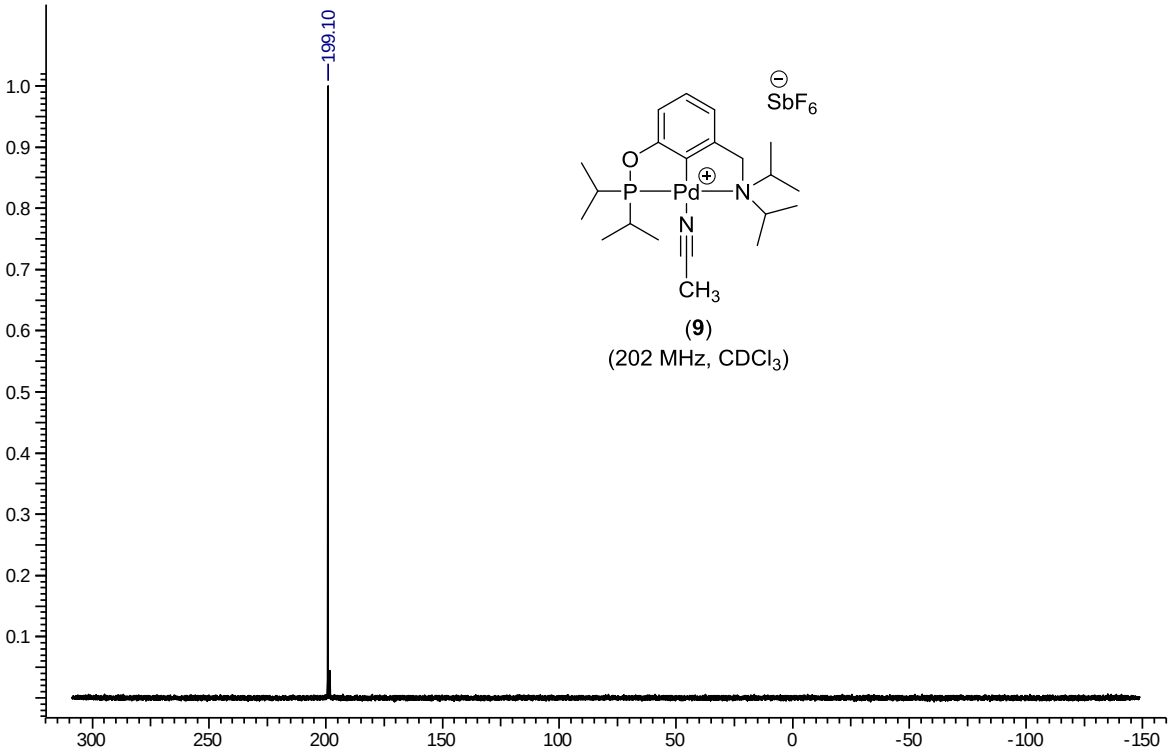
199.10
SbF6
O
P
Pd
N
N
CH3
(9)
(202 MHz, CDCl3)

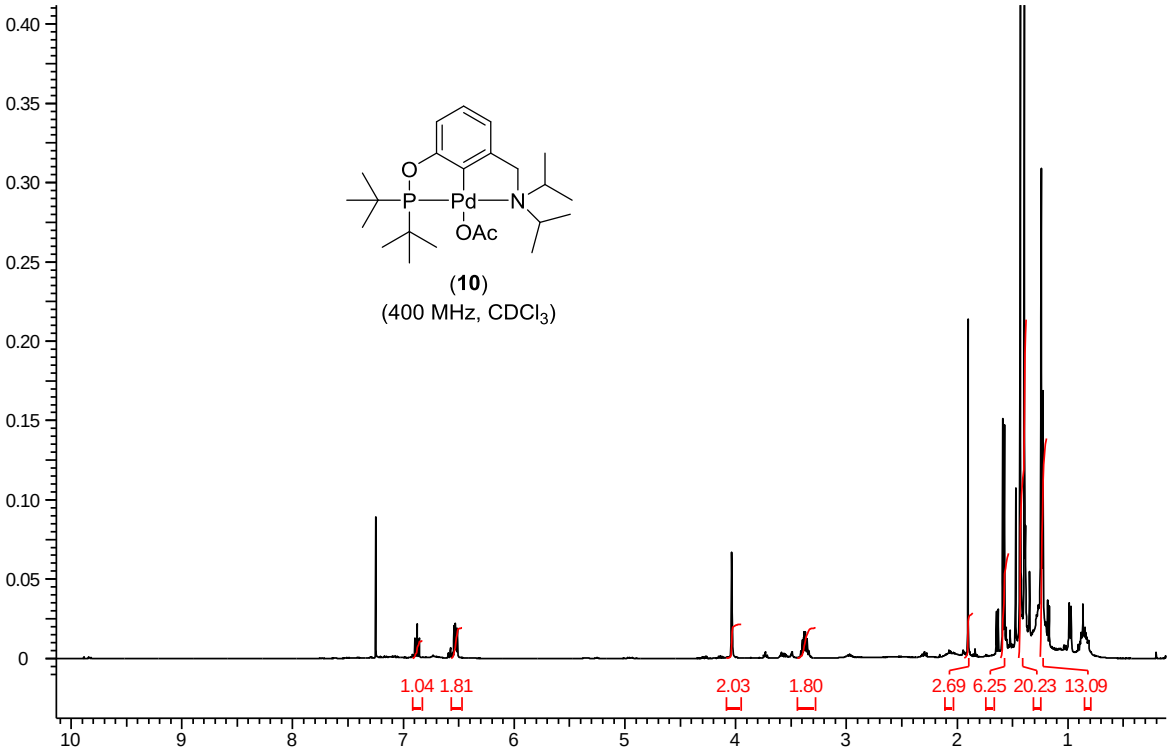
O
P
Pd
N
OAc
(10)
(400 MHz, CDCl3)
1.04
1.81
2.03
1.80
2.69
6.25
20.23
13.09

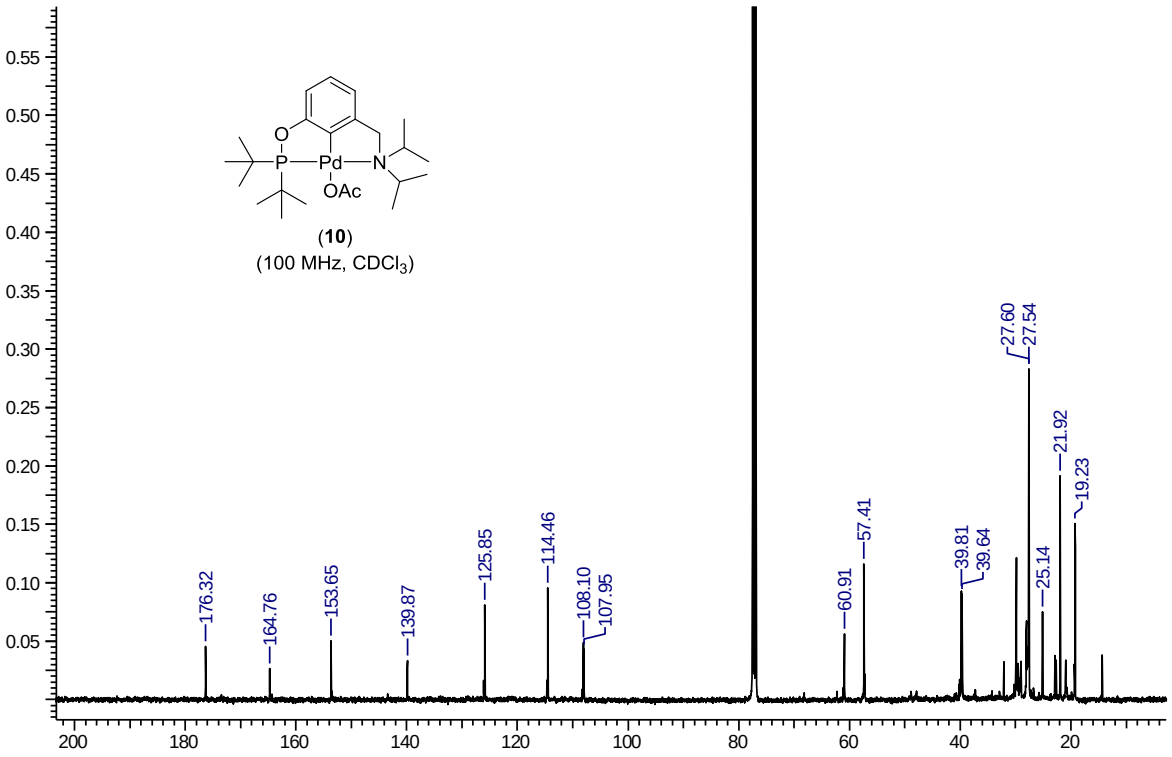
O
P
Pd
N
OAc
(10)
(100 MHz, CDCl3)
176.32
164.76
153.65
139.87
125.85
114.46
108.10
107.95
60.91
57.41
39.81
39.64
27.60
27.54
25.14
21.92
19.23

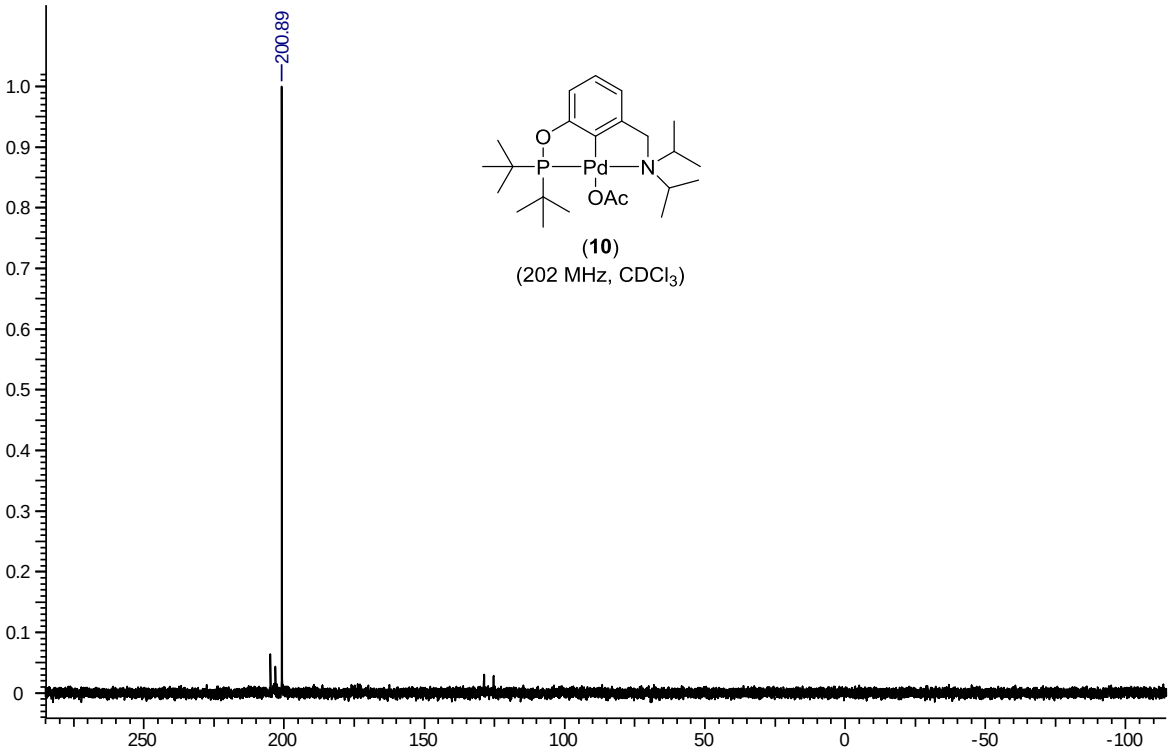
200.89
O
P
Pd
N
OAc
(10)
(202 MHz, CDCl3)

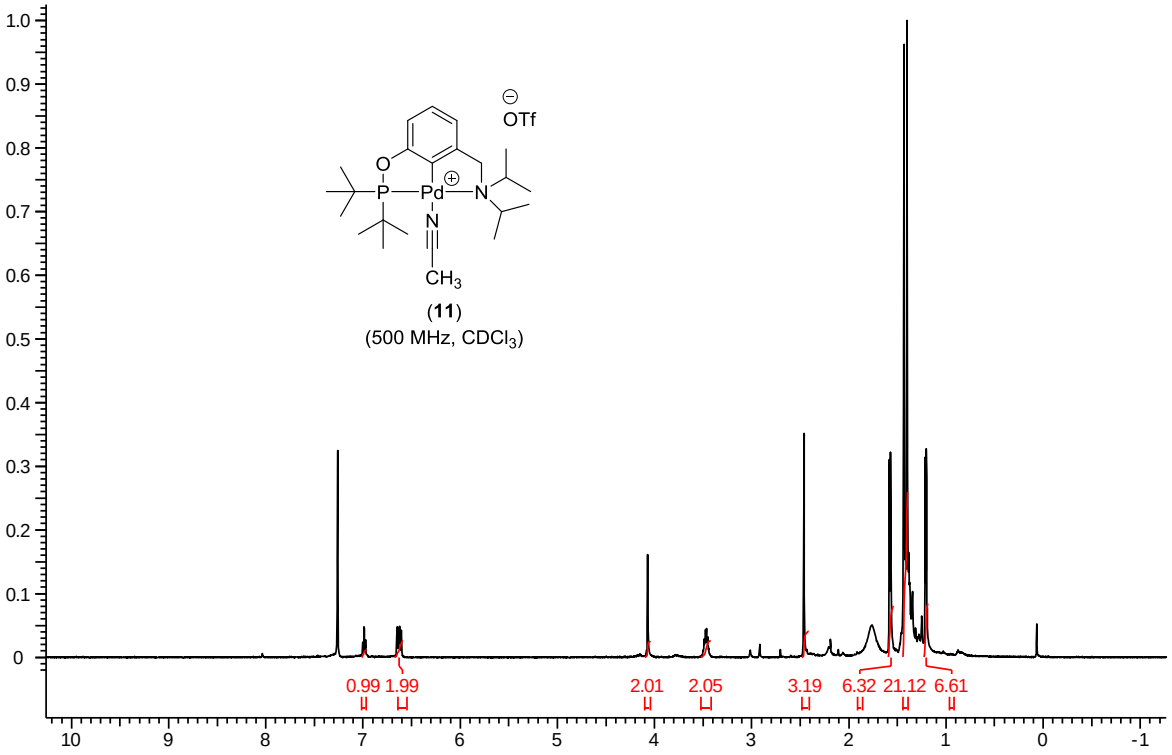
OTf
O
P
Pd
N
N
CH3
(11)
(500 MHz, CDCl3)
0.99
1.99
2.01
2.05
3.19
6.32
21.12
6.61

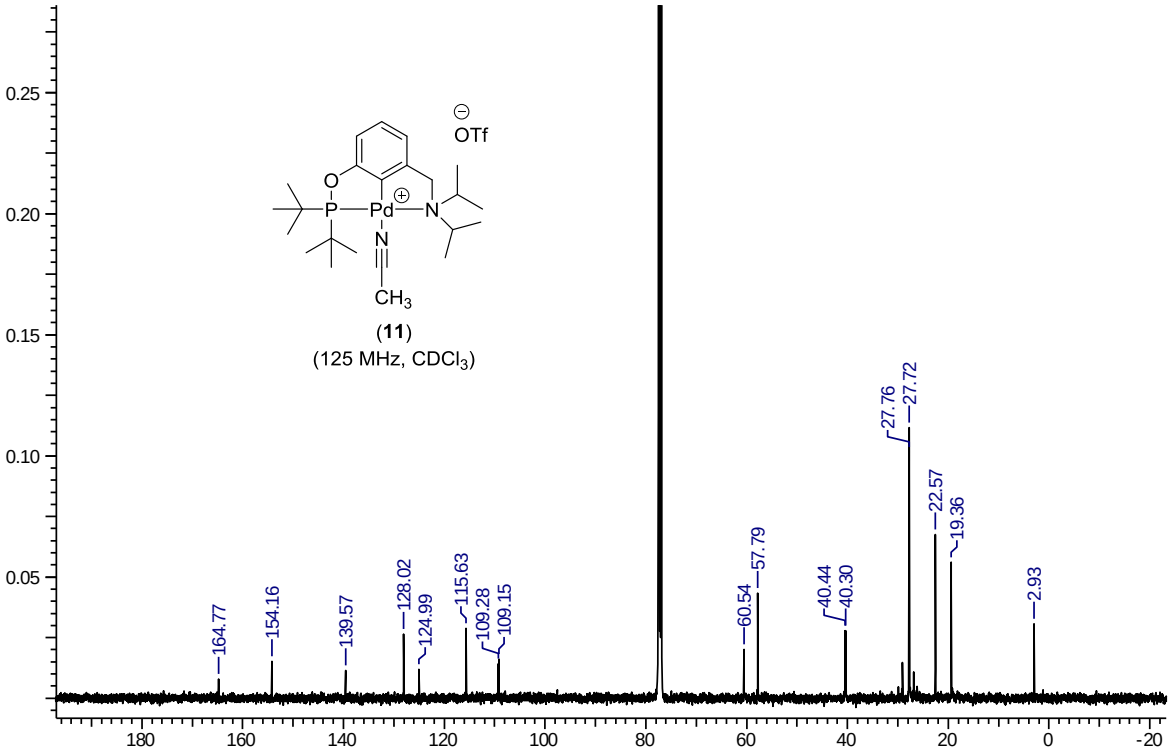
OTf
O
P
Pd
N
N
CH3
(11)
(125 MHz, CDCl3)
164.77
154.16
139.57
128.02
124.99
115.63
109.28
109.15
60.54
57.79
40.44
40.30
27.76
27.72
22.57
19.36
2.93

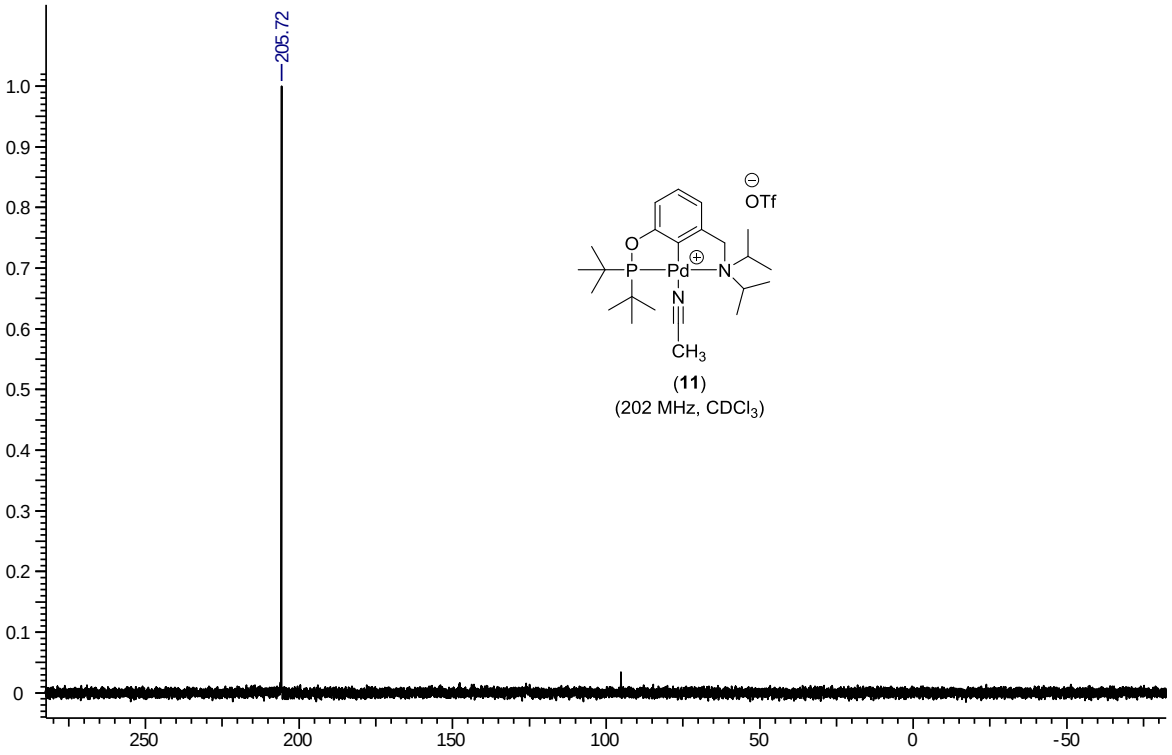
205.72
OTf
O
P
Pd
N
N
CH3
(11)
(202 MHz, CDCl3)

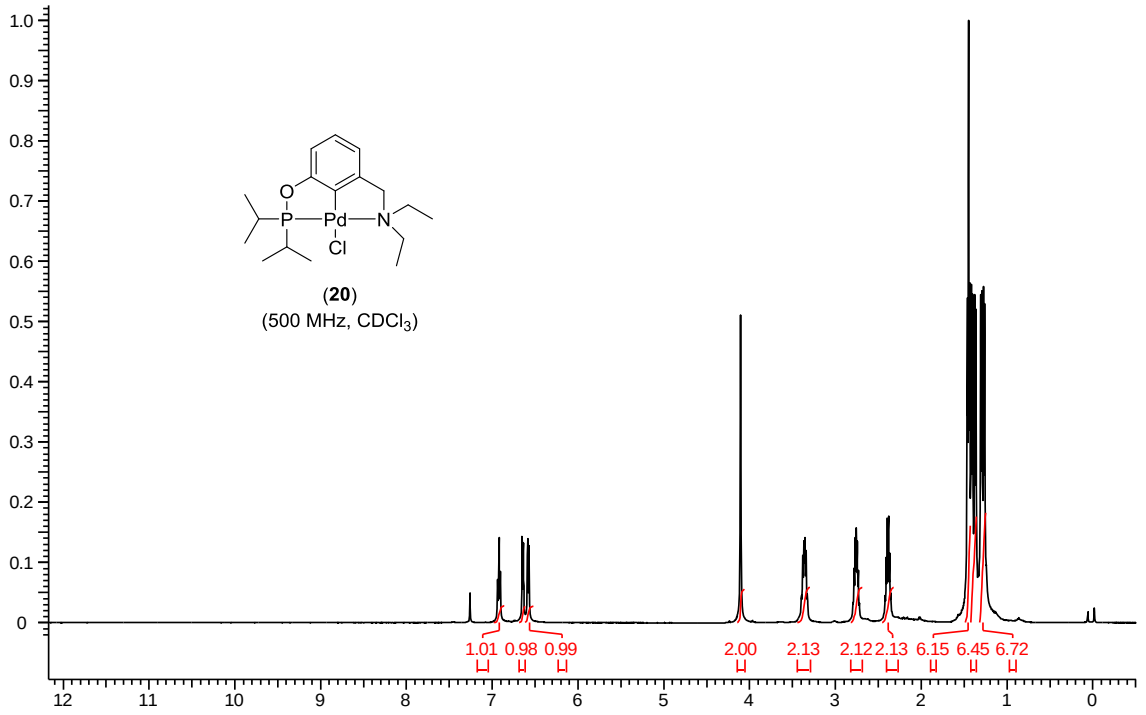
(20)
(500 MHz, CDCl3)
1.01 0.98 0.99
2.00
2.13
2.12 2.13
6.15 6.45 6.72

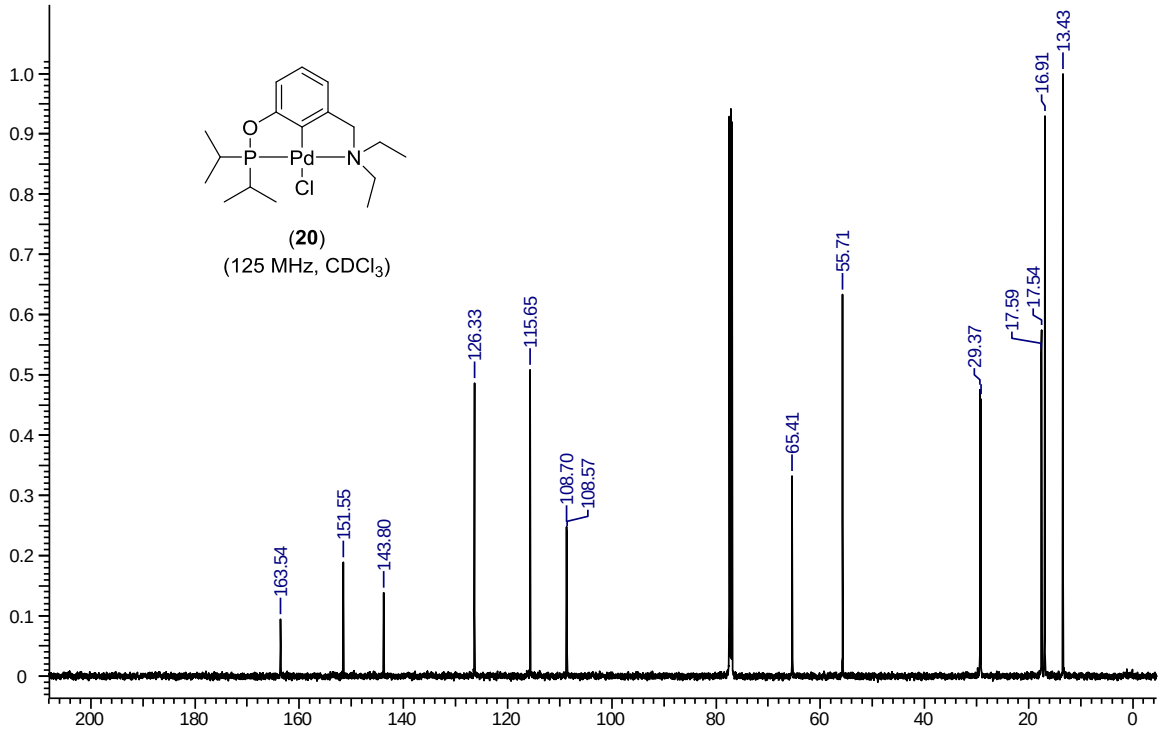
(20)
(125 MHz, CDCl3)
163.54
151.55
143.80
126.33
115.65
108.70
108.57
65.41
55.71
29.37
17.59
17.54
16.91
13.43

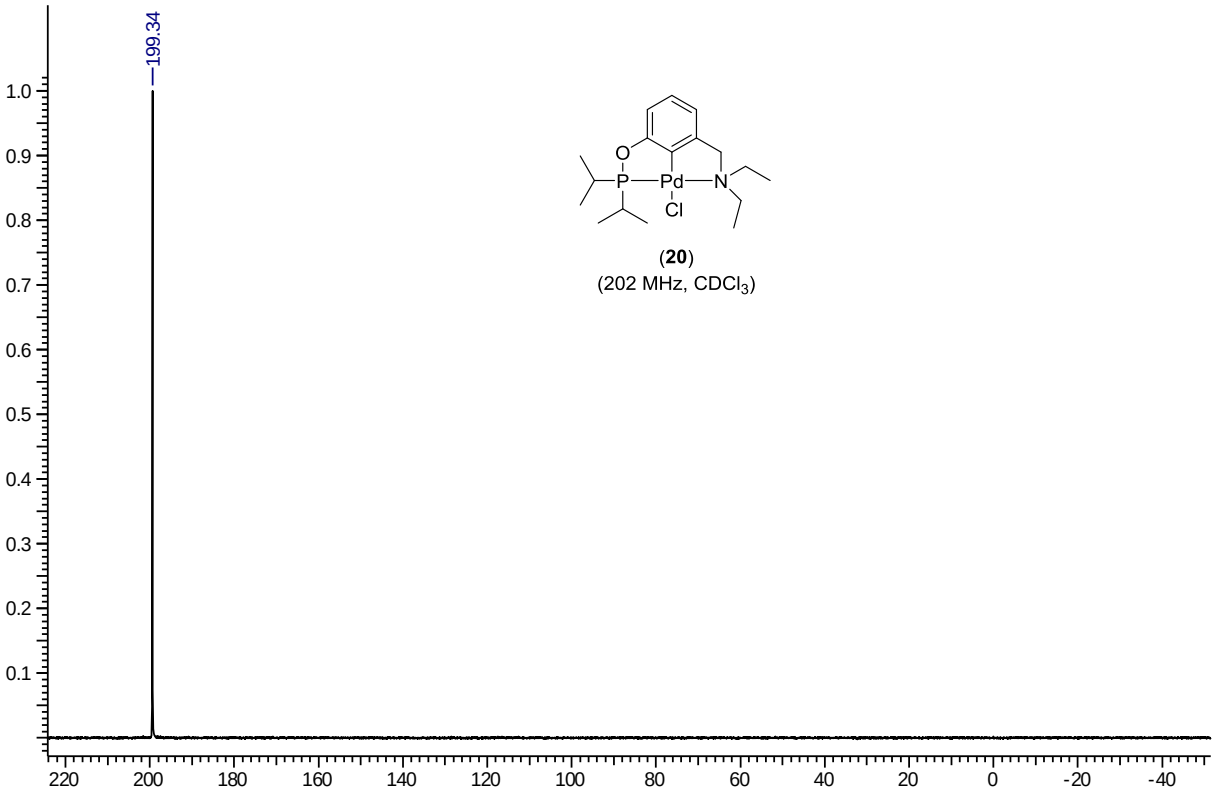

(**20**)
(202 MHz, $CDCl_3$)

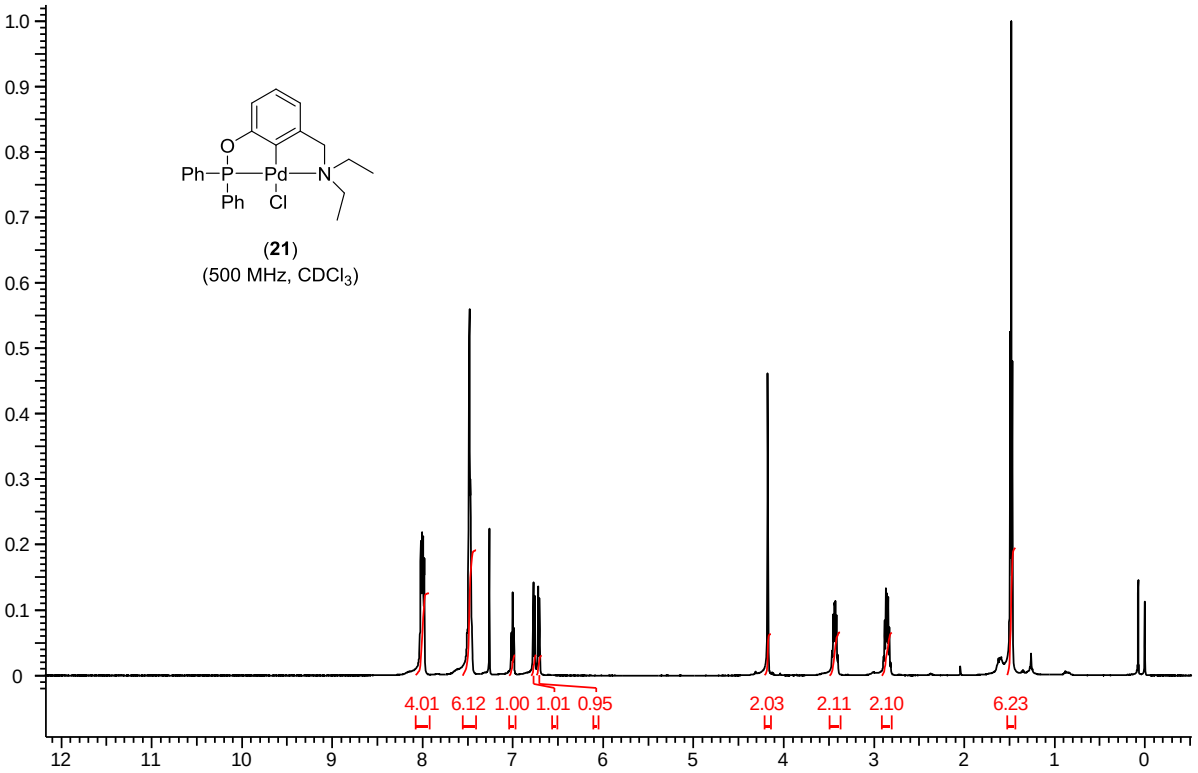

(**21**)
(500 MHz, $CDCl_3$)

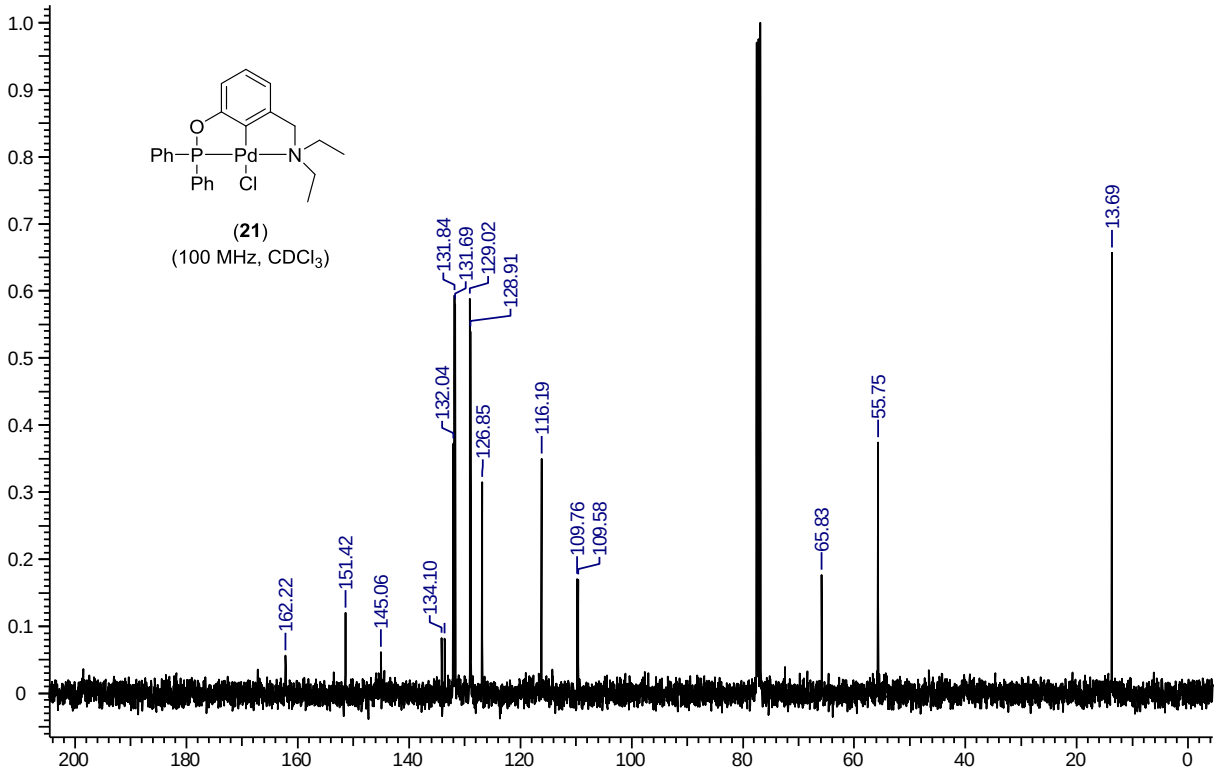
O
Ph—P—Pd—N
Ph Cl
(21)
(100 MHz, CDCl3)
162.22
151.42
145.06
134.10
132.04
131.84
131.69
129.02
128.91
126.85
116.19
109.76
109.58
65.83
55.75
13.69

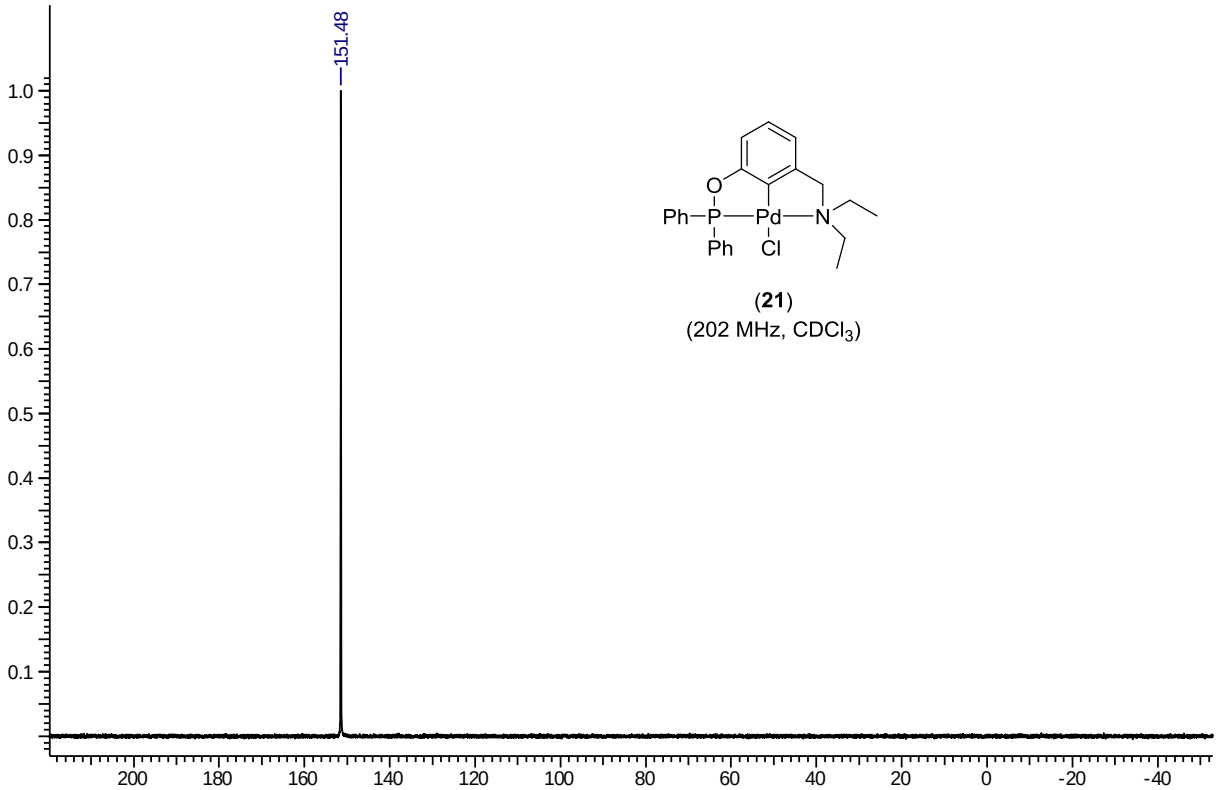
151.48
O
Ph—P—Pd—N
Ph Cl
(21)
(202 MHz, CDCl3)

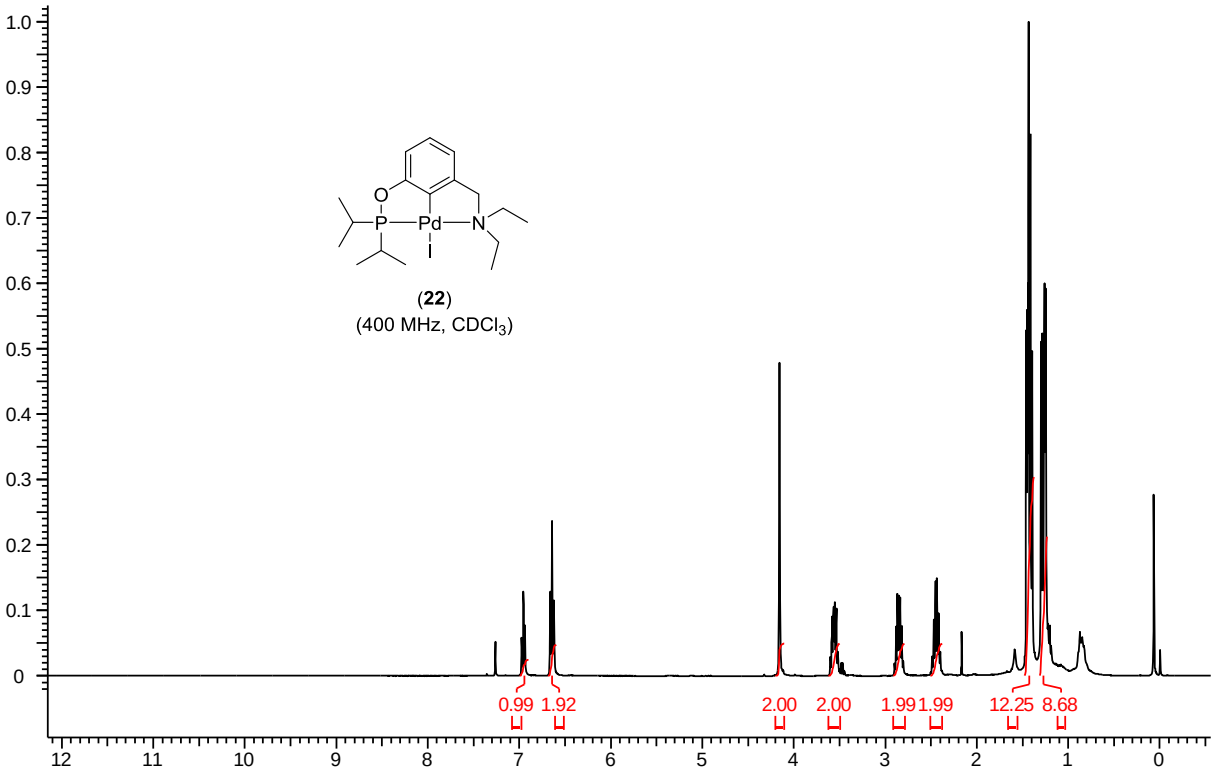
(22)
(400 MHz, CDCl3)
0.99
1.92
2.00
2.00
1.99
1.99
12.25
8.68

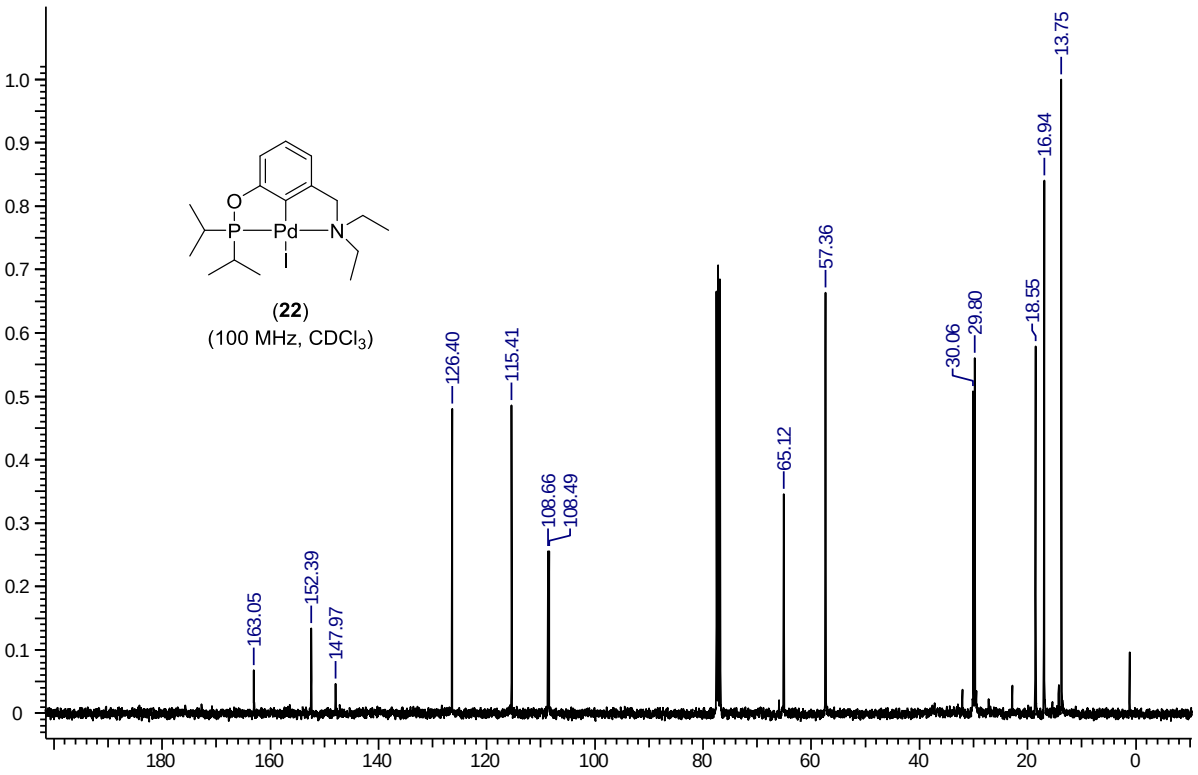
(22)
(100 MHz, CDCl3)
163.05
152.39
147.97
126.40
115.41
108.66
108.49
65.12
57.36
30.06
29.80
18.55
16.94
13.75

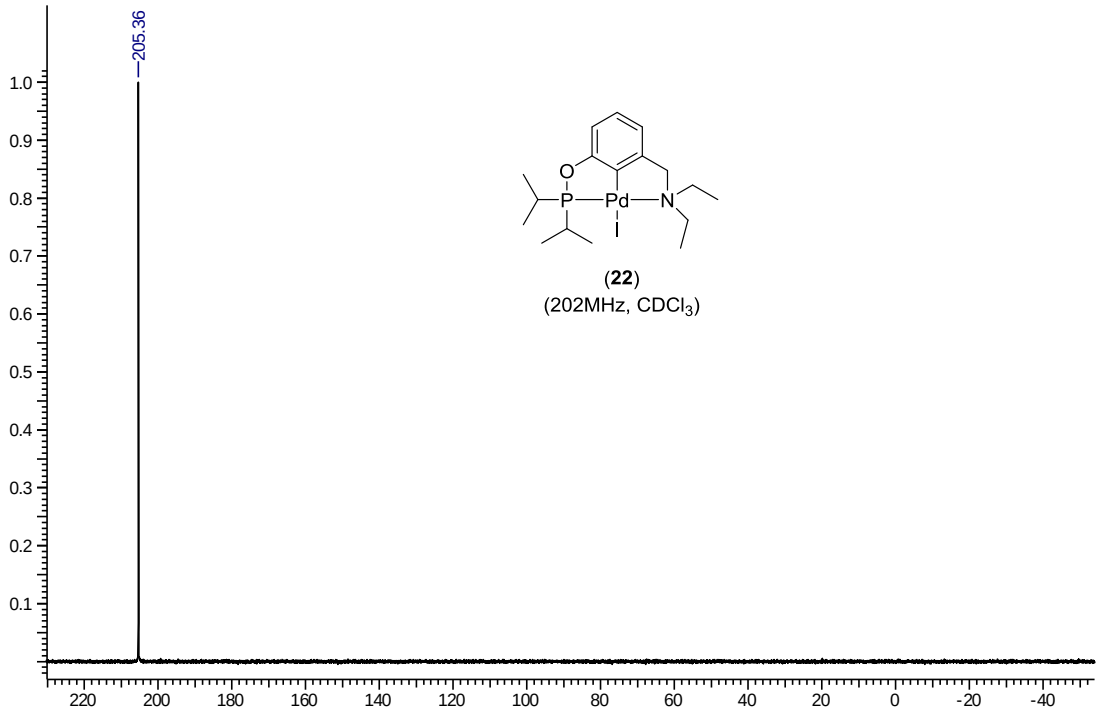

(**22**)
(202MHz, $CDCl_3$)

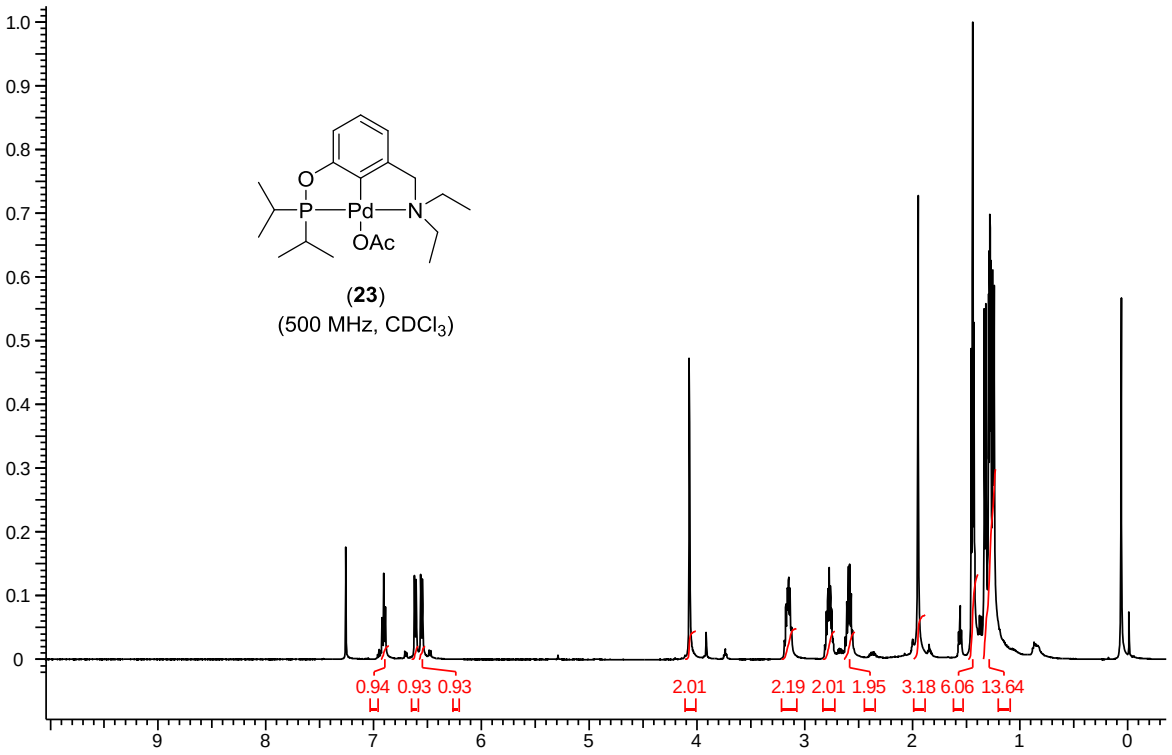

(**23**)
(500 MHz, $CDCl_3$)

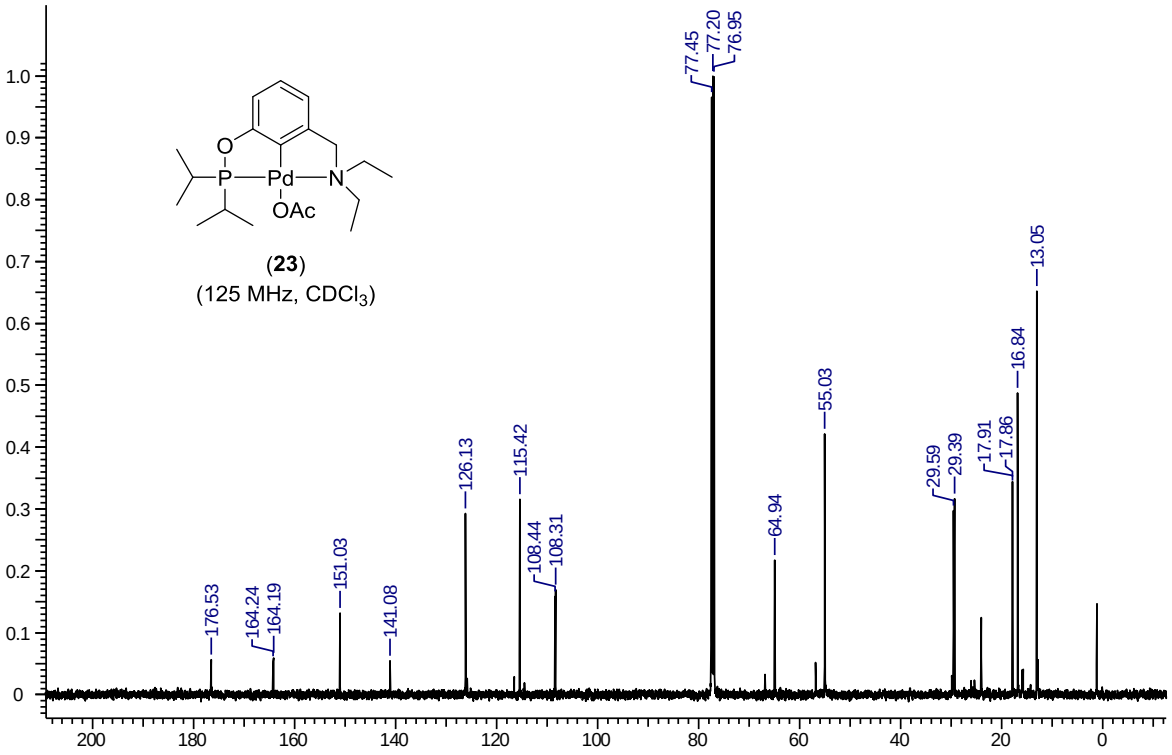
77.45
77.20
76.95
13.05
16.84
55.03
29.59
29.39
17.91
17.86
64.94
126.13
115.42
108.44
108.31
151.03
176.53
164.24
164.19
141.08
O
P
Pd
N
OAc
(23)
(125 MHz, CDCl3)

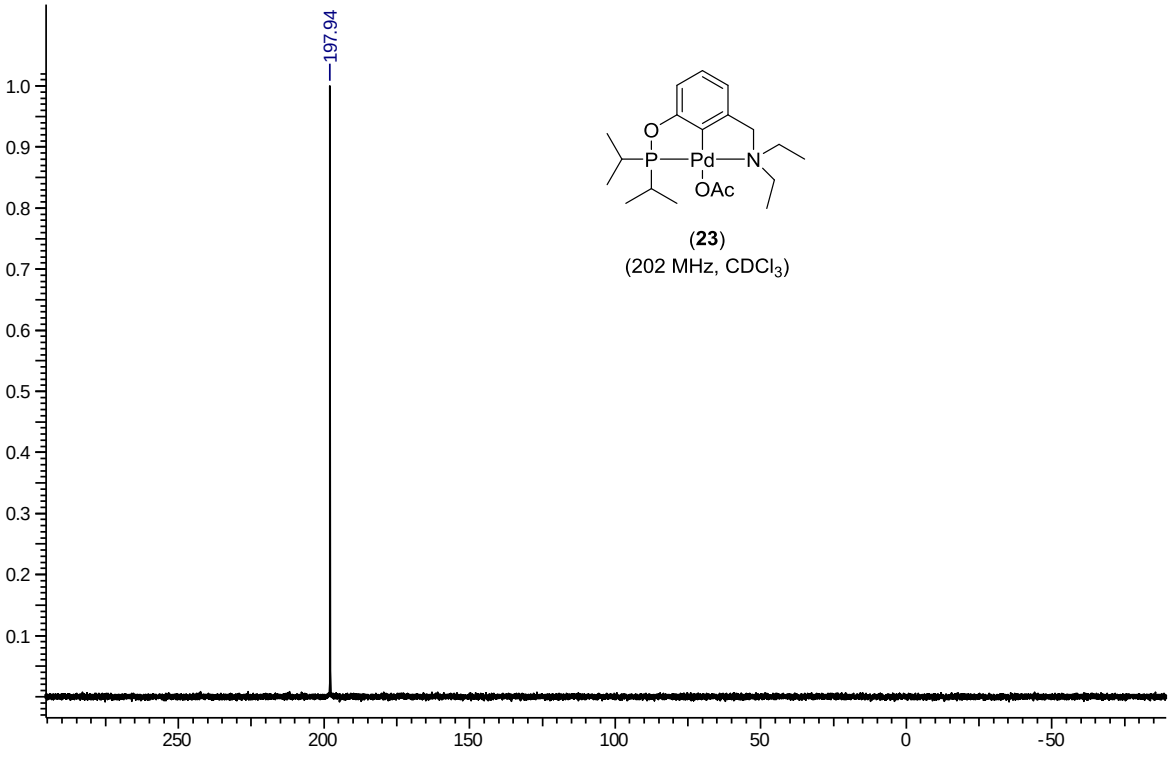
197.94
O
P
Pd
N
OAc
(23)
(202 MHz, CDCl3)

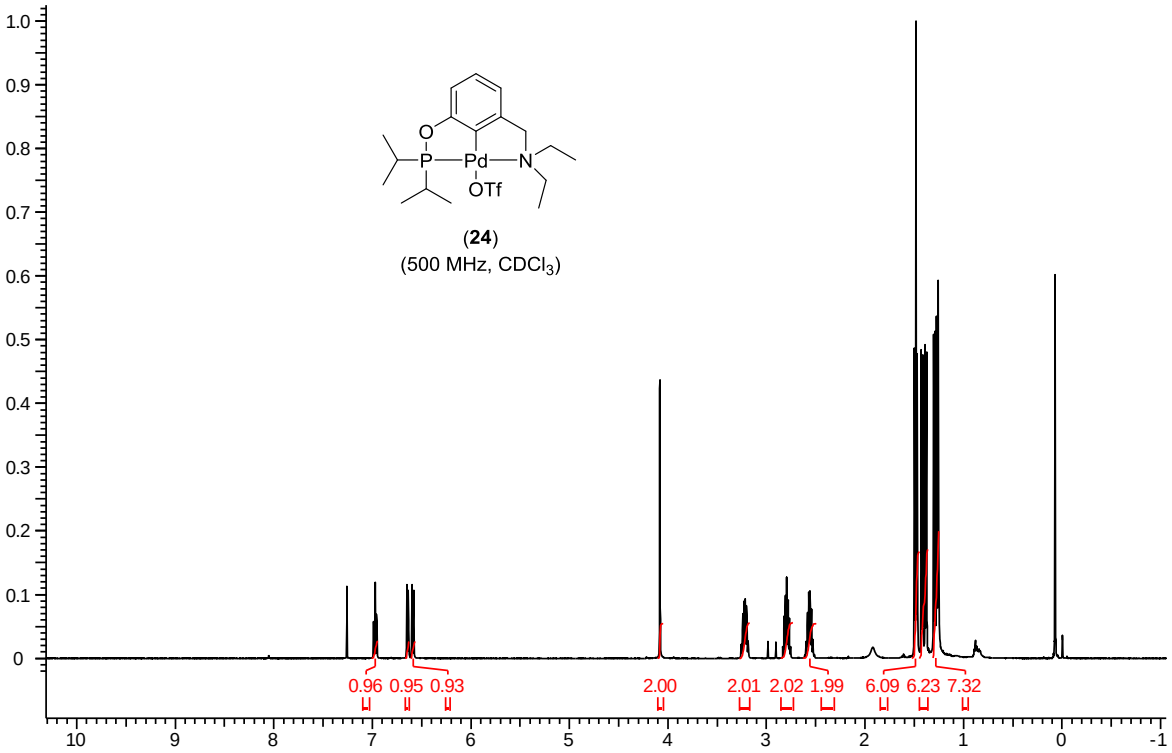
O
P
Pd
N
OTf
(24)
(500 MHz, CDCl3)
0.96 0.95 0.93
2.00
2.01 2.02 1.99
6.09 6.23 7.32

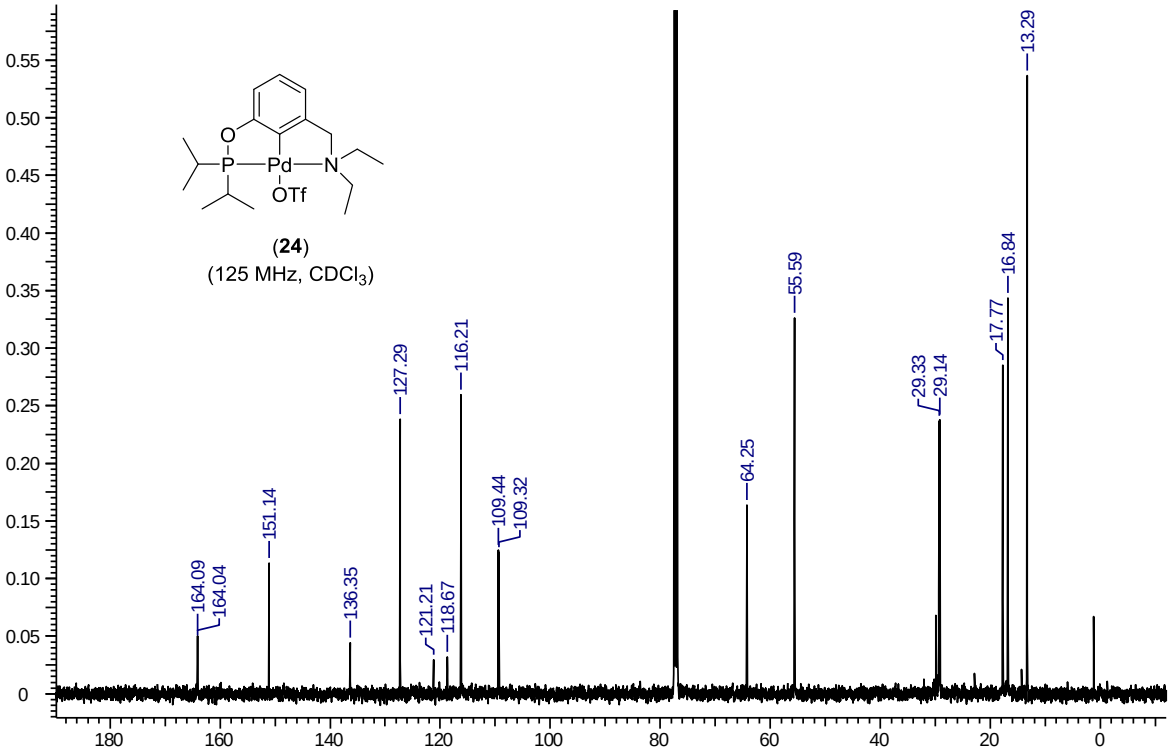
O
P
Pd
N
OTf
(24)
(125 MHz, CDCl3)
164.09
164.04
151.14
136.35
127.29
121.21
118.67
116.21
109.44
109.32
64.25
55.59
29.33
29.14
17.77
16.84
13.29

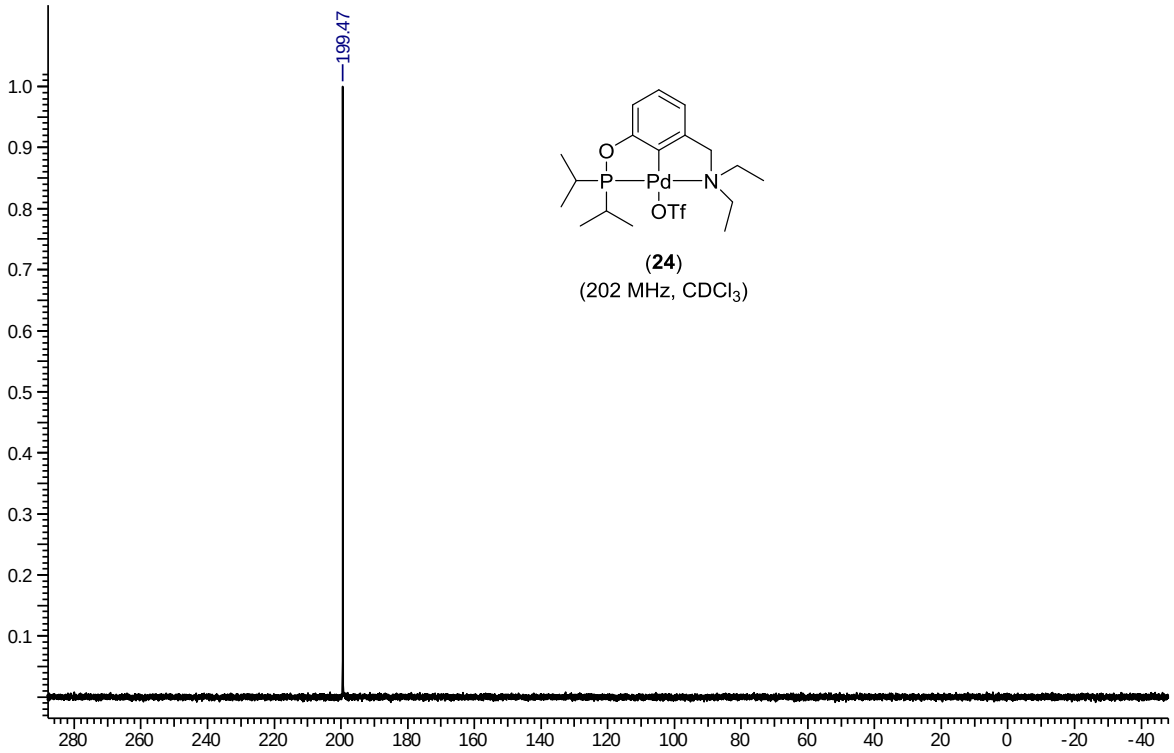

(**24**)
(202 MHz, $CDCl_3$)

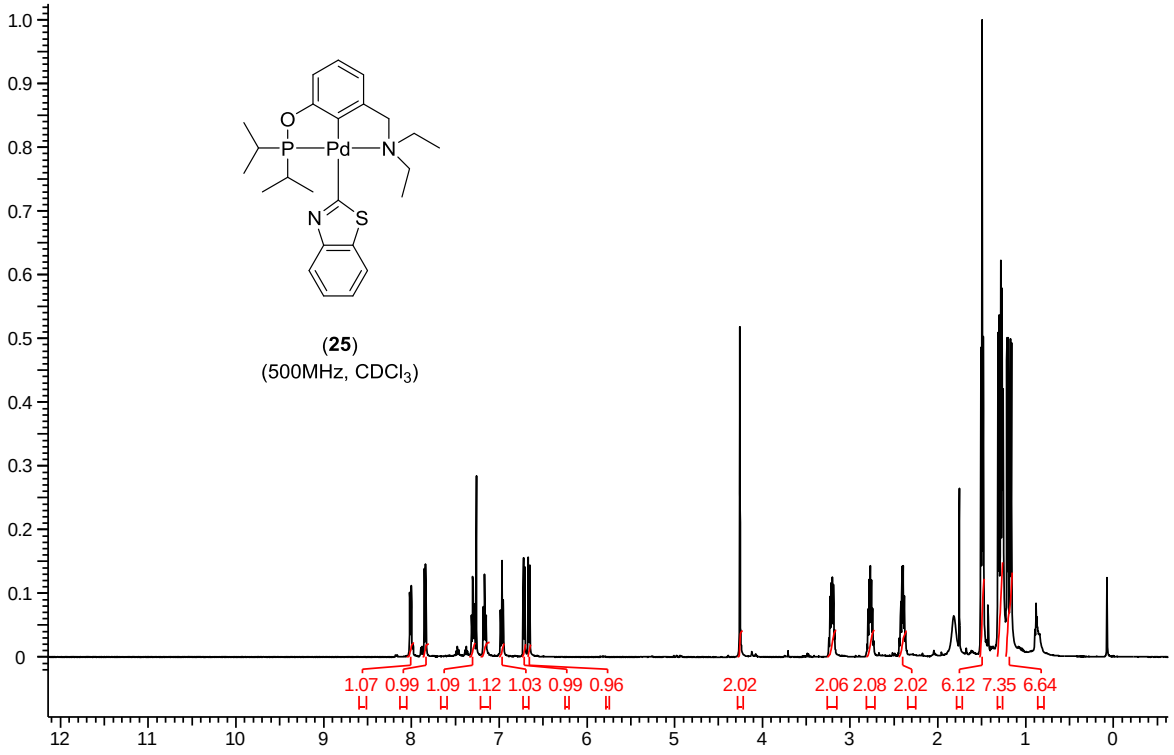

(**25**)
(500MHz, $CDCl_3$)

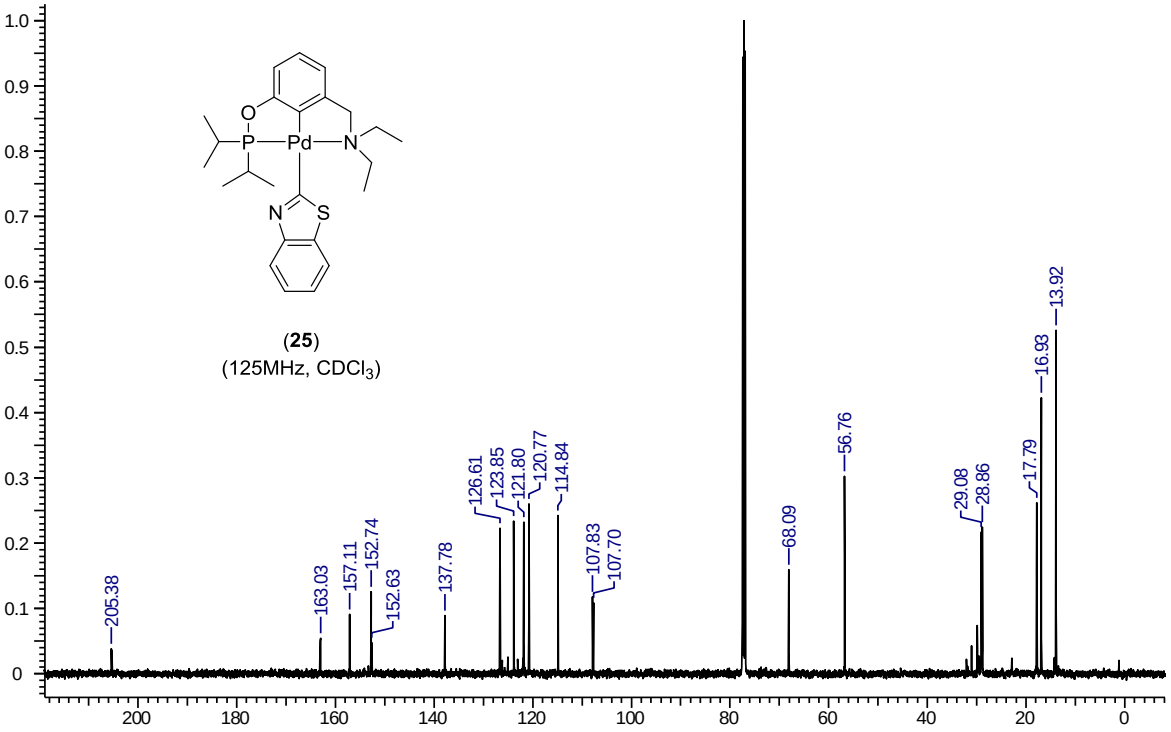

(**25**)
(125MHz, $CDCl_3$)

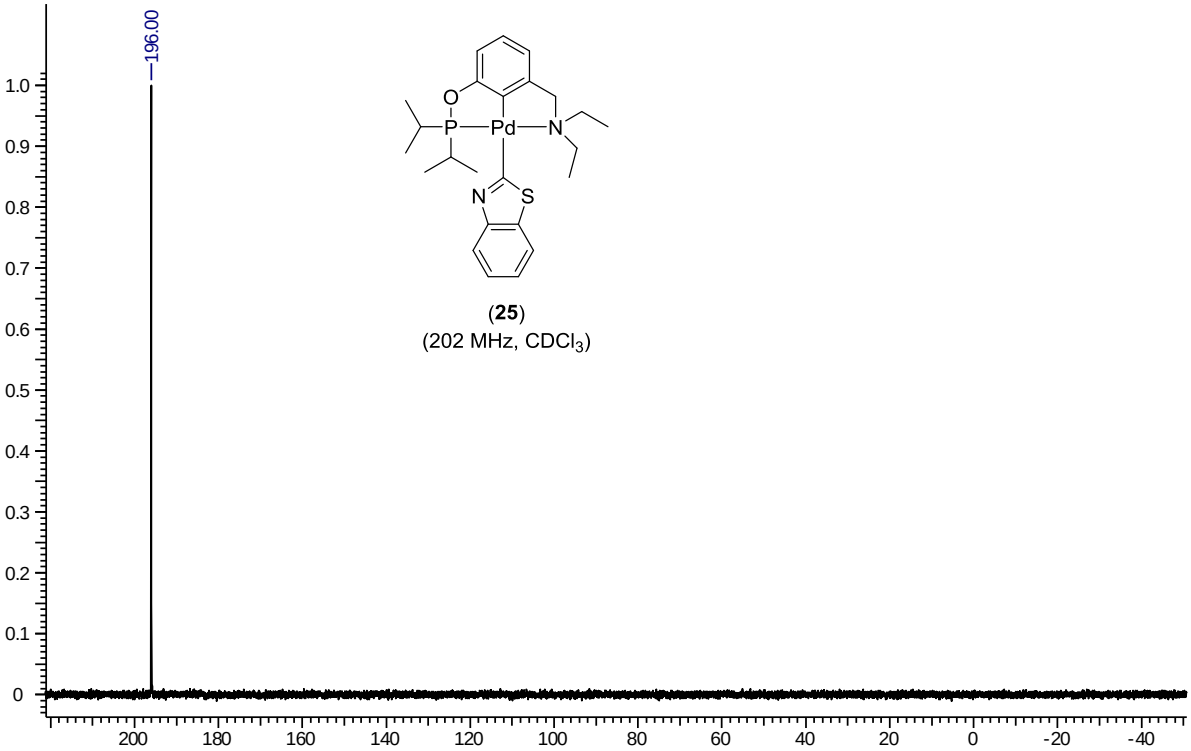

(**25**)
(202 MHz, $CDCl_3$)

HR-MS of Complexes

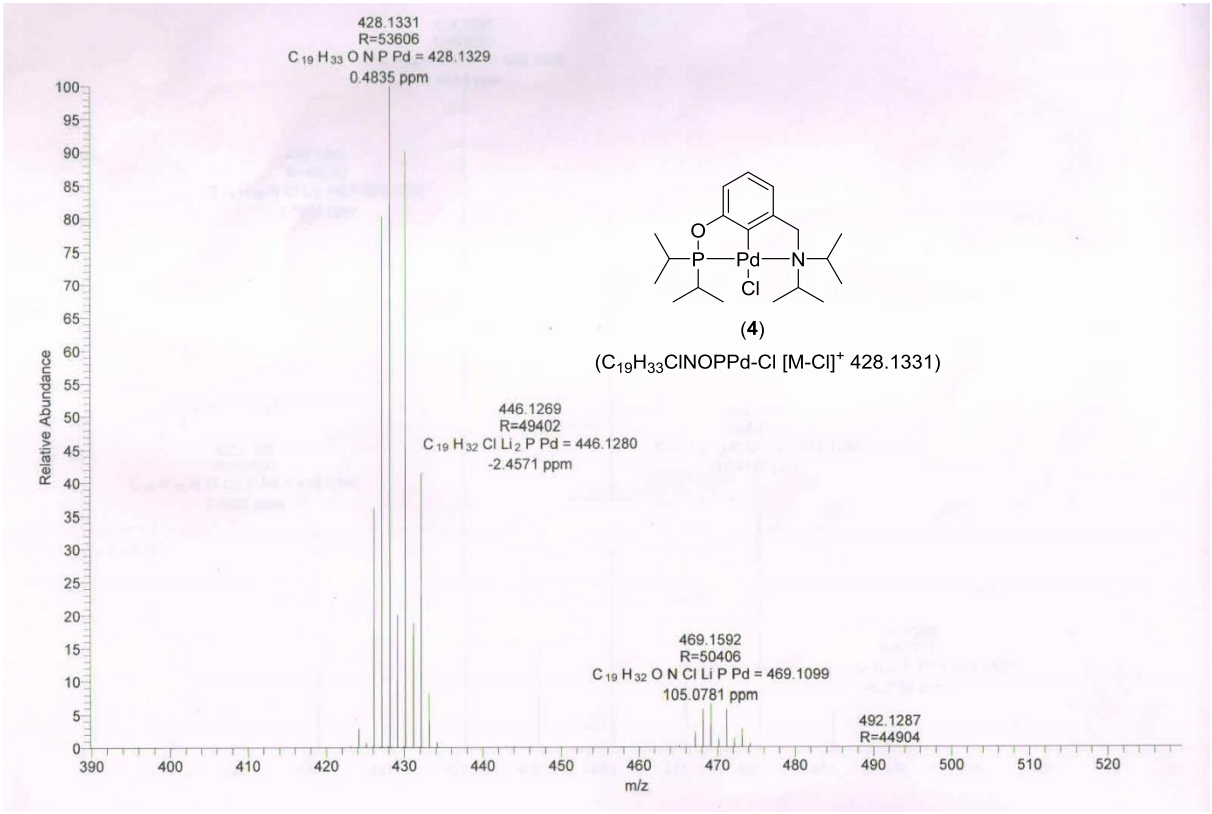

(**4**)

($C_{19}H_{33}ClNOPPd$-Cl $[M\text{-}Cl]^+$ 428.1331)

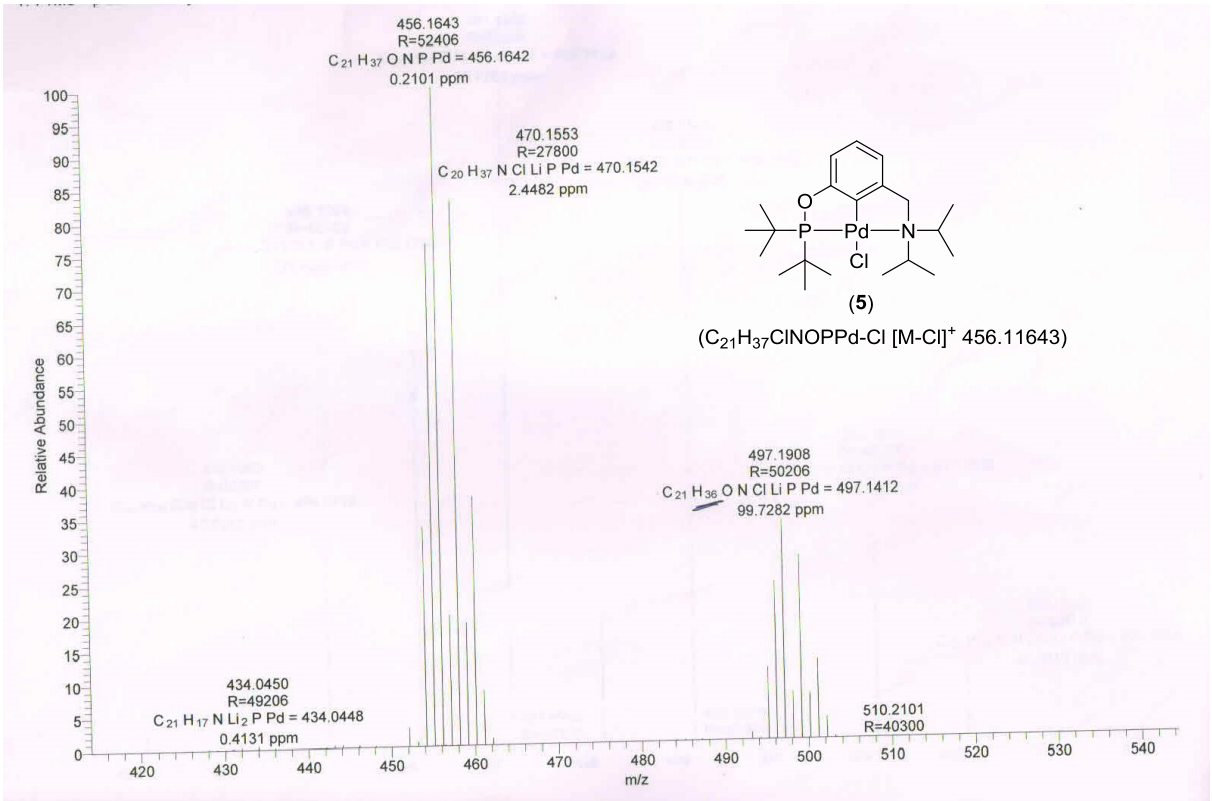

(**5**)

($C_{21}H_{37}ClNOPPd$-Cl $[M\text{-}Cl]^+$ 456.11643)

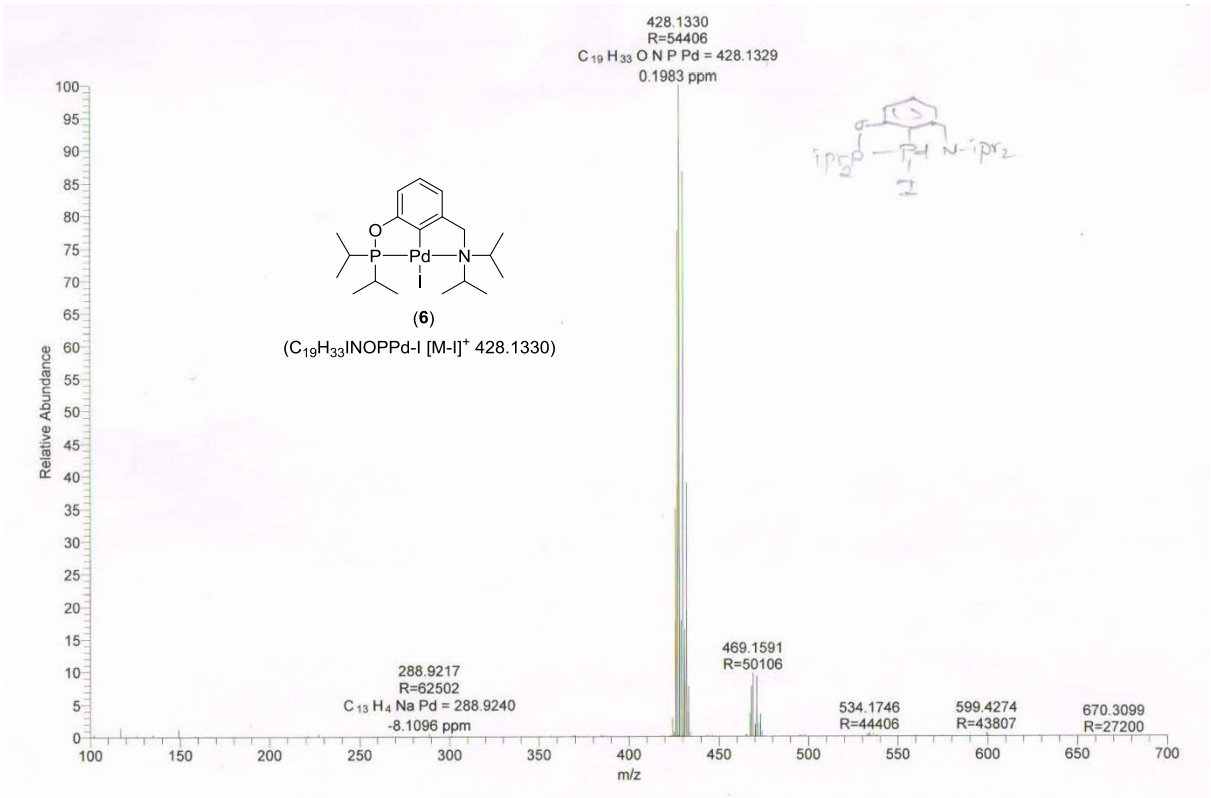
428.1330
R=54406
C 19 H 33 O N P Pd = 428.1329
0.1983 ppm
O
P
Pd
N
I
(6)
(C19H33INOPPd-I [M-I]+ 428.1330)
Relative Abundance
m/z
469.1591
R=50106
288.9217
R=62502
C 13 H 4 Na Pd = 288.9240
-8.1096 ppm
534.1746
R=44406
599.4274
R=43807
670.3099
R=27200

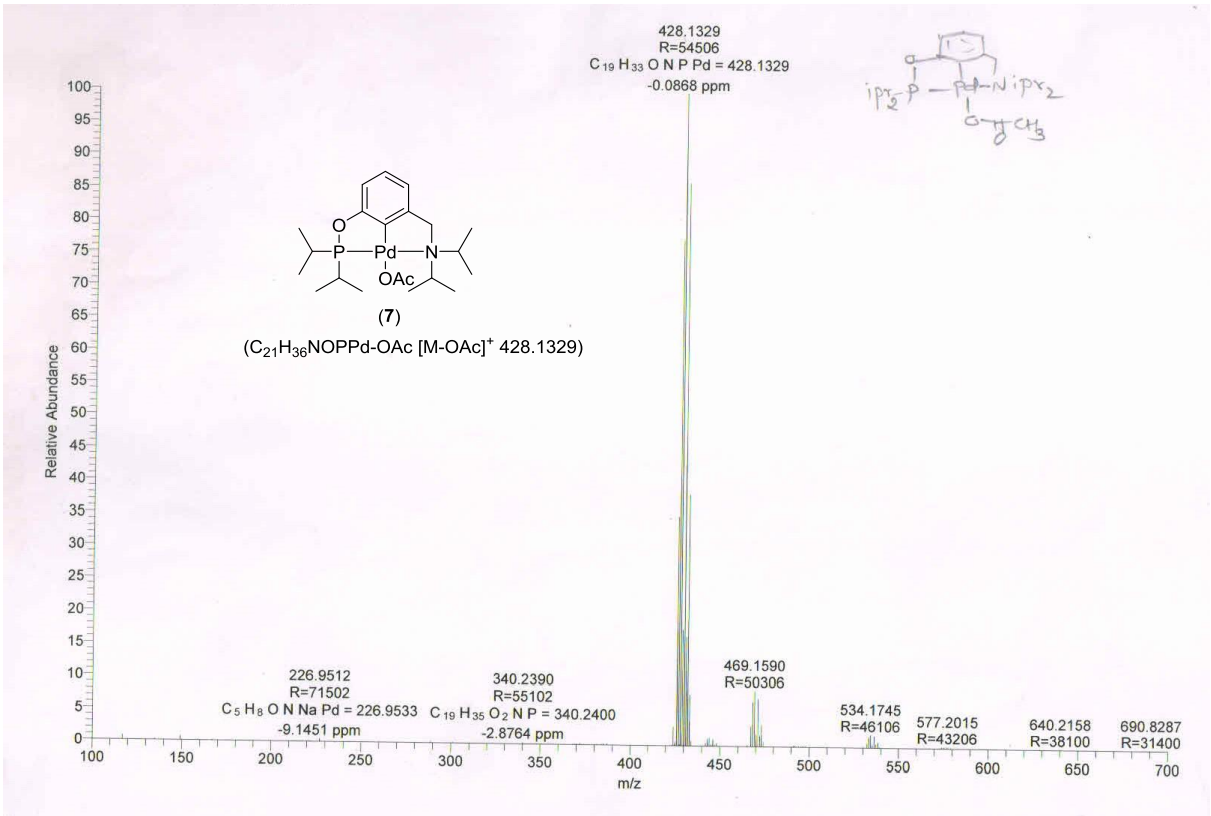
428.1329
R=54506
C 19 H 33 O N P Pd = 428.1329
-0.0868 ppm
O
P
Pd
N
OAc
(7)
(C21H36NOPPd-OAc [M-OAc]+ 428.1329)
Relative Abundance
m/z
469.1590
R=50306
226.9512
R=71502
C 5 H 8 O N Na Pd = 226.9533
-9.1451 ppm
340.2390
R=55102
C 19 H 35 O 2 N P = 340.2400
-2.8764 ppm
534.1745
R=46106
577.2015
R=43206
640.2158
R=38100
690.8287
R=31400

SK-140 #149 RT: 0.66 AV: 1 NL: 1.30E9
T: FTMS + p ESI Full ms [100.00-1500.00]

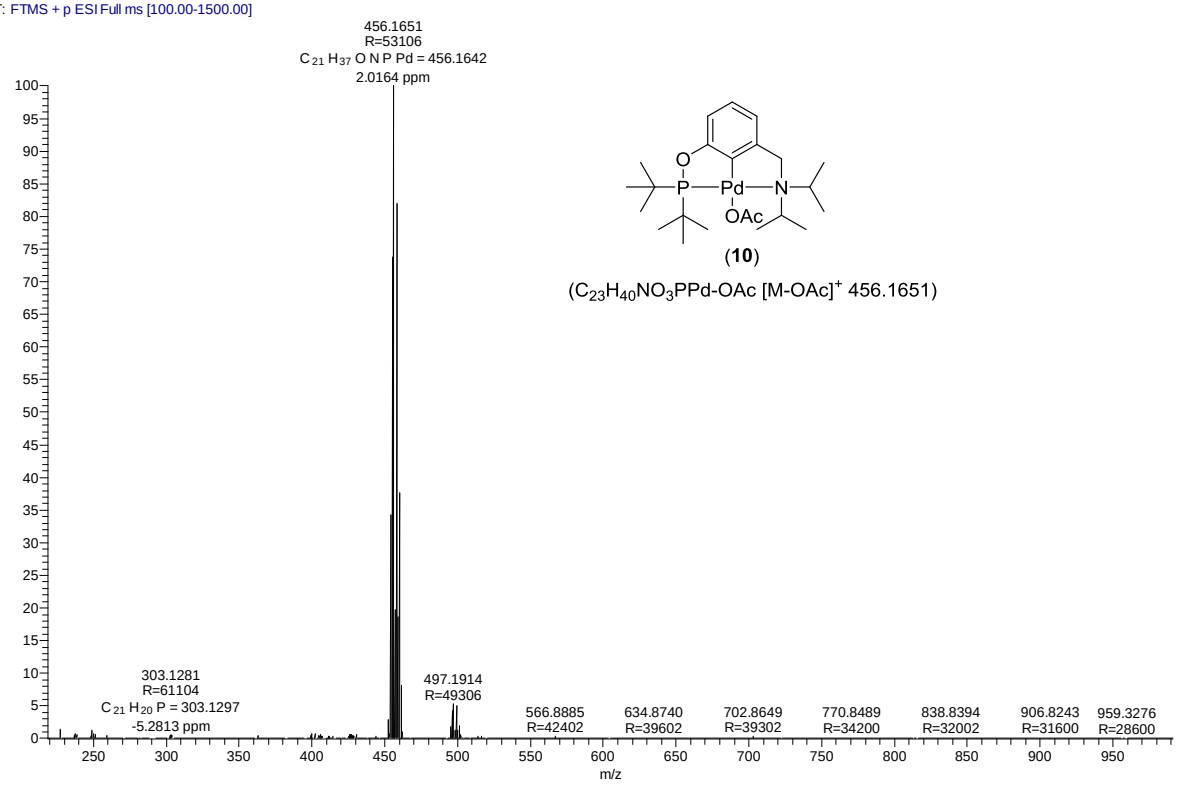

(**10**)

($C_{23}H_{40}NO_3PPd$-OAc $[M\text{-}OAc]^+$ 456.1651)

SK-139 #107 RT: 0.48 AV: 1 NL: 8.05E8
T: FTMS + p ESI Full ms [100.00-1500.00]

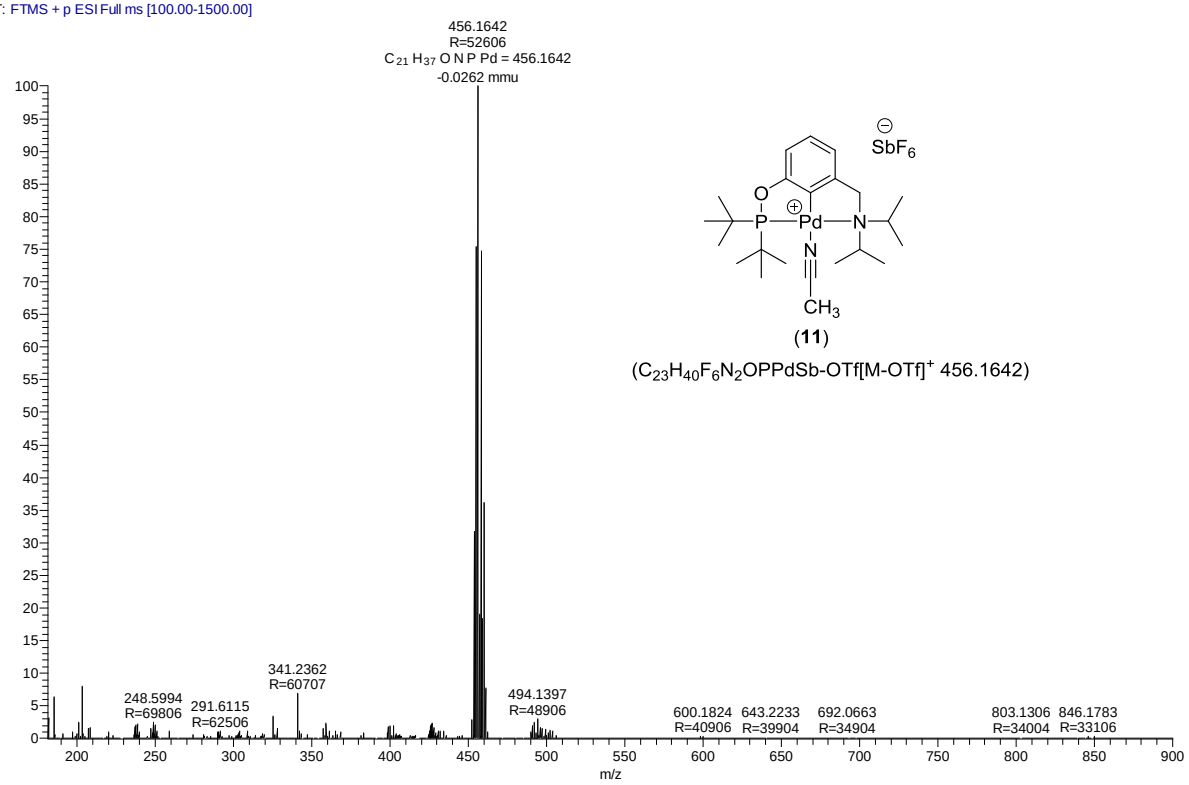

(**11**)

($C_{23}H_{40}F_6N_2OPPdSb$-OTf$[M\text{-}OTf]^+$ 456.1642)

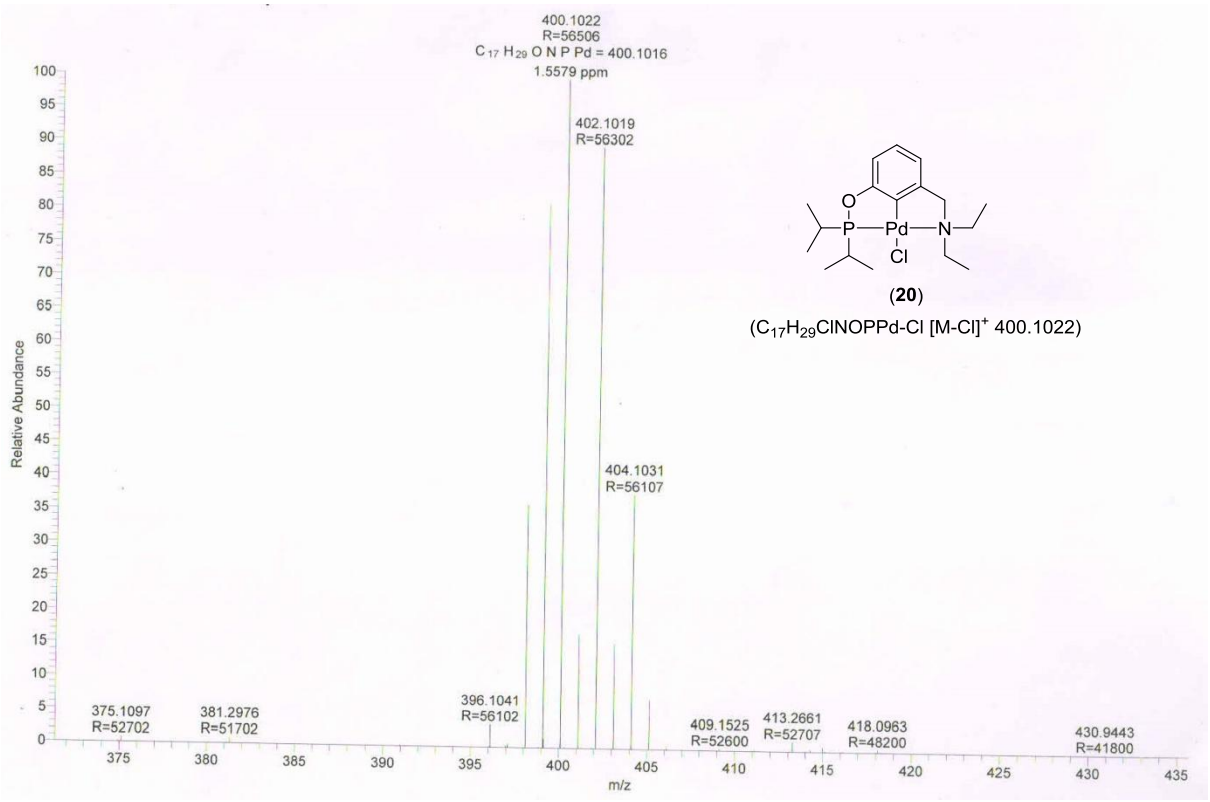

(**20**)

($C_{17}H_{29}ClNOPPd$-Cl $[M\text{-}Cl]^+$ 400.1022)

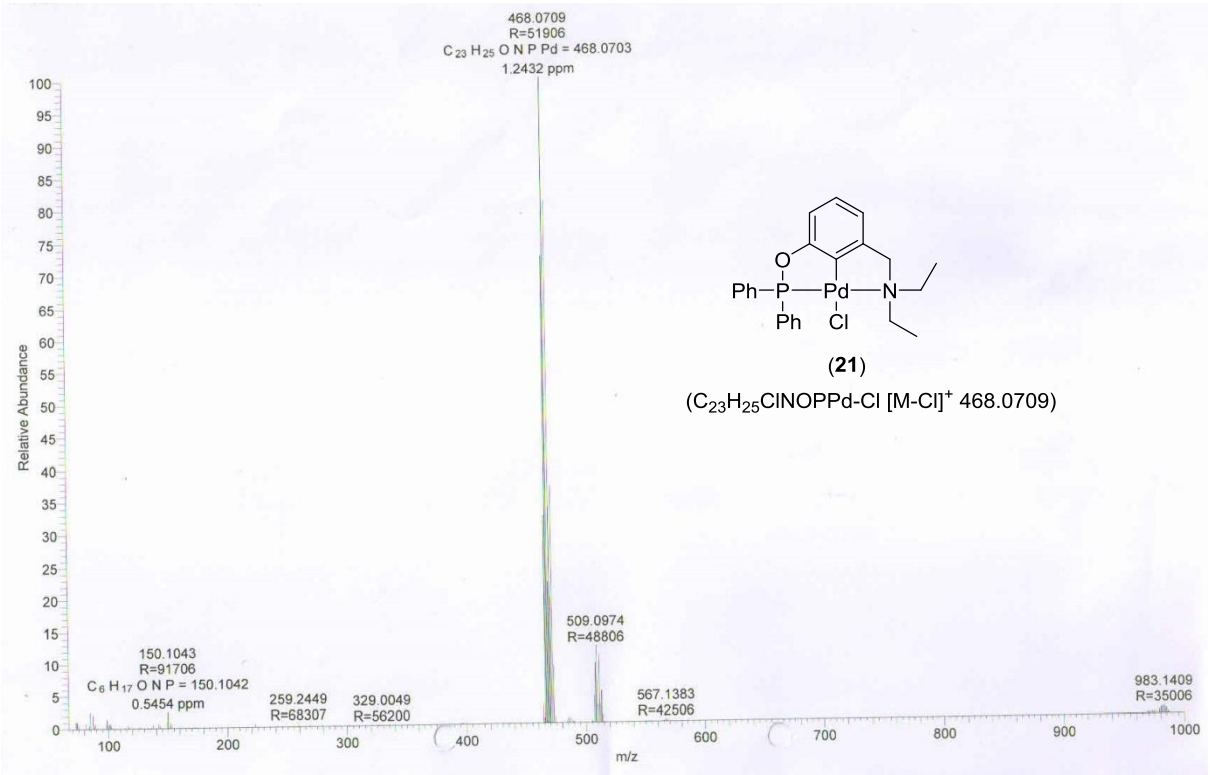

(**21**)

($C_{23}H_{25}ClNOPPd$-Cl $[M\text{-}Cl]^+$ 468.0709)

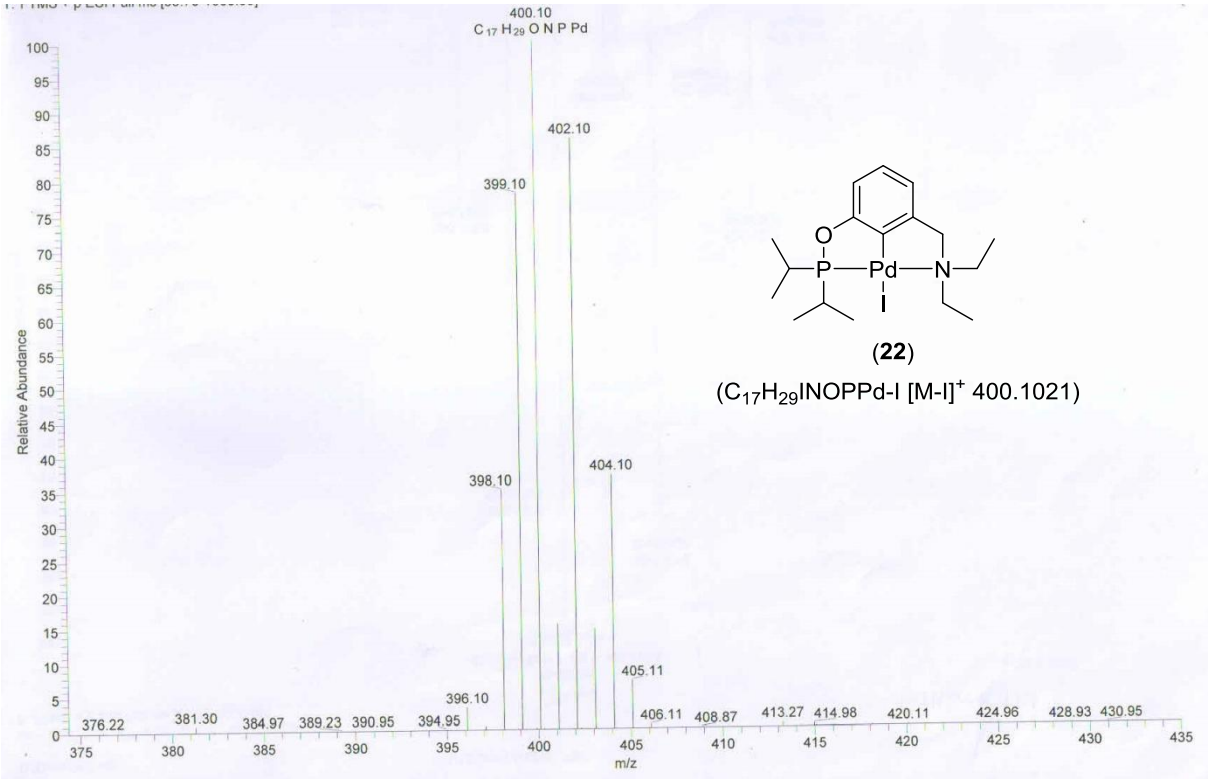

(**22**)

($C_{17}H_{29}INOPPd$-I $[M\text{-}I]^+$ 400.1021)

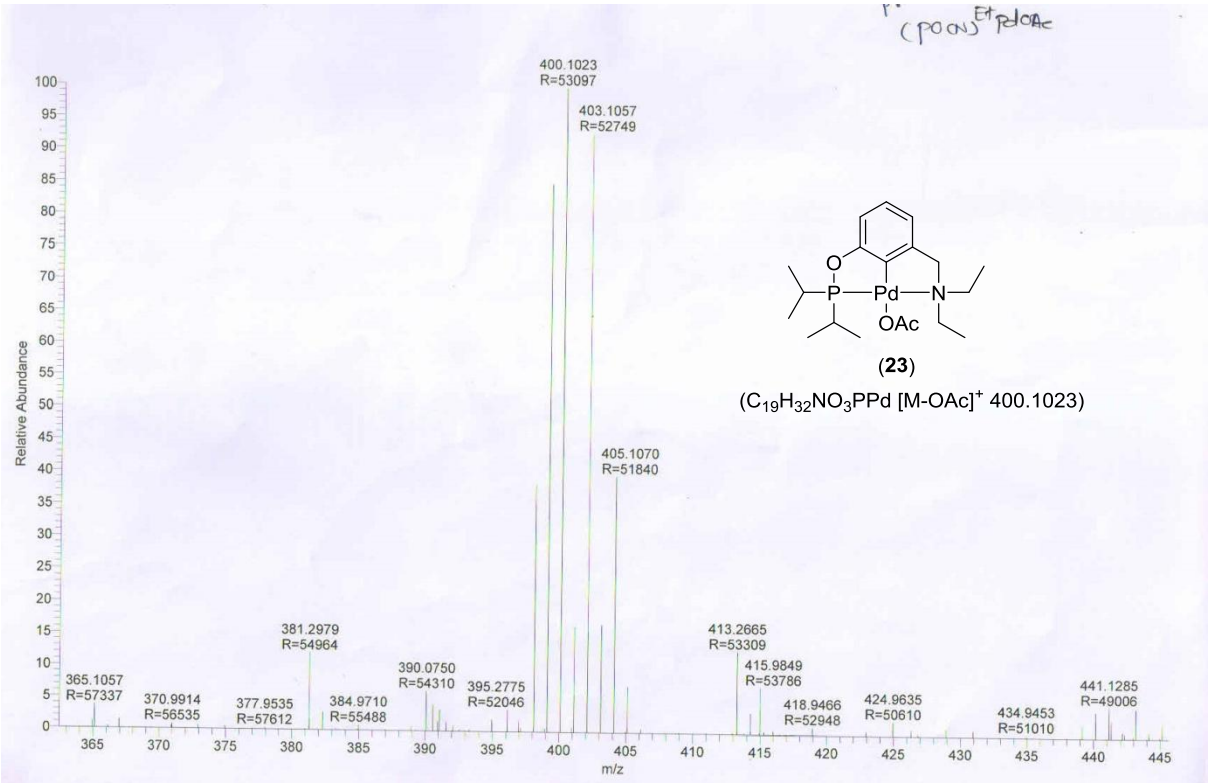

(**23**)

($C_{19}H_{32}NO_3PPd$ $[M\text{-}OAc]^+$ 400.1023)

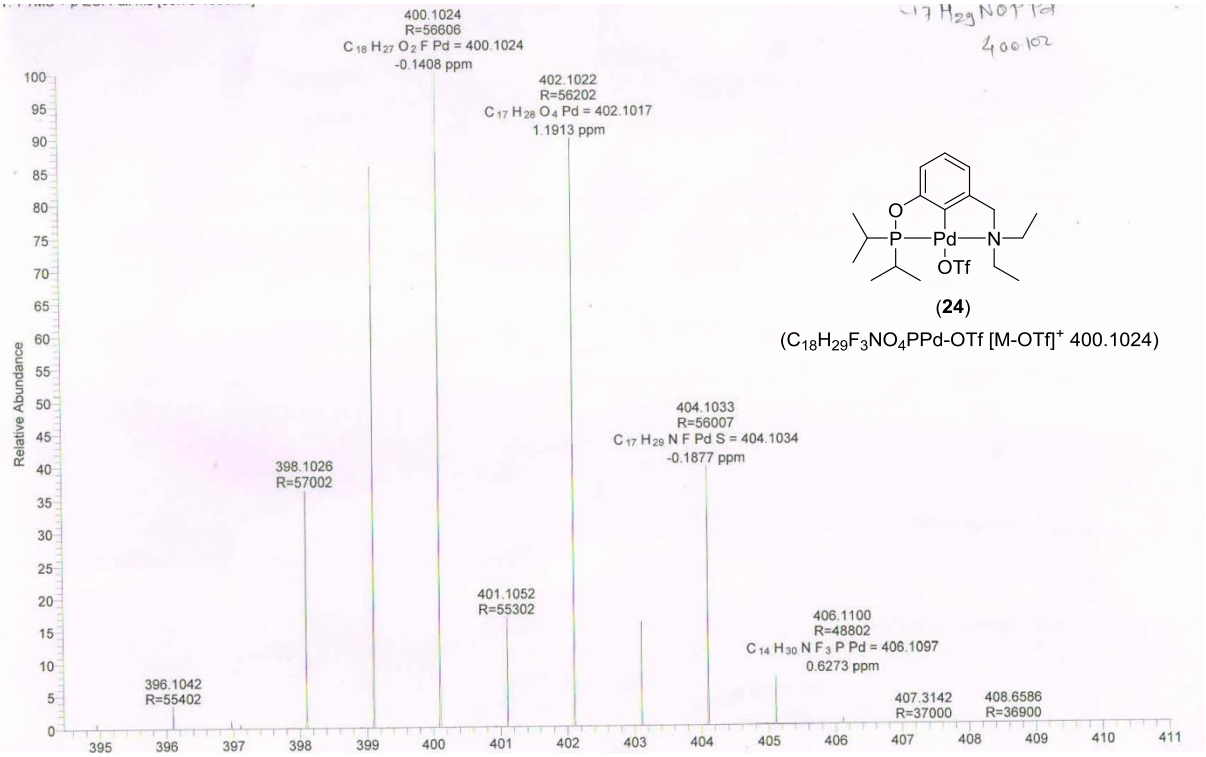

(**24**)

($C_{18}H_{29}F_3NO_4PPd$-OTf $[M\text{-}OTf]^+$ 400.1024)

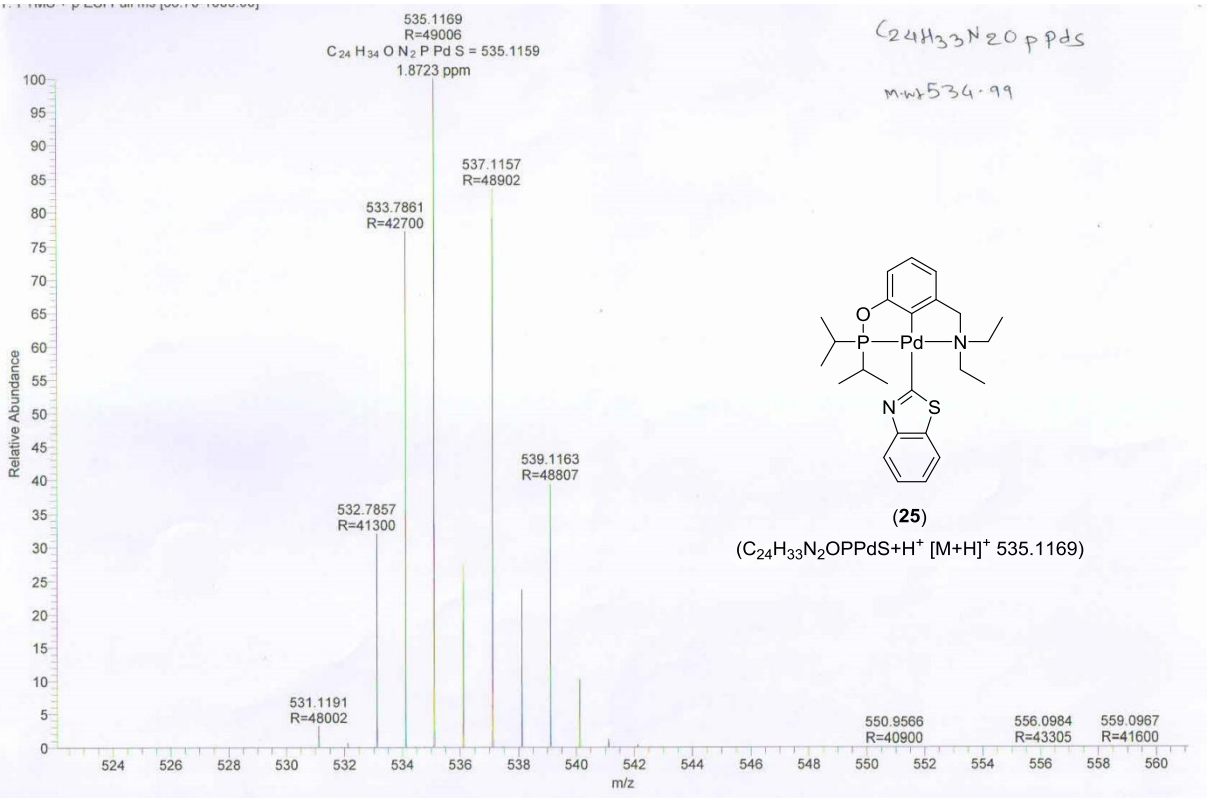

(**25**)

($C_{24}H_{33}N_2OPPdS+H^+$ $[M+H]^+$ 535.1169)

List of publications

1. Khake, S. M.; Jain, S; Vanka, K.; Gonnade, R. G.; Punji, B. "Mechanistic Aspects of Nickel-Catalyzed C(2)–H Alkynylation of Indoles", *Manuscript under preparation*.

2. Soni, V.; Khake, S. M.; Punji, B. "Nickel-Catalyzed Oxidative C(sp^2)-H/C(sp^3)-H Coupling of Indoles and Toluene Derivatives", *ACS Catal*. **2017**, *07*, 4202-4208.

3. Khake, S. M.; Soni, V.; Gonnade, R. G.; Punji, B. "A General Nickel-Catalyzed Method for C-H Bond Alkynylation of Heteroarenes through Chelation Assistance", *Chem. Eur. J.* **2017**, *23*, 2907-2914.

4. Khake, S. M.; Jagtap, R. A.; Dangat, Y. B.; Gonnade, R. G.; Vanka, K.; Punji., B., "Mechanistic Insights intoPincer-Ligated Palladium-Catalyzed Arylation of Azoles with Aryl Iodides: Evidence of a Pd(II)-Pd(IV)-Pd(II) Pathway" *Organometallics* **2016**, *35*, 875-886.

5. Pandey, D. K.; Khake, S. M.; Gonnade, R. G.; Punji, B., "Mono- and Binuclear Palladacycles via Regioselective C–H Bond Activation: Syntheses, Mechanistic Insights and Catalytic Activity in Direct Arylation of Azoles", *RSC Adv*. **2015**, *5*, 81502-81514.

6. Khake, S. M.; Soni, V.; Gonnade, R. G.; Punji, B., "Design and Development of POCN-Pincer Palladium Catalysts for C–H Bond Arylation of Azoles with Aryl Iodides", *Dalton Trans*. **2014,** *43*, 16084-16096.

7. Khake, S. M.; Soni, V.; Punji, B. "Process for the Preparation of Pincer Ligated Palladium Catalysts and Their Use for Arylation of Heterocyclic Compounds" *Indian Pat. Appl. IN 2013DE02566*, **2015**.

Highlighted Article

Chem. Eur. J. **2017**, *23*, 2907 is highlighted in *Synfacts* by Knochel, P. *SYNFACTS*, **2017**, *13*, 415.

Conference Presentations

1. Khake, S. M.; Soni. V.; Punji, B. "*Nickel-catalyzed Alkynylation of Heteroarenes and It's Mechanistic Investigation*" International Conference of Organic Synthesis-21, Indian Institute of Bombay, Maharashtra, India, December 11-16, **2016**.

2. Khake, S. M.; Punji, B. "*Mechanistic Insight into POCN-Pincer Palladium-Catalyzed Arylation of Azoles with Aryl Iodides*" Alexander von Humboldt Meet, Goa, India, November 20-22, **2015**.

3. Khake, S. M.; Punji, B. "*Mechanistic Insight into POCN-Pincer Palladium-Catalyzed Arylation of Azoles with Aryl Iodides*" 17th CRSI National Symposium in Chemistry, CSIR-National Chemical Laboratory, Pune, India, February 6-8, **2015**.

4. Khake, S. M.; Punji, B. "*Mechanistic Insight into POCN-Pincer Palladium-Catalyzed Arylation of Azoles with Aryl Iodide*" International Conference on Structural and Inorganic Chemistry, Hosted by CSIR-NCL and SP Pune university, Pune, India, December 4-5, **2014**.

5. Khake, S. M.; Soni. V.; Punji, B. "*Synthesis of Hybrid POCN-Pincer Palladium Complexes for Direct C–H Bond Arylation of Azoles*" Symposium on Modern Trends in Inorganic Chemistry-IV, Indian Institute of Roorkee, Uttarakhand, India, December 13-16, **2013**.

6. Khake, S. M.; Punji, B. "*Mechanistic Insight into POCN-Pincer Palladium-Catalyzed Arylation of Azoles with Aryl Iodides*" Poster presented on Science day held in CSIR-NCL, February 25-26, **2016**.

7. Khake, S. M.; Soni. V.; Punji, B. "*Synthesis of Hybrid POCN-Pincer Palladium Complexes for Direct C–H Bond Arylation of Azoles*" Poster presented on Science day held in CSIR-NCL, February 25-26, **2014**.

8. Khake, S. M.; Punji, B. "*Palladium Catalyzed Carbon–Carbon Bond Forming Reaction via C–H Bond Activation* " Poster presentation on CSIR foundation day in CSIR-NCL, September. **2015**

Award

Best poster prize for poster presented on science day which held on 28th February 2014 in CSIR-National Chemical Laboratory, Pune entitled as "*Synthesis of Hybrid POCN-Pincer Palladium Complexes for Direct C–H Bond Arylation of Azoles"*